Halogen- and Hydrogen-Bonding Cyclic and Interlocked Hosts for Anion Recognition and Sensing

Lydia C. Gilday

Jesus College, University of Oxford



A thesis submitted for the degree of Doctor of Philosophy

Inorganic Chemistry Laboratory

University of Oxford

Trinity Term 2013

Halogen- and Hydrogen-Bonding Cyclic and Interlocked Hosts for Anion Recognition and Sensing

Lydia C. Gilday, Jesus College, University of Oxford

Abstract of thesis submitted for the degree of Doctor of Philosophy, Trinity Term 2013

This thesis describes the synthesis of macrocyclic and interlocked receptors which exploit halogen- and hydrogen-bonding intermolecular interactions for anion recognition.

Chapter One introduces the field of supramolecular chemistry, with particular focus on applications of host–guest chemistry to anion coordination and anion templation in the construction of mechanically interlocked molecules.

Chapter Two details the synthesis of a series of cyclic and cage-like porphyrin-based receptors which bind anions through halogen- and hydrogen-bonding interactions. The ability of these receptor systems to bind and sense anionic guest species is investigated and comparisons between hydrogen- and halogen-bonding are discussed.

Chapter Three reports anion-templated pseudorotaxane assemblies stabilised by both halogen- and hydrogen-bonding. The related catenanes are also prepared and their affinity for anions is investigated. The first examples of interpenetrated and interlocked architectures constructed by a single charge-assisted halogen bond are also reported.

Chapter Four describes the synthesis of a 1,3-dialkyl-1,2,3-triazolium-containing threading component, whose anion binding properties are studied and compared with other threading molecules. The ability of this novel thread to form pseudorotaxanes is investigated and the preparation of the related rotaxane species is outlined.

Chapter Five discusses attempts to prepare rotaxanes with improved anion binding affinities through increasing the lipophilicity of the anion binding clefts. Several novel rotaxanes are described and their anion binding properties are probed.

Chapter Six describes the experimental procedures used in this work and the characterisation of compounds presented in chapters two to five.

Chapter Seven summarises the conclusions of this thesis.

Acknowledgements

I'm thankful that Paul Beer welcomed me into his group back in 2008, and for the many ideas he has provided throughout the five years I've worked for him. I'm fortunate to have such a supportive supervisor and without his encouragement and wisdom, particularly during the first year of my DPhil., I would not be here to tell the tale. I'm more grateful than I can possibly say.

As my Part II "guardian angel", Laura Hancock taught me an awful lot about lab-work and organic synthesis. Thanks for the huge amount of fun we had that year.

I've had the pleasure of working with some brilliant colleagues over the years. I'm particularly grateful to Nathan Kilah, Chris Serpell, Antonio Caballero, Fabiola Zapata, Nick Evans, Asha Brown and Graeme Spence for their advice, guidance and calming words. Neil Greenham deserves special thanks for time and again reminding me of our purpose in life. Current group members Matthew Langton, Jim Mercurio, Rich Knighton, Ben Mullaney, Sean Robinson, Tim Barendt and Stuart Cornes make S7/S8 an entertaining place to work. Thanks to Claire Carpenter, my excellent Part II student, whose collaboration and companionship made the second year of my DPhil much more enjoyable than it otherwise would have been. Special thanks also to Asha, Chris, Anna McConnell and Thomas Lang for synthetic advice and donation of compounds, to Nick White for solving crystal structures, and to Asha, Tim, Matt, Jim, Stuart, Rich and Sean for proofreading.

Journeying through this research degree without Nick White would have been unbearable. Thanks for friendship, a listening ear, discernment over synthetic ideas, encouragement when things haven't been going so well, help looking after the "kids", expanding my musical tastes, numerous Biochem coffees, and all the nick-names – a friend for life, not just for a DPhil.

I must also thank the EPSRC for funding this research, the Faulkner group for letting me use their instruments, and the various support services within the department for all their help. Specifically, Nick Rees has provided a great deal of help with NMR experiments and a lot of

football-related banter. Thanks also to Vitor Félix and Paulo Costa who were responsible for carrying out the MD Simulations described in Chapter Three.

Away from Chemistry, I owe an immense amount of gratitude to many friends. From way back when, I'd like to thank Phillida, Katie, Harriet and Joanna for friendship that has stood the test of time. I feel very blessed to have some wonderful friends from my time at Jesus College many of whom have trodden this path ahead or alongside me and understand the unique joys and challenges of research. Thanks to Scott Seamons, KWill, the Kennards, JBo, the Dollins-Nobles, and the Goddards. The past two years have been mostly Wycliffe Hall-focused and I'm grateful for the eternal friendships I've made there. Thanks to the Dysons, the Frys, Dr W., the Gallachers, the Prints, the Finlays, the Racklyefts, the Brassils, and Suzanne for your persistence in friendship and prayer on my behalf.

I'm incredibly grateful to my older and newer families for all their affection, I'm not good with words but I love you all very much. Thanks to my parents and brother for teaching me of the most important things in life, and for supporting me through eight long years in Oxford. Four years ago I acquired some wonderful in-laws – thank you for your generous welcome into the clan.

More than anything, I'm grateful for Patrick who knows me so well, loves me nevertheless, and cares for me like no-one else can: I love you. Thank you for believing in me and encouraging me to be truly myself. Thank you for letting it be my turn.

L.C.G. July 2013

"All things come from you O LORD, and of your own have we given you"

Previously published work

Some of the work described in this thesis has already been published.

Peer-reviewed journal articles

L. C. Gilday, N. G. White and P. D. Beer, *Halogen- and Hydrogen-Bonding Triazole-Functionalised Porphyrin-Based Receptors For Anion Recongition*, Dalton Trans., 2013, DOI: 10.1039/C3DT52093E.

L. C. Gilday, T. Lang, A. Caballero, P. J. Costa, V. Félix and P. D. Beer, *A Catenane Assembled through a Single Charge-Assisted Halogen Bond*, Angew. Chem. Int. Ed., 2013, **52**, 4356–4360.

L. C. Gilday, N. G. White and P. D. Beer, *Triazole- and Triazolium-Containing Porphyrin-Cages for Optical Anion Sensing*, Dalton Trans., 2012, **41**, 7092–7097.

Poster presentations

L. C. Gilday, N. G. White, and P. D. Beer, *Porphyrin-Based Cages for Anion Sensing*, International Symposium on Macrocyclic and Supramolecular Chemistry VII, Dunedin, New Zealand, February 2012.

L. C. Gilday, N. G. White and P. D. Beer, *Porphyrin-Based Anion Receptors Exploiting Halogen Bonding*, International Symposium on Macrocyclic and Supramolecular Chemistry VI, Brighton, UK, July 2011.

Oral presentations

L. C. Gilday and P. D. Beer, *Triazole- and Triazolium-Functionalised Porphyrin Receptors for Anion Recognition and Sensing*, Inorganic Chemistry Laboratory Graduate Symposium, April 2012.

Glossary

χ	electronegativity
δ	chemical shift
λ	wavelength
ε	extinction coefficient, relative permittivity
μ	micro, dipole moment
Δ	change in (a measurement), heat
°	degree
°C	degrees Celsius
4-DMAP	4-dimethylaminopyridine
Å	Ångstrom
A^-	anion
ADP	adenosine diphosphate
AN	acceptor number
anti	anticlinical
aq.	aqueous
Ar	aromatic
ATP	adenosine triphosphate
bipy	2,2'-bipyridine
Boc	di-*tert*-butyl dicarbonate
br	broad
Bu	butyl
cat.	catalytic
cf.	*confer*
c	centi
conc.	concentrated
COSY	homonuclear correlation spectroscopy
CuAAC	copper(I)-catalysed azide–alkyne cycloaddition
d	doublet, day
DBU	1,8-diazabicycloundec-7-ene
DCC	*N*,*N*'-dicyclohexylcarbodiimide
dd	doublet of doublets
DEAD	diethyl azidocarboxylate
DFT	density functional theory
D*i*BAL-H	di-*iso*-butylaluminium hydride
D*i*PEA	*N*,*N*-di-*iso*-propylethylamine
DMF	*N*,*N*-dimethylformamide
DMSO	dimethyl sulfoxide
DNA	deoxyribonucleic acid
E	standard electrode potential
e.g.	*exempli gratia*
EDCI	1-ethyl-3-(3-dimethylaminopropyl)carbodiimide

en	ethylenediamine
eq., equiv.	equivalent
ESIMS	electrospray ionisation mass spectrometry
Et	ethyl
g	gram
G	Gibbs free energy
GAFF	general amber force field
Grubbs' II	Grubbs' second generation catalyst
h	hour
HEPES	(4-(2-hydroxyethyl)-1-piperazineethanesulfonic acid
HOBt	hydroxybenzotriazole
Hz	hertz
i.e.	*id est*
J	Joule
J	coupling constant
k	kilo
K	Kelvin
K_a	association constant
K_{app}	apparent association constant
L	litre
M	molar
M	mega, molecular ion
m	milli, multiplet,
m	*meta*
m/*z*	mass-to-charge ratio
max.	maximum
MD	molecular dynamics
Me	methyl
mes	mesitylene, 1,3,5-triemethylbenzene
min	minute
MLCT	metal-to-ligand charge transfer
mol	mole
Ms, mesyl	methanesulfonyl chloride
n	nano
n	normal
NHS	*N*-hydroxysuccinimde
NMR	nuclear magnetic resonance
OAc	acetate
p	*para*
PBP	phosphate-binding protein
PET	photoinduced electron transfer
pH	$-\log_{10}[H^+]$
Ph	phenyl

phen	1,10-phenanthroline
phth	*N*-phthalimide
pK_a	$-\log_{10}K_a$
ppm	parts per million
PPTS	pyridinium *para*-toluenesulfonate
Pr	propyl
pyBOP	benzotriazol-1-yl-oxytripyrrolidinophosphonium hexafluorophosphate
q	quartet
quin.	quintet
R	chemical substituent
RCM	ring closing metathesis
R_f	Retention factor
ROESY	rotating-frame nuclear Overhauser effect correlation spectroscopy
rt	room temperature
s	second, singlet
sat.	saturated
SBP	sulfate-binding protein
sept.	septet
sic	*sic erat scriptum*
syn	synperiplanar
t	triplet
t, *tert*	tertiary
TBA	tetrabutyl ammonium
TBTA	tris[(1-benzyl-1*H*-1,2,3-triazol-4-yl)methyl]amine
TFA	trifluoroacetic acid
T_{gel}	sol-gel transition temperature
THF	tetrahydrofuran
TLC	thin layer chromatography
TMS	trimethylsilyl
TOCSY	total correlaction spectroscopy
TOF	time of flight
TPP	tetraphenylporphyrin
Ts, tosyl	*para*-toluenesulfuonyl chloride
UV	ultra-violet
V	volts
vis.	visible
wt.	weight
X	halogen atom

Contents

Chapter 1 Introduction 1

1.1 Introduction to supramolecular chemistry and its applications 1

1.2 Non-covalent forces 2

1.3 Design principles in synthetic supramolecular chemistry 5

1.3.1 Complementarity 5

1.3.2 Preorganisation and the chelate/macrocyclic effects 5

1.4 Host–guest chemistry 7

1.4.1 Cation binding 7

1.4.2 Anion binding 8

1.4.2.1 The importance of anions 8

1.4.2.2 The challenge of anions 9

1.4.2.3 Biological anion recognition 10

1.4.2.4 Synthetic anion receptor chemistry 11

1.4.2.4.1 Positively charged anion receptors 11

1.4.2.4.2 Neutral anion receptors 16

1.4.2.4.3 Lewis acid–base anion receptors. 25

1.4.3 Applications of anion recognition 26

1.4.3.1 Anion transport 26

1.4.3.2 Anion-controlled gelation 28

1.4.3.3 Anion sensors 28

1.4.3.3.1 Electrochemical anion sensors 29

1.4.3.3.2 Optical anion sensors 30

1.4.3.3.3 Displacement assays 34

1.5 Self-assembly 35

1.5.1 Templated self-assembly 35

1.5.1.1 Cation templation 36
1.5.1.2 Anion templation 37
1.5.2 Interpenetrated and interlocked structures 39
1.5.2.1 Cation-templated assembly of interlocked molecules 43
1.5.2.2 Neutral-templated assembly of interlocked molecules 47
1.5.2.3 Anion-templated assembly of interlocked molecules 48
1.5.3 Applications of interlocked molecules 50
1.5.3.1 Rotaxane shuttles 51
1.5.3.2 Rotaxane-based molecular muscles 53
1.5.3.3 Catenane-based pirouettes and shuttles 54
1.6 Project aims 55
1.7 References for Chapter One 56
Chapter 2 Triazole- and triazolium-functionalised porphyrin-based receptors for anion recognition and sensing 67
2.1 Introduction 67
2.1.1 The importance of porphyrins 67
2.1.2 The physical properties of porphyrins 69
2.1.3 Porphyrins as reporter groups for anion recognition and sensing 70
2.1.4 Triazole groups as anion recognition motifs 74
2.1.5 Chapter aims 76
2.2 Tetrapodal zinc(II)-metalloporphyrin anion receptors 77
2.2.1 Synthesis of tetrakis-triazole-functionalised zinc(II)-metalloporphyrin anion receptors 77
2.2.2 Characterisation of tetrakis-triazole-functionalised zinc(II)-metalloporphyrin anion receptors 6 and 10 82
2.2.3 Anion binding properties of neutral triazole- and iodotriazole-functionalised zinc(II)-metalloporphyrin anion receptors 84

2.2.3.1 Anion binding properties of a hydrogen-bonding triazole-functionalised anion receptor 6 84

2.2.3.2 Anion binding properties of a halogen-bonding iodotriazole-functionalised anion receptor 10 89

2.2.3.3 The effect of solvent on anion binding properties displayed by 6 and 10 .. 91

2.2.3.4 Comparing the anion binding properties of receptor 6 with its free base porphyrin analogue 93

2.2.4 Synthesis and characterisation of cationic triazolium-functionalised zinc(II)-metalloporphyrin anion receptors 95

2.2.5 Anion binding properties of cationic triazolium-functionalised zinc(II)-metalloporphyrin anion receptors 97

2.3 Cyclic functionalised-porphyrin anion receptors 101

2.3.1 Synthesis of triazole- and triazolium-functionalised zinc(II)-metalloporphyrin-cage anion receptors 101

2.3.2 Characterisation of triazole- and triazolium-functionalised zinc(II)-metalloporphyrin-cage anion receptors 105

2.3.3 Anion binding properties of triazole- and triazolium-functionalised zinc(II)-metalloporphyrin-cage anion receptors 107

2.3.4 Cation and ion-pair binding properties of neutral triazole-functionalised zinc(II)-metalloporphyrin-cage receptor 112

2.3.5 Attempted synthesis of an iodotriazole-functionalised zinc(II)-metalloporphyrin-cage for anion recognition 115

2.3.6 Characterisation of an iodotriazole-functionalised zinc(II)-metalloporphyrin-cage anion receptor 118

2.4 Conclusions and future work 119

2.5 References for Chapter Two 120

Chapter 3 Halogen-bonding threading components for anion-templated and halogen-bond-templated interpenetrated and interlocked structures 125

3.1 Introduction 125

3.1.1 The construction of interlocked structures 125

3.1.2 Halogen bonding for interpenetrated and interlocked structure assembly 126

3.1.3 Chapter aims 128

3.2 Anion-templated interpenetrated and interlocked structures exploiting halogen bonding 129

3.2.1 Synthesis of halo-functionalised pyridinium threading components 129

3.2.2 Synthesis of macrocycle components 131

3.2.3 Anion-templated pseudorotaxane formation exploiting halogen bonding 133

3.2.4 Synthesis of bis-vinyl-appended macrocycle precursors 137

3.2.5 Pseudorotaxane formation using halogen- and hydrogen-bonding bis-vinyl-appended pyridinium macrocycle precursors 140

3.2.6 Synthesis of anion-templated catenanes stabilised by halogen bonding 143

3.2.7 Characterisation of anion-templated catenanes stabilised by halogen-bonding interactions 145

3.2.8 Anion binding properties of novel [2]catenanes stabilised by halogen-bonding interactions 147

3.3 Halogen-bond-templated interlocked structures 150

3.3.1 Synthetic strategy for the formation of halogen-bond-templated catenanes 150

3.3.2 Pseudorotaxane assembly stabilised using inter-component halogen-bonding interactions 151

3.3.3 Synthesis and characterisation of a [2]catenane assembled using a single charge-assisted halogen bond 154

3.3.4 Molecular dynamics simulations of catenane 74·BF_4 carried out by Professor Vitor Félix 157

3.3.5 Towards the synthesis of anion-templated, halogen-bonding [2]rotaxanes.... 160

3.4 Towards molecular switches which operate through a combination of halogen bonding and anion binding..... 162

3.5 Conclusions and future work..... 164

3.6 References for Chapter Three..... 166

Chapter 4 Triazolium-containing interpenetrated and interlocked host structures for anion recognition.....171

4.1 Introduction and chapter aims..... 171

4.2 Acyclic 1,3-dialkyltriazolium anion receptor..... 173

4.2.1 Synthesis and characterisation of acyclic dialkyltriazolium-based anion receptors..... 173

4.2.2 Anion recognition properties of dialkyltriazolium-based anion receptors..... 175

4.2.3 Pseudorotaxane assembly studies..... 178

4.3 A rotaxane incorporating the 1,3-dialkyltriazolium anion recognition unit..... 182

4.3.1 Synthesis and characterisation of the first 1,3-disubstituted-1,2,3-triazolium-containing rotaxane..... 182

4.3.2 Anion recognition properties of novel 1,3-disubtituted triazolium-based rotaxane 100·PF_6..... 191

4.4 Macrocycles incorporating the triazolium anion recognition unit..... 193

4.4.1 1,3-Disubstituted-triazolium-based macrocycle compound..... 194

4.4.2 1,4-Disubstituted-triazolium-based macrocycle compound..... 195

4.4.3 Attempted synthesis of catenanes consisting of 1,4-disubstituted triazolium-based macrocycles..... 199

4.5 Conclusions..... 202

4.6 References for Chapter Four..... 203

Chapter 5 Shielded alkyl-functionalised rotaxane host cavities for improved anion recognition strengths 207

5.1 Introduction and chapter aims 207
5.2 Macrocycle functionalisation 208
5.2.1 Rotaxanes incorporating amino acid residues 208
5.2.1.1 Introduction 208
5.2.1.2 Synthesis of macrocycle precursor compounds 208
5.2.1.3 Synthesis of pyridinium chloride stoppered-axle component 209
5.2.1.4 Attempted synthesis of rotaxane 210
5.2.2 Rotaxanes incorporating amino ether units 212
5.2.2.1 Synthesis of macrocycle component 212
5.2.2.2 Pseudorotaxane studies 215
5.2.2.3 Synthesis and characterisation of a rotaxane incorporating an alkyl-functionalised macrocyclic component 215
5.2.2.4 Anion recognition properties of alkyl-functionalised rotaxane 218
5.3 Axle functionalisation 222
5.3.1 Rotaxanes containing alkyl-functionalised stoppers 222
5.3.1.1 Synthesis of model potential threading component 222
5.3.1.2 Pseudorotaxane formation with a model threading component 223
5.3.1.3 Synthesis of novel stoppered-axle component 225
5.3.1.4 Anion recognition properties of alkyl-functionalised axle component 226
5.3.1.5 Synthesis and characterisation of a novel rotaxane incorporating alkyl-functionalised stoppers 227
5.3.1.6 Anion binding properties of axle-functionalised rotaxane 231
5.3.2 Rotaxanes containing alkyl-functionalised axles with flexible linkages 233
5.3.2.1 Synthesis of alkyl-appended stopper groups and axle compounds 233
5.3.2.2 Anion recognition properties of new axle components 237
5.3.2.3 Synthesis and characterisation of novel rotaxanes containing alkyl-functionalised axles with flexible linkages 239

5.3.2.4 Anion recognition properties of novel rotaxanes 242

5.4 Conclusions 243

5.5 References for Chapter Five 244

Chapter 6 Experimental 249

6.1 General remarks 249

6.1.1 Reactants, reagents and solvents 249

6.1.2 Instrumental methods 249

6.2 Experimental procedures for Chapter Two 250

6.3 Experimental procedures for Chapter Three 276

6.4 Experimental procedures for Chapter Four 302

6.5 Experimental procedures for Chapter Five 325

6.6 ^{1}H NMR titration protocols 361

6.7 UV/visible titration protocols 364

6.8 References and notes for Chapter Six 364

Chapter 7 Conclusion 369

Appendices 375

A.1 Additional titration curves for titration experiments 375

A.1.1 Titration curves for Chapter Two 375

A.1.2 Titration curves for Chapter Three 378

A.2 Additional information for Chapter Five 379

A.3 Crystal structure data 379

A.3.1 General notes 379

A.3.2 Crystal structure of tetra-azide-functionalised zinc(II)-metalloporphyrin 5 .. 382

A.3.3 Crystal structure of tetrakis-iodotriazole-functionalised zinc(II)-metalloporphyrin 10 383

A.3.4 Crystal structure of triazole-functionalised zinc(II)-metalloporphyrin cage anion receptor 25 384

A.3.5 Crystal structure of 1,3-dialkyltriazolium threading species 84·Br 385

A.3.6 Crystal structure of 1,4-disubstituted triazolium-based macrocycle 113·BF_4. 386

A.3.7 Crystal structure of macrocycle 129 387

A.3.8 Crystal structure of 133·Cl 388

A.4 Molecular modelling carried out by Prof. Vitor Félix 389

A.4.1 Computational Details. 389

A.4.1.1 DFT calculations and halogen bond parameterization for Molecular Dynamics simulations 389

A.4.1.2 Generation of starting structures for the MD simulations 392

A.4.1.3 Molecular Dynamics simulations 393

A.4.2 MD simulations extended analysis 394

A.4.2.1 Extended discussion on simulations with S2A and S2B 395

A.5 References and notes for Appendices 397

Chapter One

Chapter 1 Introduction

1.1 Introduction to supramolecular chemistry and its applications

Defined as "*chemistry beyond the molecule*",[1] supramolecular chemistry is an established, wide-ranging, interdisciplinary field of scientific research concerned with non-covalent interactions between molecules, rather than more traditional covalent bonding within molecules. More rigorously, supramolecular chemistry is "*the chemistry of the intermolecular bond, covering the structures and functions of the entities formed by the association of two or more chemical species*"[1] and encompasses two main areas: host–guest chemistry and self-assembly. Host–guest chemistry covers complex formation between a receptor molecule and a smaller substrate molecule, whereas self-assembly involves the spontaneous arrangement of multiple smaller molecules to construct a higher order, more complex structure (Figure 1.1).

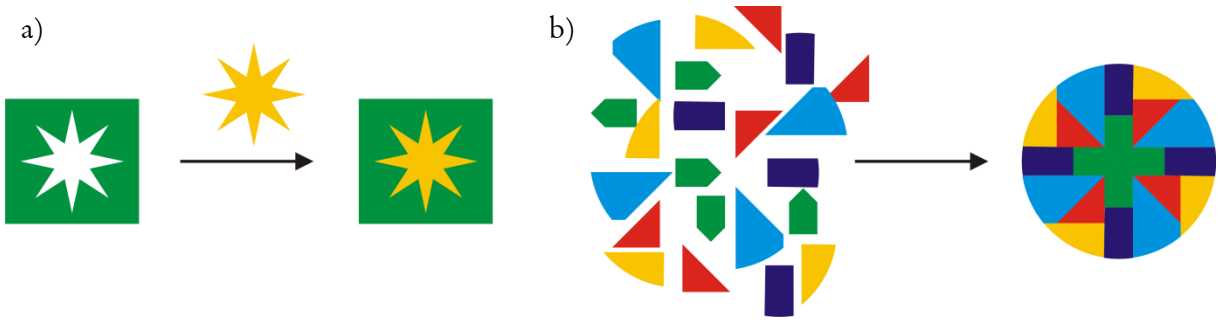


Figure 1.1. Schematic representation of the two areas of supramolecular chemistry: a) host–guest complex formation and b) self-assembly.

The intense research into this area is fuelled by the many impressive examples found in nature, where intermolecular interactions control numerous processes crucial to life. Examples include the binding of a specific substrate to an enzyme host and the construction, transcription and replication of DNA, where the specific nucleotides self-assemble via complementary hydrogen bonding into the DNA double helix.[2]

1.2 Non-covalent forces

Intermolecular non-covalent interactions are fundamental in supramolecular chemistry and the most important are discussed below. With the exception of attractive forces between opposite charges, many non-covalent interactions are weak compared with a covalent bond: hydrogen bonds are typically 4–120 kJ mol^{-1} and ion–dipole interactions 50–200 kJ mol^{-1} *versus* 300–500 kJ mol^{-1} for a carbon-carbon covalent bond. Consequently, supramolecular assemblies often rely on the cumulative effect of multiple non-covalent interactions operating in concert to facilitate the formation of stable structures.

Electrostatic interactions encompass all coulombic interactions which are usually divided into three sub-categories. *Ion–ion interactions* between oppositely charged species are the strongest but being isotropic they are often used in conjunction with other more directional forces. *Ion–dipole* and *dipole–dipole interactions* are much weaker but their utility lies in their inherent directionality arising from the orientation of the dipole (Figure 1.2).[3]

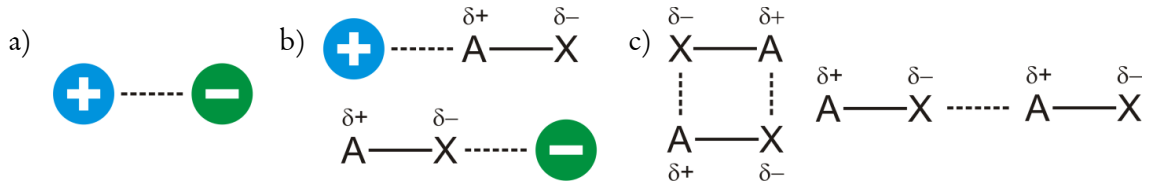


Figure 1.2. The three sub-categories of coulombic forces: a) ion-ion; b) ion-dipole; and c) dipole-dipole interactions.

Hydrogen bonding is a specific example of an ion-dipole or dipole-dipole interaction (Figure 1.3a). A hydrogen atom attached to a more electronegative atom (e.g. O, N, C; χ = 3.44, 3.04, 2.55 respectively) or electron-withdrawing group, is polarised and can interact with an anion or dipole through its partial positive charge.

Halogen bonding is analogous to hydrogen bonding where the hydrogen atom is replaced by a halogen species (Figure 1.3b). Legon has defined halogen bonding as "*an attractive interaction between a halogen atom X from a molecule or fragment R–X in which R is a group more electronegative than X or X itself, and an atom or a group of atoms A in the same molecule R–X or in a different molecule B, where there is evidence of bond formation*".[4] The forces involved in

halogen-bond formation include electrostatic, charge-transfer, electron donation and dispersion interactions. Theoretical studies reveal the electron density around the halogen atom in covalently bonded organohalides is anisotropically distributed giving rise to areas of partial positive (a "σ-hole" at the terminus of the R–X bond) and negative potential (around the equator of the halogen atom). This anisotropy is increased on moving from fluorine to iodine, and the positive potential increases further with the electron-withdrawing effect of any covalently attached groups.[5] The interaction of the σ-hole with an anion is comparable in strength to a hydrogen bond whilst being more directional. It has also been shown that the stronger the halogen bond formed, the shorter the anion···X distance, the longer the R–X bond which is more consistent with electron donation from the Lewis basic donor atom to the antibonding R–X orbital.

The ability of halogen atoms to interact with Lewis bases has been known for some time: in 1863 Guthrie reported an addition complex of diiodine and ammonium (something that would now be considered a halogen bond).[6] In the 1950s and '60s, Hassel and co-workers studied halogen-bonded complexes of inorganic and organic donors, the results of which were presented in his 1970 Nobel lecture.[7] In spite of this and further developments in the '70s and '80s, the value of halogen bonding in supramolecular chemistry remained largely unrecognised until the last 15 years. Metrangolo, Resnati and co-workers have exploited the significant directionality of halogen bonding in crystal engineering, and an example is shown in Figure 1.3b.

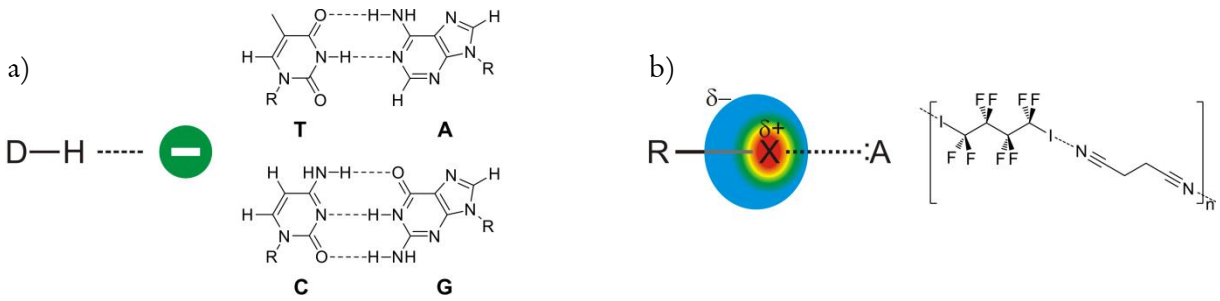


Figure 1.3. a) Hydrogen bonding: cartoon representation and hydrogen bonding between DNA base pairs.[8] b) Halogen bonding: cartoon representation showing the σ-hole (red) and halogen bonding in liquid crystals.[9]

Aromatic donor–acceptor interactions are the favourable interactions between electron-deficient and electron-rich aromatic rings which are further enhanced if one or more component is charged.[10] Previously considered as π–π stacking interactions, the parallel arrangement of aromatic rings has recently been demonstrated by theoreticians to be dominated by electrostatic and dispersion forces, with no special involvement of the π electrons, except with very large poly-aromatic systems.[11] These forces are maximised when aromatic rings stack in an off-set, face-to-face manner, though direct stacking and edge-to-face arrangements are also frequently observed (Figure 1.4a).

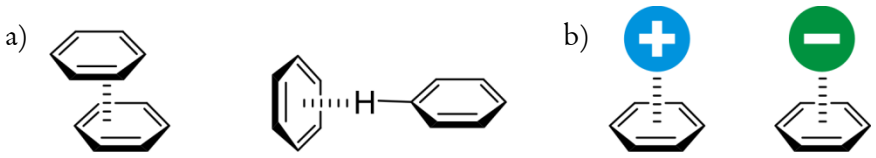


Figure 1.4. a) Aromatic donor–acceptor interactions: face-to-face and edge-to-face. b) Cation–π and anion–π interactions.

The ability of delocalised aromatic π-orbitals to interact with positively charges species has been known for some time. These *cation–π interactions* have been observed in the solid, solution and gas phases and are known to operate in nature.[12-15] In contrast, the existence of interactions between anions and electron-deficient aromatic species is a more recent discovery.[16] *Anion–π interactions* are less commonly seen in the solution phase[17] than in the gas phase[18] or solid state[17,19-23] and are usually supplemented by other non-covalent interactions.[19,24,25] As with "π–π stacking interactions", anion–π associations are dominated by electrostatic effects and anion-induced polarisation of the delocalised electron density.[26,27]

The *coordinate bond* is not strictly a supramolecular interaction since it involves a high degree of orbital overlap and consequently gives a very strong bond. Nevertheless, metal–ligand bonds and Lewis acid–base coordination are often employed in supramolecular chemistry to effect strong host–guest association or favourable self-assembly.[28]

Solvatophobic effects (or hydrophobic if water is considered), are a useful tool to be considered in supramolecular chemistry.[29] The expulsion of ordered, polar solvent molecules (usually water) from the binding site of a host receptor as a guest binds is thermodynamically

favourable. Entropically, there is an increase in disorder as the individual water molecules are released into bulk solvent; enthalpically, the removal of the weakly coordinated water molecules allows stronger non-covalent interactions to form.

1.3 Design principles in synthetic supramolecular chemistry

In addition to harnessing the individual non-covalent forces available for supramolecular assembly, it is also vital to design molecules in such a way as to optimise the concerted effect of multiple interactions between components. The principles of *complementarity* and *preorganisation* can be drawn on to achieve this goal.

1.3.1 Complementarity

In host–guest chemistry if two components are well-matched in terms of size, shape and functional groups they are said to be complementary. Almost a century before supramolecular chemistry became a well-established field, Emil Fischer suggested a "lock-and-key" model (Figure 1.5a) to describe the way in which a biological enzyme (lock) can bind a specific substrate (key).[30] Since then the concept of complementarity has been modified and expanded to an "induced-fit" model (Figure 1.5b) where small conformational changes occur upon guest binding.[31]

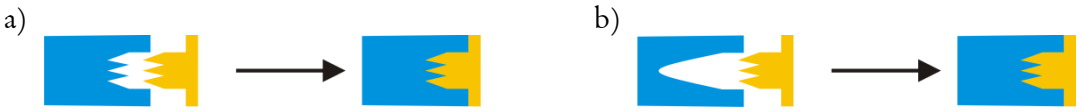


Figure 1.5. Cartoon representations showing a) 'lock-and-key' and b) 'induced-fit' complementarity.

To mimic the impressive selectivity displayed by biological enzyme–substrate binding, synthetic host molecules can be designed to incorporate a binding cavity of complementary size and shape to the target guest species.

1.3.2 Preorganisation and the chelate/macrocyclic effects

Cram proposed the principle of preorganisation which states, "*the more highly hosts and guests are organised for binding and low solvation prior to their complexation, the more stable will be*

their complexes."[32] The importance of preorganisation is illustrated by considering the chelate and macrocycle effects initially applied to cation receptor chemistry but equally valid for anion complexation.

The *chelate effect* refers to the enhanced stability of a complex containing chelate rings compared with analogous non-chelated ligands where both enthalpy and entropy contributions have been shown to be important.[33,34] Complexation by a multidentate chelating ligand releases more solvent molecules, increases the disorder of the system and is therefore, entropically favourable. Enthalpically, the energy penalty involved in bringing polar, electron-donating groups together in a complex is partially overcome when synthesising the multidentate ligand.

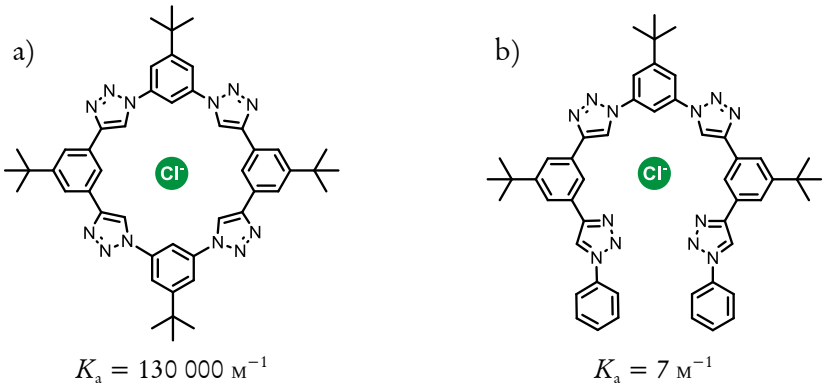


Figure 1.6. The macrocycle effect: Flood's preorganised macrocycle (a) and acyclic analogue (b).

The *macrocyclic effect* is an extension of the chelate effect and refers to the enhanced stability of a macrocyclic complex compared with an acyclic analogue.[34] Enthalpically, macrocyclic hosts tend to be less solvated than their acyclic counterparts so desolvation requires less energy; entropically, macrocyclic ligands are less flexible and so lose fewer degrees of freedom upon complex formation.[35] An example where the macrocyclic effect has been applied to anion coordination is outlined in Figure 1.6. The preorganised macrocyclic receptor has a chloride binding affinity in dichloromethane which is four orders of magnitude greater than the acyclic counterpart.

1.4 Host–guest chemistry

A plethora of synthetic host molecules have been designed which capitalise on the non-covalent interactions and design principles described above for favourable host–guest complex formation.

1.4.1 Cation binding

The importance of cations in natural processes is well-known: plants harvesting light energy in photosynthesis rely on magnesium(II) cations found in chlorophyll; iron(II) in haemoglobin is vital for respiration; and the transport of sodium(I) and potassium(I) is important for transmission of nerve impulses.[36] Furthermore, many metal cations are highly toxic (mercury(II)[37]) or radioactive (strontium-90[38] and caesium-137[39]).[40] It is no surprise, therefore, that the design and synthesis of host molecules which can encapsulate cation guests has received considerable attention.

The emergence of supramolecular chemistry, and cation binding in particular, can be traced back to the seminal work by Pedersen, who discovered that crown ethers complex alkali metal cations (Figure 1.7a).[41,42] Strong binding occurs through the cumulative effect of multiple ion–dipole interactions and in a classical demonstration of complementarity, the strongest complexes are formed with the most suitably sized cationic guest.

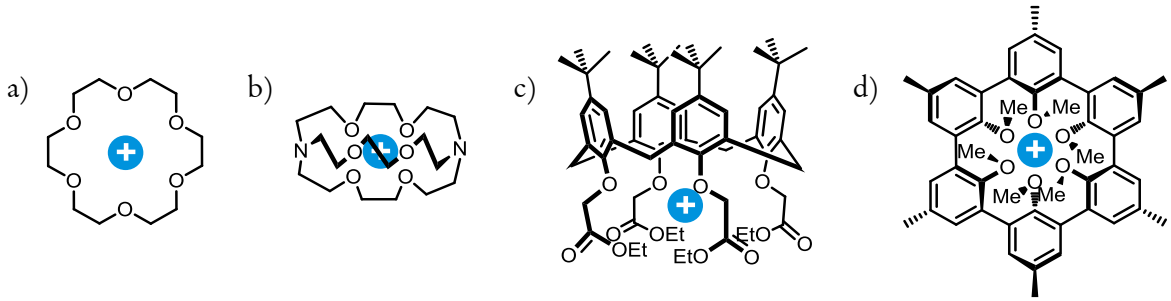


Figure 1.7. Abiotic cation receptors: a) Pedersen's crown ether; b) Lehn's cryptand; c) Shinkai's calix[4]arene; d) Cram's spherands.

Other notable examples for the recognition of group one and two metal cations include cryptands,[43] calixarenes,[44] and spherands[45]—each receptor contains similar donor atoms, but binding is enhanced by the increased preorganisation (Figure 1.7).

1.4.2 Anion binding

1.4.2.1 The importance of anions

Like cations, anionic species have essential biological, medicinal, chemical and industrial functions. The familiar DNA double helix which contains all the genetic information necessary for life to exist is a polyanion, constructed from a phosphate ester scaffold.[8] ATP and ADP contain phosphate anions at physiological pH and are involved in energy transfer and signal transmission.[36] The majority of biological enzyme substrates and co-factors are also negatively charged.[46] Bicarbonate is important for regulating physiological pH as part of the pH buffering system within the body.[47] Chloride is vital for metabolism and maintaining ionic strength.[28,48]

Altered anion regulation or concentration is a cause or symptom of many medical disorders: channelopathies are diseases where transmembrane ion transport is severely disrupted—most notably cystic fibrosis, which is triggered by faulty chloride channels;[49] problems with anion exchange procedures are linked to Alzheimer's disease;[50] and unusual pH or basic electrolyte concentration can indicate renal failure.[51]

Intense arable farming in the United Kingdom over the past 60–70 years and the consequent overuse of phosphate- and nitrate-based fertilisers to enhance food production has had a detrimental impact on the aquatic environment. These anions leach into local water supplies disrupting ecosystems, causing algal blooms – the vast growth of phytoplankton – and reducing fish populations through oxygen depletion.[52,53] Radioactive pertechnetate anions are a waste product of the nuclear fuel industry and pose a risk to human health,[54] whilst cyanide and naturally occurring arsenate are extremely toxic.[55] Hence the manufacture of artificial anion sensors and sequestering agents for medical and environmental applications is receiving an ever increasing amount of attention.

1.4.2.2 The challenge of anions

In contrast to the well-established field of cation coordination chemistry, anion coordination chemistry has been much slower to develop since many inherent properties of negatively charged species cause difficulties in the design of suitable hosts.[28]

Size: anions are larger than their isoelectronic cations (Table 1.1) owing to their diminished effective nuclear charge.[56] Consequently they have a lower charge density and any electrostatic interaction with positively charged hosts is weaker.

Table 1.1. Effective ionic radii and Gibbs free energy of hydration of isoelectronic cations and anions.

Cation	Ionic radius[a] (Å)	$\Delta_{hyd}G$ (kJ mol^{-1})[b]	Anion	Ionic radius[a] (Å)	$\Delta_{hyd}G$ (kJ mol^{-1})[b]
Na^+	1.02	−365	F^-	1.33	−465
K^+	1.38	−295	Cl^-	1.81	−340
Rb^+	1.52	–	Br^-	1.96	−315
Cs^+	1.67	−250	I^-	2.20	−275

[a]Effective ionic radii with a coordination number of six for all ions, as reported by Shannon.[56] [b]Gibbs free energy values taken from Steed and Atwood.[2]

pH dependence: many anions display a certain pH dependence, existing in their anionic state over a limited pH range. At low pH, such anions can become protonated and lose their characteristic negative charge (acetate, for example, is protonated at pH < 4). Furthermore, any positively charged hosts relying on protonated anion recognition groups can become deprotonated at higher pH. An effective anion host system, therefore, must operate within a pH window in which the target anion is deprotonated but the receptor remains protonated (section 1.4.2.4.1).[57]

Geometry: while metal cations are typically spherical, anions come in a range of geometries (Figure 1.8); spherical (halides), linear (azide, cyanide), trigonal planar (carbonate, nitrate), tetrahedral (sulfate, phosphate), and octahedral (hexafluorophosphate). This can be advantageous to some extent as the variety of anion geometries can facilitate shape- and/or size-selective anion binding. The synthetic challenge, however, is to construct host cavities of complementary size and shape to the target anion.

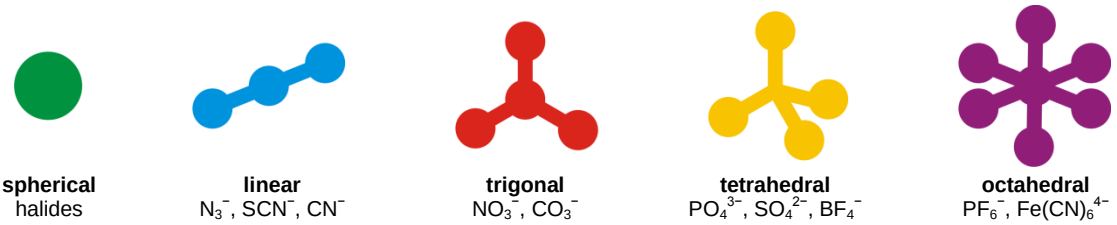


Figure 1.8. Different geometries displayed by anionic species.

Solvation: anions have large free energies of solvation in hydroxylic solvents (Table 1.1) and are more highly solvated than isoelectronic cations.[2,58] Consequently, potential anion hosts must compete effectively with the surrounding solvent media for the anionic guest: achieving strong and selective anion binding in water is a significant challenge. The *Hofmeister series*[59] (Figure 1.9) orders anions according to their decreasing hydrophobicity (i.e. increasing degree of aqueous solvation) and to achieve selectivity suitable receptors must be designed which can compete effectively with the solvent for the anionic guest.

organic anions > ClO_4^- > SCN^- > I^- > **salicylate** > NO_3^- > Br^- > Cl^- > HCO_3^- > $H_2PO_4^-$ > F^- ≈ SO_4^{2-} > HPO_4^{2-}

Figure 1.9. The Hofmeister series.

1.4.2.3 Biological anion recognition

The methods by which nature defies the difficulties associated with binding negatively charged species provide an inspiration to the synthetic chemist.

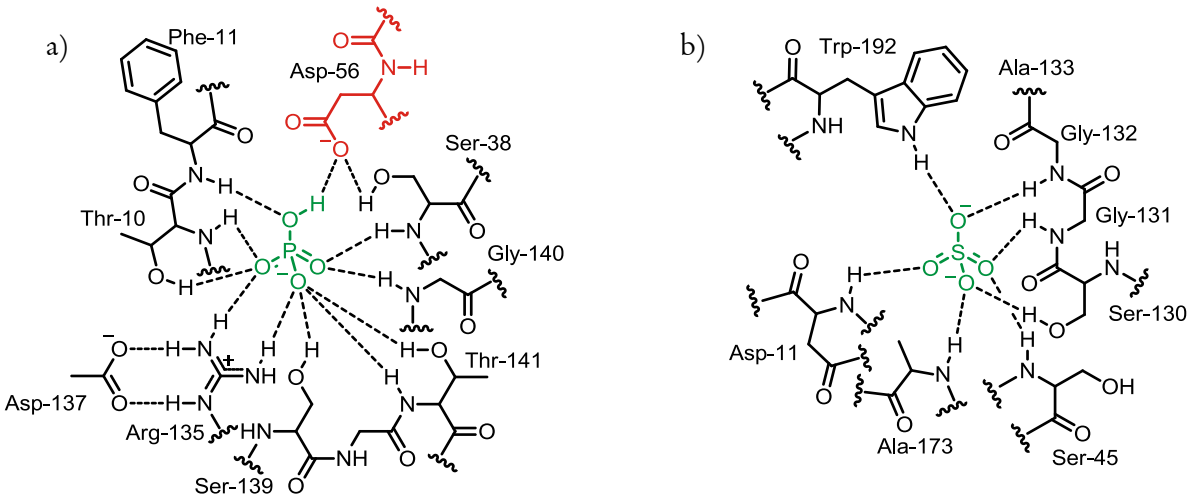


Figure 1.10. a) Phosphate- and b) sulfate-binding proteins.

The phosphate-binding protein (PBP) and sulfate-binding protein (SBP) are striking examples of selective anion host systems which transport phosphate and sulfate in bacteria. PBP (Figure 1.10a) binds the oxoanion in a cleft deep below the surface of the protein through twelve hydrogen bonds.[60] Eleven of these are protein hydrogen-bond-donor interactions whilst the twelfth, from an aspartate residue, is a protein hydrogen-bond acceptor. This carboxylate group is responsible for the selective binding of monohydrogen phosphate over sulfate despite their similar sizes and geometries; fully deprotonated sulfate being unable to act as a hydrogen-bond donor in addition to the considerable repulsion between the negative charges. In contrast SBP (Figure 1.10b) has no hydrogen-bond-acceptor residue and binds the sulfate dianion through seven neutral hydrogen-bond donors.[61]

These highly selective biological, protein-based oxoanion receptors illustrate essential features such as multiple hydrogen bonds arranged in a specific orientation forming a binding pocket shielded from solvent, to incorporate into abiotic anion receptor design.

1.4.2.4 Synthetic anion receptor chemistry

A range of functional groups and intermolecular interactions can be exploited to achieve strong, and selective, anion recognition.[28,62-66] Given anions are by definition negatively charged, many anion receptors incorporate one or more positive charges to create hosts which operate primarily through electrostatic ion–ion interactions. Various neutral host systems exist to bind anionic guests through multiple convergent hydrogen bonds or other non-covalent interactions. Another category of receptors exploit metal–ion or Lewis acid–base complexation for anion coordination. It is noteworthy that although these classifications will be dealt with sequentially, many receptors use a combination of both neutral and cationic anion binding motifs.

1.4.2.4.1 Positively charged anion receptors

Cationic motifs that have been integrated into various acyclic or macrocyclic structural frameworks employed in anion recognition include: ammonium, pyridinium, guanidinium,

and imidazolium (Figure 1.11). Positively charged receptors are typically used in polar protic solvent media, such as methanol or water, where target anions form strong hydrogen bonds to competing solvent molecules. The favourable electrostatic attraction that drives complex formation allows the penalty of host and guest desolvation to be overcome. Neutral receptors, on the other hand, function more frequently in aprotic organic solvents, although effective shielding of the binding region from competing solvent molecules may enable anion recognition to occur in more competitive media.

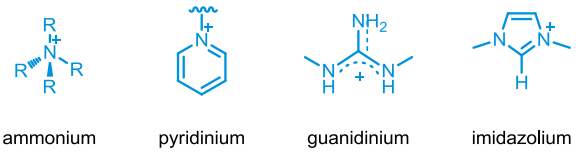


Figure 1.11. Positively charged anion binding motifs.

Polyammonium receptors

The foundations of anion receptor chemistry were laid by Park and Simmons in 1968, who reported a polyammonium system that bound halides in trifluoroacetic acid solution through a combination of electrostatics and hydrogen bonding (Figure 1.12a).[67] Subsequent crystal structure determination revealed a chloride anion encapsulated within the macrobicycle. Extending this concept, Lehn and co-workers described the anion binding properties of a range of polyammonium-containing macrocycles and macrobicycles.[68-71] The ellipsoidal hexaprotonated cryptand in Figure 1.12b is selective for linear anions such as azide [logK_a = 4.6 (azide), < 0.1 (chloride) in aqueous solution], a classic example of shape complementarity.[72]

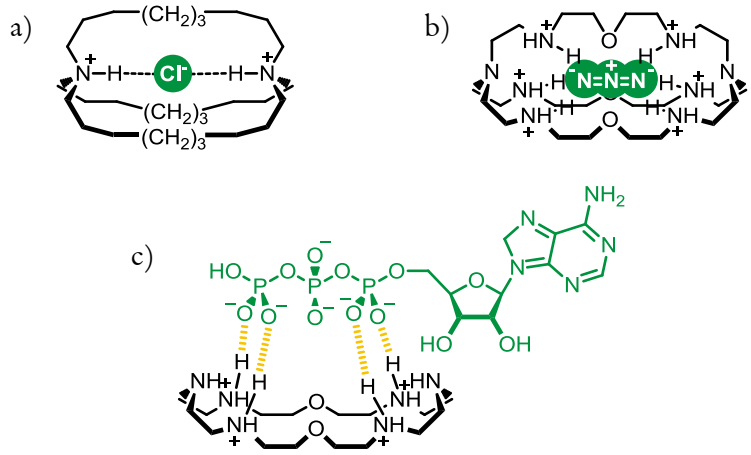


Figure 1.12. Polyammonium receptors: a) Park and Simmons' kapitand; b) Lehn's azide-selective polyammonium receptor; c) polyammonium macrocycle for ATP hydrolysis.

The polyammonium macrocycle shown in Figure 1.12c not only strongly complexes nucleotide phosphates (e.g. ATP, ADP) in water but is also a catalyst for ATP hydrolysis. This macrocycle was shown to be more efficient than other similar macrocycles containing more or fewer ammonium units which have a lower affinity for ATP, indicating the hydrolysis pathway requires the construction of a receptor–anion complex.[73]

Employing ammonium motifs for anion recognition has one distinct limitation—these host systems are pH dependent, so their optimum activity is somewhat restricted. This pH dependence may be alleviated by using quaternary ammonium groups, which, although no longer benefitting from secondary hydrogen bonding stabilisation, can nevertheless still bind anions through electrostatic attractions.

Quaternary ammonium receptors

Schmidtchen has been central in pioneering the use of alkylated quaternary ammonium moieties for anion binding. The tetrahedral cage-like receptor (Figure 1.13a) has a central cavity encompassed by four positive charges where anions are bound strongly.[74-76] By varying the length of the alkyl chain between the positive charges further "tuning" of the receptor to favour one halide over another was accomplished: R=$(CH_2)_6$, logK_a = 1.3 (chloride), 2.2 (iodide); R = $(CH_2)_8$, logK_a = <0.5 (chloride), 2.4 (iodide) in water.

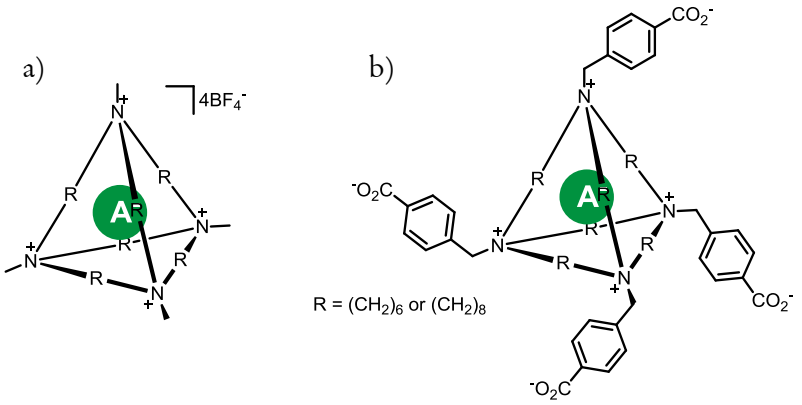


Figure 1.13. Schmidtchen's quaternary ammonium anion receptors.

With the absence of any directional intermolecular interactions arising from a lack of NH hydrogen-bond-donor groups, competition for the anion binding cleft by the counteranion is possible. Neutral zwitterionic receptors prepared by attaching borate[77] or carboxylate[78] groups (Figure 1.13b) have been prepared in which this counterion competition is alleviated and improved halide anion recognition was observed.

Pyridinium receptors

The positively charged pyridinium group has been used to construct cationic hosts for anion recognition. Shinoda and co-workers have reported a tetra-pyridinium macrocycle which exhibits a high affinity for rigid tricarboxylate anions in water (Figure 1.14a).[79]



Figure 1.14. Pyridinium-based receptors: a) Shinoda's macrocycle; and b) Steed's tripodal host.

A tripodal benzene core with pyridinium pendant arms has been prepared and studied by Steed and co-workers (Figure 1.14b).[80] In the solid state bromide complexation is observed and the receptor adopts a cone conformation. The halide anion is bound in the resultant cavity through a combination of electrostatic and C–H···anion hydrogen-bonding

interactions, and solution studies in acetonitrile gave an association constant value $K_a = 838\ M^{-1}$ for bromide complexation.

Guanidinium receptors

Employing a more basic anion recognition group is an alternative means by which pH dependence may be reduced. The guanidinium unit has a pK_a of 13.5 (*cf.* ammonium pK_a = 9.47) arising from greater charge delocalisation, and consequently it remains protonated over a much wider pH range.[81] It is often used to bind oxoanions, like carboxylate in the biologically important enzyme carboxypeptidase-A, as it can donate two hydrogen bonds in a parallel fashion.

Although Lehn's initial studies of guanidinium-based anion receptors were extensive, many of the receptors possessed relatively poor anion binding characteristics.[82,83] Improved anion affinity of guanidinium derivatives has been achieved through preorganisation of the host guanidinium group by incorporation in bicyclic systems.[84] Schmidtchen has prepared one such receptor (Figure 1.15a) which is found to form strong 1:1 host:guest complexes with hydrogen phosphate in water ($K_a = 970\ M^{-1}$).[85]

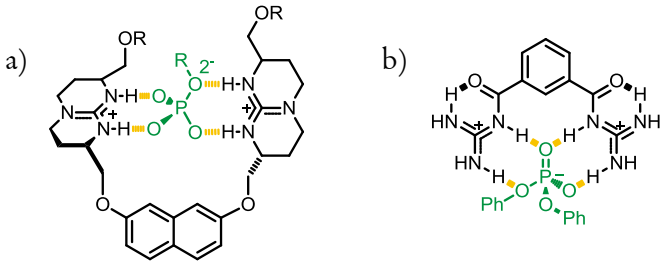


Figure 1.15. Guanidinium-based receptors: a) Schmidtchen's bipodal receptor; b) Hamilton's host system.

Hamilton and co-workers prepared an acyclic bis-guanidinium receptor which was reported to bind diphenyl phosphate ($K_a = 4.6 \times 10^4\ M^{-1}$) in acetonitrile (Figure 1.15b).[86] As well as increasing the acidity of the NH protons, the carbonyl sub-units form intramolecular hydrogen bonds endowing this receptor with a high degree of preorganisation, which contributes to its favourable binding properties.

Imidazolium receptors

1,3-Disubstituted imidazolium groups can bind anions through electrostatic interactions and hydrogen bonding from a polarised CH hydrogen-bond donor. More traditionally employed as ionic liquids and electrolytes,[87,88] in recent years attention has focused on their potential anion receptor chemistry.

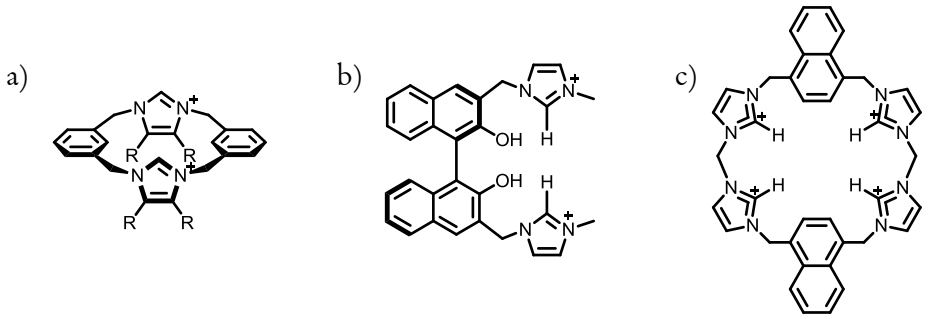


Figure 1.16. Imidazolium-based receptors: a) Alcalde's imidazolophane; b) You's bis-imidazolium receptor for α-amino acids; and c) Kim's tetra-imidazolium macrocycle.

Since the inception of imidazolium cyclophanes for anion complexation purposes by Alcalde and co-workers (Figure 1.16a),[89] a number of acyclic and macrocyclic systems incorporating the imidazolium group have been reported.[90,91]

You and co-workers have developed receptors based on the 1,1'-bi-2-naphthol scaffold with two imidazolium anion binding moieties (Figure 1.16b).[92] Titration experiments in aqueous media (10 mM HEPES buffer, pH 7.4) revealed this receptor has a strong preference for L-tryptophan over other α-amino acids studied.

Kim and co-workers have incorporated four imidazolium units into a macrocyclic anion host (Figure 1.16c).[93] The ability of this receptor to complex anions in aqueous solution (10 mM phosphate buffer, pH 7.4) was investigated and the macrocyclic selectively senses RNA through a combination of strong, complementary C–H···anion hydrogen bonding and aromatic donor–acceptor interactions ($K_a = 4.6 \times 10^6$ M^{-1}).

1.4.2.4.2 Neutral anion receptors

Numerous neutral anion receptors exist, the majority operating through hydrogen-bonding interactions. Whilst individually being much weaker than the electrostatic ion–ion

interactions previously discussed, the cumulative effects of several hydrogen bonds operating in concert, combined with their inherent directionality can bestow these receptors with strong anion recognition properties. Receptors incorporating amide, urea, pyrrole and hydroxyl functional groups are widely known and C–H···anion hydrogen-bond donors such as triazole groups have started to attract attention (Figure 1.17). In addition to hydrogen bonding, receptors relying on halogen-bond-formation and anion–π interactions have recently been reported.

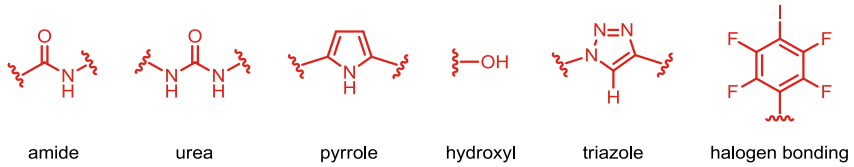


Figure 1.17. Neutral anion binding motifs.

Amide-based receptors

Given the prevalence of amide–NH···anion hydrogen bonding in nature, it is not surprising that numerous synthetic anion receptors exploiting similar interactions have been developed. Seminal reports by Crabtree and co-workers in the late 1990s highlighted the anion binding capabilities of the simple isophthalamide group.[94,95]

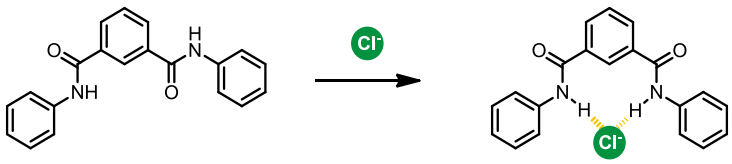


Figure 1.18. Crabtree's isophthalamide-based receptor for chloride.

This non-preorganised, bis-amide unit adopts a less favourable *syn-syn* conformation to bind anions through two convergent hydrogen bonds. The compound binds halide anions with a 1:1 stoichiometry showing a selectivity preference chloride > bromide > iodide in dichloromethane, in part due to chloride being the more complementary-sized anion (Figure 1.18). Since then this motif has been extensively exploited in many higher order supramolecular architectures.

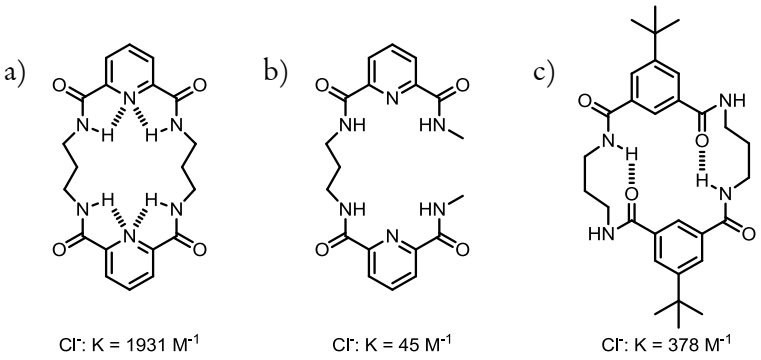


Figure 1.19. The macrocyclic effect as demonstrated by Jurczak: a) macrocycle, b) acylic analogue. The role of preorganisation demonstrated by comparing macrocycles a) and c).

Jurczak and co-workers have incorporated a bis-amide motif into several macrocycles, improving anion binding affinities through preorganisation. The pyridine-3,5-bis-amide-containing macrocycle (Figure 1.19a) binds anions in dimethyl sulfoxide and the strength of chloride anion association is much greater than that with the acyclic analogue (Figure 1.19b)—a demonstration of the macrocyclic effect in anion coordination chemistry.[96] This macrocycle is also shown to be a superior anion complexant over its carbon isophthalamide counterpart (Figure 1.19c). The authors attributed this to the greater preorganisation of the pyridine-containing macrocycle: the required *syn-syn* arrangement of amide-NH hydrogen-bond donors necessitates a greater degree of conformational change with the isophthalamide macrocycle.[97]

A rare example of anion recognition by a neutral receptor in aqueous media is provided by Kubik and co-workers. Taking inspiration from the natural world, they constructed a family of cyclopeptide receptors which bind anions in aqueous media.[98-101] The cyclic monomer (Figure 1.20a) binds large anions such as iodide (K_1 = 19 M^{-1}) and sulfate (K_1 = 95 M^{-1}) in a 1:2 host:guest stoichiometry in 4:1 water:methanol, and in the solid state the iodide complex adopts a sandwich-type structure: one iodide anion is encapsulated between two receptors by six hydrogen bonds.[98,99] The associated dimer (Figure 1.20b) was found to bind large anions in 1:1 stoichiometry and is selective for sulfate in 1:1 methanol:water, $K_a = 6.7 \times 10^6$ M^{-1} (sulfate), 5.6×10^4 M^{-1} (iodide).[101]

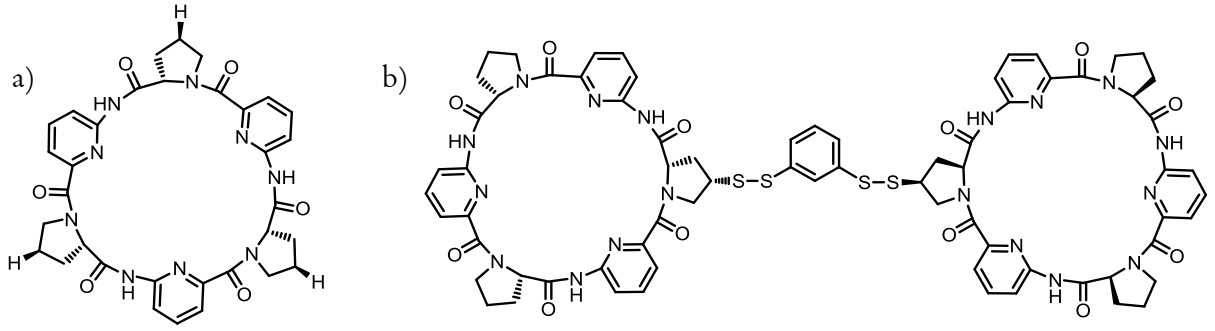


Figure 1.20. Kubik's peptide-based macrocyclic monomeric (a) and dimeric (b) anion hosts.

Urea-based receptors

A natural progression from the amide unit described above, the urea group is another potent anion recognition motif. Ureas (and thioureas) proffer two hydrogen-bond-donor groups which are appropriately oriented to bind Y-shaped anions such as carboxylates and phosphates.

Gale and co-workers investigated a series of bis-urea-containing receptors that operate in competitive media.[102-104] The receptor in Figure 1.21a shows a preference for acetate in 0.5% water:dimethyl sulfoxide (K_a = 3210 M^{-1})[103] and modification, by the addition of electron-withdrawing groups to increase the acidity of the urea protons, further enhanced anion recognition.[104]

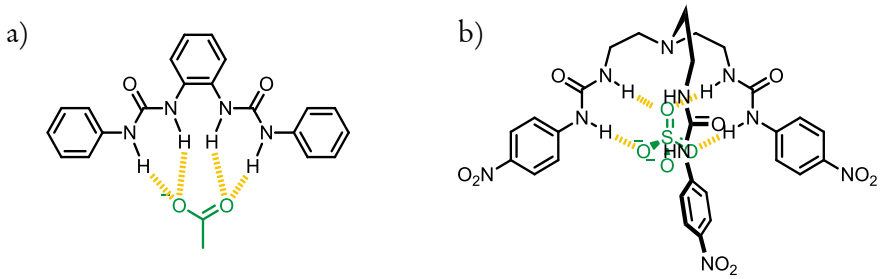


Figure 1.21. Urea-containing anion receptors: a) Gale's bis-urea acetate receptor; and b) Das and Ganguly's tren-based tris-urea host system.

The tren-based tris-urea receptor (Figure 1.21b) developed by Das and Ganguly, was found to be selective for sulfate and dihydrogen phosphate (logK_a = 4.97 and 4.26 respectively) over other oxoanions in 5% water:acetonitrile mixture. Crystal structure analysis revealed a

pseudo-capsule arrangement of two host molecules binding a sulfate-water-sulfate cluster in the solid state.[105]

Pyrrole-based receptors

Calix[4]pyrroles were the first neutral cyclic receptors incorporating pyrrole groups for anion recognition to be reported.[106] The simple *meso*-octamethylcalix[4]pyrrole binds fluoride strongly and chloride less so in dichloromethane ($K_a = 1.7 \times 10^4$ and 3.5×10^2 M^{-1} respectively). The free receptor exists in a 1,3-alternate conformation, becoming cone-shaped upon anion coordination to facilitate a convergent arrangement of hydrogen-bond donors (Figure 1.22a).

Sessler and co-workers have extended the anion binding capabilities of this simple calix[4]pyrrole system by attaching a pyrrole-containing strap (Figure 1.22b).[107] The additional NH hydrogen-bond donor confers a near 100-fold improvement in chloride binding over both a furan-strapped alternative and the original unstrapped receptor.

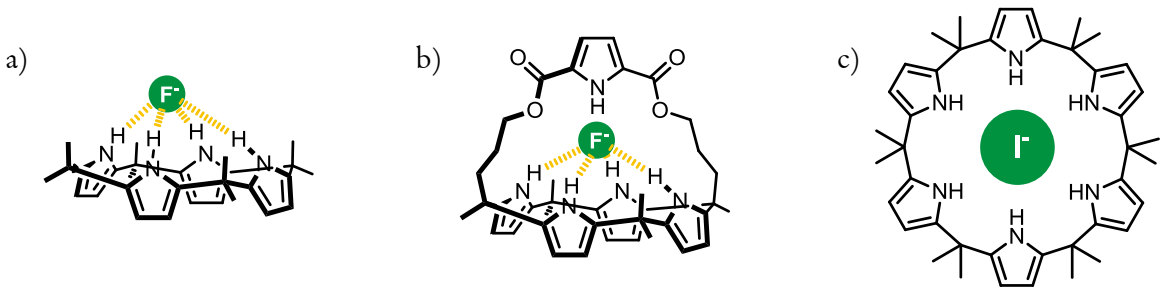


Figure 1.22. Pyrrole-based receptors: a) the first pyrrole-based anion receptor; b) Sessler's pyrrole-strapped calix[4]pyrrole; and Eichen's calix[6]pyrrole.

Higher order calix[n]pyrroles (n > 4) have also been developed and are able to bind larger anionic guest species. Eichen and co-workers prepared a calix[6]pyrrole (Figure 1.22c) that has preference for iodide over other halides; fluoride, chloride and bromide are too small to benefit from the full quota of six NH hydrogen bonds.[108]

The NH motifs of indole and indolocarbazole are more acidic than pyrrole and so form stronger hydrogen bonds to anion guests. Anion receptor molecules often combine indole sub-units with additional anion recognising functional groups. Gale and co-workers have

reported an acyclic receptor molecule which contains both amide and indole groups (Figure 1.23a). The bipyridyl core of the bis-indole-appended receptor shown becomes preorganised upon platinum(II)-coordination resulting in enhanced dihydrogen phosphate association compared with the free, unpreorganised host system (K_a = 3640 M^{-1} *versus* K_a = 90 M^{-1} in 0.5% water:dimethyl sulfoxide).[109]

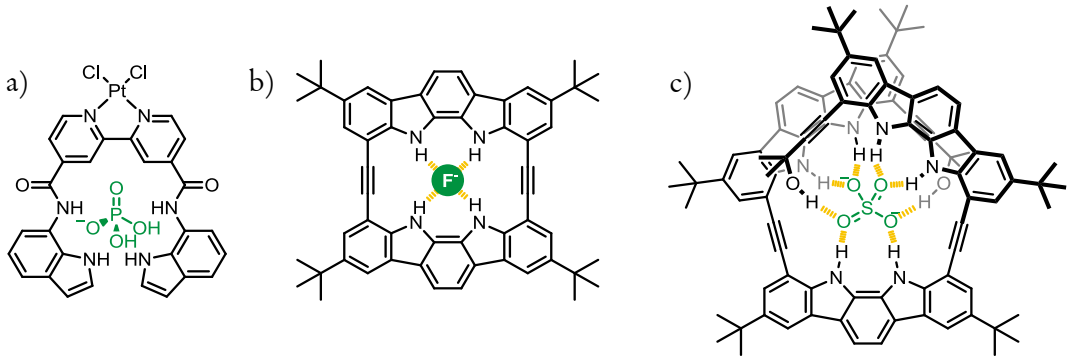


Figure 1.23. Indole- and indolocarbazole-based anion receptors: a) Gale's acyclic indole-containing receptor with Pt-induced preorganisation; b) Jeong's rigid indolocarbazole-containing macrocycle and c) Jeong's sulfate selective foldamer.

Indolocarbazole-based receptors benefit from an additional hydrogen-bond donor as well as increased rigidity of the extended aromatic-π system which serves to preorganise the host species. Following Beer's initial anion binding studies on a series of simple indolocarbazole systems,[110] Jeong and co-workers have incorporated this motif into a rigid alkyne-linked macrocycle, which exhibits strong and selective binding of fluoride in acetonitrile (Figure 1.23b).[111] Extending this work, the same group has recently reported an oligomeric indolocarbazole-based species which binds sulfate selectively in 9:1 acetonitrile:methanol solvent mixture. Anion-induced folding creates a helical binding cavity where sulfate encapsulation is stabilised by eight hydrogen bonds (Figure 1.23c).[112]

Hydroxyl-based receptors

Hydroxyl groups are potent hydrogen-bond donors in nature and thus polarised OH moieties are exploited in synthetic anion receptor chemistry. Anion coordination by a range of benzenediols has been studied by Smith and co-workers.[113,114] Both resorcinol (Figure

1.24a) and catechol (Figure 1.24b) bind chloride in acetonitrile with surprising strength (K_a = 110 and 1570 M^{-1} respectively) given the apparent simplicity of these motifs.[114]

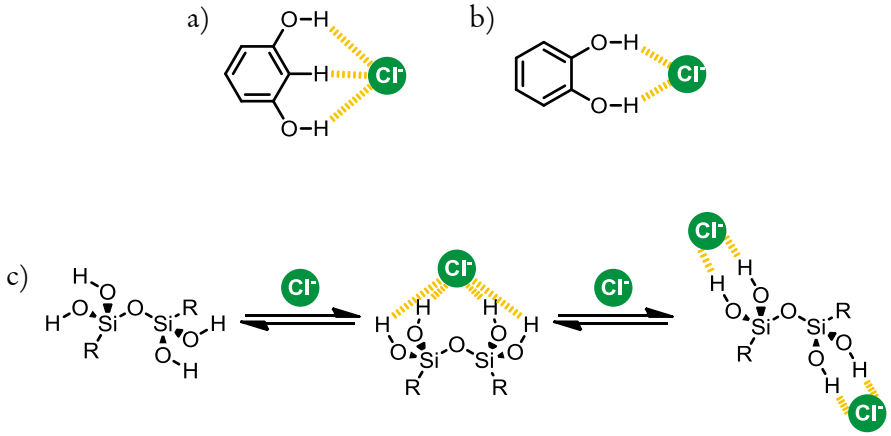


Figure 1.24. Hydroxyl-based anion receptors: a) resorcinol; b) catchecol; c) Kondo's silanediols.

Kondo, Unno and co-workers have demonstrated that silanediols can be used to bind anions in organic solvents.[115,116] Stepwise anion complexation was observed upon addition of chloride to 1,3-disiloxane-1,1,3,3-tetraols in acetonitrile (Figure 1.24c).[117]

C–H···anion hydrogen-bond-donating receptors

Typically weaker than conventional N–H···anion hydrogen bonds, C–H···anion hydrogen bonding has been used to bind anions usually in combination with stronger non-covalent forces. More recently, however, the effect of several interactions functioning together in concert has been demonstrated with the development of receptors which rely exclusively upon C–H···anion hydrogen-bonding interactions.

In 1990, a fluorinated macrocyclic ether was shown to bind fluoride through C–H···anion hydrogen bonding in tetrahydrofuran solution (Figure 1.25a).[118] It was not until almost two decades later, however, that receptors intentionally designed to exploit these interactions were reported. In 2008, several groups independently developed receptors which highlighted the potential of polytriazole hosts to complex anions in organic solvents.[35,119,120] 1,2,3-Triazole units contain a highly polarised CH bond arising from the electron-withdrawing effect of the sp^2 hybridised carbon atom and three nitrogen atoms of the heterocycle.

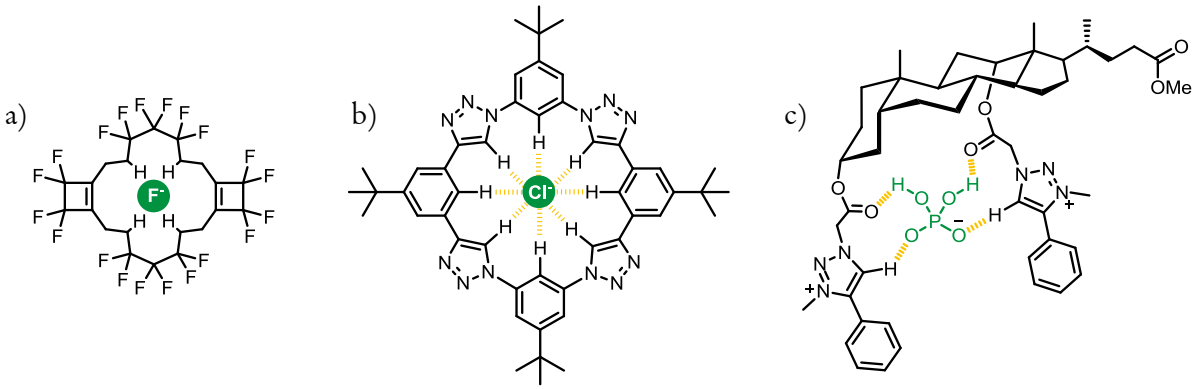


Figure 1.25. C–H···anion hydrogen-bonding receptors: a) Farnham's fluorinated macrocycle; b) Flood's tetra-triazole macrocycle; and c) Pandey's triazolium-based anion host.

Flood's tetra-triazole macrocycle forms 1:1 host:guest complexes with halide anions in dichloromethane. Size-complementarity accounts for the striking preference for chloride and bromide anions ($K_a = 1.1 \times 10^7$ and 7.5×10^6 M^{-1}) over smaller fluoride and larger iodide anions ($K_a = 2.8 \times 10^5$ and 1.7×10^4 M^{-1}).[35,121] Bachas and co-workers have developed an ion-selective electrode which incorporates this tetra-triazole macrocycle into a polyvinylchloride-based membrane for the selective detection of halide anions.[122]

Triazole groups can be alkylated to produce positively charged triazolium units which, in recent years, have also been incorporated into receptors for anion coordination: Pandey and co-workers have used the bis-triazolium receptor shown in Figure 1.25c to bind anions in chloroform solution.[123]

Halogen-bonding receptors

Whilst the scope of halogen bonding in solid-state crystal engineering has been known for some time,[124,125] the incorporation of halogen-bonding motifs into receptors for anion recognition is a relatively new venture.[126]

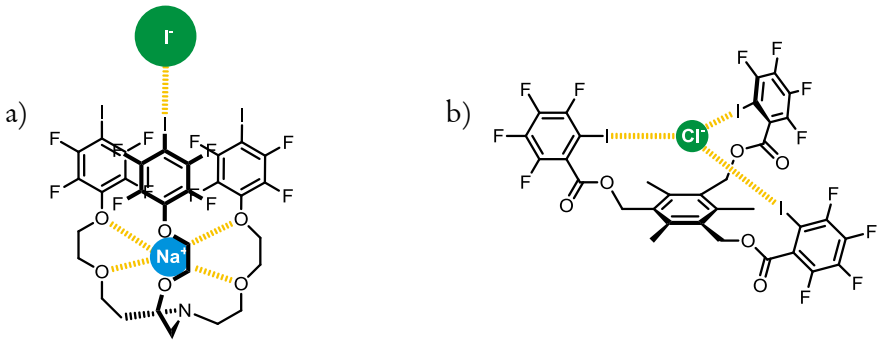


Figure 1.26. Halogen-bonding receptors: a) Resnati's ion pair receptor; b) Taylor's tridentate compound.

The first compound to deploy multiple halogen-bond donors for solution-phase anion binding was prepared by Resnati and co-workers.[127] The heteroditopic host for alkali metal halides (Figure 1.26a) showed a preference for iodide over halides bromide and chloride. Furthermore, a twenty-fold improvement in sodium iodide complexation compared with the analogous pentafluorophenyl control system was observed, which provides an estimate of the contribution of halogen bonding to the overall ion-pair binding affinity.

Taylor and co-workers have developed a library of iodotetrafluorobenzene-appended receptors for anion recognition by halogen bonding.[128] The tridentate compound shown in Figure 1.26b was found to selectively complex chloride ($K_a = 1.9 \times 10^4\ M^{-1}$) over bromide, iodide and various oxoanions in acetone solution. Furthermore, the chloride binding affinity was demonstrated to be substantially greater than similar bidentate ($K_a = 1.8 \times 10^3\ M^{-1}$) or monodentate ($K_a = 70\ M^{-1}$) hosts.[129]

Anion – π receptors

Kochi has demonstrated the formation of charge-transfer interactions between neutral π-acceptors and halide anions in acetonitrile. In the solid state, a chloride anion resides in a cavity created by four electron-deficient tetracyanopyrazine molecules (Figure 1.27a).[130] Close anion–carbon distances together with a Mulliken correlation between the charge-transfer absorption band energy and the oxidation potential of the anion are cited as evidence of complex formation.

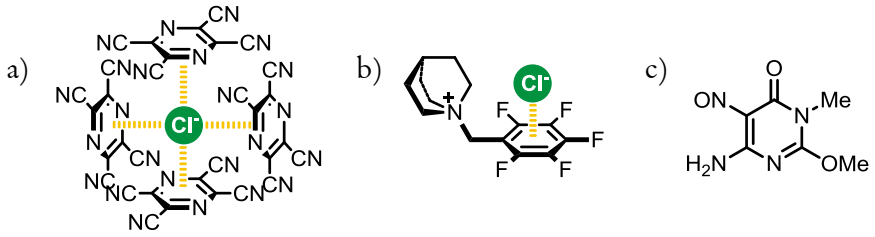


Figure 1.27. Receptors operating through anion–π interactions: a) Kochi's chloride encapsulation by four tetracyanopyrazine units; b) Albrecht's pentafluorobenzyl-substituted ammonium host; and c) Lopez-Garzón's receptor for sulfate.

Albrecht and co-workers have reported the presence of anion–π interactions between a pentafluorobenzyl-substituted ammonium compound and halide anions.[131] Crystal structures reveal chloride, bromide and iodide anions are each located above the face of the π–system (Figure 1.27b).

A recent assessment of the thermodynamics of anion–π interactions in aqueous solution was undertaken with the host molecule shown in Figure 1.27c. Isothermal titration calorimetry was undertaken to determine enthalpy and entropy contributions to the overall binding of highly negative anions such as sulfate and selinate. A favourable free energy for anion–π interactions (approximately -10 kJ mol^{-1}) was observed owing to entropic contributions and is considered to arise primarily from desolvation effects, although other factors inherent to receptor design may have smaller contributions.[132,133]

1.4.2.4.3 Lewis acid–base anion receptors.

Given an anion is intrinsically an electron-pair donor, the development of receptors incorporating Lewis acidic electron-pair-acceptor groups is logical. Since Shriver and Biallas first reported the formation of a complex between a methoxide anion and a bidentate boron derivative,[134] the scope of receptors exploiting Lewis acid–base complex formation for anion coordination has been extensively explored.

Gabbaï and co-workers have reported a series of cationic boranes which bind fluoride strongly in aqueous media (Figure 1.28a).[135] The Lewis acidity of the borane sub-unit depends upon the substitution at the neighbouring phosphorous group and increases with the hydrophobicity of the phosphonium moiety. More recently, Jäkle and co-workers have

constructed a π-expanded borazine macrocycle (Figure 1.28b) with integrated electron-deficient organoborane units and demonstrated that this receptor binds up to three cyanide anions in toluene.[136] Examples of anion receptors containing Lewis acidic metals such as mercury[137], tin[138], and germanium[139] for Lewis acid–base complex formation are also known.

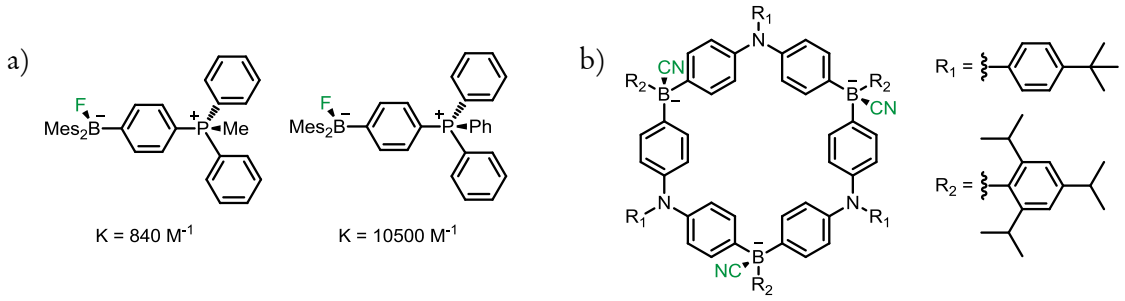


Figure 1.28. Anion receptors functioning via Lewis acid–base complex formation: a) Gabbai's cationic boranes for fluoride binding (9:1 water:methanol, pyridine buffer, pH 4.6); and b) Jäkle's π-expanded borazine macrocycle for cyanide binding.

1.4.3 Applications of anion recognition

Gaining an understanding of anion host–guest coordination enables the anion supramolecular chemist to develop host systems that have a range of potentially useful applications.

1.4.3.1 Anion transport

To be able to manipulate the transport of anions *in vivo* is a challenge that has as its goal the possibility of alleviating or curing a range of diseases (section 1.4.2.1). Synthetic compounds that artificially mimic anion transporters, functioning either as *discrete molecular carriers* or as *ion channels*, have been developed.

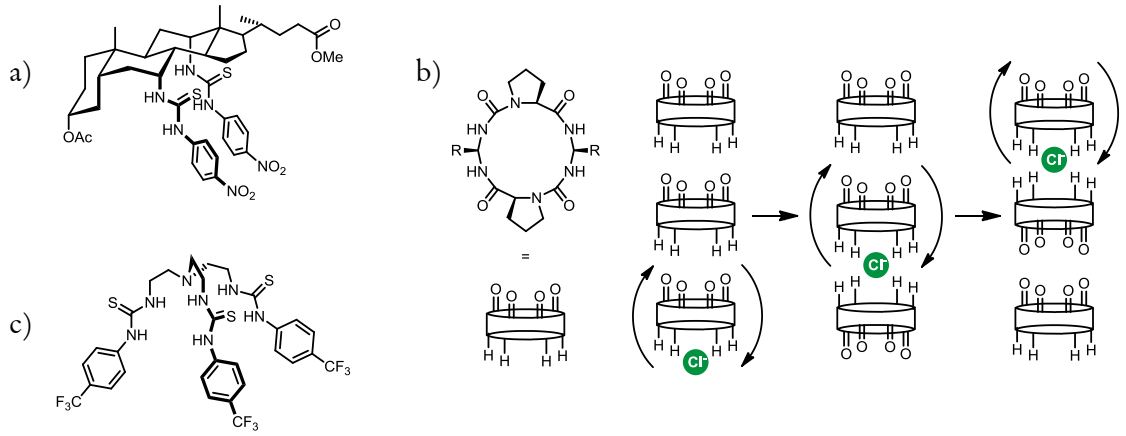


Figure 1.29. Anion transport: a) Davis's discrete anion transporter; b) Matile and Guichard's transmembrane chloride channel; and c) Gale's thiourea-containing anion transporter.

Cholapods (cyclosteroid-based anion receptors) and their ability to function as discrete carriers have been investigated by Davis and co-workers, for their potential application in channel replacement therapies for cystic fibrosis.[140,141] The lipophillic skeleton can partition into a lipid bilayer and a preorganised, tris-thiourea, hydrogen-bond-donating binding cleft forms a strong receptor:chloride complex, which is important for transporting the anion across a membrane. A structure–activity study was carried out and receptor Figure 1.29a was demonstrated to be a highly efficient chloride anion membrane transporter at very low (1:250 000) carrier:lipid concentrations.[142]

Matile and Guichard have examined the membrane transport properties of amide- and/or urea-containing macrocycles.[143] The macrocycles are thought to stack above one another forming self-assembled nanotubes that span the lipid bilayer (Figure 1.29b). These synthetic channels are able to transport anions that are larger than the macrocyclic cavity and a "Jacob's-ladder" mechanism involving individual macrocycle rotation and flipping of macrodipoles has been proposed.

Gale and co-workers have demonstrated the promising anticancer activity of several tren-based tris-thiourea derivatives.[144,145] The thiourea-containing receptors are more effective chloride/nitrate and chloride/bicarbonate exchange agents than their urea-based analogues. Fluorination of the attached phenyl groups increases the receptors' lipophillicity and

transport efficiency and the most effective anion transporter (Figure 1.29c) induces apoptosis in target cancer cells.

1.4.3.2 Anion-controlled gelation

Organogel research is a growing area under the supramolecular chemistry umbrella. Gels are everyday materials consisting of a fibrous, solid network and a solvent or liquid component held within the solid network. Heating causes a phase transition, the *gel* becoming a *sol* at temperatures above T_{gel}. Anions are increasingly being used to trigger this gel–sol transition.[146]

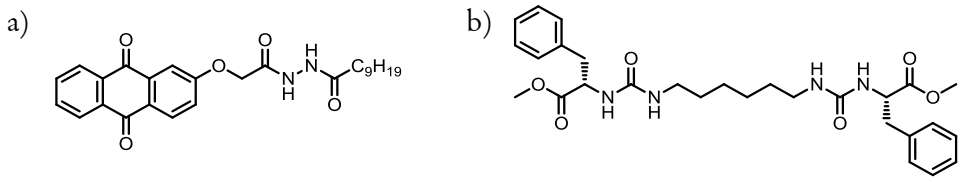


Figure 1.30. Anion-controlled gelation: a) Chen's hydrazide-anthraquinone gelator; and b) Steed's bis-urea derivative.

Chen and co-workers reported anion-induced gel-sol transitions when dihydrogen phosphate, acetate and fluoride were added to the gel formed by the hydrazine derivative in Figure 1.30a, an effect not observed with chloride, bromide and iodide.[147]

Steed and co-workers have used bis-urea gelators (Figure 1.30b) to assist crystallisation of organic compounds, in particular pharmaceuticals.[148] The gel matrix slows the crystal-growing process so larger, more uniform crystals are produced, and acetate-triggered gel–sol transitions allow easy recovery of the crystals.

1.4.3.3 Anion sensors

The ability, not only to bind anions, but also to detect and quantify their presence is a natural extension of anion recognition chemistry and the development of anion sensors which undergo a macroscopic, measurable response upon a microscopic binding event is ever-increasing. The most popular methodologies employed in the design of anion sensors are summarised in Figure 1.31.

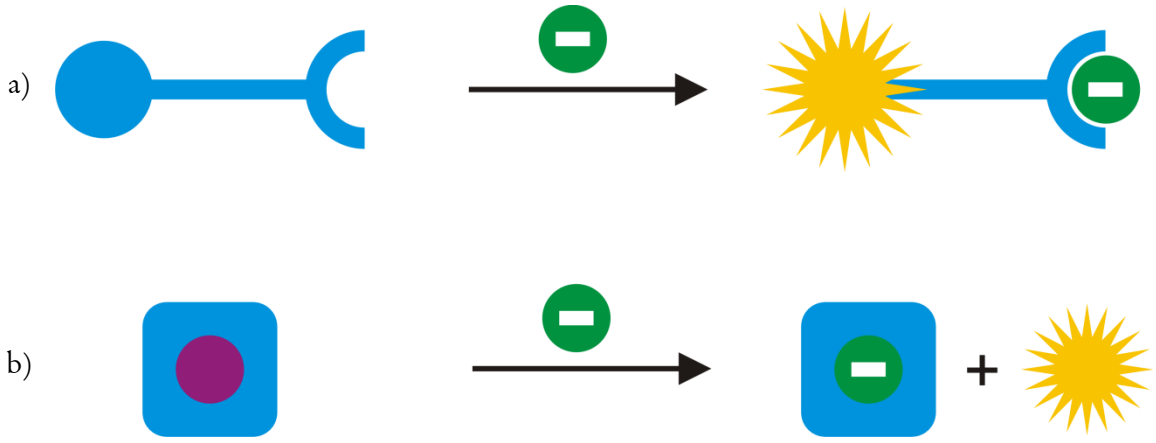


Figure 1.31. The general approaches to anion sensing: a) a discrete molecular sensor incorporating an attached reporter group; and b) a displacement assay.

Most commonly, a receptor molecule is furnished with an optical or electrochemical reporter group in proximity to the binding cleft; anion binding perturbs the electro- or photochemical properties of the host system which generates a response at the reporter group (Figure 1.31a). Alternatively, displacement assays may be used where a receptor-bound dye molecule is displaced upon anion binding, with a simultaneous change in optical properties of the dye (Figure 1.31b). Other methodologies have also been developed such as using a chemodosimeter: a sensor molecule which reacts with the target anion species inducing measurable changes in the properties of the sensor.

The ideal anion sensor combines strong and selective recognition of a target anion and a maximum response output both of which require prudent consideration of available anion binding and reporter groups.

1.4.3.3.1 Electrochemical anion sensors

Electrochemical sensors typically integrate a redox-active reporter group (such as ferrocene or cobaltocenium) into an anion host structural framework. Upon anion binding the metallocene redox couple potential of the reporter group is perturbed which can be monitored by voltammetric techniques.

Early pioneers in the development of electrochemical anion sensors were Beer and co-workers who described the anion sensing properties of several cobaltocenium-functionalised macrocyclic ester systems.[149] Since then many anion hosts incorporating redox active metal

centres such as ferrocene have been reported. A recent example is described by Molina and co-workers (Figure 1.32a) where the urea-containing cyclic structure binds fluoride ($K_a > 10^4$ M^{-1}) and dihydrogen phosphate (K_a = 405 M^{-1}) in preference to chloride, bromide and hydrogen sulfate anions in dimethyl sulfoxide.[150] Furthermore, the integrated reporter group signalled fluoride and dihydrogen phosphate binding through cathodic shifts of the ferrocene/ferrocenium redox couple: $\Delta E_{1/2}$ = 190 and 125 mV respectively in dimethyl sulfoxide.

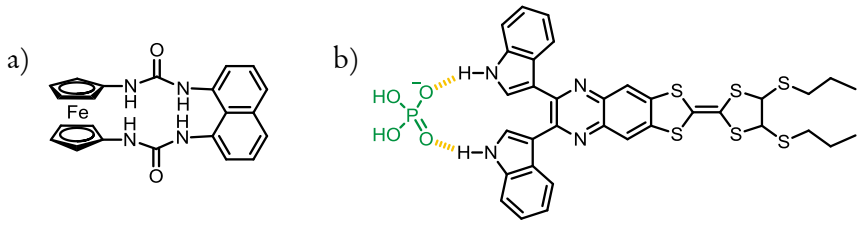


Figure 1.32. Redox-responsive anion sensors: a) Molina's ferrocene-containing receptor for fluoride; b) Sessler's tetra-thiafulvalene-containing receptor.

Sessler and co-workers employed the organic redox-active tetra-thiafulvalene unit appended to a bis-indole group (Figure 1.32b) which, upon addition of dihydrogen phosphate anions in dichloromethane, displayed a cathodic shift of 112 mV in the first oxidation wave assigned to the tetra-thiafulvalene subunit. Addition of chloride, benzoate and hydrogen sulfate, however, induced much smaller cathodic perturbations.[151]

1.4.3.3.2 Optical anion sensors

Optical sensing is usually divided into two sub-categories: *colorimetric* and *fluorescent* sensing.

Colorimetric sensing

Anion sensors incorporating chromophores are attractive as anion-induced absorbance changes can occur in the visible spectrum, and the resulting colour changes allow naked-eye detection of the anion recognition event.

Sessler and co-workers have developed a library of optical anion receptors by attaching various chromophores to a calix[4]pyrrole scaffold. In one example (Figure 1.33a), different anion-specific colour changes enabled fluoride (red to blue), chloride (red to purple) and

dihydrogen phosphate (red to dark purple) to be distinguished from one another in dichoromethane.[152]

Aldridge and co-workers have designed a variety of Lewis acidic boron-functionalised receptors for the sensing of fluoride and cyanide anions, and in some cases a ferrocene unit has been chosen as the peripheral reporter group (Figure 1.33b).[153,154] Addition of anions induced cathodic shifts in the ferrocene/ferrocenium redox couple, which occur in a window suitable for partnering to a redox-active dye and consequently the electrochemical signal of the binding event is accompanied by a colour change of the two-component system with fluoride and cyanide in 100:1 acetonitrile:methanol. Furthermore, under the same conditions, the stilbene diolate boronic ester analogue gives a colorimetric response upon addition of fluoride which is not observed in the presence of cyanide anions—these receptors are therefore able to discriminate between cyanide and fluoride by AND/NOT Boolean logic.[153]

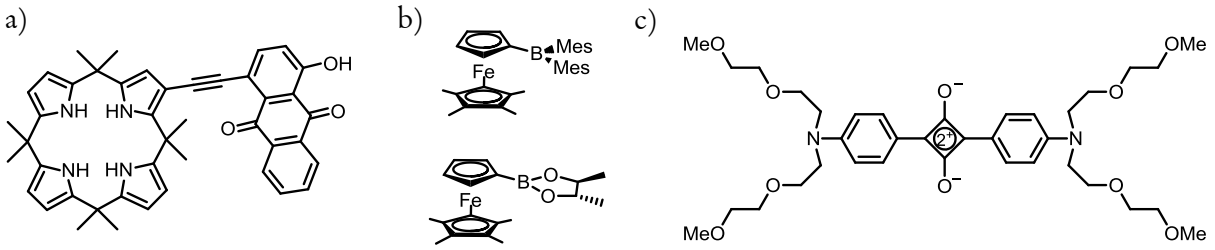


Figure 1.33. Colorimetric anion sensors: a) Sessler's anthraquinone-appended calix[4]pyrrole anion receptor; b) Aldridge's AND/NOT hosts for fluoride and cyanide; c) Martínez-Máñez's chemodosimeter.

An elegant example of a selective chemodosimeter was reported by Martínez-Máñez and co-workers.[155] The blue colour of the functionalised squaraine-dye receptor (Figure 1.33c) arises from charge transfer from the anilinium groups to the central, electron-deficient ring. The susceptibility of this central ring moiety to nucleophillic attack by cyanide causes a blue-to-colourless colour change and allows for the selective sensing of this toxic anion.

Fluorescence sensing

An abundance of anion sensors which feature inorganic or organic fluorophores have been reported in recent years. Fluorescence spectroscopy is a highly sensitive technique which can

be advantageous as sensing can occur at low anion concentrations and only small amounts of sensor are required. Changes in the fluorescence of a reporter group can arise by one of four mechanisms: photoinduced electron transfer (PET); monomer-to-excimer switching (or *vice versa*) transformation; the "rigidity effect"; and electronic energy transfer. Anion binding may either enhance or quench fluorescence of a reporter group and/or alter the emission wavelength.

Photoinduced electron transfer is a particular method of fluorescence quenching in which a proximal donor or acceptor orbital can facilitate through-space, non-radiative electron transfer to an excited fluorophore, returning it to the ground state without emission of radiation. Changes in the energy of this proximal orbital (e.g. by anion binding) can impact the extent of quenching and so the fluorescence emission.

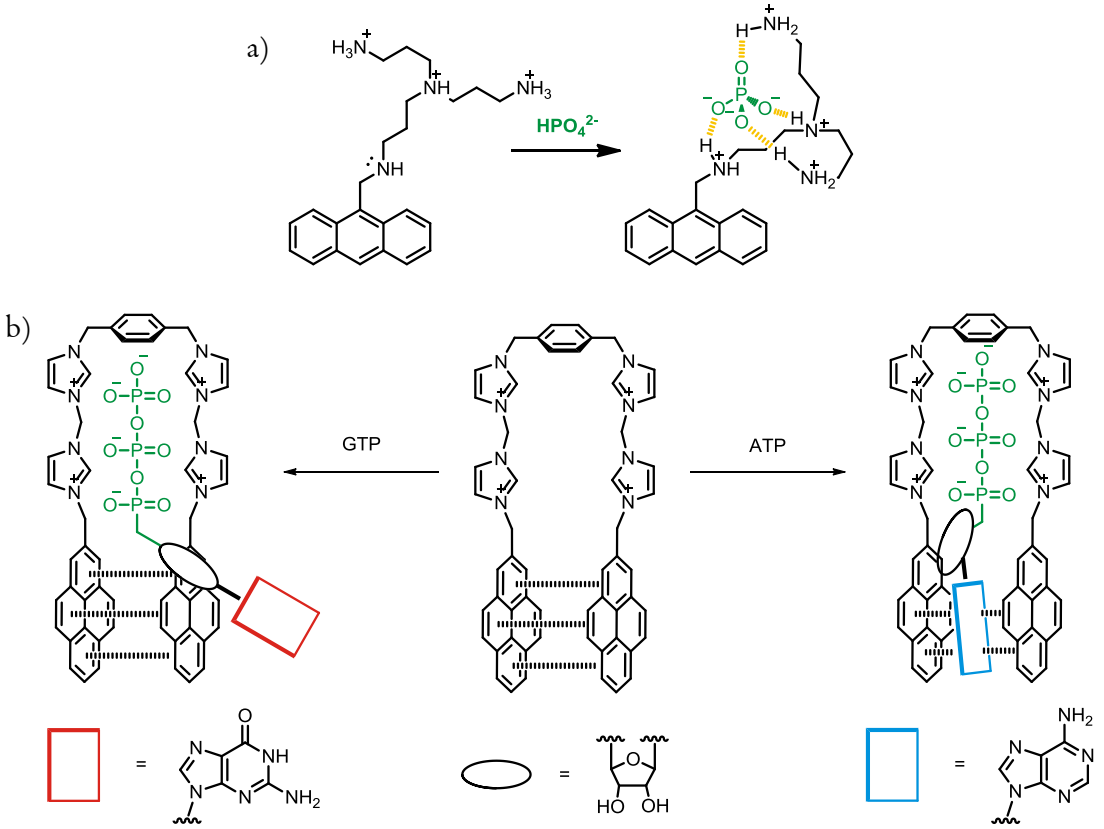


Figure 1.34. Anion sensors operating through: a) photoinduced electron transfer; and b) pyrene monomer–excimer switching.

Anthracene is an organic fluorophore extensively used in anion sensing, the first reported example is shown in Figure 1.34a.[156] In the presence of phosphate anions fluorescence

emission is enhanced due to the inhibition of photoinduced electron transfer. Anion complexation causes protonation of the neutral amino residue preventing PET quenching of the fluorescence, an effect which does not occur with sulfate and acetate.

Aromatic pyrene is known for its ability to form excited state dimers (excimers), the extent of formation depending upon the degree of overlap of monomer units. Yoon, Kim and co-workers have reported a molecular pincer-type receptor containing imidazolium anion recognition groups and terminal pyrene subunits (Figure 1.34b).[157] Upon ATP anion complexation (pH 7.4, 20 mM HEPES buffer), a decrease in excimer emission and an increase in monomer emission is observed as the adenine group disrupts dimer formation. This effect is not observed with other nucleoside triphosphates.

Numerous examples of metal-containing luminescent anion sensors exist; the ruthenium(II) tris(bipyridyl) reporter group has been much exploited for anion recognition purposes. A recent example is reported by Pinet and co-workers who constructed a guanidinium-functionalised ruthenium(II)-bipyridyl complex (Figure 1.35a) and studied its luminescence anion sensing abilities in acetonitrile.[158] Addition of L-glutamate and dihydrogen phosphate induced significant enhancements in luminescence emission and a hypsochromic shift in the maximum emission wavelength, an effect which was not observed with acetate or halide anion species. The receptor adopts a more planar conformation upon anion binding at the guanidinium units and rigidification of the transition metal bipyridyl receptor reduces energy loss through non-radiative decay pathways; the hypsochromic shift suggests anion coordination raises the energy of the MLCT band.

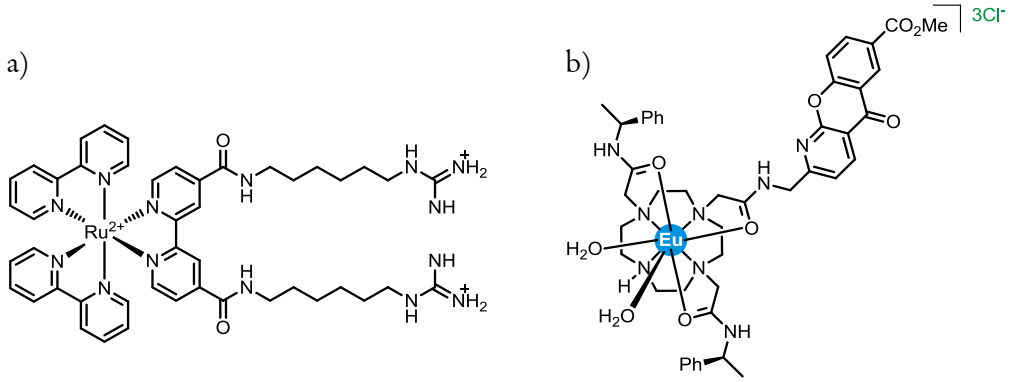


Figure 1.35. Fluorescent anion sensors: a) Pinet's ruthenium-functionalised receptor exploiting the "rigidity effect"; and b) Parker's lanthanide-containing sensor.

In addition to transition metals, lanthanides can also be used as reporter groups. Direct excitation of the lanthanide through *f-f* transitions is Laporte forbidden so another mechanism – involving sensitisation of an organic antenna located close to the lanthanide centre – enables indirect excitation via energy transfer and emission from the long-lived lanthanide can then occur.[159] Parker and co-workers have prepared a europium(III)–complex with intergrated azaxanthone sensitiser (Figure 1.35b).[160] Addition of citrate and bicarbonate caused large changes to the lanthanide emission spectral profile which was attributed to strong electrostatic interactions between host and guest as well as the entropically favourable displacement of two coordinated water molecules.

1.4.3.3.3 Displacement assays

The use of indicator-displacement assays as a method of sensing anions has been pioneered by Anslyn and co-workers. The reversible binding of boronic acids to 1,2- and 1,3-diols and of ammonium groups to carboxylates was exploited in the construction of several tripodal host systems for anion sensors.[161] By combining the receptor in Figure 1.36 with the indicator pyrocatechol violet, the binding and sensing of the anticoagulant heparin (as the sodium salt) in 1:1 water:methanol (10mM HEPES buffer at pH 7.4) was detectable by a visible colour change from grey to yellow.

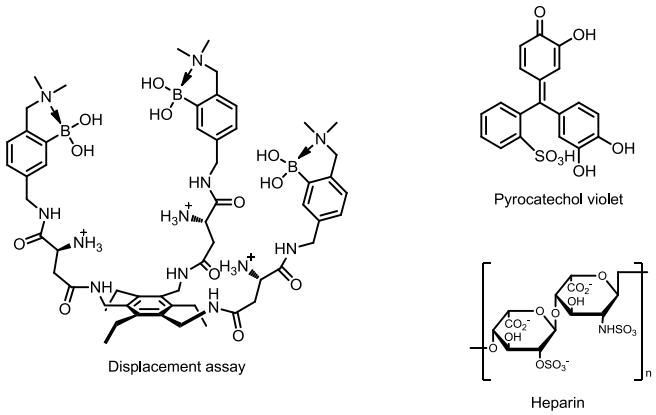


Figure 1.36. Anslyn's displacement assay for the sensing of heparin.

1.5 Self-assembly

In addition to host–guest complex formation, supramolecular chemistry also encompasses self-assembly, the spontaneous, reversible association of molecular components into well-defined more complex superstructures which are stabilised by the many non-covalent forces referred to in section 1.2. All the information required for the self-assembly process is encoded in the individual components and the resulting complex is the most thermodynamically stable aggregate that can be formed under the reaction conditions. Reversibility and thermodynamic stability enable any errors that may have occurred during the assembly process to be corrected, which is important in the assembly of biomolecules such as the DNA double helix, cell walls, viruses and multi-component enzymes. All these exemplify "strict self-assembly" as opposed to "self-assembly with covalent modification" a term applied to systems where ante- or post-assembly covalent-bond-formation enables the irreversible synthesis of a final product that is not necessarily a thermodynamically favoured architecture.[2]

1.5.1 Templated self-assembly

A template is often used in self-assembly to control the formation of a favoured product over other possible supermolecules.[162] Defined by Busch, a chemical template "*organises an assembly of atoms, with respect to one or more geometric loci, in order to achieve a particular linking of atoms*".[163] The organising role may be performed by a discrete chemical species but

in other cases the template can be thought of as "*the dominating force that orients the individual molecular units so they can collectively perform the templating function*".[164] Busch further classified templates as either kinetic or thermodynamic: a kinetic template arranges reaction precursors in such as way that the energy requirement of a particular reaction pathway is reduced, an irreversible reaction follows giving the target compound; a thermodynamic template preferentially stabilises one product in a reversible reaction, biasing the equilibrium in favour of its formation.[165] Sanders has suggested classifying templates in relation to the topology of the precursor arranged around the templating species (linear, cyclisation or interweaving templation).[166]

1.5.1.1 Cation templation

Transition metal cations have been widely employed as chemical templates, being able to form strong metal–ligand dative bonds, with varying degrees of lability, as well as preferring specific geometries in their coordination sphere through ligand field effects. Cation templation matured alongside the advances in cation coordination chemistry in the 1960s. Busch showed that nickel(II) ions could affect the product ratio of the reaction between mercaptoamines and diketones (Figure 1.37a),[165,167,168] and the size complementarity between alkali metal cations and crown ethers was exploited in the synthesis of these macrocycles (Figure 1.37b).[169]

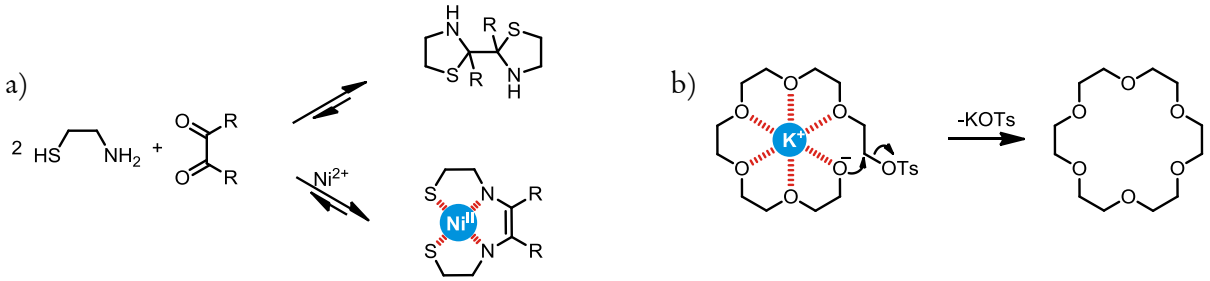


Figure 1.37. Early cation templation: a) Busch's Ni(II)-templated ligand synthesis; and b) potassium-templated synthesis of [18]crown-6.

Since then, cation templation has progressed to the formation of enormous varieties of intricate, polymetallic architectures.

Grid-like complexes have been prepared which required the orthogonal arrangement of ligands at each metal centre, usually achieved by combining ligands with either bi- or tri-dentate subunits around metal ions possessing tetrahedral or octahedral coordination preferences respectively. A number of two-dimensional square arrays (Figure 1.38) have been reported by Lehn and co-workers[170,171].

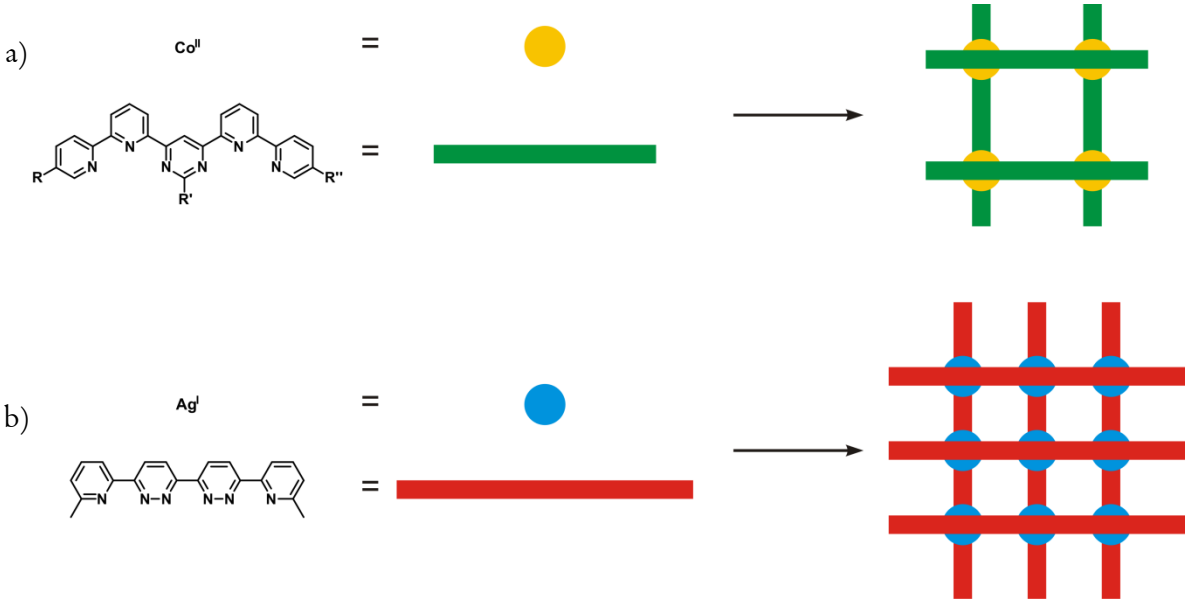


Figure 1.38. Higher order cation templation: a) Lehn's 2×2 and 3×3 grids; and b) Fujita's polyhedra.

Fujita and co-workers' seminal work exploiting nitrogen-palladium coordinate bonds and the preferred square-planar arrangement of ligands around the metal centre has resulted in the metal-directed-assembly of numerous polyhedra.[172-174] By varying the length, shape or denticity of terminal-nitrogen ligands, cages and spheres of varying sizes and shapes have been prepared. More recently, Nitschke and co-workers have constructed a cubic capsule which self-assembles from twelve bis(pyridylimine) ligands and eight iron(II) metal cations.[175]

1.5.1.2 Anion templation

The strategic use of anions to template the formation of molecular frameworks is much less developed than the field of cation templation. Many early examples of anion templation were

serendipitous discoveries, such as Lehn's archetypal formation of penta- or hexanuclear helicates by reaction of tris-bipyridyl ligands and iron(II) chloride or sulfate respectively.[176] Likewise, Dunbar and co-workers have underscored the significance of the templating anion in the formation of polymetallic macrocycles from nickel(II) salts and bidentate 3,6-bis(2-pyridyl)-1,2,4,5-tetrazine ligands (Figure 1.39). In the presence of tetrafluoroborate anions [2×2] molecular squares were obtained, yet with nitrate or hexafluoroantimonate, trimeric or pentameric macrocycles were formed exclusively. In addition, the pentagonal assembly may be converted to either other geometry in the presence of the appropriate anion in acetonitrile.[177]

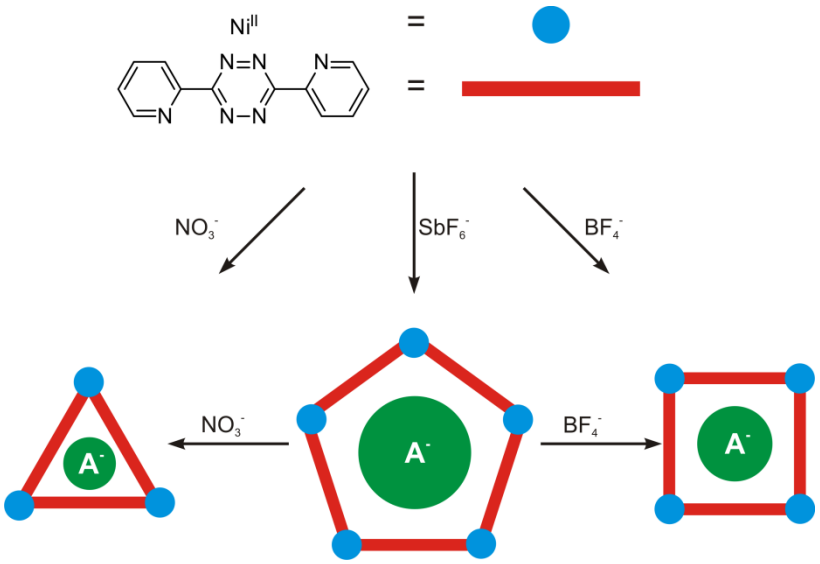


Figure 1.39. Schematic representation of Dunbar's anion-templated metallocyclophanes.

Böhmer and co-workers have incorporated multiple urea hydrogen-bond-donor groups into macrocyclic anion hosts formed by reaction between a bis-aryl ether diamine and diisocyanate in acetonitrile (Figure 1.40a). The yield of macrocycle formation was significantly enhanced by addition of templating chloride anions. Interestingly, crystal structure studies reveal one macrocycle folded in a figure-of-eight fashion creating two binding cavities each of which contain a chloride anion template.[178]

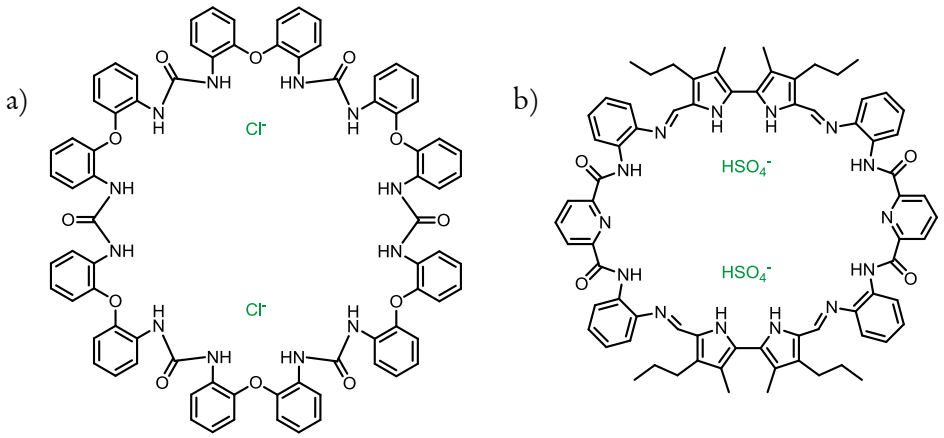


Figure 1.40. Anion-templated assemblies: a) Böhmer's chloride-templated macrocycle; b) Sessler's sulphuric-acid-templated macrocycle.

Sessler and co-workers used Schiff-base chemistry to prepare polypyrrolic macrocycles containing imine-linked bipyrrole and 2,6-pyridine bis-amide units (Figure 1.40b).[179] The condensation reactions were carried out using a range of acids and macrocycle formation proceeded cleanly, only when sulfuric acid was used; other acids giving rise to oligomeric products only.

1.5.2 Interpenetrated and interlocked structures

Self-assembly is a powerful tool which can be exploited to direct the formation of intricate, higher order structures inaccessible by traditional, stepwise synthetic methods. Mechanically interpenetrated and interlocked architectures are everywhere, from intriguing children's toys to international symbols of strength and unity as well as in domestic and industrial appliances, and biological processes (Figure 1.41). In particular, the replication of DNA involves pseudorotaxane formation for several crucial steps. For example, the enzyme DNA polymerase binds a single strand of DNA and directs the incoming individual nucleotides so that a complementary second strand is formed. Pseudorotaxane formation helps to keep the DNA strands in place to minimise errors in the synthetic process (Figure 1.41d).[180]

This Figure Has Been Removed for Copyright Reasons

Figure 1.41. Examples of interpenetrated and interlocked structures in everyday life: a) a child's toy;[181] b) Olympic rings;[182] c) a nut and bolt;[183] and d) schematic representation of DNA replication.[184]

Given the ubiquity of interlocked structures in our macroscopic world, supramolecular chemists have endeavoured to reproduce these systems at a molecular level for their synthetic non-triviality, aesthetic appeal, and potential function in molecular machinery.

An interlocked molecule has by definition a *mechanical bond*: two interlinked components cannot be separated without breaking a chemical bond, whilst not being chemically bonded themselves. The simplest and most common interlocked structures are [n]rotaxanes (a wheel threaded around a stoppered-axle; from the Latin *rota*, wheel and *axis*, axle) and [n]catenanes (interlocked rings; from the Latin *catena* meaning chain), where n represents the number of distinct components comprising the molecule, although trefoil knots (the simplest non-trivial knot, named after the three-leaf clover or trefoil plant), Solomon knots, and Borromean rings (from the Borromeo family coat of arms) are also known (Figure 1.42).[185]

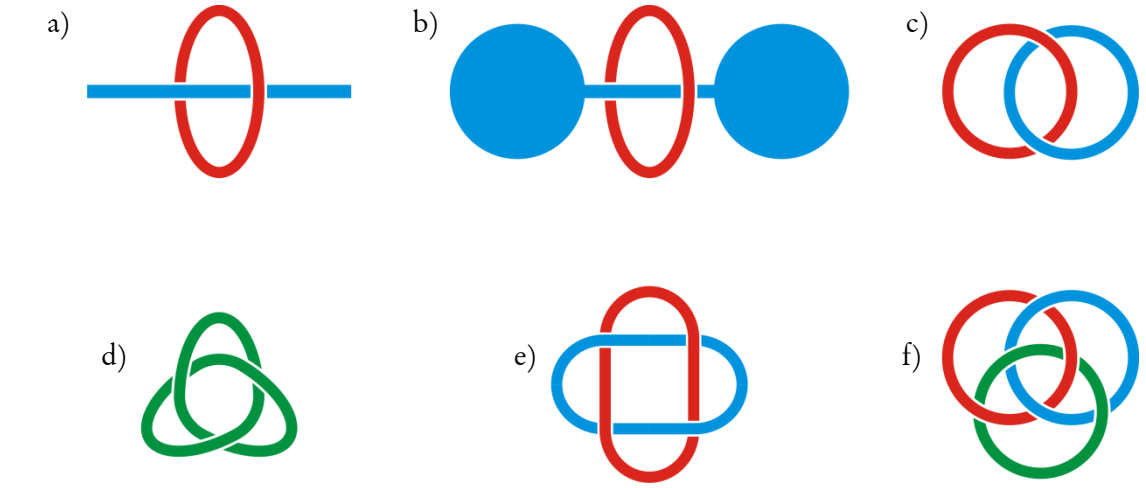


Figure 1.42. Cartoon representations of interpenetrated and interlocked architectures: a) pseudo[2]rotaxane; b) [2]rotaxane; c) [2]catenane; d) trefoil knot; e) Solomon knot; and f) Borromean rings.

Mechanically interlocked molecules can be formed in a number of ways and an overview of these is given in Figure 1.43 and Figure 1.44. Rotaxanes are most commonly formed by *clipping* or *stoppering*.[186] Clipping involves a ring-closing reaction to cyclise an acyclic macrocycle-precursor component around a stoppered-axle, the stoppers being bulky enough to prevent dethreading. In the stoppering approach a preformed pseudorotaxane assembly is functionalised by appending bulky stopper groups to the axle component. Other more obscure methods include: *slippage* of a macrocycle over suitably-sized stoppers,[†] usually achieved by thermal activation to form the rotaxane as the thermodynamic product;[187] *snapping*, where the axle is formed from two half-stoppered precursors within the macrocycle;[188,189] *swelling* the stopper groups using a dilating rearrangement once a pseudorotaxane has formed;[190] and *shrinkage* of the macrocycle component of a pseudorotaxane precursor.[191]

[†] Leigh argues that rotaxanes formed by "slippage" are not formally rotaxanes since the IUPAC definition states that rotaxanes are "*molecules in which a ring encloses another, rod-like molecule having end-groups too large to pass through the ring opening and thus holds the rod-like molecule in position without covalent bonding*". A structure cannot have end groups too large to pass through the macrocycle if it forms in such a way and instead may be considered kinetically stable pseudorotaxanes.

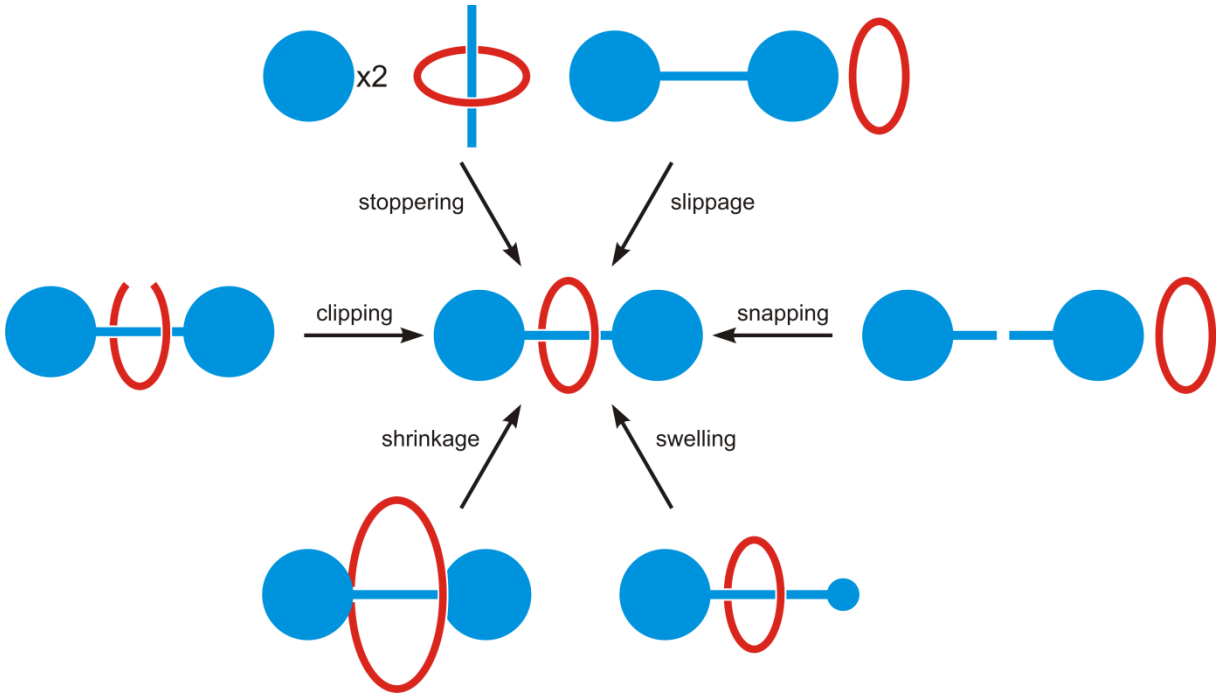


Figure 1.43. Cartoon representation of the various synthetic routes to [2]rotaxanes.

Catenanes are usually formed by cyclisation of the threading component of a pseudorotaxane or double-cyclisation of an interweaving orthogonal array of acyclic precursors.[192] Magic-ring formation of catenanes in which a macrocycle can open and then recyclise around a second cyclic component is less common.[193]

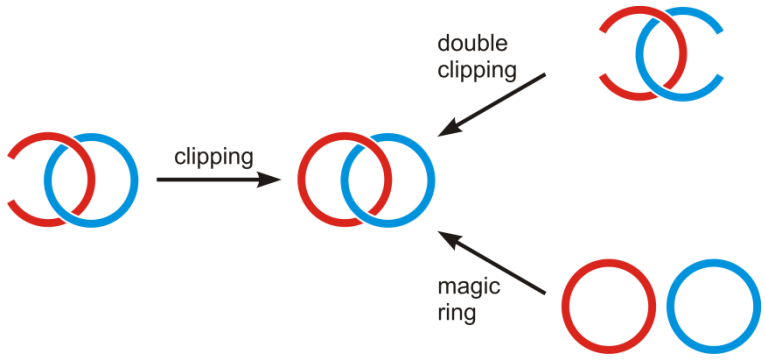


Figure 1.44. Cartoon representation of the various synthetic routes to [2]catenanes.

Historically, the synthesis of interlocked structures relied on the statistical likelihood that macrocyclisation would occur when the two precursor components were correctly interwoven. Consequently, the first catenane[194] and rotaxane[195] were isolated in very low yields (<1% and 6% respectively). Attempting to overcome the low yields of these chance formations of interlocked structures, Schill and co-workers developed a covalent-directed

templated synthesis to produce [2]catenanes.[196] This approach involved twenty-step syntheses which prevented both large scale synthesis and effective exploitation of the resulting structures. Modern syntheses almost exclusively depend on strategic cationic, neutral or anionic templation methodologies to create mechanically-bonded assemblies in higher yields.

1.5.2.1 Cation-templated assembly of interlocked molecules

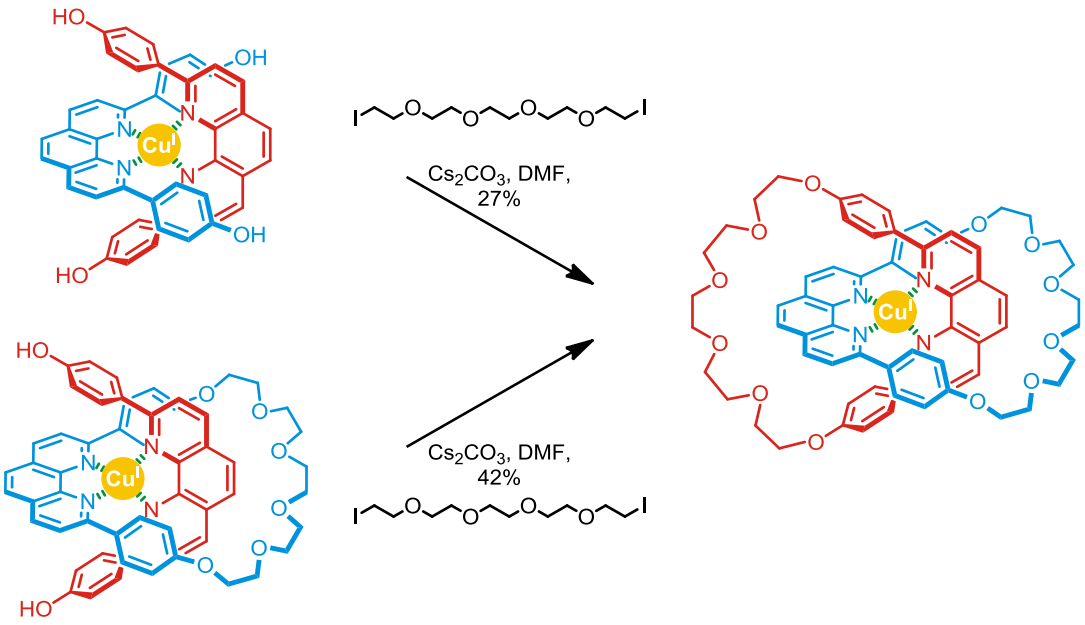


Figure 1.45. Sauvage's copper(I)-templated synthesis of a [2]catenane.

Sauvage's ground-breaking copper(I)-templated catenane formation paved the way for a number of high yielding cation-templation strategies for interlocked structure synthesis (Figure 1.45). Two bidentate phenanthroline ligands are held orthogonally by the tetrahedral coordination preference of a copper(I) templating ion. Subsequent clipping by nucleophilic substitution condensation reactions with two equivalents of pentaethyleneglycol diiodide gave the metallated [2]catenane species in 27% yield.[197] By preforming one of the macrocycle components the catenane yield was further increased to 42%.[197,198] This copper(I)-templation strategy was soon extended to produce a [3]catenane and the first molecular trefoil knot.[199]

Following on from Sauvage's use of tetrahedral-directing copper(I) ions, a number of transition metal cations with different coordination geometry preferences have been

employed in the templated-synthesis of interlocked structures (Figure 1.46). Prominent examples include: square-planar palladium(II) rotaxanes[200] and linear gold(I) rotaxanes and catenanes[201] via Grubbs' ring-closing metathesis cyclisation reactions; octahedral iron(II)-[202] and cobalt(III)-[203]templated [3]rotaxanes via a stoppering methodology; and zinc(II)-templated synthesis of a Borromean ring using reversible Schiff-base chemistry in near quantitative yield.[204]

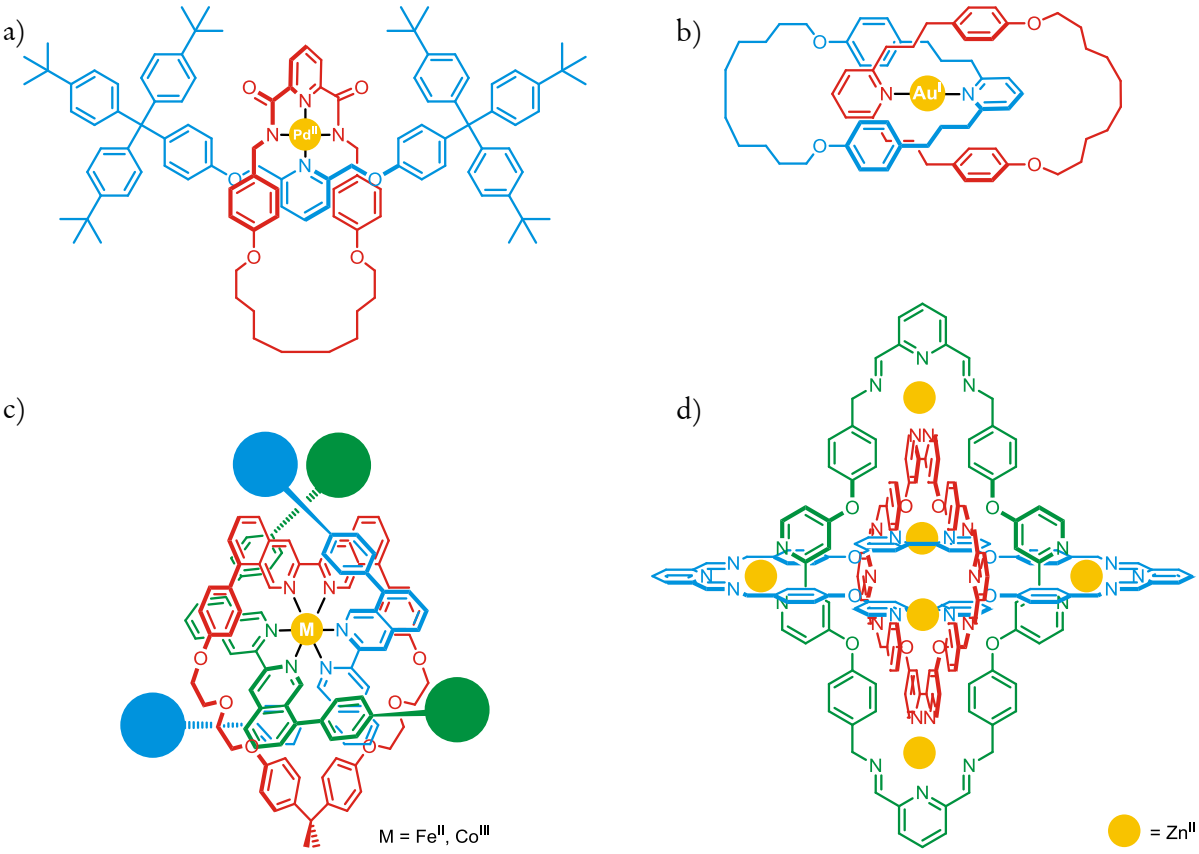


Figure 1.46. Metal-ion templated interlocked structures: a) square-planar Pd(II)-templated rotaxane; b) linear Au(I)-templated catenane; c) octahedral Fe(II)- and Co(III)-templated [3]rotaxane; Zn(II)-templated Borromean ring.

In addition to well-defined geometrical requirements, transition metals are known to catalyse a number of organic reactions. Leigh's ventures into *active metal templation* highlight the versatility of these cations in the synthesis of rotaxanes and catenanes.[205] In this methodology, the metal plays a dual role, acting both as a template for interweaving the components and as a catalyst promoting covalent-bond formation between two half threads (rotaxane) or macrocycle ring closing (catenane).

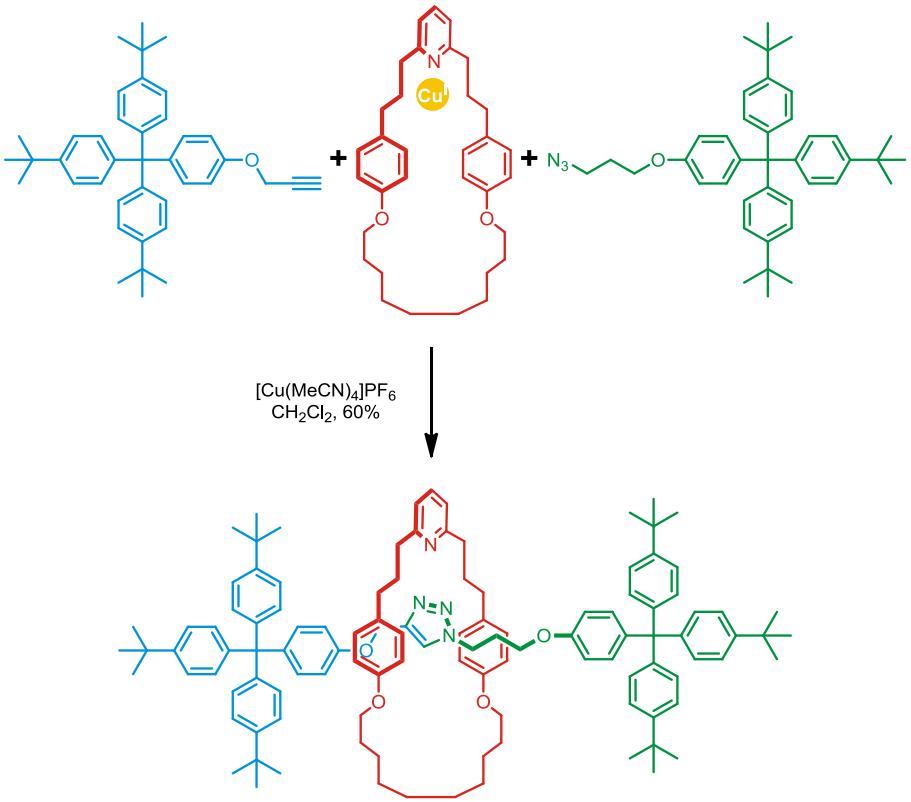


Figure 1.47. Active-metal-templated synthesis of a [2]rotaxane.

The first active-metal-templated interlocked structure was reported in 2006 by Leigh and co-workers and exploited the copper(I)-catalysed alkyne–azide cycloaddition[206] (CuAAC) in the snapping synthesis of a [2]rotaxane (Figure 1.47).[207] The concept has since been extended to exploit other transition-metal-mediated reactions such as palladium-catalysed cross-coupling,[208] copper(I)- and palladium(II)-catalysed alkyne homocouplings,[209-211] nickel-catalysed sp^3-sp^3 carbon-carbon homocoupling,[212] carbon-carbon heterocoupling,[213] and palladium-mediated Michael addition.[214]

Whilst not strictly a templation effect, metal cations have been employed in the magic ring synthesis of [2]catenanes. Fujita and co-workers have prepared [2]catenanes from a preformed macrocycle incorporating palladium(II)–pyridine dative bonds: the lability of these bonds allows dissociation of the macrocycle followed by self-assembly and cyclisation to form the interlocked species (Figure 1.48a).[215] Beer and co-workers exploited the lability of copper(II)–dithiocarbamate units in the magic ring synthesis of a tetranuclear copper(II)/copper(III)-containing catenane (Figure 1.48b).[216]

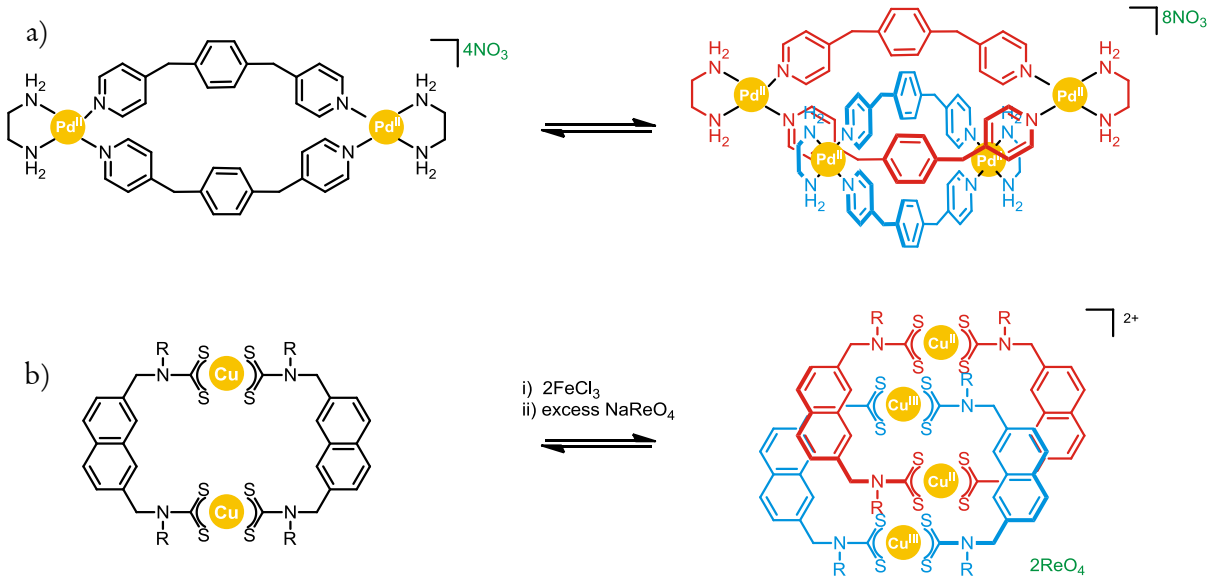


Figure 1.48. a) Fujita's and b) Beer's magic ring syntheses of [2]catenanes.

Organic cations have also been used to template the formation of interlocked molecules. The strong association between secondary ammonium cations and polyether macrocycles has been appreciated for some time,[217] and utilised in the templated assembly of pseudorotaxanes, rotaxanes and catenanes.[218,219] Stoddart and co-workers have exploited this intercomponent interaction in the synthesis of higher order rotaxanes (Figure 1.49a)[220] and a new class of interlocked molecule, suit[2]anes (Figure 1.49b).[221,222] Once mechanically bonded by an encircling macrocycle component of a rotaxane or catenane, the ammonium species can be easily deprotonated, a phenomenon exploited to great effect in molecular machine applications (section 1.5.3).

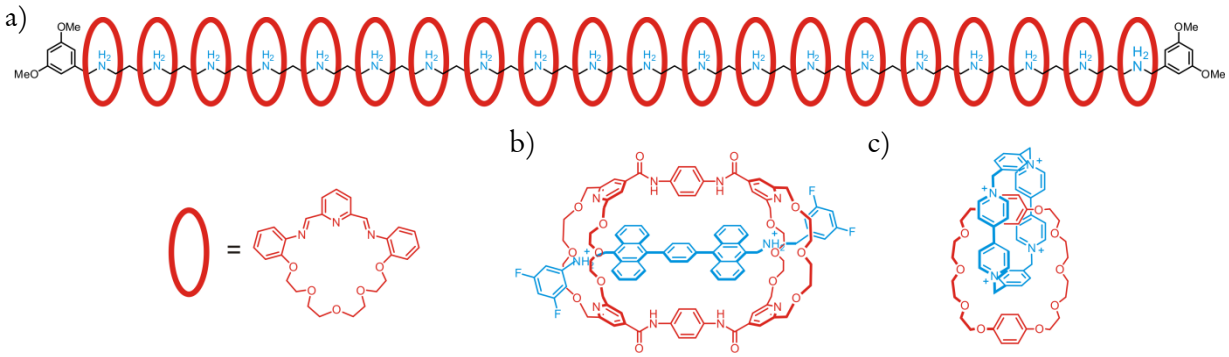


Figure 1.49. Interlocked structures templated using organic cations: Stoddart's ammonium-templated [20]rotaxane (a) and suit[2]ane (b); and Stoddart's [2]catenane templated by charge-assisted aromatic donor–acceptor interactions (c).

A macrocycle containing two viologen units (Stoddart's "blue box") has been used to assemble interlocked systems through charge-assisted donor–acceptor interactions, with electron-rich 1,4-dimethoxybenzene (Figure 1.49c),[223] tetrathiafulvalene,[224-226] and dihydroxynaphthalene[227] derivatives.

1.5.2.2 Neutral-templated assembly of interlocked molecules

In 1992 the first examples of neutral templation of catenanes were reported by the groups of Vögtle[228] and Hunter,[229] directed by intermolecular amide–amide hydrogen bonding. Hunter's catenane is prepared by a one-pot double cyclisation reaction between isophthaloyl dichloride and a bis-amine in 34% yield (Figure 1.50a). The templation does not occur prior to the reaction but instead follows the formation of one hydrogen-bond-donating amide unit. This technique has been used more recently by Leigh and co-workers to assemble both rotaxanes and catenanes.[230-232]

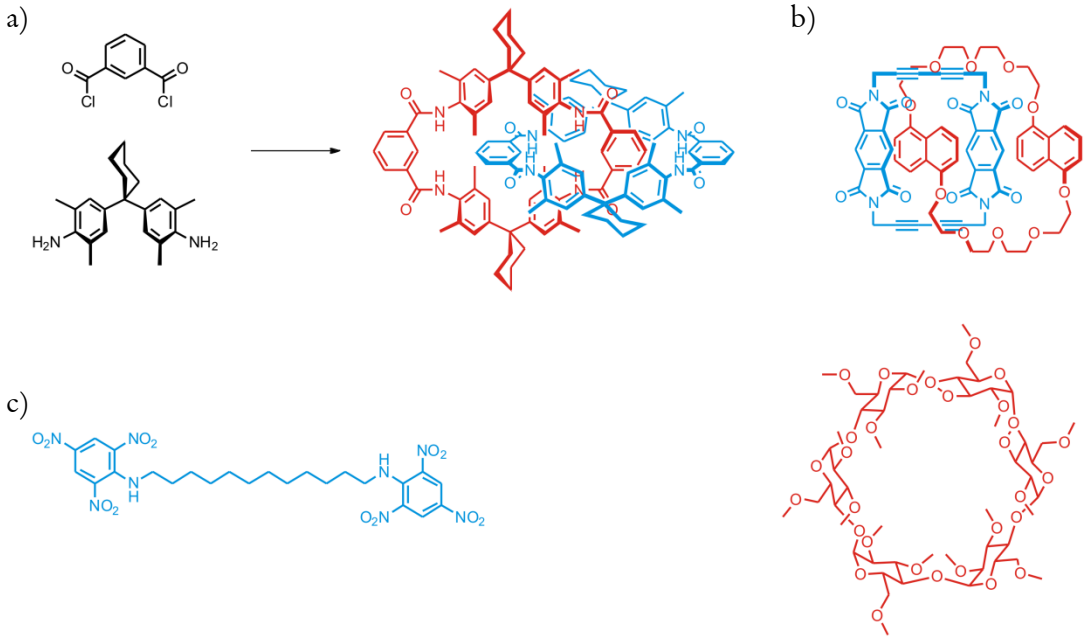


Figure 1.50. Interlocked structures templated by neutral intermolecular interactions: a) Hunter's hydrogen-bond-templated catenane; b) Sanders' catenane templated by aromatic donor–acceptor interactions; and c) Harada's [2]rotaxane assembled using the hydrophobic effect.

The stacking of electron-deficient and electron-rich arenes through donor–acceptor aromatic interactions has also been used to direct rotaxane and catenane construction. Sanders and co-

workers have used the non-covalent interactions between a dinaphthocrown macrocycle and an acetylenic aromatic diimide to assemble a pseudorotaxane species, from which the related [2]catenane was formed by a copper(I)-catalysed alkyne-coupling reaction in 25–33% yield (Figure 1.50b).[233]

Finally, the hydrophobic effect is often exploited to enhance inclusion-complex formation between cyclodextrins and a variety of guest species in aqueous solutions.[234-236] Harada and co-workers formed pseudorotaxane inclusion complexes between cyclodextrins and a long hydrocarbon molecule with terminal amine groups.[237] Irreversible stoppering with a benzenesulfonate derivative gave the interlocked rotaxane molecules in 42–48% yields (Figure 1.50c).

1.5.2.3 Anion-templated assembly of interlocked molecules

The slow beginnings witnessed in anion receptor chemistry are mirrored in anion templation, and the use of anions to template the formation of interpenetrated and interlocked structures has only become established within the past decade. Stoddart's preparation of a [5]pseudorotaxane, the crystal structure of which shows a hexafluorophosphate counteranion within the cavity, is the first anion-assisted assembly of a interpenetrated structure (Figure 1.51a).[238] The analogous assembly in the absence of the hexafluorophosphate anion was never undertaken, however, and as such its templating role was never fully established. Vögtle and co-workers reported the first anion-templated interlocked structure in 1999. A tetra-amide macrocycle was designed to hydrogen-bond to organic anions that could act as nucleophiles in substitution reactions. Reaction between a phenolate derivative and a benzylic bromo species in the presence of the macrocycle in dichloromethane afforded the neutral rotaxane system in 95% yield (Figure 1.51b).[189] Amide–oxygen hydrogen-bonding has been used to template assemblies incorporating squaraine[239], pyridine *N*-oxide[240] and phenoxide[241] functionality which maintains the anionic character of the axle component (Figure 1.51c-e).

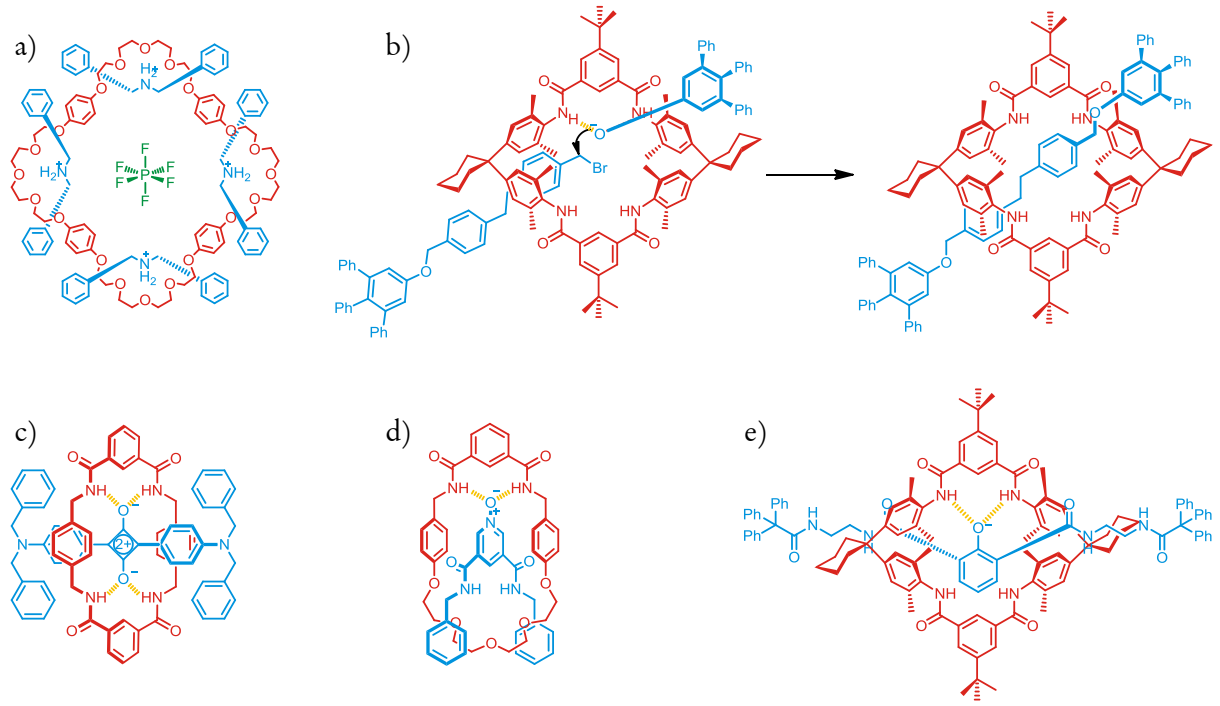


*Figure 1.51. Examples of anion templation: a) Stoddart's hexafluorophosphate-templated [5]pseudorotaxane; b) Vögtle's phenoxide-templated synthesis of a [2]rotaxane; c) Smith's squaraine [2]rotaxane; d) Jiang's pyridine-*N*-oxide-templated pseudorotaxane; and e) Schalley's phenoxide-templated rotaxane.*

These methodologies require the negatively charged template to be integrated within one component of the supramolecular assembly, and the anion consequently forms part of the product. It was Beer and co-workers who instituted *discrete anion templation* as a route to interlocked structure formation.[242] Inspired by Sauvage's copper(I)-templated catenanes, they noted that a pyridinium bis-amide ligand can complex one chloride anion, forming a tight ion pair in which the halide anion remains coordinatively unsaturated. A second bis-amide ligand can then bind to the chloride's free meridian to form an orthogonal complex with 2:1 ligand:chloride stoichiometry and an association constant K_a = 100 M^{-1} in acetone (Figure 1.52a). Replacing the neutral acyclic component with an isophthalamide-containing macrocycle species, enabled the analogous pseudorotaxane species to be assembled with an apparent association constant value of K_{app} = 2400 M^{-1} in acetone (Figure 1.52b).[243]

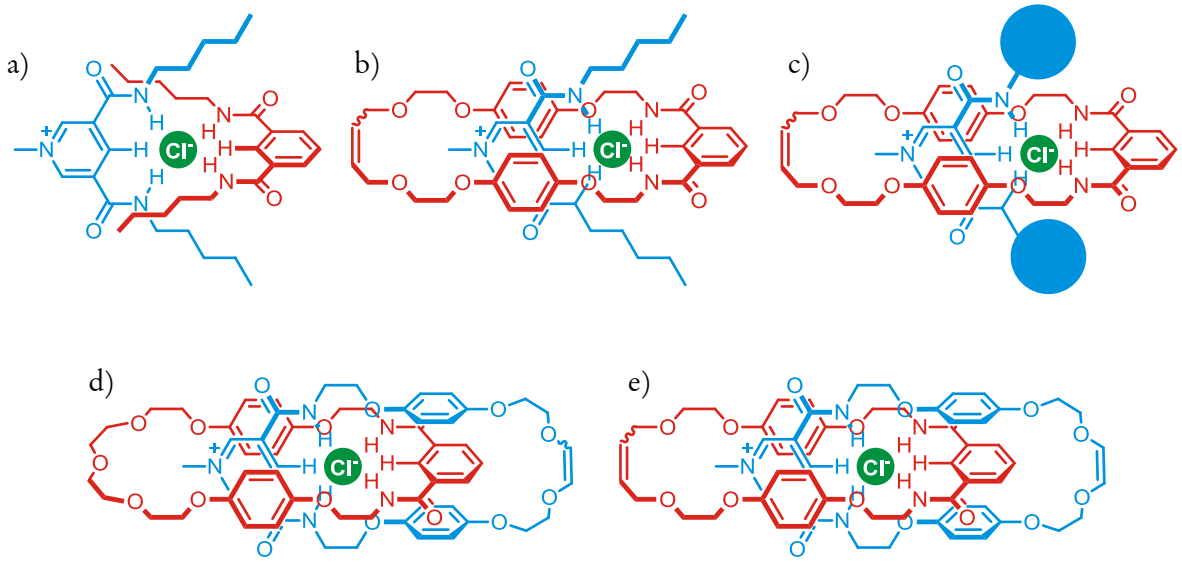


Figure 1.52. Interpenetrated and interlocked architectures assembled via Beer's discrete-chloride-template methodology: a) orthogonal precursor; b) [2]pseudorotaxane; c) Grubbs' ring-closed [2]rotaxane; d) cyclised [2]catenane; e) double-cyclised [2]catenane.

To form permanently interlocked rotaxane species the pyridinium threading component was appended with bulky stoppers and a macrocycle precursor component, functionalised with vinyl-moieties to allow cyclisation by Grubbs'-catalysed ring closing metathesis (RCM), was designed (Figure 1.52c).[244] Beer and co-workers extended this concept to produce catenanes. A bis-vinyl-appended threading component of a pseudorotaxane assembly is cyclised using Grubbs'-catalysed RCM to form the related catenane species (Figure 1.52d).[245] Likewise, double cyclisation of an orthogonal bis-vinyl-functionalised precursor assembly gave an anion-templated catenane species (Figure 1.52e).[246]

This general anion templation methodology has been implemented to prepare a range of more intricate interlocked architectures such as a sulfate-templated capsule,[247] a chloride-templated handcuff catenane,[248] and a Janus [2]rotaxane[249].

1.5.3 Applications of interlocked molecules

Mechanically bonded structures have captured chemists' imagination owing to their non-trivial topology and the promise of their potential in chemical sensor applications and nanotechnological uses as molecular switches and machines. With regard to potential sensor development, the removal of the templating ion in Beer's interlocked systems gives a

topologically unique three-dimensional hydrogen-bond-donating binding cavity which endows a rotaxane or catenane with receptor characteristics distinct from the individual parent components. The chloride-templated rotaxane (Figure 1.52c) was reported to be selective for chloride over more basic acetate and dihydrogen phosphate anions [K_a = 1130 M^{-1} (chloride), 300 M^{-1} (dihydrogen phosphate), 100 M^{-1} (acetate) in 1:1 chloroform-d:methanol-d_4] whereas the neutral isophthalamide macrocycle component did not form complexes with anions in this solvent mixture and the acyclic stoppered-pyridinium precursor preferentially bound the anions in order of basicity: acetate (K_a = 22 000 M^{-1}) > dihydrogen phosphate (K_a = 260 M^{-1}) > chloride (K_a = 125 M^{-1}).[244] The improvement in anion binding strength and the reversal of selectivity reveals the rotaxane's unique interlocked binding cleft is of complementary size and shape for the chloride anion, whereas the larger oxoanions are unable to penetrate the binding pocket. In addition, a number of rotaxanes and catenanes have been functionalised with reporter groups and can act as anion sensors. [250-254]

A significant advantage of mechanically interlocked molecules is their potential to behave as *molecular switches*.[255] Being made of multiple components, the conformation of one may be altered with respect to another, allowing rotation of a catenane macrocycle and shuttling or pirouetting of a rotaxane macrocycle (Figure 1.53). The molecular motion is usually triggered by one of several external stimuli: electrochemical, ion coordination, light, pH and solvation.[256]

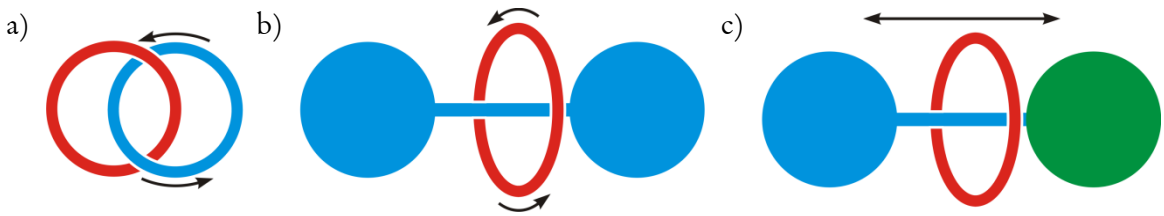


Figure 1.53. Molecular motion in simple interlocked structures: pirouetting in a) catenanes and b) rotaxanes; c) shuttling in a rotaxane.

1.5.3.1 Rotaxane shuttles

Stoddart and co-workers first reported a rotaxane molecule in which the ring component could reversibly shuttle between two stations of the axle component by either pH changes or

electrochemical means (Figure 1.54). In the ground state equilibrium position, the electron deficient tetracationic macrocycle resides preferentially over the electron-rich benzidine station. Upon oxidation or protonation with trifluoroacetic acid, the macrocycle ring shifts to the biphenol station and the shuttling process can be reversed by addition of base or reduction.[257]

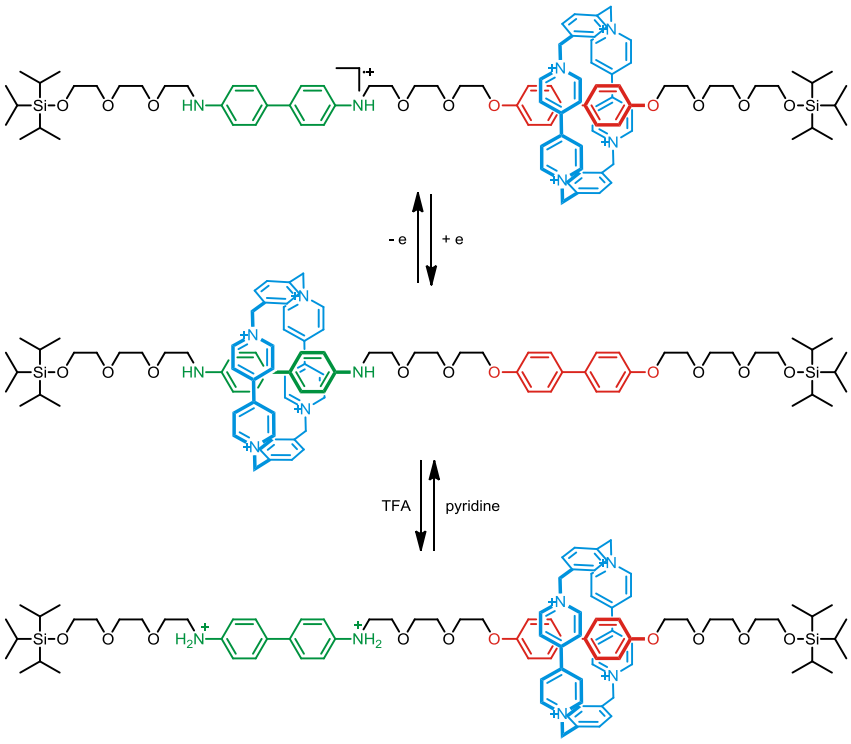


Figure 1.54. Stoddart's[2]rotaxane shuttle driven by electrochemical or pH stimuli.

Leigh and co-workers have designed a pH-stimulated molecular shuttle, where positional changes of a rotaxane's ring component can conceal or reveal an organo-catalyst (Figure 1.55a). The dibenzo[24]crown-8 macrocycle is located over the triazolium units in the unprotonated rotaxane species, allowing the secondary amine unit to catalyse Michael addition reactions between a thiol and an α,β-ketone. Following addition of acid, however, the ring component prefers to reside over the protonated ammonium group preventing access of reactants and inhibiting catalysis.[258]

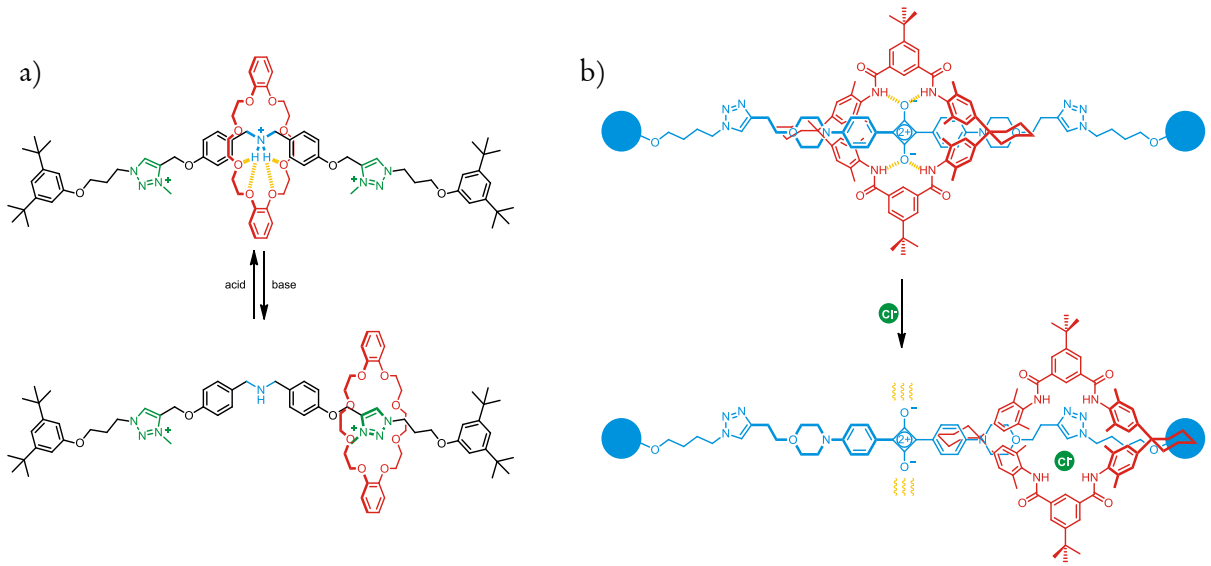


Figure 1.55. a) Leigh's acid/base switching of a macrocycle component of a [2]rotaxane enabling or inhibiting organocatalysis. b) Smith's chloride-driven rotaxane shuttle.

Anion-induced shuttling of a [2]rotaxane species has been demonstrated by Smith and co-workers. In the absence of chloride anions, the macrocycle is located at the central squaraine unit through favourable hydrogen-bonding interactions between the macrocycle's amide protons and axle's squaraine oxygens. Following addition of chloride anions in chloroform, however, the macrocycle shifts to the triazole moieties causing an increase in fluorescence intensity—a process which is reversed with removal of chloride. (Figure 1.55b).[254]

Leigh and co-workers have very recently employed a rotaxane-based molecular machine to mimic the biologically important ribosome molecule. The axle component of the rotaxane is functionalised with amino-acid units in a predetermined sequence. As the macrocycle proceeds along the axle, reaction occurs at each amino acid group in turn, forming a sequence-specific peptide molecule.[259]

1.5.3.2 Rotaxane-based molecular muscles

A type of [2]rotaxane molecule in which the two components are intertwined in a daisy chain fashion, Janus [2]rotaxanes, have been employed as *molecular muscles* capable of expanding or contracting.[260] Harada and co-workers have recently reported a Janus [2]rotaxane, the assembly of which is driven by cyclodextrin-encapsulation of a *trans*-azo derivative.

Irradiation at 365 nm triggered *trans*-to-*cis* isomerisation and the Janus [2]rotaxane contracts.[261] Sauvage used the different geometry preferences of zinc(II) and copper(II) ions to produce a Janus [2]rotaxane molecular muscle (Figure 1.56).[262] Both rotaxane components are identical and contain a 1,10-phenanthroline unit and a 2,2':6',2''-terpyridine group, and contraction or expansion of the molecular muscle is controlled by metal-ion substitution: copper(I) ions bind to two phenanthroline groups preferring a four-coordinate arrangement of nitrogen donor atoms, whereas zinc(II) has a preference for five-coordination and is complexed by both a phenanthroline unit and a terpyridine group.

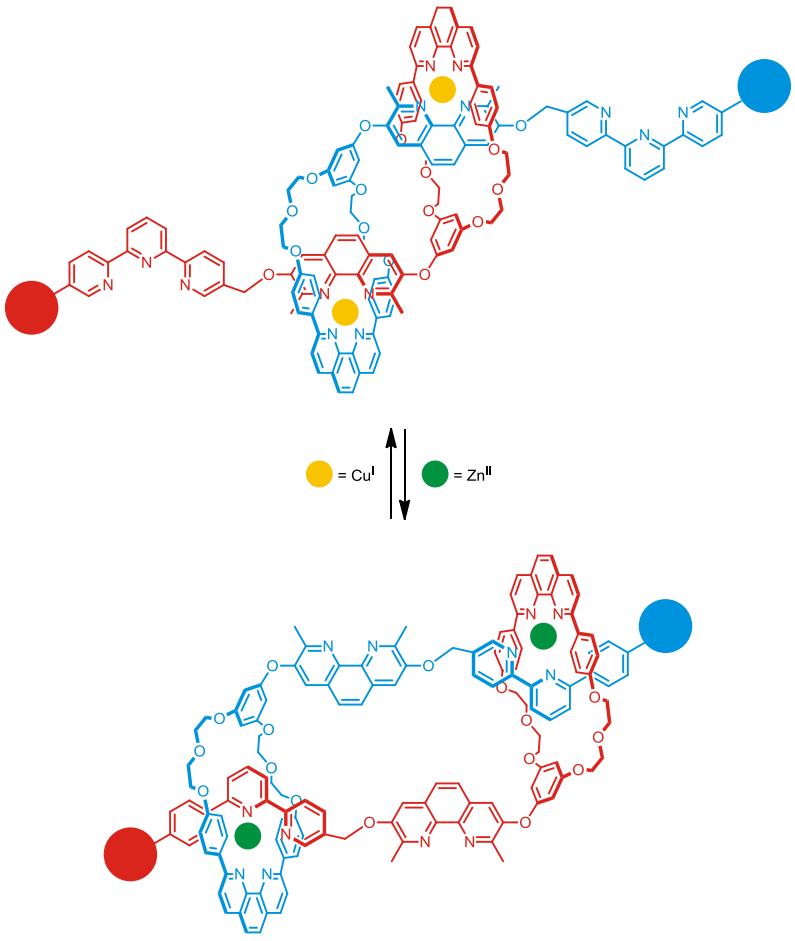


Figure 1.56. Sauvage's metal-ion-induced switching of a molecular muscle.

1.5.3.3 Catenane-based pirouettes and shuttles

A "heterocircuit" [2]catenane has been reported which undergoes a half rotation or pirouette of one component with respect to the other (Figure 1.57a). The coordination preferences of transition metal ions [octahedral cobalt(III) and square-planar palladium(II)] were used to

direct the co-conformation of the two macrocycles, which were locked in place upon metal complexation.[263]

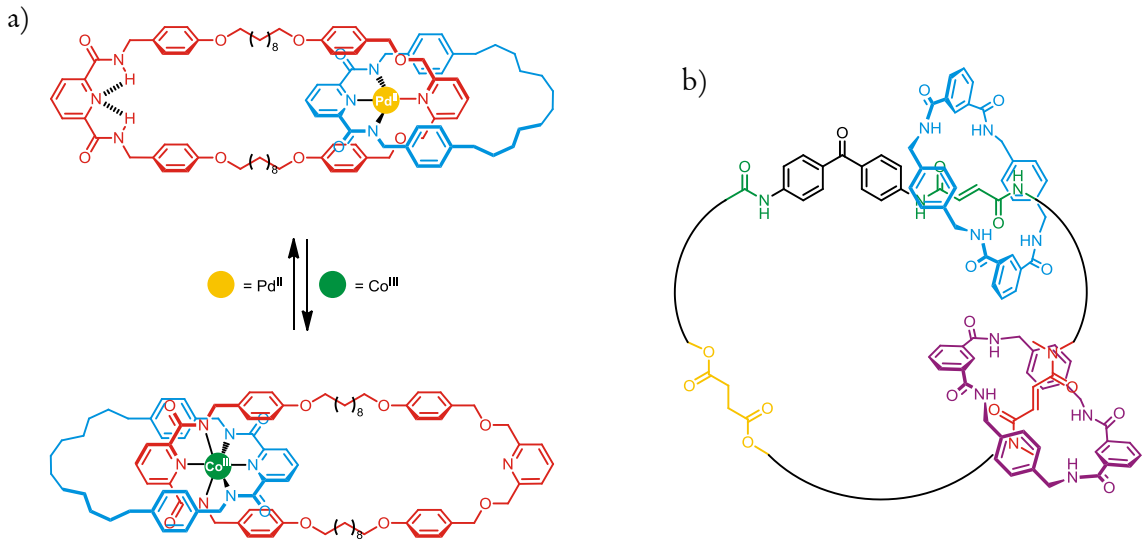


Figure 1.57. Catenane pirouettes: a) stimulated by changes in metal ion geometrical preferences; and b) unidirectional motion induced by chemical, light or heat stimuli.

Unidirectional rotation of one of two rings around discrete stations on a third, larger ring has been described by Leigh and co-workers (Figure 1.57b). Motion within the [3]catenane is driven by light, heat or chemical stimuli which changes the binding preferences of the smaller ring components.[264]

Inspired by nature's molecular walkers,[265,266] Leigh and co-workers have recently developed a number of impressive synthetic molecular walking systems.[267-269] Whilst not being based upon mechanically bonded molecules like many current molecular machines, nevertheless they reveal the power of supramolecular chemistry to direct and control processes at the molecular level.

1.6 Project aims

This thesis focuses on the development of acyclic, macrocyclic and interlocked supermolecules for the recognition and sensing of anionic guest species. In particular, halogen bonding is exploited in anion receptor design.

Chapter two details the synthesis of a series of acyclic and cage-like porphyrin-based receptors which bind anions through halogen- and hydrogen-bonding interactions. The ability of these receptor systems to bind and sense anionic guest species is investigated and comparisons between hydrogen and halogen bonding are discussed.

Chapter three reports the assembly of anion-templated pseudorotaxanes which contain both halogen- and hydrogen-bonding components. The preparation of the related catenanes is also described and their affinity for anions is investigated. The first examples of interpenetrated architectures constructed by a single charge-assisted halogen bond are detailed and the strength of the halogen-bonded assembly is utilised in the synthesis of the first example of an interlocked structure templated by a single halogen bond. Attempts to prepare a halogen-bonding catenane machine are also outlined.

Chapter four describes the synthesis of a 1,3-dialkyl-1,2,3-triazolium-containing threading component, the anion binding properties of which are determined and compared to other threading molecules. The ability of this novel thread to form pseudorotaxanes is investigated and the preparation of the related rotaxane species is outlined. Attempts to prepare macrocycles and catenanes containing this binding motif are also reported.

Chapter five discusses attempts to prepare rotaxanes with improved anion binding affinities, through increasing the lipophilicity of the anion binding clefts. Several novel rotaxanes are described and their anion binding properties studied.

1.7 References for Chapter One

[1] J.-M. Lehn, *Angew. Chem. Int. Ed. Engl.*, 1988, **27**, 89-112.
[2] J. W. Steed and J. L. Atwood, *Supramolecular Chemistry*, John Wiley & Sons, Ltd., 2000.
[3] H.-J. Schneider, *Angew. Chem. Int. Ed.*, 2009, **48**, 3924-3977.
[4] A. C. Legon, *PCCP*, 2010, **12**, 7736-7747.
[5] P. Metrangolo, F. Meyer, T. Pilati, G. Resnati and G. Terraneo, *Angew. Chem. Int. Ed.*, 2008, **47**, 6114-6127.
[6] F. Guthrie, *J. Chem. Soc.*, 1863, **16**, 239-244.
[7] O. Hassel, *Science*, 1970, **170**, 497-502.
[8] J. D. Watson and F. H. C. Crick, *Nature*, 1953, **171**, 737-738.
[9] P. Metrangolo, T. Pilati, G. Resnati and A. Stevenazzi, *Chem. Commun.*, 2004, 1492-1493.
[10] C. R. Martinez and B. L. Iverson, *Chem. Sci.*, 2012, **3**, 2191-2201.
[11] S. Grimme, *Angew. Chem. Int. Ed.*, 2008, **47**, 3430-3434.

[12] J. C. Ma and D. A. Dougherty, *Chem. Rev.*, 1997, **97**, 1303-1324.
[13] G. W. Gokel, L. J. Barbour, R. Ferdani and J. Hu, *Acc. Chem. Res.*, 2002, **35**, 878-886.
[14] L. M. Salonen, C. Bucher, D. W. Banner, W. Haap, J.-L. Mary, J. Benz, O. Kuster, P. Seiler, W. B. Schweizer and F. Diederich, *Angew. Chem. Int. Ed.*, 2009, **48**, 811-814.
[15] L. M. Salonen, M. Ellermann and F. Diederich, *Angew. Chem. Int. Ed.*, 2011, **50**, 4808-4842.
[16] B. L. Schottel, H. T. Chifotides and K. R. Dunbar, *Chem. Soc. Rev.*, 2008, **37**, 68-83.
[17] P. Phuengphai, S. Youngme, I. Mutikainen and J. Reedijk, *Inorg. Chem. Commun.*, 2012, **24**, 129-133.
[18] D. Quiñonero, C. Garau, C. Rotger, A. Frontera, P. Ballester, A. Costa and P. M. Deyà, *Angew. Chem. Int. Ed.*, 2002, **41**, 3389-3392.
[19] T. J. Mooibroek, C. A. Black, P. Gamez and J. Reedijk, *Cryst. Growth Des.*, 2008, **8**, 1082-1093.
[20] I. y. A. Gural'skiy, D. Escudero, A. Frontera, P. V. Solntsev, E. B. Rusanov, A. N. Chernega, H. Krautscheid and K. V. Domasevitch, *Dalton Trans.*, 2009, 2856-2864.
[21] S. Brooker, N. G. White, A. Bauzá, P. M. Deyà and A. Frontera, *Inorg. Chem.*, 2012, **51**, 10334-10340.
[22] Y. Li, J. C. Huffman and A. H. Flood, *Chem. Commun.*, 2007, 2692-2694.
[23] B. P. Hay and R. Custelcean, *Cryst. Growth Des.*, 2009, **9**, 2539-2545.
[24] A. Frontera, *Coord. Chem. Rev.*, 2013, **257**, 1716-1727.
[25] B. L. Schottel, H. T. Chifotides and K. R. Dunbar, *Chem. Soc. Rev.*, 2008, **37**, 68-83.
[26] C. Garau, A. Frontera, D. Quinonero, P. Ballester, A. Costa and P. M. Deya, *Chemphyschem*, 2003, **4**, 1344-1348.
[27] D. Quinonero, C. Garau, A. Frontera, P. Ballester, A. Costa and P. M. Deya, *Chem. Phys. Lett.*, 2002, **359**, 486-492.
[28] *Anion Receptor Chemistry* Ed. J. L. Sessler, P. A. Gale and W.-S. Cho, RCS, Cambridge, 2006.
[29] S. Kubik, *Chem. Soc. Rev.*, 2010, **39**, 3648-3663.
[30] E. Fischer, *Ber. Bunsen-Ges. Phys. Chem.*, 1894, **27**, 2985-2993.
[31] D. E. Koshland, *Angew. Chem. Int. Ed. Engl.*, 1995, **33**, 2375-2378.
[32] D. J. Cram, *Angew. Chem. Int. Ed. Engl.*, 1988, **27**, 1009-1020.
[33] R. D. Hancock, *J. Chem. Educ.*, 1992, **69**, 615.
[34] A. E. Martell, R. D. Hancock and R. J. Motekaitis, *Coord. Chem. Rev.*, 1994, **133**, 39-65.
[35] Y. J. Li and A. H. Flood, *Angew. Chem. Int. Ed.*, 2008, **47**, 2649-2652.
[36] J. M. Berg, J. L. Tymoczko and L. Stryer, *Biochemistry*, 6 edn., W. H. Freeman and Co., New York, 2006.
[37] http://www.nlm.nih.gov/medlineplus/ency/article/002476.htm.
[38] D. MacMahon, *Appl. Radiat. Isot.*, 2006, **64**, 1417-1419.
[39] W. H. Gries and J. Steyn, *Nuclear Instruments & Methods*, 1978, **152**, 459-462.
[40] M. Teresa Albelda, J. C. Frias, E. Garcia-Espana and H.-J. Schneider, *Chem. Soc. Rev.*, 2012, **41**, 3859-3877.
[41] C. J. Pedersen, *J. Am. Chem. Soc.*, 1967, **89**, 2495-2496.
[42] C. J. Pedersen, *J. Am. Chem. Soc.*, 1967, **89**, 7017-7036.
[43] J. M. Lehn, *Acc. Chem. Res.*, 1978, **11**, 49-57.
[44] K. Iwamoto and S. Shinkai, *J. Org. Chem.*, 1992, **57**, 7066-7073.
[45] D. J. Cram, T. Kaneda, R. C. Helgeson and G. M. Lein, *J. Am. Chem. Soc.*, 1979, **101**, 6752-6754.
[46] P. Chakrabarti, *J. Mol. Biol.*, 1993, **234**, 463-482.
[47] H. G. Hempling, in *Principles of Medical Biology*, eds. E. E. Bittar and N. Bittar, Elsevier, 1996, vol. 4, p. 217-246.
[48] W. D. McCardle, F. I. Katch and V. L. Katch, *Essentials of Exercise Physiology*, Lea & Febiger, University of Michigan, 1994.
[49] A. L. Berger, C. O. Randak, L. S. Ostedgaard, P. H. Karp, D. W. Vermeer and M. J. Welsh, *J. Biol. Chem.*, 2005, **280**, 5221-5226.
[50] G. Bosman, K. Renkawek, F. P. A. VanWorkum, I. G. P. Bartholomeus and W. J. DeGrip, *Gerontology*, 1997, **43**, 67-78.
[51] G. A. Block, T. E. Hulbert-Shearon, N. W. Levin and F. K. Port, *Am. J. Kidney Dis.*, 1998, **31**, 607-617.
[52] B. Moss, *Chem. Ind.*, 1996, 407-411.
[53] B. Moss, *Chem. Ind.*, 1996, 482-482.

[54] K. Hashimoto and K. Yoshihara, *Top. Curr. Chem.*, Springer, 1996, p. 275-291.
[55] R. Koenig, *Science*, 2000, **287**, 1737-1738.
[56] R. D. Shannon, *Acta Crystallogr. A*, 1976, **32**, 751-767.
[57] P. D. Beer, D. K. Smith and P. A. Gale, *Supramolecular Chemistry*, Oxford University Press, 1999.
[58] S. Goldman and R. G. Bates, *J. Am. Chem. Soc.*, 1972, **94**, 1476-1484.
[59] F. Hofmeister, 1888, **24**, 247-260.
[60] H. Luecke and F. A. Quiocho, *Nature*, 1990, **347**, 402-406.
[61] J. W. Pflugrath and F. A. Quiocho, *Nature*, 1985, **314**, 257-260.
[62] P. D. Beer and P. A. Gale, *Angew. Chem. Int. Ed.*, 2001, **40**, 486-516.
[63] P. A. Gale, S. E. Garcia-Garrido and J. Garric, *Chem. Soc. Rev.*, 2008, **37**, 151-190.
[64] C. Caltagirone and P. A. Gale, *Chem. Soc. Rev.*, 2009, **38**, 520-563.
[65] P. A. Gale, *Chem. Soc. Rev.*, 2010, **39**, 3746-3771.
[66] M. Wenzel, J. R. Hiscock and P. A. Gale, *Chem. Soc. Rev.*, 2012, **41**, 480-520.
[67] C. H. Park and H. E. Simmons, *J. Am. Chem. Soc.*, 1968, **90**, 2431-2432.
[68] E. Graf and J. M. Lehn, *J. Am. Chem. Soc.*, 1975, **97**, 5022-5024.
[69] E. Graf and J. M. Lehn, *J. Am. Chem. Soc.*, 1976, **98**, 6403-6405.
[70] J. P. Kintzinger, J. M. Lehn, E. Kauffmann, J. L. Dye and A. I. Popov, *J. Am. Chem. Soc.*, 1983, **105**, 7549-7553.
[71] B. Dietrich, J. Guilhem, J.-M. Lehn, C. Pascard and E. Sonveaux, *Helv. Chim. Acta*, 1984, **67**, 91-104.
[72] J. M. Lehn, E. Sonveaux and A. K. Willard, *J. Am. Chem. Soc.*, 1978, **100**, 4914-4916.
[73] M. W. Hosseini, J. M. Lehn, K. C. Jones, K. E. Plute, K. B. Mertes and M. P. Mertes, *J. Am. Chem. Soc.*, 1989, **111**, 6330-6335.
[74] F. P. Schmidtchen, *Angew. Chem. Int. Ed. Engl.*, 1977, **16**, 720-721.
[75] F. P. Schmidtchen and G. Muller, *J. Chem. Soc., Chem. Commun.*, 1984, **0**, 1115-1116.
[76] A. Ursu and F. P. Schmidtchen, *Angew. Chem. Int. Ed.*, 2012, **51**, 242-246.
[77] K. Worm, F. P. Schmidtchen, A. Schier, A. Schäfer and M. Hesse, *Angew. Chem. Int. Ed. Engl.*, 1994, **33**, 327-329.
[78] K. Worm and F. P. Schmidtchen, *Angew. Chem. Int. Ed. Engl.*, 1995, **34**, 65-66.
[79] S. Shinoda, M. Tadokoro, H. Tsukube, S. Shinoda and R. Arakawa, *Chem. Commun.*, 1998, 181-182.
[80] W. J. Belcher, M. Fabre, T. Farhan and J. W. Steed, *Org. Biomol. Chem.*, 2006, **4**, 781-786.
[81] T. H. Wirth and N. Davidson, *J. Am. Chem. Soc.*, 1964, **86**, 4325-4329.
[82] B. Dietrich, T. M. Fyles, J.-M. Lehn, L. G. Pease and D. L. Fyles, *J. Chem. Soc., Chem. Commun.*, 1978, 934-936.
[83] B. Dietrich, D. L. Fyles, T. M. Fyles and J.-M. Lehn, *Helv. Chim. Acta*, 1979, **62**, 2763-2787.
[84] G. Müller, J. Riede and F. P. Schmidtchen, *Angew. Chem. Int. Ed. Engl.*, 1988, **27**, 1516-1518.
[85] P. Schiessl and F. P. Schmidtchen, *J. Org. Chem.*, 1994, **59**, 509-511.
[86] R. P. Dixon, S. J. Geib and A. D. Hamilton, *J. Am. Chem. Soc.*, 1992, **114**, 365-366.
[87] H. Weingärtner, *Angew. Chem. Int. Ed.*, 2008, **47**, 654-670.
[88] J. Dupont and P. A. Z. Suarez, *PCCP*, 2006, **8**, 2441-2452.
[89] E. Alcalde, N. Mesquida, L. Perez-Garcia, C. Alvarez-Rua, S. Garcia-Granda and E. Garcia-Rodriguez, *Chem. Commun.*, 1999, 295-296.
[90] J. Yoon, S. K. Kim, N. J. Singh and K. S. Kim, *Chem. Soc. Rev.*, 2006, **35**, 355-360.
[91] Z. Xu, S. K. Kim and J. Yoon, *Chem. Soc. Rev.*, 2010, **39**, 1457-1466.
[92] L. Yang, S. Qin, X. Su, F. Yang, J. You, C. Hu, R. Xie and J. Lan, *Org. Biomol. Chem.*, 2010, **8**, 339-348.
[93] B. Shirinfar, N. Ahmed, Y. S. Park, G.-S. Cho, I. S. Youn, J.-K. Han, H. G. Nam and K. S. Kim, *J. Am. Chem. Soc.*, 2013, **135**, 90-93.
[94] K. Kavallieratos, S. R. deGala, D. J. Austin and R. H. Crabtree, *J. Am. Chem. Soc.*, 1997, **119**, 2325-2326.
[95] K. Kavallieratos, C. M. Bertao and R. H. Crabtree, *J. Org. Chem.*, 1999, **64**, 1675-1683.
[96] M. J. Chmielewski and J. Jurczak, *Chem. Eur. J.*, 2005, **11**, 6080-6094.
[97] M. J. Chmielewski and J. Jurczak, *Chem. Eur. J.*, 2006, **12**, 7652-7667.
[98] S. Kubik, R. Goddard, R. Kirchner, D. Nolting and J. Seidel, *Angew. Chem. Int. Ed.*, 2001, **40**, 2648-2651.
[99] S. Kubik and R. Goddard, *Proc. Natl. Acad. Sci.*, 2002, **99**, 5127-5132.

[100] S. Kubik, R. Kirchner, D. Nolting and J. Seidel, *J. Am. Chem. Soc.*, 2002, **124**, 12752-12760.
[101] S. Otto and S. Kubik, *J. Am. Chem. Soc.*, 2003, **125**, 7804-7805.
[102] S. J. Brooks, P. A. Gale and M. E. Light, *CrystEngComm*, 2005, **7**, 586-591.
[103] S. J. Brooks, P. A. Gale and M. E. Light, *Chem. Commun.*, 2005, 4696-4698.
[104] S. J. Brooks, P. R. Edwards, P. A. Gale and M. E. Light, *New J. Chem.*, 2006, **30**, 65-70.
[105] D. A. Jose, D. K. Kumar, B. Ganguly and A. Das, *Inorg. Chem.*, 2007, **46**, 5817-5819.
[106] P. A. Gale, J. L. Sessler, V. Král and V. Lynch, *J. Am. Chem. Soc.*, 1996, **118**, 5140-5141.
[107] D.-W. Yoon, D. E. Gross, V. M. Lynch, J. L. Sessler, B. P. Hay and C.-H. Lee, *Angew. Chem. Int. Ed.*, 2008, **47**, 5038-5042.
[108] B. Turner, M. Botoshansky and Y. Eichen, *Angew. Chem. Int. Ed.*, 1998, **37**, 2475-2478.
[109] C. Caltagirone, A. Mulas, F. Isaia, V. Lippolis, P. A. Gale and M. E. Light, *Chem. Commun.*, 2009, 6279-6281.
[110] D. Curiel, A. Cowley and P. D. Beer, *Chem. Commun.*, 2005, 236-238.
[111] K.-J. Chang, D. Moon, M. S. Lah and K.-S. Jeong, *Angew. Chem. Int. Ed.*, 2005, **44**, 7926-7929.
[112] J.-i. Kim, H. Juwarker, X. Liu, M. S. Lah and K.-S. Jeong, *Chem. Commun.*, 2010, **46**, 764-766.
[113] D. K. Smith, *Org. Biomol. Chem.*, 2003, **1**, 3874-3877.
[114] K. J. Winstanley, A. M. Sayer and D. K. Smith, *Org. Biomol. Chem.*, 2006, **4**, 1760-1767.
[115] S.-i. Kondo, T. Suzuki and Y. Yano, *Tetrahedron Lett.*, 2002, **43**, 7059-7061.
[116] S.-i. Kondo, T. Harada, R. Tanaka and M. Unno, *Org. Lett.*, 2006, **8**, 4621-4624.
[117] S.-i. Kondo, N. Okada, R. Tanaka, M. Yamamura and M. Unno, *Tetrahedron Lett.*, 2009, **50**, 2754-2757.
[118] W. B. Farnham, D. C. Roe, D. A. Dixon, J. C. Calabrese and R. L. Harlow, *J. Am. Chem. Soc.*, 1990, **112**, 7707-7718.
[119] H. Juwarker, J. M. Lenhardt, D. M. Pham and S. L. Craig, *Angew. Chem. Int. Ed.*, 2008, **47**, 3740-3743.
[120] R. M. Meudtner and S. Hecht, *Angew. Chem. Int. Ed.*, 2008, **47**, 4926-4930.
[121] Y. Li and A. H. Flood, *J. Am. Chem. Soc.*, 2008, **130**, 12111-12122.
[122] E. M. Zahran, Y. Hua, Y. Li, A. H. Flood and L. G. Bachas, *Anal. Chem.*, 2009, **82**, 368-375.
[123] A. Kumar and P. S. Pandey, *Org. Lett.*, 2007, **10**, 165-168.
[124] P. Metrangolo, H. Neukirch, T. Pilati and G. Resnati, *Acc. Chem. Res.*, 2005, **38**, 386-395.
[125] P. Metrangolo and G. Resnati, *Cryst. Growth Des.*, 2012, **12**, 5835-5838.
[126] T. M. Beale, M. G. Chudzinski, M. G. Sarwar and M. S. Taylor, *Chem. Soc. Rev.*, 2013, **42**, 1667-1680.
[127] A. Mele, P. Metrangolo, H. Neukirch, T. Pilati and G. Resnati, *J. Am. Chem. Soc.*, 2005, **127**, 14972-14973.
[128] M. G. Sarwar, B. Dragisić, E. Dimitrijević and M. S. Taylor, *Chem. Eur. J.*, 2013, **19**, 2050-2058.
[129] M. G. Sarwar, B. Dragisic, S. Sagoo and M. S. Taylor, *Angew. Chem. Int. Ed.*, 2010, **49**, 1674-1677.
[130] Y. S. Rosokha, S. V. Lindeman, S. V. Rosokha and J. K. Kochi, *Angew. Chem. Int. Ed.*, 2004, **43**, 4650-4652.
[131] M. Albrecht, M. Müller, O. Mergel, K. Rissanen and A. Valkonen, *Chem. Eur. J.*, 2010, **16**, 5062-5069.
[132] P. Arranz-Mascarós, C. Bazzicalupi, A. Bianchi, C. Giorgi, M.-L. Godino-Salido, M.-D. Gutiérrez-Valero, R. Lopez-Garzón and M. Savastano, *J. Am. Chem. Soc.*, 2012, **135**, 102-105.
[133] F. P. Schmidtchen, *Coord. Chem. Rev.*, 2006, **250**, 2918-2928.
[134] D. F. Shriver and M. J. Biallas, *J. Am. Chem. Soc.*, 1967, **89**, 1078-1081.
[135] Y. Kim and F. P. Gabbaî, *J. Am. Chem. Soc.*, 2009, **131**, 3363-3369.
[136] P. Chen, R. A. Lalancette and F. Jäkle, *Angew. Chem. Int. Ed.*, 2012, **51**, 7994-7998.
[137] X. Yang, C. B. Knobler and M. F. Hawthorne, *Angew. Chem. Int. Ed. Engl.*, 1991, **30**, 1507-1508.
[138] M. Newcomb, M. T. Blanda, Y. Azuma and T. J. Delord, *J. Chem. Soc., Chem. Commun.*, 1984, 1159-1160.
[139] S. Aoyagi, K. Tanaka, I. Zicmane and Y. Takeuchi, *J. Chem. Soc., Perkin Trans. 2*, 1992, 2217-2220.
[140] A. P. Davis, *Coord. Chem. Rev.*, 2006, **250**, 2939-2951.
[141] J. P. Clare, A. J. Ayling, J.-B. Joos, A. L. Sisson, G. Magro, M. N. Pérez-Payán, T. N. Lambert, R. Shukla, B. D. Smith and A. P. Davis, *J. Am. Chem. Soc.*, 2005, **127**, 10739-10746.
[142] B. A. McNally, A. V. Koulov, T. N. Lambert, B. D. Smith, J.-B. Joos, A. L. Sisson, J. P. Clare, V. Sgarlata, L. W. Judd, G. Magro and A. P. Davis, *Chem. Eur. J.*, 2008, **14**, 9599-9606.

[143] A. Hennig, L. Fischer, G. Guichard and S. Matile, *J. Am. Chem. Soc.*, 2009, **131**, 16889-16895.
[144] N. Busschaert, P. A. Gale, C. J. E. Haynes, M. E. Light, S. J. Moore, C. C. Tong, J. T. Davis and J. W. A. Harrell, *Chem. Commun.*, 2010, **46**, 6252-6254.
[145] N. Busschaert, M. Wenzel, M. E. Light, P. Iglesias-Hernández, R. Pérez-Tomás and P. A. Gale, *J. Am. Chem. Soc.*, 2011, **133**, 14136-14148.
[146] J. W. Steed, *Chem. Soc. Rev.*, 2010, **39**, 3686-3699.
[147] J.-W. Liu, Y. Yang, C.-F. Chen and J.-T. Ma, *Langmuir*, 2010, **26**, 9040-9044.
[148] J. A. Foster, M.-O. Piepenbrock, G. O. Lloyd, N. Clarke, J. A. K. Howard and J. W. Steed, *Nat Chem*, 2010, **2**, 1037-1043.
[149] P. D. Beer and A. D. Keefe, *J. Organomet. Chem.*, 1989, **375**, C40-C42.
[150] F. Oton, A. Tarraga, M. D. Velasco, A. Espinosa and P. Molina, *Chem. Commun.*, 2004, 1658-1659.
[151] C. Bejger, J. S. Park, E. S. Silver and J. L. Sessler, *Chem. Commun.*, 2010, **46**, 7745-7747.
[152] H. Miyaji, W. Sato and J. L. Sessler, *Angew. Chem. Int. Ed.*, 2000, **39**, 1777-1780.
[153] J. K. Day, C. Bresner, N. D. Coombs, I. A. Fallis, L. L. Ooi and S. Aldridge, *Inorg. Chem.*, 2008, **47**, 793-804.
[154] A. E. J. Broomsgrove, D. A. Addy, C. Bresner, I. A. Fallis, A. L. Thompson and S. Aldridge, *Chem. Eur. J.*, 2008, **14**, 7525-7529.
[155] J. V. Ros-Lis, R. Martinez-Manez and J. Soto, *Chem. Commun.*, 2002, 2248-2249.
[156] M. E. Huston, E. U. Akkaya and A. W. Czarnik, *J. Am. Chem. Soc.*, 1989, **111**, 8735-8737.
[157] Z. Xu, N. J. Singh, J. Lim, J. Pan, H. N. Kim, S. Park, K. S. Kim and J. Yoon, *J. Am. Chem. Soc.*, 2009, **131**, 15528-15533.
[158] E. Berni, I. Gosse, D. Badocco, P. Pastore, N. Sojic and S. Pinet, *Chem. Eur. J.*, 2009, **15**, 5145-5152.
[159] S. J. Butler and D. Parker, *Chem. Soc. Rev.*, 2013, **42**, 1652-1666.
[160] B. S. Murray, E. J. New, R. Pal and D. Parker, *Org. Biomol. Chem.*, 2008, **6**, 2085-2094.
[161] Z. Zhong and E. V. Anslyn, *J. Am. Chem. Soc.*, 2002, **124**, 9014-9015.
[162] R. Hoss and F. Vögtle, *Angew. Chem. Int. Ed. Engl.*, 1994, **33**, 375-384.
[163] D. H. Busch, *J. Inclusion Phenom. Mol. Recognit. Chem.*, 1992, **12**, 389-395.
[164] T. J. Hubin and D. H. Busch, *Coord. Chem. Rev.*, 2000, **200–202**, 5-52.
[165] M. C. Thompson and D. H. Busch, *J. Am. Chem. Soc.*, 1964, **86**, 213-217.
[166] S. Anderson, H. L. Anderson and J. K. M. Sanders, *Acc. Chem. Res.*, 1993, **26**, 469-475.
[167] M. C. Thompson and D. H. Busch, *J. Am. Chem. Soc.*, 1962, **84**, 1762-1763.
[168] M. C. Thompson and D. H. Busch, *J. Am. Chem. Soc.*, 1964, **86**, 3651-3656.
[169] R. N. Greene, *Tetrahedron Lett.*, 1972, **13**, 1793-1796.
[170] G. S. Hanan, D. Volkmer, U. S. Schubert, J. M. Lehn, G. Baum and D. Fenske, *Angew. Chem. Int. Ed. Engl.*, 1997, **36**, 1842-1844.
[171] A. Marquis, J.-P. Kintzinger, R. Graff, P. N. W. Baxter and J.-M. Lehn, *Angew. Chem. Int. Ed.*, 2002, **41**, 2760-2764.
[172] M. Fujita, *Chem. Soc. Rev.*, 1998, **27**, 417-425.
[173] Q. F. Sun, J. Iwasa, D. Ogawa, Y. Ishido, S. Sato, T. Ozeki, Y. Sei, K. Yamaguchi and M. Fujita, *Science*, 2010, **328**, 1144-1147.
[174] M. Fujita, M. Tominaga, A. Hori and B. Therrien, *Acc. Chem. Res.*, 2005, **38**, 369-378.
[175] C. Browne, S. Brenet, J. K. Clegg and J. R. Nitschke, *Angew. Chem. Int. Ed.*, 2013, **52**, 1944-1948.
[176] B. Hasenknopf, J. M. Lehn, B. O. Kneisel, G. Baum and D. Fenske, *Angew. Chem. Int. Ed. Engl.*, 1996, **35**, 1838-1840.
[177] C. S. Campos-Fernandez, B. L. Schottel, H. T. Chifotides, J. K. Bera, J. Bacsa, J. M. Koomen, D. H. Russell and K. R. Dunbar, *J. Am. Chem. Soc.*, 2005, **127**, 12909-12923.
[178] D. Meshcheryakov, V. Bohmer, M. Bolte, W. Hubscher-Bruder, F. Arnaud-Neu, H. Herschbach, A. Van Dorsselaer, I. Thondorf and W. Mogelin, *Angew. Chem. Int. Ed.*, 2006, **45**, 1648-1652.
[179] E. A. Katayev, G. D. Pantos, M. D. Reshetova, V. N. Khrustalev, V. M. Lynch, Y. A. Ustynyuk and J. L. Sessler, *Angew. Chem. Int. Ed.*, 2005, **44**, 7386-7390.
[180] A. Blackburn, *Chemistry in New Zealand*, 2010, **10**, 129-135.
[181] http://www.bumptobabygear.com/2012/08/toys-made-in-usa-product-find.html.

[182] http://sh.wikipedia.org/wiki/Datoteka:Olympic_rings_square.svg.
[183] http://www.keywordpicture.com/keyword/stainless%20nut/.
[184] http://cnx.org/content/m46073/latest/0323_DNA_Replication.jpg.
[185] J. F. Stoddart, *Chem. Soc. Rev.*, 2009, **38**, 1802-1820.
[186] P. L. Anelli, P. R. Ashton, R. Ballardini, V. Balzani, M. Delgado, M. T. Gandolfi, T. T. Goodnow, A. E. Kaifer, D. Philp, M. Pietraszkiewicz, L. Prodi, M. V. Reddington, A. M. Z. Slawin, N. Spencer, J. F. Stoddart, C. Vicent and D. J. Williams, *J. Am. Chem. Soc.*, 1992, **114**, 193-218.
[187] P. R. Ashton, M. Belohradsky, D. Philp and J. F. Stoddart, *J. Chem. Soc., Chem. Commun.*, 1993, 1269-1274.
[188] V. Aucagne, J. Berná, J. D. Crowley, S. M. Goldup, K. D. Hänni, D. A. Leigh, P. J. Lusby, V. E. Ronaldson, A. M. Z. Slawin, A. Viterisi and D. B. Walker, *J. Am. Chem. Soc.*, 2007, **129**, 11950-11963.
[189] G. M. Hübner, J. Gläser, C. Seel and F. Vögtle, *Angew. Chem. Int. Ed.*, 1999, **38**, 383-386.
[190] C.-W. Chiu, C.-C. Lai and S.-H. Chiu, *J. Am. Chem. Soc.*, 2007, **129**, 3500-3501.
[191] I. Yoon, M. Narita, T. Shimizu and M. Asakawa, *J. Am. Chem. Soc.*, 2004, **126**, 16740-16741.
[192] C. O. Dietrich-Buchecker and J. P. Sauvage, *Chem. Rev.*, 1987, **87**, 795-810.
[193] E. N. Guidry, S. J. Cantrill, J. F. Stoddart and R. H. Grubbs, *Org. Lett.*, 2005, **7**, 2129-2132.
[194] E. Wasserman, *J. Am. Chem. Soc.*, 1960, **82**, 4433-4434.
[195] I. T. Harrison and S. Harrison, *J. Am. Chem. Soc.*, 1967, **89**, 5723-5724.
[196] G. Schill and A. Lüttringhaus, *Angew. Chem. Int. Ed. Engl.*, 1964, **3**, 546-547.
[197] C. O. Dietrichbuchecker, J. P. Sauvage and J. P. Kintzinger, *Tetrahedron Lett.*, 1983, **24**, 5095-5098.
[198] C. O. Dietrichbuchecker, J. P. Sauvage and J. M. Kern, *J. Am. Chem. Soc.*, 1984, **106**, 3043-3045.
[199] C. O. Dietrich-Buchecker and J.-P. Sauvage, *Angew. Chem. Int. Ed. Engl.*, 1989, **28**, 189-192.
[200] A.-M. Fuller, D. A. Leigh, P. J. Lusby, I. D. H. Oswald, S. Parsons and D. B. Walker, *Angew. Chem. Int. Ed.*, 2004, **43**, 3914-3918.
[201] S. M. Goldup, D. A. Leigh, P. J. Lusby, R. T. McBurney and A. M. Z. Slawin, *Angew. Chem. Int. Ed.*, 2008, **47**, 6999-7003.
[202] A. I. Prikhod'ko, F. Durola and J.-P. Sauvage, *J. Am. Chem. Soc.*, 2007, **130**, 448-449.
[203] A. I. Prikhod'ko and J.-P. Sauvage, *J. Am. Chem. Soc.*, 2009, **131**, 6794-6807.
[204] K. S. Chichak, S. J. Cantrill, A. R. Pease, S. H. Chiu, G. W. V. Cave, J. L. Atwood and J. F. Stoddart, *Science*, 2004, **304**, 1308-1312.
[205] J. D. Crowley, S. M. Goldup, A.-L. Lee, D. A. Leigh and R. T. McBurney, *Chem. Soc. Rev.*, 2009, **38**, 1530-1541.
[206] H. C. Kolb, M. G. Finn and K. B. Sharpless, *Angew. Chem. Int. Ed.*, 2001, **40**, 2004-2021.
[207] V. Aucagne, K. D. Hänni, D. A. Leigh, P. J. Lusby and D. B. Walker, *J. Am. Chem. Soc.*, 2006, **128**, 2186-2187.
[208] J. D. Crowley, K. D. Hänni, A.-L. Lee and D. A. Leigh, *J. Am. Chem. Soc.*, 2007, **129**, 12092-12093.
[209] Y. Sato, R. Yamasaki and S. Saito, *Angew. Chem. Int. Ed.*, 2009, **48**, 504-507.
[210] J. Berná, J. D. Crowley, S. M. Goldup, K. D. Hänni, A.-L. Lee and D. A. Leigh, *Angew. Chem. Int. Ed.*, 2007, **46**, 5709-5713.
[211] S. M. Goldup, D. A. Leigh, P. R. McGonigal, V. E. Ronaldson and A. M. Z. Slawin, *J. Am. Chem. Soc.*, 2009, **132**, 315-320.
[212] S. M. Goldup, D. A. Leigh, R. T. McBurney, P. R. McGonigal and A. Plant, *Chem. Sci.*, 2010, **1**, 383-386.
[213] J. Berná, S. M. Goldup, A.-L. Lee, D. A. Leigh, M. D. Symes, G. Teobaldi and F. Zerbetto, *Angew. Chem. Int. Ed.*, 2008, **47**, 4392-4396.
[214] S. M. Goldup, D. A. Leigh, P. J. Lusby, R. T. McBurney and A. M. Z. Slawin, *Angew. Chem. Int. Ed.*, 2008, **47**, 3381-3384.
[215] M. Fujita, F. Ibukuro, H. Hagihara and K. Ogura, *Nature*, 1994, **367**, 720-723.
[216] M. E. Padilla-Tosta, O. D. Fox, M. G. B. Drew and P. D. Beer, *Angew. Chem. Int. Ed.*, 2001, **40**, 4235-4239.
[217] J. M. Timko, R. C. Helgeson, M. Newcomb, G. W. Gokel and D. J. Cram, *J. Am. Chem. Soc.*, 1974, **96**, 7097-7099.
[218] P. R. Ashton, P. J. Campbell, P. T. Glink, D. Philp, N. Spencer, J. F. Stoddart, E. J. T. Chrystal, S. Menzer, D. J. Williams and P. A. Tasker, *Angew. Chem. Int. Ed. Engl.*, 1995, **34**, 1865-1869.

[219] M. C. T. Fyfe and J. F. Stoddart, *Acc. Chem. Res.*, 1997, **30**, 393-401.
[220] M. E. Belowich, C. Valente, R. A. Smaldone, D. C. Friedman, J. Thiel, L. Cronin and J. F. Stoddart, *J. Am. Chem. Soc.*, 2012, **134**, 5243-5261.
[221] B. H. Northrop, F. Aricó, N. Tangchiavang, J. D. Badjić and J. F. Stoddart, *Org. Lett.*, 2006, **8**, 3899-3902.
[222] A. R. Williams, B. H. Northrop, T. Chang, J. F. Stoddart, A. J. P. White and D. J. Williams, *Angew. Chem. Int. Ed.*, 2006, **45**, 6665-6669.
[223] P. R. Ashton, T. T. Goodnow, A. E. Kaifer, M. V. Reddington, A. M. Z. Slawin, N. Spencer, J. F. Stoddart, C. Vicent and D. J. Williams, *Angew. Chem. Int. Ed. Engl.*, 1989, **28**, 1396-1399.
[224] Z.-T. Li, P. C. Stein, J. Becher, D. Jensen, P. Mørk and N. Svenstrup, *Chem. Eur. J.*, 1996, **2**, 624-633.
[225] W. Devonport, M. A. Blower, M. R. Bryce and L. M. Goldenberg, *J. Org. Chem.*, 1997, **62**, 885-887.
[226] M. Asakawa, P. R. Ashton, V. Balzani, A. Credi, C. Hamers, G. Mattersteig, M. Montalti, A. N. Shipway, N. Spencer, J. F. Stoddart, M. S. Tolley, M. Venturi, A. J. P. White and D. J. Williams, *Angew. Chem. Int. Ed.*, 1998, **37**, 333-337.
[227] M. Asakawa, W. Dehaen, G. L'Abbé, S. Menzer, J. Nouwen, F. M. Raymo, J. F. Stoddart and D. J. Williams, *J. Org. Chem.*, 1996, **61**, 9591-9595.
[228] F. Vögtle, S. Meier and R. Hoss, *Angew. Chem. Int. Ed. Engl.*, 1992, **31**, 1619-1622.
[229] C. A. Hunter, *J. Am. Chem. Soc.*, 1992, **114**, 5303-5311.
[230] D. A. Leigh, A. Murphy, J. P. Smart and A. M. Z. Slawin, *Angew. Chem. Int. Ed. Engl.*, 1997, **36**, 728-732.
[231] F. G. Gatti, D. A. Leigh, S. A. Nepogodiev, A. M. Z. Slawin, S. J. Teat and J. K. Y. Wong, *J. Am. Chem. Soc.*, 2001, **123**, 5983-5989.
[232] D. A. Leigh, A. Venturini, A. J. Wilson, J. K. Y. Wong and F. Zerbetto, *Chem. Eur. J.*, 2004, **10**, 4960-4969.
[233] D. G. Hamilton, J. K. M. Sanders, J. E. Davies, W. Clegg and S. J. Teat, *Chem. Commun.*, 1997, 897-898.
[234] K. A. Connors, *Chem. Rev.*, 1997, **97**, 1325-1358.
[235] M. V. Rekharsky and Y. Inoue, *Chem. Rev.*, 1998, **98**, 1875-1918.
[236] H.-J. Schneider, F. Hacket, V. Rüdiger and H. Ikeda, *Chem. Rev.*, 1998, **98**, 1755-1786.
[237] A. Harada, J. Li and M. Kamachi, *Chem. Commun.*, 1997, 1413-1414.
[238] M. C. T. Fyfe, P. T. Glink, S. Menzer, J. F. Stoddart, A. J. P. White and D. J. Williams, *Angew. Chem. Int. Ed. Engl.*, 1997, **36**, 2068-2070.
[239] E. Arunkumar, C. C. Forbes, B. C. Noll and B. D. Smith, *J. Am. Chem. Soc.*, 2005, **127**, 3288-3289.
[240] M. Chen, S. Han, L. Jiang, S. Zhou, F. Jiang, Z. Xu, J. Liang and S. Zhang, *Chem. Commun.*, 2010, **46**, 3932-3934.
[241] P. Ghosh, O. Mermagen and C. A. Schalley, *Chem. Commun.*, 2002, **0**, 2628-2629.
[242] M. D. Lankshear and P. D. Beer, *Acc. Chem. Res.*, 2007, **40**, 657-668.
[243] J. A. Wisner, P. D. Beer and M. G. B. Drew, *Angew. Chem. Int. Ed.*, 2001, **40**, 3606-3609.
[244] J. A. Wisner, P. D. Beer, M. G. B. Drew and M. R. Sambrook, *J. Am. Chem. Soc.*, 2002, **124**, 12469-12476.
[245] M. R. Sambrook, P. D. Beer, J. A. Wisner, R. L. Paul and A. R. Cowley, *J. Am. Chem. Soc.*, 2004, **126**, 15364-15365.
[246] K.-Y. Ng, A. R. Cowley and P. D. Beer, *Chem. Commun.*, 2006, 3676-3678.
[247] Y. Li, K. M. Mullen, T. D. W. Claridge, P. J. Costa, V. Felix and P. D. Beer, *Chem. Commun.*, 2009, 7134-7136.
[248] N. H. Evans, C. J. Serpell and P. D. Beer, *Angew. Chem. Int. Ed.*, 2011, **50**, 2507-2510.
[249] N. H. Evans and P. D. Beer, *Chem. Eur. J.*, 2011, **17**, 10542-10546.
[250] D. Curiel and P. D. Beer, *Chem. Commun.*, 2005, 1909-1911.
[251] S. R. Bayly, T. M. Gray, M. J. Chmielewski, J. J. Davis and P. D. Beer, *Chem. Commun.*, 2007, 2234-2236.
[252] N. H. Evans and P. D. Beer, *Org. Biomol. Chem.*, 2011, **9**, 92-100.
[253] N. H. Evans, H. Rahman, A. V. Leontiev, N. D. Greenham, G. A. Orlowski, Q. Zeng, R. M. J. Jacobs, C. J. Serpell, N. L. Kilah, J. J. Davis and P. D. Beer, *Chem. Sci.*, 2012, **3**, 1080-1089.
[254] J. J. Gassensmith, S. Matthys, J.-J. Lee, A. Wojcik, P. V. Kamat and B. D. Smith, *Chem. Eur. J.*, 2010, **16**, 2916-2921.

[255] E. R. Kay, D. A. Leigh and F. Zerbetto, *Angew. Chem. Int. Ed.*, 2007, **46**, 72-191.
[256] R. Ballardini, V. Balzani, A. Credi, M. T. Gandolfi and M. Venturi, *Acc. Chem. Res.*, 2001, **34**, 445-455.
[257] R. A. Bissell, E. Cordova, A. E. Kaifer and J. F. Stoddart, *Nature*, 1994, **369**, 133-137.
[258] V. Blanco, A. Carlone, K. D. Hänni, D. A. Leigh and B. Lewandowski, *Angew. Chem. Int. Ed.*, 2012, **51**, 5166-5169.
[259] B. Lewandowski, G. De Bo, J. W. Ward, M. Papmeyer, S. Kuschel, M. J. Aldegunde, P. M. E. Gramlich, D. Heckmann, S. M. Goldup, D. M. D'Souza, A. E. Fernandes and D. A. Leigh, *Science*, 2013, **339**, 189-193.
[260] R. E. Dawson, S. F. Lincoln and C. J. Easton, *Chem. Commun.*, 2008, 3980-3982.
[261] S. Li, D. Taura, A. Hashidzume and A. Harada, *Chem. Asian J.*, 2010, **5**, 2281-2289.
[262] M. C. Jimenez-Molero, C. Dietrich-Buchecker and J.-P. Sauvage, *Chem. Eur. J.*, 2002, **8**, 1456-1466.
[263] D. A. Leigh, P. J. Lusby, A. M. Z. Slawin and D. B. Walker, *Chem. Commun.*, 2012, **48**, 5826-5828.
[264] D. A. Leigh, J. K. Y. Wong, F. Dehez and F. Zerbetto, *Nature*, 2003, **424**, 174-179.
[265] R. D. Vale, *Cell*, 2003, **112**, 467-480.
[266] *Molecular Motors* Ed. M. Schliwa, Wiley-VCH, Weinheim, 2003.
[267] M. von Delius, E. M. Geertsema and D. A. Leigh, *Nat Chem*, 2010, **2**, 96-101.
[268] M. J. Barrell, A. G. Campaña, M. von Delius, E. M. Geertsema and D. A. Leigh, *Angew. Chem. Int. Ed.*, 2011, **50**, 285-290.
[269] M. von Delius, E. M. Geertsema, D. A. Leigh and D.-T. D. Tang, *J. Am. Chem. Soc.*, 2010, **132**, 16134-16145.

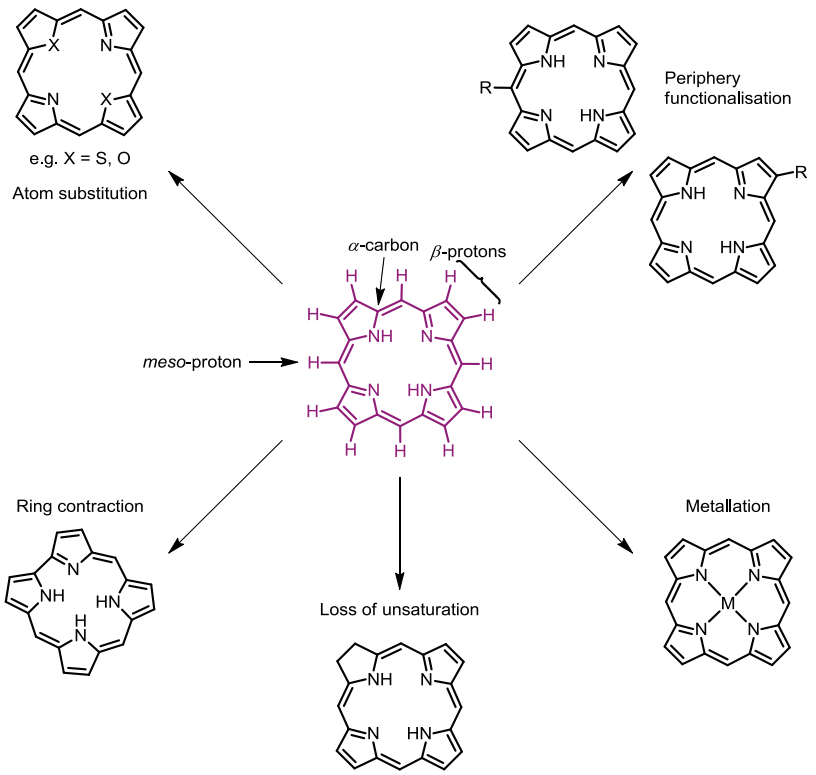
Chapter Two

Chapter 2 Triazole- and triazolium-functionalised porphyrin-based receptors for anion recognition and sensing

2.1 Introduction

2.1.1 The importance of porphyrins

Porphyrins are biologically important molecules derived from the $C_{20}H_{14}N_4$ porphine heterocyclic macrocycle. The structure was described by Küster in 1912 and consists of four pyrrole subunits connected at the α-carbon by methine bridges.[1] Modification of the macrocycle scaffold is often achieved by substitution at any of the 12 exocyclic *meso*- or β-hydrogen atoms and by chelation of the four central nitrogen atoms to metal cations (Scheme 2.1). Further alterations to the porphyrin macrocycle by ring contraction or expansion, substitution of atoms comprising the ring or loss of unsaturation can occur to produce related species.



Scheme 2.1. The porphine macrocycle and the routes by which it may be modified.

Haemoproteins are a class of porphyrin-containing superstructures which are fundamental in physiology. The toxicity of heavy metals like lead arises through their ability to diminish the activity of the haem-synthesising enzyme porphobilinogen synthase,[2,3] and many life-limiting conditions are caused by disruption to the production of haem: new-born jaundice (from an excess of bilirubin in the body),[4] sickle cell anaemia (sickle-cell variety of haemoglobin is less soluble than regular haemoglobin),[5] porphyrias (defects in the biosynthesis of haem),[6,7] nerve damage (from a shortage of red blood cells),[8] and methaemoglobinaemia (from oxidation of iron(II) to iron(III)).[9,10] Haemoglobin (Figure 2.1a) is essential for respiration in mammals, transporting oxygen and carbon dioxide around the body. Reduction in the oxygen-carrying capabilities of the blood, for example through poisoning by carbon monoxide which coordinates to haemoglobin 240 times more strongly than oxygen,[11] can cause hypoxia and death. Other vital biomolecules incorporating the porphyrin scaffold include vitamin B12 (for metabolism and proton transfer),[12] cytochrome-c (electron transfer for cell respiration),[13] myoglobin (oxygen storage),[14] and superoxide dismutase, peroxidise and catalase (to quench

intermediate oxides in the conversion from oxygen to water).[15] Finally, chlorophyll (Figure 2.1b) is involved in photosynthesis, enabling plants to extract energy from light.[16]

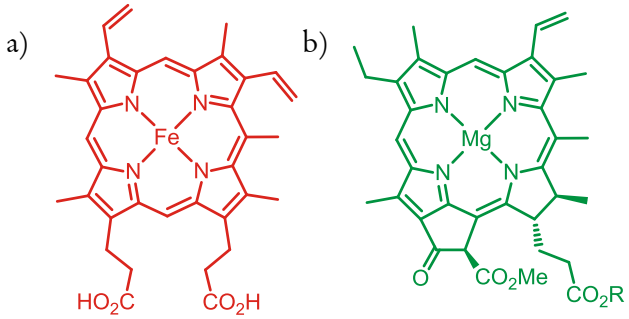


Figure 2.1. The structures of a) haem and b) chlorophyll.

2.1.2 The physical properties of porphyrins

The etymology of the word "porphyrin" gives insight into its physical properties. Derived from the Greek word πορφυρα *porphyra* meaning "purple",[17] porphyrins are characterised by their deep purple colour. This colour arises from intense absorbances in the visible region which are due to electronic transitions between highly delocalised π orbitals. Eighteen of a possible 26 π electrons are considered to participate in this delocalisaion and porphyrins are widely accepted to obey Hückel's rule for aromaticity.[18-20] The strongest absorption, the fully allowed Soret band, is observed between 400 and 450 nm and weaker (quasi-allowed) bands occurring in the region 550–630 nm are the α and β Q bands (Figure 2.2). Gouterman's *four orbital model*, which considers electronic transitions between the two highest occupied and two lowest unoccupied molecular orbitals, helps to explain the absorption spectra observed for porphyrin molecules. In addition porphyrins display characteristic emission spectra.[21-23]

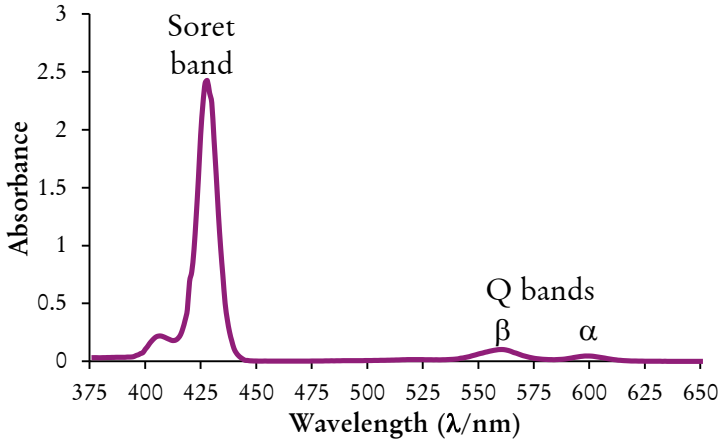


Figure 2.2. UV/visible spectrum of a typical zinc(II)-metalloporphyrin (DMSO, 293 K, 5 × 10^{-6} M).

The similar energies of the porphyrin's frontier energy levels allows access to a number of oxidation states (usually +2 to −2). Porphyrin derivatives can undergo multiple redox processes which depend on the exact structure of the molecule, the central metal ion, and any axially coordinating ligands.

The unique optical and redox properties of porphyrins give rise to a variety of useful applications.[24,25] Being light sensitive, porphyrins have been used as photosensitisers for photodynamic therapy: after intravenous administration of the drug, the tumour is selectively exposed to light and the drug reacts to produce cytotoxic singlet oxygen which destroys cancerous cells.[26] Visudyne® (to treat retina damage),[27] Cysview® (to detect bladder cancer)[28] and Photofrin® (for palliative treatment of oesophageal cancer)[29] are all porphyrin-based pharmaceuticals approved for clinical use.

In recent years porphyrin derivatives have found use in solar photochemical cells (where inspiration is drawn from light-harvesting chlorophyll),[30] molecular wires,[31] liquid crystals,[32,33] haemoproteins models,[34] and dyes (phthalocyanines).[35]

2.1.3 Porphyrins as reporter groups for anion recognition and sensing

Functionalised-porphyrin derivatives have also found use in anion recognition applications. Sanders and Anderson employed protonated porphyrins to bind anions through strong electrostatic interactions.[36] The hexaprotonated porphyrin trimer in Figure 2.3a was isolated in 47% yield by copper(I)-catalysed Glaser coupling of three bis-acetylinic zinc(II)-

porphyrin precursors, followed by addition of dilute acid.[37] Fast atom bombardment mass spectrometry was used to demonstrate host–guest complex formation with giant cluster anions such as $PW_{12}O_{40}^{4-}$, $SiW_{12}O_{40}^{4-}$ and $Os_{10}C(CO)_{24}^{2-}$. Control experiments revealed no anion complexation occurred with smaller anions such as chloride, triflate or sulfate, highlighting the importance of charge-, size-, and shape-complementarity of the binding domain for large anionic clusters.

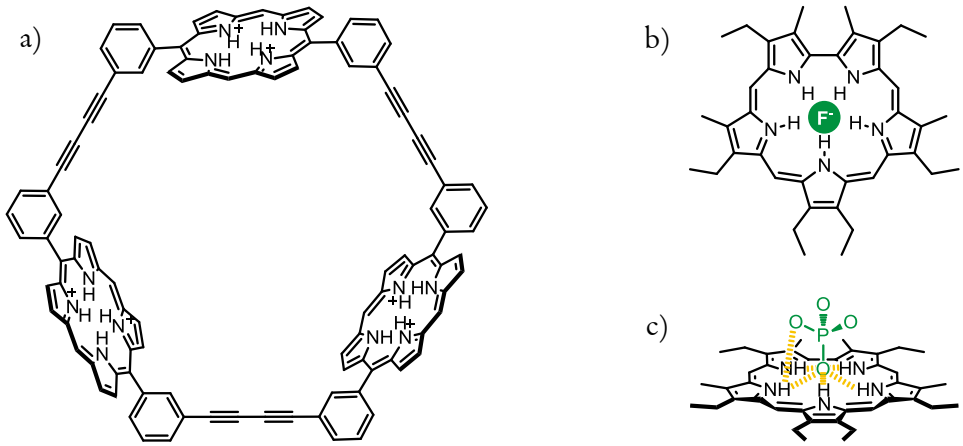


Figure 2.3. Porphyrin-based anion receptors: a) Sanders and Anderson's hexaprotonated porphyrin trimer; b) Sessler's fluoride–sapphyrin complex; c) Sesslers's phosphate–sapphyrin complex.

Since Sessler's serendipitous discovery of fluoride-encapsulation within the central core of an expanded porphyrin (Figure 2.3b),[38] these motifs have been widely used in anion binding. The same sapphyrin molecule (a pentapyrrolic analogue of porphine) was shown to bind halides fluoride, chloride and bromide in methanol, the smaller fluoride anion being more suitably sized for the macrocycle cavity.[39] The possibility of phosphate binding was revealed by the formation of 1:1 sapphyrin:phosphate species in the solid state (Figure 2.3c).[40] As part of their general investigations into phosphate binding, Sessler and co-workers probed the interactions between sapphyrins and DNA. When a sapphyrin molecule was added to an aqueous solution of DNA, green fibres precipitated from solution.[41] Crystal structure analysis suggested "phosphate chelation" was occurring, where individual phosphate subunits along the DNA backbone were bound by sapphyrin molecules through multiple hydrogen

bonds. Further evidence was provided by ^{31}P NMR spectroscopy, circular dichroism and UV/visible spectroscopy.

Alternatively, porphyrin subunits may be functionalised with pendant anion recognition groups attached to the periphery to construct rigid, preorganised anion receptors (Figure 2.4). Metallated porphyrins are generally stronger anion complexants as anion recognition is enhanced through metal Lewis acid–anion interactions. Furthermore, anion coordination to the metal centre induces changes in the physical properties of the porphyrin unit, providing a pathway by which the anion binding event may be signalled.[42,43]

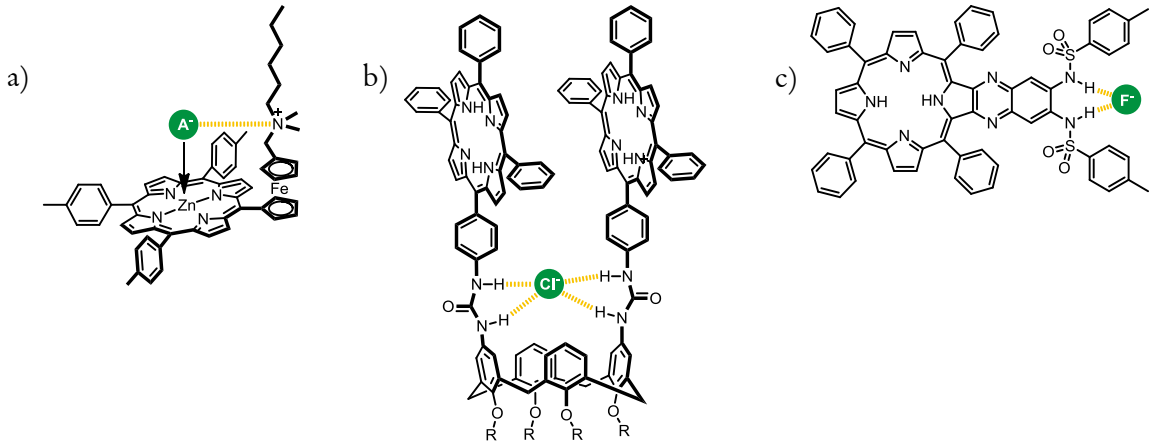


Figure 2.4. Porphyrin molecules with attached anion recognition groups: a) Moutet's ferrocene-functionalised porphyrin; b) Dudic's bis-porphyrin-appended calix[4]arene; c) Starnes's β,β'-disulfonamide porphyrin conjugate.

Moutet and co-workers have prepared a metalloporphyrin–ferrocene–alkylammonium conjugate which recognised and detected anions in dichloromethane through a combination of electrostatic interactions with the alkylammonium group and axial coordination to the zinc metal centre (Figure 2.4a).[44] Cathodic shifts in the ferrocene/ferrocenium and porphyrin oxidation potentials ($P/P^{+\bullet}$ and $P^{+\bullet}/P^{2+}$) were observed upon addition of anions, as were bathochromic shifts in the porphyrin absorption spectrum.

Upper-rim calix[4]arene–porphyrin conjugates containing urea mtoifs were reported to bind anions in dichloromethane.[45] ^{1}H NMR spectroscopy was used to confirm 1:1 stoichiometric halide binding by the bis-porphyrin-functionalised calix[4]arene receptor (Figure 2.4b) which

bound chloride more strongly than other halide anions: K_a = 1.4 × 10^6 (chloride), 2.2 × 10^5 (bromide), 2.9 × 10^4 (iodide) M^{-1}.

Starnes and co-workers designed a *β,β*-disubstituted porphyrin receptor incorporating two sulfonamide motifs attached to the porphyrin via a rigid, conjugated spacer (Figure 2.4c).[46] Anion binding occurs through hydrogen bonding to the bis-sulfonamide motif and concomitant changes in the UV/visible absorption spectrum enabled 1:1 and 1:2 receptor:anion association constants to be determined. A preference for basic anions such as fluoride (K_a = 255 000 M^{-1}) and dihydrogen phosphate (K_a = 70 000 M^{-1}) was observed in dichloromethane.

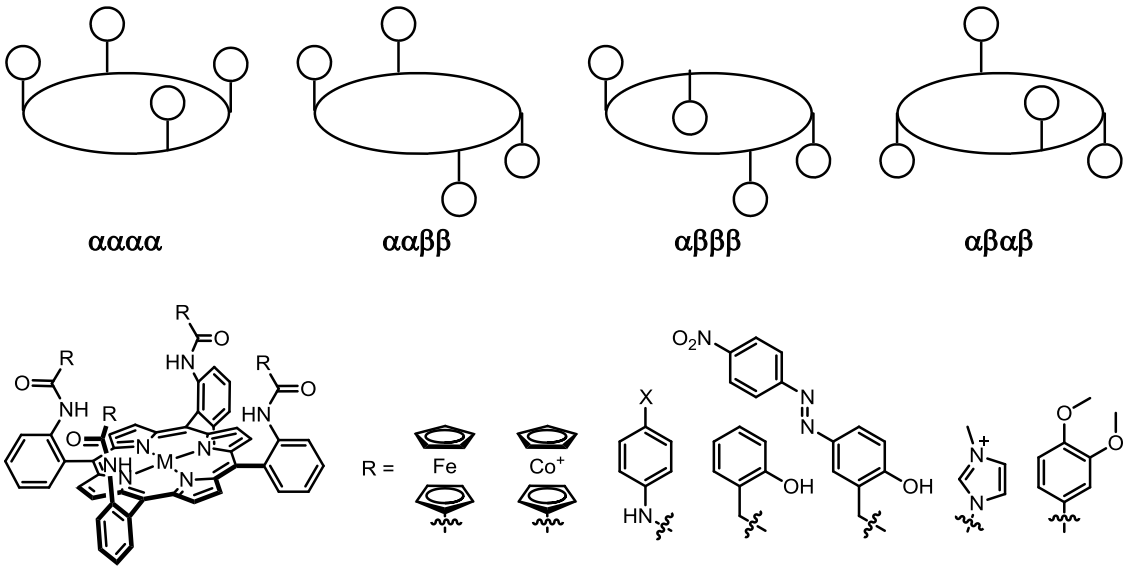


Figure 2.5. Cartoon illustrating the atropisomers of α,α,α,α-H_2TAPP. Anion receptor molecules based on this scaffold.

The *α,α,α,α*-atropisomer of 5,10,15,20-tetakis(2-aminophenyl)porphyrin (H_2TAPP) can be used as a tetrapodal building block for "picket-fence" anion receptors. The four amino units in this isomer are oriented on the same face of the porphyrin macrocycle and attaching anion binding motifs effectively traps the porphyrin derivative in this preorganised conformation. Picket fence zinc(II)-metalloporphyrin receptors incorporating amide, urea, hydroxyl, and imidazolium anion recognition groups, as well as redox active motifs such as ferrocene and cobaltocenium, have been reported (Figure 2.5).[47-53] Since the four anion binding groups are located on the same face of the porphyrin macrocycle, recognition occurs through multiple

cooperative anion binding interactions, in addition to coordination at the Lewis-acidic porphyrin-complexed zinc(II) metal centre.

2.1.4 Triazole groups as anion recognition motifs

The Huigsen [3+2] cycloaddition between an azide and a terminal alkyne is a very effective synthetic methodology for the preparation of five-membered 1,2,3-triazole heterocycles. Sharpless and co-workers have recently shown that, in the presence of a copper(I) catalyst, the cycloaddition reaction regioselectively forms the 1,4-disubstituted-1,2,3-triazole species (Figure 2.6a).[54,55] This reaction route falls under the umbrella of *click chemistry*: idealised chemical reactions which allow a "*fast, modular, process-driven approach to molecular chemistry*" and form products which can be easily isolated in high yields. Before then, azide–alkyne cycloadditions required elevated temperatures and gave a mixture of 1,4- and 1,5-substituted triazole groups. The advent of the copper(I)-catalysed azide–alkyne cycloaddition (CuAAC) reaction has resulted in triazole groups being widely exploited in chemical synthesis, particularly in supramolecular chemistry, where the mild reaction conditions and substantial tolerance of other functional groups contribute to its utility.

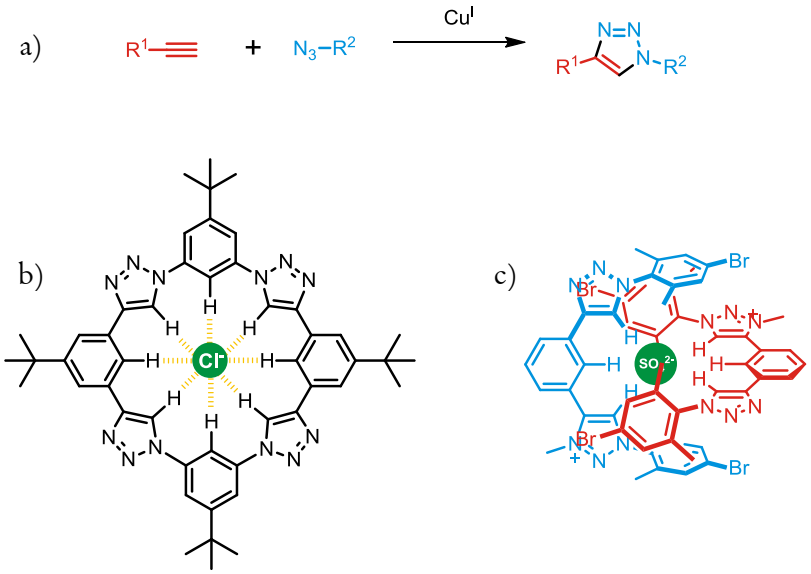


Figure 2.6. a) The copper(I)-catalysed azide–alkyne cycloaddition forming a 1,4-disubstituted-1,2,3-triazole. b) Flood's chloride-binding tetra-triazole macrocycle. c) Schubert's orthogonal assembly of two triazole-triazolium hosts around a sulfate anion.

The 1,4-disubstituted-1,2,3-triazole moiety has traditionally been used as a convenient covalent linker, with no particular function in the resulting organic framework. In recent years, however, the anion binding ability of this motif has been studied, and several receptors incorporating multiple triazole units were shown to effectively complex anions in non-polar organic solvents through polarised C–H···anion hydrogen bonding.[56-58] The three electronegative nitrogen atoms within the heterocycle polarise the CH bond, which increases the acidity of the hydrogen atom and its affinity for negatively charged species. A triazole-based anionophore was reported by Flood and co-workers (section 1.4.2.4.2 and Figure 2.6b).[56] The tetra-triazole macrocycle forms 1:1 macrocycle:halide complexes and is selective for chloride in dichloromethane, binding the anionic guest species through the concerted effect of multiple C–H···anion hydrogen bonds. Furthermore, both Pandey and Schubert have alkylated neutral triazole groups to produce positively charged triazolium units, and demonstrated their ability to bind anions through a combination of electrostatics and hydrogen bonding (see section 1.4.2.4.2 and Figure 2.6c).[59,60]

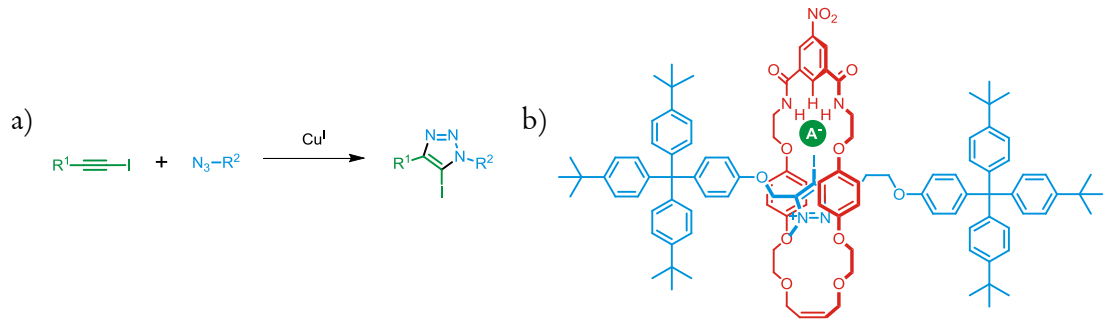


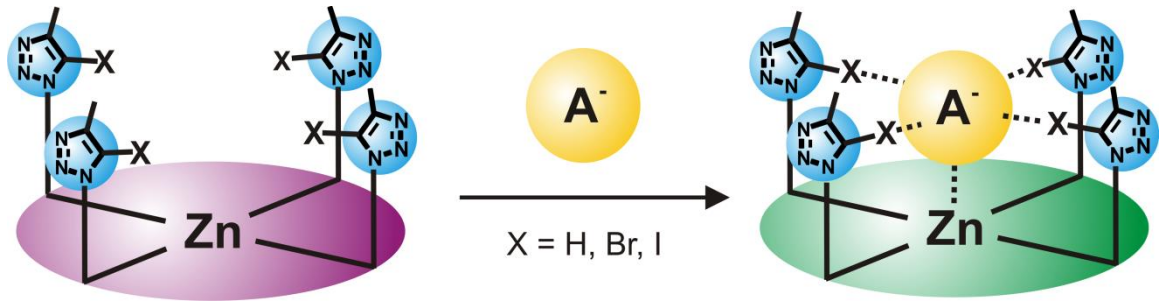
Figure 2.7. a) The synthesis 5-iodotriazole motif by copper(I) catalysis and b) an iodotriazolium-containing rotaxane.

In 2009, Hein, Fokin and co-workers reported a straightforward synthetic route to 5-iodo-1,4,5-trisubstituted-1,2,3-triazoles (Figure 2.7a).[61] A [3+2] cycloaddition reaction between substituted azides and iodoalkynes was shown to proceed with regiocontrol in the presence of a catalytic amount of copper(I) iodide and an amine ligand to produce 5-iodotriazoles in high yields. Within a year, the first receptor incorporating the 5-iodotriazolium group for anion recognition through halogen bonding was reported by Beer and co-workers (Figure 2.7b).[62]

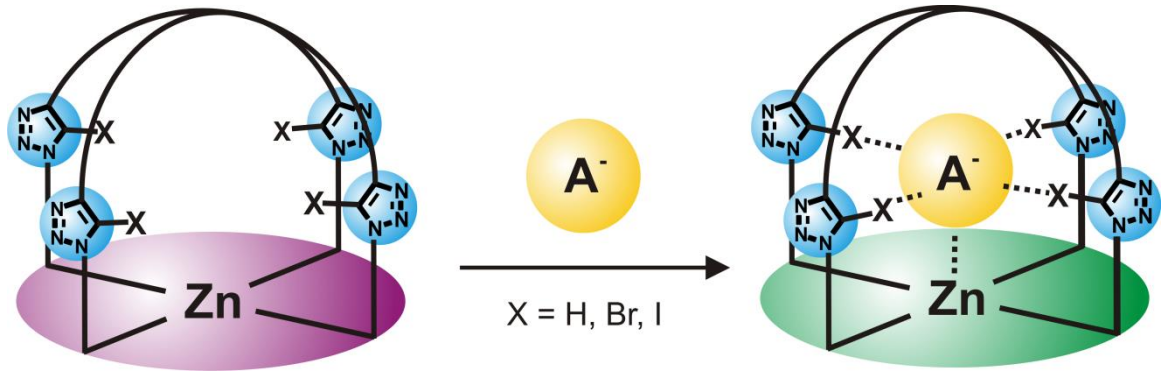
This rotaxane was assembled using solution-phase, halogen-bonding and bromide anion templation, the first example of interlocked structure formation directed by halogen bonding. The incorporation of the halotriazolium unit into the anion receptor was shown to enhance bromide and iodide anion binding affinity, in comparison with the protic rotaxane analogue. Since then modified reaction conditions, using copper(I) bromide and copper(II) acetate have been successfully employed to prepare 5-bromotriazole derivatives.[63]

2.1.5 Chapter aims

The aim of this chapter was to attach hydrogen- and halogen-bonding triazole and triazolium groups to a porphyrin scaffold to produce novel host molecules which are capable of anion recognition and sensing (Scheme 2.2). In addition, the construction of second generation, preorganised cage-like porphyrin analogues was undertaken and their anion binding properties investigated (Scheme 2.3).



Scheme 2.2. Cartoon representation of the target hydrogen- and halogen-bonding triazole-based zinc(II)-metalloporphyrin anion receptors.



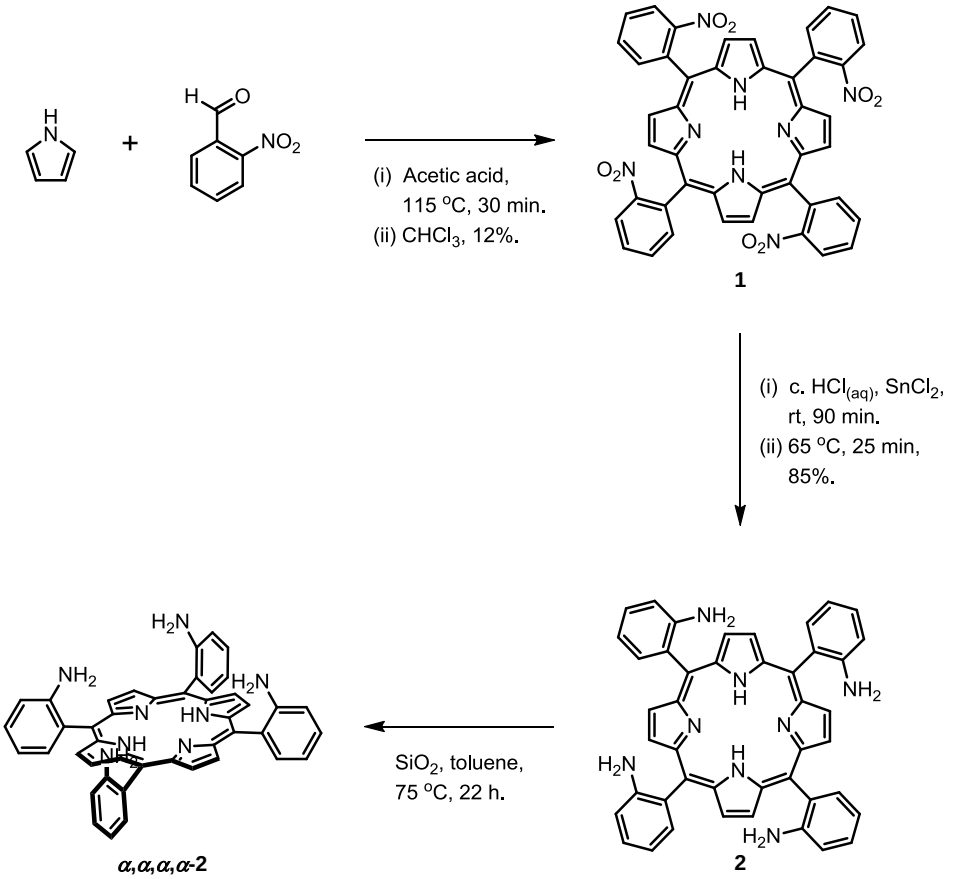
Scheme 2.3. Cartoon representation of the target hydrogen- and halogen-bonding triazole-based zinc(II)-metalloporphyrin cage anion receptors.

2.2 Tetrapodal zinc(II)-metalloporphyrin anion receptors

2.2.1 Synthesis of tetrakis-triazole-functionalised zinc(II)-metalloporphyrin anion receptors

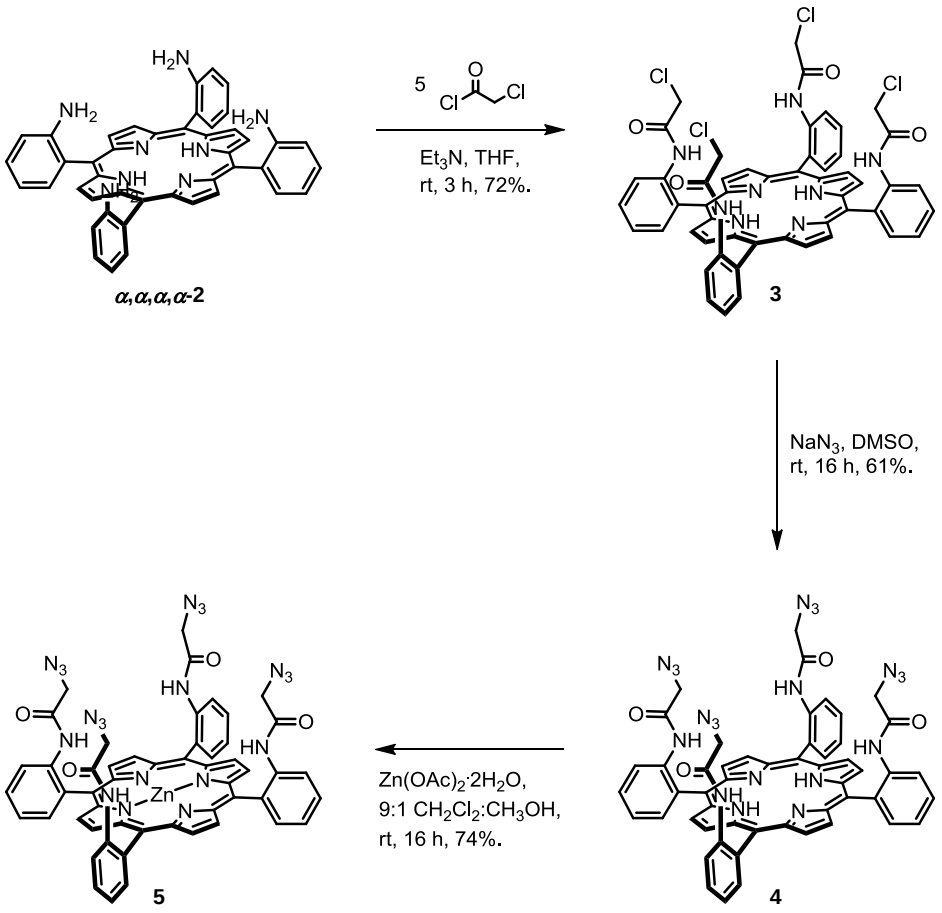
It was envisaged that the target tetrapodal triazole-containing zinc(II)-metalloporphyrin anion receptor would be prepared via a CuAAC reaction between a tetra-azido zinc(II)-porphyrin species and a suitable alkyne molecule. The multistep synthesis of the azide precursor is outlined in Schemes 2.4 and 2.5.

5,10,15,20-Tetrakis(2-nitrophenyl)porphyrin 1 was prepared according to the procedure reported by Sorrell (Scheme 2.4).[64] A heated solution of 2-nitrobenzaldehyde and freshly distilled pyrrole afforded porphyrin 1 in 12% yield. Reducing the nitro group to the corresponding amine (H_2TAPP) was achieved by the Collman method[65] using tin(II) chloride in concentrated hydrochloric acid to produce tetra-amine porphyrin 2 in 85% yield. At room temperature, the four possible atropisomers of H_2TAPP exist in a 1:2:4:1 (α_4:$\alpha_2\beta_2$;$\alpha\beta_3$;$\alpha\beta\alpha\beta$) statistical mixture (Figure 2.5). The proportion of the desired $\alpha,\alpha,\alpha,\alpha$-isomer, however, was increased using the Lindsey method.[66] H_2TAPP 2 and silica were heated in toluene for 22 hours. Column chromatographic separation gave the desired $\alpha,\alpha,\alpha,\alpha$-isomer 2, which was used immediately in the next step.



Scheme 2.4. Synthesis of α,α,α,α-*5,10,15,20-tetakis(2-aminophenyl)porphyrin 2.*

α,α,α,α-Tetrakis(2-chloroacetamidophenyl)porphyrin was synthesised according to the procedure reported by Collman *et al*.[67] The condensation of ***α,α,α,α***-2 with five equivalents of chloroacetyl chloride in the presence of base gave porphyrin 3 in 72% isolated yield. A nucleophilic substitution reaction between compound 3 and sodium azide in dimethyl sulfoxide afforded the tetra-azide porphyrin 4 in 61% yield. Metallation with zinc, to give 5 was achieved by stirring porphyrin 4 with a ten-fold excess of zinc(II) acetate dihydrate in 9:1 dichloromethane:methanol (Scheme 2.5).



Scheme 2.5. Synthesis of tetra-azide-functionalised porphyrin 5.

Small, poor quality crystals of compound 5 were grown by slow evaporation of a chloroform solution and the single crystal X-ray crystallographically determined solid state structure was solved by Dr Nicholas White (Figure 2.8).

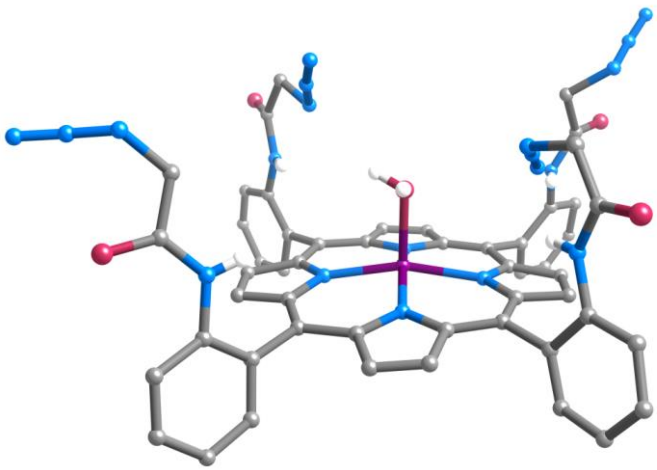
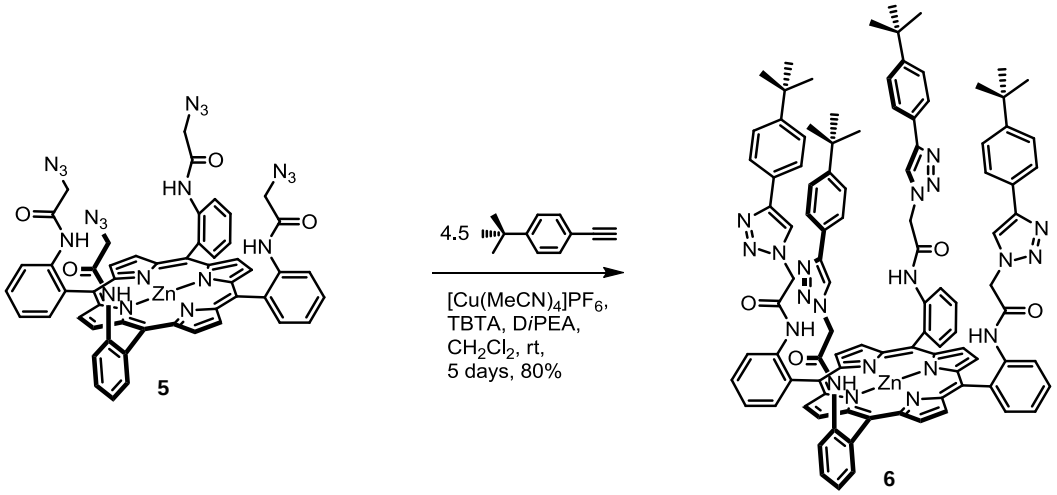


Figure 2.8. Solid state structure of porphyrin 5. Chloroform solvate and hydrogen atoms except those belonging to amide or water molecules are omitted for clarity. Colour scheme: grey=C, white=H, blue=N, red=O, violet=Zn.

The structure confirms the molecule has a *syn*-conformation with all of the azide-functionalised appendages on the same face of the porphyrin ring as anticipated for a picket fence structure. All four amide hydrogen-bond donors point into the centre of the cavity formed by the pendant arms and a pocket is created where an anion may potentially bind. A water molecule is axially-coordinated to the zinc metal centre, displacing the zinc from the plane of the macrocycle. The crystallographic data from this structure may be found in Appendix A.5.2.

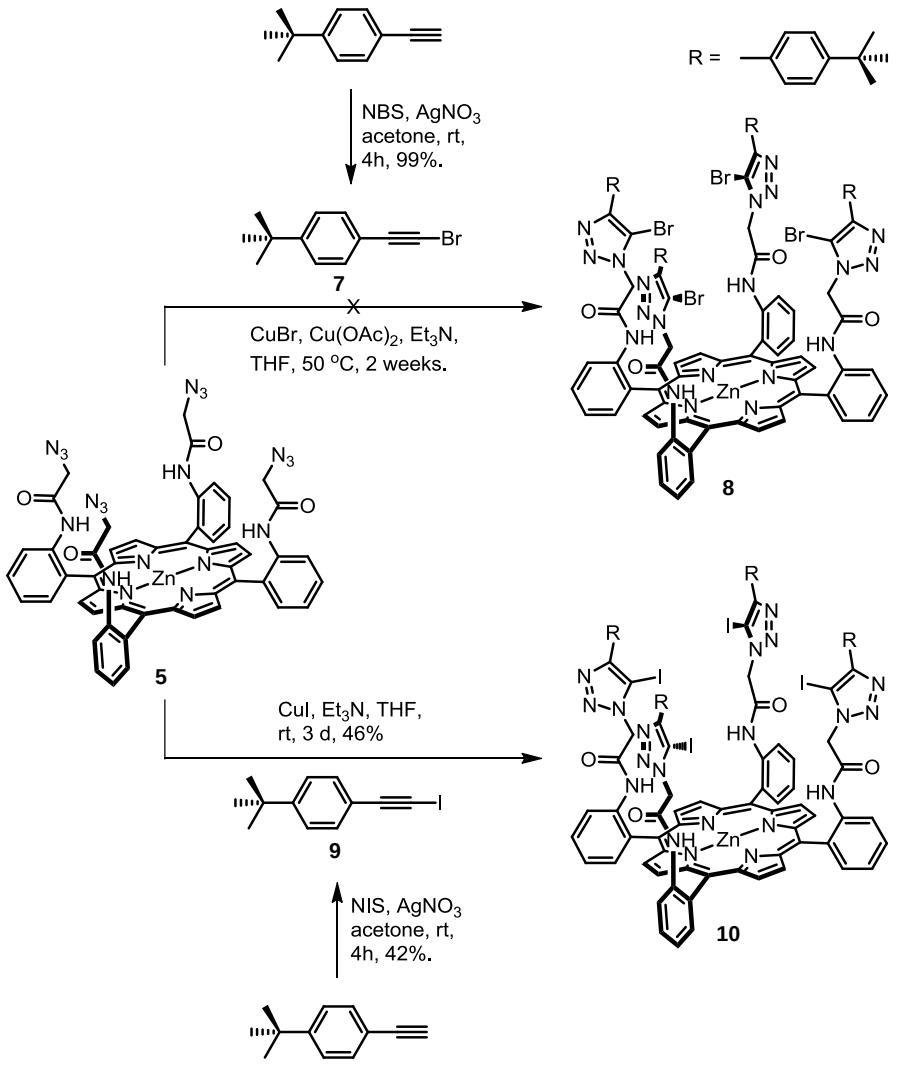
A copper(I)-catalysed azide–alkyne cycloaddition was carried out to prepare the target tetrakis-triazole-appended zinc(II)-metalloporphyrin. Tetra-azide porphyrin 5 and four-and-a-half equivalents of 4-*tert*-butylphenylacetylene were stirred in the presence of copper(I)tetrakis-acetonitrile hexafluorophosphate, TBTA and *N*,*N*-di-*iso*-propylethylamine in anhydrous dichloromethane for five days in the dark. Purification by column chromatography gave the desired tetrakis-triazole zinc(II)-porphyrin anion receptor 6 in 80% isolated yield (Scheme 2.6).



Scheme 2.6. Synthesis of triazole-functionalised porphyrin 6.

Attempts to prepare bromo- and iodotriazole zinc(II)-metalloporphyrin analogues were undertaken as outlined in Scheme 2.7. 4-*Tert*-butylphenylacetylene, *N*-bromosuccinimide and silver(I) nitrate were stirred in acetone to produce the required bromoalkyne 7 which was isolated in 99% yield, and used immediately in the following step.[68] Tetra-azide porphyrin 5

and four-and-a-half equivalents of bromoalkyne 7 were stirred in tetrahydrofuran in the presence of copper(I) bromide, copper(II) acetate and triethylamine in the dark.[63] Although a peak at m/z = 2040.2 corresponding to bromotriazole-porphyrin species was detected in the electrospray mass spectrum, the bromotriazole-porphyrin 8 could not be isolated which suggests it was formed in negligible yield.



Scheme 2.7. Synthesis of bromo- and iodotriazole-functionalised porphyrins 8 and 10.

A similar reaction to prepare the analogous iodotriazole-functionalised zinc(II)-metalloporphyrin compound by stirring tetra-azide porphyrin 5 and four-and-a-half equivalents of iodooalkyne 9 (prepared from 4-*tert*-butylphenylacetylene and N-iodosuccinide)[61] in the presence of copper(I) iodide and triethylamine in anhydrous tetrahydrofuran was successfully carried out.[62] Purification by column chromatography gave

the target iodotriazole-functionalised zinc(II)-metalloporphyrin **10** in 46% yield (Scheme 2.7).

2.2.2 Characterisation of tetrakis-triazole-functionalised zinc(II)-metalloporphyrin anion receptors 6 and 10

All compounds were characterised by ^{1}H NMR spectroscopy, electrospray mass spectrometry, and ^{13}C NMR spectroscopy where novel. The assigned ^{1}H NMR spectra of compounds 6 and **10** in chloroform-d are shown in Figure 2.9.

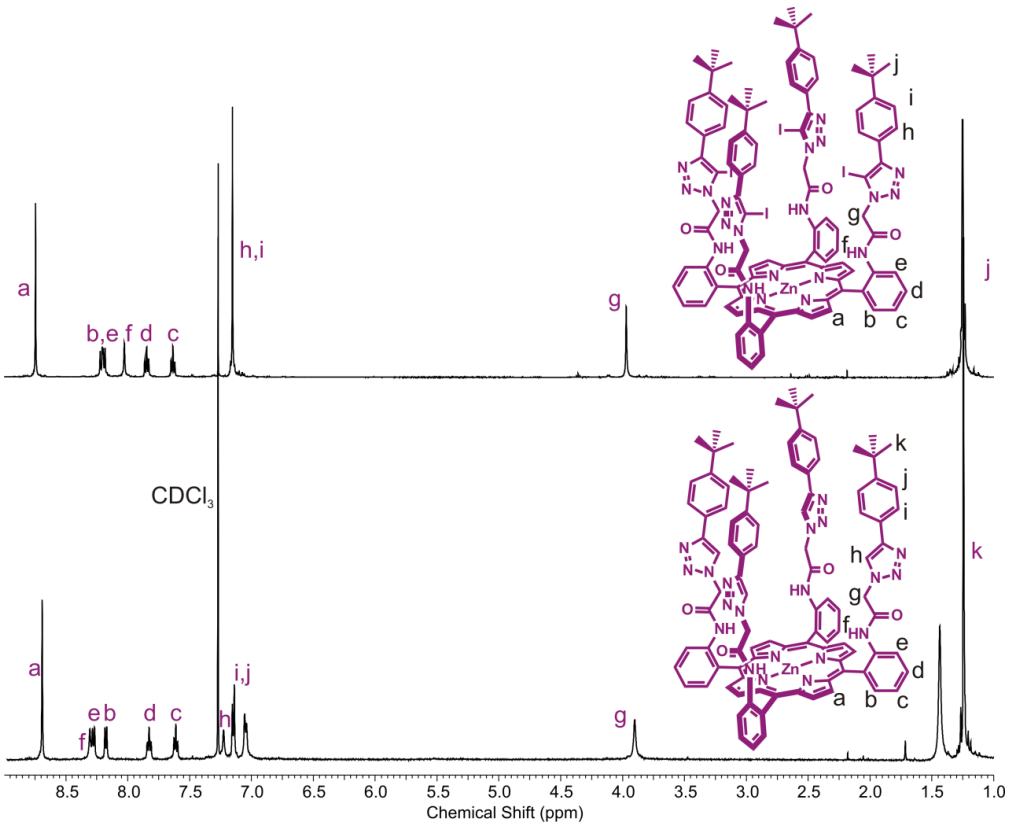


*Figure 2.9. ^{1}H NMR spectra of porphyrins 6 (bottom) and **10** (top) showing peak assignments (500 MHz, $CDCl_3$, 293 K).*

In both spectra, the eight equivalent *β*-pyrrole protons *a* appear as a singlet around 8.7 ppm, and the porphyrin *meso* aromatic protons (*b*, *c*, *d* and *e*) show the expected doublet and triplet resonances characteristic of *meso*-(*ortho*-substituted phenyl)porphyrin compounds between 7.5 and 9.0 ppm. Of particular importance is the presence of a triazole proton signal *h* in the spectrum of triazole-porphyrin 6 and its corresponding absence in the spectrum of iodotriazole-porphyrin **11**, confirming the successful formation of a halotriazole-

functionalised porphyrin. Furthermore, addition of D_2O to an NMR sample of compound 6 resulted in the loss of amide proton signal *f* through deuterium exchange enabling amide and triazole proton singlets to be distinguished.

Crystals of iodotriazole-porphyrin **10** of suitable quality for single crystal X-ray structural determination were grown by slow diffusion of diethyl ether into a tetrahydrofuran solution, and the structure solved by Dr Nicholas White (Figure 2.10).

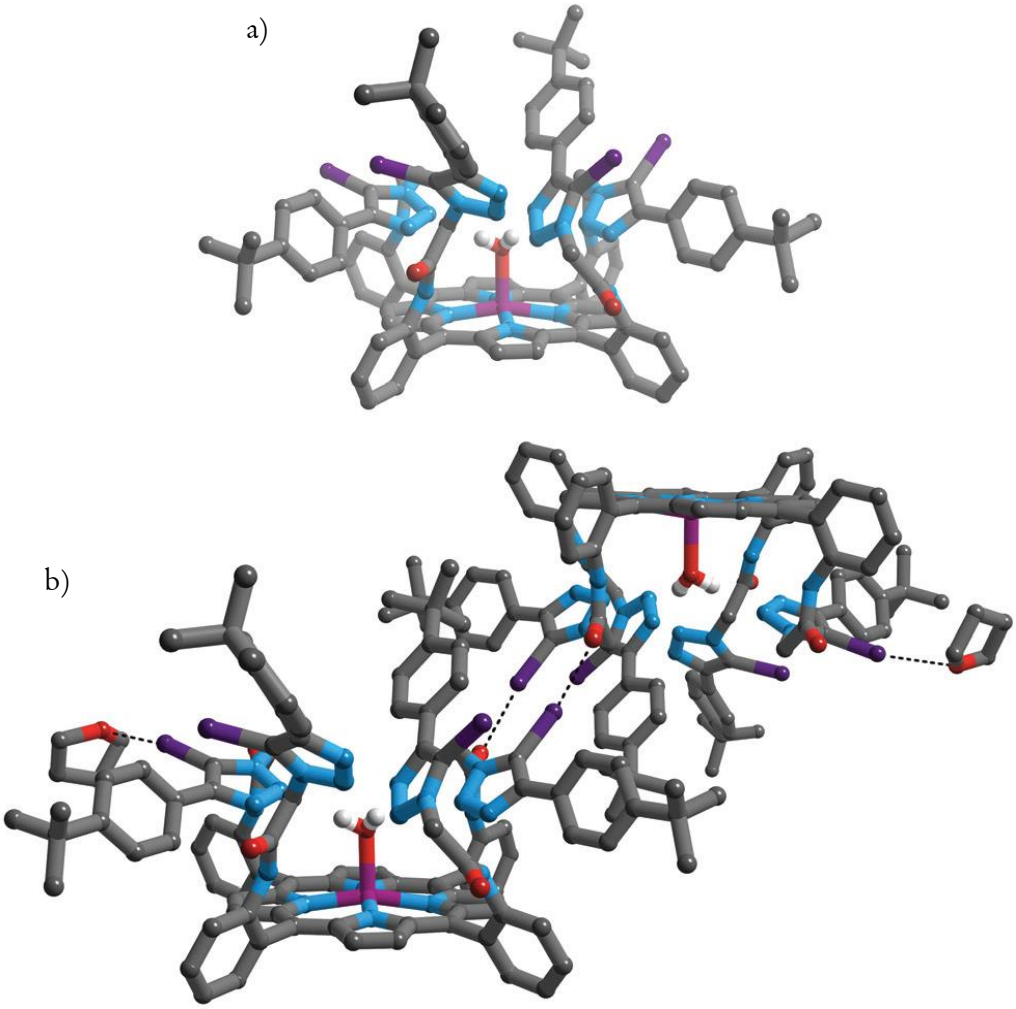


Figure 2.10. Structure of compound 5 (top); and diagram showing formation of dimers in the solid state. Halogen bonding interactions are shown as black dotted lines. Hydrogen atoms, except those on coordinated water and amide moieties are omitted for clarity, as are both (top) or one (bottom) of the crystallographically independent THF solvates. Key: grey = C, white = H, blue = N, red = O, violet = Zn, purple = I.

The structure (Figure 2.10a) reveals a picket-fence porphyrin molecule with all amide and iodotriazole anion recognition motifs on the same side with respect to the porphyrin motif. Intermolecular XB interactions are present between an iodotriazole iodine atom of the

receptor and a symmetry-related amide carbonyl group of the adjacent molecule (Figure 2.10b). Another iodine atom forms a halogen bond to a THF solvate. In both cases the interactions are close to linear, and the iodine···oxygen distance is significantly shorter than the sum of the van der Waals radii [C–I···O_{amide} = 2.920(5) Å, 83% of sum of vdW radii, ∠C–I···O_{amide} = 171.2(2)°; C–I···O_{THF} = 2.961(10) Å, 85% of sum of vdW radii, ∠C–I···O_{amide} = 167.7(3)°].

2.2.3 Anion binding properties of neutral triazole- and iodotriazole-functionalised zinc(II)-metalloporphyrin anion receptors

2.2.3.1 Anion binding properties of a hydrogen-bonding triazole-functionalised anion receptor 6

Initially, the anion binding properties of this novel class of anion receptor were assessed using ^{1}H NMR spectroscopy. In a NMR spectrum, the chemical shift of a particular proton resonance depends on electron density, electronegativity of neighbouring atoms or groups and local magnetic field effects. The binding of anions causes diagnostic changes to a receptor's NMR spectrum which can indicate the location of anion coordination and allow association constants for the equilibrium process (Scheme 2.8) to be determined.

$$\text{Host} + \text{Guest} \underset{}{\overset{K_a}{\rightleftharpoons}} \text{Host:Guest}$$

$$K_a = \frac{[\text{Host:Guest}]}{[\text{Host}][\text{Guest}]}$$

Scheme 2.8. Definition of association constant for 1:1 host:guest complex formation.

A typical ^{1}H NMR titration experiment involves adding aliquots of a solution of guest to a solution of host at 293 K and changes in the NMR spectrum are monitored and analysed. Host:guest complexation is usually fast on the NMR timescale and so chemical shift values are a weighted average between the chemical shift of the free and bound species. Anions are added as their tetrabutylammonium (TBA) salts as the TBA cation is essentially non-competitive for the counter anion to be studied.

Analysis of the observed proton shifts in the ^{1}H NMR spectrum of compound 6 after addition of increasing equivalents of anions in chloroform-d gives an insight into the mode of anion complexation. For example with chloride, downfield shifts in the receptor's triazole *h*, methylene *g* and phenyl *i* protons were observed (Figure 2.11). Furthermore, there is a much smaller perturbation of the amide proton signal *f* which suggests the halide anion is binding within the pocket formed by the four arms of the picket-fence architecture, in the vicinity of the triazole groups through C–H···anion hydrogen bonds.

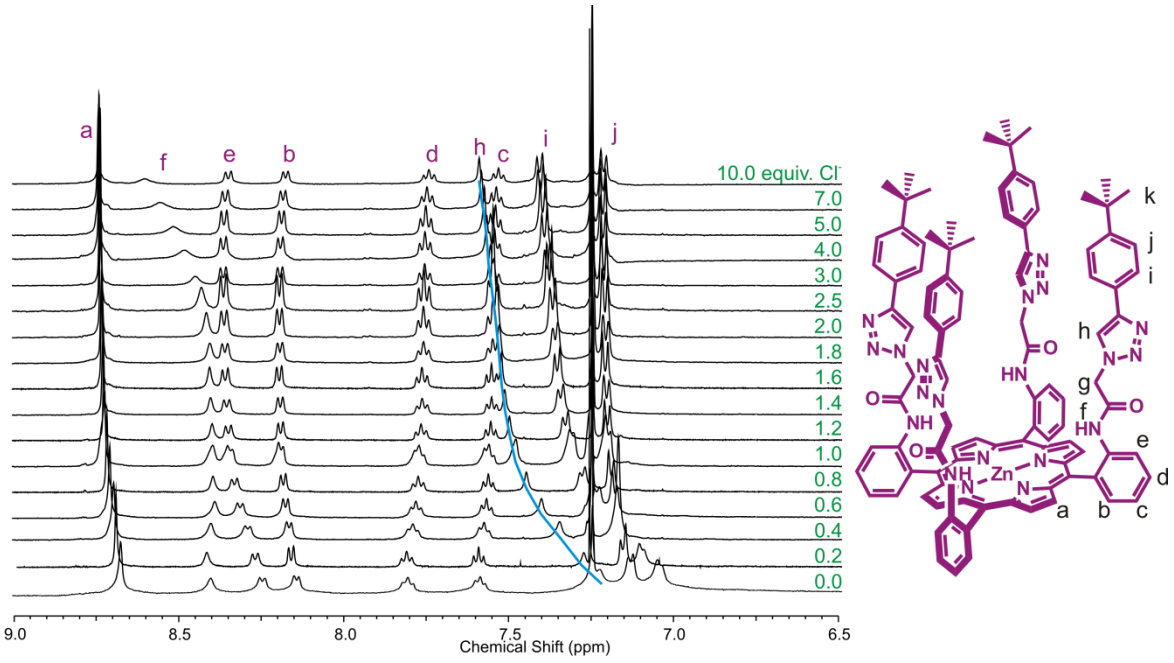


Figure 2.11. Partial ^{1}H NMR spectra of receptor 6 upon addition of equivalents of TBA·Cl (500 MHz, $CDCl_3$, 293 K).

The observed chemical shift perturbations of the triazole proton *h* with ten equivalents of anion (Table 2.1) reveal dihydrogen phosphate causes the largest magnitude of perturbation and the shifts are in general larger for oxoanions than less basic halides. Moreover, no evidence of complex formation was observed with hexafluorophosphate, an anion which typically associates weakly with traditional anion receptors and which is often used as a non-competitive counteranion with positively charged receptors.

Quantitative binding data for the complexation process was determined from the titration data obtained by monitoring the shift of the porphyrin's triazole proton *h* as a function of the

concentration of anion (Figure 2.12). Non-linear least squares analysis of the titration data using WinEQNMR[69] gave 1:1 stoichiometric association constants for anion complexation shown in Table 2.1.

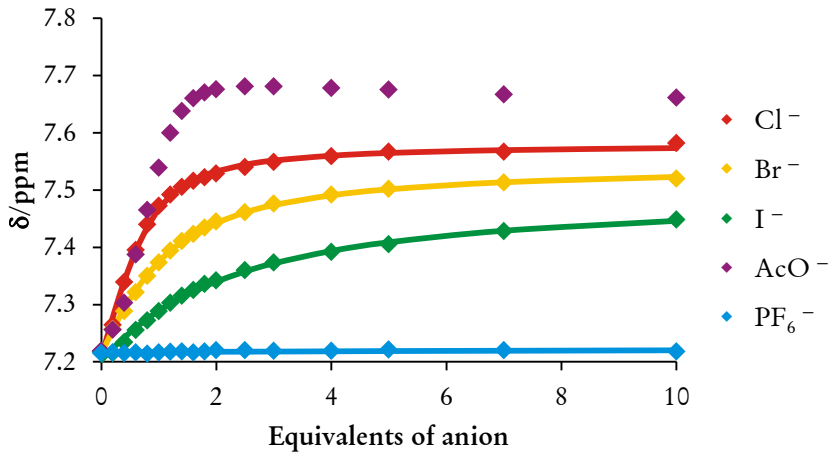


Figure 2.12.Titration curves for complex formation between porphyrin 6 and various anions obtained by monitoring triazole proton h. *$CDCl_3$, 293 K. Square data points represent experimental data; continuous lines represent theoretical binding isotherms.*

Table 2.1. Association constants, K_a *(M^{-1}), for 1:1 complexes of porphyrin host 6 with various anions.*

Anion	$\Delta\delta$ (ppm)	$K_a(M^{-1})^a$
Cl^-	0.37	2226(183)
Br^-	0.30	662(23)
I^-	0.23	224(23)
AcO^-	0.45	$>10^4$
$H_2PO_4^-$	0.65	*b*
PF_6^-	*c*	*c*

[a]All anions added as their TBA salt. Association constants were determined by monitoring the downfield shift of the triazole proton h. *Estimated standard errors are given in parentheses. $CDCl_3$, 293 K. [b]Overlapping peaks in the NMR spectra prevented quantitative binding data from being obtained. [c]Chemical shift changes too small to allow an accurate association constant to be determined.*

The porphyrin host 6 forms the most stable complex with acetate, followed by chloride > bromide > iodide. This anion selectivity trend in general correlates with anion basicity. Hexafluorophosphate binding was extremely weak as anticipated. Addition of dihydrogen phosphate caused changes in the chemical shifts which could not be accurately monitored on account of overlapping signals, so quantitative data for this anion could not be obtained.

Having established by ^{1}H NMR spectroscopy that 6 was capable of binding anions in chloroform solution, analogous UV/visible spectroscopic titration experiments were undertaken to investigate the potential optical sensing capabilities of this receptor.

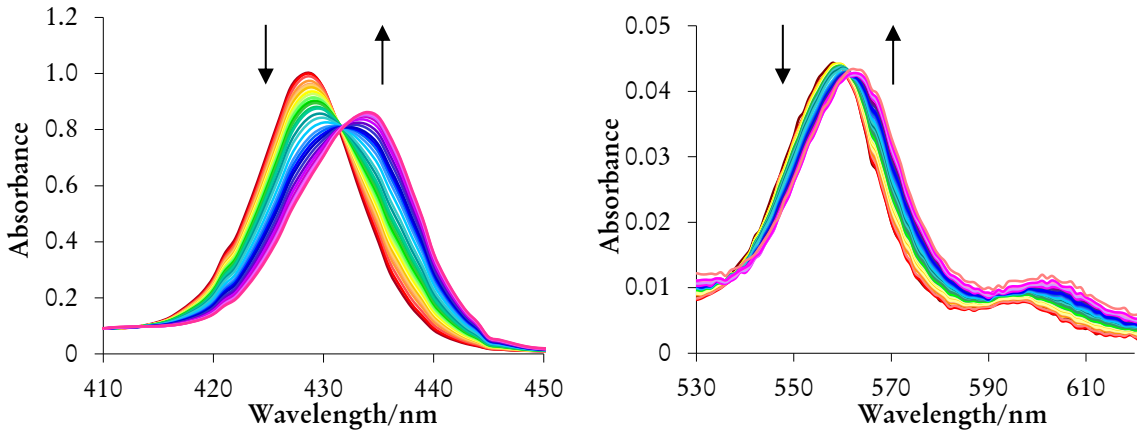


Figure 2.13. Changes in the a) Soret band and b) Q band components of the UV/visible absorption spectrum of a 2 μM solution of porphyrin 6 upon addition of TBA·Br. $CHCl_3$, 293 K.

Anion titration experiments induced significant perturbations of the receptor's absorbance spectrum. In a typical titration experiment (Figure 2.13) bathochromic shifts in the Soret and Q bands are observed upon addition of anions, which arise from axial ligation to the Lewis acidic zinc metal centre and correspond to similar observations described by Valentine for addition of anions to zinc(II)-tetraphenylporphyrin.[42] An isobestic point is observed with increasing anion concentration which corresponds to a 1:1 receptor:anion binding stoichiometry.

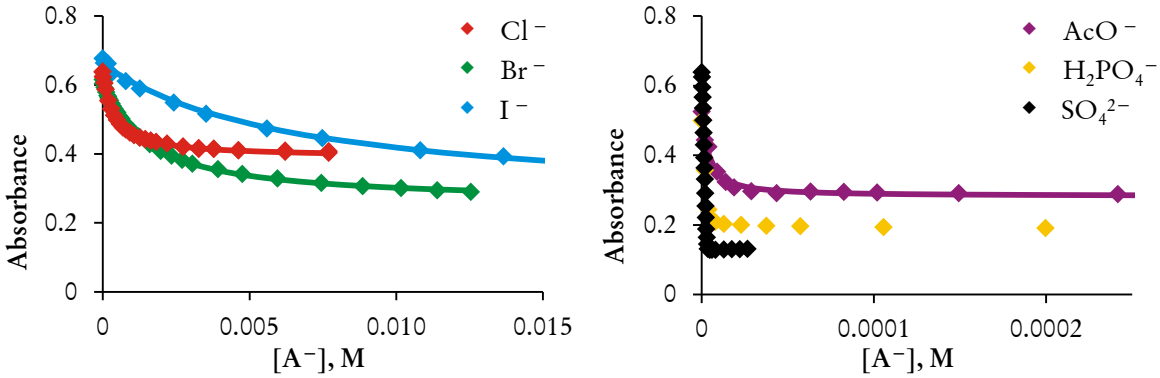


Figure 2.14. Titration curves for complex formation between porphyrin 6 and various anions obtained by monitoring perturbations of the Soret band at 425 nm. $CHCl_3$, 293 K. Square data points represent experimental data; continuous lines represent theoretical binding isotherms.

Association constants for 1:1 stoichiometric complexes were determined using the Specfit® computer program[70] to analyse the titration data (Figure 2.14) and are reported in Table 2.2. Pleasingly, UV/visible spectroscopy enabled quantitative data for dihydrogen phosphate binding to be obtained.

Table 2.2. Association constants, K_a *(*M^{-1}*), for 1:1 complexes of porphyrin host 6 with various anions.*

Anion	K_a $(M^{-1})^a$
Cl^-	2587(128)
Br^-	685(16)
I^-	150(5)
AcO^-	335 660(7383)
$H_2PO_4^-$	$>10^6$
SO_4^{2-}	$>10^6$
PF_6^-	[b]

[a]All anions added as their TBA salt. Association constants were determined by monitoring the perturbations of the Soret band. Estimated standard errors are given in parentheses. $CHCl_3$*, 293 K. [b]No evidence of binding.*

Sulfate is bound most strongly by porphyrin 6 as a consequence of its higher charge. Of the singly charged anions, a general preference for oxoanions over halides is observed, which may be explained in terms of anion basicity, with the receptor displaying relatively low binding affinity for larger, more diffuse bromide and iodide. It is interesting to note that there is almost an order of magnitude preference for dihydrogen phosphate over acetate, despite acetate being the more basic anion, which suggests the receptor prefers to bind anions of tetrahedral rather than trigonal geometry.

Importantly, these association constant values are in good agreement with those determined using ^{1}H NMR spectroscopy. UV/visible titration experiments are particularly attractive as they require only a small amount of the precious anion receptor species. Moreover, the absence of a triazole proton in iodotriazole zinc(II)-metalloporphyrin **10**, and relatively smaller anion-binding-induced shifts of other protons mean errors will be larger if ^{1}H NMR spectroscopic titrations are undertaken with receptor **10**.

2.2.3.2 *Anion binding properties of a halogen-bonding iodotriazole-functionalised anion receptor 10*

Initially, a qualitative ^{1}H NMR titration experiment of iodotriazole porphyrin **10** and chloride in chloroform-d was undertaken. Upon addition of one equivalent of chloride, downfield shifts of *meso*-phenyl proton *e*, methylene proton *g* and phenyl proton *h*, and relatively smaller perturbation of the amide proton *f* was observed, which indicates the chloride anion is being bound in the vicinity of the iodotriazole groups by four C–I···chloride halogen bonds (Figure 2.15).

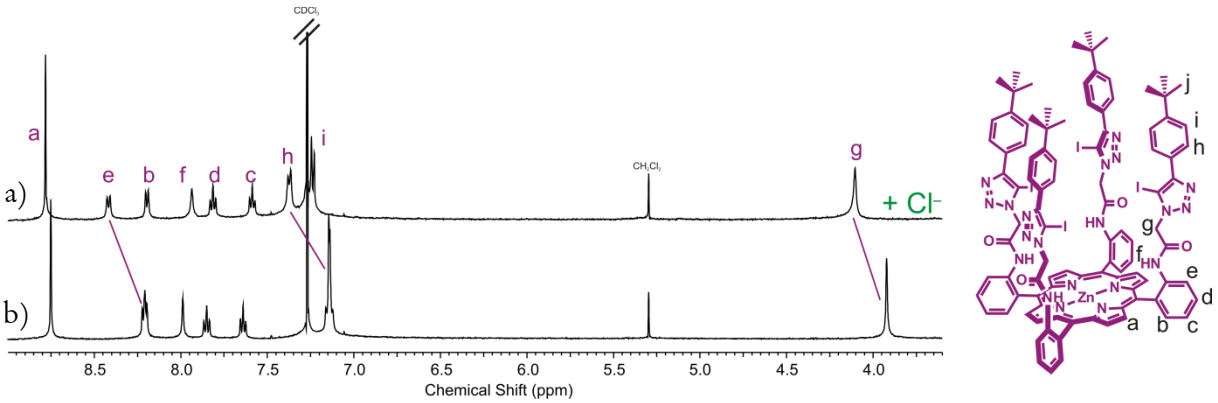


*Figure 2.15. Partial ^{1}H NMR spectra of a) receptor **10** and b) receptor **10** and one equivalent of TBA chloride. (500 MHz, $CDCl_3$, 293 K).*

UV/visible titrations were undertaken with iodotriazole porphyrin **10** to determine the ability of the halogen-bonding porphyrin-based anion receptor to bind anionic species, using the same protocol as that for triazole porphyrin 6 described above. Addition of anions to solutions of receptor **10** induced bathochromic shifts of the Soret and Q bands (*e.g.* Figure 2.16a) and monitoring these shifts as a function of the concentration of anion gave the titration data shown in Figure 2.16b. Association constants for 1:1 stoichiometric receptor:anion complex formation were obtained by Specfit® analysis of the titration data and are reported in Table 2.3.

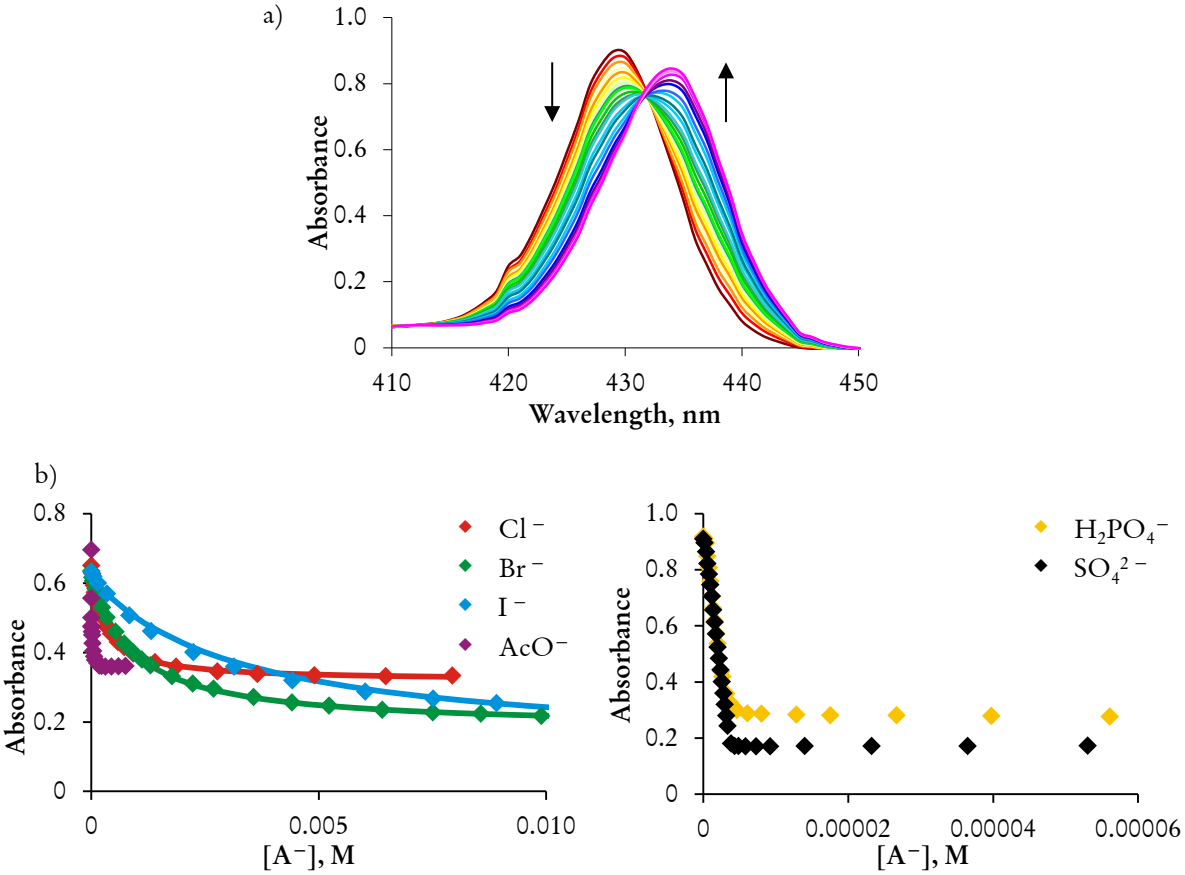


Figure 2.16. a) Changes in the Soret band of the UV/visible absorption spectrum of porphyrin **10** *upon addition of TBA·Cl. b) Titration curves for complex formation between porphyrin* **10** *and anions obtained by monitoring perturbations of the Soret band at 425 nm. $CHCl_3$, 293 K. Square data points represent experimental data; continuous lines represent theoretical binding isotherms.*

Table 2.3. Association constants, K_a *(M^{-1}), for 1:1 complexes of porphyrin host* **10** *with various anions.*

Anion	K_a (M^{-1})[a]
Cl^-	3592(31)
Br^-	1132(11)
I^-	305(23)
AcO^-	258 642(7578)
$H_2PO_4^-$	$>10^6$
SO_4^{2-}	$>10^6$
PF_6^-	[b]

[a]*All anions added as their TBA salt. Association constants were determined by monitoring the perturbations of the Soret band. Estimated standard errors are given in parentheses. $CHCl_3$, 293 K.* [b]*No evidence of binding.*

As for the protic analogue 6, this host displays a preference for basic oxoanions over halides, with the strongest binding being observed with doubly charged sulfate and tetrahedral

dihydrogen phosphate. Of the halides, chloride is bound most strongly followed by bromide and iodide, in order of decreasing anion basicity. Comparing Table 2.2 and Table 2.3 there are some interesting differences between the anion binding affinities of the hydrogen- and halogen-bonding receptors. It is noteworthy that the halogen-bonding iodotriazole host **10** has a greater affinity for chloride and bromide—with the strength of bromide association almost double in magnitude of that with the protic species (K_a = 1132 M^{-1} *versus* 685 M^{-1}). There is also a reduction in the acetate recognition strength with the halogen bonding receptor. Enhanced halide anion recognition together with reduced oxoanion affinity is consistent with that observed for other known halogen-bonding anion receptors.[71]

2.2.3.3 The effect of solvent on anion binding properties displayed by 6 and 10

The anion binding behaviour of halogen-bonding receptors in different solvents has not as yet been widely studied. The anion binding properties of porphyrin-based receptors 6 and **10** in acetone and acetonitrile were elucidated and compared to give an insight into solvent effects on anion binding in general and hydrogen *versus* halogen bonding in particular. UV/visible spectroscopic titrations were undertaken monitoring the Soret band with increasing anion concentration, producing titration curves (reported in Appendix A.3.1) from which Specfit® analysis determined quantitative data reported in Table 2.4.

*Table 2.4. Association constants, K_a (M^{-1}), for 1:1 complexes of porphyrin host 6 and **10** with anions in various solvents.*

K_a (M^{-1})[a]		Cl^-	Br^-	I^-	AcO^-	$H_2PO_4^-$	SO_4^{2-}
$CHCl_3$ ε = 4.81 μ = 1.15 AN = 23.1	6	2587(128)	685(16)	150(5)	335 660(7383)	$>10^6$	$>10^6$
	10	3592(31)	1132(11)	305(23)	258 642(7578)	$>10^6$	$>10^6$
MeCN ε = 37.5 μ = 3.45 AN = 18.9	6	34 626(184)	4494(369)	396(8)	$>10^6$	$>10^{6b}$	$>10^6$
	10	272 144(2613)	13 589(91)	656(11)	805 378(19 409)	$>10^{6b}$	$>10^6$
Acetone ε = 20.7 μ = 2.85 AN = 12.5	6	$>10^6$	721 938(9818)	14 659(846)	$>10^6$	$>10^6$	$>10^6$
	10	$>10^6$	$>10^6$	60 339(2009)	$>10^6$	$>10^6$	$>10^6$

[a]*All anions added as their TBA salt. Association constants were determined by monitoring the perturbations of the Soret band. Estimated standard errors are given in parentheses. 293 K.* [b]*Fitted better to a 1:2 host:guest model. ε = relative permittivity, μ = dipole moment, AN = acceptor number.*

As expected there are significant differences in the magnitude of the association constant values obtained in the three solvents. It is important to note, however, that the selectivity trends in anion binding strength remain the same in all cases, where in general, oxoanions are bound more strongly than halides with sulfate and dihydrogen phosphate displaying the largest association constant values, presumably on account of their tetrahedral shape.

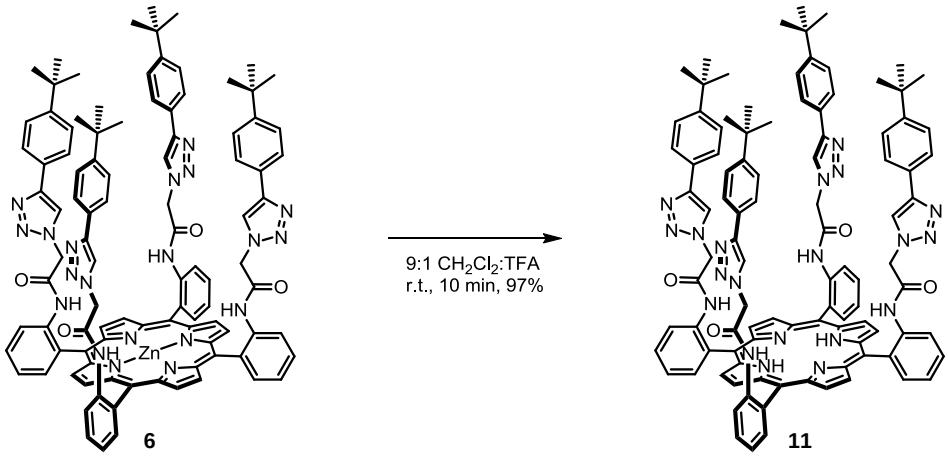
Anion binding strength is maximised by receptors 6 and **10** in acetone, followed by acetonitrile and chloroform. This anion binding behaviour does not correlate with bulk solvent properties such as relative permittivity (ε) or dipole moment (μ). There is however, a correlation between Gutmann's *acceptor number* (AN) of the solvent,[72] which gives a measure of the hydrogen-bond-donor ability of a solvent. As the hydrogen-bond-donor strength of the solvent increases (larger AN), anion affinity decreases: competing anion–solvent interactions are strongest in chloroform, and weakest in acetone.[73]

One final observation to note is the magnitude of enhancement of chloride and bromide halide anion recognition that occurs upon changing the solvent from chloroform to acetonitrile is more pronounced with the halogen-bonding receptor **10** than the hydrogen-bonding analogue 6. Indeed, chloride anion binding affinity increases 75-fold with halogen-bonding porphyrin **10** but only 13-fold with hydrogen-bonding receptor 6. Future, indepth

thermodynamic investigations will be required to help rationalise these observations, through the determination of entropic and enthalpic contributions of halogen-bonding anion recognition in a range of solvent media.

2.2.3.4 Comparing the anion binding properties of receptor 6 with its free base porphyrin analogue

To assess the contribution of the Lewis-acidic zinc(II) metal centre to the overall anion binding process, the free base analogue of receptor 6 was prepared as outlined in Scheme 2.9.



*Scheme 2.9. Synthesis of tetra-triazole free-base porphyrin **11**.*

Zinc(II)-metalloporphyrin compound 6 was stirred in the presence of trifluoroacetic acid in dichloromethane to afford the free base porphyrin **11** in 97% yield. Successful demetallation was confirmed by the presence of a singlet at $\delta = -2.3$ ppm corresponding to the two pyrrole NH protons *k* in the ^{1}H NMR spectrum (Figure 2.17).

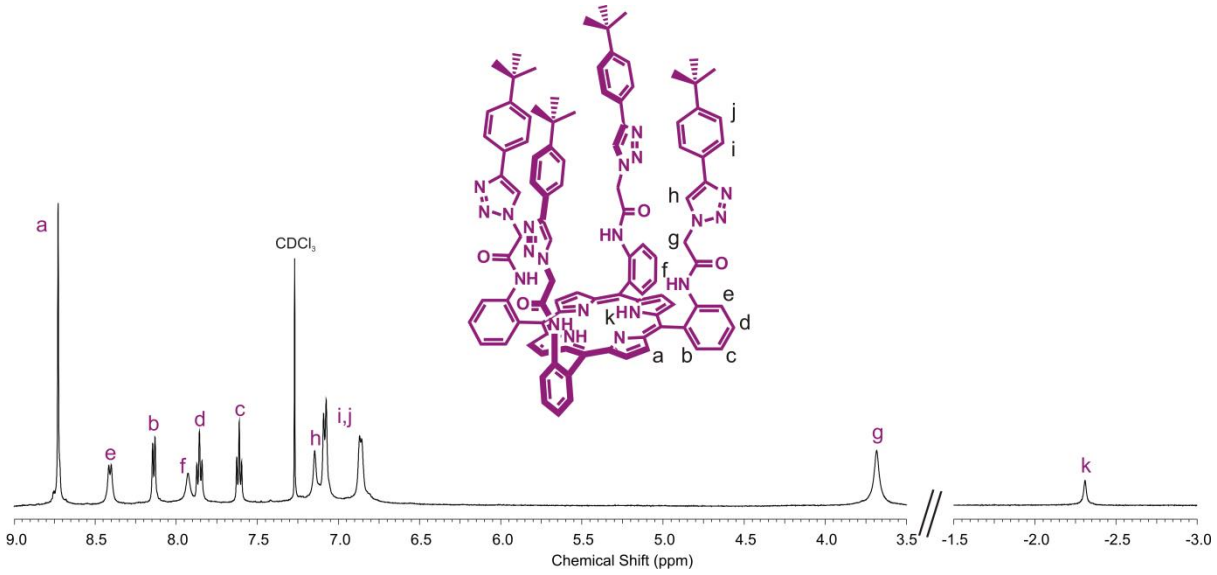


*Figure 2.17. [1]HNMR spectra of triazole-functionalised free base porphyrin **11** showing peak assignments (500 MHz, $CDCl_3$, 293 K).*

*Table 2.5. Association constants, K_a (M^{-1}), for 1:1 complexes of porphyrin host **11** with various anions.*

Anion	K_a $(M^{-1})^a$
Cl^-	358(21)
Br^-	167(9)
I^-	66(6)

[a]All anions added as their TBA salt. Association constants were determined by monitoring the perturbations of the triazole proton. Estimated standard errors are given in parentheses. $CDCl_3$, 293 K.

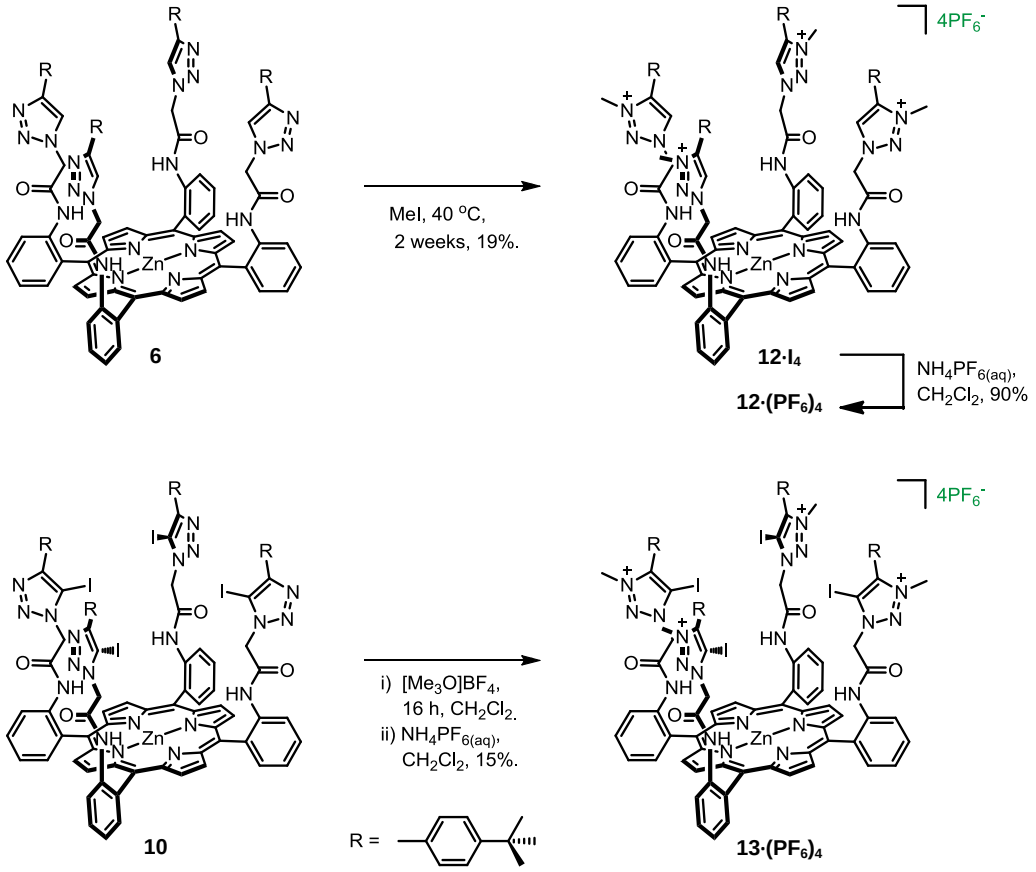
^{1}H NMR spectroscopic titrations in chloroform-d were undertaken to investigate the anion binding properties of this free-base triazole-porphyrin species **11**. The association constants for halide anion binding obtained by monitoring the chemical shift perturbations of the triazole proton *g* are reported in Table 2.5. As expected, these values are lower than those for the zinc(II)-porphyrin analogue 6 which indicates that anion ligation to the zinc(II) metal centre is significant and is an important contribution to the overall anion binding strengths of porphyrin-based receptors. The same trend in halide anion recognition chloride > bromide > iodide is observed which is dictated by the pendant triazole anion recognition groups cooperatively binding the halide guest species.

2.2.4 Synthesis and characterisation of cationic triazolium-functionalised zinc(II)-metalloporphyrin anion receptors

The triazole- and iodotriazole-containing zinc(II)-metalloporphyrin species described above have proven to be effective anion host systems. Alkylating these triazole-porphyrin architectures to produce tetra-triazolium-porphyrin analogues is expected to increase anion binding affinity through favourable electrostatic interactions.

The synthesis of cationic triazolium-porphyrin-based receptors is outlined in Scheme 2.10. The reaction of 6 with excess methyl iodide proved to be extremely slow under the mild reaction conditions required to prevent demetallation and alkylation at the pyrrole nitrogens from occurring. After two weeks and chromatographic purification the iodide salt was isolated in 19% yield. Following anion exchange by repeatedly washing a dichloromethane solution of **12·I$_4$** with aqueous ammonium hexafluorophosphate, the target tetra-triazolium-porphyrin species **12·(PF$_6$)$_4$** was isolated in 90% yield.

Analogous alkylation reaction conditions with the iodotriazole-porphyrin compound **10** failed and an alternative approach using trimethyloxonium tetrafluoroborate, a more potent methylating agent, was undertaken. Iodotriazole-porphyrin compound **10** and five equivalents of trimethyloxonium tetrafluoroborate were dissolved in anhydrous dichloromethane and, following anion exchange and purification by preparative thin layer chromatography, iodotriazolium-porphyrin compound **13·(PF$_6$)$_4$** was obtained in 15% yield.



Scheme 2.10. Synthesis of triazolium- and iodotriazolium-porphyrin anion receptors ***12·(PF$_6$)$_4$*** *and* ***13·(PF$_6$)$_4$****.*

Both triazolium-containing receptors were characterised by ^{1}H, ^{13}C, ^{19}F and ^{31}P NMR spectroscopy. The ^{1}H NMR spectra of triazolium-porphyrins **12·I$_4$** and **12·(PF$_6$)$_4$** are shown in Figure 2.18. In the absence of axial-coordinated anionic guests, the ^{1}H NMR spectrum of **12·(PF$_6$)$_4$** in chloroform-d contained a number of broad peaks so pyridine-d$_5$ was added to help produce a sharper spectrum. Significant downfield shifts of signals corresponding to amide proton *f*, triazole proton *h*, and methylene protons *g* are observed in the presence of iodide. These changes are consistent with these proton residues forming hydrogen-bonding interactions with the complexed the iodide anion.

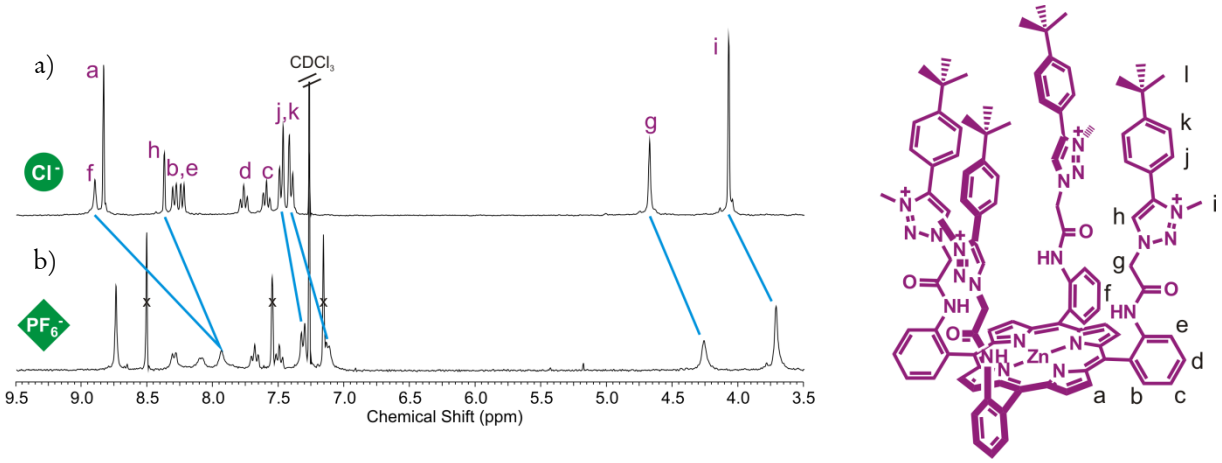


*Figure 2.18. Partial ^{1}H NMR spectra of triazolium-porphyrin compounds a) **12·I$_4$** ($CDCl_3$) and b) **12·(PF$_6$)$_4$** (9:1 $CDCl_3$:pyridine-d_5). (300 MHz, 293 K).*

A similar spectrum was obtained for iodotriazolium-porphyrin compound **13·(PF$_6$)$_4$** the most notable feature of which is the absence of a triazolium proton signal in this system (Figure 2.19).

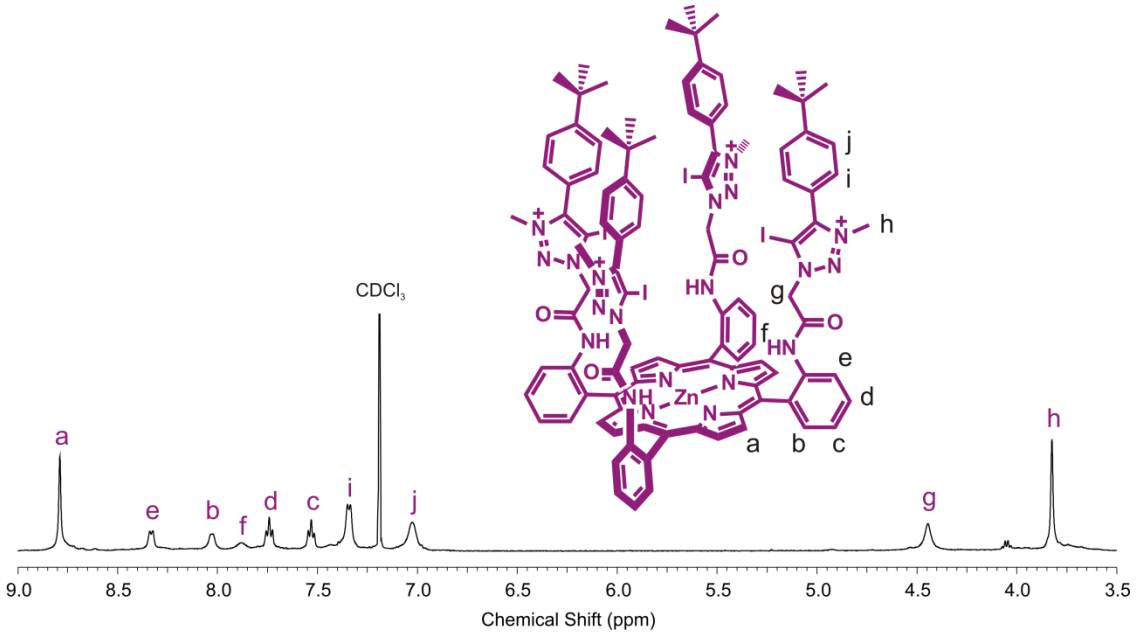


*Figure 2.19. Partial ^{1}H NMR spectra of iodotriazolium-porphyrin compound **13·(PF$_6$)$_4$**. (500 MHz, $CDCl_3$, 293 K).*

2.2.5 Anion binding properties of cationic triazolium-functionalised zinc(II)-metalloporphyrin anion receptors

Owing to the limited supply of compounds **12·(PF$_6$)$_4$** and **13·(PF$_6$)$_4$**, the anion binding properties of these systems were only investigated by UV/visible spectroscopy. Anion

titration experiments were carried out in dimethylsulfoxide solution as it was anticipated that the positively charged receptors would prove to be potent anion complexants in this competitive solvent medium.

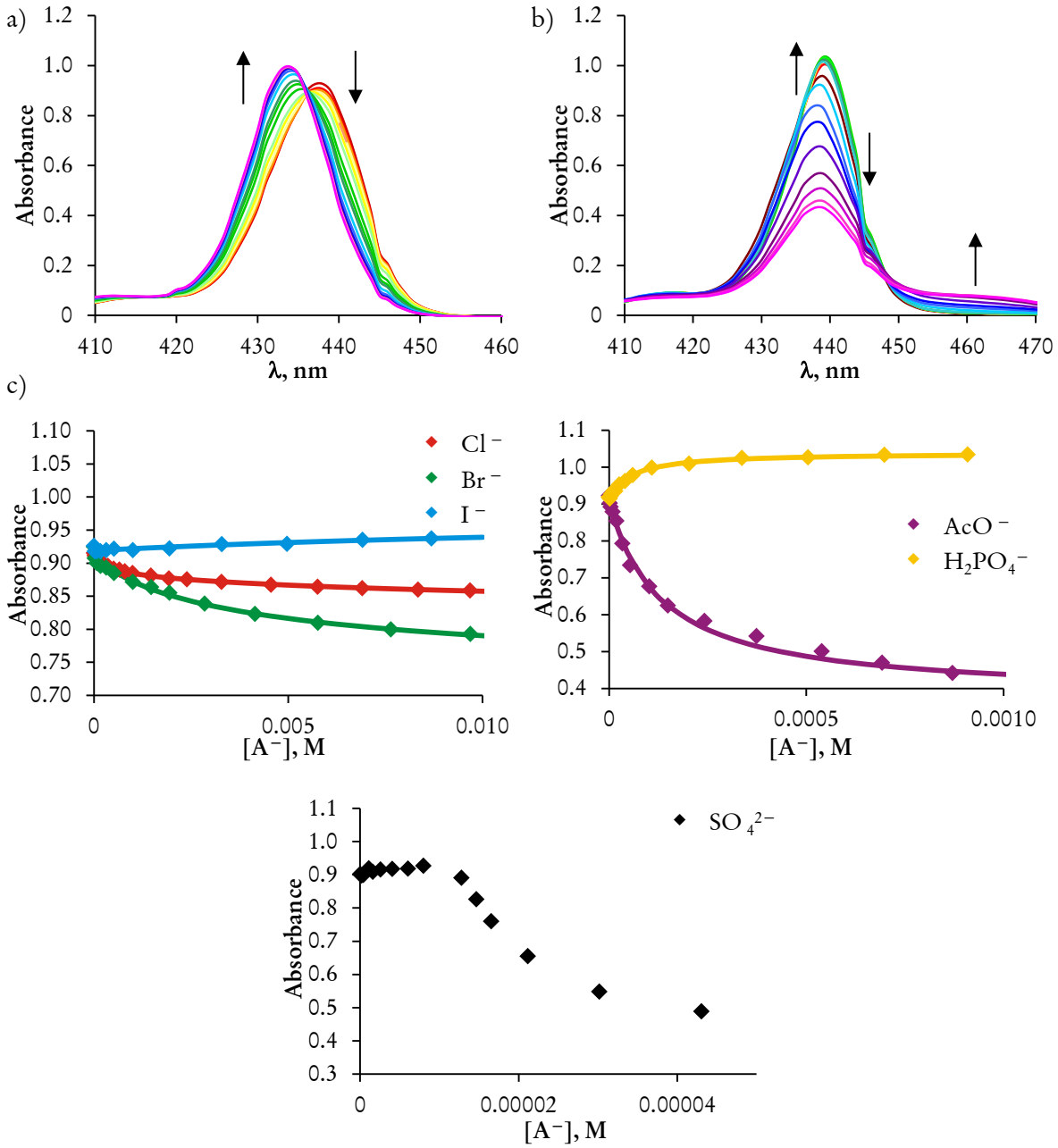


Figure 2.20. Changes in the Soret band of the UV/visible absorption spectrum of a 2 μM solution of porphyrin ***12*·(PF$_6$)$_4$** *upon addition of a) TBA·Br and b) [TBA]$_2$[SO$_4$]. c) Titration curves for complex formation between porphyrin* ***12*·(PF$_6$)$_4$** *and various anions obtained by monitoring perturbations of the Soret band at 437 nm. DMSO, 293 K. Square data points represent experimental data; continuous lines represent theoretical binding isotherms.*

Addition of anions to solutions of **12**·$(PF_6)_4$ and **13**·$(PF_6)_4$ caused shifts in the receptors' absorbance spectra. Monitoring changes in the Soret band as a function of the concentration of anion gave titration curves shown in Figures 2.20 and 2.21. Specfit® analysis of the titration data determined, in the majority of cases, 1:1 host:guest stoichiometric association constant values (Table 2.6).

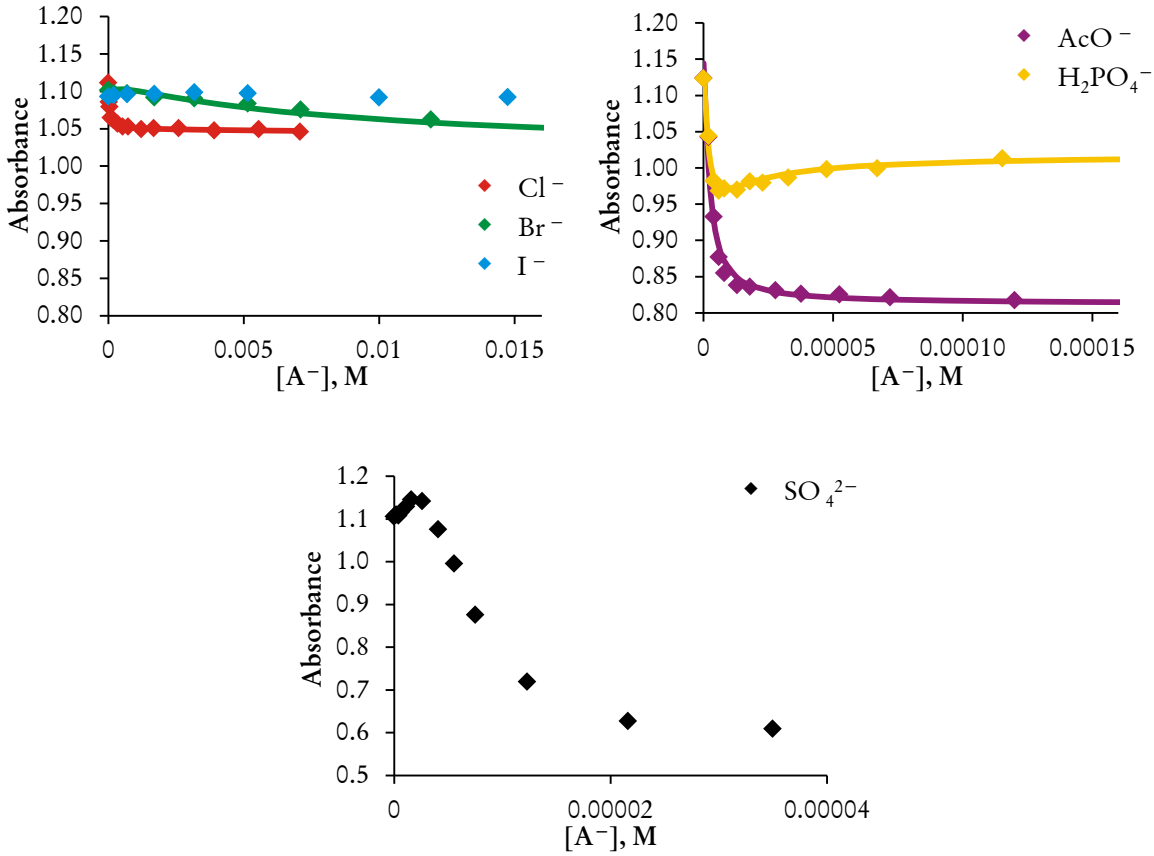


Figure 2.21. Titration curves for complex formation between porphyrin ***13***·$(PF_6)_4$ *and various anions obtained by monitoring perturbations of the Soret band at 437 nm. DMSO, 293 K. Square data points represent experimental data; continuous lines represent theoretical binding isotherms.*

*Table 2.6. Association constants, K_a (M^{-1}), for complexes of porphyrin host **12·(PF$_6$)$_4$** and **13·(PF$_6$)$_4$** with various anions.*

Anion	K_a (M^{-1})[a] **12·(PF$_6$)$_4$**	K_a (M^{-1})[a] **13·(PF$_6$)$_4$**
Cl^-	K_1 = 3177(12) K_2 = 85 (0.3)	K_1 = 26 393(117) K_2 = 25(1)
Br^-	664(7)	K_1 = 3297(29) K_2 = 109(1)
I^-	50(0.7)	[b]
AcO^-	K_1 = >10^6 K_2 = 7599 (216)	721 440 (16 087)
$H_2PO_4^-$	K_1 = >10^6 K_2 = 18980(93)	K_1 >10^6 K_2 = 82 395 (975)
SO_4^{2-}	[c]	[c]

[a]*All anions added as their TBA salt. Association constants were determined by monitoring the perturbations of the Soret band. Estimated standard errors are given in parentheses. DMSO, 293K.* [b]*Shifts in the Soret band were too small to allow an association constant to be accurately determined.* [c]*Titration data could not be accurately fitted to a simple 1:1 or 1:2 binding model.*

The general trends observed in association constant values for anion binding by these positively charged receptors are similar to those displayed by their neutral analogues; the addition of charge serves to enable anion recognition to occur in the competitive solvent dimethyl sulfoxide. Of the singly charged anions, acetate and dihydrogen phosphate binding strength is significantly greater than halide anion recognition owing to their more basic nature. Specifically, dihydrogen phosphate is bound more favourably than acetate, a result of the cavity's shape complementarity for tetrahedral guests: K_a ($H_2PO_4^-$) = >10^6 M^{-1} *versus* K_a (AcO^-) = 7.2 × 10^5 M^{-1} for the iodotriazolium-porphyrin host system. As for the neutral systems, substantial improvement in halide anion recognition is observed when the triazole proton is replaced by an iodine atom while oxoanion recognition strength is somewhat reduced. Addition of sulfate induced changes in the porphyrin's UV/visible spectrum which could not be fitted to a simple binding modelling, suggesting the presence of complicated, competing equilibria.

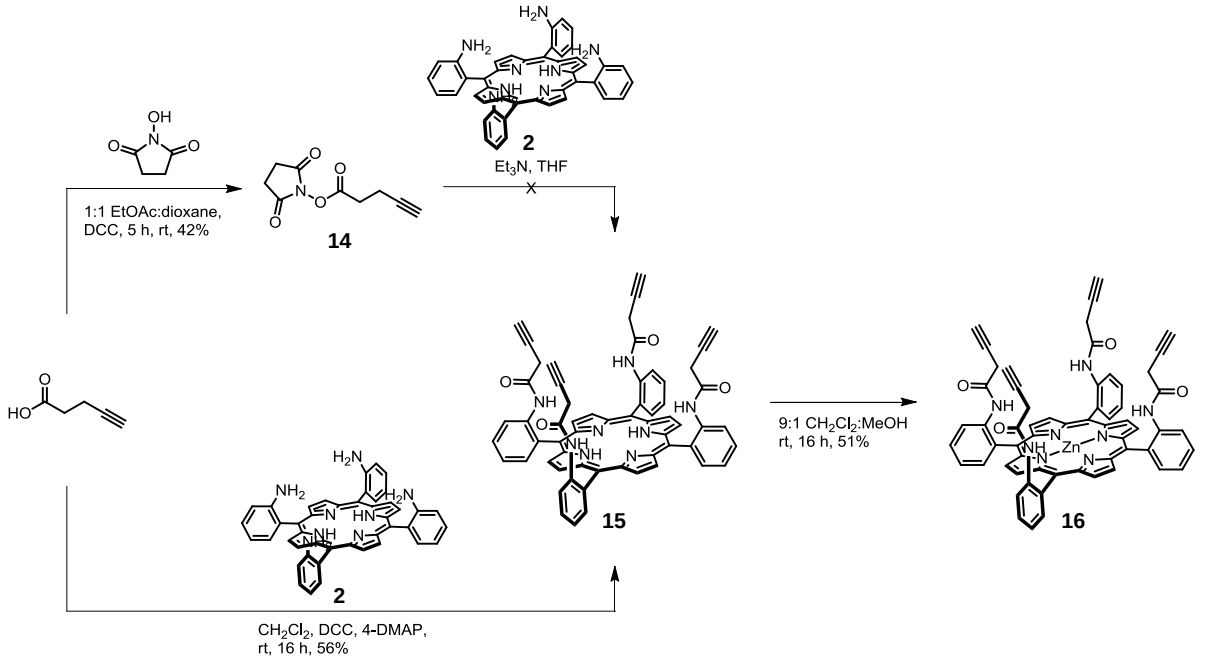
2.3 Cyclic functionalised-porphyrin anion receptors

2.3.1 Synthesis of triazole- and triazolium-functionalised zinc(II)-metalloporphyrin-cage anion receptors

The principle of preorganisation was introduced in Chapter One, along with the macrocyclic and chelate effects, as concepts which may be exploited to effect stronger association between host and guest. It was envisaged that integrating triazole and iodotriazole recognition groups into zinc(II)-metalloporphyrin-based cage-like structures would produce anion receptors with enhanced anion recognition properties.

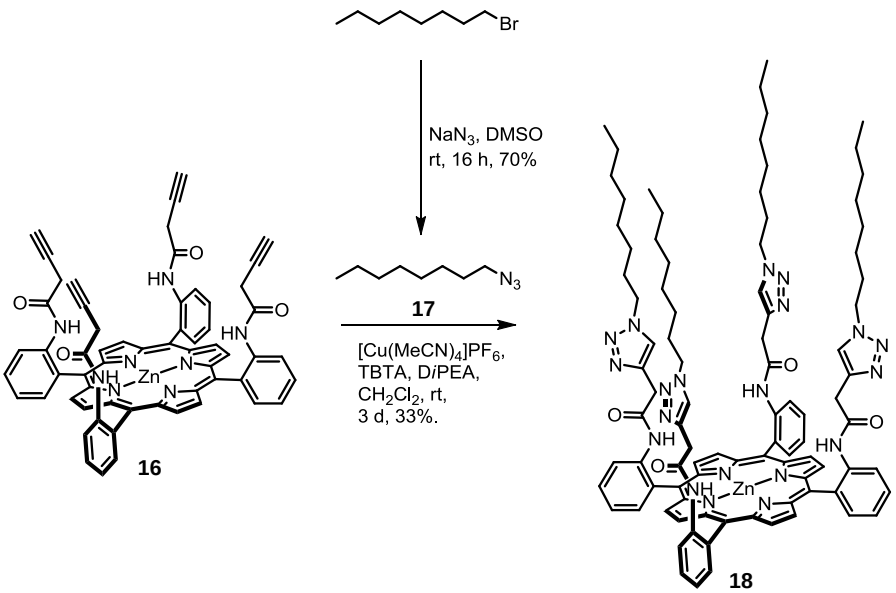
Initial attempts to prepare a porphyrin-containing cage focused on the design of an appropriate alkyne-functionalised porphyrin species which could be coupled with tetra-azide porphyrin 5 to form a novel bis-porphyrin host system using CuAAC reactions.

The preparation of alkyne-functionalised porphyrin **16** is outlined in Scheme 2.11. Stirring pent-4-ynoic acid, *N*-hydroxysuccinimide and *N*,*N*'-dicyclohexylcarbodiimide in 1:1 ethyl acetate:dioxane afforded activated ester compound **14** in 42% yield.[74] Four equivalents of **14** were added to porphyrin $\alpha,\alpha,\alpha,\alpha$-2 in the presence of triethylamine in tetrahydrofuran. After several days, however, no evidence of alkyne-porphyrin formation was observed by mass spectrometry or thin layer chromatography so an alternative approach was undertaken. A peptide coupling reaction between pent-4-ynoic acid and amino-porphyrin $\alpha,\alpha,\alpha,\alpha$-2 using *N*,*N*'-dicyclohexylcarbodiimide 4-dimethylaminopyridine in dichloromethane gave the alkyne-functionalised porphyrin **15** in 56% yield and metallation to produce tetra-alkyne zinc(II)-metalloporphyrin **16** was achieved in 51% yield with zinc(II) acetate in 1:1 dichloromethane:methanol.



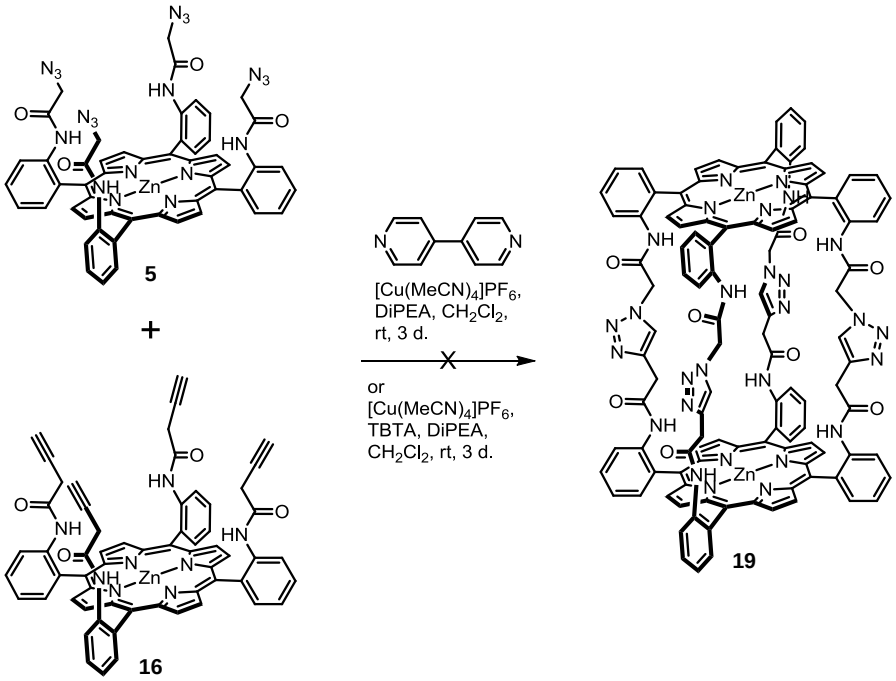
*Scheme 2.11. Synthesis of alkyne-functionalised porphyrin **16**.*

A model CuACC reaction was initially carried out to investigate whether triazole forming reactions were possible with porphyrin **16**. Reaction between alkyne porphyrin **16** and four equivalents of 1-*n*-octylazide **17** (prepared in 70% yield by stirring 1-*n*-octylbromide and sodium azide in dimethyl sulfoxide)[75] in the presence of copper(I)tetrakis-acetonitrile hexafluorophosphate, TBTA and *N*,*N*-di-*iso*-propylethylamine in dichloromethane afforded triazole-appended zinc(II)-metalloporphyrin compound **18** in 33% yield (Scheme 2.12).



*Scheme 2.12. Synthesis of model triazole-porphyrin compound **18**.*

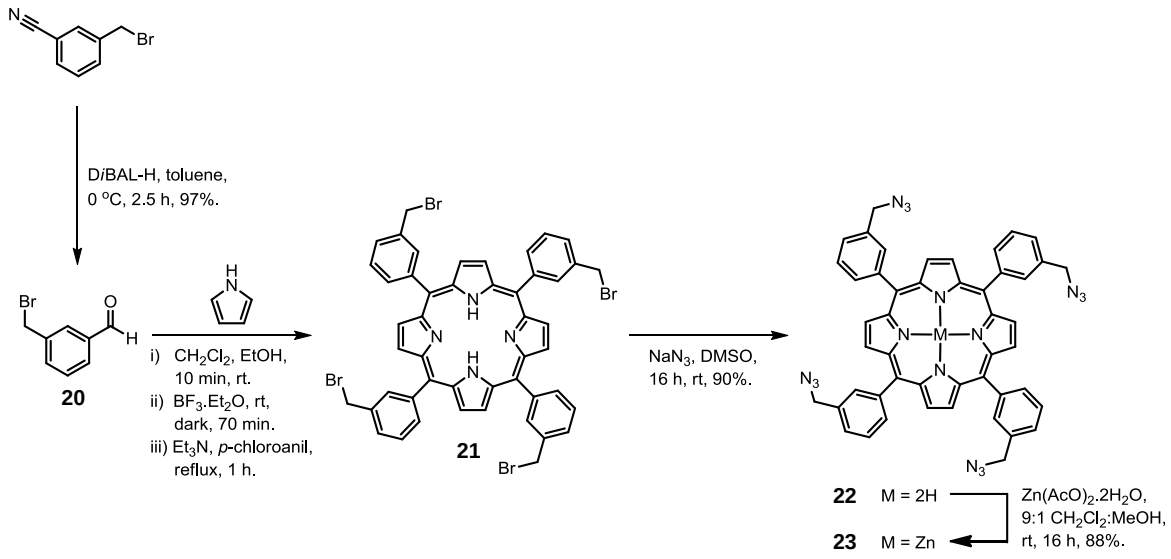
Attempts to prepare a bis-porphyrin-containing cage structure are detailed in Scheme 2.13. Equimolar amounts of azido-porphyrin **5** and alkyne-porphyrin **16** were stirred in the presence of copper(I)tetrakis-acetonitrile hexafluorophosphate, *N*,*N*-di-*iso*-propylethylamine and TBTA in dichloromethane. After three days, there was no evidence of product formation in the crude mass spectra or by thin layer chromatography. The reaction was repeated with one equivalent of 4,4'-bipyridine with the intention that it might template the assembly of the two components through zinc–pyridine acid–base chelation. Disappointingly, this still failed to produce any identifiable target compound.



Scheme 2.13. Attempted synthesis of a bis-porphyrin cage.

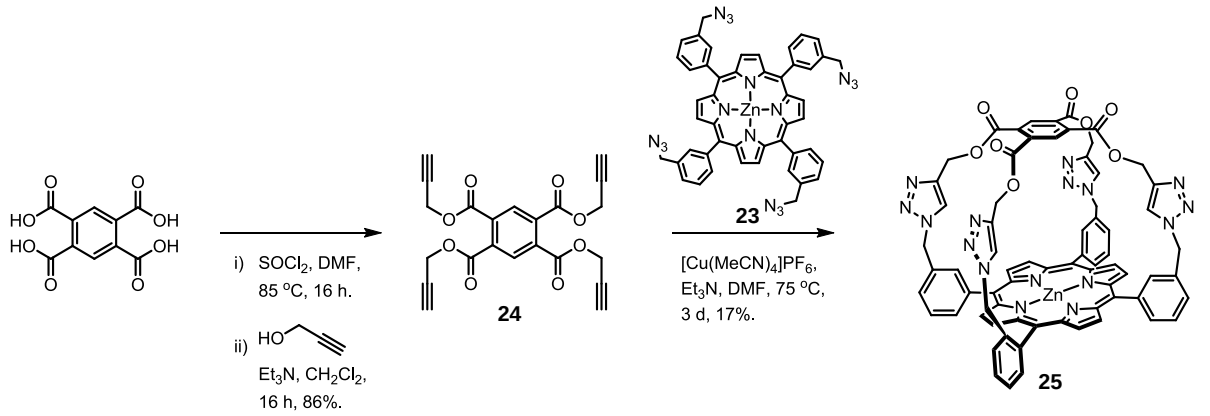
Alternative means of preparing a triazole-porphyrin-cage species were considered and a search of the literature revealed the synthesis of a suitable triazole-porphyrin-cage compound. The target triazole-containing zinc(II)-metalloporphyrin-cage receptor **25** was prepared via modification of Crossley's synthetic procedure[76] which involves a copper(I)-catalysed azide–alkyne cycloaddition (CuAAC) reaction[54,77] between a tetra-*meso*-substituted azide-functionalised porphyrin and a capping aryl-alkyne (Schemes 2.14 and 2.15).

3-(Bromomethyl)benzaldehyde **20** was prepared in 97% yield by reduction of commercially available 3-(bromomethyl)benzonitrile using di-*iso*butylaluminium hydride in toluene.[78] Reaction with pyrrole in the presence of catalytic boron trifluoride etherate afforded porphyrin **21** via a modification of the Lindsey protocol.[79,80] Stirring porphyrin **21** with sodium azide in dimethyl sulfoxide gave tetra-azide porphyrin **22** in 90% yield. Azide-porphyrin **22** was metallated using zinc(II) acetate in 9:1 dichloromethane:methanol giving the zinc(II)-metalloporphyrin derivative **23** in 88% yield (Scheme 2.14).



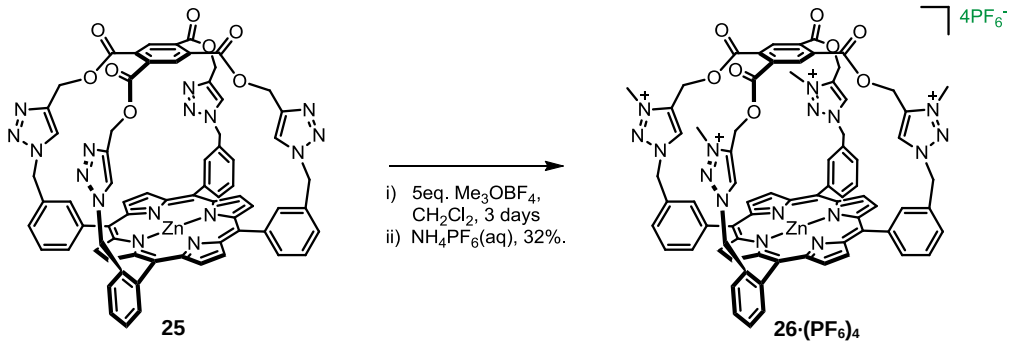
*Scheme 2.14. Synthesis of tetra-azide porphyrin **23**.*

The required tetra-alkyne aryl capping group **24** was prepared in 86% yield by condensation of ten equivalents of propargyl alcohol with benzene-1,2,4,5-tetracarbonyl chloride, formed by heating benzene-1,2,4,5-tetracarboxylic acid and thionyl chloride.[76] Zinc(II)-porphyrin-cage **25** was prepared via a CuAAC reaction between 5,10,15,20-tetrakis(*α*-azido-*m*-tolyl)zinc porphyrin **23** and capping group **24** in the presence of copper(I)tetrakis-acetonitrile hexafluorophosphate and triethylamine in dimethylformamide. After purification using preparative thin layer chromatography (95:5 dichloromethane:methanol), the zinc(II)-porphyrin-cage compound **25** was isolated in 17% yield (Scheme 2.15).



Scheme 2.15. Synthesis of triazole-porphyrin cage compound ***25****.*

Alkylation of the zinc(II)-porphyrin-cage **25** to produce the novel tetra-triazolium cage receptor **26·$(PF_6)_4$** was achieved in 32% yield via reaction of **25** with five equivalents of trimethyloxonium tetrafluoroborate in anhydrous dichloromethane followed by purification and anion exchange to the hexafluorophosphate salt (Scheme 2.16).



Scheme 2.16. Synthesis of tetra-triazolium porphyrin-cage ***26·$(PF_6)_4$****.*

2.3.2 Characterisation of triazole- and triazolium-functionalised zinc(II)-metalloporphyrin-cage anion receptors

Both porphyrin-cage receptors **25** and **26·$(PF_6)_4$** were characterised by NMR spectroscopy, mass spectrometry and UV/visible spectroscopy.

The ^{1}H NMR spectrum of zinc(II)-porphyrin-cage receptor **25** is shown in Figure 2.22. All salient proton environments are present: *β*-pyrrole *a*,*a*', *meso*-phenyl proton doublets *b* and *d*, and triplet *c*, and aromatic singlets corresponding to triazole *g*, *meso*-phenyl *e*, and capping-group proton *i*. It is interesting to note the desymmetrisation of signals corresponding to the

methylene protons *f,f'* and *h,h'*, and the *β*-pyrrole protons *a,a'* arising from the inequivalence of these protons as a result of the C_{2v} symmetry of this molecule.

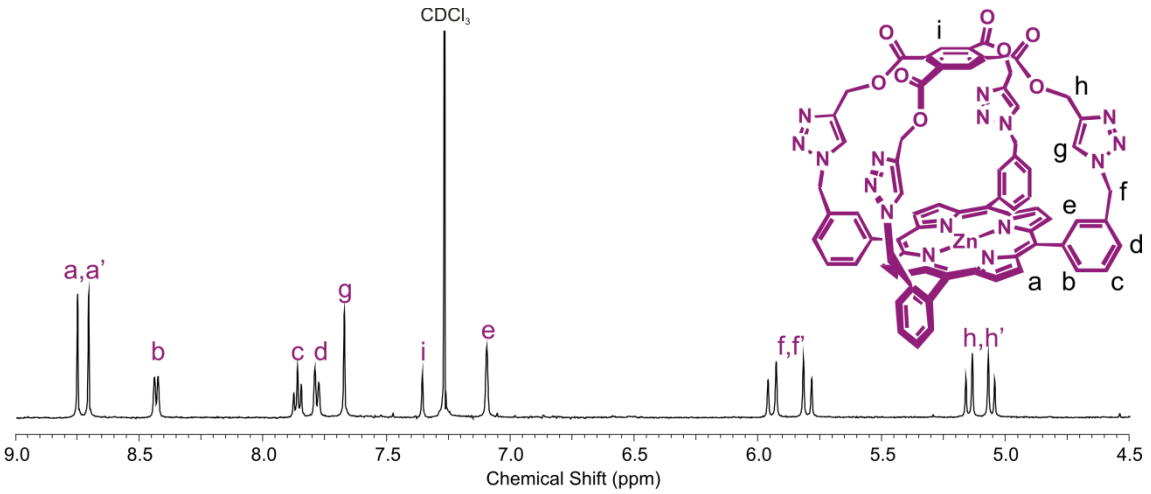


*Figure 2.22. Partial ^{1}H NMR spectrum of **25** showing peak assignments (500 MHz, $CDCl_3$, 293 K).*

Proton peak assignments were confirmed by ^{1}H–^{1}H TOCSY and ROESY two dimensional spectroscopy. Important through space cross–coupling interactions are highlighted in Figure 2.23. In particular, interaction **1** enabled methylene protons *f* and *h* to be identified, and interaction **3** allowed the singlet at 6.93 ppm to be assigned to the *meso*-phenyl proton *e* resonance.

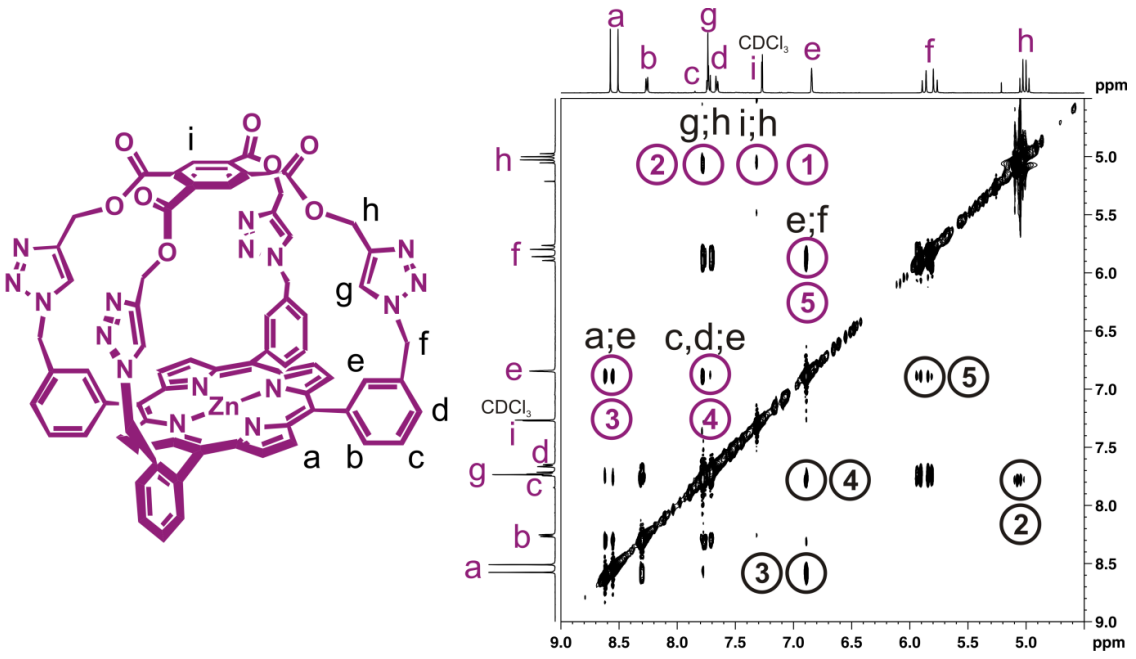


*Figure 2.23. Partial ^{1}H–^{1}H ROESY spectra of **25** showing important cross-coupling interactions. (500 MHz, 9:1 $CDCl_3$:CD_3OD, 293 K).*

Crystals of zinc(II)-metalloporphyrin cage **25** suitable for single crystal X-ray diffraction structural analysis were grown by the slow evaporation of an acetone solution of the cage receptor. The structure (Figure 2.24) reveals the open nature of the three-dimensional cavity where an anion can potentially be bound. The four triazole groups are aligned perpendicular to the cage in the solid state but the flexibility of the receptor should allow for strong induced-fit anion binding. It can be seen that the four *meso*-phenyl protons pointing into the cavity, together with the triazole protons provide a suitable binding pocket for anion coordination to the porphyrin-bound zinc(II) centre. The presence of five-coordinate zinc(II), with an acetone solvent molecule as the axial-coordinating ligand, is also apparent.

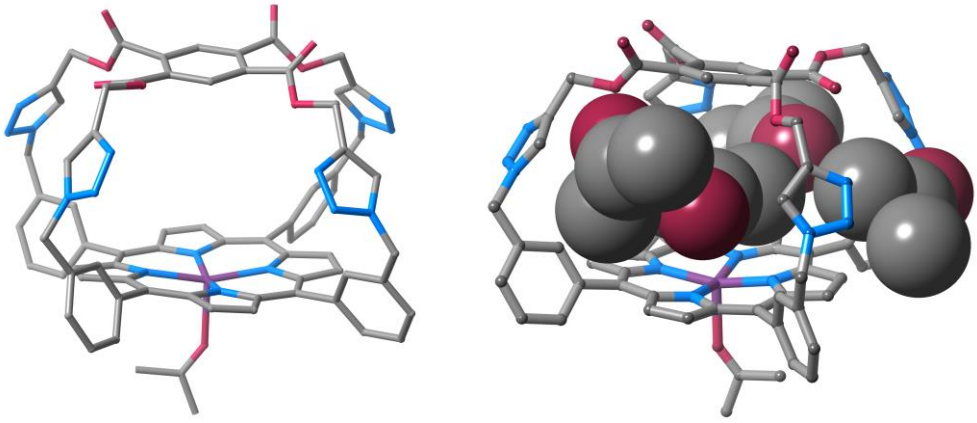


Figure 2.24. Capped stick model (left) and space filling representation (right) of the X-ray crystal structure of ***25***$\cdot 5(C_3H_6O)$*. Colour scheme: grey=C, blue=N, red=O, purple=Zn.*

2.3.3 Anion binding properties of triazole- and triazolium-functionalised zinc(II)-metalloporphyrin-cage anion receptors

A preliminary ^{1}H NMR anion binding investigation of **25** and tetrabutylammonium chloride was undertaken in acetone-d_6 solution. Upon addition of chloride significant downfield shifts in the receptor's triazole *g* and *meso*-phenyl *e* cavity protons were observed (Figure 2.25). This suggests the chloride anion is binding within the cage, coordinating to both the triazole and phenyl CH groups through the cumulative effects of multiple hydrogen-bonding interactions. WinEQNMR[69] analysis of the titration data gave an association constant value, $K_a > 10^4$ M^{-1} following the *meso*-phenyl proton *e*.

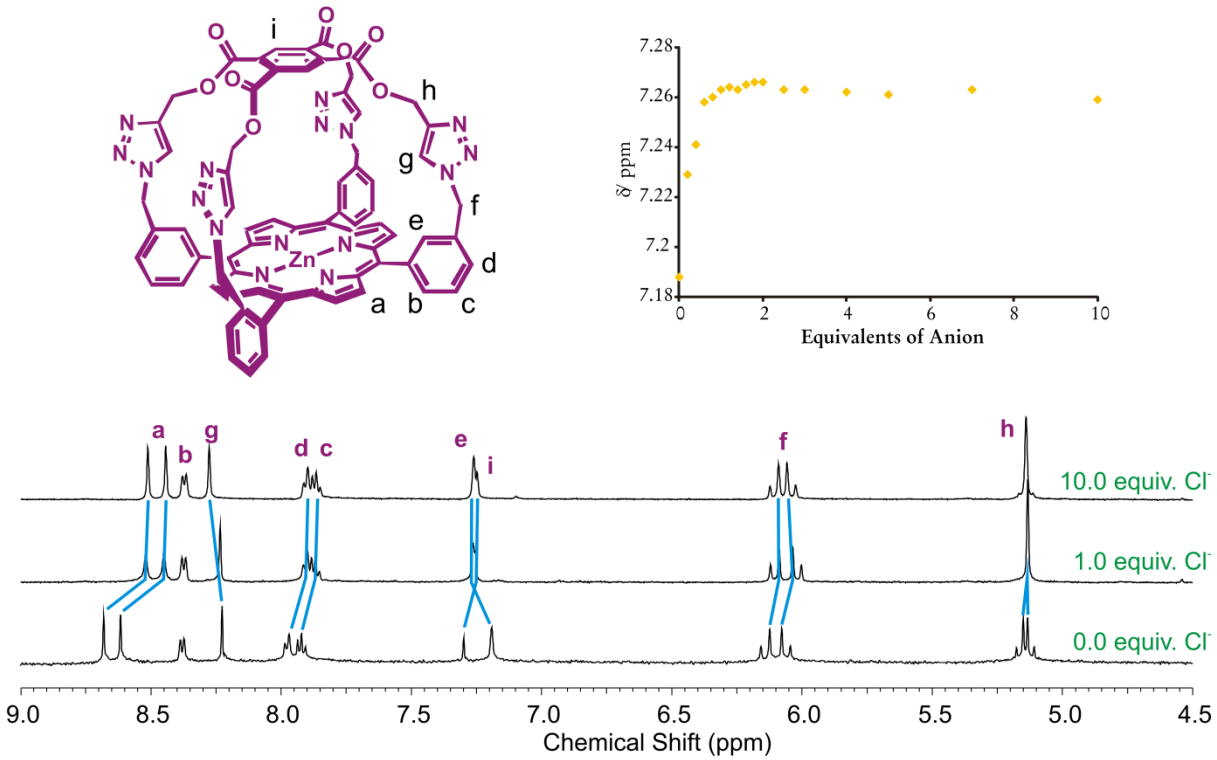


*Figure 2.25. Partial ^{1}H NMR spectra of a solution of porphyrin **25** in the presence of 0, 1 and 10 equivalents of TBA·Cl in acetone-d_6 at 293 K. Changes in chemical shift of proton* e *on addition of TBA·Cl.*

The anion recognition properties of cage porphyrins **25** and **26**·$(PF_6)_4$ were investigated by UV/visible spectroscopic titrations. Both receptors exhibit characteristic metalloporphyrin absorption spectra with strong Soret band absorbances in the 400–450 nm region as well as weaker Q band absorbances in the 500–650 nm region.

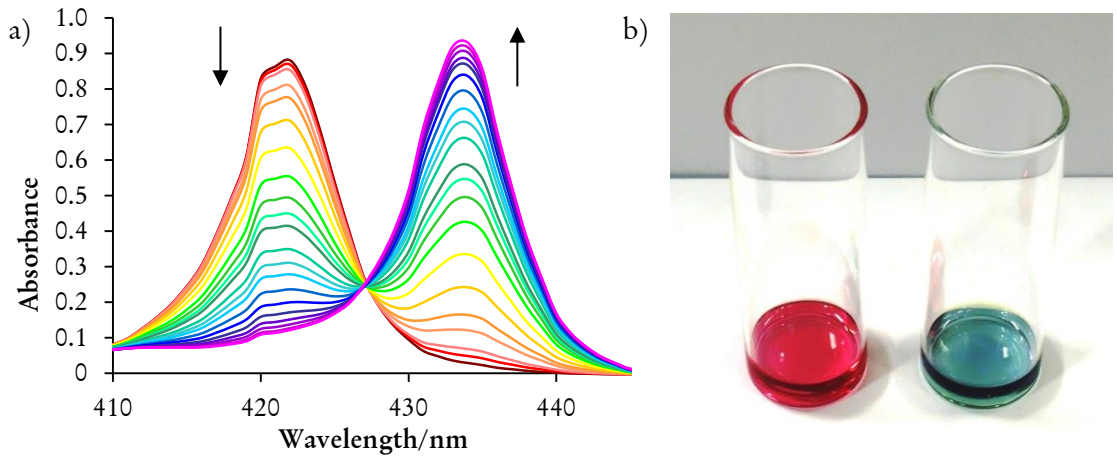


*Figure 2.26. a) Changes in the Soret band component of the UV/visible absorption spectrum of a 2 μM solution of porphyrin **25** upon addition of TBA·Cl (acetone, 293 K).*

Anion titration experiments in acetone and acetone/water solvent mixtures revealed significant perturbations of the respective porphyrin receptor's Soret band as a function of concentration of TBA·A salts. In a typical titration experiment (Figure 2.26), upon addition of chloride, a bathochromic shift in the maxima of the absorbance bands is observed as the halide anion coordinates to the zinc(II) metal centre.[81] An isobestic point is observed with increasing anion concentration which corresponds to a 1:1 receptor:anion binding stoichiometry. It is noteworthy that acetone solutions of zinc(II)-metalloporphyrin anion receptor **25** are pink in colour and addition of anions resulted in the solutions changing colour detectable by the naked eye (Figure 2.27).

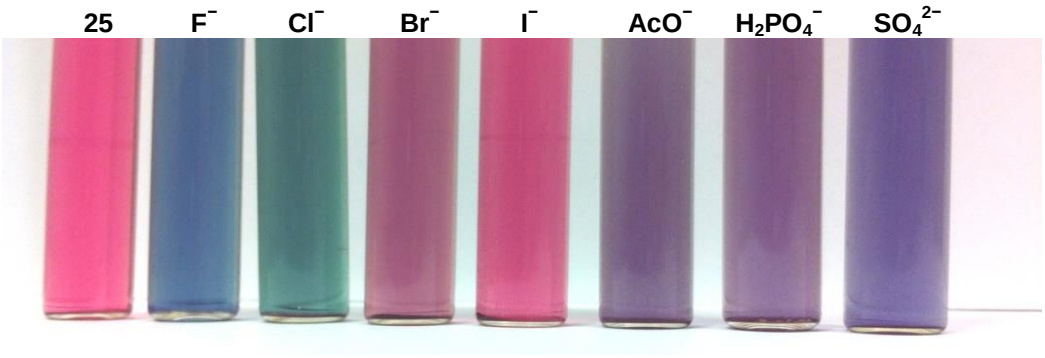


*Figure 2.27. Colour of receptor **25** before and after addition of 10 equivalents of anions in acetone.*

The anion binding properties of zinc(II)-tetraphenylporphyrin[82-84] (ZnTPP, a sample was kindly provided by Dr. Asha Brown) were also investigated as a control, in order to elucidate the contribution of the triazole-capping framework of receptor **25** on anion binding strength and selectivity. Monitoring the perturbations of the Soret band as a function of anion concentration gave the titration curves reported in Figure 2.28 for **25** and Figure 2.29 for ZnTPP and association constants for 1:1 stoichiometric complexes, determined using the Specfit® computer program,[70] are reported in Table 2.7.

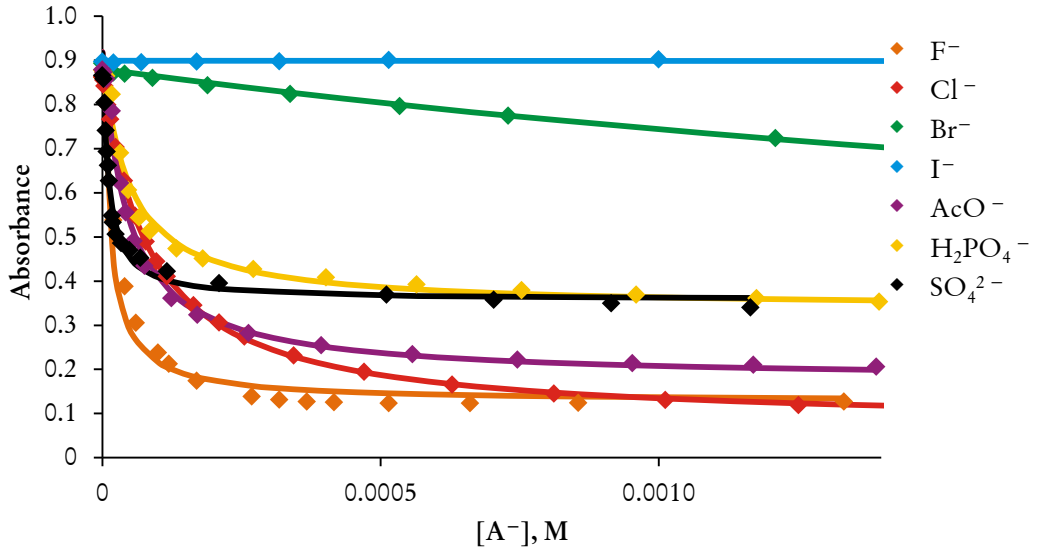


Figure 2.28. Titration curves for complex formation between porphyrin ***25*** *and various anions obtained by monitoring perturbations of the Soret band at 421 nm. Acetone, 293 K. Square data points represent experimental data; continuous lines represent theoretical binding isotherms.*

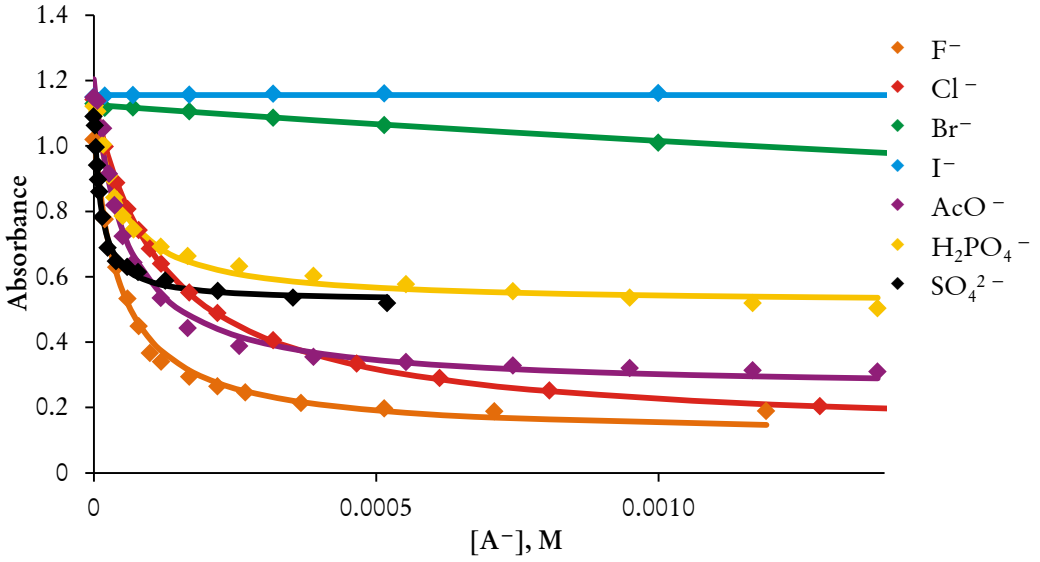


Figure 2.29 Titration curves for complex formation between ZnTPP and various anions obtained by monitoring perturbations of the Soret band at 420 nm. Acetone, 293 K. Square data points represent experimental data; continuous lines represent theoretical binding isotherms.

*Table 2.7. Association constants, K_a (M^{-1}), for 1:1 complexes of porphyrin-cage **25** and ZnTPP with various anions.*

Anion	**25** K_a (M^{-1})[a]	ZnTPP K_a (M^{-1})[a]
F^-	79 707 (8989)	20 850 (988)
Cl^-	12 191 (159)	8092 (318)
Br^-	255 (13)	149 (5)
I^-	<50	<50
AcO^-	22 202 (893)	18 971 (786)
$H_2PO_4^-$	21 657 (989)	23 691 (801)
SO_4^{2-}	100 785 (4858)	91 537 (2556)

[a]*All anions added as their TBA salt. Association constants were determined by monitoring the perturbations of the Soret band. Estimated standard errors are given in parentheses. Acetone, 293 K.*

Neutral cage host **25** was found to bind anions strongly in acetone with, in particular, large association constant values for fluoride and sulfate. Indeed, the receptor is shown to be selective for fluoride over other halide anions, despite its small size. This is likely to be a result of fluoride's greater basicity and possibly it is bound as the trihydrate complex. Receptor **25** exhibits low binding affinity for larger, more diffuse bromide and iodide anions. Sulfate is bound very strongly with an association constant an order of magnitude higher than for the other basic oxoanions, which is presumably a consequence of the sulfate anion's higher charge. Amongst the singly charged anions, the anion selectivity trend displayed by **25** in general correlates with anion basicity.

The data in Table 2.7 also highlight a significant increase in anion binding strength for cage receptor **25** compared with ZnTPP, particularly for fluoride and chloride, where additional hydrogen-bond-donating triazole units provide a complementary binding cleft for harder, spherical anions.

The anion recognition properties of the positively charged, tetra-triazolium zinc(II)-porphyrin-cage **26·$(PF_6)_4$** were also probed using UV/visible spectroscopy and the association constants for complex formation in 5% water:acetone are reported in Table 2.8. As anticipated, even in the presence of water, the tetracationic cage **26·$(PF_6)_4$** is a potent anion receptor. In this aqueous media the binding affinity of **26·$(PF_6)_4$** for fluoride and chloride is

of similar magnitude and is significantly larger than with bromide or iodide. All oxoanions are bound strongly in 5% water:acetone with **26·(PF$_6$)$_4$** exhibiting a clear preference for the dianionic sulfate anion guest species.

Table 2.8. Association constants, K_a *(M^{-1}), for 1:1 complexes of porphyrin host* ***26·(PF$_6$)$_4$*** *with various anions.*[a]

Anion	K_a (M^{-1}) 5% H_2O:acetone	K_a (M^{-1}) 15% H_2O:acetone
F^-	8666 (312)	[d]
Cl^-	7449 (112)	[d]
Br^-	<50	-
I^-	<50	-
AcO^-	134 214 (1060)	[b]
$H_2PO_4^-$	123 452 (12 221)	[b]
SO_4^{2-}	517 726 (73 517)	252 988 (1426)

[a]*All anions added as their TBA salt. Association constants were determined by monitoring the perturbations of the Soret band. Estimated standard errors are given in parentheses.* [b]*Soret band perturbations too small to determine an association constant.*

The optical anion sensing properties of **26·(PF$_6$)$_4$** were also assessed in 15% water:acetone for fluoride, chloride, acetate, dihydrogen phosphate and sulfate (Table 2.8). The caged receptor displays strong and selective sulfate binding whereas, with the singly charged anions, minimal perturbations of the Soret band were observed which suggests these anions are not bound in this more competitive aqueous solvent mixture.

2.3.4 Cation and ion-pair binding properties of neutral triazole-functionalised zinc(II)-metalloporphyrin-cage receptor

Triazole units are known to be ambidentate being able to bind anions at the polarised CH bond or transition metal cations at the nitrogen atoms. The ability of neutral triazole-porphyrin-cage **25** to complex metal ions silver(I) and copper(I) was studied through ^{1}H NMR spectroscopic titration experiments. The metal ions were added as their hexafluorophosphate salts to prevent any potential competition for counteranion species.

Addition of copper(I) to an acetone-d_6 solution of receptor **25** resulted in substantial changes to the ^{1}H NMR spectrum as shown in Figure 2.30. Downfield perturbation of the signal corresponding to the triazole proton *g* is observed, which is consistent with metal chelation at the nitrogen atoms. The concomitant downfield shifts of the methylene proton signals *h* and *f*, and upfield shift of cavity phenyl proton *e* are likely to be due to conformational changes upon cation coordination.

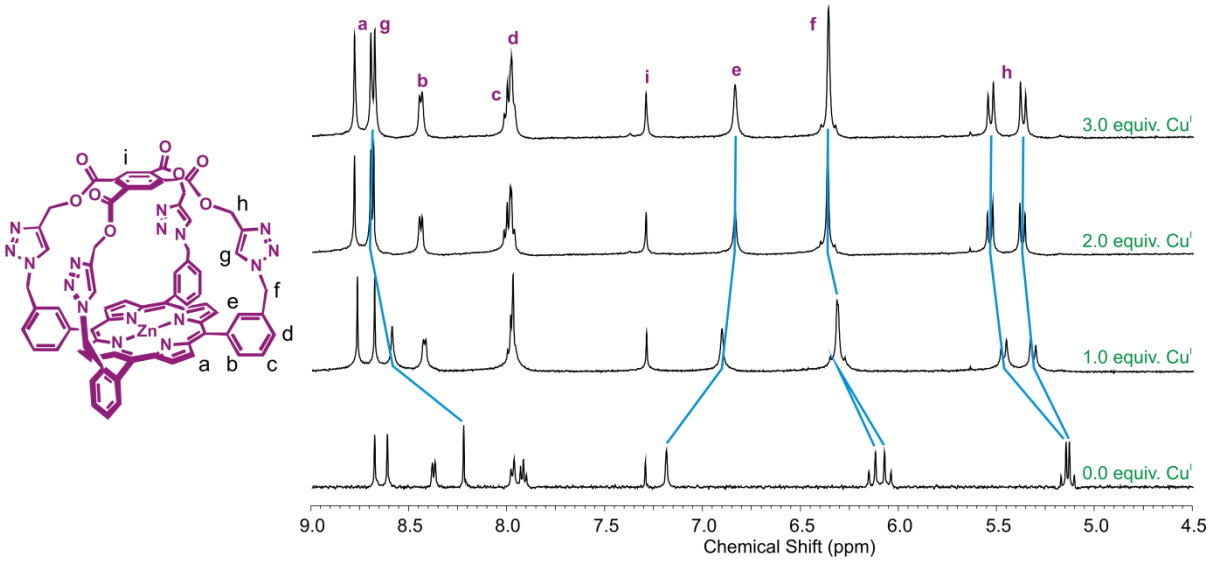


*Figure 2.30. Partial ^{1}H NMR spectra of receptor **25** upon addition of various equivalents of $[Cu(MeCN)_4]PF_6$ (500 MHz, acetone-d_6, 293 K).*

The titration curves for copper(I)- and silver(I)-addition to porphyrin cage **25** obtained by monitoring the changes in triazole proton chemical shift with increasing equivalents of cation are shown in Figure 2.31. It is interesting to note that the titration curves plateau after addition of one equivalent of silver(I) ions and two equivalents of copper(I) ions, which is indicative of the respective transition metal cation binding stoichiometries. Copper(I) is smaller than silver(I) (77 pm and 115 pm respectively for the hexaaqua complex)[85] and so is probably too small to allow for optimal complexation by all four triazole groups. Analysis of the titration data using the winEQNMR computer program gave association constants values $K_a > 10^4$ M^{-1} in both cases. The available data preclude the drawing of any conclusions about the naure of binding, although the 1:1 association of silver(I) may be consistent with cation association occuring within the cavity.

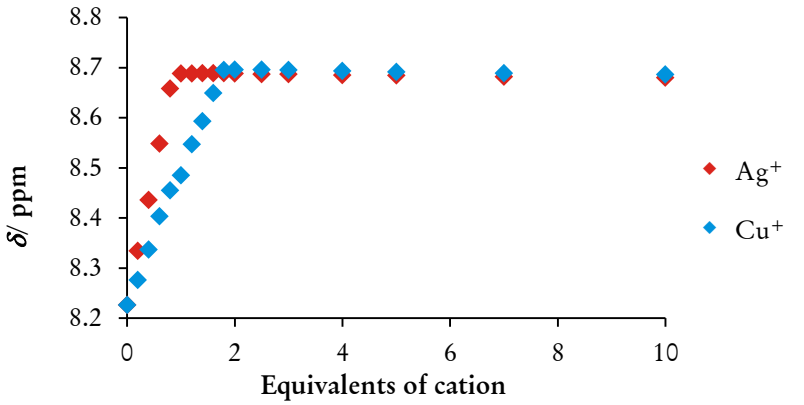


*Figure 2.31. Titration curves for complex formation between porphyrin **25** and Ag(I) or Cu(I) obtained by monitoring perturbations of the triazole proton signal* g. *(500 MHz, acetone-d_6, 293 K). Square data points represent experimental data.*

The possibility of enhanced anion sensing of a **25**:Cu(I) complex was investigated by UV/visible titrations in acetone. Aliquots of TBA chloride were added to an equimolar solution of **25** and copper(I)tetrakis-acetonitrile hexafluorophosphate and changes in the UV/visible spectrum were monitored. Specfit analysis of the titration data gave an apparent association constant value of K_a = 11 797(233) M^{-1}, substantially lower than in the absence of copper(I) ions. Chloride complexation is therefore less favourable in this system possibly as a result of copper–chloride ion-pairing or chloride association occurring outside the binding cavity. Complications arising from the preferential formation of a 1:2 receptor:copper(I) complex may also be significant.

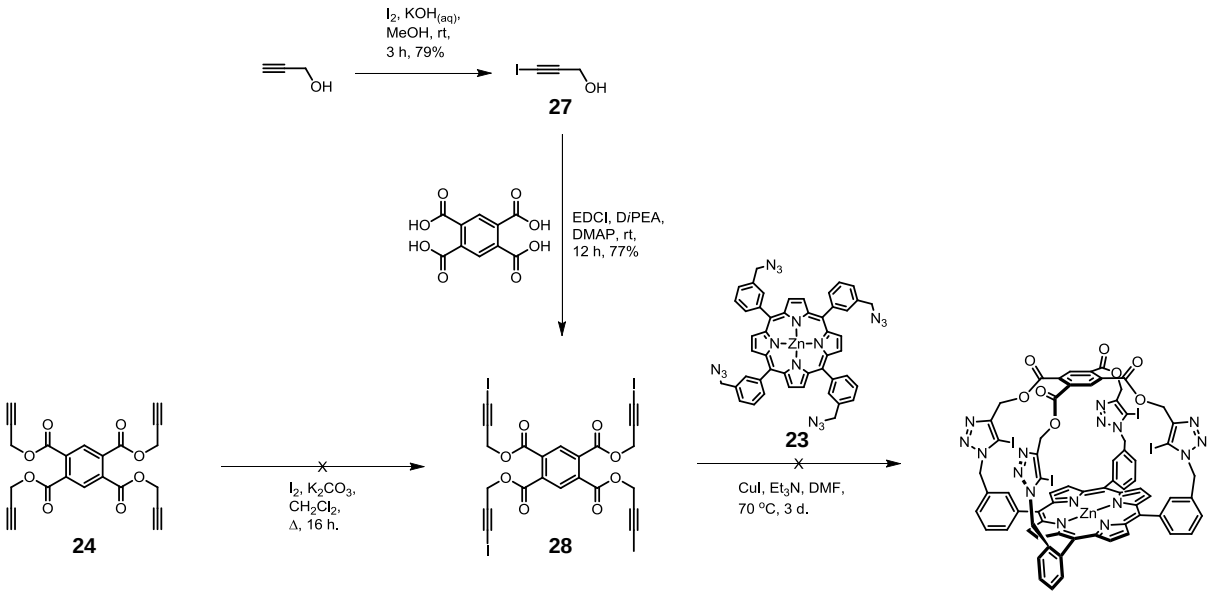
Alkali metal cations are well known to be strongly complexed by crown ether ligands. The four ester linkages of the cage receptor's capping group may be able to complex sodium or potassium in a similar manner. A ^{1}H NMR titration experiment with sodium cations was undertaken in acetone-d_6. With increasing equivalents of cationic guest, however, no changes to the ^{1}H NMR spectrum of **25** was observed, which indicates no sodium binding is occurring.

In summary, ^{1}H NMR and UV/visible titration experiments have demonstrated that triazole-porphyrin-cage receptor **25** is capable of strong cation or anion binding at the triazole units. Preliminary ion-pair binding studies with copper(I):**25** and chloride, however, suggest the caged cavity is too small for cooperative ion pair binding to occur.

2.3.5 Attempted synthesis of an iodotriazole-functionalised zinc(II)-metalloporphyrin-cage for anion recognition

Attempts to prepare an equivalent iodotriazole porphyrin cage system are outlined in Scheme 2.17.

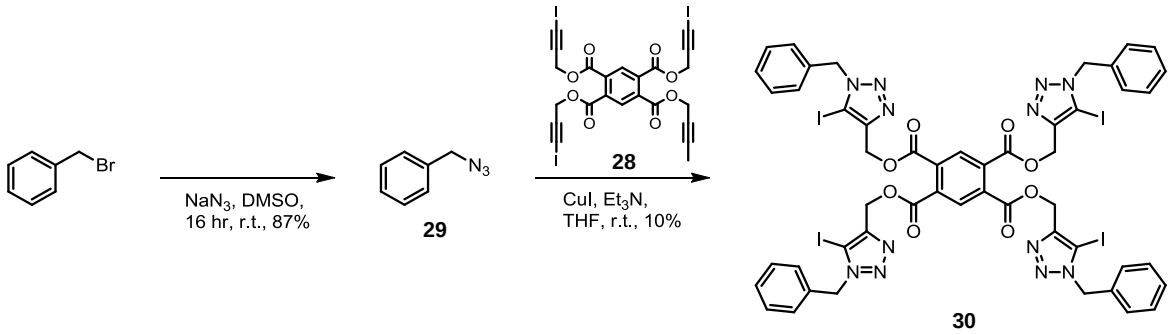
Initially, it was envisaged that a copper(I)-catalysed cycloaddition reaction (similar to that used to prepare iodotriazole-porphyrin species **10**) between azide-porphyrin **23** and an iodoalkyne-functionalised analogue of capping group **24** could be used to prepare the target iodotriazole-porphyrin-cage system.



*Scheme 2.17. Synthesis of iodoalkyne-functionalised capping group **28**, and attempted preparation of an iodotriazole-porphyrin-cage receptor.*

With a view to preparing an iodoalkyne-functionalised capping group, compound **24** and iodine were heated in the presence of base in dichloromethane. No evidence of iodoalkyne formation was observed however, possibly because a stronger base was needed. To avoid any possibility of ester hydrolysis in the presence of a strong base, 3-iodoprop-2-yn-1-ol **27** was first prepared in 79% yield by stirring propargyl alcohol, iodine and potassium hydroxide in methanol. Compound **27** was then coupled with 1,2,4,5-benzenetetracarboxylic acid using 1-ethyl-3-(3-dimethylaminopropyl)carbodiimde, *N*,*N*-di-*iso*-propylethylamine and 4-dimethylaminopyridine in dichloromethane to form the iodoalkyne-capping group **28** in 77% yield. A cycloaddition reaction between azido-porphyrin **23** and iodoalkyne derivative **28** in

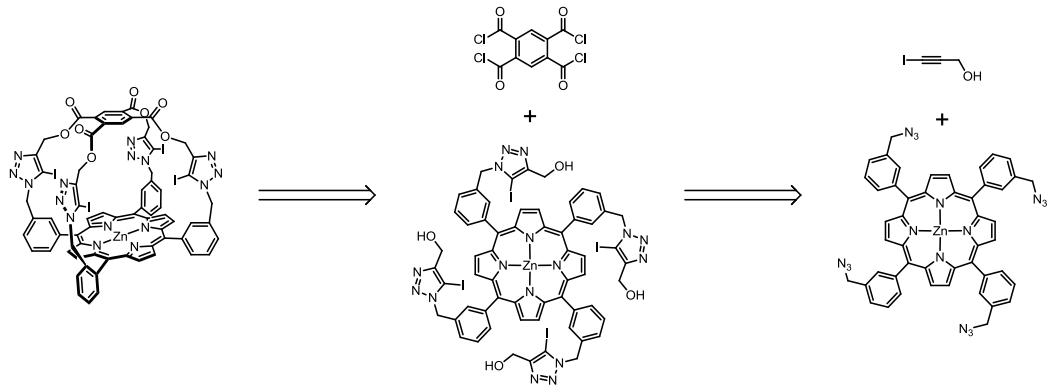
the presence of copper(I) iodide and triethylamine in dimethylformamide was then undertaken. After three days, however, analysis of the reaction mixture revealed only starting materials were present.



Scheme 2.18. Synthesis of model iodotriazole-functionalised capping group ***30****.*

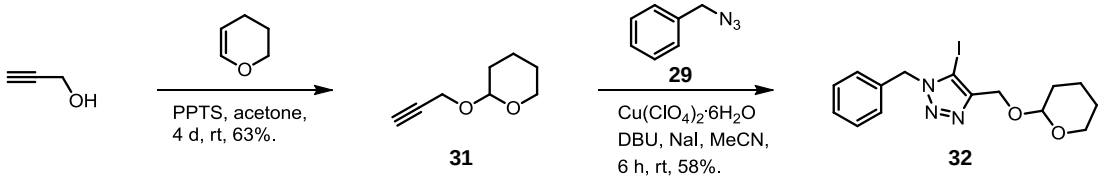
The ability of this new iodoalkyne-functionalised capping group to form iodotriazoles by copper(I)-catalysed cycloaddition reactions was investigated using benzyl azide as a model system (Scheme 2.18). Stirring tetra-iodoalkyne **28** with four equivalents of benzyl azide **29** in the presence of copper(I) iodide and triethylamine in tetrahydrofuran afforded the model tetrakis-iodotriazole compound **30** in 10% yield. Other fractions isolated were revealed to be tetra-triazole species with only one, two or three iodine atoms.

The low yield of this reaction together with the mixture of products formed prompted the consideration of an alternative synthetic route (Scheme 2.19). This approach required the formation of a precursor molecule with four iodotriazole-containing pendant arms from iodoalkyne **27** and azide porphyrin **23** which can then be capped with 1,2,4,5-benzenetetracarbonyl chloride.



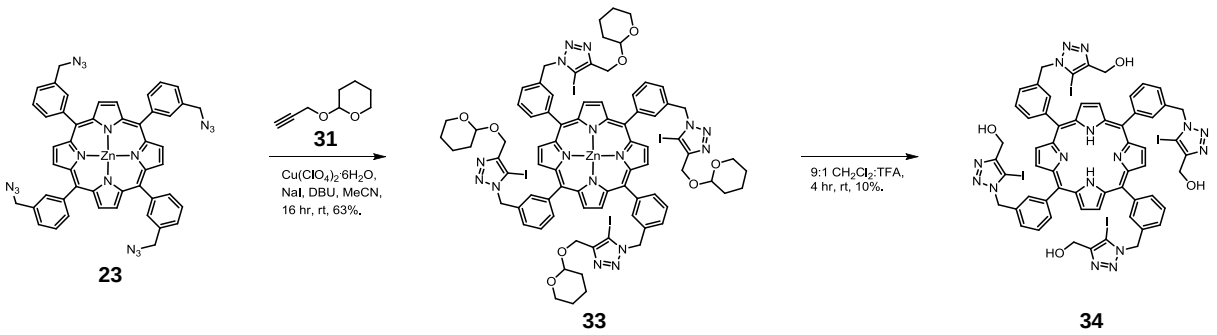
Scheme 2.19. Retro-synthesis of an iodotriazole-porphyrin-cage.

In the course of these synthetic investigations, a new route to iodotriazoles was reported by Brotherton and co-workers, which involves formation of the required iodoalkyne *in situ*.[86] A test reaction between benzyl azide and protected propargyl alcohol – to avoid any complications from the alcohol functionality – was undertaken (Scheme 2.20). Propargyl alcohol and pyridinium *p*-toluenesulfonate were dissolved in degassed acetone, 3,4-dihydro-2*H*-pyran was added and after stirring for four days at room temperature THP-protected propargyl alcohol **31** was isolated in 63% yield. This was then stirred with benzyl azide **29**, in the presence of sodium iodide, copper(II) perchlorate and 1,8-diazabicycloundec-7-ene in acetonitrile and after purification, the model system **32** was isolated in 58% yield.



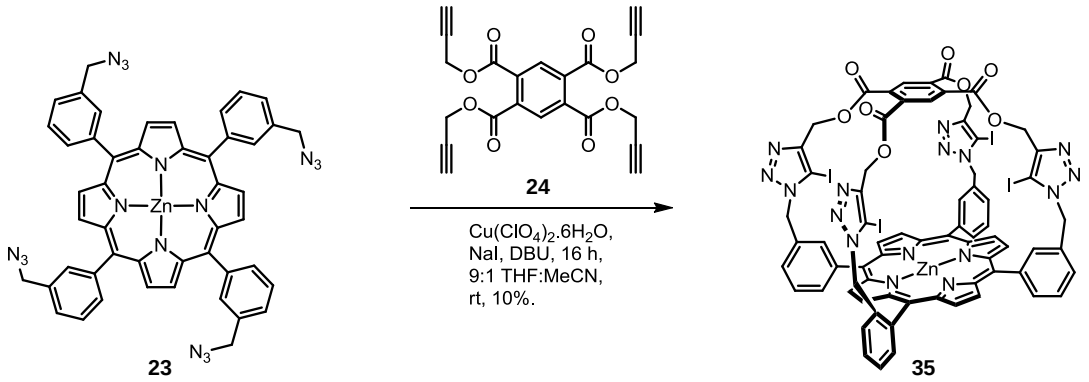
*Scheme 2.20. Synthesis of a model iodotriazole-containing species **32**.*

Encouraged by the success of this model compound synthesis, an analogous reaction with azide porphyrin **23** was pursued (Scheme 2.21). Compound **23** and THP-protected propargyl alcohol **31** were stirred together in the presence of copper(I) perchlorate, sodium iodide and 1,8-diazabicycloundec-7-ene and following purification tetra-iodotriazole-porphyrin **33** was isolated in 63% yield. Attempts to remove the THP protecting group trifluoroacetic acid in dichloromethane, however, afforded only a small amount of deprotected iodotriazole porphyrin **34** in overall 10% yield, which was considered too low for subsequent reactions.



Scheme 2.21. Synthesis of an iodotriazole-functionalised porphyrin species.

A final attempt to prepare the target iodotriazole-functionalised cage receptor was undertaken using the reaction conditions newly reported by Brotherton[86] – in a direct reaction between azido-porphyrin **23** and alkyne-functionalised capping group **24** (Scheme 2.22). Stirring zinc(II)-metalloporphyrin **23** and compound **24** with sodium iodide, copper(I) perchlorate and 1,8-diazabicycloundec-7-ene in 9:1 tetrahydrofuran:acetonitrile produced a small amount of the target halogen-bonding porphyrin-cage **35** in 10% isolated yield.



*Scheme 2.22. Synthesis of target iodotriazole-containing porphyrin cage **35**.*

2.3.6 Characterisation of an iodotriazole-functionalised zinc(II)-metalloporphyrin-cage anion receptor

Iodotriazole-porphyrin-cage **35** was characterised by ^{1}H NMR spectroscopy and high resolution mass spectrometry. The molecular ion peak at m/z = 1828.8728 is readily observed, the high-resolution mass spectrum revealing the isotopic distribution of the porphyrin-cage species is in good agreement with the theoretical spectrum.

In chloroform-d solution, at room temperature, the ^{1}H NMR spectrum of compound **35** is surprisingly broad possibly owing to aggregation of porphyrin molecules in solution. The

spectrum (Figure 2.32) reveals all the salient proton environments of this species; most notably the absence of a signal corresponding to any triazole protons. The low yield and limited supply of porphyrin **35** prevented any extensive, in depth anion binding titration experiments from being undertaken.

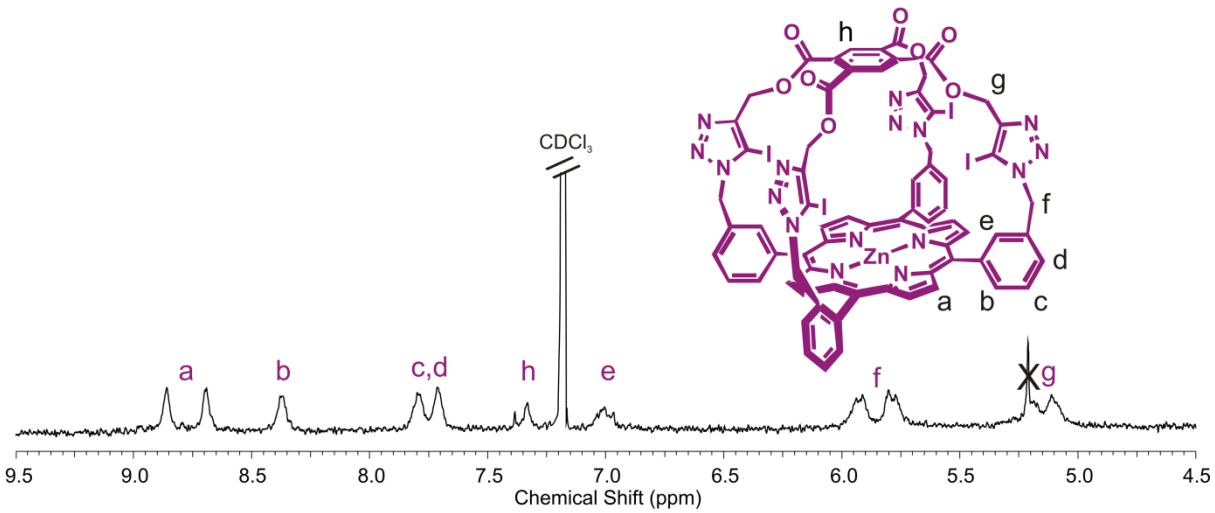


*Figure 2.32. Partial ^{1}H NMR spectrum of iodotriazole-porphyrin-cage **35** showing peak assignments (500 MHz, $CDCl_3$, 293 K).*

2.4 Conclusions and future work

Four novel triazole- and triazolium-containing zinc(II)-metalloporphyrin-based acyclic anion receptors were prepared and their anion recognition and sensing properties studied. Importantly, the halogen-bonding iodotriazole-porphyrin-based anion host displayed halide anion binding affinities which were substantially larger than the protic-functionalised hydrogen-bonding analogue and a reduced strength of acetate oxoanion complexation. The effect of solvent on halogen bonding *versus* hydrogen bonding was also investigated, which revealed the strength of anion recognition correlated with the hydrogen-bond-donor ability of the solvent, the Gutmann acceptor number. The enhancement of anion binding affinity by the halogen-bonding receptor was more pronounced in acetonitrile (AN = 18.9) than chloroform (AN = 23.1). Alkylation to form the related triazolium- and iodotriazolium-porphyrin compounds was achieved. These positively charged host systems exhibited stronger binding in more competitive solvent and similar trends in anion binding properties to those of the neutral triazole systems were also observed.

Two cyclic triazole- and triazolium-porphyrin-cage anion receptors were also successfully prepared for anion recognition and sensing purposes. A neutral triazole-porphyrin-cage receptor was revealed to be a potent colorimetric anion sensor allowing naked-eye detection of the anion binding event. The anion binding ability of a related positively charged triazolium-porphyrin-cage species was investigated and the receptor was able to sense anions in competitive aqueous solvent media and displayed an impressive selectivity for sulfate in a 15% water/acetone solvent mixture. The ambidentate nature of the triazole moiety was also explored: receptor **25** strongly complexed both silver(I) and copper(I) metal cations although it was unable to effect strong, cooperative ion-pair binding.

Finally, an iodotriazole-containing porphyrin-cage compound was also prepared but the low reaction yield precluded comparable anion association data from being obtained.

Initial future work could involve varying the Lewis-acidic metal complexed within the porphyrin macrocycle and the effect on the hydrogen- and halogen-bonding receptors' anion recognition properties investigated.

The nature of the capping group within the porphyrin-cage systems **25** and **26·$(PF_6)_4$** could potentially be varied. For example, by incorporating amide anion recognition units within the molecular framework, the hosts' anion binding strength and selectivity may be enhanced. Furthermore, integrating proven cation-binding units or increasing the size of the caged host system through the use of larger capping groups may enable ion-pair binding to occur.

2.5 References for Chapter Two

[1] W. Küster, *Hoppe-Seyler's Z. Physiol. Chem.*, 1912, **82**, 463.
[2] L. Patrick, *Altern, Med. Rev.*, 2006, **11**, 2-22.
[3] L. Patrick, *Altern, Med. Rev.*, 2006, **11**, 114-127.
[4] J. Dalton, L. R. Milgrom and R. Bonnett, *Chem. Phys. Lett.*, 1979, **61**, 242-244.
[5] H. Lehman and R. G. Huntsman, 1974, 144.
[6] L. R. Milgrom, in *The Colours of Life: An Introduction to the Chemistry of Porphyrins and Related Compounds*, Oxford University Press, Oxford, 1997, p. 186-190.
[7] L. Eals, in *The Porphyrins*, ed. D. Dolphin, 1978, vol. 6.
[8] L. R. Milgrom, in *The Colours of Life: An Introduction to the Chemistry of Porphyrins and Related Compounds*, Oxford University Press, Oxford, 1997, p. 14.
[9] L. R. Milgrom, in *The Colours of Life: An Introduction to the Chemistry of Porphyrins and Related Compounds*, Oxford University Press, Oxford, 1997, p. 182.

[10] C. E. Castro, in *The Porphyrins*, 1978, vol. 5, p. 18.
[11] J. B. West, *Respiratory Physiology - the essentials*, Lippincott, Williams & Wilkins, 2012, p. 82.
[12] D. C. Hodgkin, J. Kamper, M. Mackay, J. Pickworth, K. N. Trueblood and J. G. White, *Nature*, 1956, **178**, 64-66.
[13] T. L. Poulos, B. C. Finzel and A. J. Howard, *J. Mol. Biol.*, 1987, **195**, 687-700.
[14] J. C. Kendrew, G. Bodo, H. M. Dintzis, R. G. Parrish, H. Wyckoff and D. C. Phillips, *Nature*, 1958, **181**, 662-666.
[15] L. R. Milgrom, in *The Colours of Life: An Introduction to the Chemistry of Porphyrins and Related Compounds*, Oxford University Press, Oxford, 1997, p. 19.
[16] L. R. Milgrom, in *The Colours of Life: An Introduction to the Chemistry of Porphyrins and Related Compounds*, Oxford University Press, Oxford, 1997, p. 178-190.
[17] *The Oxford English Dictionary*, 2nd edn., Clarendon Press, Oxford, 1989, p. 138-140.
[18] F. Sondheimer, R. Wolovsky and Y. Amiel, *J. Am. Chem. Soc.*, 1962, **84**, 274-284.
[19] E. Vogel, *J. Heterocycl. Chem.*, 1996, **33**, 1461-1487.
[20] T. D. Lash, *Eur. J. Org. Chem.*, 2007, **2007**, 5461-5481.
[21] M. Gouterman, *J. Mol. Spectrosc.*, 1961, **6**, 138-163.
[22] *The Porphyrins* Ed. M. Gouterman, Academic Press, New York, 1978, vol. 3.
[23] L. R. Milgrom, in *The Colours of Life: An Introduction to the Chemistry of Porphyrins and Related Compounds*, Oxford University Press, Oxford, 1997, p. 65-98.
[24] L. R. Milgrom, in *The Colours of Life: An Introduction to the Chemistry of Porphyrins and Related Compounds*, Oxford University Press, Oxford, 1997, p. 191-243.
[25] *The Porphyrin Handbook* Ed. K. M. Kadish, K. M. Smith and R. Guilard, Academic Press, 2000, vol. 6.
[26] M. Ethirajan, Y. Chen, P. Joshi and R. K. Pandey, *Chem. Soc. Rev.*, 2011, **40**, 340-362.
[27] http://www.rxlist.com/visudyne-drug.htm.
[28] http://www.cysview.net/.
[29] http://www.rxlist.com/photofrin-drug.htm.
[30] L. R. Milgrom, in *The Colours of Life: An Introduction to the Chemistry of Porphyrins and Related Compounds*, Oxford University Press, Oxford, 1997, p. 201-227.
[31] J. P. Collman, J. T. McDevitt, K. Kim, J. M. Garner, M. B. Zisk, C. R. Leidner, G. T. Yee, J. W. Prodolliet and W. A. Little, in *Organic Superconductivity*, eds. V. Z. Kresin and W. A. Little, Plenum Press, New York, p. 359-366.
[32] D. W. Bruce, D. A. Dunmur, L. S. Santa and M. A. Wali, *J. Mater. Chem.*, 1992, **2**, 363-364.
[33] L. R. Milgrom, in *The Colours of Life: An Introduction to the Chemistry of Porphyrins and Related Compounds*, Oxford University Press, Oxford, 1997, p. 238-242.
[34] L. R. Milgrom, in *The Colours of Life: An Introduction to the Chemistry of Porphyrins and Related Compounds*, Oxford University Press, Oxford, 1997, p. 216-230.
[35] A. H. Jackson, in *The Porphyrins*, 1978, vol. 1, p. 374.
[36] H. L. Anderson and J. K. M. Sanders, *J. Chem. Soc., Chem. Commun.*, 1992, 946-947.
[37] H. L. Anderson and J. K. M. Sanders, *J. Chem. Soc., Chem. Commun.*, 1989, 1714-1715.
[38] J. L. Sessler, M. J. Cyr, V. Lynch, E. McGhee and J. A. Ibers, *J. Am. Chem. Soc.*, 1990, **112**, 2810-2813.
[39] M. Shionoya, H. Furuta, V. Lynch, A. Harriman and J. L. Sessler, *J. Am. Chem. Soc.*, 1992, **114**, 5714-5722.
[40] V. Král, H. Furuta, K. Shreder, V. Lynch and J. L. Sessler, *J. Am. Chem. Soc.*, 1996, **118**, 1595-1607.
[41] B. L. Iverson, K. Shreder, V. Kral and J. L. Sessler, *J. Am. Chem. Soc.*, 1993, **115**, 11022-11023.
[42] M. Nappa and J. S. Valentine, *J. Am. Chem. Soc.*, 1978, **100**, 5075-5080.
[43] A. S. Hinman and B. J. Pavelich, *J. Electroanal. Chem.*, 1989, **269**, 53-61.
[44] C. Bucher, C. H. Devillers, J. C. Moutet, G. Royal and E. Saint-Aman, *New J. Chem.*, 2004, **28**, 1584-1589.
[45] M. Dudic, P. Lhotak, I. Stibor, K. Lang and P. Proskova, *Org. Lett.*, 2003, **5**, 149-152.
[46] S. D. Starnes, S. Arungundram and C. H. Saunders, *Tetrahedron Lett.*, 2002, **43**, 7785-7788.
[47] P. D. Beer, M. G. B. Drew, D. Hesek and R. Jagessar, *J. Chem. Soc., Chem. Commun.*, 1995, 1187-1189.
[48] R. C. Jagessar, M. Y. Shang, W. R. Scheidt and D. H. Burns, *J. Am. Chem. Soc.*, 1998, **120**, 11684-11692.

[49] C. Lee, D. H. Lee and J. I. Hong, *Tetrahedron Lett.*, 2001, **42**, 8665-8668.
[50] P. D. Beer, D. P. Cormode and J. J. Davis, *Chem. Commun.*, 2004, 414-415.
[51] D. P. Cormode, S. S. Murray, A. R. Cowley and P. D. Beer, *Dalton Trans.*, 2006, 5135-5140.
[52] D. P. Cormode, M. G. B. Drew, R. Jagessar and P. D. Beer, *Dalton Trans.*, 2008, 6732-6741.
[53] P. D. Beer, M. G. B. Drew and R. Jagessar, *J. Chem. Soc., Dalton Trans.*, 1997, 881-886.
[54] H. C. Kolb, M. G. Finn and K. B. Sharpless, *Angew. Chem. Int. Ed.*, 2001, **40**, 2004-2021.
[55] B. T. Worrell, J. A. Malik and V. V. Fokin, *Science*, 2013, **340**, 457-460.
[56] Y. J. Li and A. H. Flood, *Angew. Chem. Int. Ed.*, 2008, **47**, 2649-2652.
[57] H. Juwarker, J. M. Lenhardt, D. M. Pham and S. L. Craig, *Angew. Chem. Int. Ed.*, 2008, **47**, 3740-3743.
[58] R. M. Meudtner and S. Hecht, *Angew. Chem. Int. Ed.*, 2008, **47**, 4926-4930.
[59] A. Kumar and P. S. Pandey, *Org. Lett.*, 2007, **10**, 165-168.
[60] B. Schulze, C. Friebe, M. D. Hager, W. Günther, U. Köhn, B. O. Jahn, H. Görls and U. S. Schubert, *Org. Lett.*, 2010, **12**, 2710-2713.
[61] J. E. Hein, J. C. Tripp, L. B. Krasnova, K. B. Sharpless and V. V. Fokin, *Angew. Chem. Int. Ed.*, 2009, **48**, 8018-8021.
[62] N. L. Kilah, M. D. Wise, C. J. Serpell, A. L. Thompson, N. G. White, K. E. Christensen and P. D. Beer, *J. Am. Chem. Soc.*, 2010, **132**, 11893-11895.
[63] B. H. M. Kuijpers, G. C. T. Dijkmans, S. Groothuys, P. Quaedflieg, R. H. Blaauw, F. L. van Delft and F. Rutjes, *Synlett*, 2005, 3059-3062.
[64] T. N. Sorrell, *Inorg. Synth.*, 1980, **20**, 161.
[65] J. P. Collman, R. R. Gagne, C. Reed, T. R. Halbert, G. Lang and W. T. Robinson, *J. Am. Chem. Soc.*, 1975, **97**, 1427-1439.
[66] J. Lindsey, *J. Org. Chem.*, 1980, **45**, 5215-5215.
[67] J. P. Collman, B. Boitrel, L. Fu, J. Galanter, A. Straumanis and M. Rapta, *J. Org. Chem.*, 1997, **62**, 2308-2309.
[68] J. Leroy, *Synth. Commun.*, 1992, **22**, 567-572.
[69] M. J. Hynes, *J. Chem. Soc., Dalton Trans.*, 1993, 311-312.
[70] *Specfit v. 2.02 ed*, Spectrum Software Associates Chapel Hill, NC, USA.
[71] M. G. Chudzinski, C. A. McClary and M. S. Taylor, *J. Am. Chem. Soc.*, 2011, **133**, 10559-10567.
[72] U. Mayer, V. Gutmann and W. Gerger, *Monatshefte für Chemie / Chemical Monthly*, 1975, **106**, 1235-1257.
[73] P. D. Beer and M. Shade, *Chem. Commun.*, 1997, **0**, 2377-2378.
[74] D. C. Kennedy, C. S. McKay, M. C. B. Legault, D. C. Danielson, J. A. Blake, A. F. Pegoraro, A. Stolow, Z. Mester and J. P. Pezacki, *J. Am. Chem. Soc.*, 2011, **133**, 17993-18001.
[75] S. G. Alvarez and M. T. Alvarez, *Synthesis-Stuttgart*, 1997, 413-414.
[76] J. E. A. Webb, F. Maharaj, I. M. Blake and M. J. Crossley, *Synlett*, 2008, 2147-2149.
[77] V. D. Bock, H. Hiemstra and J. H. van Maarseveen, *Eur. J. Org. Chem.*, 2006, 51-68.
[78] L. Q. Wen, M. Li and J. B. Schlenoff, *J. Am. Chem. Soc.*, 1997, **119**, 7726-7733.
[79] J. S. Lindsey and R. W. Wagner, *J. Org. Chem.*, 1989, **54**, 828-836.
[80] B. C. Bookser and T. C. Bruice, *J. Am. Chem. Soc.*, 1991, **113**, 4208-4218.
[81] M. Nappa and J. S. Valentine, *J. Am. Chem. Soc.*, 1978, **100**, 5075-5080.
[82] A. D. Adler, F. R. Longo, Finarell.Jd, Goldmach.J, J. Assour and Korsakof.L, *J. Org. Chem.*, 1967, **32**, 476.
[83] G. H. Barnett, M. F. Hudson and K. M. Smith, *J. Chem. Soc., Perk. Trans. 1*, 1975, 1401-1403.
[84] M. Pineiro, A. L. Carvalho, M. M. Pereira, A. Gonsalves, L. G. Arnaut and S. J. Formosinho, *Chem. Eur. J.*, 1998, **4**, 2299-2307.
[85] R. D. Shannon, *Acta Crystallogr. A*, 1976, **32**, 751-767.
[86] W. S. Brotherton, R. J. Clark and L. Zhu, *J. Org. Chem.*, 2012, **77**, 6443-6455.

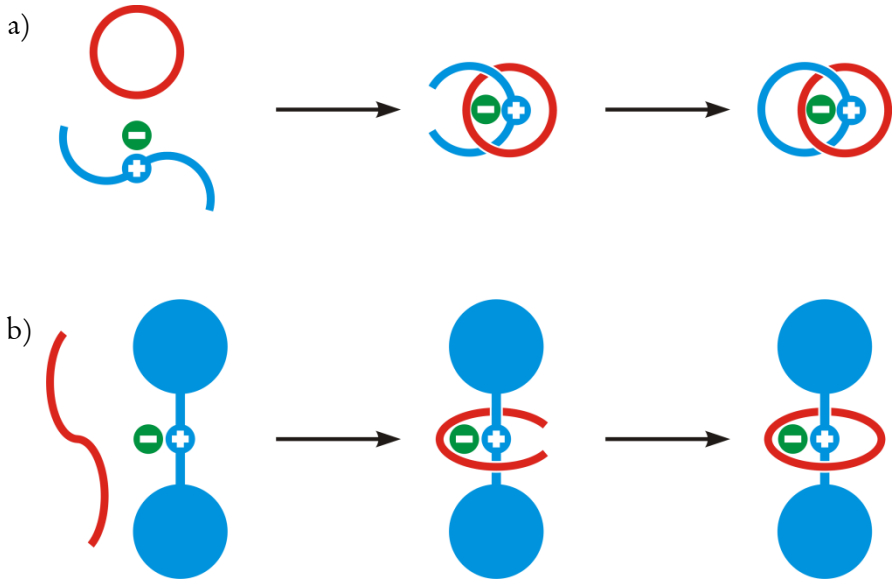
Chapter Three

Chapter 3 Halogen-bonding threading components for anion-templated and halogen-bond-templated interpenetrated and interlocked structures

3.1 Introduction

3.1.1 The construction of interlocked structures

Interlocked molecules have captured chemists' imagination owing to their non-trivial topology and the promise of their potential nanotechnological uses as molecular machines,[1-3] and in chemical sensor applications.[4-8] The synthesis of such sophisticated architectures is a challenge and as a consequence this has necessitated the implementation of imaginative cation, anion and neutral templation methodologies (Chapter One).



Scheme 3.1. Cartoon representation of the discrete anion templation methodologies for the assembly of catenanes (a) and rotaxanes (b).

Over the past decade, Beer and co-workers have developed *discrete anion templation* approaches for the anion-templated assembly of interpenetrated and interlocked structures (Scheme 3.1).[9] The general strategy requires the preparation of a positively charged threading component which can form a tight ion-pair with the templating anion by a combination of

electrostatics and hydrogen bonding. Crucially, this templating anion is coordinatively unsaturated and can associate with a second anion recognition unit, which may be part of a macrocyclic (forming a pseudorotaxane) or an acyclic component (forming an orthogonal array), and a subsequent cyclisation reaction follows to produce the related interlocked species.

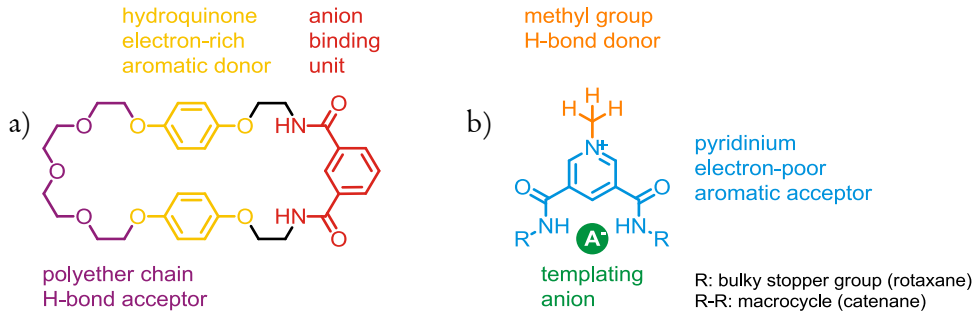


Figure 3.1. a) Macrocycle and b) ion-pair threading components highlighting important motifs for stable inter-component assembly.

The assembly of the interpenetrative or interlocked structure is driven by anion templation, although secondary non-covalent interactions are also important in stabilising the multi-component assembly (Figure 3.1). In particular, hydroquinone units are often incorporated into the macrocyclic component, providing electron-rich surfaces which form strong aromatic donor–acceptor interactions with electron-poor, positively charged aromatic regions on the threading component. Additional stabilisation may arise from hydrogen-bonding interactions between the oxygen atoms of a macrocycle's polyether linkage and the *N*-methyl pyridinium group of the ion-pair threading component.

3.1.2 Halogen bonding for interpenetrated and interlocked structure assembly

A range of macrocycle and threading components incorporating various anion recognition groups have since been designed and which use a combination of complementary electrostatic and hydrogen-bonding interactions for anion-templated component assembly. Halogen bonding is the attractive, highly directional, non-covalent interaction between an electron-deficient halogen atom and a Lewis base.[10] The scope of halogen bonding in solid state crystal engineering has been intensively explored for a number of years.[11-16] In spite of the

complementary analogy to ubiquitous hydrogen bonding, however, it is only in recent times that investigations into the application of solution phase halogen-bonding interactions to molecular recognition processes, self-assembly and catalysis have resulted in this field developing rapidly.[17-23] Indeed, in conjunction with anion templation, halogen bonding has been exploited recently to assemble interpenetrated and interlocked molecular frameworks (Figure 3.2).[18-20]

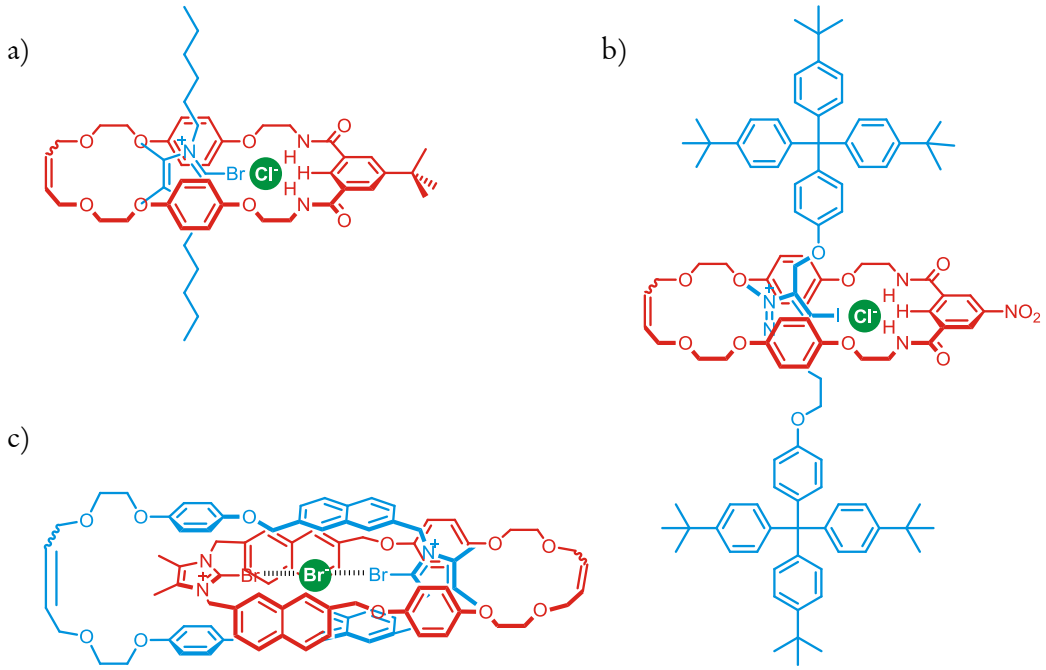


Figure 3.2 Halogen-bonding anion-templated interpenetrated and interlocked structures: a) a bromoimidazolium-based pseudorotaxane; b) an iodotriazolium-containing rotaxane; and c) a bromoimidazolium-based catenane.

In 2010, Beer and co-workers reported the first anion-templated interpenetrated pseudorotaxane assembly to be stabilised by halogen bonding.[19] A bromo-functionalised imidazolium derivative was threaded through an isophthalamide-containing macrocycle by a chloride-anion template (Figure 3.2a). Furthermore, the bromoimidazolium pseudorotaxane architecture was found to be more stable than the equivalent hydrogen-bonded assembly formed from an analogous protic imidazolium threading component (K_a = 254 M^{-1} and 97 M^{-1} respectively in chloroform-d solution). The isolation of the related interlocked rotaxane structure, however, was never successfully achieved.

As outlined in Chapter Two, Beer and co-workers employed a facile CuAAC synthetic strategy for preparing 5-iodo-1,4,5-trisubstituted-1,2,3-triazoles to construct a stoppered-axle with an integrated 5-iodotriazolium unit. The related rotaxane (Figure 3.2b) was the first reported interlocked structure to be assembled using halogen bonding in conjunction with anion-templation, and displayed vastly improved anion recognition properties in comparison with the hydrogen-bonding analogue: for bromide $K_a = >10^4\ M^{-1}$, compared with $K_a = 970\ M^{-1}$ in 1:1 chloroform-d/methanol-d_4.[18] In addition, in aqueous solvent the iodotriazolium rotaxane was found to bind halides in the order iodide > bromide > chloride a reversal of that expected on anion basicity grounds.

The first halogen-bonding catenane was also prepared by Beer and co-workers and is shown in Figure 3.2c. The bromoimidazolium-containing interlocked species recognises chloride and bromide anions in acetonitrile solely by halogen-bonding interactions and the incorporation of naphthalene units enabled optical anion sensing to be achieved.

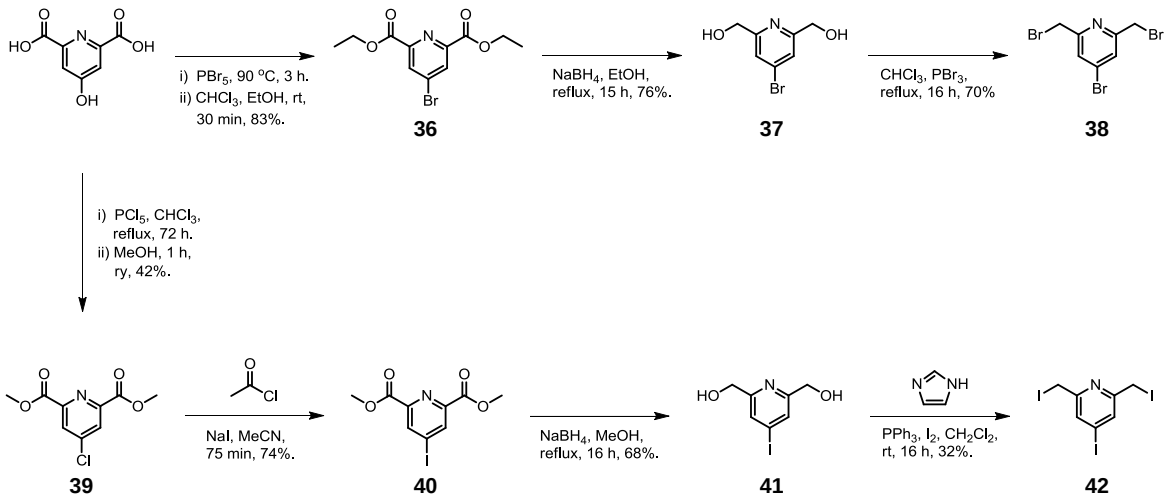
3.1.3 Chapter aims

In addition to triazolium and imidazolium anion-recognition groups, pyridinium units have been widely used in the effective construction of anion-templated interlocked assemblies. To date, however, no functionalised pyridinium-based halogen-bond donors for anion recognition have been reported. The research outlined in this chapter initially focused on the preparation of new bromo- and iodo-functionalised pyridinium-containing threading components as well as a protic analogue. The early sections of this chapter concentrate on attempts to exploit halogen bonding in the anion-templated assembly of interpenetrated and interlocked structures between halogen-bond-donor pyridinium threading components and an isophthalamide-based macrocycle. Work towards the formation of pseudorotaxane, rotaxane and catenane assemblies which are stabilised through intercomponent halogen-bond formation, in the absence of any anion templating effects, is then outlined and compared to the hydrogen-bond-templated counterpart. Finally, molecular switches which operate through halogen- and/or hydrogen-bonding interactions are also targeted.

3.2 Anion-templated interpenetrated and interlocked structures exploiting halogen bonding

3.2.1 Synthesis of halo-functionalised pyridinium threading components

The halopyridinium threading components were prepared as outlined in Schemes 3.2 and 3.3. 4-Halopyridinium derivatives were initially targeted as important intermediate compounds which could then be functionalised as required.

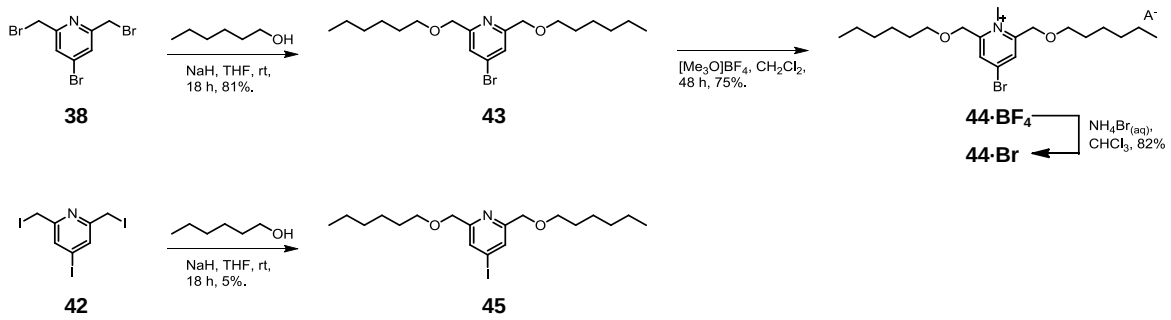


*Scheme 3.2. Synthesis of important intermediate halopyridinium compounds **38** and **42**.*

4-Bromo-2,6-bis(bromomethyl)pyridine **38** was prepared according to literature procedures.[24] Heating chelidamic acid hydrate and phosphorous pentabromide gave compound **36** in 83% yield. The ester functionalities were reduced using sodium borohydride in ethanol and a Soxhlet extraction afforded compound **37** in 76% yield. Bromination to give 4-bromo-2,6-bis(bromomethyl)pyridine **38** was achieved using phosphorous tribromide in chloroform in 70% yield.

4-Iodo-2,6-bis(bromomethyl)pyridine **42** was prepared by a similar route. Chelidamic acid hydrate and phosphorous pentachloride were heated in chloroform giving compound **39** in 42% yield. Chlorine–iodine exchange was carried out in 74% yield by sonicating an acetonitrile solution of compound **39** in the presence of sodium iodide and acetyl chloride.[25] Compound **40** was reduced in 68% yield with sodium borohydride in methanol. Finally, stirring bis-hydroxyl-functionalised 4-iodopyridine **41** and iodine in the presence of imidazole

and triphenylphosphine in dichloromethane afforded 4-iodo-2,6-bis(bromomethyl)pyridine **42** in 32% yield.



38 **43** **44·BF$_4$** **44·Br** **42** **45**

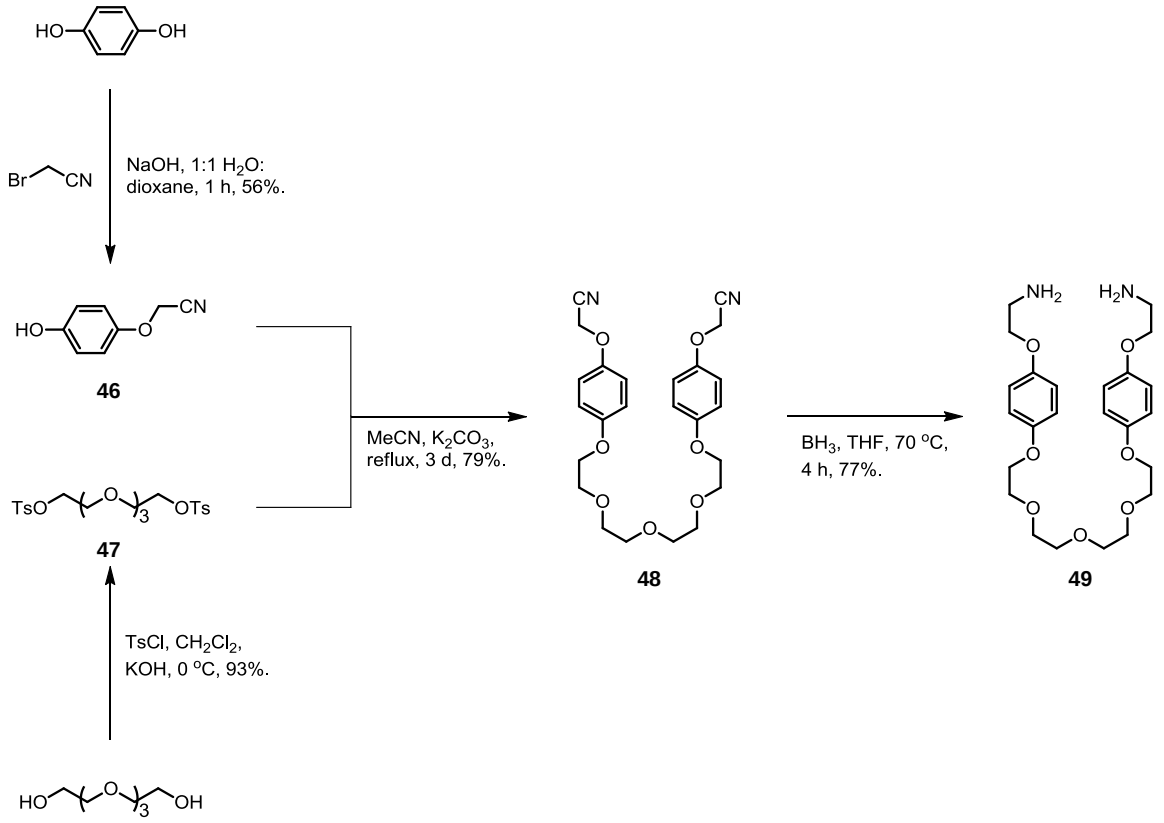
*Scheme 3.3. Synthesis of 4-bromopyridinium threading component **44·A**.*

Functionalisation with alkyl groups to produce suitable threading components was then undertaken (Scheme 3.3). A nucleophilic substitution reaction between 4-bromo-2,6-bis(bromomethyl)pyridine **38** and two equivalents of 1-hexanol in the presence of sodium hydride in tetrahydrofuran afforded compound **43** in 81% yield. Methylation of **43** using trimethyloxonium tetrafluoroborate in dichloromethane was successfully achieved and the bromopyridinium compound **44·BF$_4$** isolated in 75% yield. Exchanging the non-coordinating tetrafluoroborate anion for a chloride anion template by repeated washing of a chloroform solution of compound **44·BF$_4$** with aqueous ammonium chloride was attempted. Some evidence of bromine–chlorine exchange was observed by mass spectrometry and ^{1}H NMR spectroscopy, however, so anion exchange to the bromide salt was instead undertaken and compound **44·Br** obtained in 82% yield.

The preparation of the analogous iodopyridinium threading compound was also attempted. Stirring 4-iodo-2,6-bis(bromomethyl)pyridine **42** and two equivalents of 1-hexanol in the presence of sodium hydride in tetrahydrofuran produced the required bis-alkyl-functionalised 4-iodopyridine species **45** which was isolated in only 5% yield. As a result of this low yield, anion-templated pseudorotaxane studies exploiting halogen bonding focused on the bromopyridinium threading component.

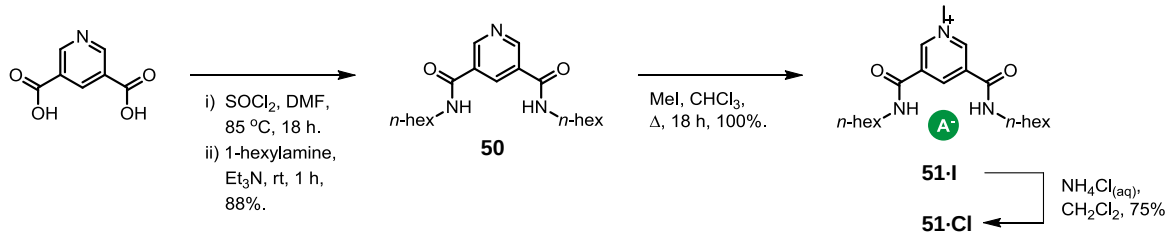
3.2.2 Synthesis of macrocycle components

In order to study the ability of halogen bonding to stabilise interpenetrated assemblies, a suitable isophthalamide-containing macrocycle was prepared which has been demonstrated to be capable of forming anion-templated assemblies with pyridinium-3,5-bis-amide threading components. The target macrocycle **52** was synthesised via a known template procedure[26] as summarised in Schemes 3.4 and 3.6.



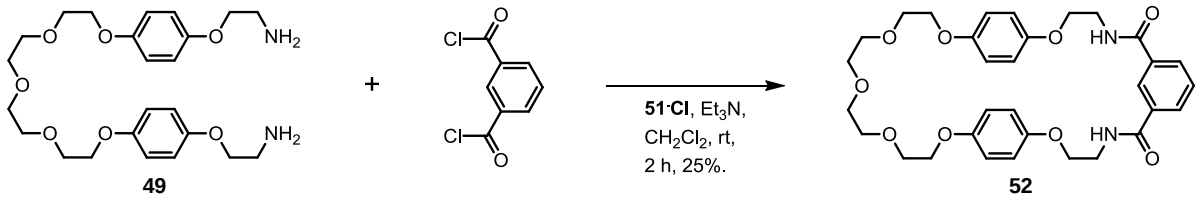
*Scheme 3.4. Synthesis of macrocycle precursor compound **49**.*

Hydroquinone was monofunctionalised using bromoacetonitrile and sodium hydroxide in a 1:1 water:dioxane solvent mixture to give compound **46** in 56% yield. Tosylation of tetraethylene glycol using potassium hydroxide and *p*-toluenesulfonyl chloride in dichloromethane gave compound **47** in 93% yield. Monofunctionalised hydroquinone **46** and ditosylate **47** were heated in the presence of potassium carbonate in acetonitrile, producing compound **48** which was isolated in 79% yield. The bis-amine macrocycle precursor compound **49** was prepared in 77% yield by reducing **48** using borane in tetrahydrofuran.



*Scheme 3.5. Synthesis of the pyridinium chloride template **51·Cl**.*

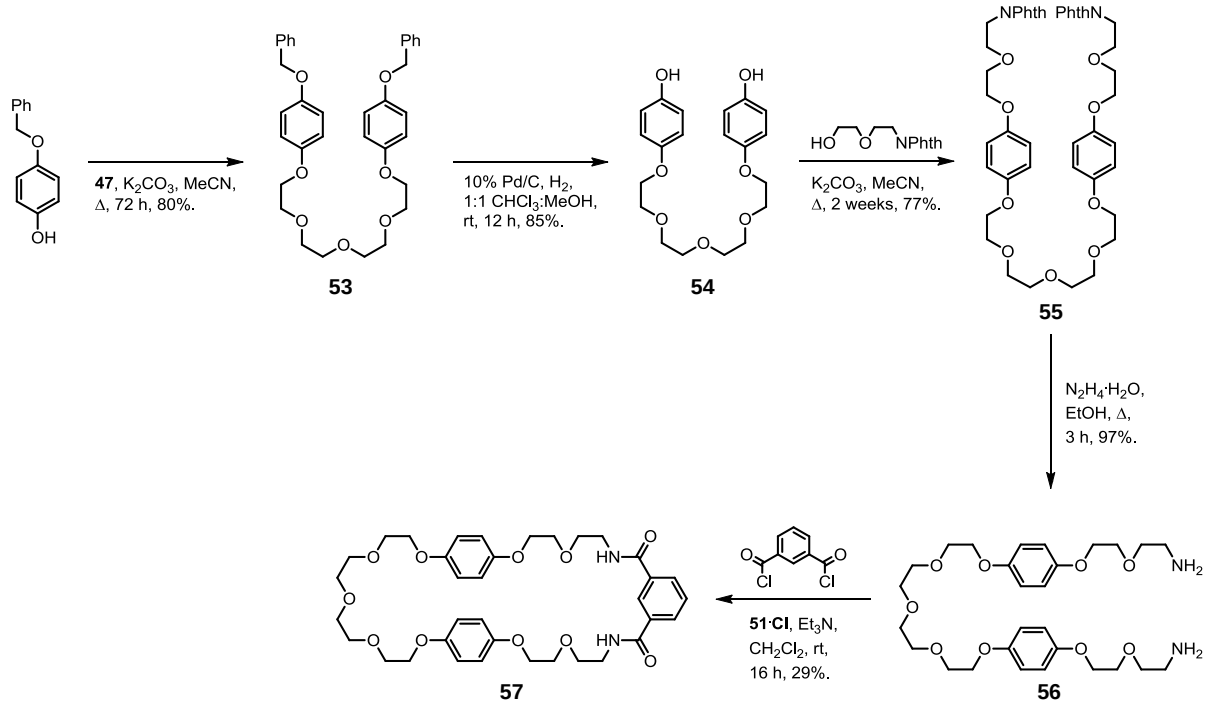
The acid-chloride–bis-amine cyclisation reaction is carried out in the presence of a pyridinium chloride template **51·Cl**, which was synthesised as shown in Scheme 3.5. Heating pyridine-3,5-dicarboxylic acid in thionyl chloride afforded the corresponding bis-acid-chloride which was used immediately in the next step. Acid-chloride-condensation with two equivalents of 1-hexylamine in the presence of triethylamine in dichloromethane gave compound **50** in 88% yield. Methylation was achieved by heating with methyl iodide in chloroform to give **51·I** which was converted to the chloride template **51·Cl** in 75% yield by repeated washing of a chloroform solution of the iodide salt with aqueous ammonium chloride.



*Scheme 3.6. Synthesis of macrocycle component **52**.*

The target macrocycle **52** was successfully prepared as summarised in Scheme 3.6. The condensation reaction between bis-amine compound **49** and isophthaloyl dichloride in the presence of pyridinium chloride template **51·Cl** and triethylamine in anhydrous dichloromethane afforded, after purification by column chromatography, the target isophthalamide-based macrocycle compound **52** in 25% isolated yield.

Since the bromine atom substituent of the potential bromopyridinium threading compound $\mathbf{44}^+$ is significantly larger in size than a proton, a new, expanded isophthalamide macrocycle was also prepared as outlined in Scheme 3.7

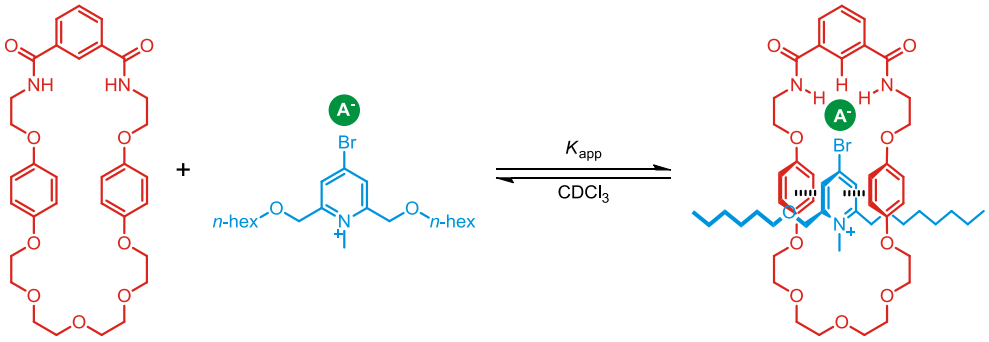


*Scheme 3.7. Synthesis of larger isophthalamide macrocycle **57**.*

4-Benzyloxyphenol and tetraethylene ditosylate **47** were heated in the presence of potassium carbonate in acetonitrile to give compound **53** in 80% yield. Hydrogenation using palladium on carbon in 1:1 chloroform:methanol removed the benzyl protecting groups to produce bis-hydroxyl compound **54** in 85% yield. A nucleophillic substitution reaction between compound **54** and *N*-phthalimidoethoxyl ethanol[27] (kindly donated by Dr A. McConnell) under basic conditions in acetonitrile gave phthalimide-protected macrocycle precursor **55** in 77% yield, which was deprotected using hydrazine monohydrate in ethanol affording compound **56** in 97% yield. Stirring bis-amine **56** and pyridinium chloride template **51·Cl** in the presence of isophthaloyl dichloride and triethylamine in anhydrous dichloromethane gave larger macrocycle **57** in 29% yield after acidic work up and purification by column chromatography.

3.2.3 Anion-templated pseudorotaxane formation exploiting halogen bonding

With two macrocycles, **52** and **57**, and bromopyridinium threading components **44·A** in hand the anion-templated assembly of pseudorotaxanes (Scheme 3.8) using halogen-bonding interactions to stabilise the interpenetrated assemblies was investigated.



*Scheme 3.8. Pseudorotaxane formation between bromopyridinium threading component **44**·**A** and macrocycle **52**.*

^{1}H NMR spectroscopic pseudorotaxane assembly titration experiments provide an insight into the strength of association between the macrocycle and potential threading components. Typically, aliquots of a solution of threading component are added to a solution of macrocycle and any changes in the ^{1}H NMR spectrum are monitored for evidence of interpenetration (Figure 3.3).

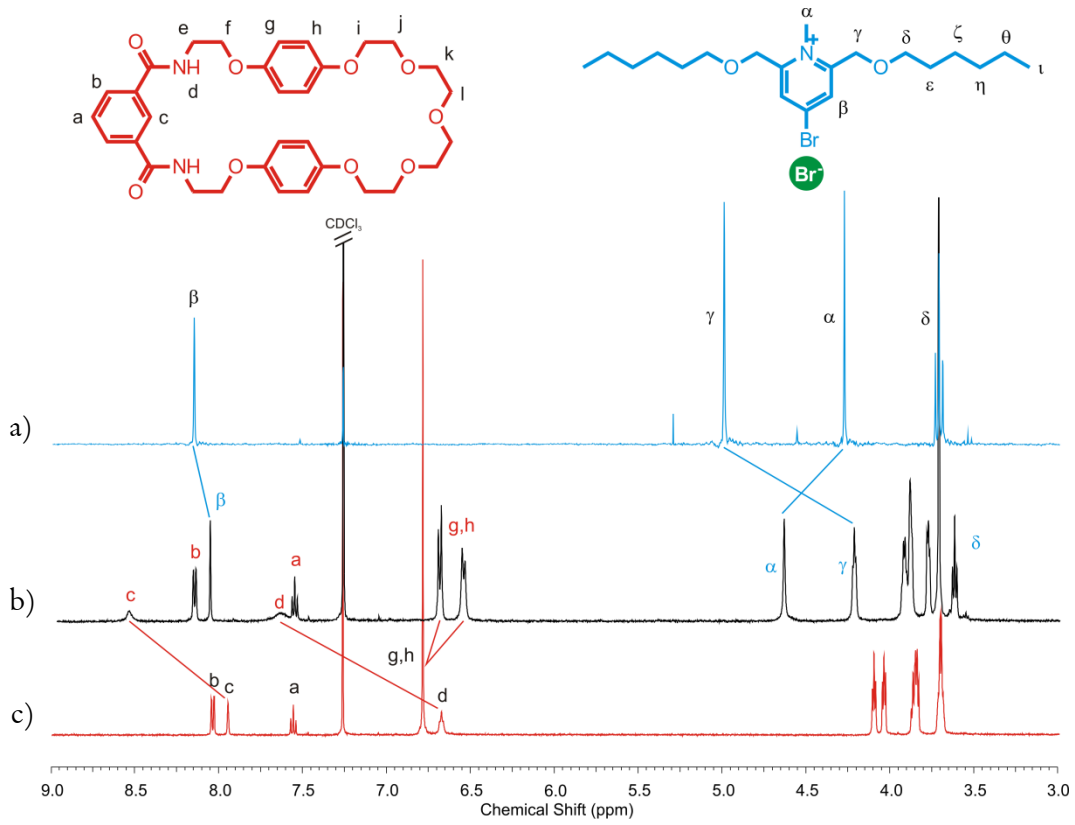


*Figure 3.3. Partial ^{1}H NMR spectra of: a) bromopyridinium thread **44**·**Br**; b) pseudorotaxane; and c) macrocycle **52** (500 MHz, $CDCl_3$, 293 K).*

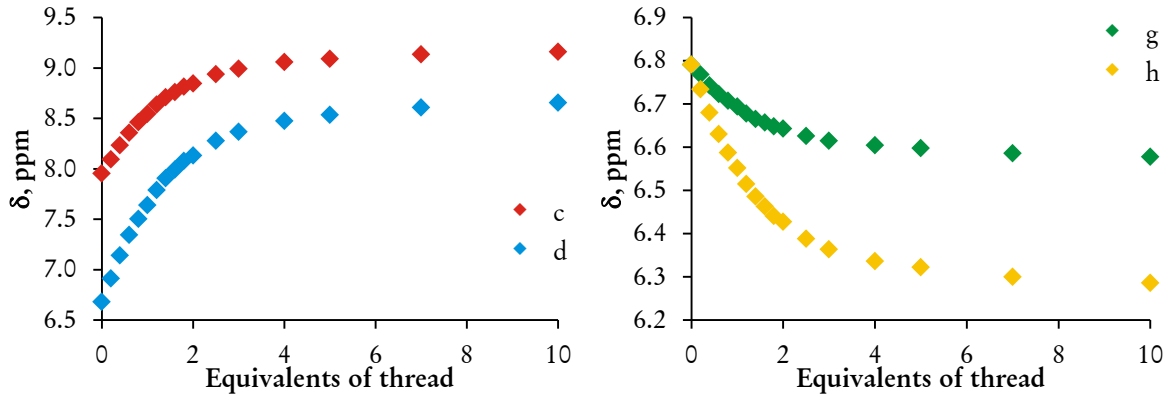


Figure 3.4. Chemical shift perturbations of important protons upon addition of threading component ***44·Br*** *to macrocycle* ***52****. $CDCl_3$, 293 K.*

Addition of threading compound **44·Br** to macrocycle **52** caused shifts in a number of signals in the ^{1}H NMR spectrum (Figures 3.3 and 3.4). Downfield perturbations in the macrocycle cavity proton signal *c* and amide protons signal *d* is indicative of bromide anion binding within the macrocycle's isophthalamide binding cleft. These shifts in macrocycle cavity protons could be caused by halide anion abstraction by the macrocycle rather than pseudorotaxane formation. A more reliable change in the ^{1}H NMR spectrum which signifies pseudorotaxane assembly is the observed upfield shift and splitting of the signal corresponding to the macrocycle hydroquinone protons *g* and *h*. These shifts are consistent with the formation of aromatic donor–acceptor intermolecular interactions between the macrocycle's electron-rich hydroquinone units and the electron-deficient threading component's pyridinium group. Additionally, the downfield shift in the signal corresponding to the *N*-methyl pyridinium protons α arises as a result of hydrogen bonding to the polyether oxygen atoms. Finally, upfield shifts in the signals corresponding to the threading component protons β and γ are a result of both aromatic donor–acceptor interactions and the bromide anion template binding to the isophthalamide domain.

The chemical shift perturbations of the macrocycle's hydroquinone protons were monitored as a function of the concentration of threading compound giving the titration curves reported in Figure 3.5. WinEQNMR[28] analysis of the titration data gave the apparent association constants K_{app} reported in Table 3.1.

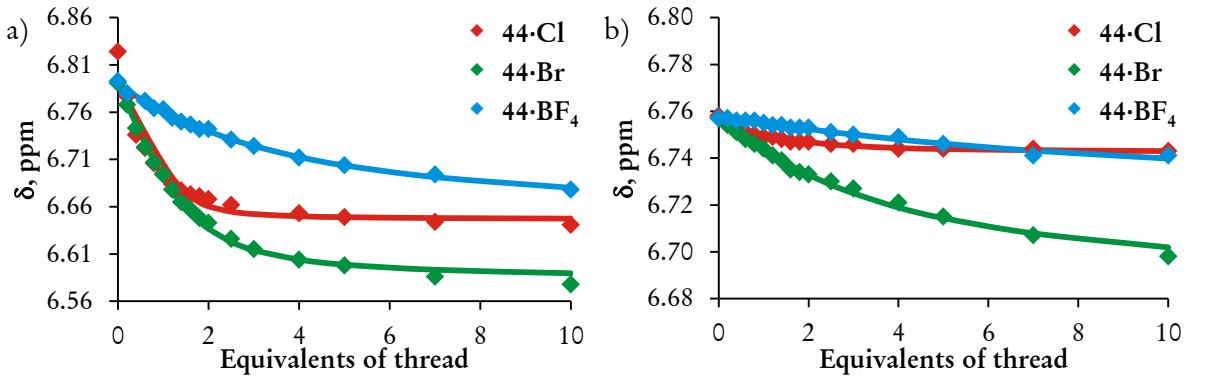


*Figure 3.5. Titration curves for pseudorotaxane formation between a) macrocycle **52** and b) macrocycle **57**, and threading compounds obtained by monitoring perturbations of the hydroquinone protons. 500 MHz $CHCl_3$, 293 K. Square data points represent experimental data; continuous lines represent theoretical binding isotherms.*

*Table 3.1. Association constants, K_{app} (M^{-1}), for pseudorotaxane formation between macrocycles **52** and **57**, and threading components **44·A**.*

Thread	Macrocycle **52** K_{app} (M^{-1})[a]	Macrocycle **57** K_{app} (M^{-1})[a]
44·Br	1463(21)	140(7)
44·BF_4	149(8)	33(1)
TBA·Cl	36(1)	50(2)
44·Cl[b]	6873(127)	1044(6)

*[a]Association constants were determined by monitoring the perturbations of the macrocycle hydroquinone protons. [b]Thread **44·BF_4** added to an equimolar mixture of macrocycle and TBA·Cl. Estimated standard errors are given in parentheses. $CDCl_3$, 293 K.*

Importantly, pseudorotaxane assembly between the smaller macrocycle **52** and bromopyridinium threading components is strongest in the presence of the templating bromide anion: K_{app} (**44·Br**) = 1463 M^{-1} > K_{app} (**44·BF_4**) = 149 M^{-1}. Macrocycle **52** contains an isophthalamide anion recognition motif which is able to associate with a spherical halide anion. The much smaller association constant value for the bromopyridinium tetrafluoroborate threading species is consistent with the non-coordinating nature of the tetrafluoroborate anion. A similar trend is observed with the larger macrocycle **57**.

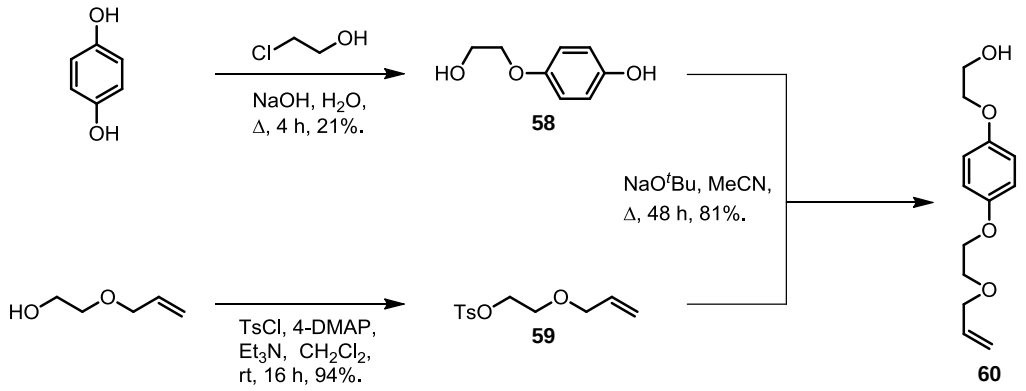
The pseudorotaxane assemblies formed with the smaller macrocycle **52** are significantly stronger than with the larger macrocycle **57** as shown by the strength of association with bromopyridinium bromide **44·Br** [K_a (**52**) 1463 M^{-1} > K_a (**57**) 140 M^{-1}]. This indicates that

the smaller macrocycle **52** is more suitably sized for anion-templated pseudorotaxane assembly, and is able to maximise the stabilising contributions of secondary aromatic donor–acceptor and *N*-methyl-pyridinium–oxygen hydrogen-bonding interactions.

Since some evidence of bromine–chlorine halogen atom exchange was observed in the attempted preparation of the chloride salt of 4-bromopyridinium threading species **44·Cl**, chloride-templated pseudorotaxane assembly studies were carried out using a modified titration protocol by adding threading component **44·BF_4** to an equimolar solution of macrocycle and TBA chloride. The apparent association constant value reveals the interpenetrative assembly is more stable with a chloride anion template than with bromide. The use of a modified titration procedure, however, means the association constant values cannot be directly compared. The relatively weak association of chloride with macrocycle **52** serves to highlight the fact that it is the effect of cumulative contributions of multiple non-covalent interactions operating in concert that result in the overall stability of the chloride-anion-templated interpenetrated assembly.

3.2.4 Synthesis of bis-vinyl-appended macrocycle precursors

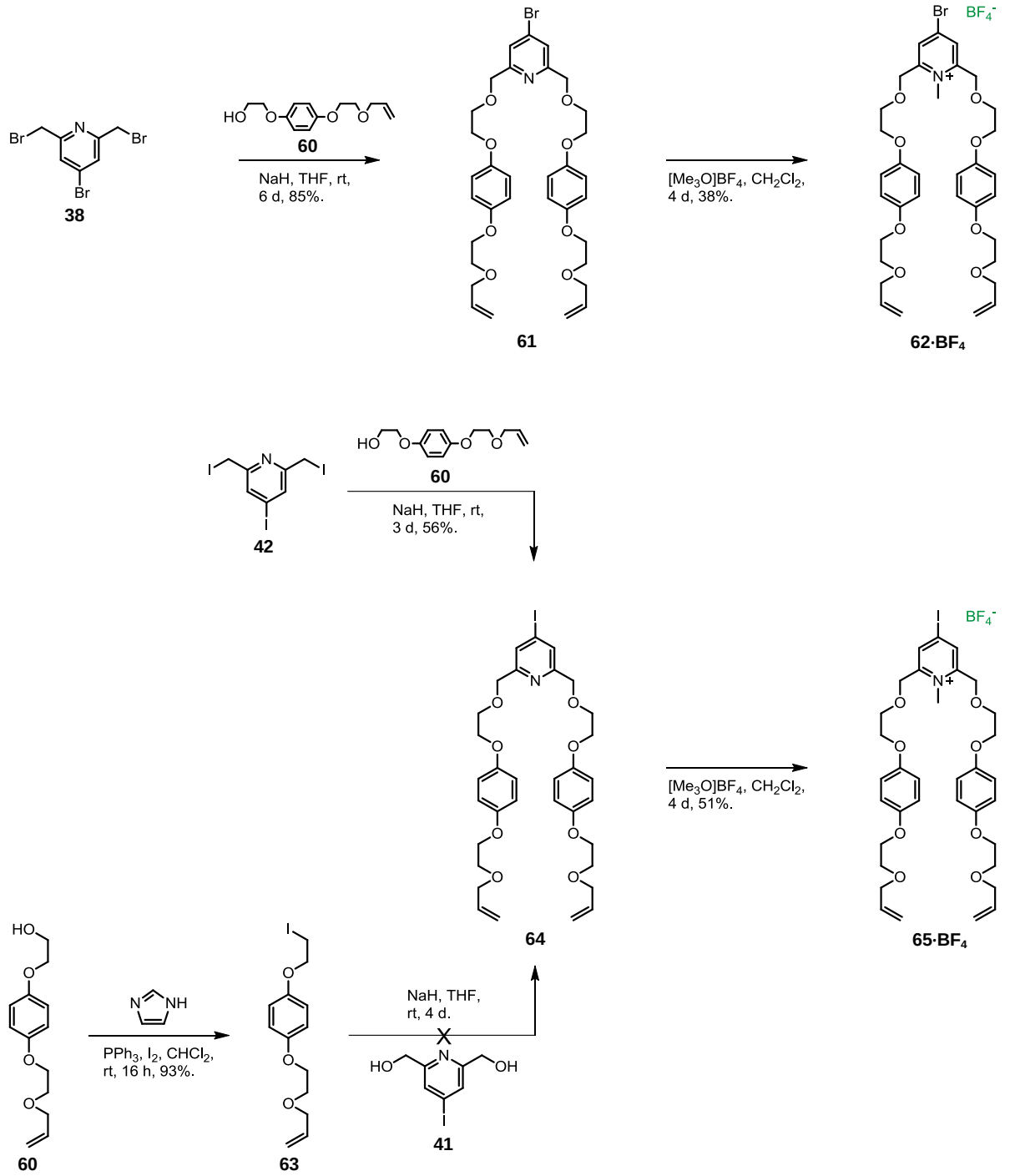
Given the encouraging results reported in section 3.2.3 for anion-templated assembly of pseudorotaxanes exploiting halogen-bonding interactions, it was anticipated that by replacing the threading component with a suitable bis-vinyl-functionalised halopyridinium derivative it may be possible to prepare a related interlocked catenane species through an anion-templated threading-then-clipping methodology.



Scheme 3.9. Synthesis of vinyl-appended intermediate compound **60**.

A suitable vinyl-appended, hydroquinone-containing hydroxyl species designed to undergo nucleophilic substitution reactions with 4-halo-2,6-bis(halomethyl)pyridine species **38** and **42** was prepared as a useful intermediate synthon (Scheme 3.9). Hydroquinone and 2-chloroethanol were heated in water in the presence of sodium hydroxide and following purification using column chromatography compound **58** was isolated in 21% yield.[29] Tosylation of 2-allyloxyethanol, to give compound **59** was achieved in 94% yield using *p*-toluenesulfonyl chloride, triethylamine and 4-dimethylaminopyridine in dichloromethane.[30] A nucleophilic substitution reaction between monofunctionalised hydroquinone compound **58** and tosylated compound **59** in the presence of base in acetonitrile afforded compound **60** in 81% yield.

The target bis-vinyl-appended, halopyridinium macrocycle precursor components were synthesised as described in Scheme 3.10.

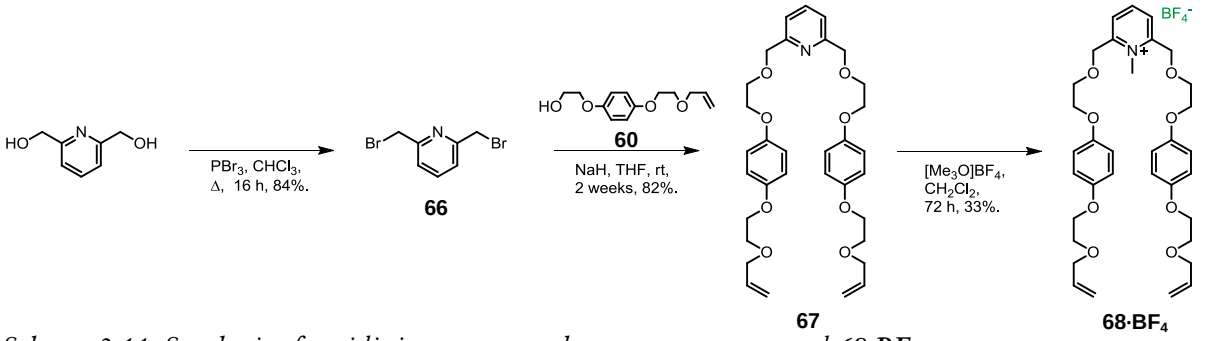


Scheme 3.10. Synthesis of vinyl-appended, halopyridinium macrocycle precursor compounds ***62·BF$_4$*** *and* ***65·BF$_4$****.*

Stirring 4-bromo-2,6-bis(bromomethyl)pyridine **38** and two equivalents of vinyl-appended hydroquinone derivative **60** in the presence of sodium hydride in tetrahydrofuran produced bis-vinyl-functionalised bromopyridine species **61** in 85% yield. Alkylation using trimethyloxonium tetrafluoroborate in anhydrous dichloromethane afforded the target bromopyridinium macrocycle precursor compound **62·BF$_4$** in 38% yield.

In spite of the low yielding preparation of the 4-iodopyridine threading compound **45**, attempts to prepare the equivalent bis-vinyl-appended macrocycle precursor were undertaken. 4-Iodo-2,6-bis(bromomethyl)pyridine **42**, two equivalents of compound **60** and sodium hydride were stirred in anhydrous tetrahydrofuran giving iodopyridine compound **64** in 56% yield. An alternative synthetic approach to prepare compound **64** in potentially higher yields was also undertaken. A nucleophilic substitution reaction between hydroxyl-functionalised 4-iodopyridine **41** and two equivalents of compound **63** (prepared in 93% yield via iodination of compound **60** using imidazole, triphenyl phosphine and iodine in dichloromethane) in the presence of sodium hydride in tetrahydrofuran was undertaken. After four days, however, thin layer chromatographic analysis of the reaction mixture revealed only a small amount of mono-substituted product had formed and therefore this alternative route to compound **64** was abandoned. Methylation of iodopyridine compound **64** with trimethyloxonium tetrafluoroborate in anhydrous dichloromethane gave iodopyridinium compound **65·BF$_4$** in 51% yield.

An equivalent proton-containing pyridinium threading species was also prepared (Scheme 3.11) which would allow for comparison with the anion-templated pseudorotaxane assembly investigations stabilised by halogen bonding.

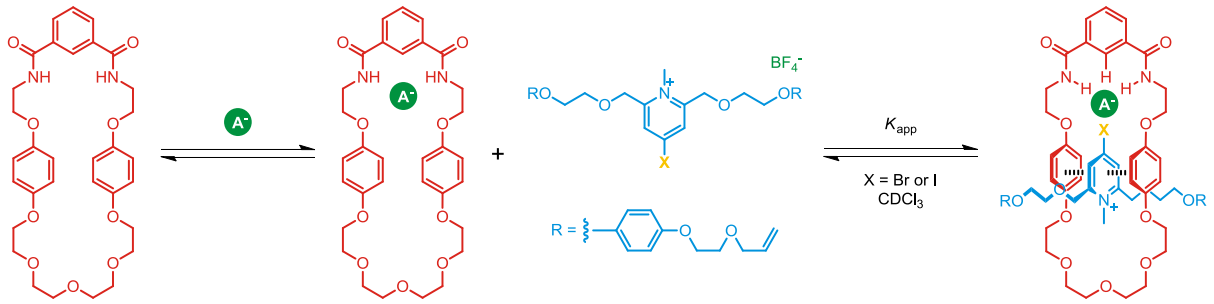


*Scheme 3.11. Synthesis of pyridinium macrocycle precursor compound **68·BF$_4$**.*

3.2.5 Pseudorotaxane formation using halogen- and hydrogen-bonding bis-vinyl-appended pyridinium macrocycle precursors

Following the successful isolation of a potential iodopyridinium threading species in section 3.2.4, further anion-templated interpenetrative ^{1}H NMR titration studies were undertaken

with compounds **62·A** and **65·A** to establish how the nature of the halogen-bond donor and halide anion template affects the strength of pseudorotaxane formation.



Scheme 3.12. Pseudorotaxane formation between threading components ***62·BF*** $_4$*,* ***65·BF*** $_4$ *or* ***68·BF*** $_4$ *and macrocycle* ***52*** *in the presence of TBA·A.*

Owing to the possibility of halogen-atom exchange, anion-templated investigations were restricted to using halides bromide and iodide and compared with tetrafluoroborate as a control species. Importantly, to ensure there is no possibility of halide substitution between the templating halide anion and the halogen-bond-donor atom, some evidence of which was unexpectedly observed in attempts to prepare the chloride salt of bromopyridinium derivative **44**$^+$ (see section 3.2.1), the titration protocol was modified. Aliquots of threading components as their tetrafluoroborate salts were added to an equimolar solution of macrocycle and TBA halide salt in chloroform-d (Scheme 3.12). Addition of bis-vinyl-appended halopyridinium components **62·BF**$_4$ and **65·BF**$_4$ to macrocycle **52** in the presence of bromide or iodide caused similar changes in the macrocycle's ^{1}H NMR spectrum to those observed for pseudorotaxane formation with threading component **44·BF**$_4$ (Figure 3.6). In particular, the diagnostic upfield shift and splitting of the macrocycle hydroquinone proton signal *g*,*h* arising from the formation of aromatic donor–acceptor interactions, confirms the formation of an anion-templated interpenetrated assembly.

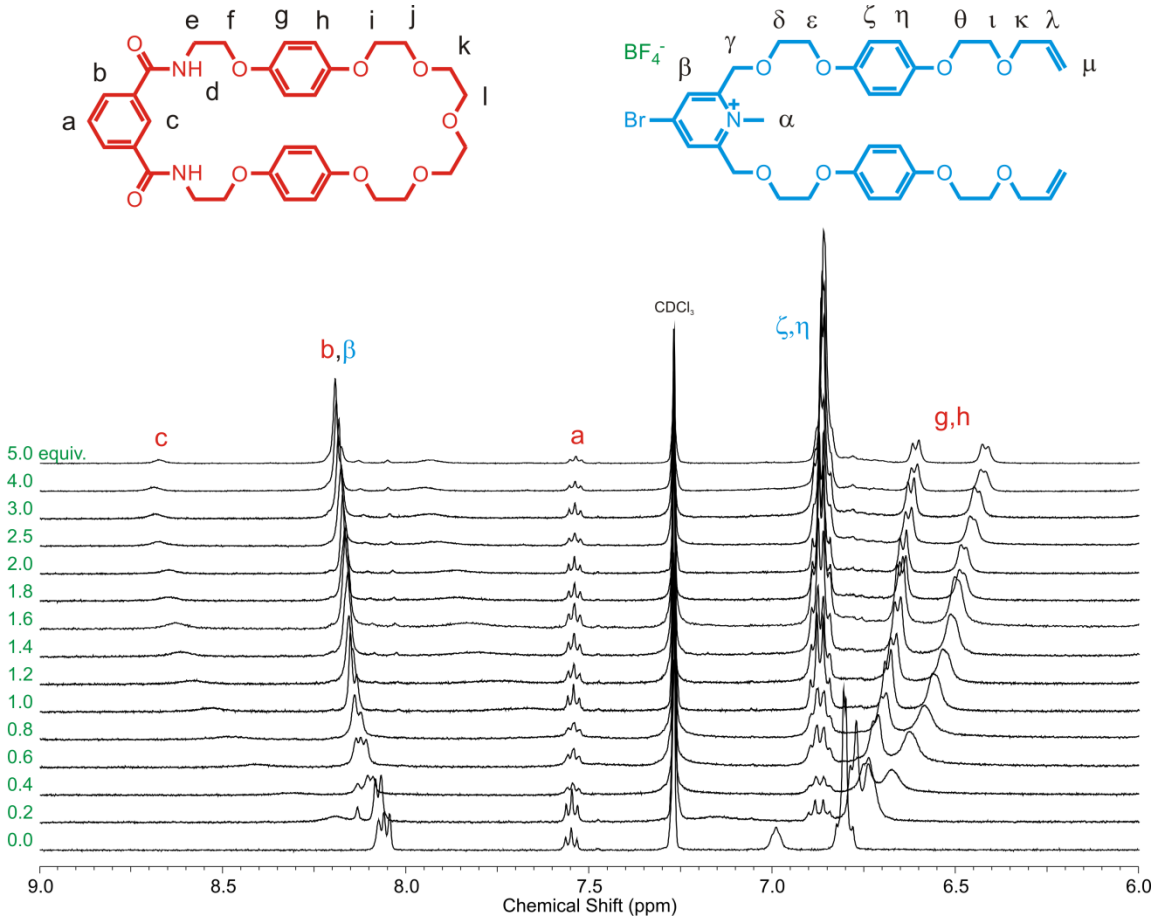


*Figure 3.6. Partial ^{1}H NMR spectra of an equimolar mixture of macrocycle **52** and TBA·Br with equivalents of threading component **62·BF$_4$** (500 MHz, CDCl$_3$, 293 K).*

Monitoring the perturbations of the macrocycle's hydroquinone protons as a function of concentration of threading component gave the titration curves shown in Appendix A.3.2, and analysis of the titration data using the winEQNMR2 computer program gave the apparent association constants, K_{app}, for pseudorotaxane formation reported in Table 3.2.

*Table 3.2. Apparent association constants, K_{app} (M^{-1}), for pseudorotaxane formation between threading components **62·A**, **65·A** or **68·A** and macrocycle **52**.*

Threading component	Macrocycle **52** + Br^- K_{app} (M^{-1})[a]	Macrocycle **52** + I^- K_{app} (M^{-1})[a]	Macrocycle **52** K_{app} (M^{-1})[a]
62·BF_4 (X=Br)	2328(135)	777(36)	272(26)
65·BF_4 (X=I)	3279(772)	1527(59)	249(27)
68·BF_4 (X=H)	1019(98)	341(19)	215(32)

[a]*Apparent association constants were determined by monitoring the perturbations of the macrocycle hydroquinone protons upon addition of threading species to an equimolar mixture of macrocycle and TBA·A. Estimated standard errors are given in parentheses. $CDCl_3$, 293 K.*

Importantly, the most stable pseudorotaxane assemblies are found with the iodopyridinium threading component **65·A** with apparent association constants larger in magnitude than with the analogous halogen-bonding bromopyridinium threading component **62·A** (K_{app} = 1527 M^{-1} and 777 M^{-1} respectively for templation with iodide). This is attributed to the greater halogen-bond-donor ability of the more polarisable iodine atom compared with bromine. Moreover, the interpenetrative assembly with the equivalent protic pyridinium species **68·BF_4** is significantly weaker (K_{app} = 341 M^{-1} with iodide) which demonstrates that the halogen-bonding, halide-anion-templated pseudorotaxanes are more stable than their hydrogen-bonding counterparts.

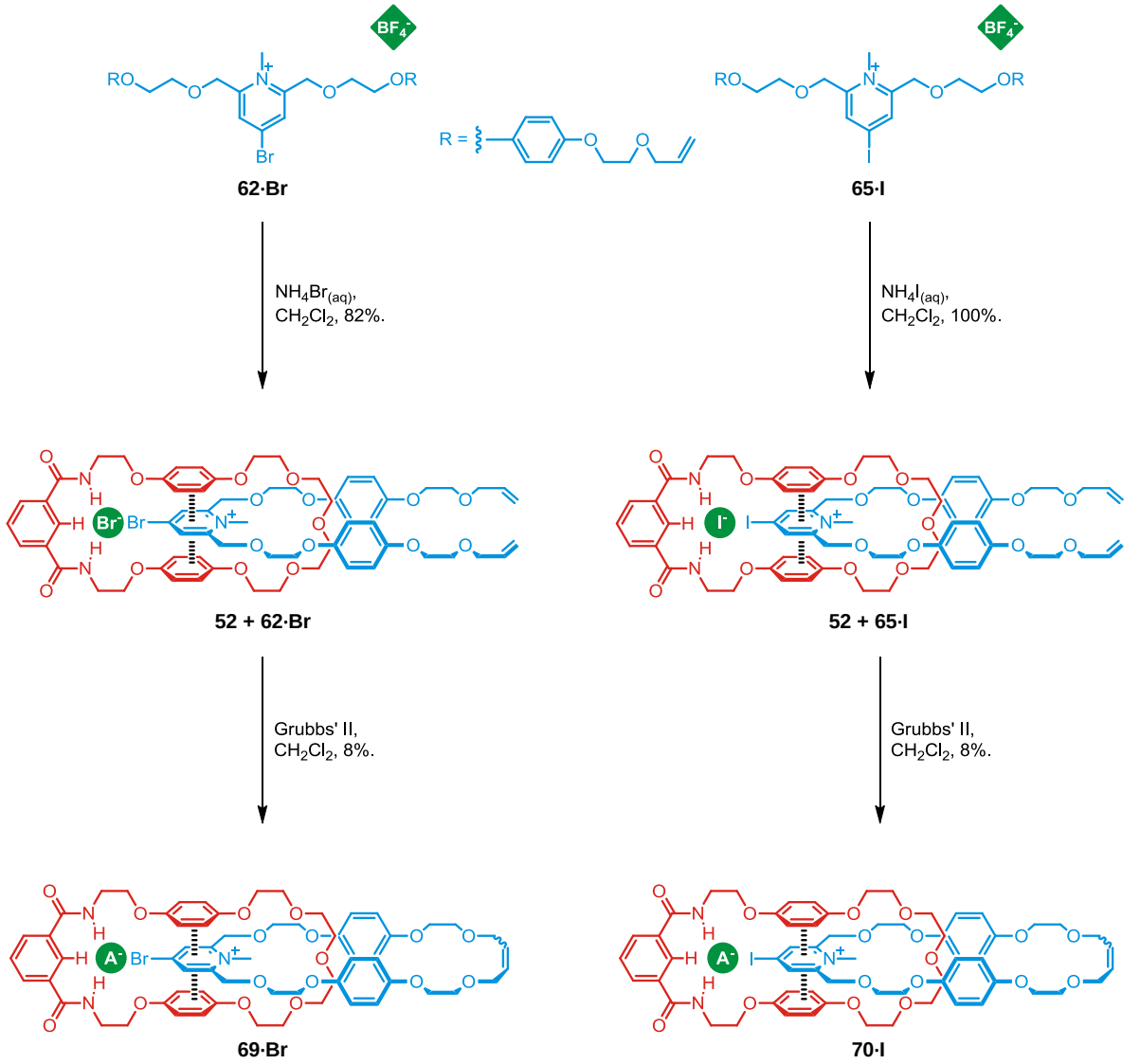
It is noteworthy that pseudorotaxane assembly is stronger when a bromide anion template is employed instead of iodide: K_{app} (**62·A**) = 2328 M^{-1} *versus* 777 M^{-1}. This suggests the relatively smaller bromide anion is more suitably sized to bind to the isophthalamide anion recognition cleft than the larger iodide anion.

Finally, in the absence of a halide anion template, the interpenetrative assemblies with the halo- and protic-functionalised pyridinium tetrafluoroborate salts are all much less stable and are of similar modest stability.

3.2.6 Synthesis of anion-templated catenanes stabilised by halogen bonding

Encouraged by the favourable anion-templated association between macrocycle **52** and macrocycle precursor compounds **62·BF_4** and **65·BF_4** the synthesis of novel anion-templated,

halogen-bonding [2]catenanes using a Grubbs'-catalysed RCM reaction was undertaken (Scheme 3.13).



*Scheme 3.13. Synthesis of novel anion-templated, halogen-bonding catenanes **69·Br** and **70·I**.*

The required templating macrocycle precursor components were prepared by anion exchanging the non-coordinating tetrafluoroborate anion for either bromide or iodide. Given the potential possibilities of halogen atom exchange, bromide was used as the anion template with bromopyridinium species **62** and iodide with the iodopyridinium compound **65**. Anion exchange was achieved by repeated washing of a dichloromethane solution of the pyridinium species with aqueous ammonium bromide or iodide: the target threading species, **62·Br** and **65·I**, were isolated in 81% and quantitative yields respectively.

Macrocycle **52** and 1.1 equivalents of macrocycle precursor **62·Br** in anhydrous dichloromethane were stirred at room temperature for four days in the presence of Grubbs' second generation catalyst (10% by weight). Following purification using repeated preparative thin layer chromatography the target catenane **69·Br** was isolated in 8% yield.

The synthesis of the related iodopyridinium-containing catenane species was undertaken using similar reaction conditions and iodopyridinium catenane **70·I** was isolated in 8% yield.

3.2.7 Characterisation of anion-templated catenanes stabilised by halogen-bonding interactions

Evidence of successful interlocked structure formation was provided by high-resolution electrospray mass spectrometry and ^{1}H NMR spectroscopy. The cationic molecular ion peaks of both catenanes are easily observed in the mass spectrum which suggests the presence of a single interlocked species and the high-resolution mass spectra reveal the isotopic distribution of the catenanes **69·PF$_6$** and **70·PF$_6$** are in good agreement with the theoretical spectra (Figure 3.7).

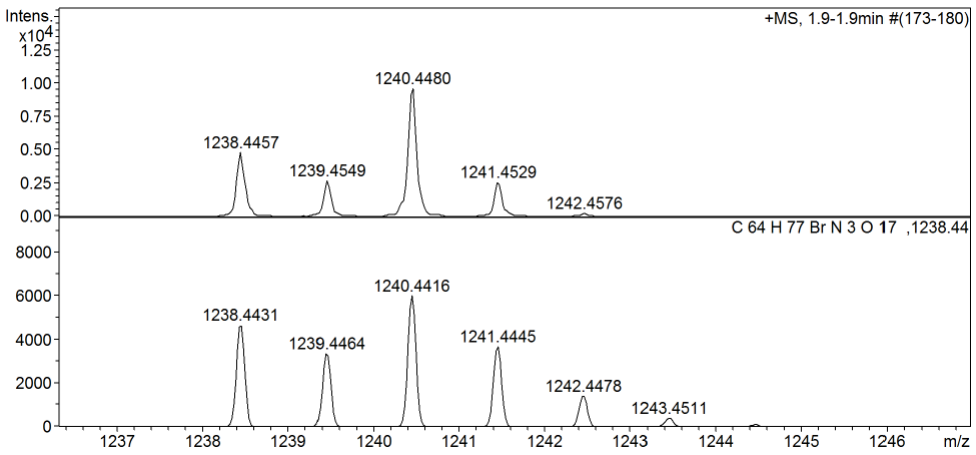


*Figure 3.7. High-resolution mass spectrum of catenane **69·Br**.*

The ^{1}H NMR spectrum of bromopyridinium-containing catenane **69·Br** together with those for the component macrocycle and bis-vinyl-appended precursor for comparison are shown in Figure 3.8. The disappearance of the vinylic multiplet μ and the convergence of multiplet λ into a pseudo-singlet in the catenane spectrum are attributed to cyclisation of the acyclic

precursor. Crucially, the upfield shift and splitting of the macrocycle hydroquinone protons *g* and *h* is indicative of aromatic donor–acceptor interactions between the electron-rich macrocycle hydroquinone units and the electron-poor pyridinium group. Downfield shifts of signals corresponding to the macrocycle cavity protons *ortho*-isophthalamide proton *c* and amide protons *d* are caused by the formation of hydrogen-bonding interactions between these protons and the bromide anion template. Additionally, upfield shift of the pyridinium methyl proton signal α is observed which is attributed to hydrogen-bonding interactions between the pyridinium methyl group and the isophthalamide macrocycle's polyether linkage. Finally, the upfield perturbation of the *meta*-pyridinium proton β is consistent with the bromide anion guest being shared with the amide binding cleft and also a result of the formation of aromatic donor–acceptor interactions.

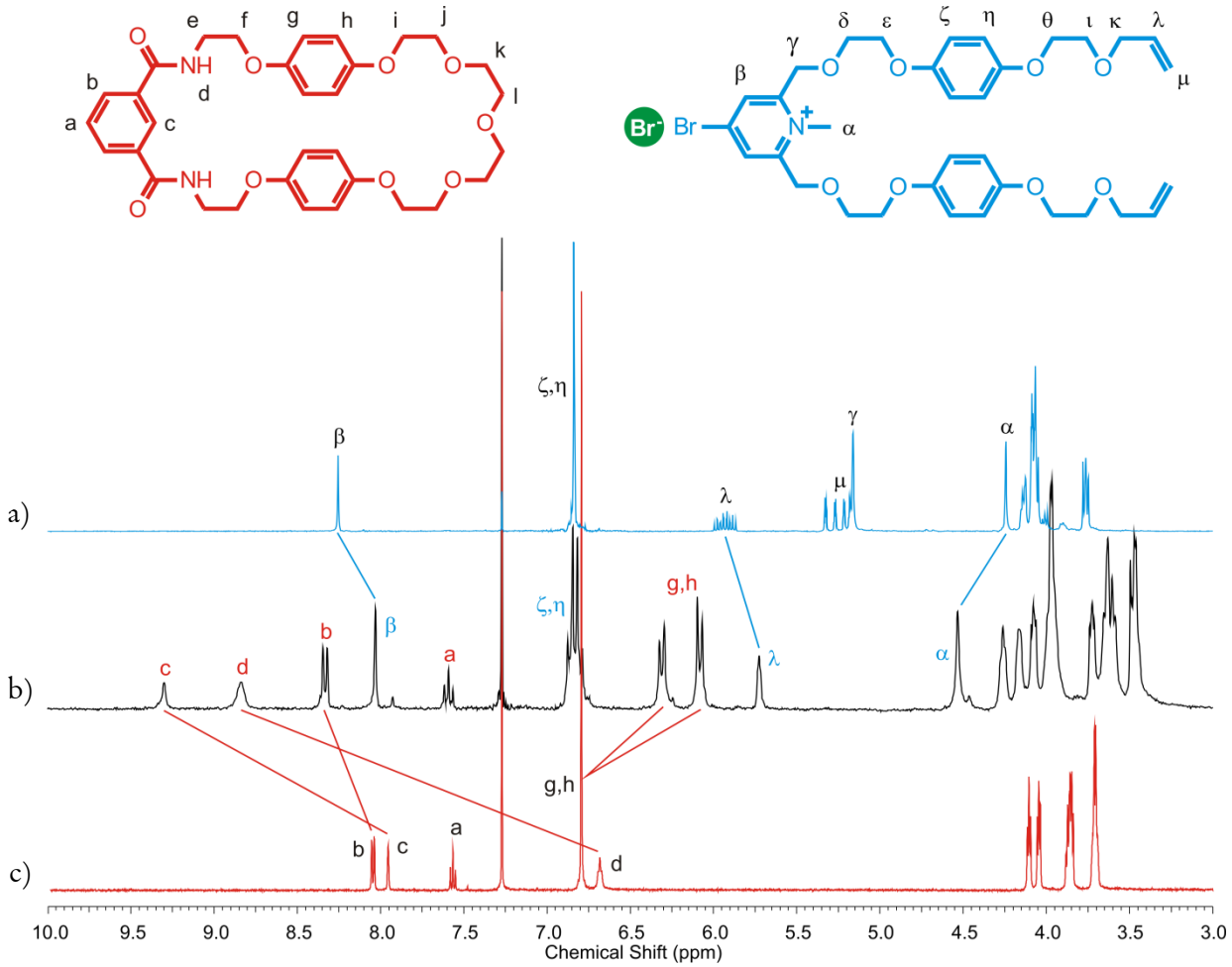


Figure 3.8. Partial ^{1}H NMR spectra of: a) bromopyridinium macrocycle precursor ***62·Br****; b) catenane* ***69·Br****; and c) macrocycle* ***52*** *(500 MHz, $CDCl_3$, 293 K).*

Two dimensional ^{1}H–^{1}H ROESY NMR spectroscopy provides further evidence of the interlocked nature of the [2]catenane **69·Br** (Figure 3.9).

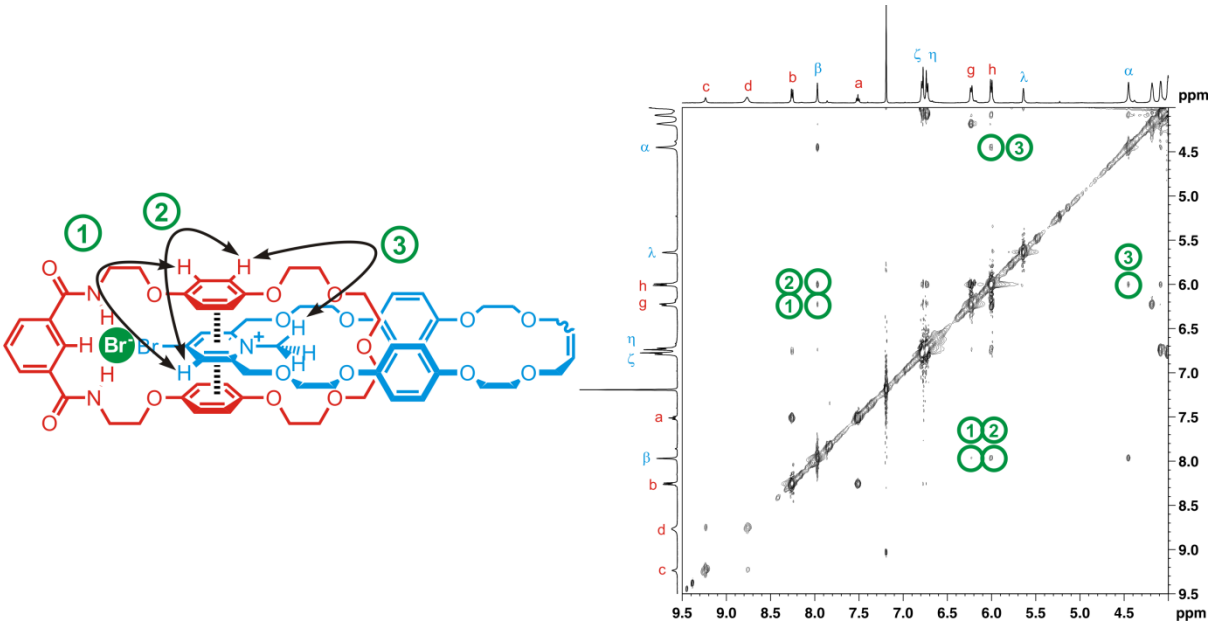


*Figure 3.9. ^{1}H–^{1}H ROESY NMR spectrum of catenane **69·Br**. Assignable inter-component through-space interactions are highlighted.*

The ^{1}H–^{1}H ROESY spectrum displays several through space cross-coupling interactions between the two components of the catenane. Important interactions include **1** ($\beta \rightarrow g$) and **2** ($\beta \rightarrow h$) which confirm the electron-rich hydroquinone units and the electron-poor pyridinium moiety are close in space, as would be expected if the macrocycle components are interlocked with respect to one another. Interaction **3** ($\alpha \rightarrow h$) also demonstrates the hydroquinone and pyridinium aromatic units are in close proximity.

3.2.8 Anion binding properties of novel [2]catenanes stabilised by halogen-bonding interactions

To study the anion recognition properties of the novel catenanes, the respective templating halide guests were exchanged for the non-coordinating hexafluorophosphate anion. This was achieved by repeatedly washing a dichloromethane solution of the catenane with aqueous ammonium hexafluorophosphate to give catenanes **69·PF$_6$** or **70·PF$_6$** in 81% or quantitative yields respectively. Figure 3.10 shows the ^{1}H NMR spectra of catenane **69·A** before and after anion exchange with ammonium hexafluorophosphate.

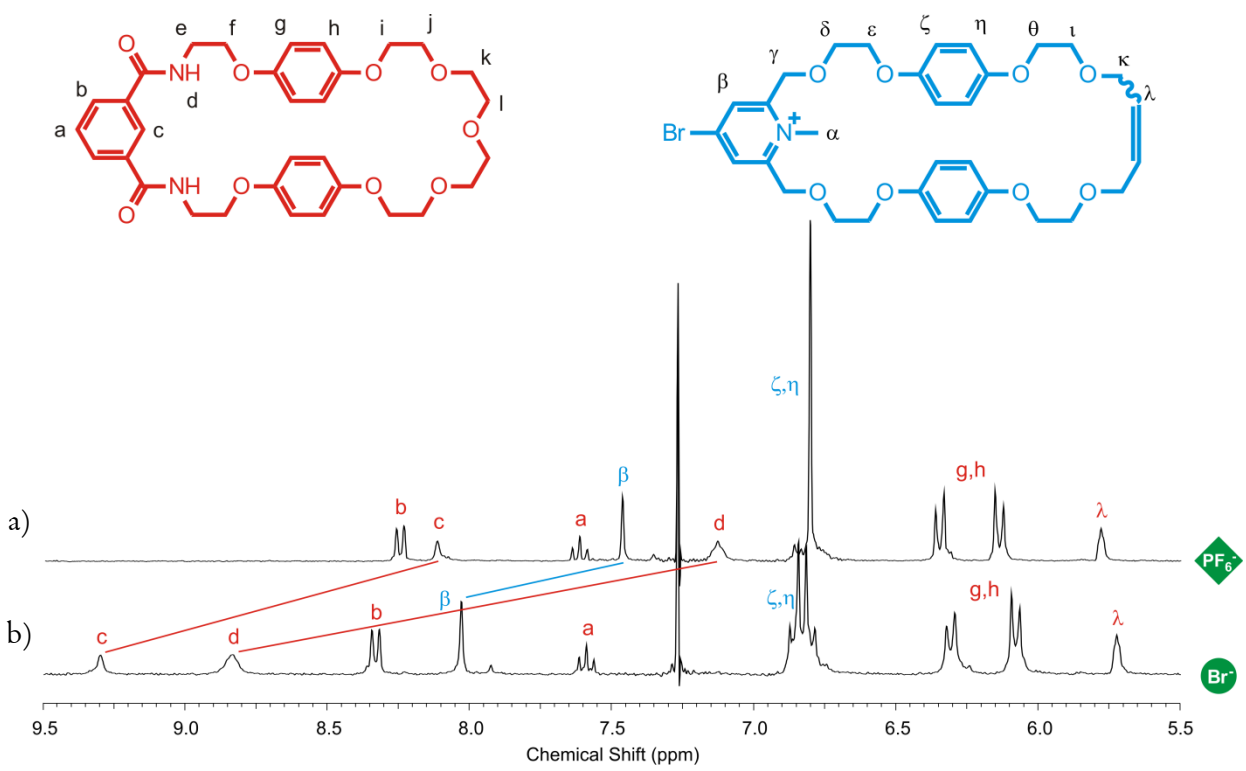


Figure 3.10 Partial ^{1}H NMR spectra of: a) catenane ***69·PF$_6$*** *and; b) catenane* ***69·Br*** *(300 MHz, $CDCl_3$, 293 K).*

Appreciable upfield shifts of the catenane signals corresponding to the *ortho*-isophthalamide and amide cavity protons, *c* and *d*, and the *meta*-pyridinium proton *β* were observed in the ^{1}H NMR spectrum, which are consistent with the removal of bromide from the interlocked binding pocket. Most importantly, despite the very small shifts of the hydroquinone protons *g* and *h* (probably a result of slight conformational changes within the interlocked structure) they still remain split and further upfield compared with their chemical shift value in the free macrocycle, indicating that the catenane remains interlocked following removal of the bromide anion template.

The anion binding properties of the catenanes **69·PF$_6$** and **70·PF$_6$** were investigated using ^{1}H NMR spectroscopic titration experiments with TBA halide salts in the competitive solvent mixture 1:1 chloroform-d:methanol-d$_4$. Upon addition of anions to both catenane species, downfield chemical shift perturbations of the *ortho*-isophthalamide proton *c* and pyridinium proton *β* were observed with increasing anion concentration. It was not possible to monitor the chemical shift values of the amide protons *d* as these were exchanged for deuterium in this

solvent mixture. WinEQNMR analysis of the titration curves obtained for chloride, bromide and iodide binding (Figure 3.11) gave the 1:1 stoichiometric association constants reported in Table 3.3.

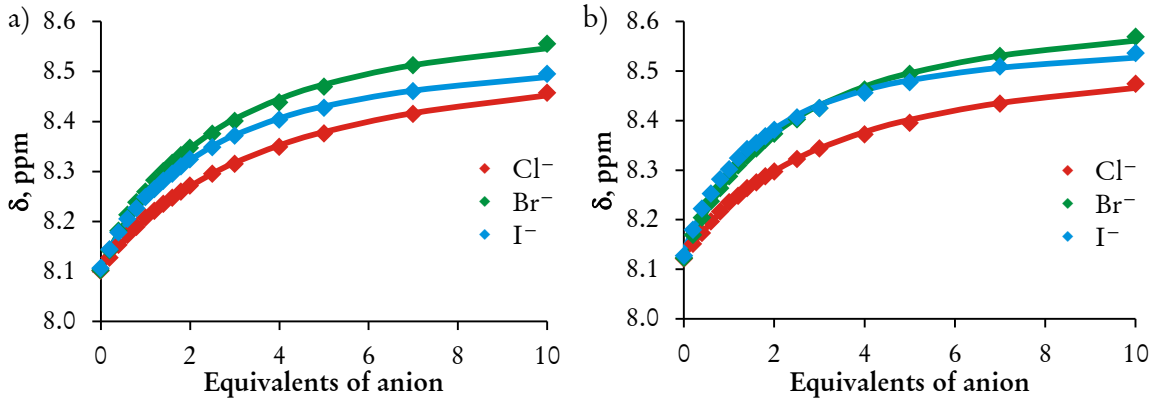


*Figure 3.11. Titration curves for addition of various anions to a) catenane **69·PF$_6$** and b) catenane **70·PF$_6$** obtained by monitoring the macrocycle cavity proton c. 1:1 $CDCl_3$:CD_3OD, 293 K. Square data points represent experimental data; continuous lines represent theoretical binding isotherms.*

*Table 3.3. Association constants, K_a (M^{-1}), for addition of various anions to catenanes **69·PF$_6$** and **70·PF$_6$**.*

Anion	Catenane **69·PF$_6$** K_a (M^{-1})[a]	Catenane **70·PF$_6$** K_a (M^{-1})[a]
Cl^-	127(5)	156(6)
Br^-	197(8)	226(11)
I^-	217(9)	335(21)

[a]*All anions added as their TBA salt. Association constants were determined by monitoring the perturbations of isophthalamide cavity proton c. Estimated standard errors are given in parentheses. 1:1 $CDCl_3$:CD_3OD, 293 K.*

The association constant values reveal both catenanes complex halide anions chloride, bromide and iodide with moderate affinity in this competitive solvent system. The iodopyridinium-containing catenane **70·PF$_6$** is a superior halide anion host to the bromopyridinium functionalised catenane **69·PF$_6$** (K_a = 335 M^{-1} *versus* 217 M^{-1} for iodide association) which reflects the greater halogen-bond-donor ability of the iodine atom compared with bromine. Interestingly, for both catenanes the strongest host–guest association is with iodide, followed by bromide and chloride: K_a = 335 M^{-1} (iodide), 226 M^{-1} (bromide), and 156 M^{-1} (chloride) for catenane **70·PF$_6$**. This is the reverse of what is expected on anion basicity grounds and may be attributed to a combination of factors including an

interlocked binding domain more suited to the larger halide anions, a higher penalty for desolvation of chloride than bromide or iodide in this competitive protic solvent mixture and possibly a greater degree of charge-transfer-type halogen-bonding interaction, between the respective catenane's bromo- and iodopyridinium halogen-bond-donor motif and the larger halide anions.

3.3 Halogen-bond-templated interlocked structures

The use of halogen bonding to bind anions has been well-demonstrated throughout Chapters Two and Three. Polarised halogen atoms, however, are able to form strong halogen-bonding interactions with *neutral* Lewis bases—an approach much exploited in the field of crystal engineering.

By incorporating a suitable neutral Lewis basic halogen-bond acceptor, such as pyridine,[12,31] into a macrocyclic framework, it may prove possible to assemble interpenetrated and interlocked architectures that are stabilised through halogen-bond formation between the two components within the superstructure. An investigation into the construction of a [2]catenane using halogen-bonding is described in the following sections.

3.3.1 Synthetic strategy for the formation of halogen-bond-templated catenanes

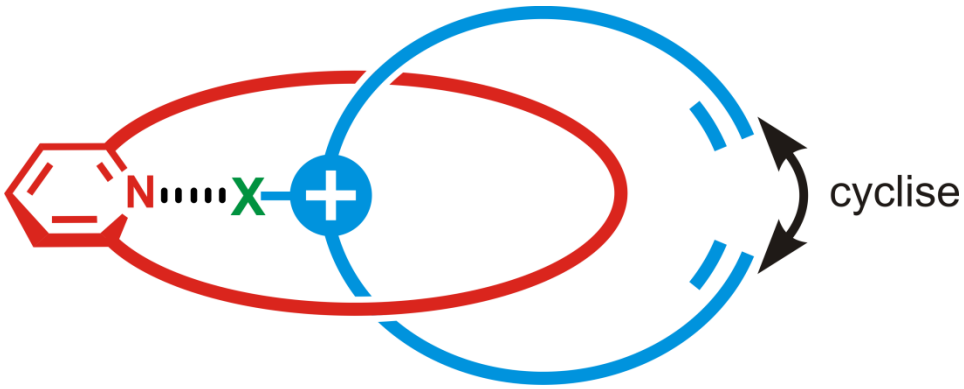


Figure 3.12. Cartoon representation of orthogonal halogen-bond-templated pseudorotaxane species. X is a halogen atom.

The synthetic strategy employed to construct the target catenane is outlined in Figure 3.12. An acyclic, positively charged halogen-bond-donor component threads through a

complementary halogen-bond-accepting pyridine-containing macrocycle forming an orthogonal interpenetrative assembly which is stabilised by a charge-assisted halogen-bonding interaction. In addition to the incorporated pyridine halogen-bond-acceptor motif, the macrocycle component **71** (kindly provided by Dr T. Lang) contains electron-rich hydroquinone groups to facilitate supplementary secondary aromatic donor–acceptor interactions with electron-deficient positively charged heterocyclic halogen-bond-donor threading derivatives. The bromo- and iodo-functionalised pyridinium compounds were studied as potential threading components with this pyridine macrocycle and compared with analogous halogen-functionalised triazolium species prepared by Dr A. Caballero. These potential thread components (Figure 3.13) contain terminal vinyl functional groups which, following successful pseudorotaxane assembly with macrocycle **71**, could be used for catenane synthesis through ring-closing metathesis (RCM) cyclisation.

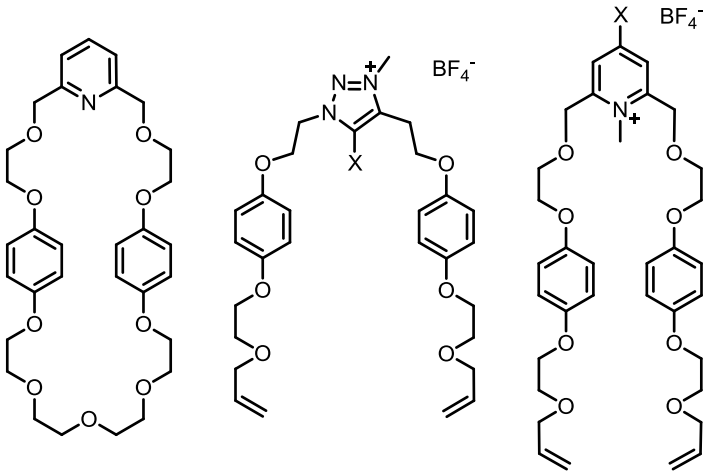
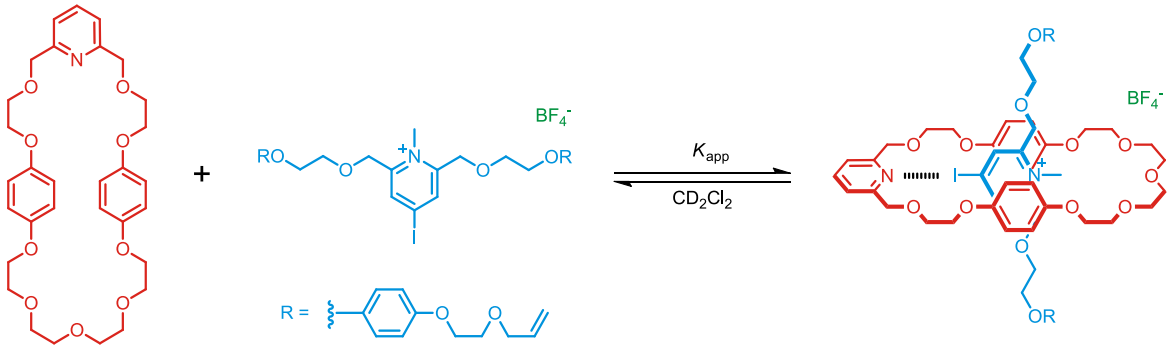


*Figure 3.13. Structures of pyridine-containing macrocycle **71** and various potential threading components.*

3.3.2 Pseudorotaxane assembly stabilised using inter-component halogen-bonding interactions

To establish solution phase evidence for interpenetrative assembly (Scheme 3.14) and also determine the strength of any association between respective macrocycle halogen-bond-acceptor and potential halogen-bond-donor heterocyclic thread components, the

pseudorotaxane assembly between macrocycle **71** and halo-functionalised triazolium and pyridinium compounds in dichloromethane-d_2 solution were investigated using ^{1}H NMR spectroscopy.



*Scheme 3.14. Pseudorotaxane assembly between macrocycle **71** and iodopyridinium threading component **65·BF$_4$**.*

Upon addition of thread components **73·BF$_4$**, **62·BF$_4$**, and **65·BF$_4$** to macrocycle **71**, the signals corresponding to the macrocycle hydroquinone protons were shifted upfield, which is attributed to aromatic donor–acceptor interactions with the respective electron-deficient heterocyclic aromatic surface.

These diagnostic changes in the macrocycle's ^{1}H NMR spectrum are highly indicative of the successful formation of an interpenetrated species via threading through the annulus of the macrocycle component. The observed chemical shift perturbations of the hydroquinone protons with ten equivalents of thread component (Table 3.4) reveal the iodopyridinium derivative **65·BF$_4$** causes the largest magnitude of perturbation; the chemical shift perturbation diminishes with the halogen-bond-donor capability of the substituent X, as observed for **62·BF$_4$ > 65·BF$_4$**. Furthermore, these $\Delta\delta_{ppm}$ values are greater for the pyridinium species than for the triazolium analogues. Notably, no significant evidence of interpenetration was observed with the bromotriazolium **72·BF$_4$** derivative.

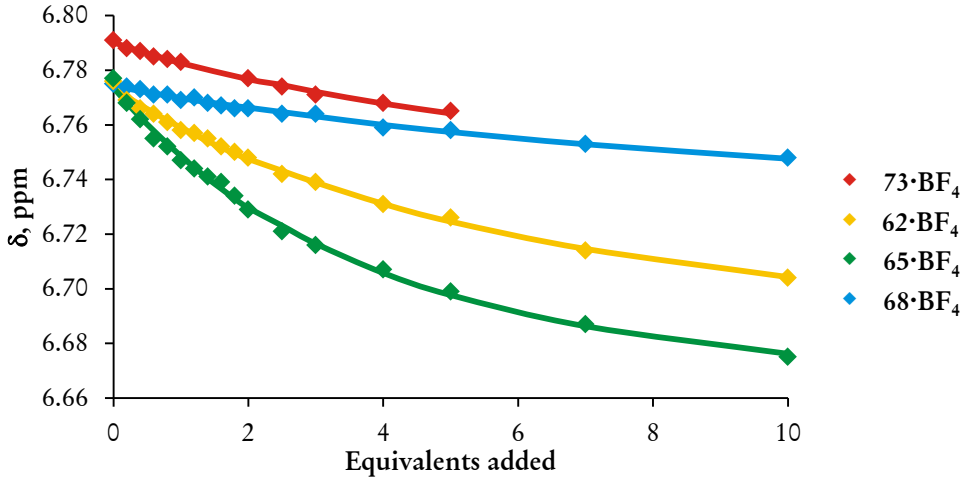


*Figure 3.14. Titration curves for pseudorotaxane assembly between macrocycle **71** and various threading components.*

*Table 3.4. Observed chemical shift perturbations (Δδ) of hydroquinone protons and association constants, K_a (M^{-1}), for macrocycle **71** with various threading components.*

Thread	**73·BF$_4$**	**62·BF$_4$**	**65·BF$_4$**	**68·BF$_4$**
Δδ (ppm)[a]	0.03[b]	0.07	0.10	0.03
K_a (M^{-1})[c]	55(3)	80(2)	180(20)	30(2)

[a]After addition of ten equivalents of threading species. [b]After addition of five equivalents of threading species. [c]Association constants were determined by monitoring the perturbations of hydroquinone protons. Estimated standard errors are given in parentheses. CD_2Cl_2, 293 K.

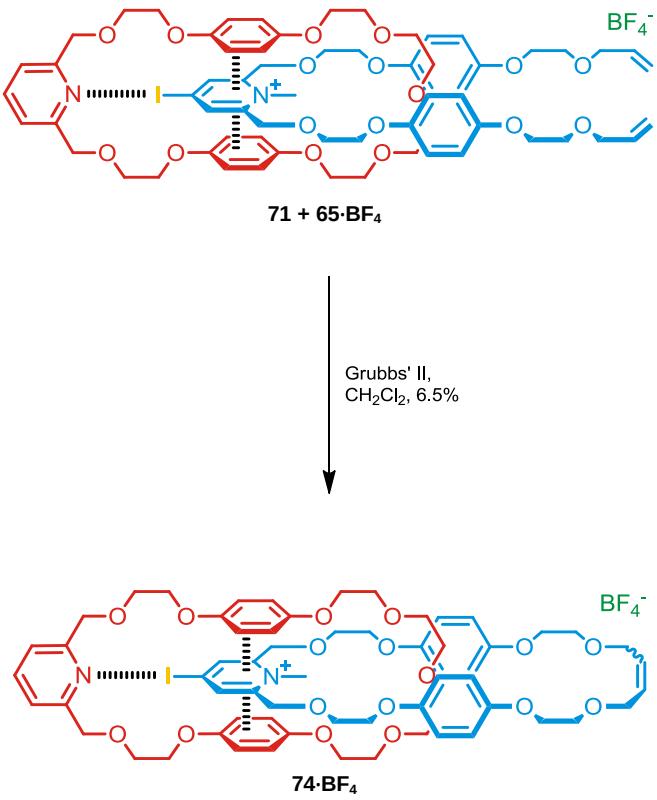
Quantitative analysis of the pseudorotaxane assembly process was achieved by monitoring the macrocycle's hydroquinone protons as a function of thread concentration and winEQNMR2 analysis of the titration data (Figure 3.14) gave 1:1 stoichiometric association constants for pseudorotaxane formation shown in Table 3.4. Importantly, the most stable interpenetrative assembly with macrocycle **71** is found with the iodopyridinium thread **65·BF$_4$** with an association constant value (K_a = 180 M^{-1}) more than double that of the pseudorotaxane assembly observed with bromopyridinium thread **62·BF$_4$** (K_a = 80 M^{-1}). This can be attributed to the greater halogen-bond-donor ability of the more polarisable iodine substituent as compared to bromine. Notably, the interpenetrative assembly with the corresponding protic-pyridinium analogue **68·BF$_4$** is significantly weaker (K_a = 30 M^{-1}), thus

highlighting the essential contribution of the halogen-bonding interaction in stabilising the overall pseudorotaxane assembly process.

Of the triazolium derivatives, Table 3.4 shows that although the iodotriazolium compound **73·BF$_4$** forms a measurable pseudorotaxane association with the pyridine macrocycle **71**, the extremely small chemical shift perturbations noted in the titration experiment with the bromotriazolium analogue **72·BF$_4$** suggest interpenetration is not occurring. The reduced supplementary secondary aromatic donor–acceptor interactions of the triazolium motif with the macrocycle's hydroquinone groups in comparison with pyridinium will also be a contributing factor.

3.3.3 Synthesis and characterisation of a [2]catenane assembled using a single charge-assisted halogen bond

Encouraged by the favourable association between macrocycle **71** and iodopyridinium thread **65·BF$_4$**, the synthesis of a novel [2]catenane using a RCM clipping reaction in the presence of Grubbs' catalyst was undertaken (Scheme 3.15).



*Scheme 3.15. Synthesis of a novel halogen-bond-templated catenane **74·BF$_4$**.*

Macrocycle **71** and 1.1 equivalents of iodopyridinium thread component **65·BF$_4$** in anhydrous dichloromethane solution were stirred at room temperature in the presence of Grubbs' second generation catalyst (10% by weight). Following purification using repeated preparative thin layer chromatography the target [2]catenane **74·BF$_4$** was isolated in 6.5% yield.

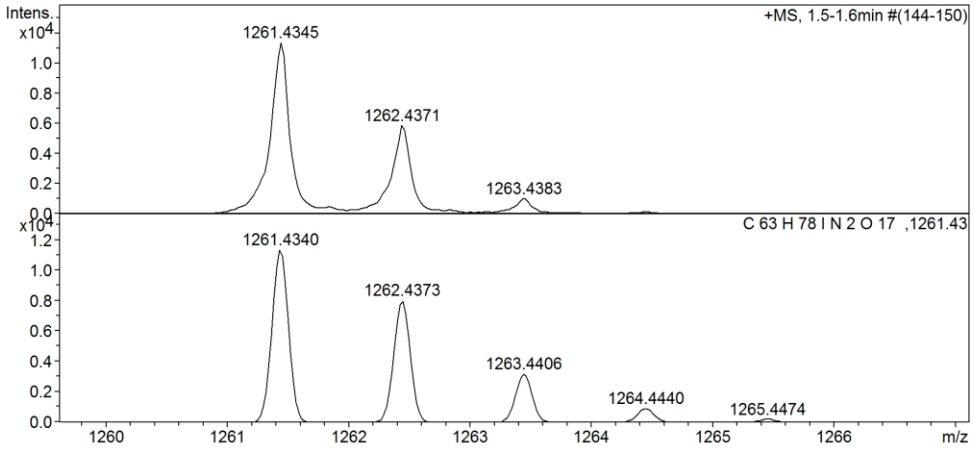


*Figure 3.15. High-resolution mass spectrum of catenane **74·BF$_4$**.*

Evidence for the successful formation of a halogen-bonded [2]catenane species is provided by electrospray mass spectrometry (Figure 3.15) and ^{1}H NMR spectroscopy (Figure 3.16).

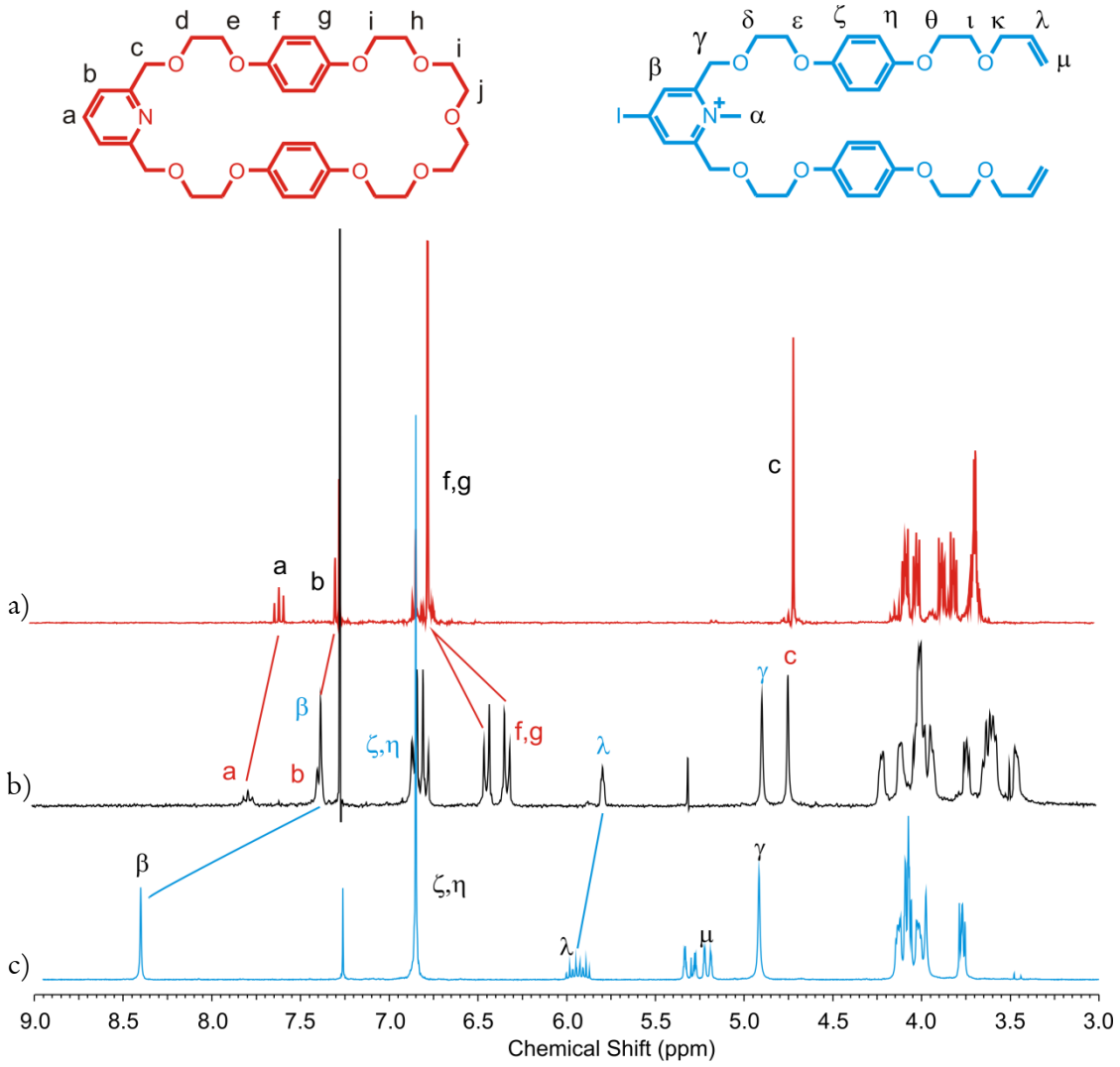


*Figure 3.16. Partial ^{1}H NMR spectra of a) pyridine macrocycle **71**, b) halogen-bonded [2]catenane **74·BF$_4$**, c) iodopyridinium ring closing metathesis precursor **65·BF$_4$** (300 MHz, $CDCl_3$, 293 K).*

The ^{1}H NMR spectrum of the [2]catenane and those of the component macrocycle and vinyl-appended precursor are shown in Figure 3.16. The disappearance of the multiplet *μ* and the convergence of multiplet *λ* into a pseudo-singlet in the catenane spectrum are attributed to cyclisation of the acyclic precursor. Most importantly, the upfield shift and splitting of the macrocycle hydroquinone protons *f* and *g* is indicative of aromatic donor–acceptor interactions between the electron-rich macrocycle hydroquinone units and the electron-poor pyridinium group. The downfield shift of pyridine protons *a* and *b* is consistent with the withdrawal of electron density by the formation of the halogen bond. Finally, the upfield shift of pyridinium proton signal *β* is a result of catenane inter-ring halogen-bond formation between the pyridine nitrogen and the iodine substituent.

Two dimensional ^{1}H–^{1}H ROESY spectroscopy was used to confirm the interlocked nature of the catenane. At 500 MHz, the spectrum in chloroform-d is broader than at 300 MHz which is indicative of dynamic behaviour on the NMR timescale. Heating to 70 °C in acetonitrile-d_3 gave a sharper one-dimensional ^{1}H NMR spectrum and through-space correlations between protons in the two ring components were identified in the ^{1}H–^{1}H ROESY spectrum (Figure 3.17).

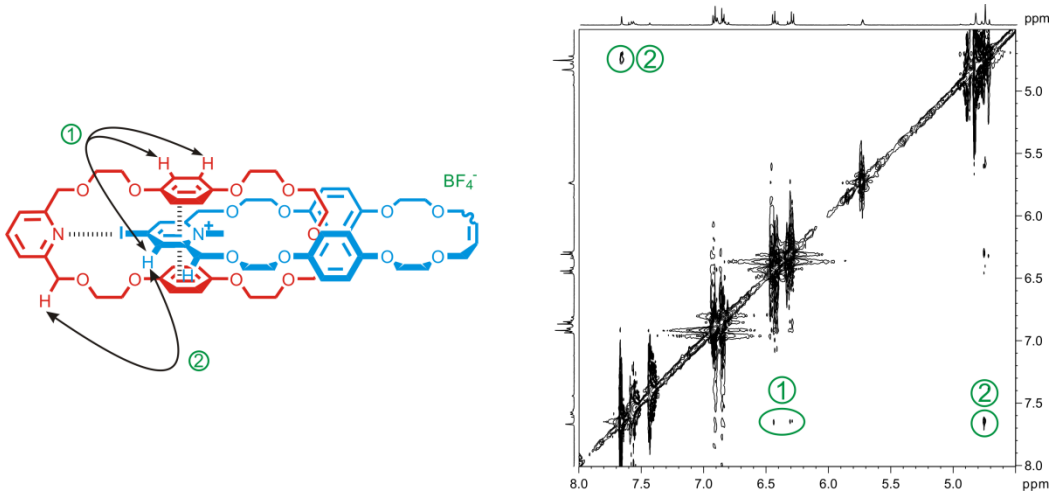


*Figure 3.17. ^{1}H–^{1}H ROESY NMR spectrum of catenane **74·BF$_4$**. Assignable inter-component through-space interactions are highlighted (500 MHz, CD_3CN, 343 K).*

The synthesis of the related protic and bromopyridinium functionalised catenanes were also attempted with threading components **62·BF$_4$** and **68·BF$_4$** by employing analogous Grubbs'-catalysed RCM reaction conditions. Although no evidence of catenane formation was observed with protic pyridinium thread **68·BF$_4$**, with the bromopyridinium thread **62·BF$_4$** a peak at m/z = 1213.4 corresponding to the [2]catenane species was detected by electrospray mass spectrometry. In spite of numerous attempts, however, the catenane could not be isolated which suggests it is produced in negligible yield.

3.3.4 Molecular dynamics simulations of catenane 74·BF$_4$ carried out by Professor Vitor Félix

In order to obtain further insights on the structure of catenane **74·BF$_4$**, molecular dynamics (MD) simulations were performed in explicit chloroform using the Amber 12[32] accelerated GPU code. The C–I···N halogen-bonding interaction was added to the general Amber force

field (GAFF)[33] via a dummy atom[34,35] which was parameterised as described in Appendix A.6. Four starting co-conformations were generated in the gas phase and are presented in Figure 3.18.

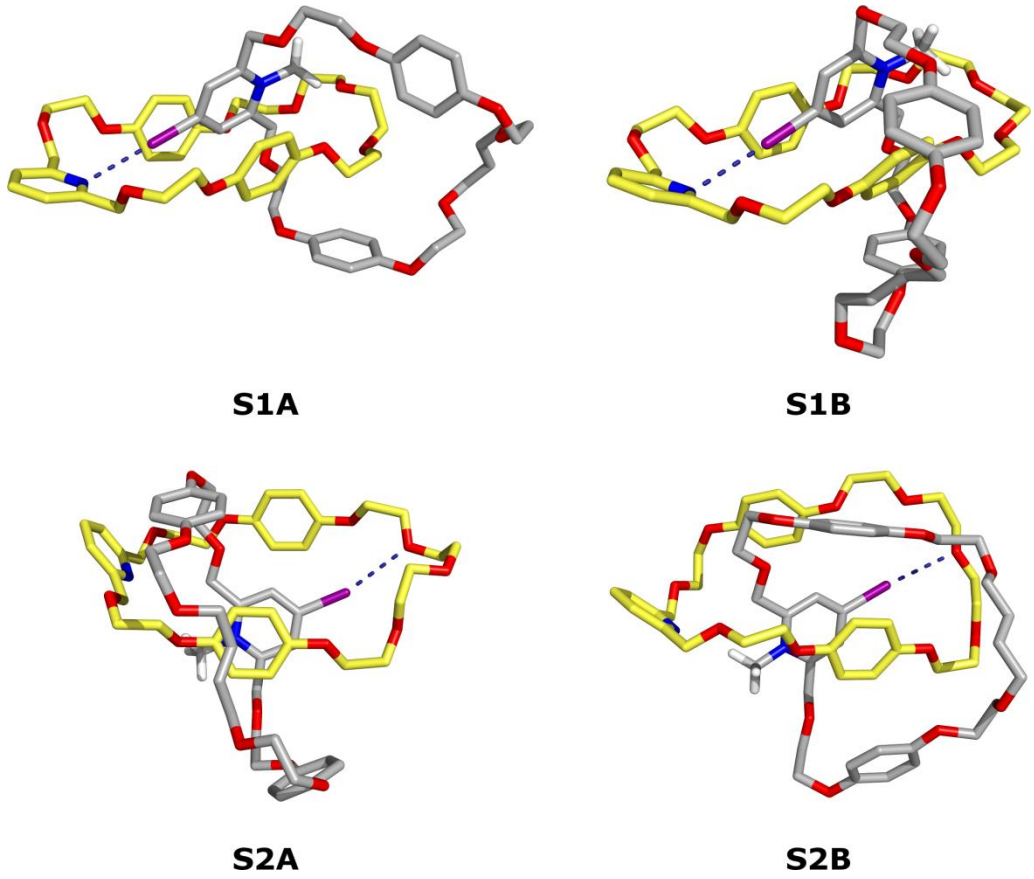


*Figure 3.18. Starting co-conformations used in the MD simulations, **S1A** and **S1B** exhibit a C–I···N halogen bond and **S2A** and **S2B** present a C–I···O halogen bond.*

These structures, **S1A**, **S1B**, **S2A**, and **S2B** correspond to two main arrangements: in **S1** (**A** and **B**) there is an I···N halogen bond as represented in Scheme 3.15 whereas in **S2** (**A** and **B**) co-conformations the iodopyridinium macrocycle is rotated with the C–I bond pointing towards the polyether loop of the pyridine macrocycle **71**. Within the two alternative binding scenarios, **A** and **B** differ mainly on the conformation of the iodopyridinium macrocycle. Subsequently, these four co-conformations were subjected to MD runs in chloroform for 50 ns.

The I···N halogen bond is highly stable throughout the course of the simulation time in both **S1A** and **S1B** co-conformations as evident by the plot of the I···N distances *versus* the C–I···N angles presented in Figure A.19. A narrow spot centred at a I···N distance of 3.19 Å and

a C–I···N angle of 173° is observed, which is indicative of the existence of a persistent halogen bond. A representative co-conformation of **74·BF$_4$** in chloroform solution for simulation **S1A** is presented in Figure 3.19. Simulation **S1B** yields a virtually identical co-conformation (see Figure A.20). In this representative frame, as mentioned earlier, an I···N halogen bond is established between the iodopyridinium derivative and the pyridine ring of the macrocycle. Additionally, this co-conformation is stabilised by the stacking interactions between the iodopyridinium moiety and the hydroquinone rings, in total agreement with the NMR findings.

The alternative **S2** scenarios (**A** and **B**) allow the existence of C–I···O halogen bonds between the iodopyridinium and the oxygen atoms of the polyether loop of the pyridine macrocycle. Indeed, these non-covalent interactions were intermittently observed during the MD simulations undertaken with both binding arrangements. This type of halogen bond is more labile than the C–I···N ones leading to a diffuse distribution of the I···O distances and C–I···O angles when they are plotted together as can be seen in Figure A.21, and therefore, are not sufficiently stable for halogen-bond templation. See Appendix A.6 for a full discussion of the MD simulations carried out with **S2A** and **S2B**.

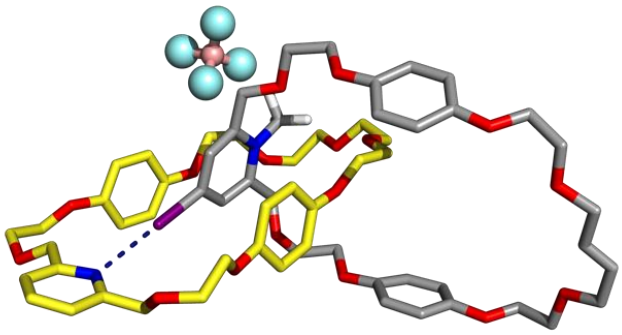


*Figure 3.19. Representative co-conformation of **74·BF$_4$** in chloroform solution for simulation **S1A**. Hydrogen atoms apart those from the methyl groups were omitted for clarity. The C–I···N halogen bond is drawn as blue dashed lines. Colour scheme: yellow or grey=C, red=O, blue=N, purple=I, light blue=F, light pink=B.*

3.3.5 Towards the synthesis of anion-templated, halogen-bonding [2]rotaxanes

It was envisaged that pyridine-based macrocycle precursor compound **67** could also be used to form a halogen-bond-templated [2]rotaxane species by a ring closing metathesis clipping reaction if an appropriate halogen-bond-donating axle component were prepared (Figure 3.20).

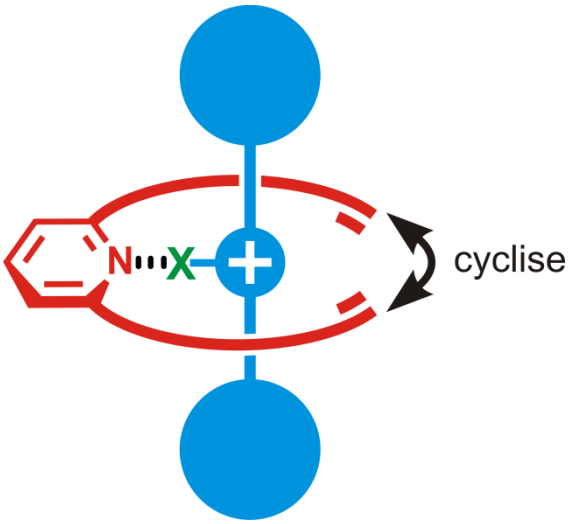
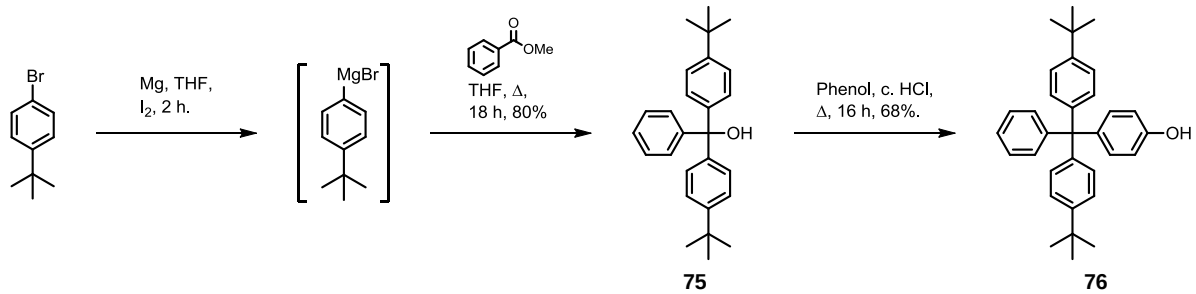


Figure 3.20. Cartoon representation of orthogonal halogen-bond-templated rotaxane species. X is a halogen atom.

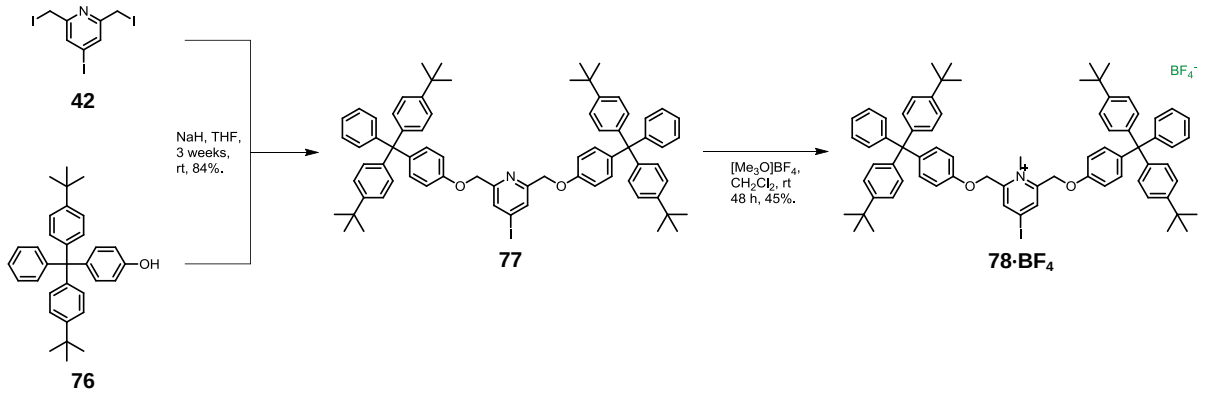
The required stoppered-axle component was prepared as outlined in Schemes 3.16 and 3.17.



Scheme 3.16. Synthesis of axle stopper compound ***76****.*

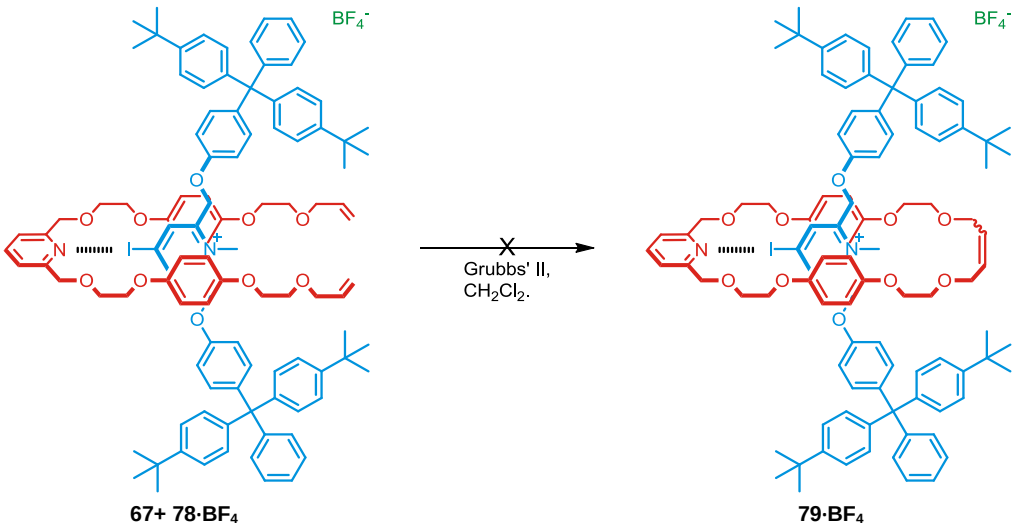
Heating 1-bromo-4-*tert*-butyl benzene and magnesium turnings in the presence of iodine in tetrahydrofuran afforded the Grignard intermediate, which was then reacted with methyl benzoate in tetrahydrofuran to give compound **75** in 80% yield. The required stopper phenol compound **76** was prepared in 68% yield by heating compound **75** in phenol in the presence of a catalytic amount of concentrated hydrochloric acid.

A nucleophilic substitution reaction between iodopyridine precursor compound **42** and stopper compound **76** in the presence of sodium hydride in tetrahydrofuran afforded the stoppered-pyridine compound **77** in 84% yield. Methylation using trimethyloxonium tetrafluoroborate in dichloromethane produced the required iodopyridinium axle component **78** in 45% yield.



Scheme 3.17. Synthesis of iodopyridinium-containing stoppered-axle compound ***78·BF*** $_4$.

With both the required axle and macrocycle precursor compounds in hand the attempted synthesis of a halogen-bond-templated rotaxane was undertaken (Scheme 3.18).



Scheme 3.18. Attempted synthesis of halogen-bond-templated [2]rotaxane ***79·BF*** $_4$.

Halogen-bond-donating iodopyridinium tetrafluoroborate axle **78·BF**$_4$ and two equivalents of halogen-bond-accepting pyridine-containing macrocycle precursor species **67** were stirred in the presence of Grubbs' second generation catalyst (10% by weight) in dichloromethane at room temperature. Evidence of successful rotaxane formation was provided by electrospray

mass spectrometry, where the cationic molecular ion peak is readily observed, which suggests the presence of a single interlocked species. Purification proved problematic, however, and despite numerous attempts the rotaxane species could not be isolated, which suggests it is formed in a low yield. A high-resolution mass spectrum of the rotaxane species was obtained (Figure 3.21) and shows the isotopic distribution of the interlocked rotaxane is in good agreement with the theoretical spectrum.

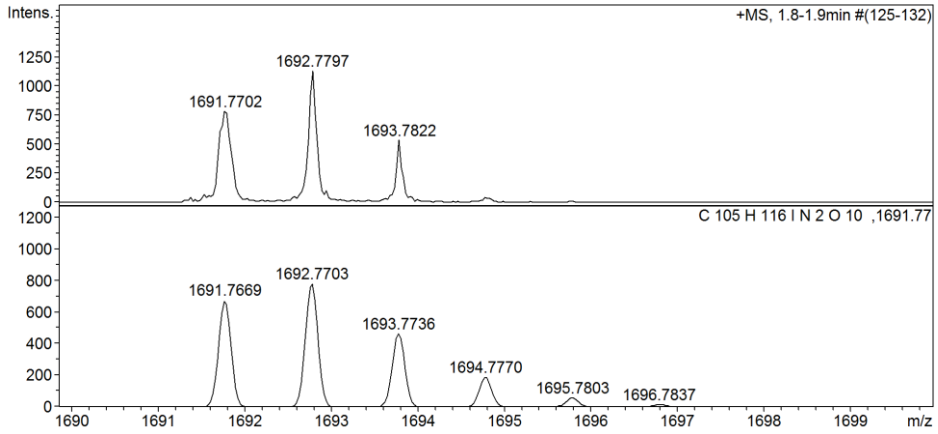


Figure 3.21. High-resolution mass spectrum of rotaxane ***79·BF$_4$****.*

3.4 Towards molecular switches which operate through a combination of halogen bonding and anion binding

The power of halogen bonding to direct the assembly of anion-templated interlocked structures has been highlighted and the ability of the resulting catenanes to complex halide anionic guests in competitive 1:1 chloroform-d:methanol-d_4 solution was revealed in section 3.2. Moreover, by designing a suitable macrocycle with an integrated halogen-bond-accepting pyridine unit, the construction of interpenetrated and interlocked architectures templated by a single charge-assisted halogen bond was achieved. It was envisaged that, through the design and synthesis of a suitable macrocycle containing both an isophthalamide anion recognition motif and a pyridine unit, a potential conformationally switchable [2]catenane could be prepared, designed to undergo anion-binding-induced pirouetting of one macrocycle with respect to another through inter-ring halogen-bond breaking and inter-ring anion binding (Figure 3.22).

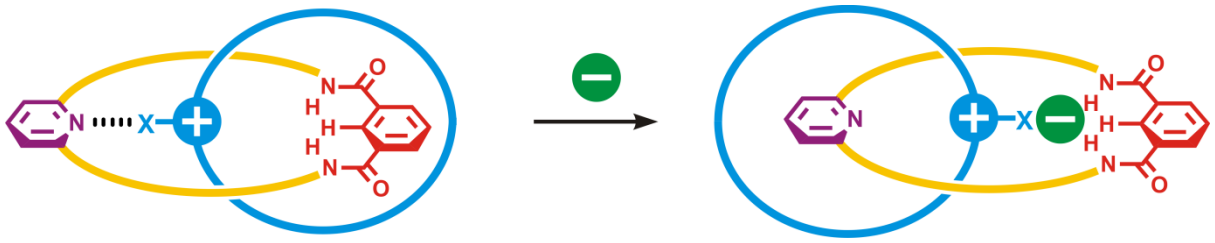
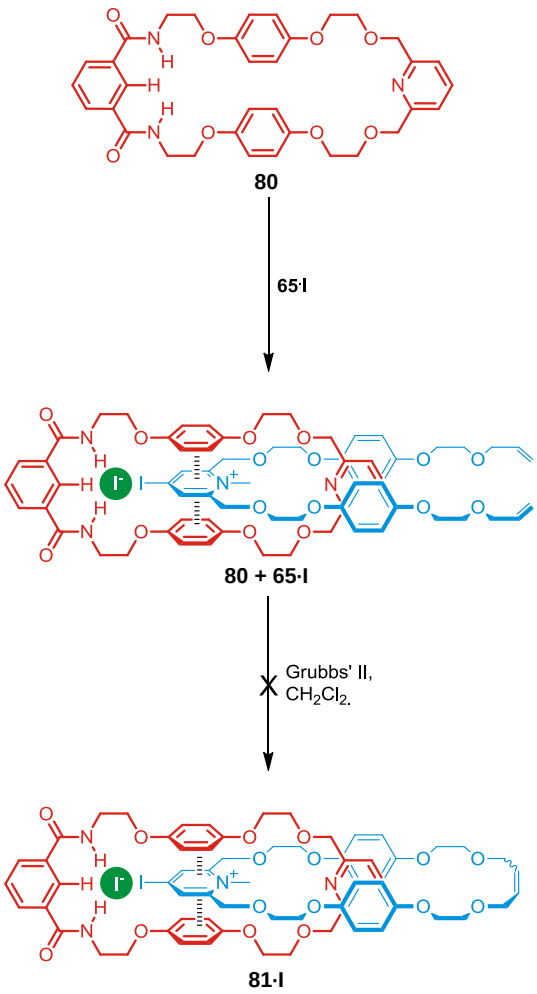


Figure 3.22. Cartoon representation of a halogen-bonding catenane which can undergo anion-induced switching.

The attempted synthesis of the target catenane is outlined in Scheme 3.19. Heteroditopic macrocycle **80** was prepared and donated by Dr T. Lang. Macrocycle **80** and 1.1 equivalents of iodopyridinium iodide macrocycle precursor **65·I** were stirred in the presence of Grubbs' second generation catalyst (10% by weight) in dichloromethane. Pleasingly, a peak corresponding to the catenane species **81·I** was observed in the crude mass spectrum confirming the successful formation of the interlocked structure.



*Scheme 3.19. Attempted synthesis of catenane **81·I**.*

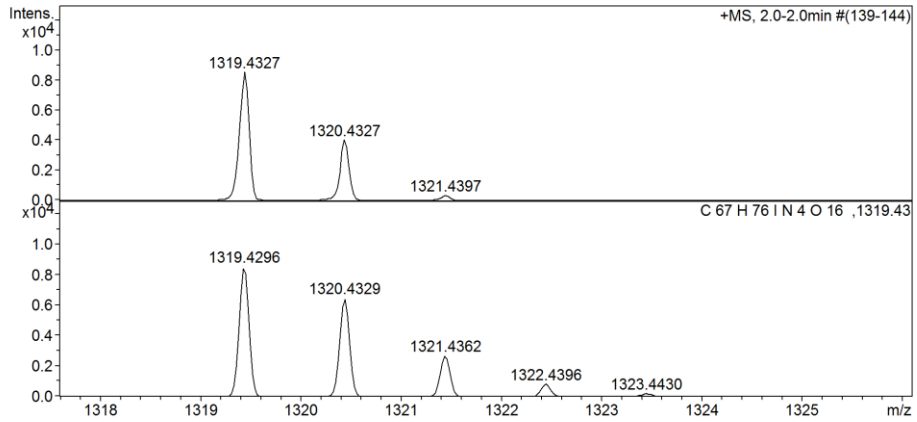


*Figure 3.23. High-resolution mass spectrum of rotaxane **81·I**.*

In spite of a number of attempts, however, it was not possible to isolate the target compound suggesting it did not form in particularly high yield.

3.5 Conclusions and future work

A series of new iodo- and bromo-functionalised pyridinium threading components and macrocycle precursor species were designed and synthesised, and their ability to form halide-anion-templated interpenetrative pseudorotaxane assemblies with an isophthalamide-containing macrocycle was explored. Pseudorotaxane formation was more favourable when halogen-bonding was employed—specifically, the more stable bromide- and iodide-templated interpenetrated assemblies were found with the iodopyridinium species, which reflects the greater halogen-bond-donor ability of the more polarisable iodine atom. The stability of the anion-templated halogen-bonding pseudorotaxanes was utilised in the construction of two novel halogen-bonding catenane architectures, whose halide anion recognition properties were probed in competitive solvent mixture. The strength of anion binding was found to be similar for both bromine and iodine halogen-bond-donor catenanes which each display anion affinities iodide > bromide> chloride; the opposite of those expected on anion basicity grounds.

Through the use of a suitable halogen-bond-acceptor pyridine-containing macrocycle, the formation of pseudorotaxane assemblies with halogen-bond-donating bromo- and iodo-functionalised pyridinium threading components was achieved, which are stabilised by a

single charge-assisted halogen-bonding interaction. The strength of the halogen-bond-templated interpenetrative assembly between the pyridine macrocycle and iodopyridinium thread was exploited in the Grubbs'-catalysed RCM clipping synthesis of a novel [2]catenane. The crucial importance of the single charge-assisted halogen-bonding interaction between the two components was highlighted by the fact that no evidence of catenane formation was observed in an analogous RCM reaction of the pyridine macrocycle with the corresponding protic-pyridinium reactant. The construction of a similar halogen-bond-templated rotaxane species was explored but the reaction occurred in a prohibitively low yield to allow facile purification of the interlocked product.

Finally, an ambitious attempt to prepare the first halogen-bonding, anion-triggered molecular switch where halogen bonding is used to bind the anionic guest was undertaken. A ditopic macrocycle containing both an isophthalamide anion recognition site and a pyridine halogen-bond-acceptor motif was prepared by Dr T. Lang. Disappointingly, however, the Grubbs'-catalysed RCM clipping reaction to produce the target catenane framework did not proceed in sufficient yield to enable isolation of pure product, although evidence of its formation was provided by both ^{1}H NMR and mass spectroscopy.

Halogen bonding has been shown to have real potential in the templation of interlocked structures and in anion recognition applications. Future work could pursue the construction of halogen-bonding, anion-templated rotaxane species. An anion-templated orthogonal complex could be assembled between the halogen-bonding iodopyridinium (or analogous bromopyridinium) axle component (prepared in Scheme 3.17) and an appropriate isophthalamide-containing bis-vinyl-appended macrocycle precursor, and cyclisation using Grubbs'-catalysed RCM to give the interlocked host could then be undertaken. The anion recognition properties of such interlocked systems could then be investigated and compared to the catenanes reported above. Further attempts to prepare the halogen-bonding molecular switch could be undertaken, perhaps on a larger scale using bromide anion-templation.

3.6 References for Chapter Three

[1] E. R. Kay, D. A. Leigh and F. Zerbetto, *Angew. Chem. Int. Ed.*, 2007, **46**, 72-191.
[2] S. Saha and J. F. Stoddart, *Chem. Soc. Rev.*, 2007, **36**, 77-92.
[3] J. D. Crowley, E. R. Kay and D. A. Leigh, in *Intelligent Materials*, eds. M. Shahinpoor and H.-J. Schneider, RSC Publiching, Cambridge, 2008, p. 1-47.
[4] S. R. Bayly, T. M. Gray, M. J. Chmielewski, J. J. Davis and P. D. Beer, *Chem. Commun.*, 2007, 2234-2236.
[5] D. Curiel and P. D. Beer, *Chem. Commun.*, 2005, 1909-1911.
[6] J. J. Gassensmith, S. Matthys, J.-J. Lee, A. Wojcik, P. V. Kamat and B. D. Smith, *Chem. Eur. J.*, 2010, **16**, 2916-2921.
[7] N. H. Evans and P. D. Beer, *Org. Biomol. Chem.*, 2011, **9**, 92-100.
[8] M. J. Chmielewski, J. J. Davis and P. D. Beer, *Org. Biomol. Chem.*, 2009, **7**, 415-424.
[9] M. D. Lankshear and P. D. Beer, *Acc. Chem. Res.*, 2007, **40**, 657-668.
[10] P. Metrangolo, F. Meyer, T. Pilati, G. Resnati and G. Terraneo, *Angew. Chem. Int. Ed.*, 2008, **47**, 6114-6127.
[11] D. Cincic, T. Friscic and W. Jones, *Chem. Eur. J.*, 2008, **14**, 747-753.
[12] L. C. Roper, C. Prasang, V. N. Kozhevnikov, A. C. Whitwood, P. B. Karadakov and D. W. Bruce, *Cryst. Growth Des.*, 2010, **10**, 3710-3720.
[13] N. S. Goroff, S. M. Curtis, J. A. Webb, F. W. Fowler and J. W. Lauher, *Org. Lett.*, 2005, **7**, 1891-1893.
[14] R. Liantonio, P. Metrangolo, T. Pilati, G. Resnati and A. Stevenazzi, *Cryst. Growth Des.*, 2003, **3**, 799-803.
[15] D. W. Bruce, P. Metrangolo, F. Meyer, C. Prasang, G. Resnati, G. Terraneo and A. C. Whitwood, *New J. Chem.*, 2008, **32**, 477-482.
[16] M. T. Johnson, Z. Džolić, M. Cetina, O. F. Wendt, L. Öhrström and K. Rissanen, *Cryst. Growth Des.*, 2011, **12**, 362-368.
[17] M. G. Sarwar, B. Dragisic, S. Sagoo and M. S. Taylor, *Angew. Chem. Int. Ed.*, 2010, **49**, 1674-1677.
[18] N. L. Kilah, M. D. Wise, C. J. Serpell, A. L. Thompson, N. G. White, K. E. Christensen and P. D. Beer, *J. Am. Chem. Soc.*, 2010, **132**, 11893-11895.
[19] C. J. Serpell, N. L. Kilah, P. J. Costa, V. Felix and P. D. Beer, *Angew. Chem. Int. Ed.*, 2010, **49**, 5322-5326.
[20] A. Caballero, F. Zapata, N. G. White, P. J. Costa, V. Felix and P. D. Beer, *Angew. Chem. Int. Ed.*, 2012, **51**, 1876-1880.
[21] M. Erdelyi, *Chem. Soc. Rev.*, 2012, **41**, 3547-3557.
[22] F. Zapata, A. Caballero, N. G. White, T. D. W. Claridge, P. J. Costa, V. Felix and P. D. Beer, *J. Am. Chem. Soc.*, 2012, **134**, 11533-11541.
[23] T. M. Beale, M. G. Chudzinski, M. G. Sarwar and M. S. Taylor, *Chem. Soc. Rev.*, 2013, **42**, 1667-1680.
[24] H. Takalo, P. Pasanen and J. Kankare, *Acta Chem. Scand. Ser. B.*, 1988, **42**, 373-377.
[25] A. Picot, C. Feuvrie, C. Barsu, F. Malvolti, B. Le Guennic, H. Le Bozec, C. Andraud, L. Toupet and O. Maury, *Tetrahedron*, 2008, **64**, 399-411.
[26] L. M. Hancock and P. D. Beer, *Chem. Eur. J.*, 2009, **15**, 42-44.
[27] J. W. Lown, R. Rao Koganty and A. V. Joshua, *J. Org. Chem.*, 1982, **47**, 2027-2033.
[28] M. J. Hynes, *J. Chem. Soc., Dalton Trans.*, 1993, 311-312.
[29] L. Crombie, A. P. Ryan, D. A. Whiting and S. O. Yeboah, *J. Chem. Soc., Perkin Trans. 1*, 1987, 2783-2786.
[30] P. Nilsson, M. Larhed and A. Hallberg, *J. Am. Chem. Soc.*, 2001, **123**, 8217-8225.
[31] F. Zordan, L. Brammer and P. Sherwood, *J. Am. Chem. Soc.*, 2005, **127**, 5979-5989.
[32] D. A. Case, T. A. Darden, I. T. E. Cheatham, C. L. Simmerling, J. Wang, R. E. Duke, R. Luo, R. C. Walker, W. Zhang, K. M. Merz, B. Roberts, S. Hayik, A. Roitberg, G. Seabra, J. Swails, A. W. Götz, I. Kolossváry, K. F. Wong, F. Paesani, J. Vanicek, R. M. Wolf, J. Liu, X. Wu, S. R. Brozell, T. Steinbrecher, H. Gohlke, Q. Cai, X. Ye, J. Wang, M.-J. Hsieh, G. Cui, D. R. Roe, D. H. Mathews, M. G. Seetin, R. Salomon-Ferrer, C. Sagui, V. Babin, T. Luchko, S. Gusarov, A. Kovalenko and P. A. Kollman, *AMBER12*, University of California, San Francisco, 2012.
[33] J. Wang, R. M. Wolf, J. W. Caldwell, P. A. Kollman and D. A. Case, *J. Comput. Chem.*, 2004, **25**, 1157-1174.

[34] M. A. A. Ibrahim, *J. Comput. Chem.*, 2011, **32**, 2564-2574.
[35] S. Rendine, S. Pieraccini, A. Forni and M. Sironi, *PCCP*, 2011, **13**, 19508-19516.

Chapter Four

Chapter 4 Triazolium-containing interpenetrated and interlocked host structures for anion recognition†

4.1 Introduction and chapter aims

In recent years the 1,4-dialkyl-1,2,3-triazole and related triazolium motifs have emerged as effective anion binding units, and not simply as convenient covalent linkers in organic structures.[1] As outlined in Chapters One and Two, the advent of the copper(I)-catalysed cycloaddition reaction (Figure 4.1a) between a terminal alkyne and an azide has been central to the surge in popularity of the 1,2,3-triazole group in supramolecular chemistry applications. Indeed, various receptors incorporating the 1,2,3-triazole and -triazolium groups have been reported; in particular, Flood's macrocycle (Figure 4.1b) and Beer's rotaxane (Figure 4.1c) represent significant developments in this area.[2,3] To date, only receptors incorporating 1,4-disubstituted triazole and triazolium units have been prepared for anion recognition purposes.

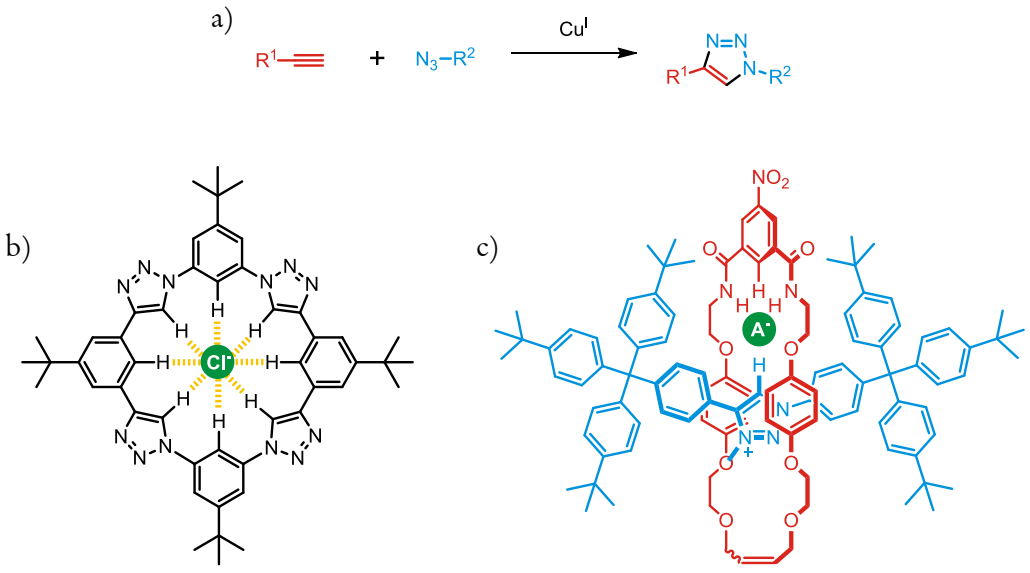
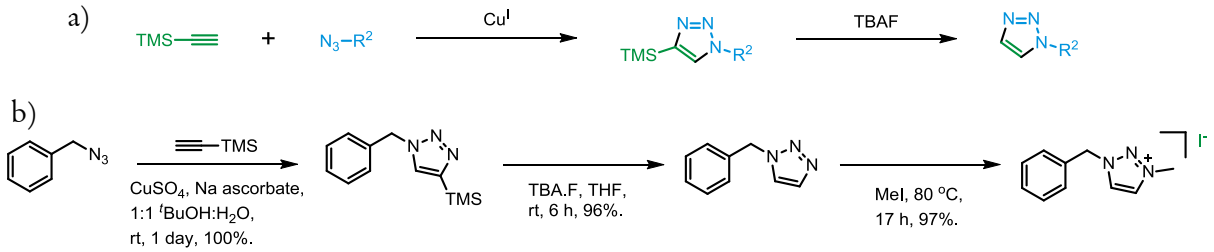


Figure 4.1. a) Schematic representation of the CuAAC reaction forming a 1,4-dialky-1,2,3-triazole. b) Flood's triazolophane for chloride recognition. c) One of Beer's triazolium-containing [2]rotaxanes.

†Some of the synthetic investigations and anion binding studies in this chapter were carried out in collaboration with Part II undergraduate student Claire Carpenter.

In 2010, it was reported that by replacing the terminal alkyne species with trimethylsilylacetylene, 1,3-disubstituted-1,2,3-triazolium moieties can be prepared for use as ionic liquids and solvents in organic synthesis (Scheme 4.1a).[4] Their use as anion receptor groups, however, has not been explored.



Scheme 4.1. a) Schematic representation of the copper(I)-catalysed synthesis of a 1,3-diazlkyl-1,2,3-triazole. b) Ryu and co-workers' preparation of a 1,3-dialkyl-1,2,3-triazolium ionic liquid.

The synthesis involves a copper(I)-catalysed 1,3-dipolar cycloaddition reaction between a terminal azide and trimethylsilylacetylene. The trimethylsilyl group is subsequently removed using tetrabutylammonium fluoride in tetrahydrofuran, and alkylation affords the 1,3-dialkyl-1,2,3-triazolium ion pair (Scheme 4.1b).

This 1,3-disubstituted-triazolium motif (Figure 4.2a) deploys two polarised C–H hydrogen-bond donors which may give rise to enhanced anion recognition compared with the 1,4-disubstituted-triazolium group (Figure 4.2b), which only proffers one hydrogen-bond-donor atom. In addition, the three sp^2 hybridised nitrogen atoms could potentially polarise the C–H bonds more strongly than in the topologically similar 2-methylimidazolium anion binding unit (Figure 4.2c), which has been shown to bind anions in chloroform.[5,6]

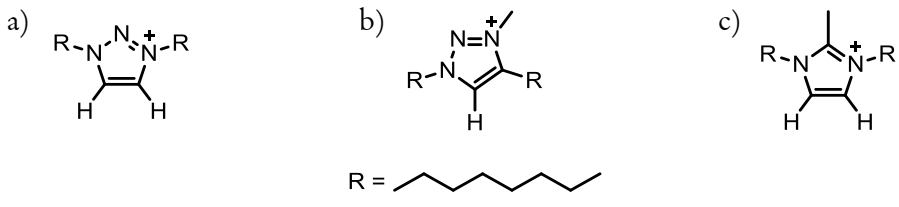


Figure 4.2. a) The target 1,3-dialkyl-1,2,3-triazolium group. b) The analogous 1,4-dialkyl-1,2,3-triazolium group. c) The equivalent 1,3-dialkyl-2-methylimidazolium group.

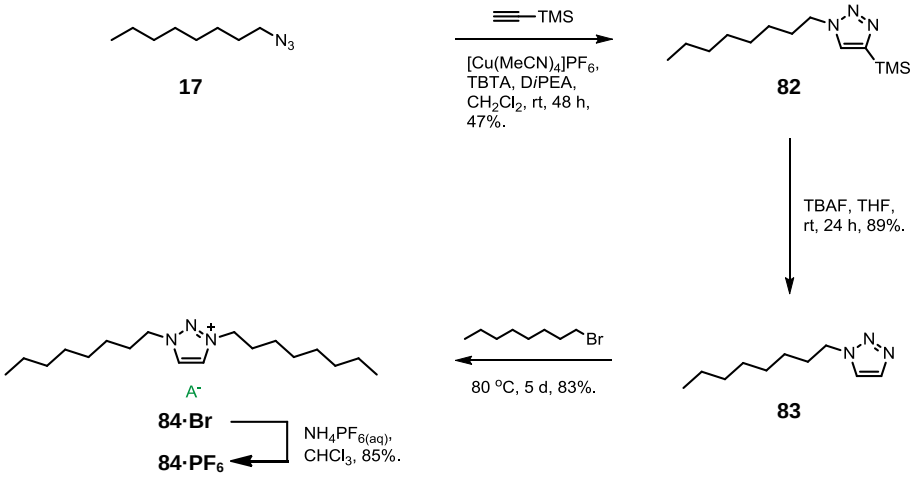
The aim of this chapter was to incorporate this under-exploited 1,3-dialkyltriazolium moiety into interpenetrated and interlocked molecular architectures for anion recognition

applications. The preparation of a novel acyclic 1,3-dialkyltriazolium receptor is undertaken initially and its anion binding properties elucidated. Anion-templated pseudorotaxane assembly studies with such derivatives are carried out and the synthesis of an interlocked [2]rotaxane system is attempted. Finally, the preparation of new macrocyclic receptors containing 1,3- and 1,4-dialkyltriazolium anion recognition motifs is also described and the synthesis of interlocked structures containing these cyclic components investigated.

4.2 Acyclic 1,3-dialkyltriazolium anion receptor

4.2.1 Synthesis and characterisation of acyclic dialkyltriazolium-based anion receptors

The synthesis of an acyclic 1,3-dialkyltriazolium anion receptor was accomplished as outlined in Scheme 4.2.

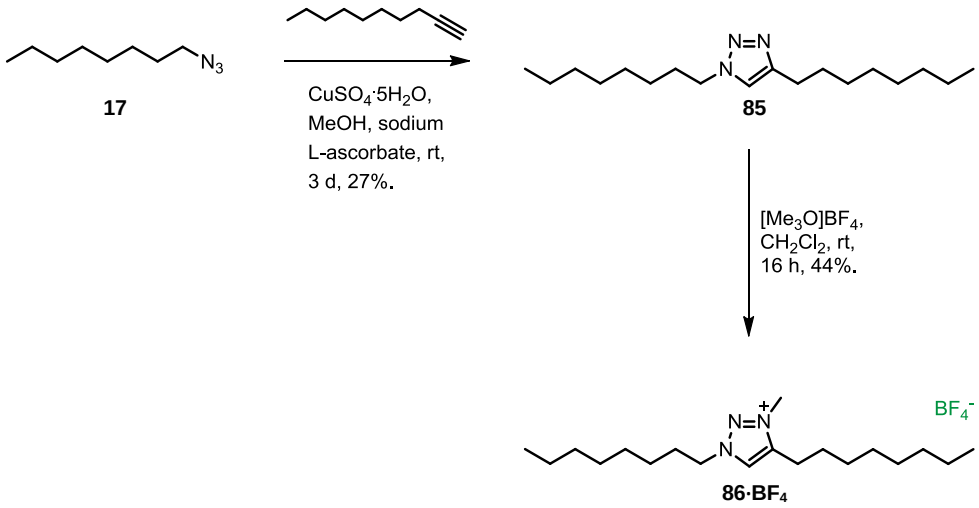


Scheme 4.2. Synthesis of acyclic 1,3-dialkyltriazolium anion receptor ***84·PF$_6$***.

A CuAAC reaction between azide **17** and trimethylsilylacetylene in the presence of copper(I)tetrakis-acetonitrile hexafluorophosphate, *N*,*N*-di-*iso*-propylethylamine and TBTA in dichloromethane gave the triazole compound **82** in 47% yield after column chromatographic purification. Trimethylsilyl-deprotection was achieved using tetrabutylammonium fluoride in tetrahydrofuran, producing compound **83** in 89% yield. Heating triazole compound **83** in 1-*n*-octylbromide afforded the triazolium compound **84·Br**

in 83% yield, which was then anion exchanged to the non-coordinating hexafluorophosphate salt to enable anion binding properties to be elucidated.

The synthesis of the related 1,4-dialkyltriazolium anion receptor for comparison is described in Scheme 4.3. A cycloaddition reaction between 1-azidooctane **17** and 1-decyne using copper sulfate and sodium L-ascorbate in methanol gave triazole species **85** in 27% yield. Alkylation was achieved in 44% yield by stirring compound **85** with trimethyloxonium tetrafluoroborate in dichloromethane giving triazolium compound **86·BF$_4$** which has the added advantage that the counter anion is the non-coordinating tetrafluoroborate anion.



*Scheme 4.3. Synthesis of 1,4-dialkyltriazolium receptor **86·BF$_4$**.*

Both dialkyltriazolium-based anion receptors were characterised by ^{1}H, ^{13}C NMR spectroscopy and electrospray mass spectrometry.

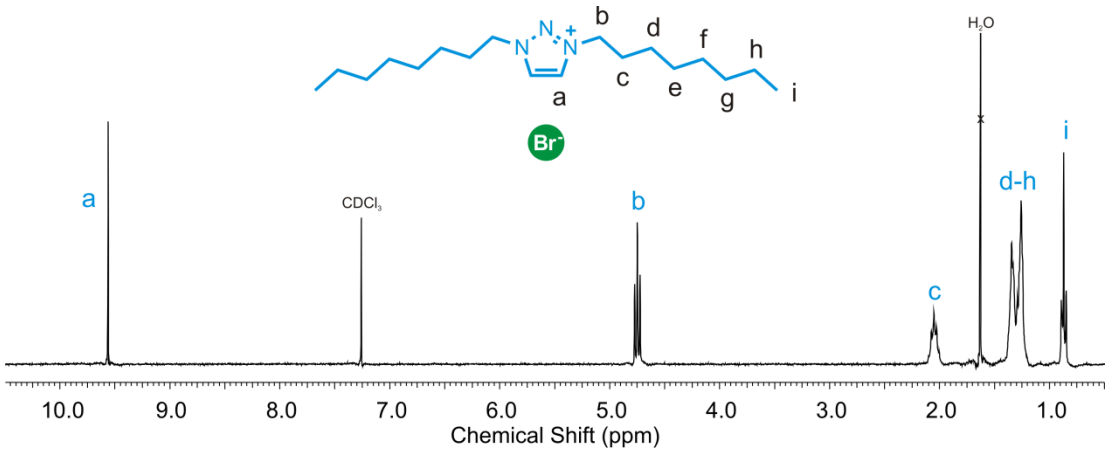


*Figure 4.3. ^{1}H NMR spectrum of 1,3-dialkyltriazolium bromide compound **84·Br*** (300 MHz, $CDCl_3$, 293 K).

The assigned ^{1}H NMR spectrum of compound **84·Br** is shown in Figure 4.3. Of particular importance is the singlet corresponding to the two triazolium protons *a*, which is consistent with the formation of a symmetric molecule as well as with bromide binding equally to both triazolium protons through two C–H···bromide hydrogen-bonding interactions.

This symmetric halide binding by two hydrogen bonds was corroborated by the solid state structure of compound **84·Br** (Figure 4.4). Single crystals suitable for X-ray diffraction structural determination were grown by slow vapour diffusion of di-*iso*-propyl ether into a chloroform solution of **84·Br**. The structure (solved by Dr Nicholas White) reveals C–H···bromide hydrogen bonding between the two triazolium protons *a* and the bromide anion guest: C–H···Br = 3.461(7) Å and 3.610(7) Å.

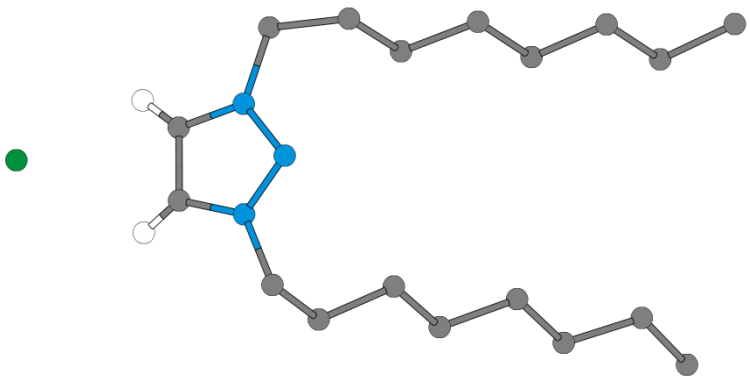


*Figure 4.4. Ball and stick plot of 1,3-dialkyltriazolium bromide compound **84·Br**. Colour scheme: grey=C, blue=N, green=Br, white=H.*

4.2.2 Anion recognition properties of dialkyltriazolium-based anion receptors

The anion binding affinities of the dialkyltriazolium receptors **84·PF$_6$** and **86·BF$_4$** were investigated using ^{1}H NMR spectroscopic titrations in chloroform-d solution. Following addition of anions to both receptors, significant downfield shift perturbation of the respective triazolium proton signal is observed which is consistent with the deshielding of these protons through hydrogen bonding to the anion guest species (Figure 4.5).

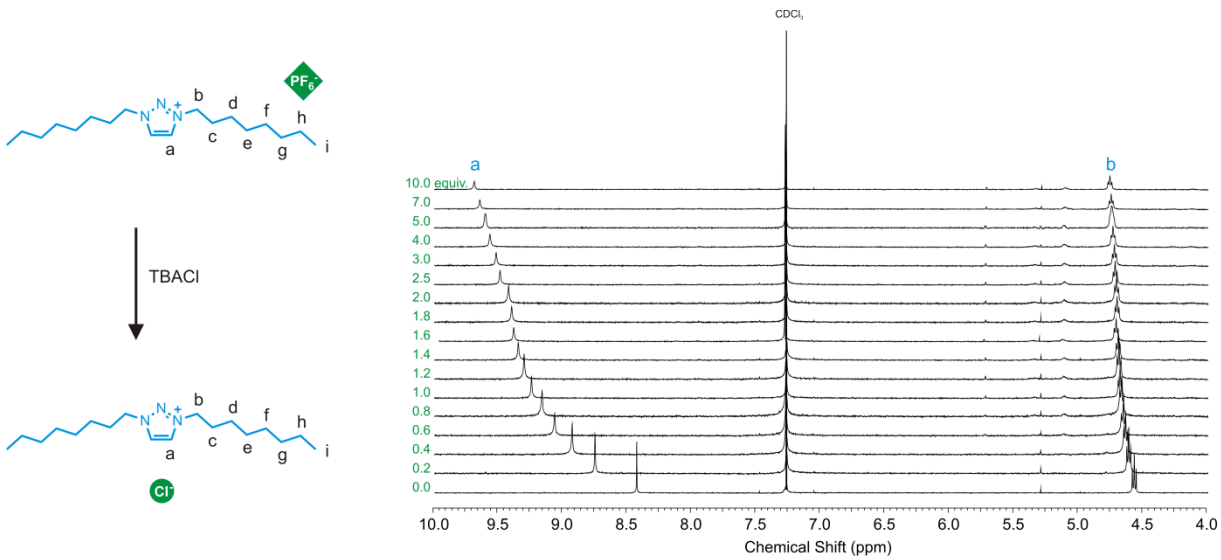


*Figure 4.5. Partial ^{1}H NMR spectra of receptor **84·PF$_6$** and equivalents of TBA·Cl (500 MHz, $CDCl_3$, 293 K).*

Monitoring these shifts as a function of the concentration of anion produced the titration curves shown in Figure 4.6 and winEQNMR[7] analysis of the titration data determined 1:1 stoichiometric association constants reported in Table 4.1.

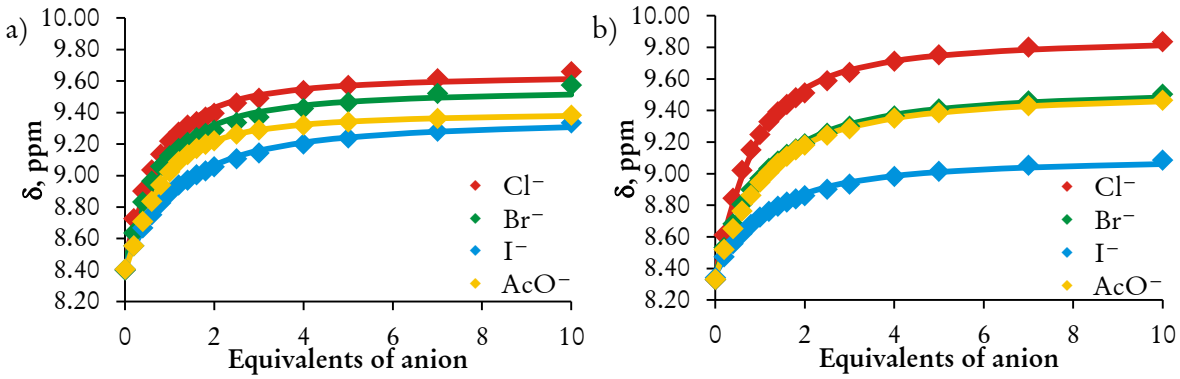


*Figure 4.6. Titration curves for addition of various anions to receptors a) **84·PF$_6$** and b) **86·BF$_4$** obtained by monitoring the triazolium protons. $CDCl_3$, 293 K. Square data points represent experimental data; continuous lines represent theoretical binding isotherms.*

*Table 4.1. Anion association constants, K_a (M^{-1}), for **84·PF$_6$**, **86·BF$_4$**, and a 2-methylimidazolium analogue.*

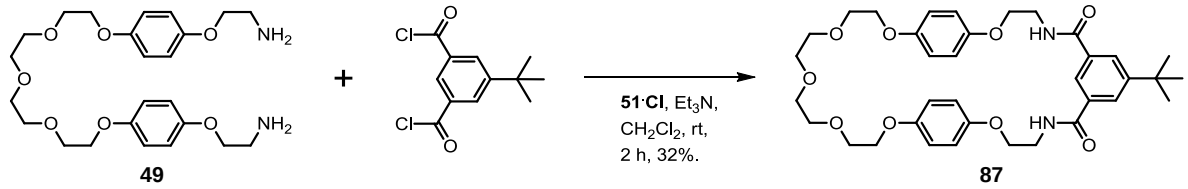
Anion	**84·PF$_6$** K_a(M^{-1})[a]	**86·BF$_4$** K_a(M^{-1})[a]	*2-methylimidazolium*[b] K_a(M^{-1})[a]
Cl^-	1372(209)	1085(77)	782(42)
Br^-	1147(175)	710(47)	523(60)
I^-	600(43)	627(33)	402(44)
AcO^-	1374(34)	721(19)	827(69)

[a]*All anions added as their TBA salt. Association constants were determined by monitoring the downfield shift of the triazolium or imidazolium proton.* [b]*Association constants take from reference* [6]*. Estimated standard errors are given in parentheses. $CDCl_3$, 293 K.*

Importantly, 1,3-dialkyltriazolium species **84·PF$_6$** is a more potent anion complexant than the 1,4-dialkytriazolium host **86·BF$_4$**: for example, with chloride $K_a = 1372$ and 1085 M^{-1} respectively. This may be attributed to the ability of the 1,3-dialkyltriazolium receptor **84·PF$_6$** to contribute two hydrogen-bond-donor groups to the anion binding process and the additional C–H···anion hydrogen-bonding interaction leads to stronger anion recognition. These data also highlight the importance of hydrogen bonding to the overall strength of the anion–receptor complex—the binding is not simply electrostatic in origin. Interestingly, the strength of bromide association is significantly greater with 1,3-dialkyltriazolium receptor **84·PF$_6$** which suggests the formation of two hydrogen-bonding interactions improves the affinity for this larger halide anion. It is worth noting the doubling in the strength of acetate binding with the 1,3-dialkyltriazolium-based species **84·PF$_6$**, which is possibly on account of the two complementary hydrogen-bond donors being more favourably oriented for the 'Y'-shaped acetate anion. In addition, the triazolium analogue **84·PF$_6$** also binds anions more strongly than the topologically equivalent 2-methylimidazolium receptor (for chloride association $K_a = 1372$ *versus* 782 M^{-1}), which is presumably a consequence of the electron-withdrawing effect of an additional nitrogen atom in the heterocycle further polarising the C–H hydrogen-bond-donor groups.

4.2.3 Pseudorotaxane assembly studies

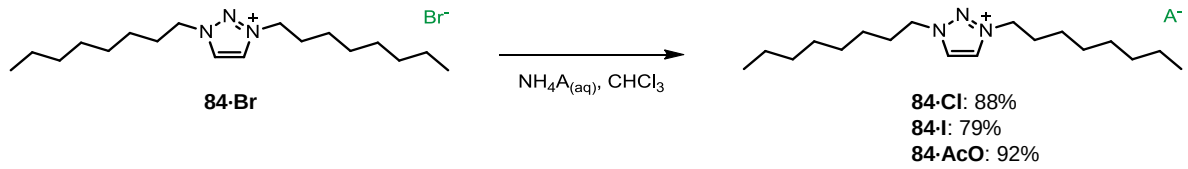
Pseudorotaxane formation between a 2-methylimidazolium chloride threading component and a 5-*tert*-butyl-isophthalamide-containing macrocycle has previously been studied.[5,6] To enable direct comparison with the potential dialkyltriazolium threading components, the 5-*tert*-butyl-isophthalamide macrocycle species **87** was prepared according to a known literature procedure as outlined in Scheme 4.4.[8,9]



Scheme 4.4. Synthesis of macrocycle 87.

Macrocycle precursor bis-amine **49** was condensed with one equivalent of 5-*tert*-butyl-isophthaloyl dichloride (prepared by heating the bis-acid in thionyl chloride) in the presence of pyridinium chloride template **51·Cl** and triethylamine in anhydrous dichloromethane. Following purification by column chromatography the target macrocycle **87** was isolated in 32% yield.[8,9]

The chloride, iodide, and acetate salts of 1,3-dialkylimidazolium derivative **84·A** were prepared in order to probe the strength of pseudorotaxane assembly between **84·A** and macrocycle **87** with a range of anion templates. The required anion exchanges were achieved by repeated washing of a chloroform solution of **84·Br** with the appropriate aqueous ammonium salt to give compounds **84·Cl**, **84·I** and **84·AcO** in 88%, 79% and 92% yields respectively (Scheme 4.5).



Scheme 4.5. Anion exchange of compound 84·Br.

With both macrocycle and potential 1,3-dialkyltriazolium threading components in hand ^{1}H NMR titration pseudorotaxane assembly studies were undertaken. A qualitative ^{1}H NMR

investigation was initially carried out; Figure 4.7 shows the ^{1}H NMR spectrum of an equimolar mixture of macrocycle **87** and **84·Cl** in chloroform-d solution together with those of component macrocycle and threading species for comparison.

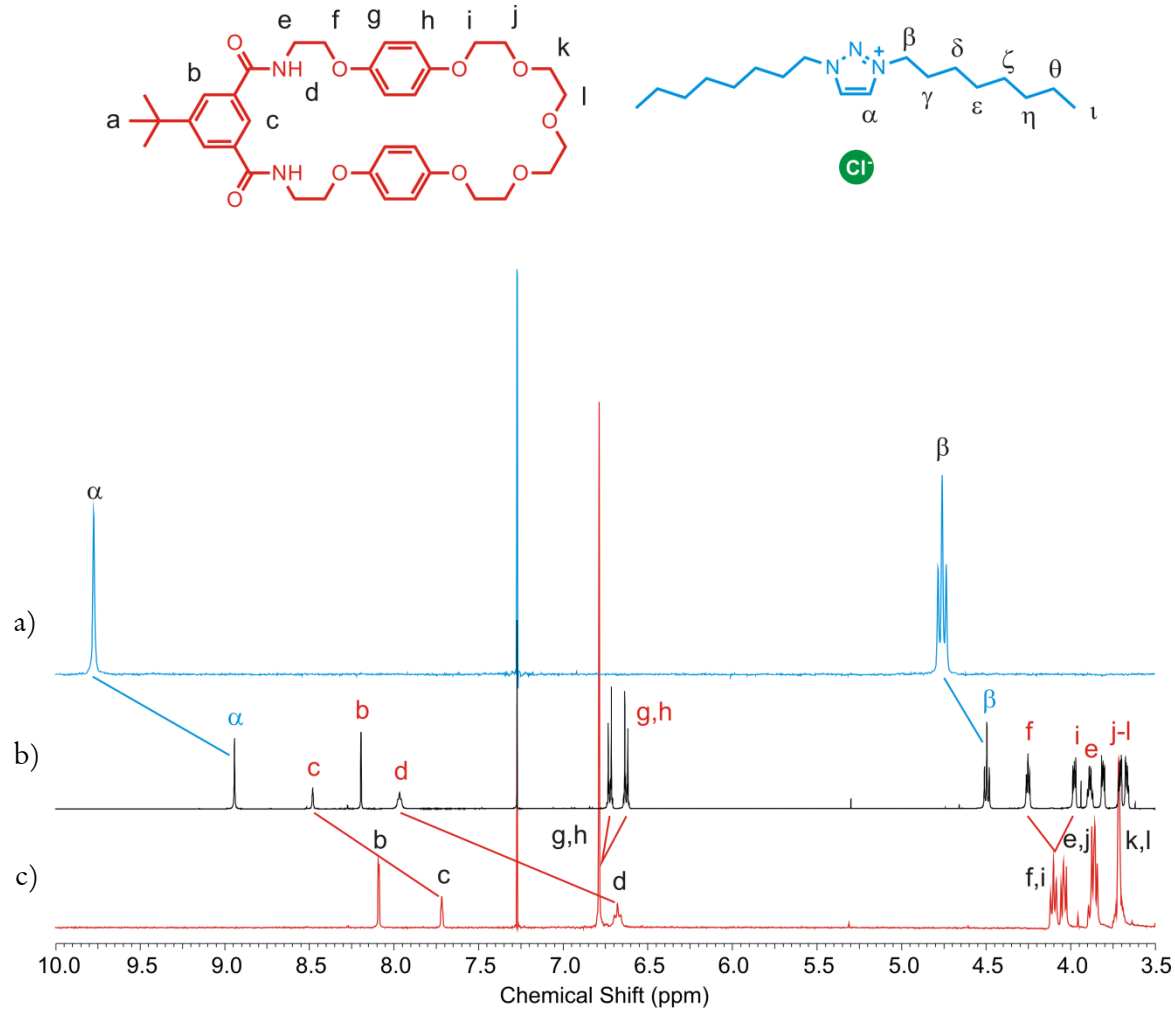


*Figure 4.7. Partial ^{1}H NMR spectra of: a) threading component **84·Cl**; b) pseudorotaxane 1:1 **84·Cl**:**87**; and c) macrocycle **87** (300 MHz, $CDCl_3$, 293 K).*

Evidence of successful pseudorotaxane formation is demonstrated by the upfield shift and splitting of the hydroquinone protons signal *g,h* which is diagnostic of aromatic donor–acceptor interactions between the electron-deficient triazolium group and the electron-rich hydroquinone residues of the macrocycle. In addition, the upfield shift of the triazolium protons *α* and the downfield shifts of macrocycle cavity proton *c* and amide protons *d* are consistent with the templating chloride anion being complexed by both the macrocycle isophthalamide and the thread triazolium anion recognition groups.

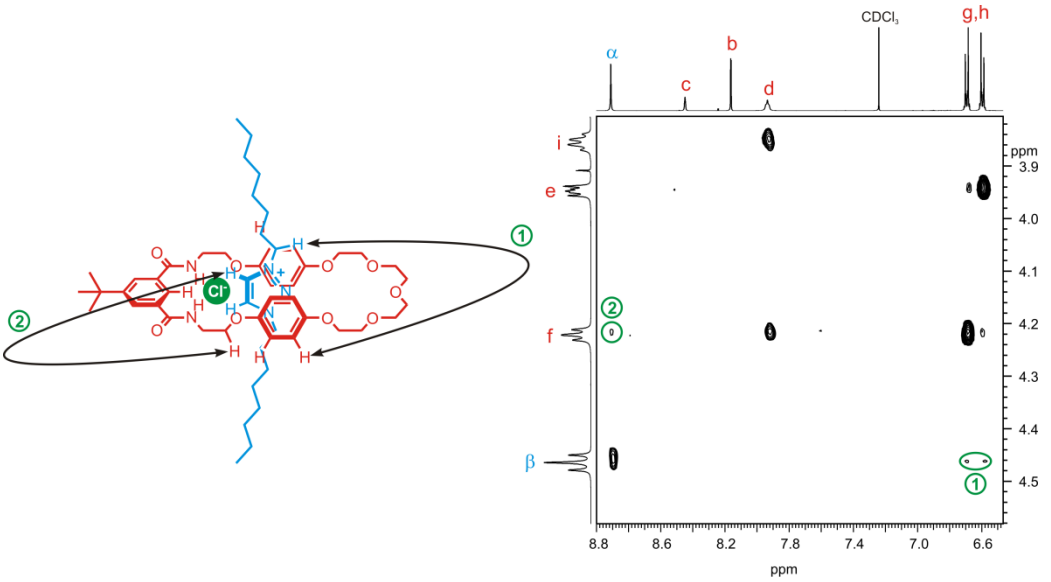


*Figure 4.8. ^{1}H–^{1}H ROESY NMR spectrum of pseudorotaxane 1:1 **84·Cl:87**. Assignable inter-component through-space interactions are highlighted (500 MHz, $CDCl_3$, 293 K).*

Further evidence of the interpenetrated nature of the supramolecular assembly is provided by two-dimensional ^{1}H–^{1}H ROESY NMR spectroscopy. The fingerprint region (Figure 4.8) shows important through-space cross-coupling interactions between protons of the threading and macrocycle components in the pseudorotaxane. Interaction **1** ($\beta \rightarrow g,h$) reveals the protons adjacent to the thread's triazolium unit are in close proximity to both the macrocycle hydroquinone protons and interaction **2** ($f \rightarrow \alpha$) demonstrates that the triazolium group is near to the macrocycle methylene protons. Both these cross-coupling interactions are consistent with the formation of an interpenetrated supramolecular assembly.

Quantitative analysis of the pseudorotaxane assembly process between macrocycle **87** and the various 1,3-dialkyltriazolium salts **84·A** (Figure 4.9) was undertaken using ^{1}H NMR titration experiments in chloroform-d. Addition of aliquots of threading species to a chloroform solution of macrocycle **87** induced changes in the macrocycle's ^{1}H NMR spectrum. In all cases except **84·PF$_6$**, upfield shift and splitting of the macrocycle's hydroquinone protons signal *g,h* was observed which is consistent with the triazolium species being threaded through the annulus of the macrocycle. Monitoring this chemical shift perturbation as a function of anion concentration gave the titration data shown in Figure 4.10, winEQNMR analysis of which gave apparent association constant values reported in Table 4.2.

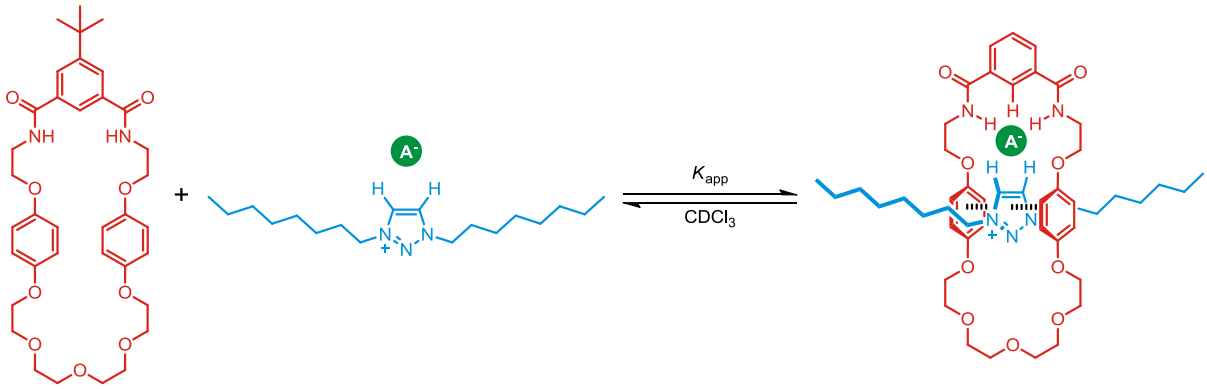


Figure 4.9. Pseudorotaxane formation between 1,3-disubstituted-triazolium threading component ***84·A*** *and macrocycle* ***87****.*

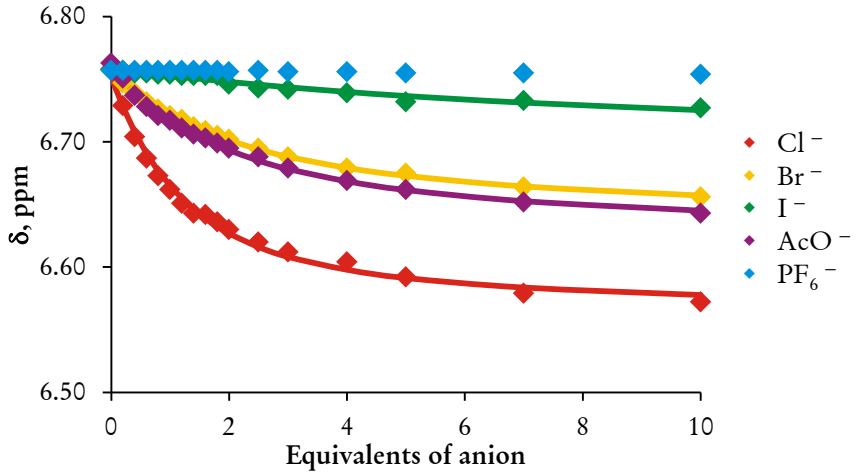


Figure 4.10. Titration curves for pseudorotaxane formation between macrocycle ***87*** *and threading components* ***84·A*** *obtained by monitoring the macrocycle hydroquinone protons.* $CDCl_3$*, 293 K. Square data points represent experimental data; continuous lines represent theoretical binding isotherms.*

*Table 4.2. Apparent association constants, K_{app} (M^{-1}), for pseudorotaxane formation between macrocycle **87** and threading components **84·A**.*

Threading species	Macrocycle **87** $K_{app}(M^{-1})$[a]
84·Cl	578(63)
84·Br	216(11)
84·I	35(5)
84·AcO	252(6)
84·PF_6	[b]

[a]*Association constants were determined by monitoring the downfield shift of the macrocycle hydroquinone protons.* [b]*Chemical shift perturbations too small to allow an association constant to be accurately determined. Estimated standard errors are given in parentheses. $CDCl_3$, 293 K.*

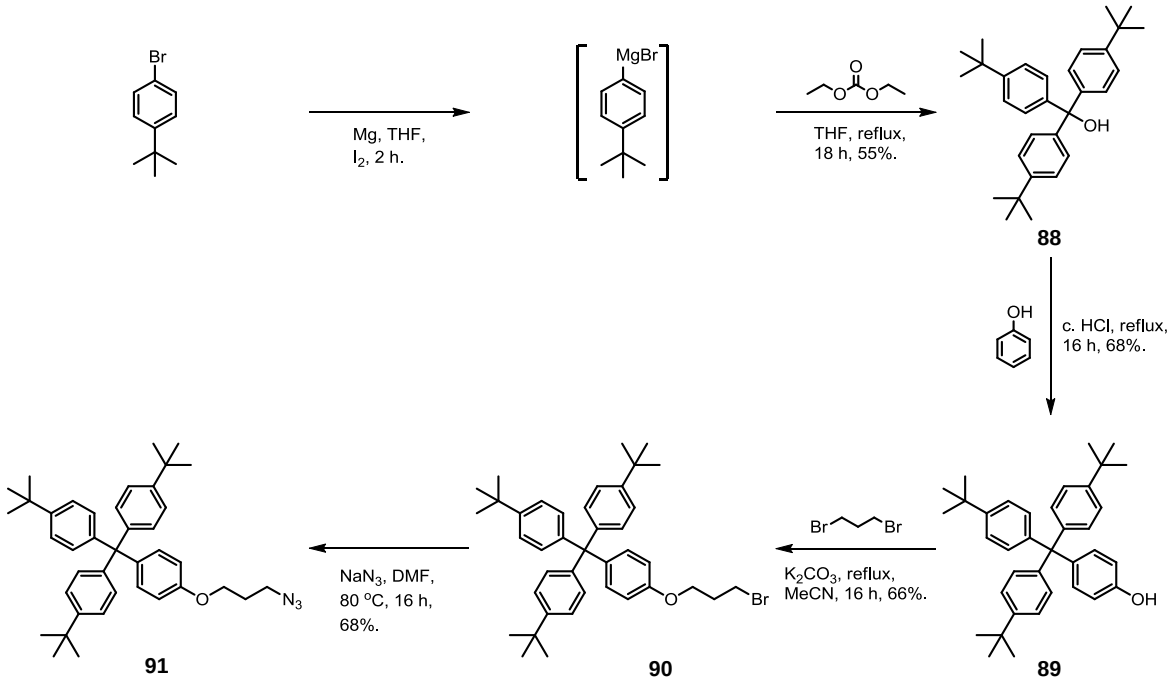
The strongest pseudorotaxane assembly is formed with the triazolium chloride threading species **84·Cl**, with relatively weaker association with bromide and iodide triazolium salts, which is attributed to the size-complementarity of the macrocycle isophthalamide binding cleft for the smaller chloride anion. Interestingly, the stability of the interpenetrated assembly with 1,3-dialkyltriazolium chloride threading species **84·Cl** (K_{app}= 578 M^{-1}) is greater than with either the 1,4-dialkyltriazolium chloride species **86·Cl** (K_{app} = 499 M^{-1}) or the 2-methylimidazolium chloride threading component (K_{app} = 245 M^{-1}) which also reflects their chloride anion binding affinities (Table 4.1).[6] No evidence of interpenetration is observed with the hexafluorophosphate salt **84·PF_6**, which confirms the non-coordinating nature of the hexafluorophosphate anion. Finally, the pseudorotaxane assembly templated with acetate is weaker than that with chloride (K_{app} = 252 *versus* 578 M^{-1}) which is possibly because a different binding mode or threading conformation is occurring with the bidentate oxoanion.

4.3 A rotaxane incorporating the 1,3-dialkyltriazolium anion recognition unit

4.3.1 Synthesis and characterisation of the first 1,3-disubstituted-1,2,3-triazolium-containing rotaxane

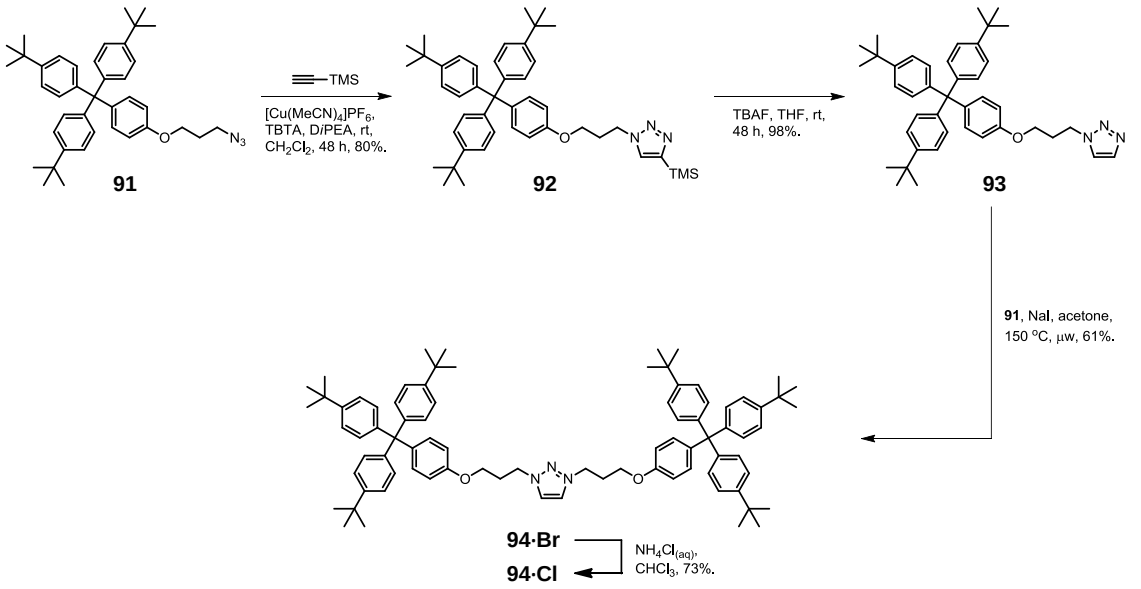
By replacing the threading component **84·A** with an appropriate stoppered-axle, the preparation of the first 1,3-disubstituted-triazolium-containing interlocked architecture was

undertaken. Since the most stable pseudorotaxane assembly was found with **84·Cl**, chloride was chosen as the templating anion in the rotaxane synthesis. The preparation of the required 1,3-disubstituted-triazolium chloride axle species is outlined in Schemes 4.6 and 4.7.



*Scheme 4.6. Synthesis of azide-functionalised stopper intermediate **91**.*

1-Bromo-4-*tert*-butylbenzene was added to magnesium turnings to produce the corresponding Grignard reagent, which was immediately heated with diethyl carbonate in tetrahydrofuran giving compound **88** in 55% yield. Compound **88** was heated in phenol in the presence of catalytic hydrochloric acid and the corresponding stopper-alcohol **89** was obtained in 68% yield. Heating compound **89** and 1,3-dibromopropane in the presence of potassium carbonate in acetonitrile gave compound **90** in 66% yield. Azide-functionalised stopper compound **91** was prepared in 68% yield using sodium azide in dimethylformamide.[10] The synthesis of the required triazolium-based axle compound was completed as outlined in Scheme 4.7.



Scheme 4.7. Synthesis of 1,3-disubstituted-triazolium chloride axle ***94·Cl****.*

A CuAAC reaction between stopper-azide compound **91** and trimethylsilylacetylene in the presence of copper(I)tetrakis-acetonitrile hexafluorophosphate, TBTA and *N*,*N*-di-*iso*-propylethylamine in dichloromethane gave protected-triazole **92** in 80% yield. The trimethylsilyl group was removed to produce compound **93** in 98% yield, using TBA fluoride in tetrahydrofuran. Alkylation was achieved by heating triazole compound **93** with stopper-bromide **90** in the presence of sodium iodide in acetone under microwave radiation, producing the axle bromide **94·Br** in 15% yield. The low yield in this alkylation step was not improved by increased reaction times. By recycling the starting materials, however, the overall reaction yield was increased to 61%. Anion exchange to the templating chloride anion was achieved in 73% yield by repeated washing of a chloroform solution of **94·Br** with aqueous ammonium chloride.

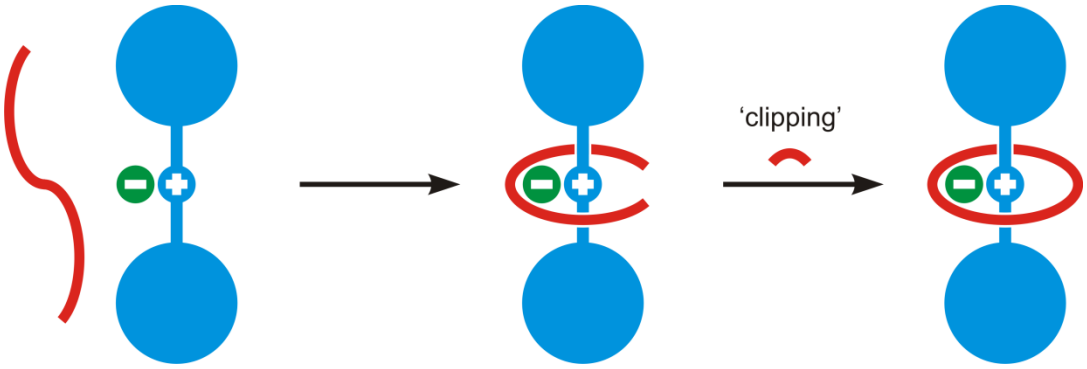
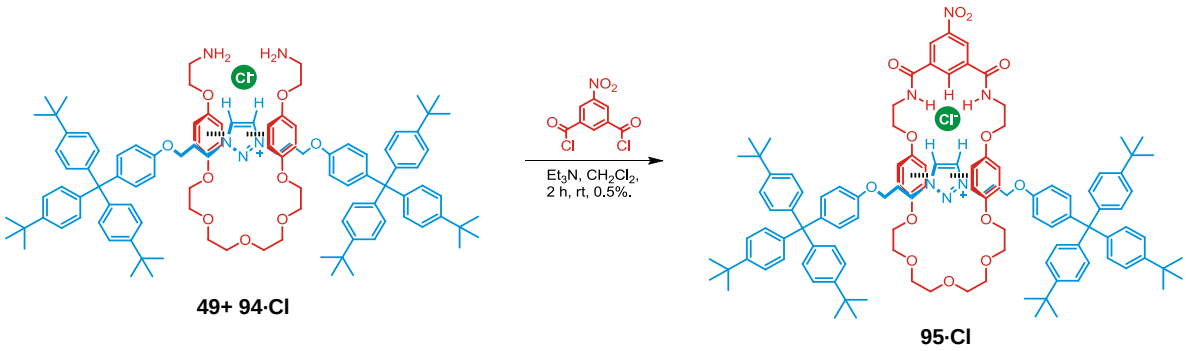


Figure 4.11. Cartoon representation of the recently developed anion-templated clipping methodology for the assembly of a [2]rotaxane.

In recent years, a new anion-templation route to interlocked structure formation has been developed which involves a clipping condensation reaction between a bis-amine macrocycle precursor compound and a bis-acid-chloride (Figure 4.11).[8,11] This route is similar to the macrocycle synthesis described earlier (section 3.2.2), where the pyridinium chloride template is replaced with a bulky stoppered-axle, and avoids using expensive Grubbs' catalyst and is, in general, higher yielding.[8,11,12]

Attempts to prepare the target rotaxane species incorporating a 1,3-disubstituted-triazolium axle using this clipping methodology are outlined in Scheme 4.8.



Scheme 4.8. Synthesis of 1,3-disubstituted-triazolium rotaxane ***95·Cl****.*

The acid-chloride-condensation reaction between an equimolar solution of bis-amine macrocycle precursor **49** and 5-nitroisophthaloyl dichloride (prepared by heating 5-nitroisophthalic acid in thionyl chloride) in the presence of triazolium axle **94·Cl**, and triethylamine in anhydrous dichloromethane afforded both macrocycle side-product and the target rotaxane species which, after purification using column and preparative thin layer chromatography, was isolated in only 0.5% yield.

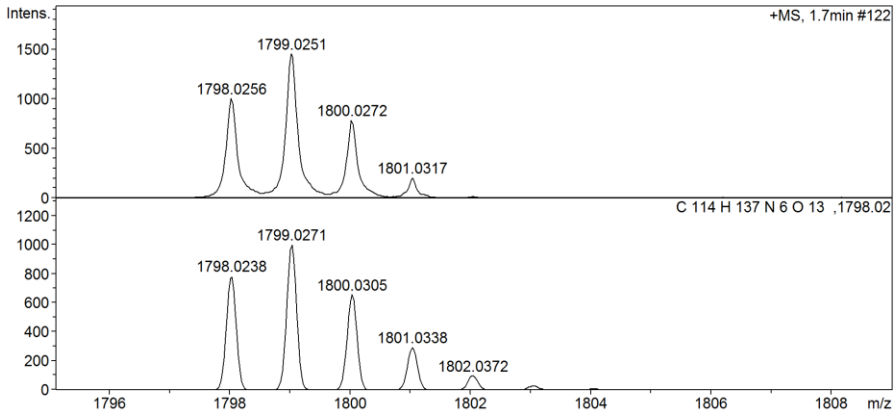


Figure 4.12. High-resolution mass spectrum of rotaxane ***95·Cl****.*

The rotaxane was characterised by electrospray mass spectroscopy and ^{1}H NMR spectrometry. The cationic molecular ion peak is readily observed in the mass spectrum which suggests the presence of a single interlocked species and the high-resolution mass spectrum reveals the isotopic distribution of the [2]rotaxane is in good agreement with the theoretical spectrum (Figure 4.12).

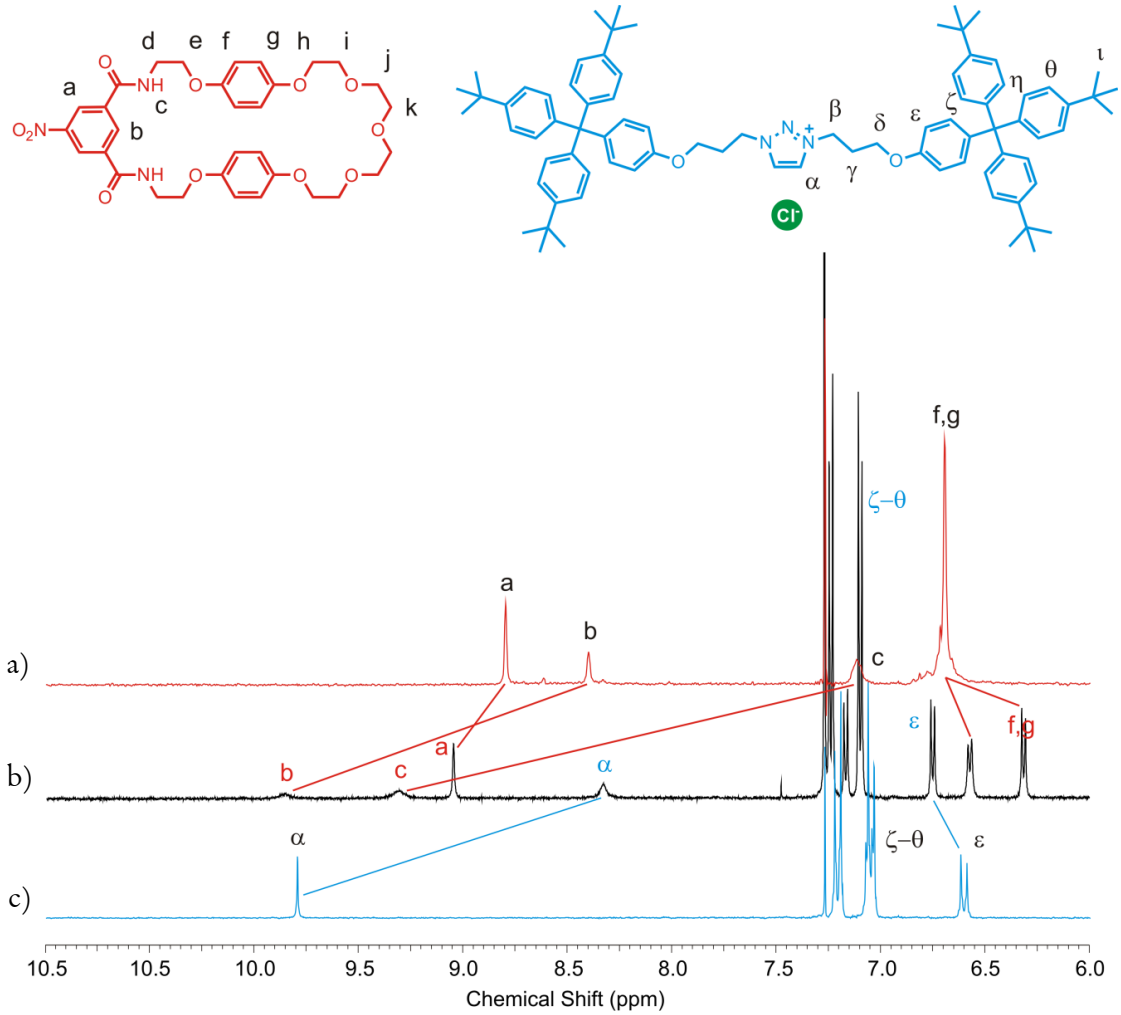
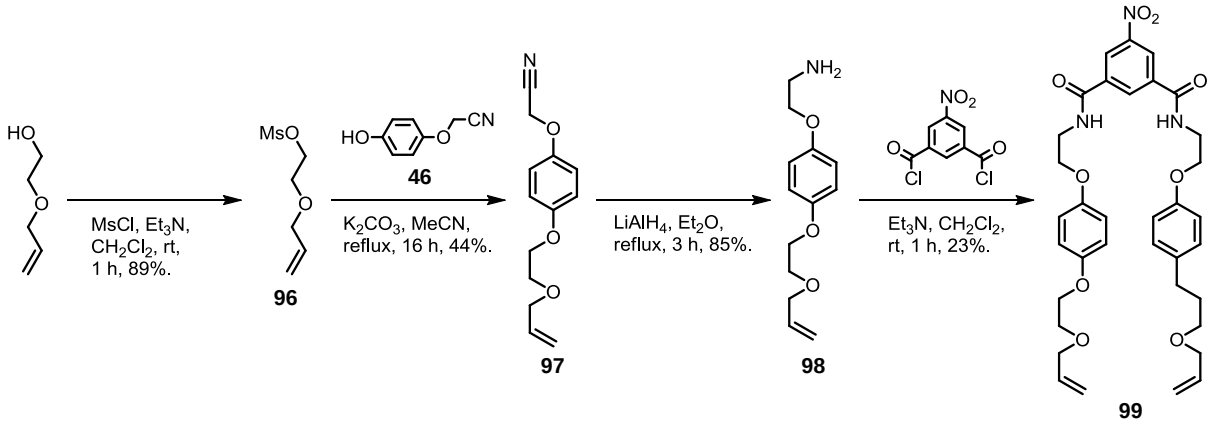


Figure 4.13. Partial ^{1}H NMR spectra of: a) macrocycle component; b) rotaxane ***95·Cl****; and c) axle component* ***94·Cl*** *(300 MHz, $CDCl_3$, 293 K).*

The ^{1}H NMR spectrum of the [2]rotaxane and those of component axle and macrocycle are shown in Figure 4.13. Diagnostic changes in the rotaxane spectrum provide evidence for the interlocked nature of compound **95·Cl**. Most importantly, the upfield shift and splitting of the signal corresponding to the macrocycle hydroquinone protons *f* and *g* is indicative of aromatic donor–acceptor interactions between the electron-rich hydroquinone units and the axle's electron-poor triazolium group, a result of the axle being interlocked through the macrocycle ring. Furthermore, the downfield shift of macrocycle internal proton *b* and amide protons *c*, together with the upfield shift of the triazolium proton signal *α* is consistent with the templating chloride anion being bound in the rotaxane's unique interlocked binding domain through hydrogen-bonding interactions with both the isophthalamide and triazolium anion recognition groups.

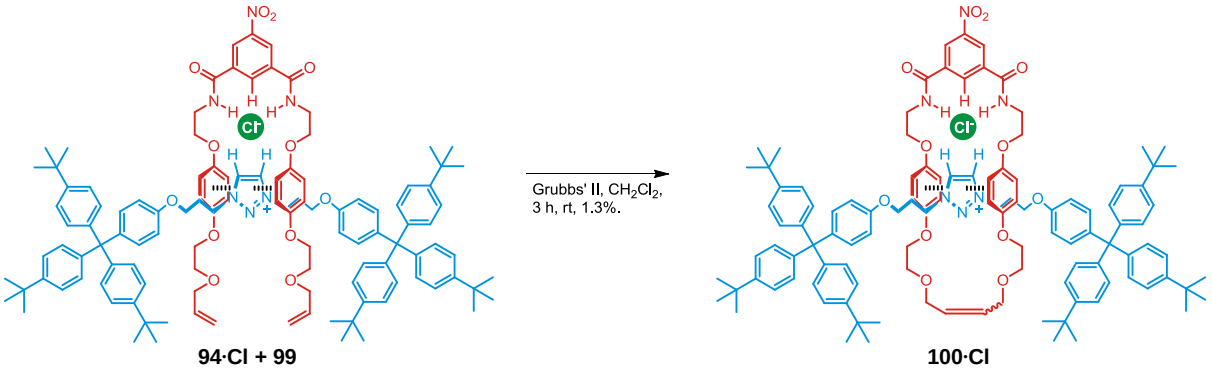
The small amount of rotaxane **95·Cl** obtained by this synthetic route was not sufficient to allow anion recognition investigations to be carried out. The reduced stability of the pseudorotaxane assembly with this triazolium-chloride species compared with traditional pyridinium-3,5-bis-amide chloride template,[9] a result of weaker aromatic donor–acceptor interactions and lower anion recognition strength of triazolium moieties compared with pyridinium surfaces, may account for the low yield of rotaxanation using this synthetic methodology (*c.f.* section 3.3.2). Consequently, the traditional Grubbs'-catalysed RCM clipping route for the preparation of rotaxanes was undertaken, in which the two components are assembled in an orthogonal orientation by the templating anion prior to the cyclisation reaction. This synthetic methodology requires the preparation of an appropriate, bis-vinyl-appended isophthalamide-containing macrocycle precursor. The preparation of such a compound is outlined in Scheme 4.9.[13]



Scheme 4.9. Synthesis of bis-vinyl-appended isophthalamide-based macrocycle precursor compound ***99****.*

Mesylation of 2-allyloxyethanol to produce **96** was achieved in 89% yield by stirring with methanesulfonyl chloride in dichloromethane. A nucleophilic substitution reaction between mesylate **96** and monofunctionalised hydroquinone **46** under basic conditions afforded compound **97** in 44% yield. The nitrile group was reduced to the corresponding amine with lithium aluminium hydride to give amine **98** in 85% yield. The required macrocycle precursor compound **99** was prepared in 23% yield via an acid-chloride-condensation reaction between 5-nitroisophthaloyl dicarbonyl chloride and two equivalents of amine **98** in the presence of triethylamine in dichloromethane.

Having successfully prepared a suitable bis-vinyl-appended macrocycle precursor compound, the synthesis of the corresponding [2]rotaxane species using triazolium chloride axle **94·Cl** was achieved as shown in Scheme 4.10.



*Scheme 4.10. Synthesis of rotaxane **100·Cl**.*

Stoppered-axle **94·Cl** and two equivalents of macrocycle precursor compound **99** were stirred in the presence of Grubbs' second generation catalyst (10% by weight) in anhydrous dichloromethane. Following purification using column and preparative thin layer chromatography the target rotaxane **100·Cl** was isolated in an improved yield of 1.3%! Anion exchange to the non-coordinating hexafluorophosphate was also carried out by repeated washing of a chloroform solution of rotaxane **100·Cl** with aqueous ammonium hexafluorophosphate, giving **100·PF$_6$** in 90% yield.

Evidence of successful rotaxane formation was provided by high-resolution electrospray mass spectrometry (Figure 4.14), and one- and two-dimensional ^{1}H NMR spectroscopy.

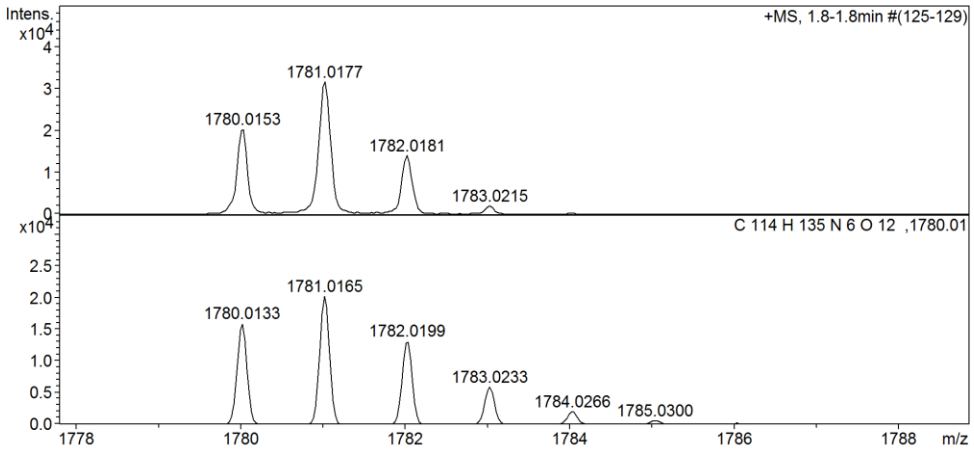


*Figure 4.14. High-resolution mass spectrum of rotaxane **100·PF$_6$**.*

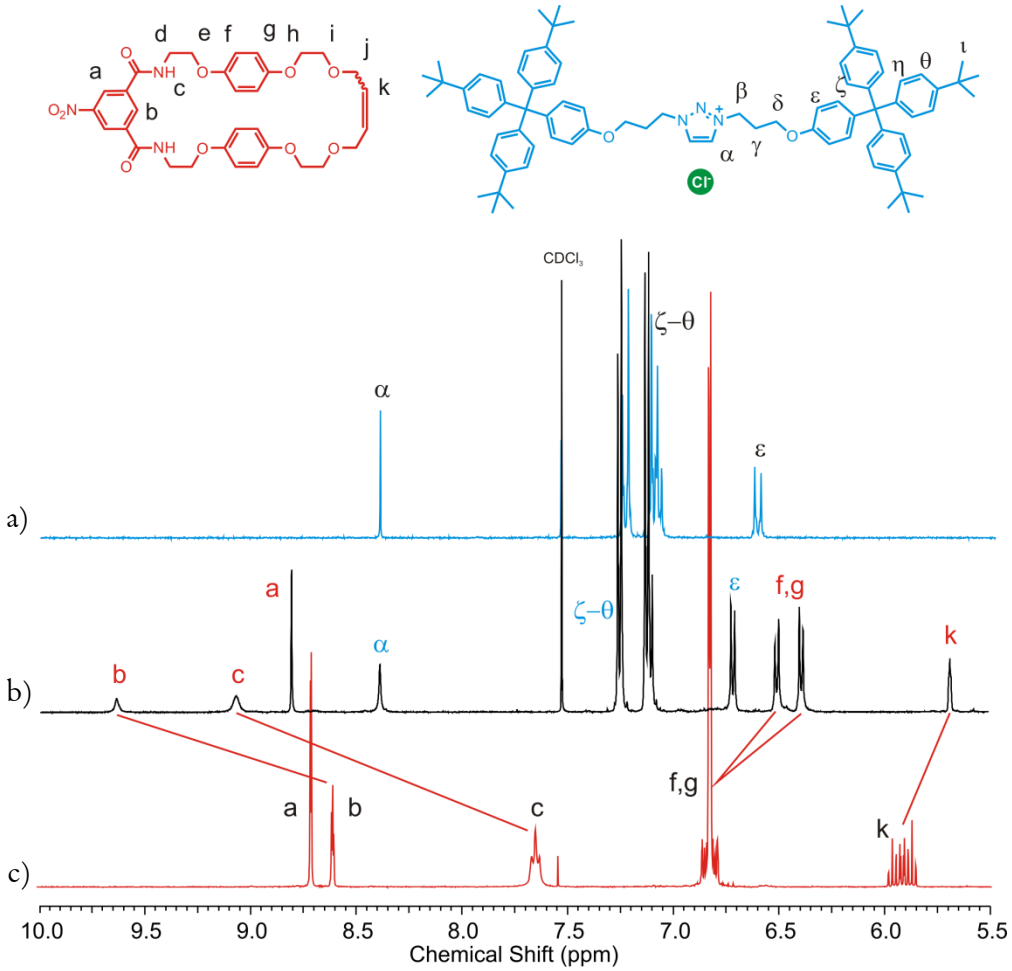


Figure 4.15. Partial ^{1}H NMR spectra of: a) axle component ***94·Cl****; b) rotaxane* ***100·Cl****; and c) macrocycle precursor component* ***99*** *(500 MHz, 4:1 CD_3CN:$CDCl_3$, 293 K).*

The ^{1}H NMR spectrum of the rotaxane species **100·Cl** (Figure 4.15) displays the convergence of multiplet *k* into a pseudo-singlet which confirms the Grubbs'-catalysed RCM reaction was successful. The presence of diagnostic upfield shift and splitting of the macrocycle hydroquinone proton signal *f,g* compared with the free macrocycle spectrum is consistent with the interlocked rotaxane adopting a conformation in which there are aromatic donor–acceptor interactions between the triazolium unit and the hydroquinone groups. The downfield shift of macrocycle internal proton *b* and amide protons *c* indicates chloride is now being bound by the isophthalamide anion recognition group through hydrogen bonding to these protons.

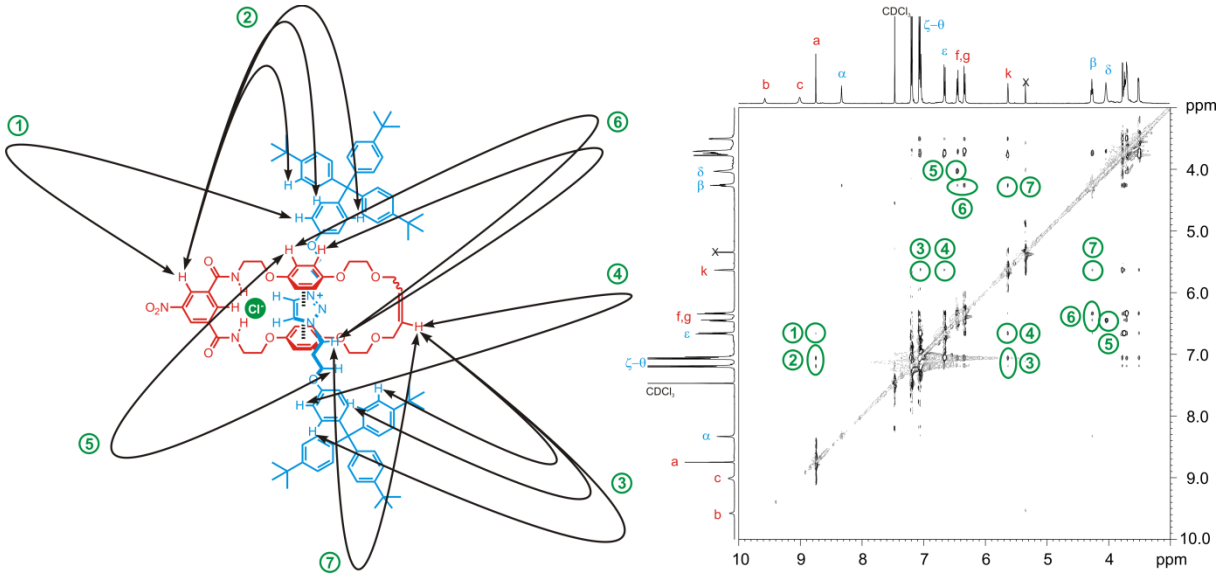


Figure 4.16. ^{1}H–^{1}H ROESY NMR spectrum of rotaxane ***100·Cl****. Assignable inter-component through-space interactions are highlighted (500 MHz, 4:1 CD_3CN:$CDCl_3$, 293 K).*

The two-dimensional ^{1}H–^{1}H ROESY NMR spectrum of rotaxane **100·Cl** shown in Figure 4.16 displays a number of through-space cross-coupling interactions which further demonstrate the mechanically bonded nature of this molecular framework. Interactions **5** (*f* → *δ*) and **6** (*f*,*g* → *β*) reveal the hydroquinone groups are in close proximity to the axle methylene moieties. The alkene protons *k* are demonstrated to be near to the stopper groups and axle methylene units by interactions **3** (*k* → *ζ*–*θ*), **4** (*k* → *ε*) and **7** (*k* → *β*). Finally, interactions **1** (*a* → *ε*) and **2** (*a* → *ζ*–*θ*) highlight the stopper groups are proximal to the isophthalamide group.

4.3.2 Anion recognition properties of novel 1,3-disubtituted triazolium-based rotaxane 100·PF_6

Owing to the very small amount of [2]rotaxane isolated in section 4.2.4, only the chloride recognition ability of **100·PF_6** was investigated by ^{1}H NMR spectroscopic titration experiments.

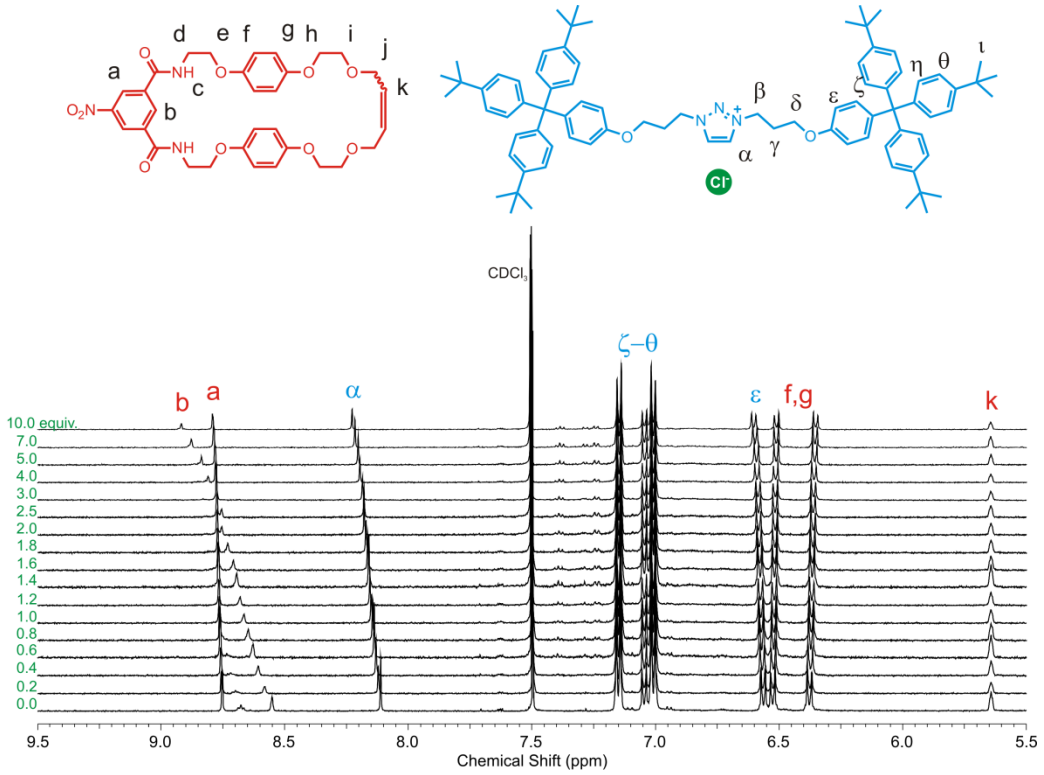


*Figure 4.17. Partial ^{1}H NMR spectra of receptor **100·PF$_6$** and equivalents of TBA·Cl (500 MHz, 1:1 $CDCl_3$:CD_3OD, 293 K).*

Upon addition of TBA chloride to a solution of rotaxane in 1:1 chloroform-d:methanol-d_4, downfield shifts of the signals corresponding to the protons comprising the binding domain (*ortho*-isophthalamide *b* and triazolium proton α) were observed as the chloride anion binds in the interlocked cavity (Figure 4.17). The changes in the triazolium proton signal as a function of anion concentration were monitored, giving the titration data shown in Figure 4.19, winEQNMR analysis of which gave a 1:1 stoichiometric association constant value of $K_a = 170(3)\ \text{M}^{-1}$.

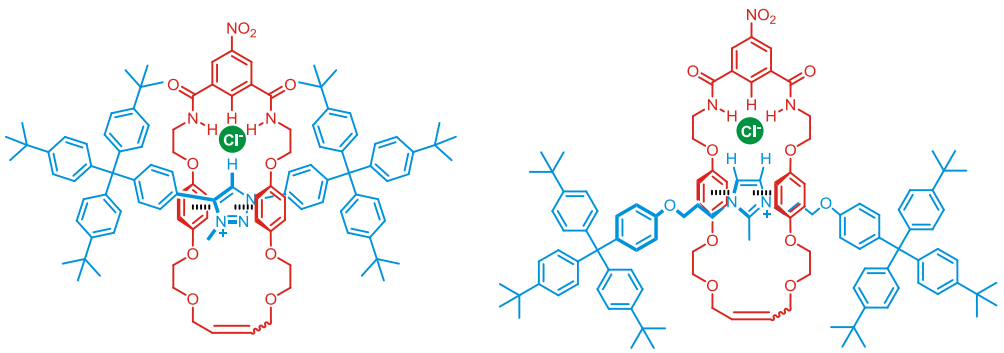


Figure 4.18. Structure of rotaxanes containing a) 1,4-disubstituted-triazolium or b) 2-methylimidazolium anion recognition groups.

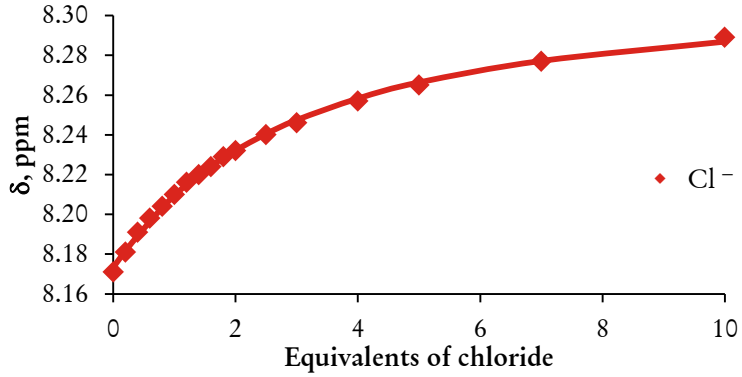


Figure 4.19. Titration curve for ***100·PF$_6$*** *and chloride obtained by monitoring the triazolium proton α. 1:1 $CDCl_3$:CD_3OD, 293 K. Square data points represent experimental data; continuous lines represent theoretical binding isotherms.*

It is interesting to note that the affinity of rotaxane **100·PF$_6$** for chloride is lower than for the equivalent rotaxanes with either a 1,4-disubstituted-triazolium or 2-methylimidazolium-containing axle component: K_a = 424(20) M^{-1} and K_a = 360(24) M^{-1} respectively.[6,14] The weaker chloride anion binding strength displayed by rotaxane **100·PF$_6$** may be attributed to the absence of an incorporated methyl group in the positively charged heterocyclic motif of the axle component which could hydrogen-bond to the macrocycle polyether oxygen atoms. These hydrogen-bonding interactions are thought to preorganise the rotaxane into a more favourable conformation for anion complexation and thus serve to enhance the anion recognition strength of an interlocked rotaxane host system. Alternatively, it is possible that the lone pair of electrons on the N(2) atom of the 1,3-disubtituted-triazolium motif may give rise to unfavourable repulsions with the macrocycle's polyether oxygen atoms which may somehow destabilise the rotaxane–chloride complex.

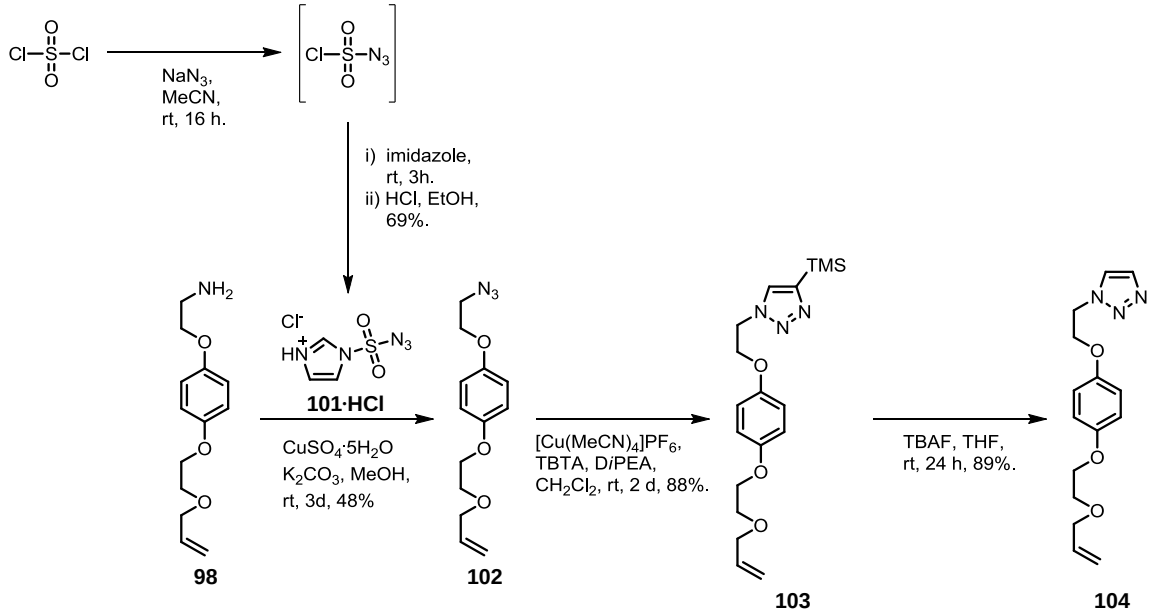
4.4 Macrocycles incorporating the triazolium anion recognition unit

The incorporation of the 1,4-disubstituted-1,2,3-triazole motif into receptors for anion recognition is a relatively new venture. Flood's tetratriazolophane is the archetypical example (section 1.3.2) where four triazole groups were able to bind chloride in dichloromethane with an impressive association constant value of $K_a = 1.1 \times 10^7$ M^{-1}.[2] To date only a few examples of triazolium-containing macrocyclic structures for anion recognition have been prepared, all

of which have been reported since the start of this project.[15-18] Furthermore, no examples of 1,3-disubtituted triazolium-based macrocycles for anion recognition have been described.

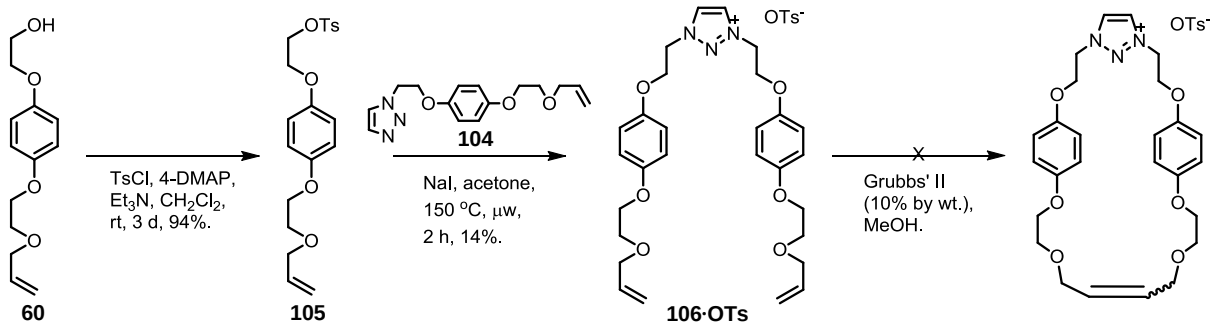
4.4.1 1,3-Disubstituted-triazolium-based macrocycle compound

It was envisaged that the preparation of a bis-vinyl-appended 1,3-disubstituted-triazolium-containing macrocycle precursor component would facilitate the preparation of the macrocycle, and possibly a related catenane molecular framework via anion templation. The synthesis of such a precursor molecule is outlined in Schemes 4.11 and 4.12.



*Scheme 4.11. Synthesis of vinyl-appended triazole compound **104**.*

The vinyl-appended triazole compound **104** was prepared as outlined in Scheme 4.11. Amine **98** was converted to the azide-functionalised compound **102** in 48% yield using the azide transfer agent **101** (prepared from sulfuryl chloride using sodium azide, and imidazole in acetonitrile),[19] copper(II) sulfate, and potassium carbonate in methanol. A CuAAC reaction between azide **102** and trimethylsilylacetylene using copper(I)tetrakis-acetonitrile hexafluorophosphate in the presence of TBTA, *N*,*N*-di-*iso*-propylethylamine in dichloromethane afforded the trimethylsilyl-protected triazole compound **103** in 88% yield. Removal of the trimethylsilyl group to give derivative **104** was achieved in 89% yield by stirring with TBA fluoride in tetrahydrofuran.



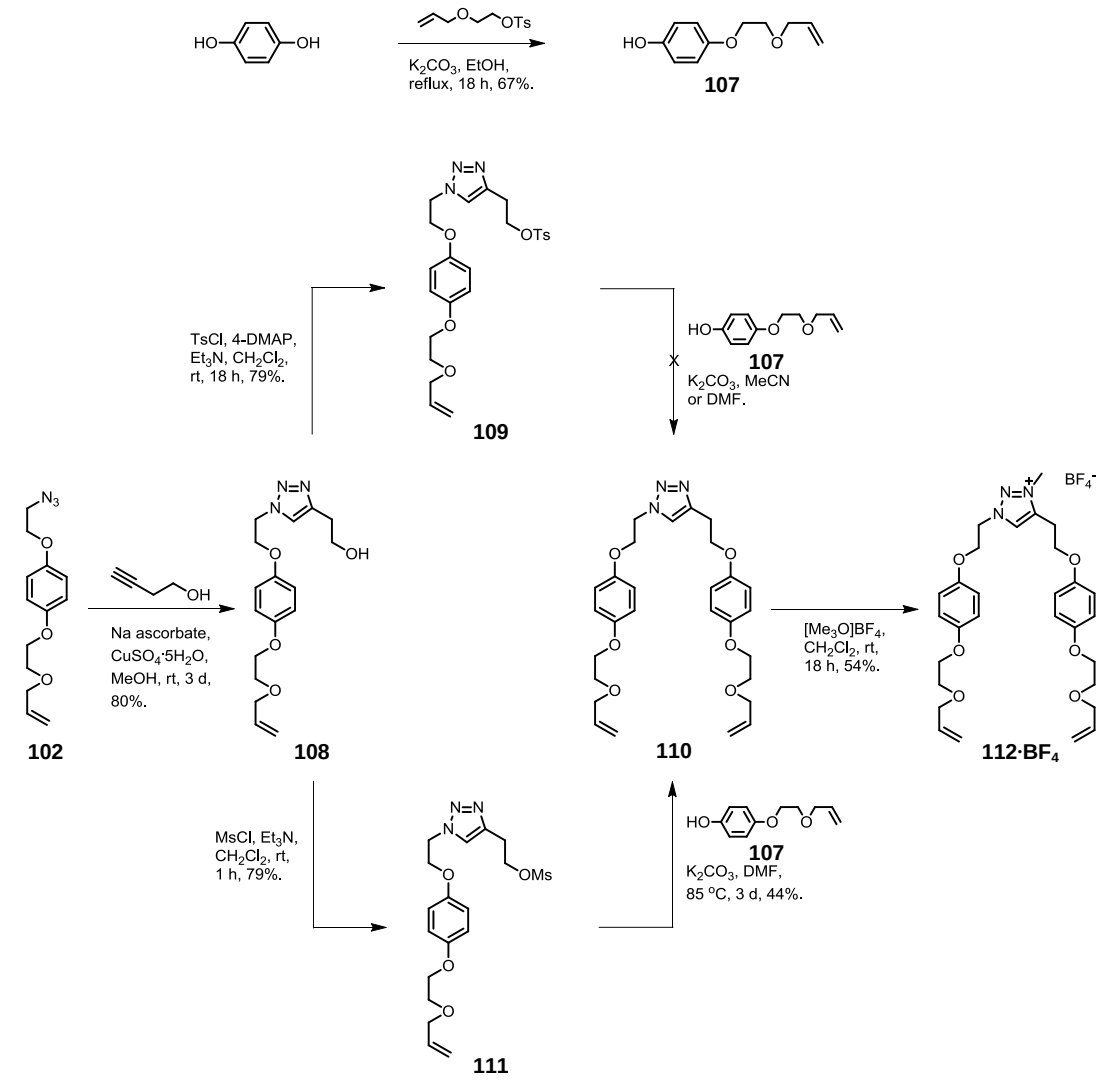
Scheme 4.12. Attempted synthesis of triazolium-based macrocycle.

The synthesis of a 1,3-disubstituted-triazolium-based macrocycle was attempted as shown in Scheme 4.12. Tosylate **105** was prepared from compound **60** in 94% yield using *p*-toluenesulfonyl chloride, 4-dimethylaminopyridine and triethylamine in dichloromethane. Heating tosylate **105** and triazole compound **104** in the presence of a catalytic amount of sodium iodide in acetone afforded triazolium species **106·OTs** in only 14% yield. The insolubility of this compound in chlorinated solvents prevented it being anion exchanged to the chloride salt. Since Grubbs'-catalysed RCM reactions in methanol have been reported,[20] cyclisation of triazolium macrocycle precursor compound **106·OTs** in methanol was attempted. No evidence of cyclisation, however, was detected by either electrospray mass spectrometry or ^{1}H NMR spectroscopy of the crude reaction mixture. As a result, attention turned to preparing the corresponding bis-vinyl-appended 1,4-disubstituted triazolium derivative.

4.4.2 1,4-Disubstituted-triazolium-based macrocycle compound

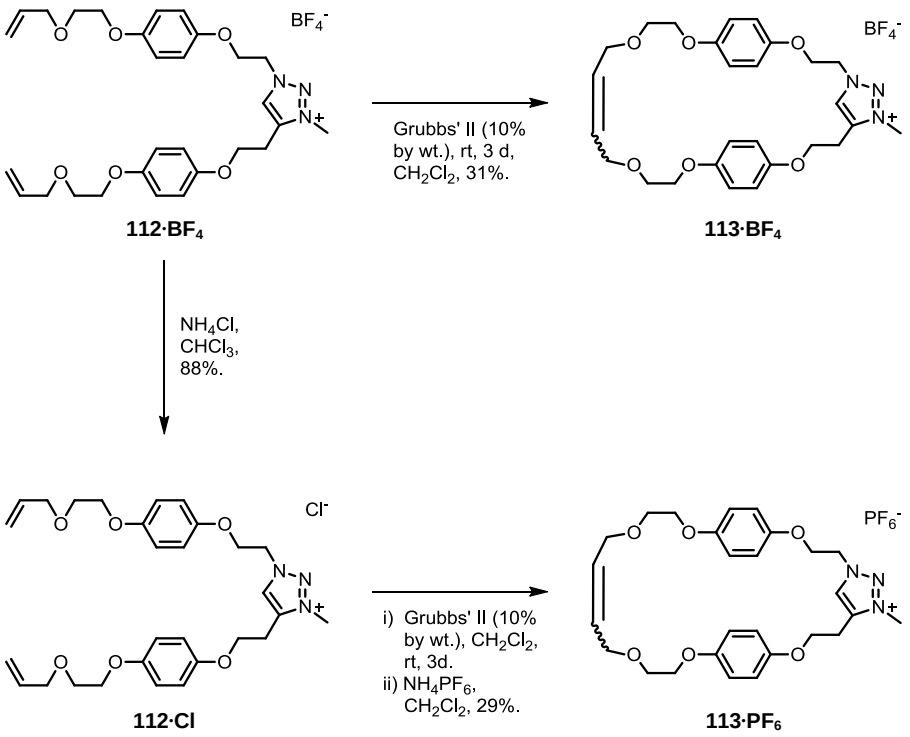
The synthesis of the 1,4-triazolium-based macrocycle precursor compound is summarised in Scheme 4.13. A CuAAC reaction between azide-functionalised allyl compound **102** and 3-butyn-1-ol using copper(II) sulfate and sodium L-ascorbate in methanol, afforded triazole compound **108** in 80% yield. This was converted to the tosylate derivative in 79% yield using *p*-toluenesulfonyl chloride in dichloromethane. A nucleophilic substitution reaction between tosylate **109** and vinyl-appended hydroquinone **107** (prepared from hydroquinone and 2-allyloxyethyl tosylate by heating with potassium carbonate in ethanol)[21] was attempted in the presence of potassium carbonate in both acetonitrile and dimethylformamide. Whilst

evidence of product formation was provided by both ^{1}H NMR and mass spectrometry, the isolation of target compound **110** from starting material could not be achieved. A modified synthesis was therefore carried out. Mesylate compound **111** was prepared in 79% yield from hydroxyl species **108** using methanesulfonyl chloride and triethylamine in dichloromethane. Heating compounds **111** and **107** in the presence of potassium carbonate in dimethylformamide produced the target bis-vinyl-appended triazole compound **110** in 44% yield. Alkylation to give the corresponding triazolium species **112·BF$_4$** was successfully accomplished in 54% yield by stirring with two equivalents of trimethyloxonium tetrafluoroborate.



*Scheme 4.13. Synthesis of 1,4-disubtituted triazolium-containing macrocycle precursor **112·BF$_4$**.*

The synthesis of the triazolium-based macrocycle species **113·BF$_4$** was successfully completed via cyclisation of the bis-vinyl compound **112·BF$_4$** using Grubbs' second generation catalyst (10% by weight) in dichloromethane (Scheme 4.14). Interestingly, the yield was found to almost double under more dilute conditions which favour intramolecular cyclisation over polymerisation. Increasing the yield of macrocyclisation using a templating anion was also investigated. The chloride salt of the macrocycle precursor was prepared by repeated washing a chloroform solution of **112·BF$_4$** with aqueous ammonium chloride, producing **112·Cl** in 88% yield. Grubbs'-catalysed RCM cyclisation of macrocycle precursor **112·Cl**, followed by anion exchange to the hexafluorophosphate gave the corresponding macrocycle **113·PF$_6$** in 29% yield. The similar yields produced by both synthetic routes suggest the chloride anion is not acting as a template in the cyclisation process.



Scheme 4.14. Synthesis of macrocycle 113·A.

Crystals of macrocycle **113·BF$_4$** suitable for single crystal X-ray diffraction structural analysis were grown by slow evaporation of a solution of **113·BF$_4$** in chloroform. The structure (Figure 4.20), solved by Dr Nicholas White, confirms the successful synthesis of the target triazolium-based macrocycle. Notably, in the solid state, the triazolium proton is directed

into the centre of the macrocyclic cavity and the non-coordinating tetrafluoroborate anion is located on the periphery of the macrocyclic structure.

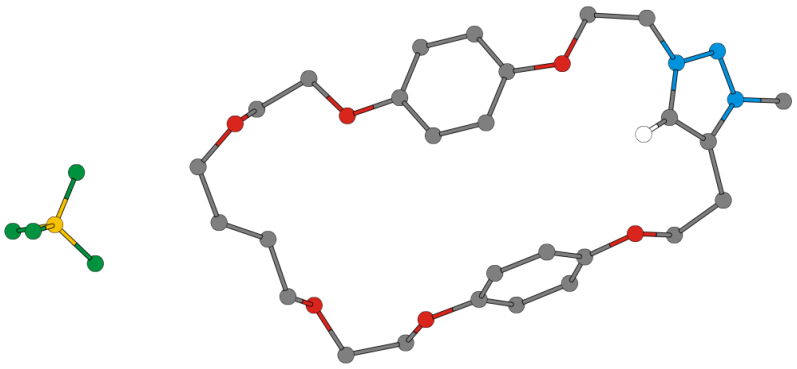


Figure 4.20. Ball and stick plot of ***113·BF$_4$****. Colour scheme: grey=C, blue=N, red=O, white=H, yellow=B, and green=F.*

Both the tetrafluoroborate and hexafluorophosphate salts of macrocycle **113**$^+$ proved insoluble in commonly used organic solvents. Addition of one equivalent of TBA chloride, however, helped to alleviate this problem, enabling both macrocycles to be characterised by NMR spectroscopy. The ^{1}H NMR spectrum of macrocycle **113·BF$_4$** with one equivalent of chloride is shown in Figure 4.21 and displays all the salient proton environments. Importantly, the presence of four signals corresponding to the hydroquinone protons *e*,*f*,*o*,*p* arises as a result of the asymmetry of this macrocycle.

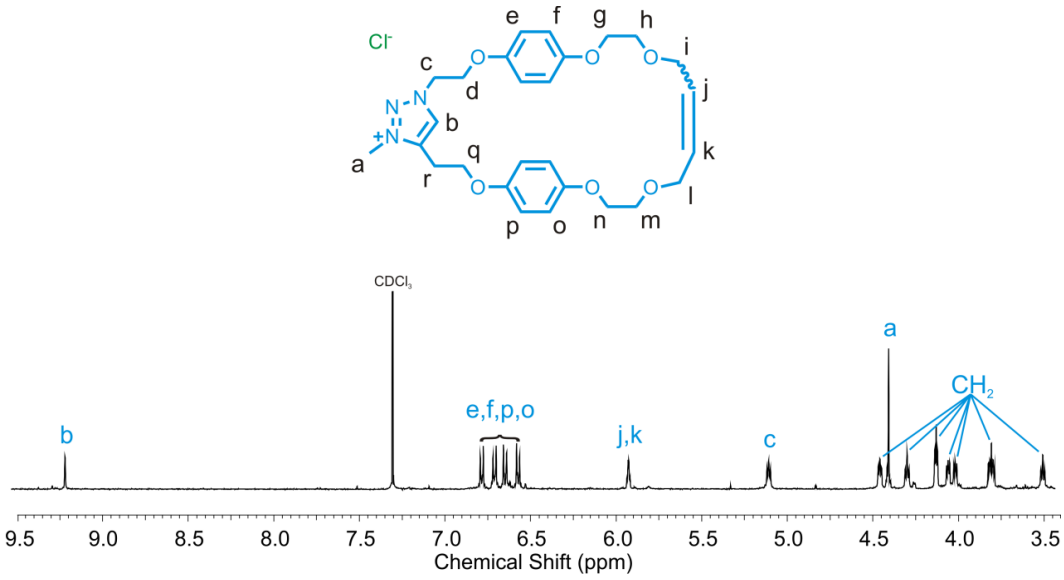


Figure 4.21. ^{1}H NMR spectrum of 1:1 macrocycle ***113·BF$_4$****:Cl$^-$ showing peak assignments (500 MHz, CDCl3, 293 K).*

4.4.3 Attempted synthesis of catenanes consisting of 1,4-disubstituted triazolium-based macrocycles

The possibility of pseudorotaxane formation between triazolium macrocycle **113·A** and the potential triazolium threading species **86·BF$_4$** was investigated using ^{1}H NMR spectroscopy. The insolubility of macrocycle **113·BF$_4$** prevented any quantitative data for the assembly process from being obtained. Figure 4.22 shows the ^{1}H NMR spectrum of an equimolar mixture of macrocycle **113·BF$_4$**, **86·BF$_4$** and TBA chloride, together with spectra of the individual components.

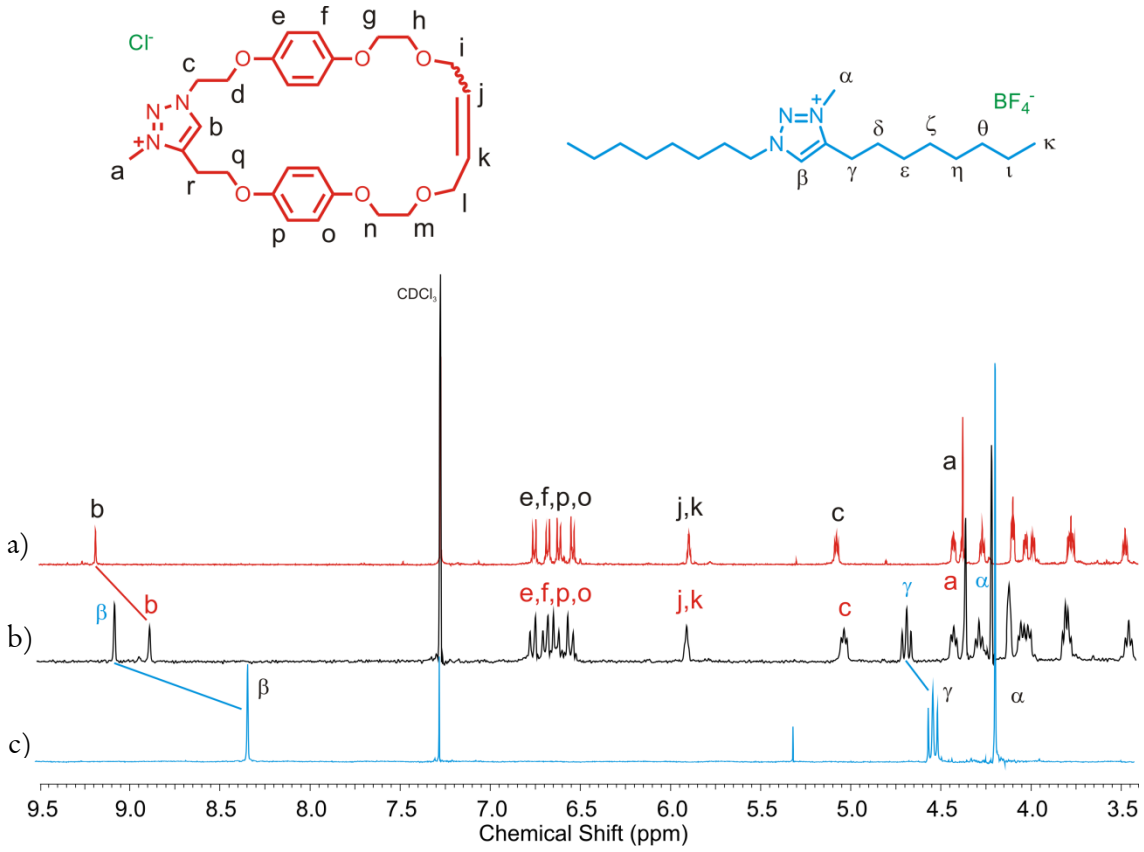
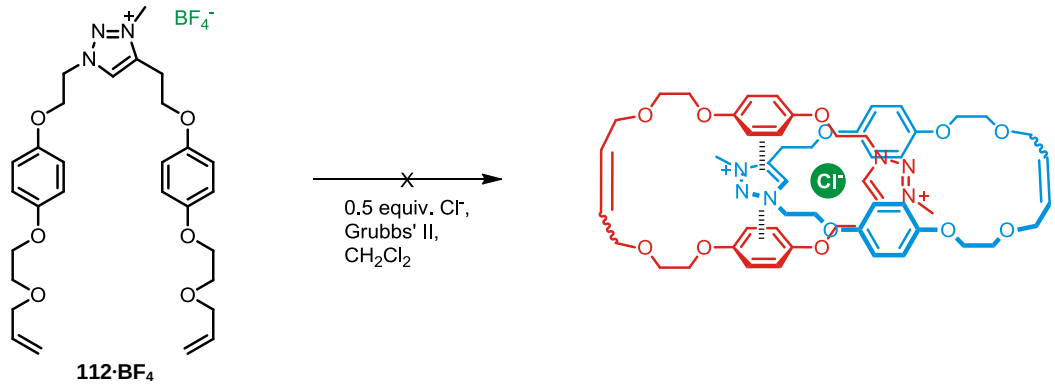


*Figure 4.22. ^{1}H NMR spectra of: a) macrocycle **113·BF$_4$** and TBA·Cl; b) pseudorotaxane; and c) thread **86·BF$_4$** (300 MHz, $CDCl_3$, 293 K).*

The asymmetry of the macrocycle gives rise to multiple signals corresponding to the hydroquinone protons *e*,*f*,*p*,*o* which makes it difficult to determine whether any diagnostic upfield shift and splitting of the signals, typical of pseudorotaxane formation, is evident. The downfield shift of the triazolium proton *β* and methylene proton *γ* arises from coordination of chloride to the threading component **86·BF$_4$** and the concomitant upfield shift of the

macrocycle's triazolium proton *b* is a consequence of the halide being shared with the threading species.

Despite the absence of definitive evidence for pseudorotaxane formation with this system, the preparation of a homocatenane was attempted as outlined in Scheme 4.15. Initially, the homocatenane was targeted via a chloride-anion-templated double cyclisation reaction. Two equivalents of bis-vinyl-appended triazolium **112·BF$_4$** and one equivalent of TBA chloride were stirred in anhydrous dichloromethane in the presence of Grubbs's second generation catalyst (10% by weight). After stirring at room temperature for three days, however, no evidence of catenane formation was detected by either electrospray mass spectrometry or ^{1}H NMR techniques.



112·BF$_4$

Scheme 4.15. Attempted synthesis of a triazolium-containing homocatenane.

This synthetic route to a homocatenane species requires the double cyclisation reaction of both components of an orthogonal 2:1 receptor:chloride complex. The failure to produce any catenane by this methodology may be a consequence of the relatively weak chloride anion binding affinity of the triazolium components, which reduces the stability of the required orthogonal intermediate.

The preparation of a heterocatenane species, where one component is a preformed macrocycle that is known to complex chloride strongly, was therefore considered. Before any synthetic attempts were undertaken, however, a qualitative ^{1}H NMR pseudorotaxane investigation was carried out to probe whether chloride-templated threading occurs between

isophthalamide-based macrocycle **87** and triazolium threading component **112·Cl** (Figure 4.23).

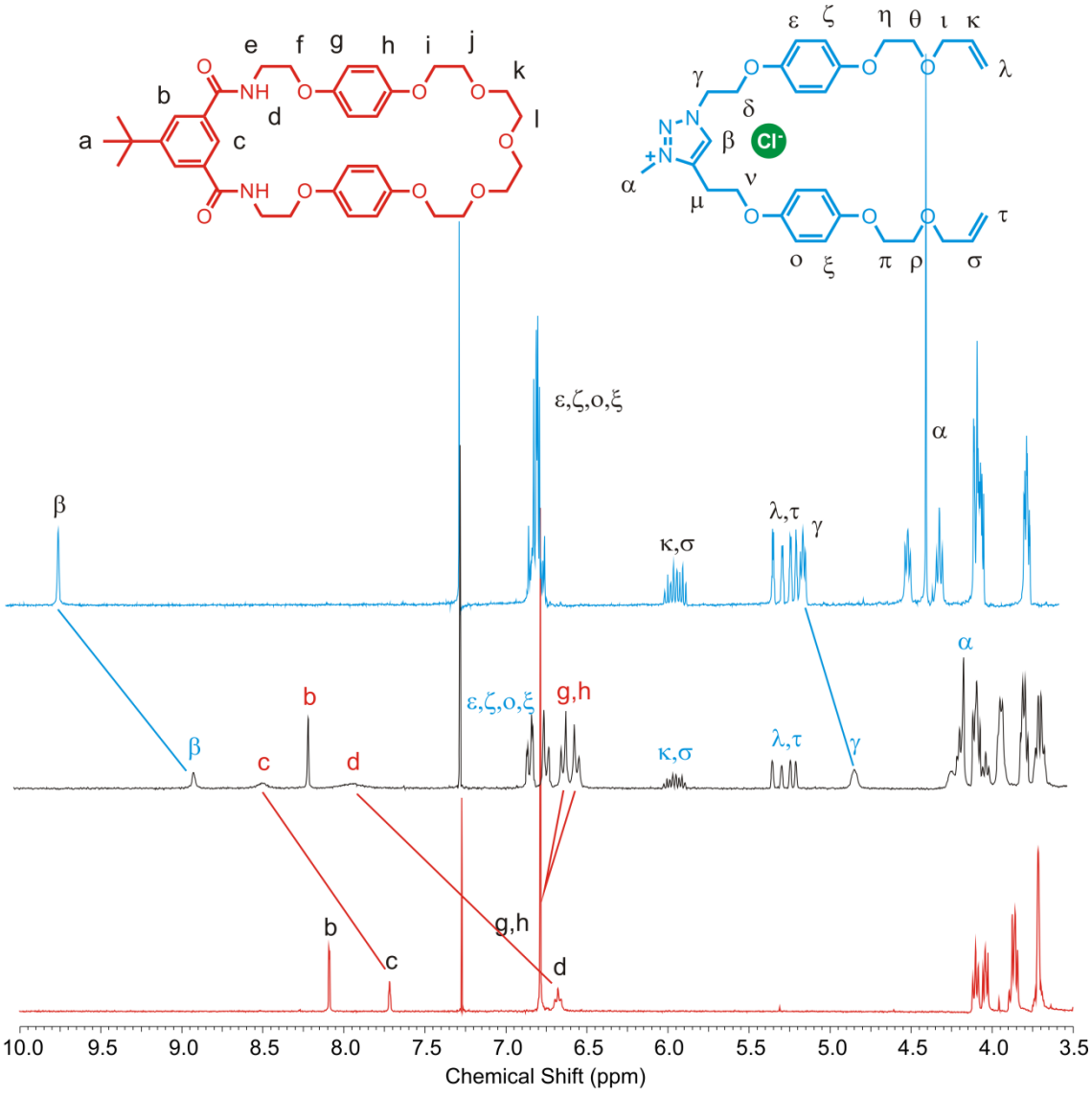
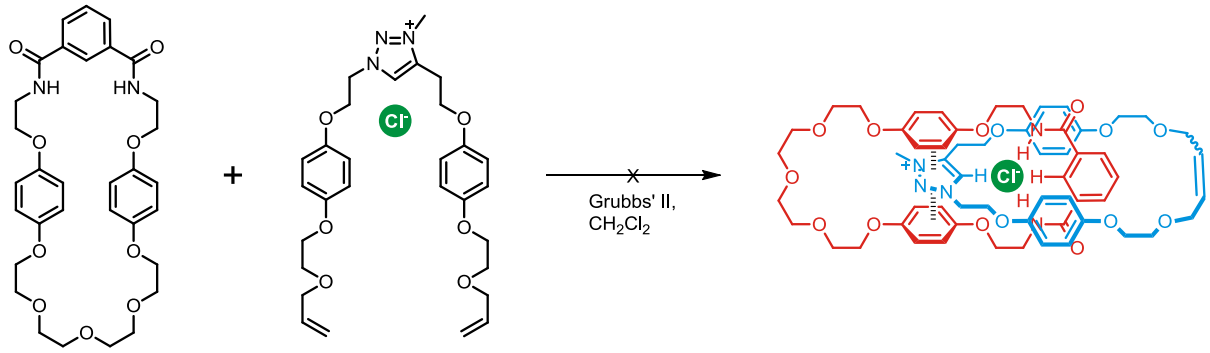


*Figure 4.23. [1]H NMR spectra of: a) macrocycle precursor **112·Cl**; b) pseudorotaxane; and c) macrocycle **87** (300 MHz, $CDCl_3$, 293 K).*

The [1]H NMR of an equimolar mixture of macrocycle precursor **112·Cl** and isophthalamide-containing macrocycle **87** in chloroform-d is shown in Figure 4.23. Evidence of pseudorotaxane formation is provided by the upfield shift and splitting of the hydroquinone protons signal *g,h* compared with the corresponding signal for the free macrocycle, which is characteristic of aromatic donor–acceptor interactions between the electron-rich hydroquinone units and the electron-poor triazolium group. Additionally, the downfield shift

of the macrocycle's internal cavity proton *c* and amide protons *d*, together with the upfield shift of the triazolium proton *β* are consistent with coordination of the templating chloride anion by both the triazolium proton and the isophthalamide binding cavity through hydrogen-bonding interactions.

Given the evidence for successful pseudorotaxane assembly between macrocycle **87** and triazolium derivative **112·Cl**, an attempt to prepare the corresponding catenane was undertaken. To avoid any complications through unfavourable steric interactions with the tertiary butyl group of macrocycle **87**, the related isophthalamide macrocycle **52** was used for catenane assembly (Scheme 4.16).



Scheme 4.16. Attempted synthesis of a triazolium-containing heterocatenane.

The synthesis of the target catenane was undertaken by stirring macrocycle **52** with bis-vinyl-appended macrocycle precursor compound **112·Cl** in the presence of Grubb's second generation catalyst (10% by weight) in anhydrous dichloromethane. Mass spectroscopic analysis of the crude mixture revealed a peak at m/z = 1090.6 providing evidence of the successful formation of an interlocked catenane species. Numerous attempts to purify the catenane failed, however, and only the component macrocycles could be isolated.

4.5 Conclusions

A simple 1,3-dialky-1,2,3-triazolium anion receptor has been successfully prepared and the anion binding properties of this new anion recognition motif were probed using ^{1}H NMR titration experiments. The 1,3-dialkyltriazolium motif was found to possess a greater halide

and acetate anion binding affinity than the analogous 1,4-dialkyltriazolium and 2-methylimidazolium host systems; anion binding occurs at two polarised C–H hydrogen-bond-donor groups. The first anion-templated interpenetrated architectures incorporating a 1,3-disubstituted-triazolium threading component were successfully assembled and the most stable pseudorotaxane species was obtained when a templating chloride anion was employed. The construction of the analogous interlocked structure comprising a 1,3-triazolium-based axle component was also achieved. The rotaxane displayed a moderate affinity for chloride in competitive 1:1 chloroform:methanol solvent, which was lower than with similar 1,4-disubstituted-triazolium- or 2-methylimidazolium-containing rotaxanes.

Further exploitation of the 1,3-disubstituted-triazolium anion binding unit through incorporation into macrocycle precursor components was accomplished but attempts to prepare the related anion-templated cyclic or interlocked structures were thwarted by the low solubility of this compound. Attention turned to the preparation of a novel 1,4-triazolium macrocycle precursor compound and the corresponding macrocycle was successfully isolated. The preparation of a chloride-templated homocatenane from two equivalents of 1,4-disubstituted-triazolium macrocycle precursor was attempted, although no evidence of successful interlocked-structure formation was obtained by either mass spectrometry or NMR spectroscopy. Promising evidence of pseudorotaxane assembly with a preformed, isophthalamide macrocycle was obtained using ^{1}H NMR spectroscopy and the chloride-templated synthesis of an analogous catenane species was successful; although the target interlocked species could not be isolated.

4.6 References for Chapter Four

[1] Y. Hua and A. H. Flood, *Chem. Soc. Rev.*, 2010, **39**, 1262-1271.
[2] Y. Li and A. H. Flood, *J. Am. Chem. Soc.*, 2008, **130**, 12111-12122.
[3] K. M. Mullen, J. Mercurio, C. J. Serpell and P. D. Beer, *Angew. Chem. Int. Ed.*, 2009, **48**, 4781-4784.
[4] Y. Jeong and J.-S. Ryu, *J. Org. Chem.*, 2010, **75**, 4183-4191.
[5] C. J. Serpell, N. L. Kilah, P. J. Costa, V. Felix and P. D. Beer, *Angew. Chem. Int. Ed.*, 2010, **49**, 5322-5326.
[6] G. T. Spence, C. J. Serpell, J. Sardinha, P. J. Costa, V. Félix and P. D. Beer, *Chem. Eur. J.*, 2011, **17**, 12955-12966.
[7] M. J. Hynes, *J. Chem. Soc., Dalton Trans.*, 1993, 311-312.

[8] L. M. Hancock and P. D. Beer, *Chem. Eur. J.*, 2009, **15**, 42-44.
[9] M. R. Sambrook, P. D. Beer, J. A. Wisner, R. L. Paul, A. R. Cowley, F. Szemes and M. G. B. Drew, *J. Am. Chem. Soc.*, 2005, **127**, 2292-2302.
[10] H. Zheng, W. Zhou, J. Lv, X. Yin, Y. Li, H. Liu and Y. Li, *Chem. Eur. J.*, 2009, **15**, 13253-13262.
[11] L. M. Hancock, L. C. Gilday, S. Carvalho, P. J. Costa, V. Felix, C. J. Serpell, N. L. Kilah and P. D. Beer, *Chem. Eur. J.*, 2010, **16**, 13082-13094.
[12] L. M. Hancock, L. C. Gilday, N. L. Kilah, C. J. Serpell and P. D. Beer, *Chem. Commun.*, 2011, **47**, 1725-1727.
[13] M. R. Sambrook, P. D. Beer, M. D. Lankshear, R. F. Ludlow and J. A. Wisner, *Org. Biomol. Chem.*, 2006, **4**, 1529-1538.
[14] N. G. White, DPhil. Thesis, University of Oxford, 2012.
[15] R. K. Chhatra, A. Kumar and P. S. Pandey, *J. Org. Chem.*, 2011, **76**, 9086-9089.
[16] N. G. White and P. D. Beer, *Beilstein J. Org. Chem.*, 2012, **8**, 246-252.
[17] N. G. White, S. Carvalho, V. Felix and P. D. Beer, *Org. Biomol. Chem.*, 2012, **10**, 6951-6959.
[18] J. Cai, B. P. Hay, N. J. Young, X. Yang and J. L. Sessler, *Chem. Sci.*, 2013, **4**, 1560-1567.
[19] E. D. Goddard-Borger and R. V. Stick, *Org. Lett.*, 2007, **9**, 3797-3800.
[20] S. J. Connon, M. Rivard, M. Zaja and S. Blechert, *Adv. Synth. Catal.*, 2003, **345**, 572-575.
[21] M. D. Lankshear, N. H. Evans, S. R. Bayly and P. D. Beer, *Chem. Eur. J.*, 2007, **13**, 3861-3870.

Chapter Five

Chapter 5 Shielded alkyl-functionalised rotaxane host cavities for improved anion recognition strengths

5.1 Introduction and chapter aims

The attraction of mechanically interlocked molecules, in their capacity to act as chemical sensors as well as their potential nanotechnological uses as molecular switches and machines, was outlined in Chapter One. A particularly appealing characteristic of rotaxane interlocked host structures for anion binding is that they exhibit superior anion recognition properties compared with their macrocycle and axle components. This is a consequence of the unique interlocked binding domain which is of complementary size and shape for the templating anion used to construct the mechanically bonded structure, typically the chloride anion. Such systems display pronounced chloride anion selectivity over basic oxoanions, which are too large to penetrate the shielded binding pocket.[1-3]

The concept of shielding a binding cleft from solvent to produce a complementary binding domain for the target guest species is not new. Nature provides inspiration through the strong and specific binding of certain substrates to enzymes. Sulfate- and phosphate-binding proteins contain intricate hydrogen-bonding active sites which are deeply buried below the protein surface and well-shielded from competing water molecules. Multiple hydrogen-bond donors combine to strongly complex the oxoanion. The exact number and nature of the hydrogen-bond-donor groups, together with additional amino acid residues enables the protein to discriminate between the oxoanion guest species (see section 1.4.2.3).

With this in mind, the aim of this chapter was to construct rotaxane host molecules containing additional alkyl functionality which is designed to perform the role of shielding the binding cavity from solvent and so produce interlocked anion receptors with improved anion recognition capabilities. Various synthetic approaches to integrate alkyl functionality

into the macrocycle (Figure 5.1a) and axle (Figure 5.1b) components were undertaken prior to rotaxane construction.

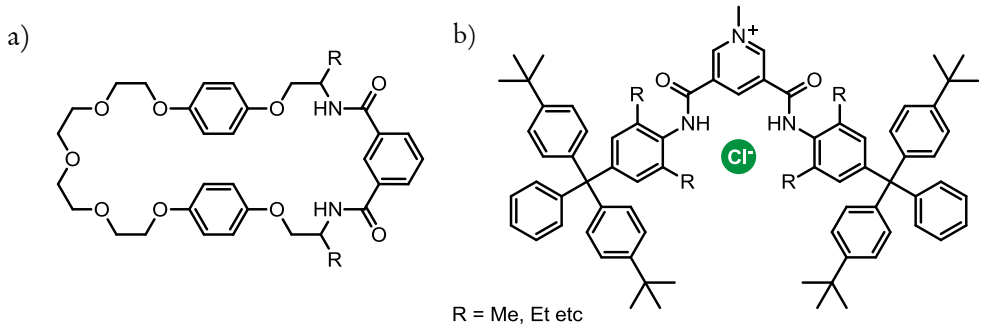


Figure 5.1. Structures of target alkyl-functionalised macrocycle (a) or axle (b) components of a rotaxane.

5.2 Macrocycle functionalisation

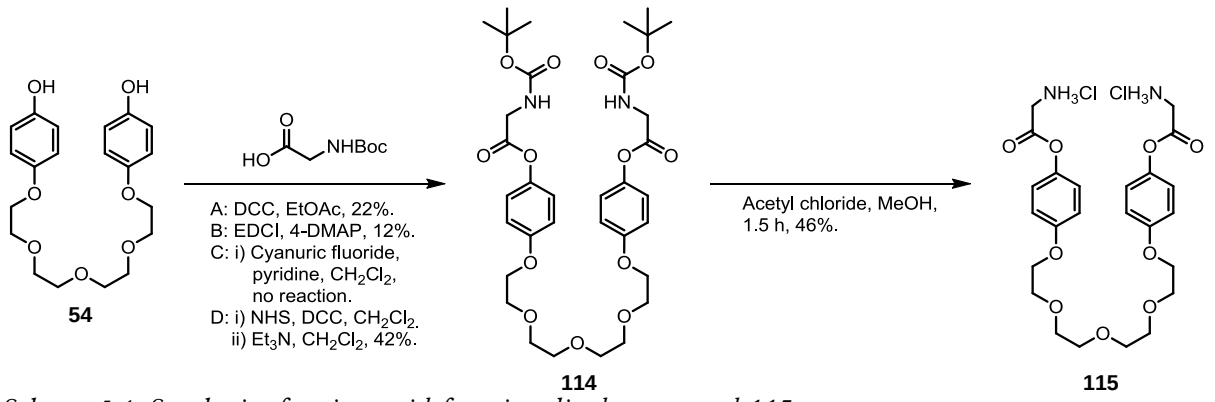
5.2.1 Rotaxanes incorporating amino acid residues

5.2.1.1 Introduction

One method by which additional alkyl groups may be incorporated into a macrocyclic component is by replacing the two amide groups with amino acid peptide linkages. The variety of amino acids available provides a straightforward method for preparing a range of macrocycle components from which an assortment of rotaxanes could be prepared and the effect of the different alkyl groups on the anion recognition properties investigated.

5.2.1.2 Synthesis of macrocycle precursor compounds

A variety of synthetic procedures for coupling *N*-Boc protected amino acid derivatives to bis-phenolic compound **54** were undertaken, initially with commercially available *N*-Boc-glycine as a model system (Scheme 5.1).

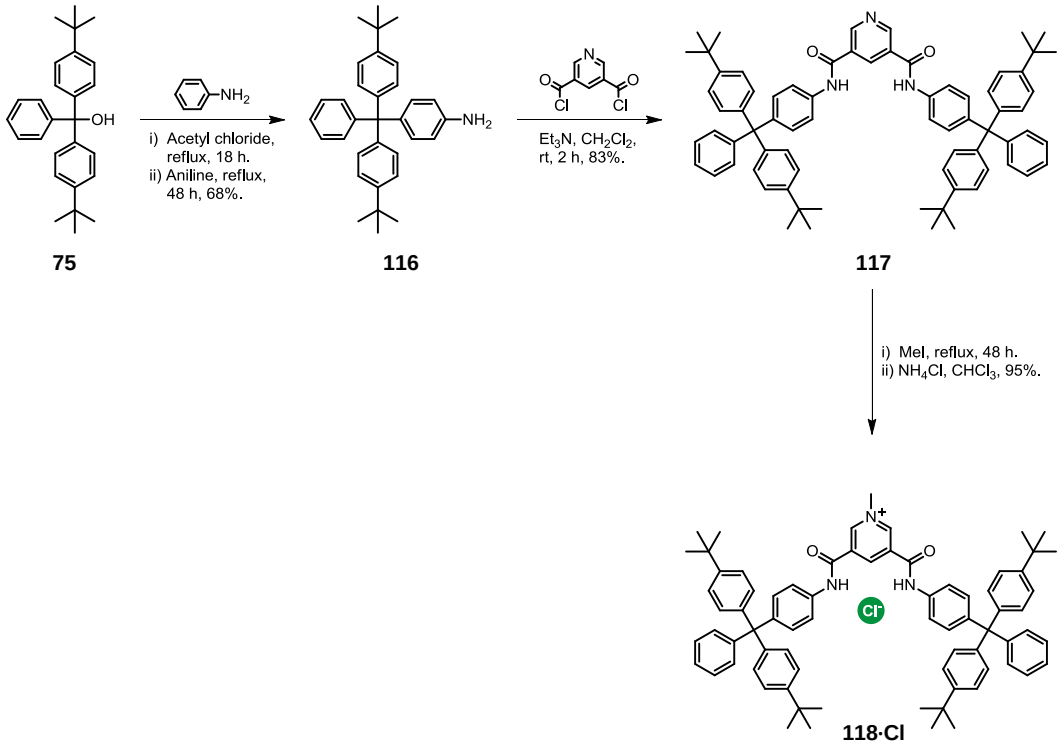


*Scheme 5.1. Synthesis of amino-acid-functionalised compound **115**.*

Stirring **54** and *N*-Boc-glycine in the presence of *N*,*N*'-dicyclohexylcarbodiimide in ethyl acetate afforded compound **114** in 22% yield. Attempts to prepare this Boc-protected amino acid compound in higher yield were also investigated. *N*-Boc-glycine and **54** were stirred in the presence of 1-ethyl-3-(3-dimethylaminopropyl)carbodiimide and a catalytic amount of 4-dimethylaminopyridine in 1:1 dimethylformamide:ethyl acetate giving compound **114** in 12% yield. An acid fluoride condensation reaction between **54** and *N*-Boc-glycine fluoride (prepared using cyanuric fluoride in pyridine) was also undertaken but was unsuccessful. An activated ester approach was then employed. Stirring *N*-Boc-glycine, *N*-hydroxysuccinimide and *N*,*N*'-dicyclohexylcarbodiimide in anhydrous dichloromethane overnight afforded the corresponding activated ester compound in quantitative yield which, upon condensation with **54** in the presence of triethylamine in anhydrous dichloromethane, gave **114** in an improved yield of 42%. Boc-deprotection with anhydrous hydrogen chloride (formed *in situ* by reaction between acetyl chloride and methanol) afforded the hydrochloride salt **115** in 46% yield.

5.2.1.3 Synthesis of pyridinium chloride stoppered-axle component

To allow for direct comparison with rotaxanes previously reported by Beer and co-workers, the synthesis of the pyridinium-containing axle component **118·Cl** was undertaken according to literature procedures[3] as outlined in Scheme 5.2.



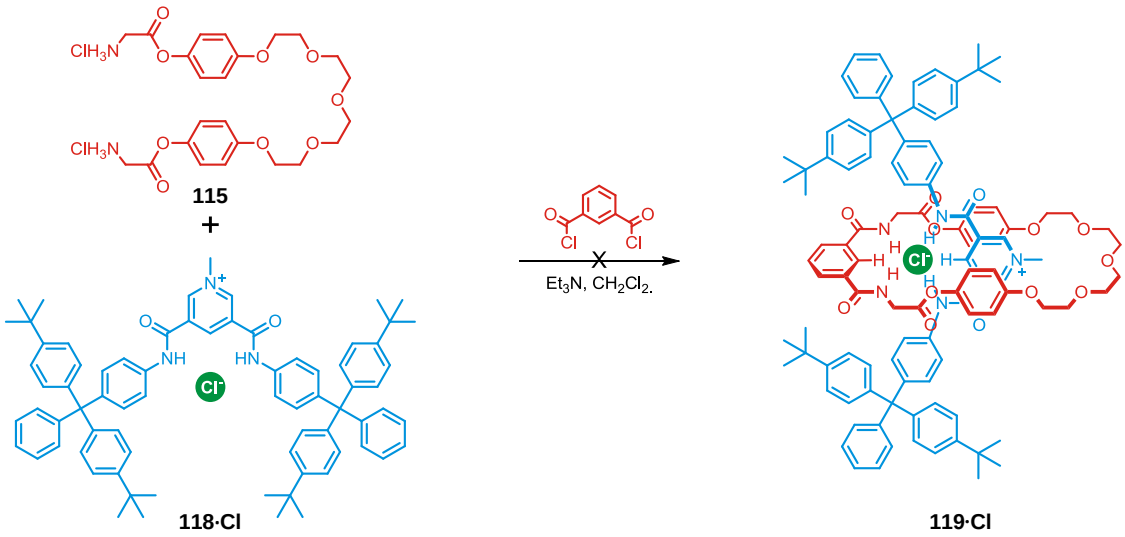
75 **116** **117** **118·Cl**

*Scheme 5.2. Synthesis of pyridinium chloride axle compound **118·Cl**.*

Compound **75** was heated in acetyl chloride followed by neat aniline to afford the terphenyl amine derivative **116** in 68% yield after recrystallisation. Condensation of two equivalents of **116** with pyridine-3,5-dicarbonyl chloride (prepared by heating pyridine-3,5-dicarboxylic acid in thionyl chloride) in the presence of triethylamine in dichloromethane gave pyridine-3,5-bis-amide **117** in 83% yield. Alkylation of the pyridine nitrogen by heating in methyl iodide produced the pyridinium iodide derivative **118·I** which was converted to the chloride salt in 95% yield by repeated washing of a chloroform solution of **118·I** with aqueous ammonium chloride.[3,4]

5.2.1.4 Attempted synthesis of rotaxane

Having successfully prepared the glycine-containing macrocycle precursor and pyridinium chloride axle components, the preparation of a [2]rotaxane was attempted using Beer and Hancock's acid-chloride-condensation clipping methodology (Scheme 5.3).[5]



*Scheme 5.3. Synthesis of [2]rotaxane **119·Cl**.*

An equimolar solution of macrocycle precursor compound **115** and pyridinium chloride axle species **118·Cl** was stirred in the presence of triethylamine and isophthaloyl dichloride in dichloromethane. A peak in the mass spectrum at m/z = 1662.0 corresponding to the interlocked species suggested the rotaxane synthesis had been achieved. Purification was undertaken using thin layer chromatography and initial separation of the rotaxane from the contaminating axle component was successful. Additional attempts to purify the rotaxane, however, revealed further contamination by the axle component as evidenced by ^{1}H NMR spectroscopy and thin layer chromatographic analysis, which suggested the rotaxane was decomposing.

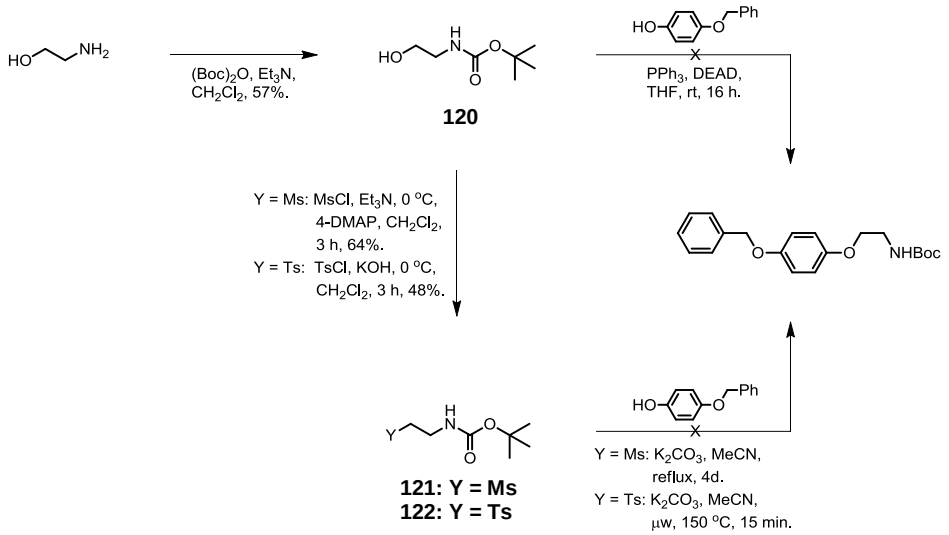
To probe this behaviour, the stability of the macrocycle precursor compound **115** was investigated. The hydrochloride salt **115** and triethylamine were stirred in anhydrous dichloromethane and then washed with water to remove the triethylammonium chloride species. The ^{1}H NMR spectrum of the product revealed multiple signals in the aromatic region (instead of the expected singlet) and the relative intensities of aromatic and aliphatic signals indicated a loss of CH_2 protons. Also the mass spectrum displayed a peak at m/z = 401.16 corresponding to the bis-phenolic species **54.** This spectroscopic evidence suggested that the phenolic ester linkage of the macrocycle component was susceptible to

base hydrolysis, which may account for the observed instability of the rotaxane product **119·Cl**.

5.2.2 Rotaxanes incorporating amino ether units

5.2.2.1 Synthesis of macrocycle component

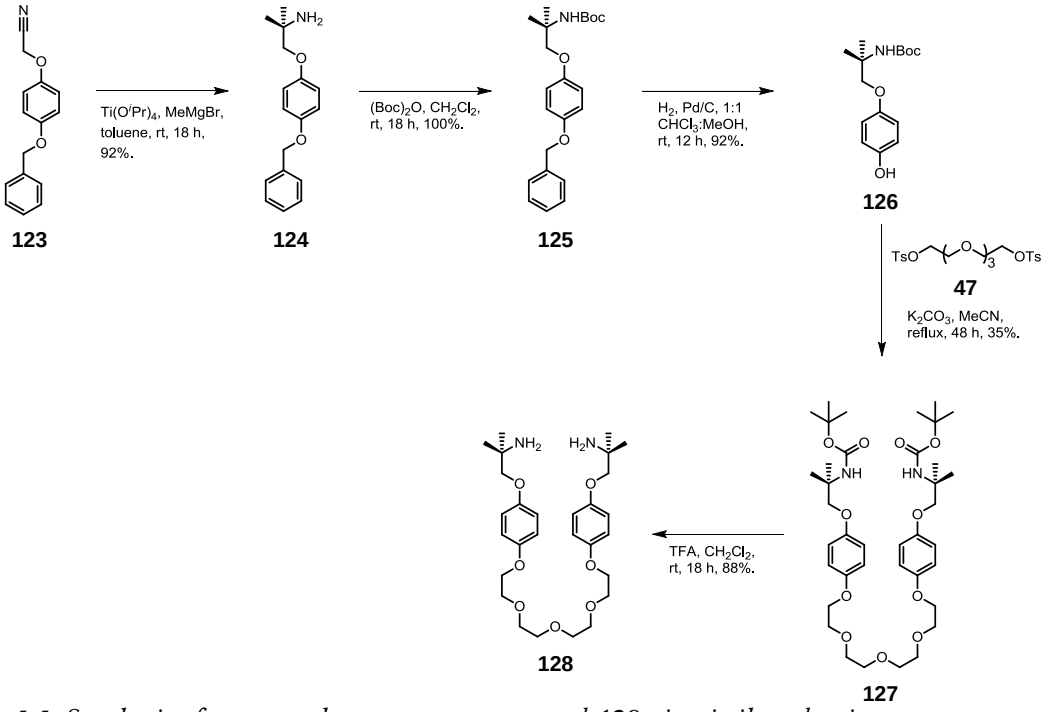
Replacing the ester moiety with a more stable ether linkage should surmount the rotaxane decomposition problem. Alternative syntheses involving *N*-protected amino alcohols were therefore undertaken (Scheme 5.4).



Scheme 5.4. Attempted synthesis of amino ether compounds.

Boc-protection of 2-ethanolamine to give compound **120** was achieved in 57% yield by stirring with di-*tert*-butyl dicarbonate and triethylamine in dichloromethane. A Mitsunobu reaction with 4-benzyloxyphenyl was attempted, however, there was no evidence of reaction either by ^{1}H NMR spectroscopic or thin layer chromatographic analysis of the crude reaction mixture. Mesylation or tosylation, using methanesulfonyl chloride or *p*-toluenesulfonyl chloride respectively, in the presence of base in dichloromethane, gave the corresponding compounds **121** and **122**. Reaction with 4-benzyloxyphenol by heating in acetonitrile with potassium carbonate, however, failed to give the target compound.

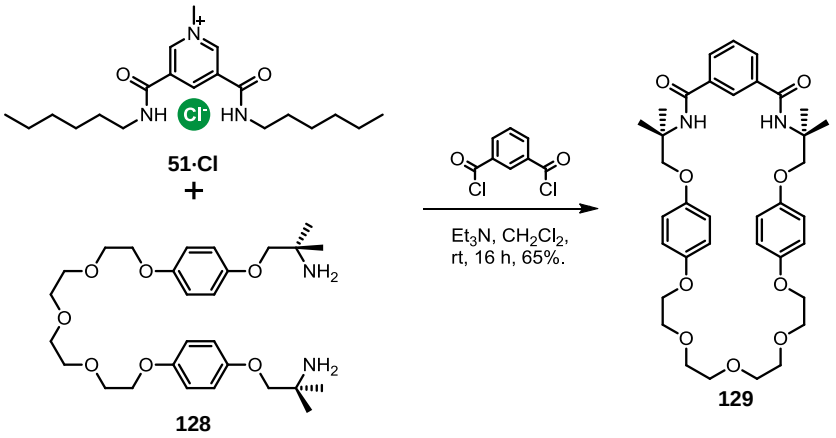
Alternative routes to functionalisation at the α-carbon were sought and the possibility of double nucleophilic addition to a nitrile group by a Grignard reagent was considered. A suitable macrocycle precursor was prepared by this synthetic route as outlined in Scheme 5.5



*Scheme 5.5. Synthesis of macrocycle precursor compound **128** via nitrile reduction.*

Reaction of two equivalents of methylmagnesium bromide and benzyl-protected nitrile-functionalised hydroquinone **123** (kindly donated by Dr Chris Serpell) in the presence of titanium(IV)-*iso*propoxide in toluene, produced the dimethyl-amine derivative **124** in 92% yield.[6] Boc-protection of this compound using di-*tert*-butyl dicarbonate in dichloromethane, gave **125** in quantitative yield. Hydrogenation to remove the benzyl group with 10% palladium/carbon under an atmosphere of hydrogen afforded compound **126** in 92% yield. A nucleophilic substitution reaction between **126** and ditosylate **47** under basic conditions in acetonitrile gave compound **127** in 35% yield. Boc-deprotection using trifluoroacetic acid in dichloromethane produced the target macrocycle precursor compound **128** in 88% yield.

The anion-templated acid-chloride–amine condensation synthesis of the new macrocycle was achieved as shown in (Scheme 5.6).



*Scheme 5.6. Anion-templated synthesis of compound **129**.*

After stirring an equimolar solution of **128** and isophthaloyl dichloride in the presence of templating agent **51·Cl** and triethylamine in anhydrous dichloromethane at room temperature for 16 hours, macrocycle species **129** was isolated in 65% yield following purification by column chromatography.

Crystals of macrocycle **129** suitable for single crystal X-ray diffraction structural analysis were grown by slow evaporation of a chloroform solution of the macrocycle. The solid state structure, solved by Dr Nicholas White, is shown in Figure 5.2 and reveals the convergence of the amide protons into the cyclic cavity which is partially screened by the methyl group functionalities.

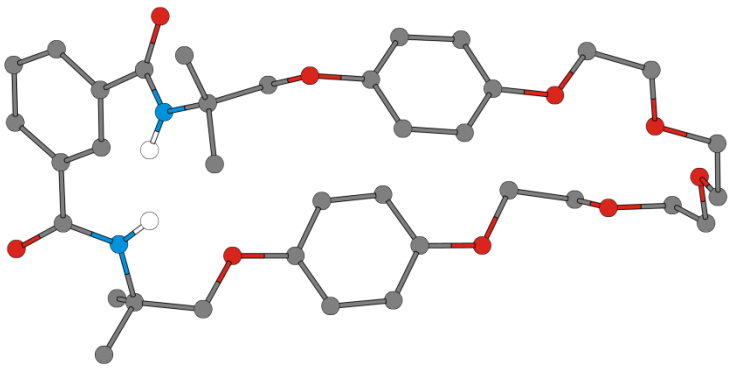


*Figure 5.2. Ball and stick plot of macrocycle **129**. Chloroform solvate and hydrogen atoms except those belonging to amide groups are omitted for clarity. Colour scheme: grey=C, white=H, blue=N, red=O.*

5.2.2.2 *Pseudorotaxane studies*

Following the successful preparation of the new alkyl-functionalised macrocycle **129**, a ^{1}H NMR pseudorotaxane assembly titration experiment with potential pyridinium chloride threading component **51·Cl** was undertaken. Upon addition of aliquots of **51·Cl** to a solution of macrocycle in chloroform-d, characteristic downfield shifts in the macrocycle's internal cavity and amide protons were observed, as well as diagnostic upfield shifts and splitting of the hydroquinone proton signals. In both chloroform-d and dichloromethane-d_2, however, the spectra became very broad and it was difficult to monitor accurately the perturbations of any signals corresponding to macrocycle protons involved in the interpenetration process. Consequently, no quantitative data could be obtained for the assembly process, although qualitatively, the partial titration curves (Figure 5.3) suggest there is strong association between the two components.

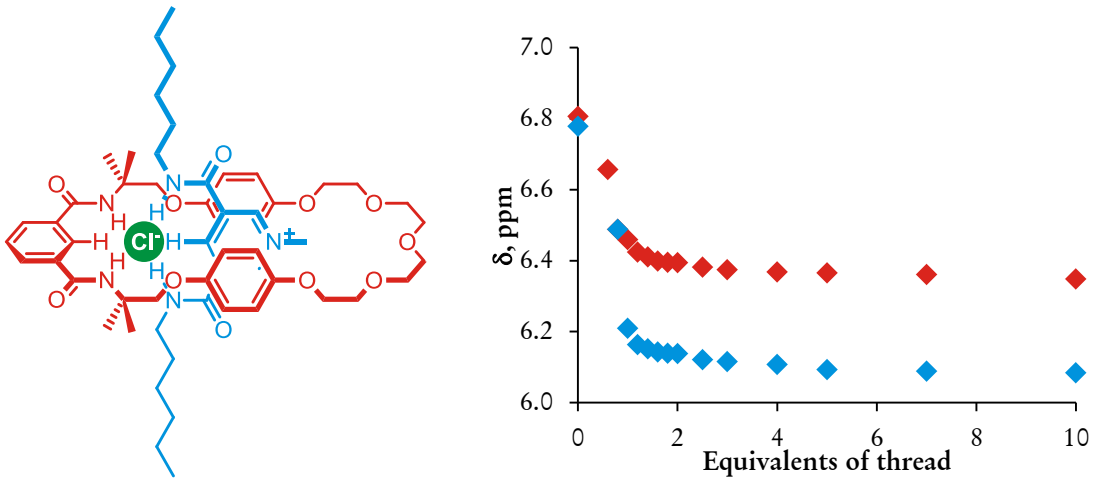
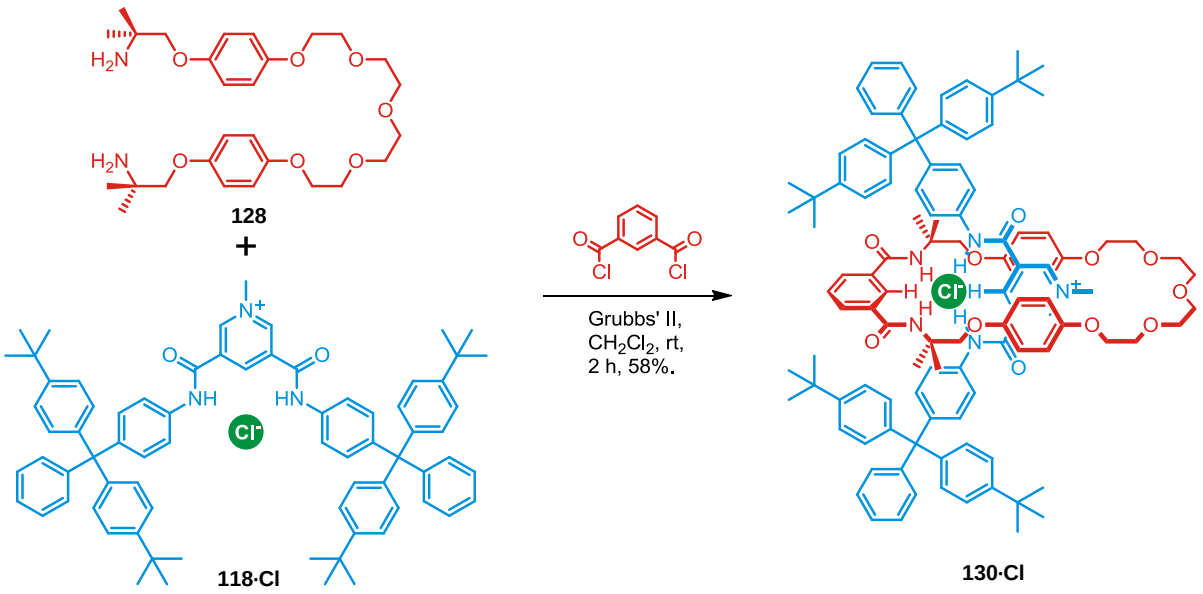


Figure 5.3. Chemical shift perturbations of hydroquinone protons upon addition of threading component ***51·Cl*** *to macrocycle* ***129*** *(500 MHz, $CDCl_3$, 293 K).*

5.2.2.3 *Synthesis and characterisation of a rotaxane incorporating an alkyl-functionalised macrocyclic component*

The synthesis of the target interlocked rotaxane species was achieved as outlined in Scheme 5.7. Stirring bis-amine compound **128** and pyridinium chloride axle component **118·Cl** in the presence of triethylamine and isophthaloyl dichloride afforded the target rotaxane **130·Cl**,

which was isolated in 58% yield following purification using preparative thin layer chromatography.



Scheme 5.7. Synthesis of target rotaxane ***130·Cl****.*

Evidence for the successful formation of an interlocked structure was provided initially by electrospray mass spectrometry and ^{1}H NMR spectroscopy.

The cationic molecular ion peak is readily observable in the mass spectrum which indicates the presence of a single molecular entity and the isotopic distribution revealed in the high-resolution mass spectrum is in good agreement with the theoretical model.

The ^{1}H NMR spectrum of the rotaxane is shown in Figure 5.4 along with spectra of the component macrocycle and axle for comparison. Several distinctive changes are displayed in the rotaxane's ^{1}H NMR spectrum, which are consistent with the formation of an interlocked species. Significant downfield perturbations of the signals corresponding to the macrocycle's internal proton *c* and amide protons *d* are observed as the isophthalamide motif associates with the chloride anion template through hydrogen bonding by these protons. This is further substantiated by the corresponding upfield shifts in the pyridinium axle cavity proton peak γ and amide signal δ as the chloride anion is polarised away from these protons, and they become less deshielded. The singlet in the macrocycle ^{1}H NMR spectrum corresponding to the hydroquinone protons *g* and *h* is split and shifted upfield in the rotaxane spectrum which

is characteristic of aromatic donor–acceptor interactions formed between the macrocycle's electron-rich hydroquinone units and the axle's electron-deficient pyridinium group. Finally, the pyridinium methyl protons signal α is shifted downfield as these protons are deshielded through hydrogen-bonding to the polyether oxygens of the macrocycle ring.

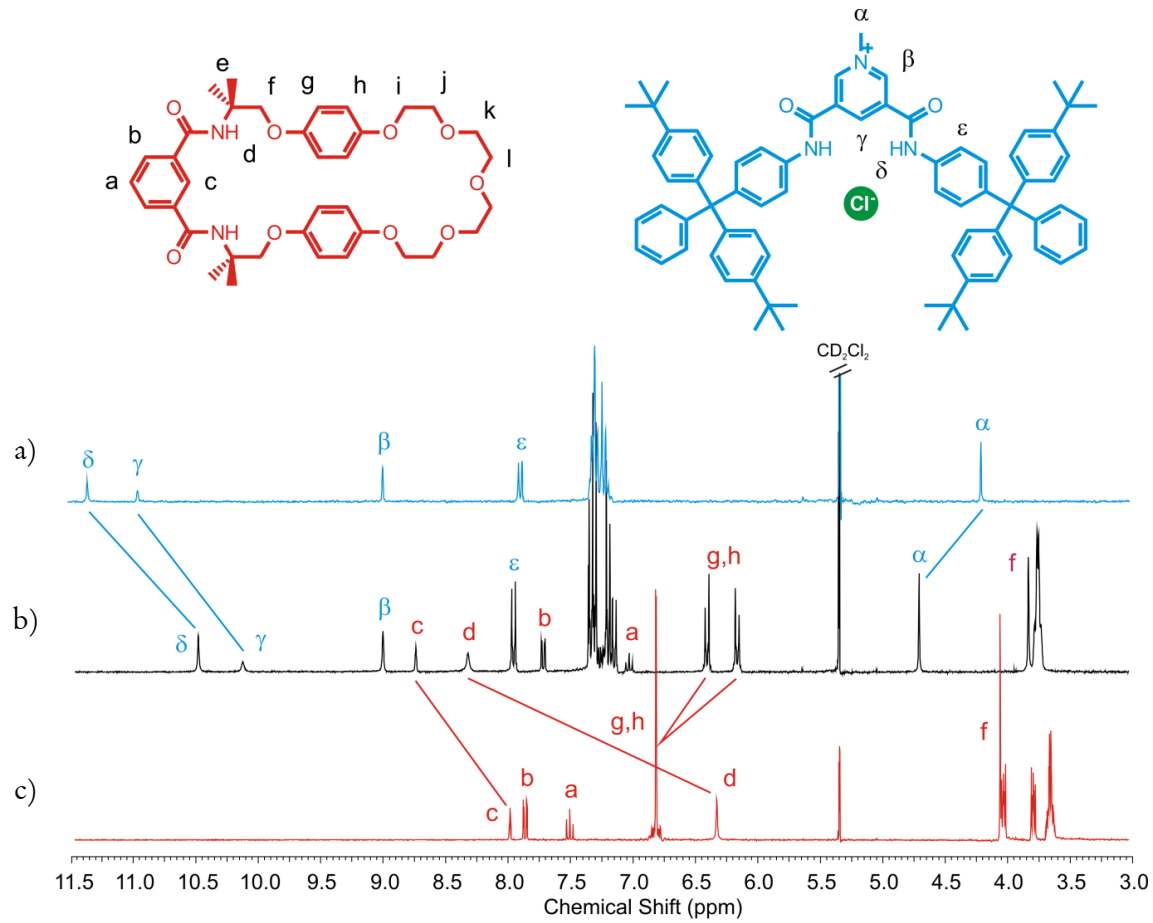


Figure 5.4. ^{1}H NMR spectra of a) pyridinium chloride axle ***118·Cl****, b) [2]rotaxane* ***130·Cl****, c) macrocycle* ***129*** *(500 MHz, CD_2Cl_2, 293 K).*

Further evidence for the interlocked nature of rotaxane **130·Cl** was provided by two-dimensional ^{1}H–^{1}H ROESY NMR spectroscopy (Figure 5.5). The spectrum reveals a number of through-space cross-coupling interactions between the two distinct components of the rotaxane. Notable interactions include **6** ($\beta \rightarrow h$) and **7** ($\delta \rightarrow g$) which are consistent with the axle pyridinium unit intercalating between the macrocycle hydroquinone groups through the formation of aromatic donor–acceptor interactions. Interactions **5** ($\varepsilon \rightarrow g$,*h*), **3** ($\varepsilon \rightarrow f$, *i–l*) and **8** ($\varepsilon \rightarrow c$) confirm the protons of the axle stopper groups are in close proximity to the macrocycle's hydroquinone, methylene and internal isophthalamide cavity protons

respectively. The pyridinium methyl protons are found to be near to both the macrocycle polyether chain, by interaction **1** ($\alpha \rightarrow i$–l), and the macrocycle hydroquinone protons, through interaction **2** ($\alpha \rightarrow h$). Cross-coupling interaction **4** ($\beta \rightarrow i$–l), between the *ortho*-axle pyridinium protons and the macrocycle polyether chain, also suggests the axle is threaded through the macrocyclic ring in the orientation depicted.

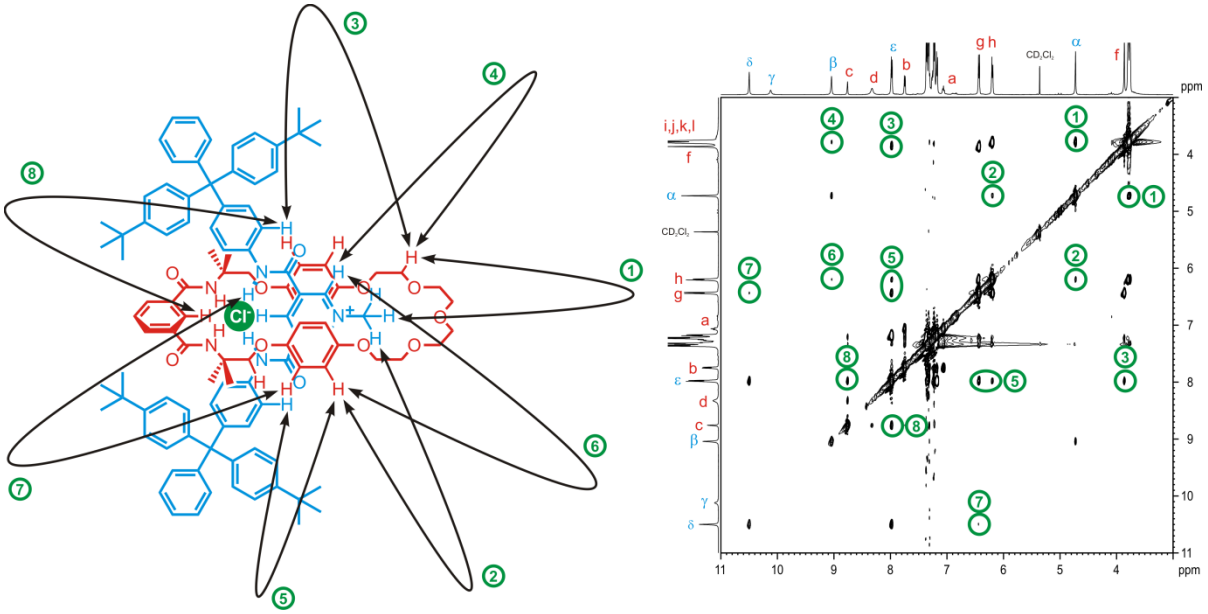


*Figure 5.5. ^1H–^1H ROESY NMR spectrum of rotaxane **130·Cl**. Assignable inter-component through-space interactions are highlighted (500 MHz, CD_2Cl_2, 293 K).*

5.2.2.4 Anion recognition properties of alkyl-functionalised rotaxane

In order to assess the anion recognition properties of the new rotaxane incorporating the tetra-methyl-functionalised macrocycle component, it was necessary to exchange the templating chloride anion for the non-coordinating hexafluorophosphate anion. This was achieved in 96% yield by repeatedly washing a chloroform solution of rotaxane **130·Cl** with aqueous ammonium hexafluorophosphate and the ^{1}H NMR spectra of the rotaxane with both chloride (**130·Cl**) and hexafluorophosphate (**130·PF$_6$**) are shown in Figure 5.6.

The most distinctive changes displayed in the ^{1}H NMR spectrum upon anion exchange to the hexafluorophosphate counteranion are the large upfield shifts of the protons comprising the interlocked binding cleft *c*, *d*, γ and δ which are indicative of chloride having been removed from the anion binding domain. These protons are no longer hydrogen bonding to the halide

anionic guest so are less deshielded, and shifted upfield. It is also worth noting the smaller upfield shifts of the pyridinium methyl protons *α* and downfield shift of the hydroquinone proton signals *g,h* which is possibly a result of small conformational changes between the rotaxane's axle and macrocycle components.

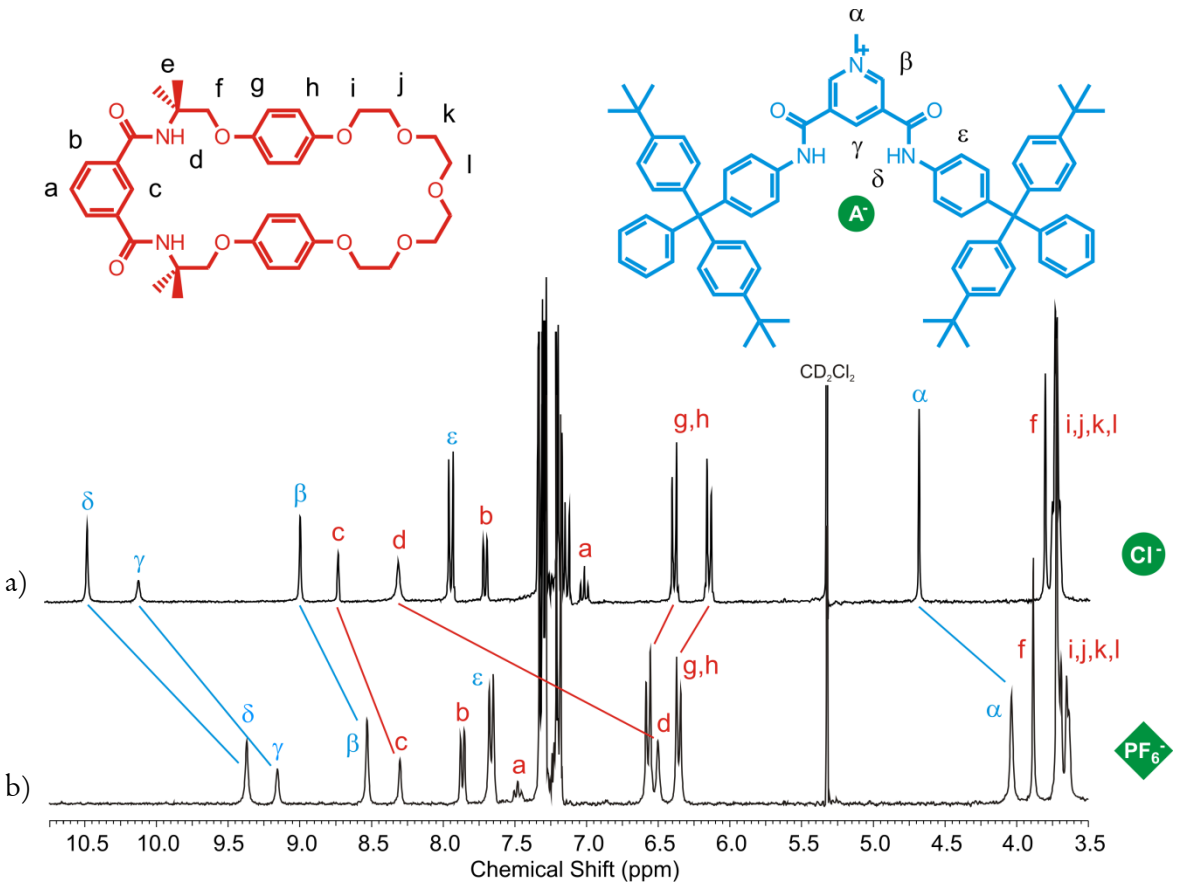


Figure 5.6. [1]H NMR spectra of: a) rotaxane ***130·Cl*** *and; b) rotaxane* ***130·PF$_6$*** *(300 MHz, CD_2Cl_2, 293 K).*

The anion recognition properties of this novel rotaxane were investigated by ^{1}H NMR spectroscopic titrations with chloride, acetate and dihydrogen phosphate in both 1:1 chloroform-d:methanol-d_4 and 45:45:10 chloroform-d:methanol-d_4:water-d_2 to enable comparison with a rotaxane previously reported by Beer and co-workers.[7]

Addition of anions to a solution of **130·PF$_6$** induced chemical shift perturbations in the signals corresponding to the cavity protons *c* and *γ*, and *ortho*-pyridinium protons *β* (Figure 5.7). It was not possible to monitor shifts of the amide protons *d* and *δ* as they were exchanged for deuterium.

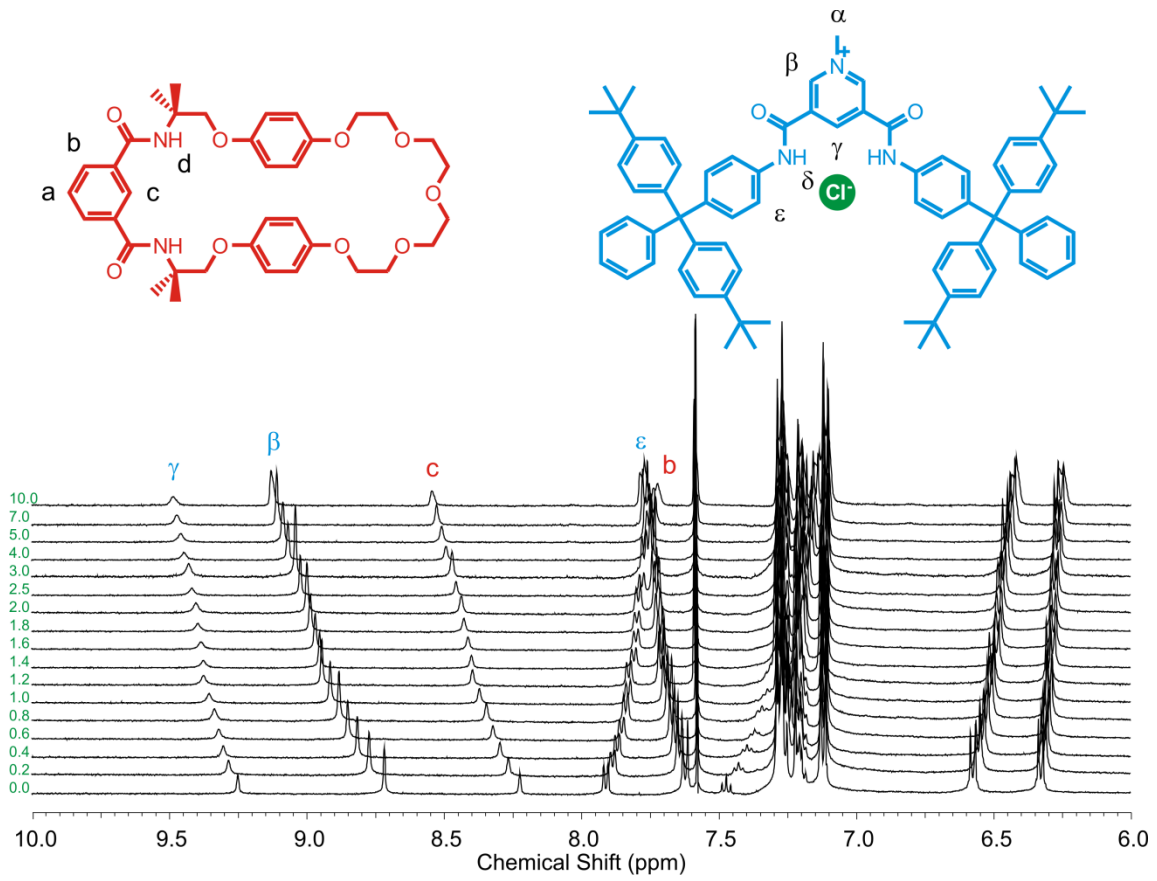


Figure 5.7. Partial ^1H NMR spectra of rotaxane ***130·PF$_6$*** *and various equivalents of TBA·Cl (500 MHz, 1:1 $CDCl_3$:CD_3OD, 293 K).*

To allow for direct comparison with the analogous unfunctionalised rotaxane, titration curves (Figure 5.8) and winEQNMR association constant values (Table 5.1) were determined by monitoring the perturbations of the ortho-pyridinium proton *β* as a function of the concentration of anion.

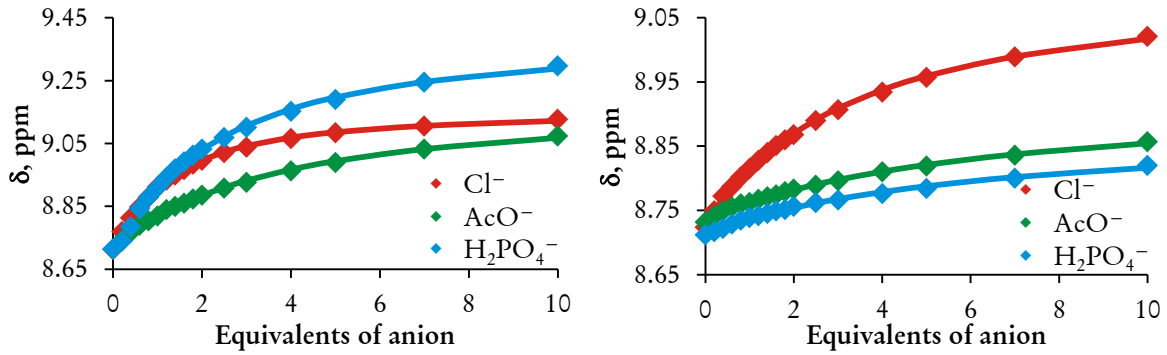
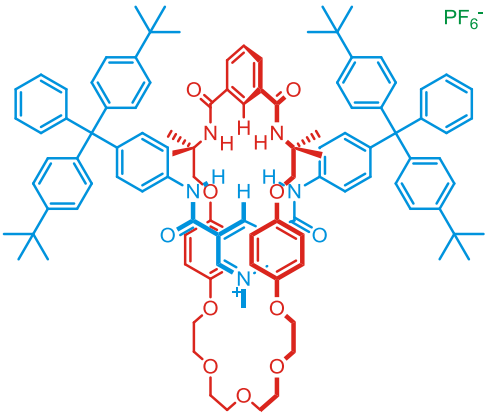
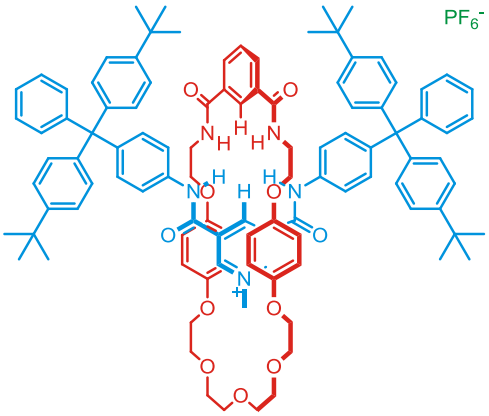


Figure 5.8. Titration curves for complex formation between rotaxane ***130·PF$_6$*** *and various anions obtained by monitoring* ortho*-pyridinium proton* β*. 500 MHz, 293 K, solvent: a) 1:1 $CDCl_3$:CD_3OD; b) 45:45:10 $CDCl_3CD_3OD$:D_2O. Square data points represent experimental data; continuous lines represent theoretical binding isotherms.*

Table 5.1. Association constants, K_a (M^{-1}), for 1:1 complexes of rotaxane hosts ***130·PF$_6$*** *and* ***131·PF$_6$*** *with various anions.*[a]



130·PF$_6$



131·PF$_6$

Anion	K_a(M^{-1})[a,b] 1:1 $CDCl_3$:CD_3OD		K_a(M^{-1})[a,b] 45:45:10 $CDCl_3$:CD_3OD:D_2O	
	130·PF$_6$	**131·PF$_6$**[c]	**130·PF$_6$**	**131·PF$_6$**[c]
Cl^-	475(14)	$>10^4$	137(5)	1190
AcO^-	124(7)	[d]	61(4)	120
$H_2PO_4^-$	215(12)	[d]	65(8)	180

[a]*All anions added as their TBA salt.* [b]*Association constants were determined by monitoring the downfield shift of the* ortho*-pyridinum proton* β*. Estimated standard errors are given in parentheses. $CDCl_3$, 293 K.* [c]*Association constants taken from reference* [7] *.* [d]*Not reported.*

The 1:1 stoichiometric association constants reported in Table 5.1 demonstrate that, whilst rotaxane **130·PF$_6$** is capable of binding anions in these competitive solvent mixtures, the interlocked host does not bind as strongly as the unfunctionalised rotaxane **131·PF$_6$**. In 1:1 chloroform-d:methanol-d_4 chloride binding by rotaxane **131·PF$_6$** is extremely strong, too strong to allow an accurate association constant to be determined ($K_a > 10^4$ M^{-1}), whereas the alkyl-functionalised rotaxane **130·PF$_6$** binds substantially more weakly (K_a = 475 M^{-1}). In the still more competitive aqueous solvent mixture, affinity for all anions is much lower with the alkyl-functionalised rotaxane **130·PF$_6$** than the traditional analogue. The macrocycle's additional methyl functionalities may simply be providing a steric barrier that prevents the anionic guests from penetrating the interlocked cavity, rather than shielding the cavity from solvent molecules as was hoped.

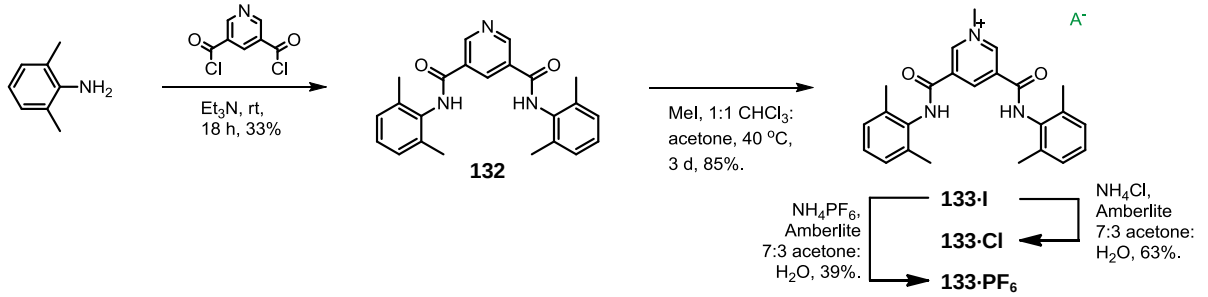
It was postulated that attaching additional methyl groups to the axle component, rather than the macrocycle, may provide an alternative route to enhancing anion recognition through shielding the cavity from competing solvent molecules and this avenue of research is discussed in the following section.

5.3 Axle functionalisation

5.3.1 Rotaxanes containing alkyl-functionalised stoppers

5.3.1.1 Synthesis of model potential threading component

It was envisaged that replacing the aniline moiety used in the preparation of the bulky stopper group (**116**, Scheme 5.2) with 2,6-dimethyl aniline would produce a corresponding terphenyl derivative with additional methyl groups which would enable an alkyl-functionalised axle component to be prepared. A model threading component containing 2,6-dimethylaniline groups was initially prepared, as outlined in Scheme 5.8, in order to examine the possibility of pseudorotaxane assembly with an isophthalamide macrocycle.



Scheme 5.8. Synthesis of 2,6-dimethylaniline-containing model threading compound ***133·Cl****.*

Two equivalents of 2,6-dimethylaniline were condensed with one equivalent of pyridine-3,5-dicarbonyl chloride in the presence of triethylamine in dichloromethane, forming 2,6-dimethylaniline-functionalised pyridine species **132** in 33% yield. Methylation using methyl iodide in 1:1 chloroform:acetone afforded the pyridinium iodide salt **133·I** which was converted to the chloride salt **133·Cl** in 63% yield by passing through an Amberlite® anion exchange column.

Crystals of compound **133·Cl** suitable for single crystal X-ray diffraction structural analysis were grown by slow evaporation of a chloroform solution of **133·Cl**. The structure, solved by Dr Nicholas White, reveals a chloride anion guest is coordinated in the bis-amide binding domain through hydrogen bonds to the two amide NH groups and the *para*-pyridinium CH moiety. It is interesting to note the twisted aniline rings, which lie out of the plane of the rest of the molecule, effectively protecting two faces of the chloride anion guest whilst leaving sufficient space for a second, orthogonal isophthalamide-containing species to satisfy the coordination sphere of the chloride anion.

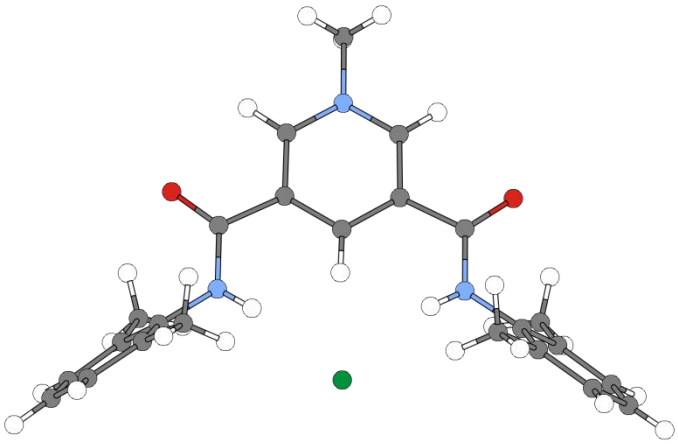
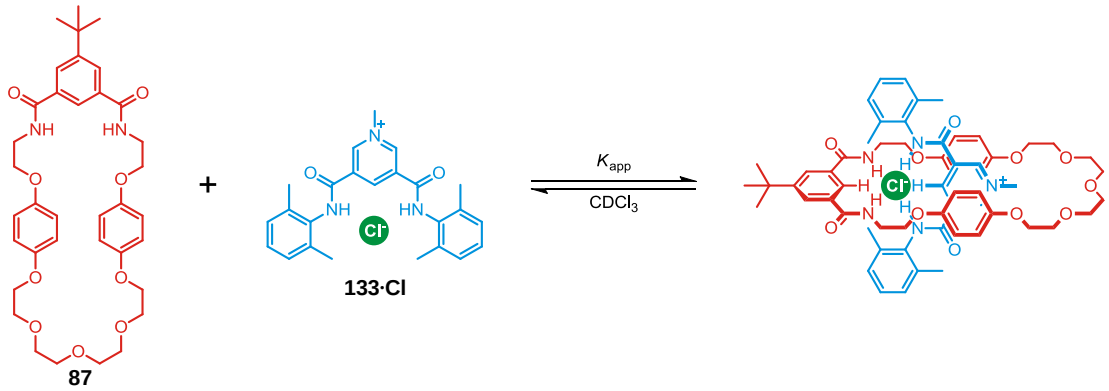


Figure 5.9. Crystal structure of model thread compound ***133·Cl****. Solvent molecules are omitted for clarity. Colour scheme: black=C, white=H, blue=N, red=O, green=Cl⁻.*

5.3.1.2 Pseudorotaxane formation with a model threading component

A chloride-anion-templated pseudorotaxane assembly study between potential threading component **133·Cl** and isophthalamide-containing macrocycle **87** was undertaken using a ^{1}H NMR spectroscopic titration experiment.



*Scheme 5.9. Pseudorotaxane formation between macrocycle **87** and threading component **133·Cl**.*

Unfortunately, compound **133·Cl** was found to exhibit limited solubility at the concentrations required for the ^{1}H NMR titrations in solvents such as acetone, chloroform or dichloromethane. As a consequence, the hexafluorophosphate salt was also prepared with a view to adding aliquots of **133·PF$_6$** to an equimolar solution of macrocycle and TBA chloride. This was achieved in 39% yield by passing a solution of **133·I** through an Amberlite® exchange column, preloaded with hexafluorophosphate. Compound **133·PF$_6$** was no more soluble than the chloride salt, however, and so quantitative analysis of the pseudorotaxane assembly process could not be undertaken. A ^{1}H NMR spectrum of an equimolar mixture of macrocycle **87**, **133·PF$_6$** and TBA chloride is shown in Figure 5.10.

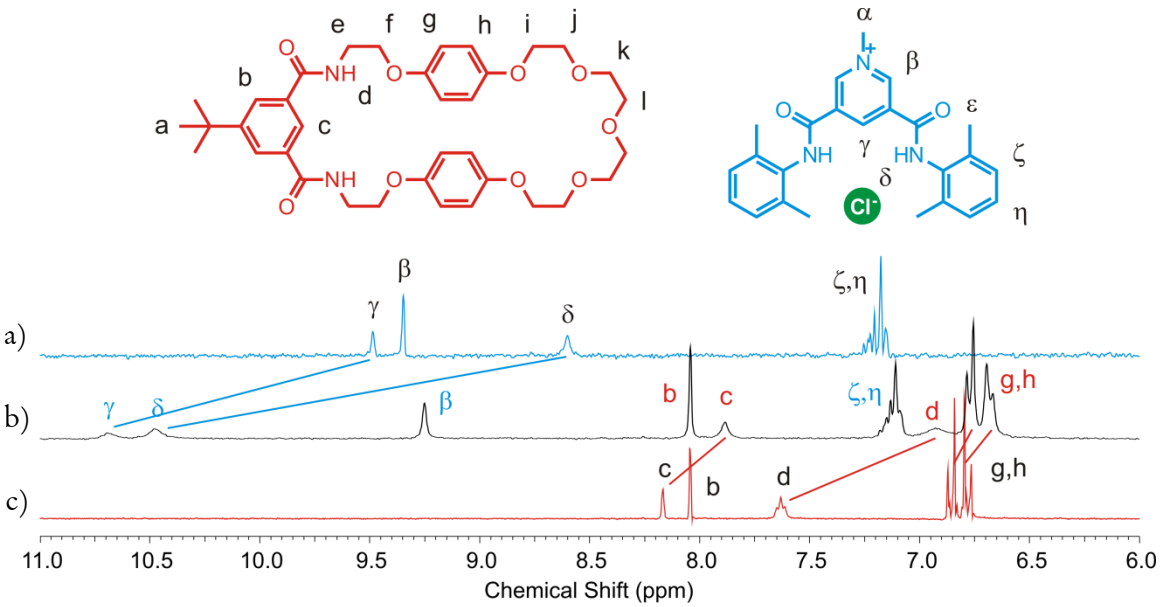
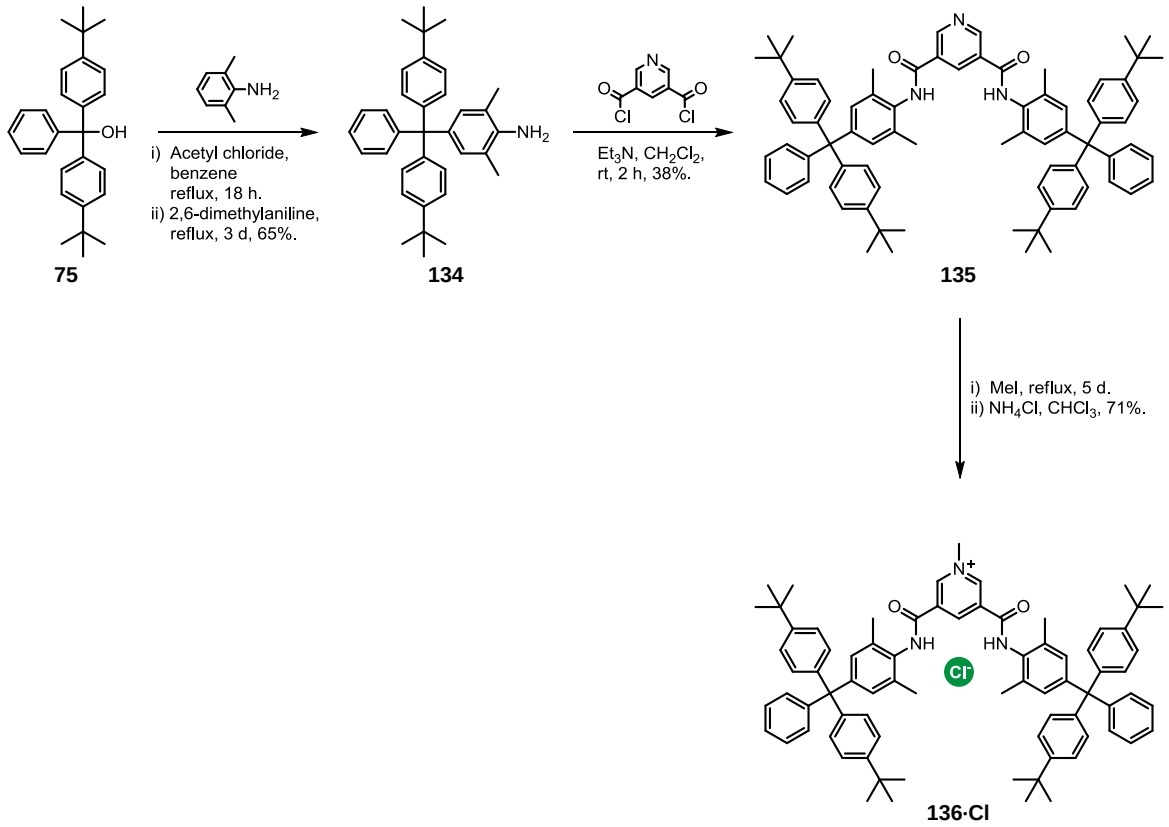


*Figure 5.10. Partial ^{1}H NMR spectra of a) pyridinium chloride thread **133·PF$_6$**, b) 1:1:1 **133·PF$_6$**:Cl^-:**87** 'pseudo[2]rotaxane', c) macrocycle **87** (300 MHz, CD_2Cl_2, 293 K).*

Crucially, the upfield shift of the macrocycle hydroquinone proton signal *g*,*h* is indicative of aromatic donor–acceptor interactions between the macrocycle's electron-rich hydroquinone and the thread's electron-poor pyridinium units, consistent with the formation of an interpenetrated assembly. The upfield shift of macrocycle cavity proton *c* and amide protons *d*, together with the downfield shift of threading component's internal proton *γ* and amide protons *δ* further corroborate the formation of a pseudorotaxane species as the chloride anion becomes complexed by both individual components of the supramolecular assembly.

5.3.1.3 Synthesis of novel stoppered-axle component

Following the ^{1}H NMR spectroscopic evidence of pseudorotaxane formation between model threading component **135·Cl** and macrocycle **87**, the preparation of a 2,6-dimethylaniline-containing stoppered-axle derivative was undertaken as outlined in Scheme 5.10.



Scheme 5.10. Synthesis of pyridinium chloride axle compound ***136·Cl****.*

Heating stopper precursor compound **75** and acetyl chloride in anhydrous benzene gave the chloro intermediate compound which was immediately dissolved in 2,6-dimethylaniline

affording the dimethylaniline stopper derivative **134** in 65% yield. This was then condensed with half an equivalent of pyridine-3,5-dicarbonyl chloride (formed by heating pyridine-3,5-dicarboxylic acid in thionyl chloride) in the presence of triethylamine in anhydrous dichloromethane to give the stoppered-pyridine compound **135** in 38% yield. Alkylation, followed by anion exchange, afforded the target axle component **136·Cl** in 71% yield over two steps.

5.3.1.4 Anion recognition properties of alkyl-functionalised axle component

Prior to commencing attempts to prepare the interlocked rotaxane architectures with the novel methyl-functionalised axle component **136·PF_6**, its anion binding properties were investigated to determine whether the additional methyl groups have any influence on the anion binding affinity of the pyridinium axle species. ^{1}H NMR spectroscopic titration experiments were undertaken in 1:1 chloroform-d:methanol-d_4 and monitoring the *para*-pyridinium proton γ gave the titration curves reported in Figure 5.11. WinEQNMR analysis of the titration data gave 1:1 stoichiometric association constants which are reported in Table 5.2 along with those for the traditional axle component **118·PF_6** for comparison.

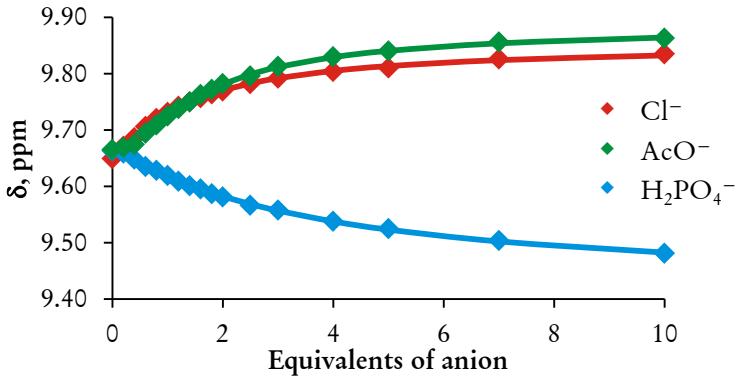


*Figure 5.11. Titrations curves for complex formation between pyridine axle compound **136·PF_6** and various anions. 1:1 $CDCl_3$:CD_3OD, 293 K. Square data points represent experimental data; continuous lines represent theoretical binding isotherms.*

Table 5.2. Association constants, K_a (M^{-1}), for addition of various anions to axle compound ***136·PF$_6$.***

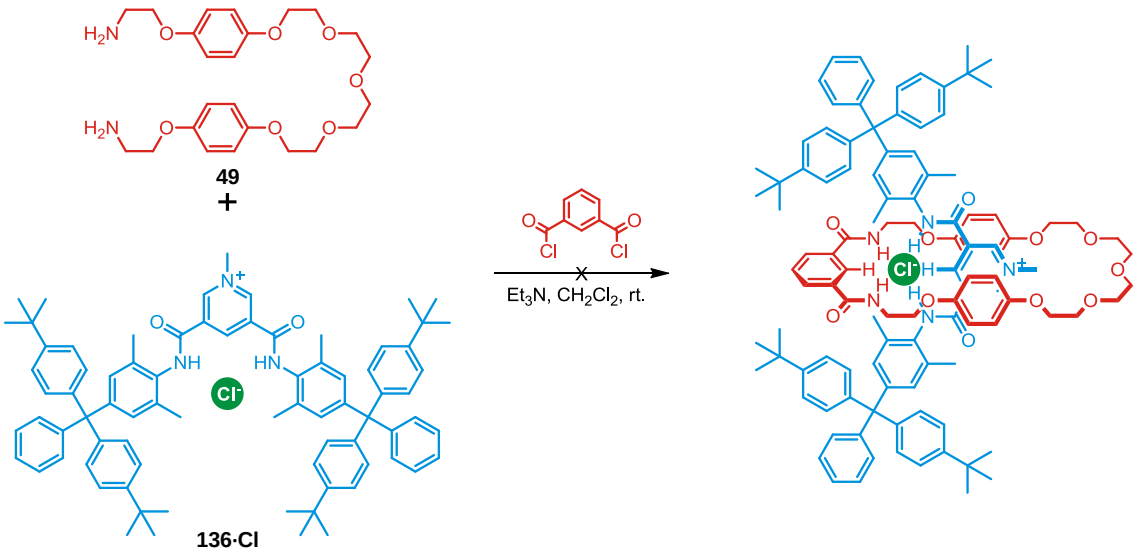
Anion	K_a (M^{-1})[a]	
	136·PF$_6$	**118·PF$_6$**[b]
Cl^-	394(15)	125
AcO^-	K_{11}: 814(42) K_{12}: 26(4)	K_{11}: 2200 K_{12}: 140
$H_2PO_4^-$	119(3)	260

[a]*All anions added as their TBA salt. Association constants were determined by monitoring the downfield shift of the para-pyridinum proton γ.* [b]*Association constant values taken from reference* [2]*. Estimated standard errors are given in parentheses. 1:1 $CDCl_3$:CD_3OD, 293 K.*

The strength of chloride association is larger with the functionalised axle component **136·PF$_6$** than the original axle species **118·PF$_6$**: K_a = 394 M^{-1} *versus* K_a = 125 M^{-1} respectively. This promising result suggests the additional methyl groups are contributing to enhanced chloride affinity with this system as was hoped. Additionally, there is a reduction in acetate binding affinity and little change to the strength of dihydrogen phosphate binding which suggests the additional methyl groups may aid selectivity for the smaller, more suitably sized yet less basic chloride anion when the axle is incorporated into a rotaxane host system.

5.3.1.5 Synthesis and characterisation of a novel rotaxane incorporating alkyl-functionalised stoppers

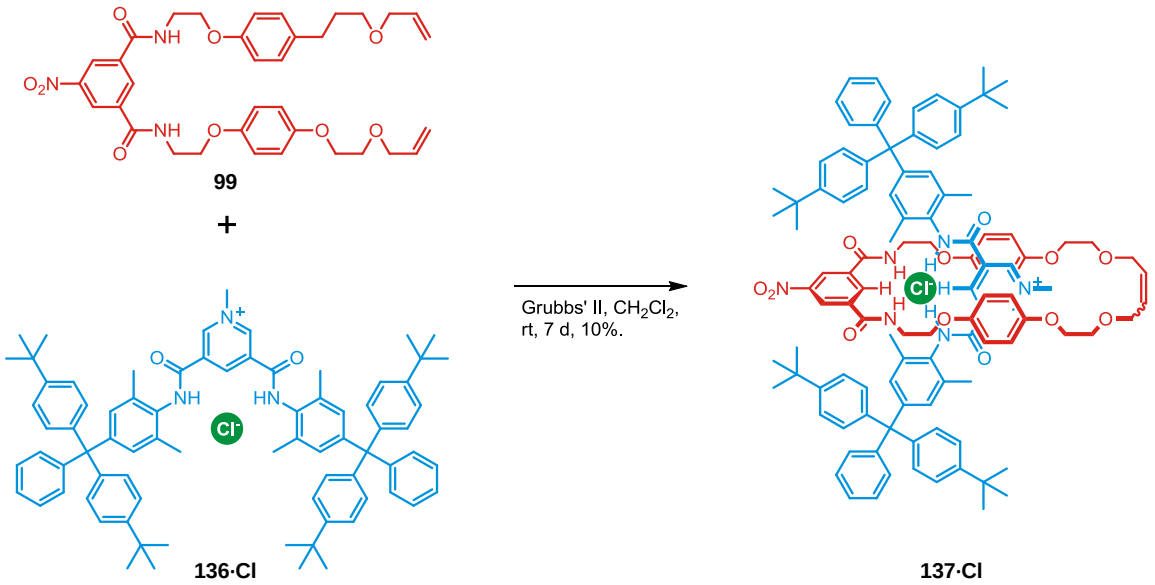
Following the successful synthesis of the required novel axle component and its promising anion recognition characteristics, the anion-templated synthesis of the corresponding [2]rotaxane was undertaken by using the acid-chloride-condensation methodology (Scheme 5.11).



Scheme 5.11. Attempted synthesis of a novel [2]rotaxane.

Axle compound **136·Cl** and bis-amine macrocycle precursor **49** were stirred in the presence of triethylamine and isophthaloyl dichloride in anhydrous dichloromethane. A peak in the mass spectrum at m/z = 1725.9 indicated some rotaxane had formed, although the rotaxane species could not be identified in the crude ^{1}H NMR spectrum suggesting it may have been produced in very small yield. Despite repeated attempts to purify the rotaxane species using preparative thin layer chromatography, it proved impossible to isolate any rotaxane. The presence of the additional methyl groups on the bulky stoppers may be sterically hindering the acid-chloride-condensation reaction. An alternative clipping route for rotaxane formation which makes use of a Grubbs'-catalysed RCM reaction was therefore undertaken (Scheme 5.12).

The synthesis of the target rotaxane **137·Cl** was successfully achieved by stirring a dichloromethane solution of bis-vinyl-appended macrocycle precursor **99** and stoppered-axle compound **136·Cl** in the presence of Grubbs' second generation catalyst (10% by weight) at room temperature for seven days. Following purification using repeated preparative thin layer chromatography, the rotaxane was isolated in 10% yield.



*Scheme 5.12. Synthesis of rotaxane **137·Cl**.*

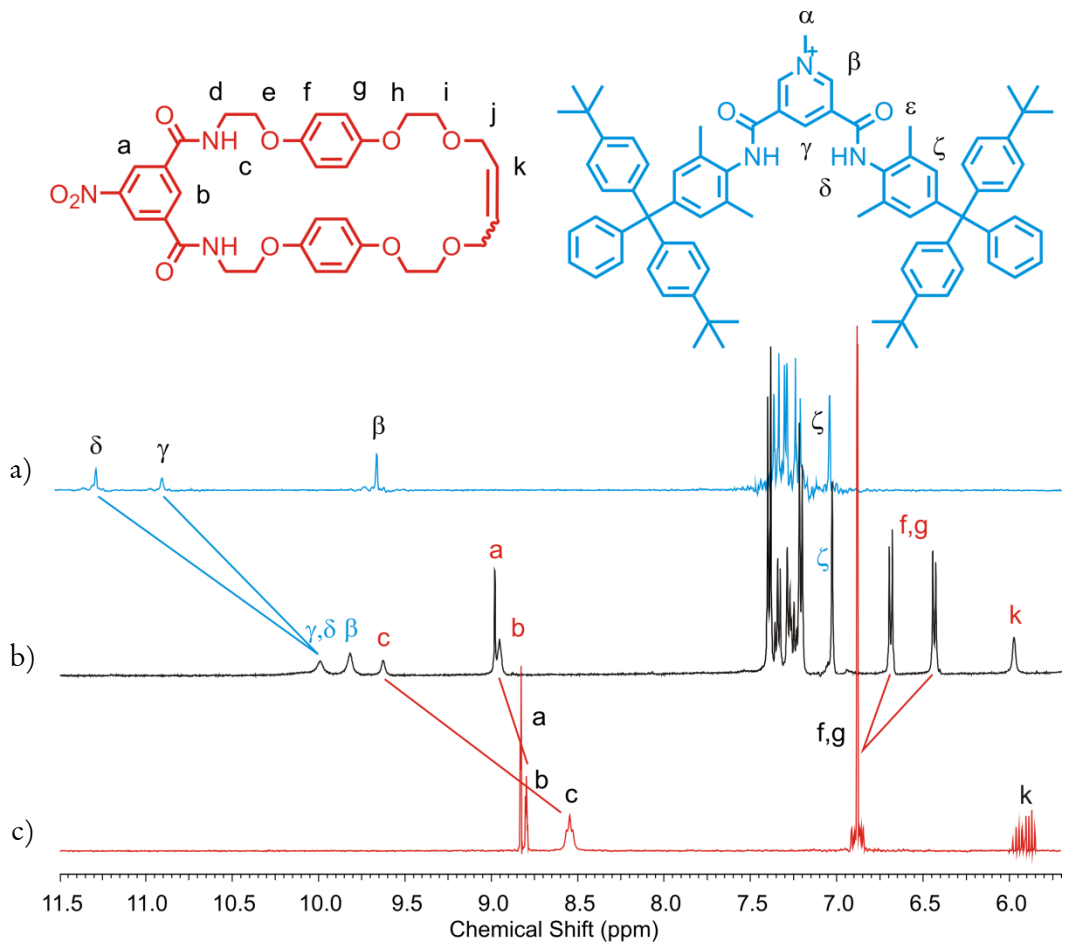


*Figure 5.12. Partial ^{1}H NMR spectra of a) pyridinium chloride axle **136·Cl**, b) rotaxane **137·Cl**, c) macrocycle precursor **99** (300 MHz, acetone-d_6, 293 K).*

The ^{1}H NMR spectra in acetone-d_6 of rotaxane **137·Cl** and those of component axle and macrocycle for comparison are shown in Figure 5.12. Several important features are worthy of

note. The convergence of the vinylic multiplet into a pseudo-singlet *k* in the rotaxane spectrum is attributed to the cyclisation of the acyclic precursor. More importantly, the diagnostic upfield shift and splitting of the hydroquinone proton signal *f*,*g* from the formation of aromatic donor–acceptor interactions between electron-rich hydroquinone and electron-poor pyridinium groups confirms the interlocked nature of the rotaxane structure. Finally, the upfield shift of pyridinium proton signals *γ* and *δ*, and the downfield shifts of macrocycle proton signal *c* are consistent with the templating chloride anion now no longer binding solely to the pyridinium axle component but being shared with the macrocycle isophthalamide moiety and residing in the pseudotetrahaedral binding domain formed between the two components.

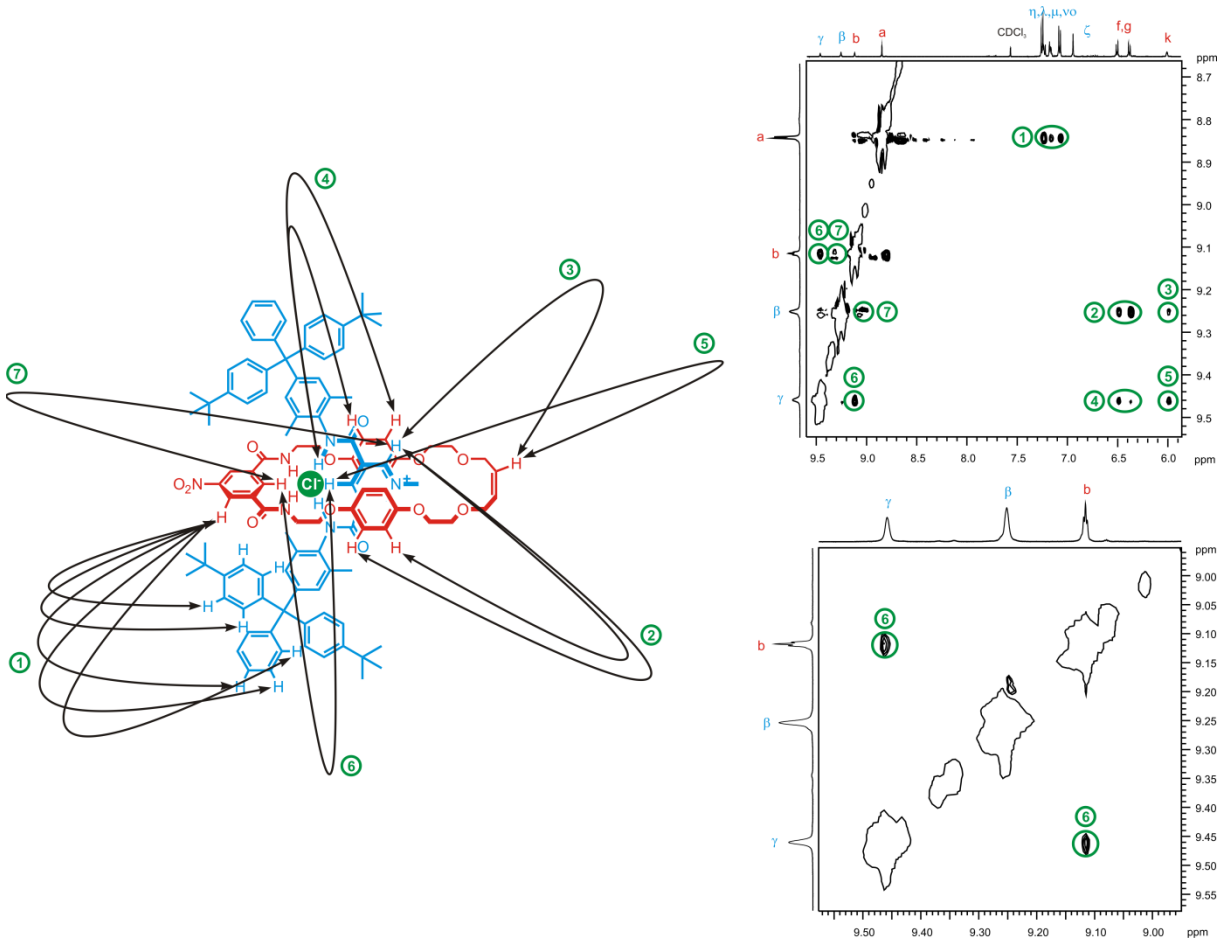


*Figure 5.13. ^{1}H–^{1}H ROESY NMR spectrum of rotaxane **137·Cl**. Assignable inter-component through-space interactions are highlighted (500 MHz, 1:1 $CDCl_3$:CD_3OD, 293 K).*

Further evidence confirming the interlocked nature of rotaxane **137·Cl** was provided by two-dimensional NMR spectroscopy: the ^{1}H–^{1}H ROESY NMR spectrum (Figure 5.13) displays

several significant through-space cross-coupling interactions between the two mechanically bonded components. Cross coupling interactions **2** ($\beta \rightarrow f,g$) and **4** ($\gamma \rightarrow f,g$) reveal the axle *ortho*- and *para*-pyridinium protons are in close proximity to the macrocycle hydroquinone groups, indicating the axle is threaded through the annulus of the cyclic species. Interactions **3** ($k \rightarrow \beta$) and **5** ($k \rightarrow \gamma$) show the axle pyridinium protons are near to the alkene protons of the macrocycle group. Macrocycle proton *a* is shown to be in the vicinity of the axle stopper groups by interaction **1** ($a \rightarrow \eta,\lambda,\mu,\nu,o$). Finally, interaction **6** ($b \rightarrow \gamma$) confirms the axle and macrocycle cavity protons are proximal as they converge into the interlocked cavity to bind chloride, and interaction **7** ($b \rightarrow \beta$) suggests the axle pyridinium group is in close proximity to the macrocycle isophthalamide unit.

5.3.1.6 Anion binding properties of axle-functionalised rotaxane

The anion binding properties of rotaxane **137·PF$_6$**, prepared by repeated washing of a chloroform solution of rotaxane **137·Cl** with aqueous ammonium hexafluorophosphate, were studied via ^{1}H NMR spectroscopic titration experiments with chloride, acetate and dihydrogen phosphate in the competitive solvent mixture 1:1 chloroform-d:methanol-d$_4$. Monitoring the chemical shift perturbations of axle pyridinium protons β and γ as a function of anion concentration gave the titration curves shown in Figure 5.14.

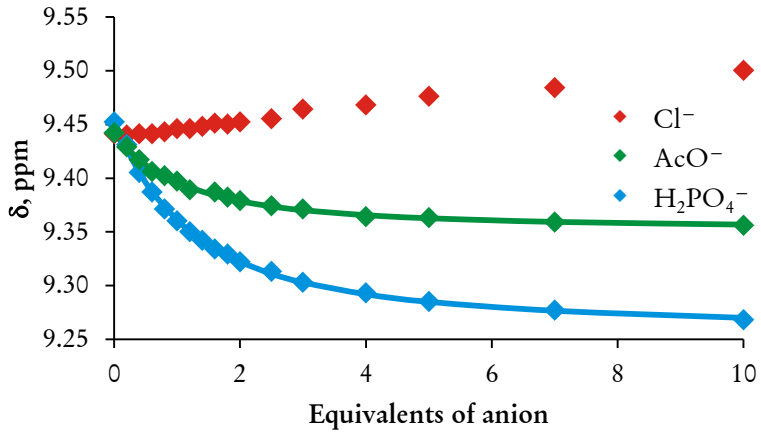
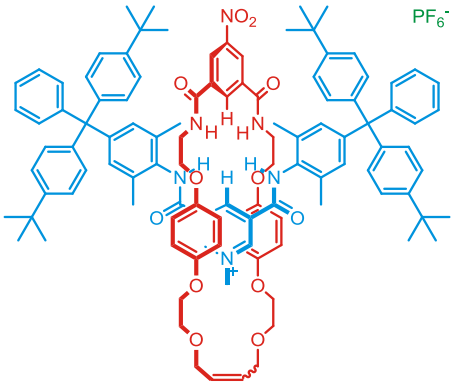
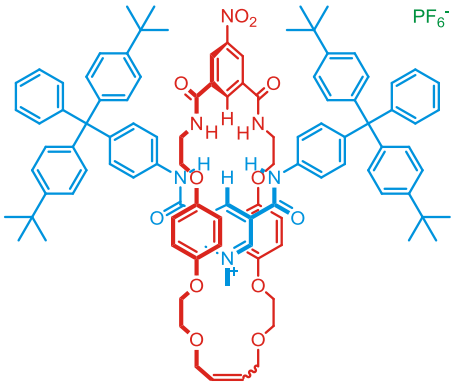


*Figure 5.14. Titration curves for addition of various anions to rotaxane **137·PF$_6$** obtained by following the axle cavity proton γ. 1:1 CDCl$_3$:CD$_3$OD, 293 K. Square data points represent experimental data; continuous lines represent theoretical binding isotherms.*

*Table 5.3. Association constants, K_a (M^{-1}), for addition of various anions to rotaxanes **137·PF$_6$** and **138·PF$_6$**.*



137·PF$_6$



138·PF$_6$

Anion	Axle **136·PF$_6$**	Rotaxane **137·PF$_6$**	Rotaxane **138·PF$_6$**[a]
	K_a(M^{-1})[b]	K_a(M^{-1})[b]	K_a(M^{-1})[b]
Cl^-	394(15)	[c]	4500
AcO^-	814(2)	626(46)	725
$H_2PO_4^-$	119(3)	400(41)	1500

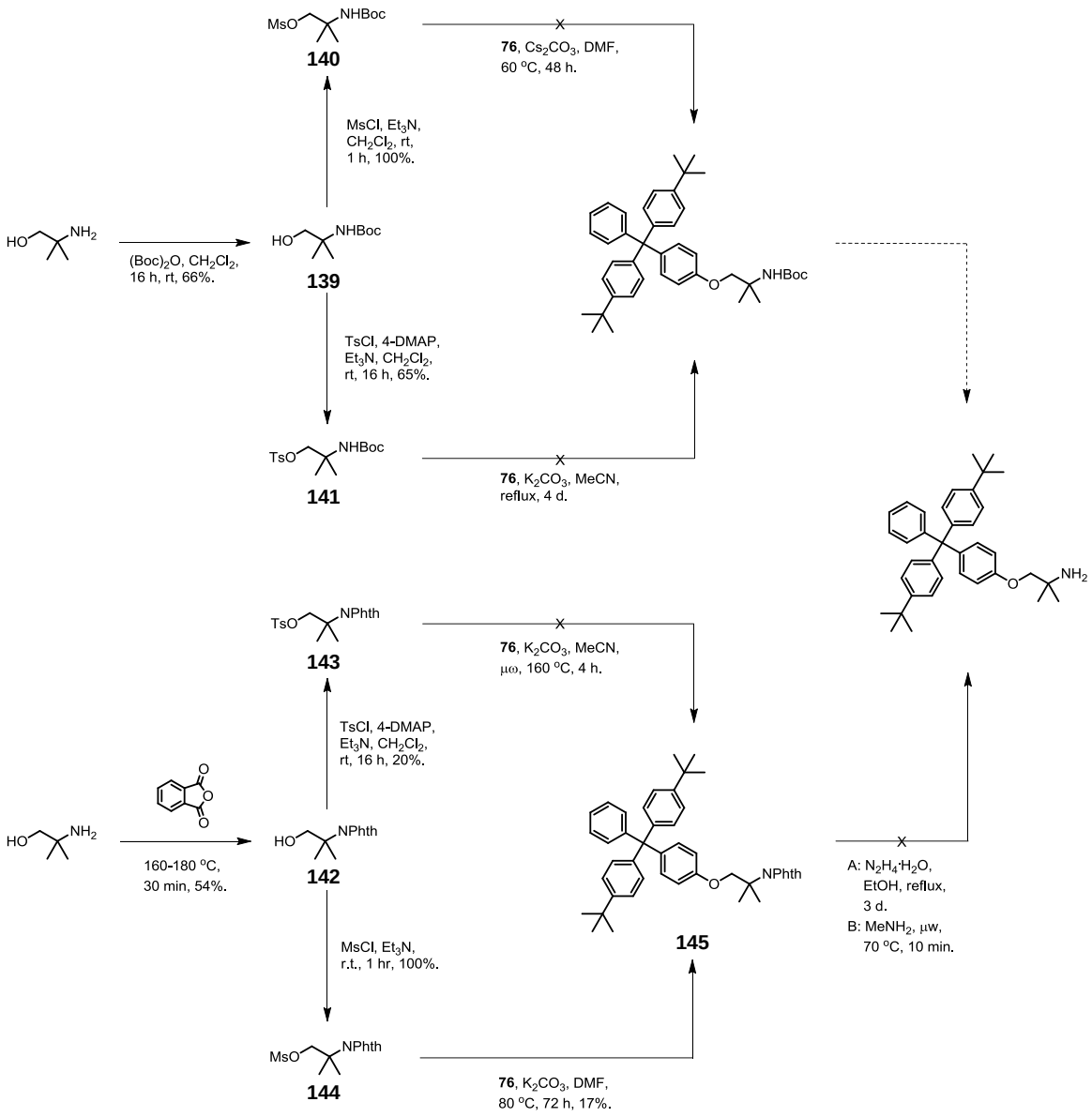
[a]Association constant values taken from reference [2]. [b]All anions added as their TBA salt. Association constants determined by monitoring the para*-pyridinium proton γ. [c]Chemical shift perturbations too small to allow an association constant to be determined. Estimated standard errors are given in parentheses. 1:1 $CDCl_3$:CD_3OD, 293 K.*

Anion complexation by new, methyl-functionalised rotaxane **137·PF$_6$** is significantly weaker than the traditional rotaxane **138·PF$_6$**. The chemical shift perturbations induced upon chloride anion addition to methyl-functionalised rotaxane **137·PF$_6$** were too small to allow an association constant value to be determined accurately, in contrast to a chloride binding affinity of K_a = 4500 M^{-1} for unfunctionalised rotaxane **138·PF$_6$**. The chloride and acetate anion binding affinities of rotaxane **137·PF$_6$** are also significantly weaker than that of axle component **136·PF$_6$**. In addition, the strength of dihydrogen phosphate complexation is also reduced with the methyl-functionalised rotaxane: K_a = 400 M^{-1} (**137·PF$_6$**) compared with 1500 M^{-1} for rotaxane **138·PF$_6$**. These observations suggest that the tetra-methyl-funcationalised axle component of rotaxane **137·PF$_6$** is sterically hindering access to the interlocked cavity to such an extent that chloride is unable to penetrate the rotaxane's binding domain, whereas oxoanions are still able to associate peripherally.

5.3.2 Rotaxanes containing alkyl-functionalised axles with flexible linkages

5.3.2.1 Synthesis of alkyl-appended stopper groups and axle compounds

The disappointing anion recognition properties of rotaxane **137·PF$_6$** may be improved if the methyl groups are incorporated into a more flexible axle component, which may result in a more sterically accessible binding domain. Attempts to prepare suitable alkyl-functionalised stopper groups are outlined in Schemes 5.14 and 5.15.



Scheme 5.13. Attempted synthesis of a new alkyl-appended stopper compound.

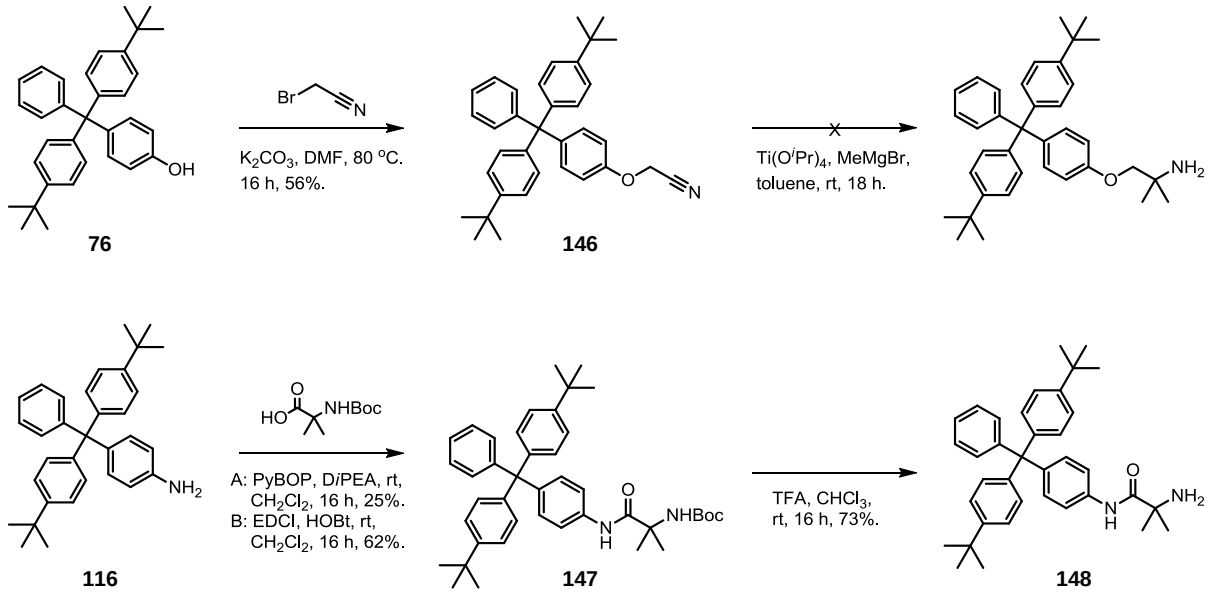
2-Amino-2-methyl propanol was Boc-protected to give **139** in 66% yield using di-*tert*-butyl dicarbonate in dichloromethane. Mesylation (to form compound **140**) or tosylation (to

produce compound **141**) were achieved in quantitative and 65% yields respectively by stirring with either methane- or *p*-toluenesulfonyl chloride in dichloromethane. Nucleophilic substitution reaction between compound **140** or **141** with stopper-phenol compound **76** in the presence of base and at elevated temperatures failed to produce any of the target Boc-protected alkyl-stopper compound.

Similar syntheses were carried out using phthalimide amine-protecting group. 2-Amino-2-methyl propanol was protected by heating with phthalic anhydride, giving compound **142** in 54% yield. Tosylation (using *p*-toluenesulfonyl chloride) or mesylation (using methanesulfonyl chloride) afforded compounds **143** and **144** in 20% and quantitative yields respectively. A nucleophilic substitution reaction between stopper-phenol **76** and tosylate **143** failed, although the target compound **145** was successfully prepared in 17% yield using mesylate derivative **144** under basic conditions in acetonitrile. Phthalimide-deprotection using either hydrazine monohydrate or methylamine in ethanol was unsuccessful, however, with evidence of cleavage of the C–O bond to produce the stopper-phenol precursor **76** provided by thin layer chromatography and mass spectrometry of the reaction mixture.

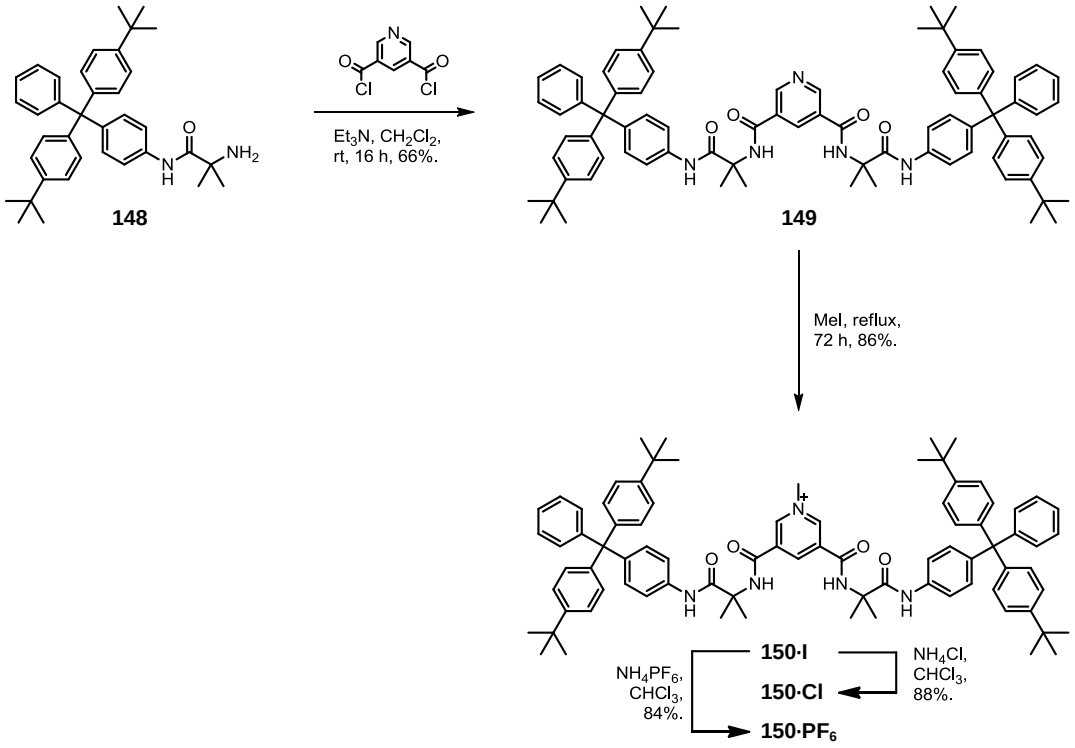
Alternative synthetic approaches were considered as reported in Scheme 5.14. The nitrile-functionalised stopper compound **146** was prepared in 56% yield by heating with bromoacetonitrile in the presence of potassium carbonate in acetonitrile. Nucleophilic addition to the nitrile group using methylmagnesium bromide and titanium(IV)-*iso*propoxide (c.f. Scheme 5.5) was attempted, however, only starting materials were recovered. Finally, the synthesis of an alkyl-stopper group was successfully accomplished using an amide-acid condensation approach to form the peptide derivative. Stopper-amine compound **116** and Boc-α-methylamine (Boc-Aib-OH) were stirred in the presence of peptide-coupling agent benzotriazol-1-yl-oxytripyrrolidinophosphonium hexafluorophosphate (PyBOP) and di-*iso*-propylethylamine and following purification by column chromatography, the target Boc-protected alkyl-stopper species **147** was isolated in 25% yield. A similar reaction using 1-ethyl-3-(3-dimethylaminopropyl)carbodiimide hydrochloride (EDCI·HCl) and

hydroxybenzotriazole in dichloromethane afforded compound **147** in an improved yield of 62% yield. Boc-deprotection by stirring with trifluoroacetic acid in dichloromethane produced the alkyl-appended stopper-amine compound **148** in 73% yield.



*Scheme 5.14. Synthesis of allyl-appended stopper compound **148**.*

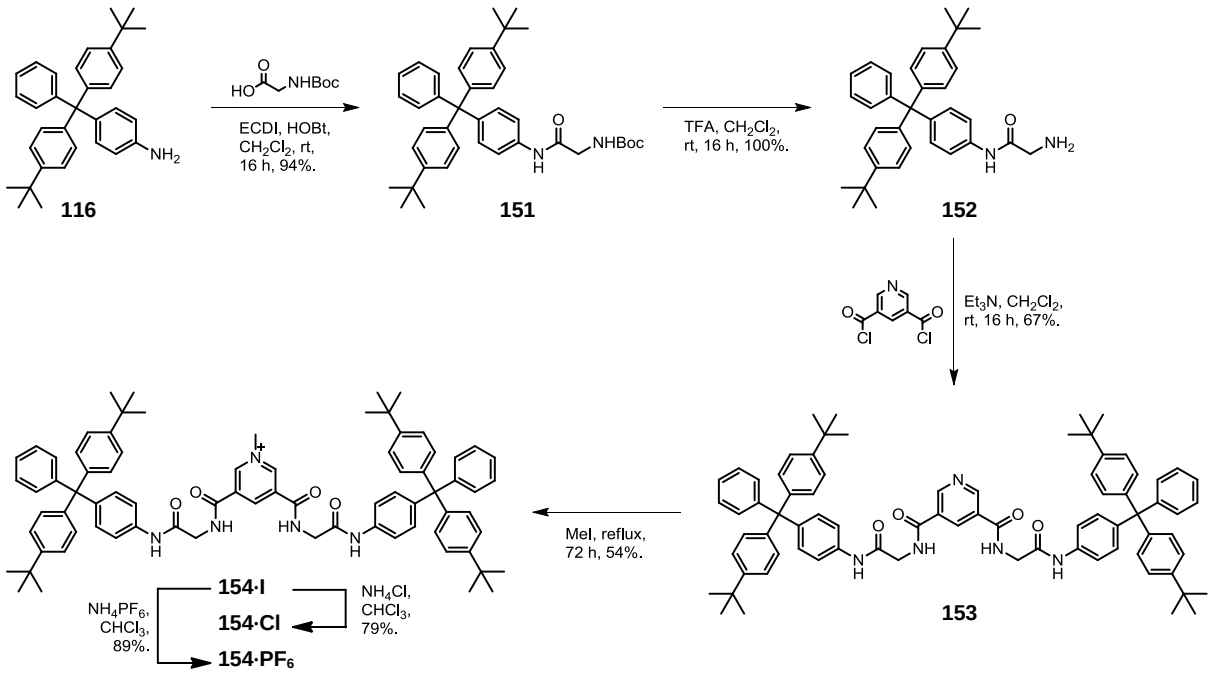
The preparation of the corresponding axle component is described in Scheme 5.15. An acid-chloride-condensation reaction between pyridine-3,5-dicarbonyl chloride and two equivalents of stopper-amine **148** in the presence of triethylamine in dichloromethane afforded compound **149** in 66% yield. Methylation using methyl iodide gave the iodide salt **150·I** in 86% yield. Exchanging the iodide anion for the templating chloride anion or the non-coordinating hexafluorophosphate anion was achieved by repeated washing a chloroform solution of compound **150·I** with the appropriate aqueous ammonium salt to give **150·Cl** and **150·PF_6** in 88% and 84% yields respectively.



*Scheme 5.15. Synthesis of axle component **150·A**.*

Before embarking on the rotaxane synthesis with this novel axle compound, the preparation of a control axle derivative without the additional methyl groups was also targeted (Scheme 5.16).

Stopper-amine compound **116** and *N*-Boc-glycine were coupled using EDCI·HCl and hydroxybenzotriazole in dichloromethane to give compound **151** in 94% yield. Boc-deprotection of compound **151** was achieved by stirring with trifluoroacetic acid in dichloromethane and produced compound **152** in quantitative yield. Condensation of two equivalents of amine **152** and pyridine-3,5-dicarbonyl chloride in the presence of triethylamine in dichloromethane afforded stoppered-pyridine compound **153**, which was alkylated to give compound **154·I** in 54% yield. Anion exchange to either the chloride or hexafluorophosphate salts was again achieved by repeated washing of a chloroform solution of **154·I** with ammonium chloride or hexafluorophosphate giving **154·Cl** and **154·PF$_6$** in 79% and 89% yields respectively.



*Scheme 5.16. Synthesis of control axle component **154·A**.*

5.3.2.2 Anion recognition properties of new axle components

The anion binding properties of novel axle component **150·PF$_6$** were studied using ^{1}H NMR spectroscopic titration experiments in 1:1 chloroform-d:methanol-d$_4$. Upon addition of chloride, acetate and dihydrogen phosphate downfield shift perturbations of the signal corresponding to the *para*-pyridinium proton were observed. Monitoring this proton signal as a function of anion concentration gave the titration curves reported in Figure 5.15 and winEQNMR analysis of the titration data gave the association constant values reported in Table 5.4. Unfortunately, the control axle species **154·PF$_6$** was only soluble in dimethylsulfoxide-d$_6$ and, owing to time constraints, anion binding studies with both axles in dimethylsulfoxide were not undertaken.

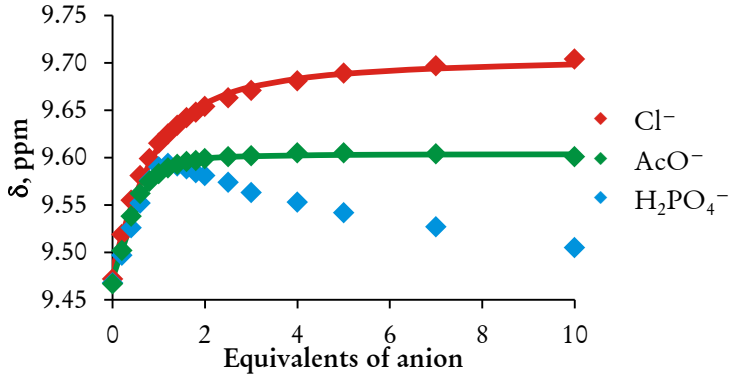


Figure 5.15. Titration curves for addition of various anions to axle compound ***150·PF$_6$*** *obtained by following the* para*-pyridinium proton. 1:1 $CDCl_3$:CD_3OD, 293 K. Square data points represent experimental data; continuous lines represent theoretical binding isotherms.*

Table 5.4. Association constants, K_a *(M^{-1}), for addition of various anions to axle compound* ***150·PF$_6$***.

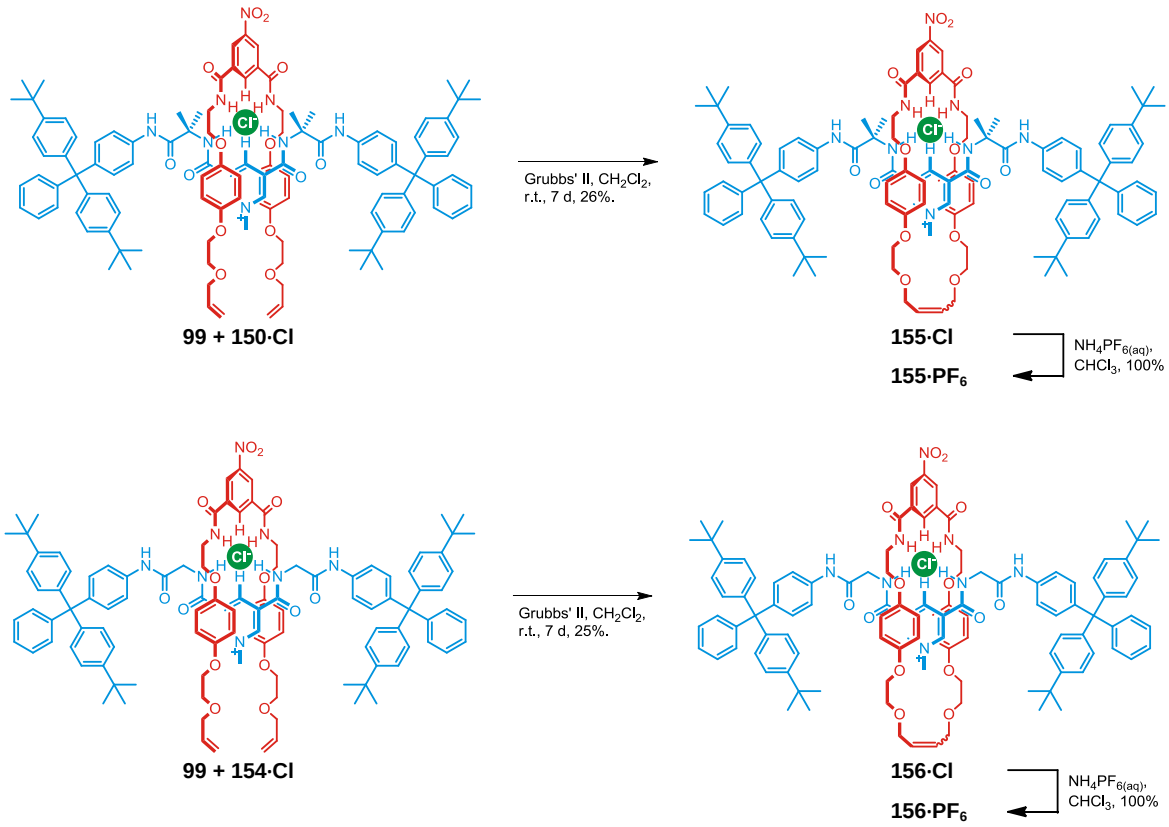
Anion	$K_a(M^{-1})^a$
Cl^-	1071(31)
AcO^-	9080(581)
$H_2PO_4^-$	*b*

[a]All anions added as their TBA salt. Association constants were determined by monitoring the downfield shift of the para-pyridinium proton. [b]Could not fit to a simple 1:1 or 1:2 binding model. Estimated standard errors are given in parentheses. 1:1 $CDCl_3$:CD_3OD, 298 K.

The association constant values in Table 5.4 demonstrate the flexible axle component is able to bind anions strongly even in this competitive solvent system. It is interesting to note that the anion binding affinity of this system is greater than any of the other axles or rotaxanes discussed previously in this chapter. This may be a result of the incorporation of two additional amide anion recognition motifs in the axle's structural framework. Acetate association is more favourable than chloride anion recognition, which is to be expected since acetate is the more basic anion—a trend commonly observed with acyclic, non-preorganised hydrogen-bond-donor systems. Dihydrogen phosphate binding also appears to be very strong although the induced chemical shift perturbations could not be fitted to a simple 1:1 or 1:2 host:guest binding model.

5.3.2.3 *Synthesis and characterisation of novel rotaxanes containing alkyl-functionalised axles with flexible linkages*

Having successfully prepared two new axle components, the synthesis of the related rotaxane species was attempted (Scheme 5.17).



*Scheme 5.17. Synthesis of alkyl-linkage-containing rotaxanes **155·A** and **156·A**.*

Axle component **150·Cl** and bis-vinyl-appended macrocycle precursor **99** were dissolved in anhydrous dichloromethane, Grubbs' second generation catalyst (10% by weight) was added and the solution stirred at room temperature for seven days. Following purification by repeated preparative thin layer chromatography, the target rotaxane host system **155·Cl** was isolated in 26% yield. Anion exchange to the non-coordinating hexafluorophosphate salt **155·PF$_6$** was achieved in quantitative yield. Analogous reaction conditions were employed in the preparation of control rotaxane **156·PF$_6$** in 25% yield over two steps.

The two new rotaxanes were characterised by ^{1}H, ^{13}C, ^{1}H–^{1}H COSY and ^{1}H–^{1}H ROESY NMR spectroscopy and electrospray mass spectrometry. The ^{1}H NMR spectrum of rotaxane

155·Cl together with those of component axle and macrocycle precursor for comparison are shown in Figure 5.16.

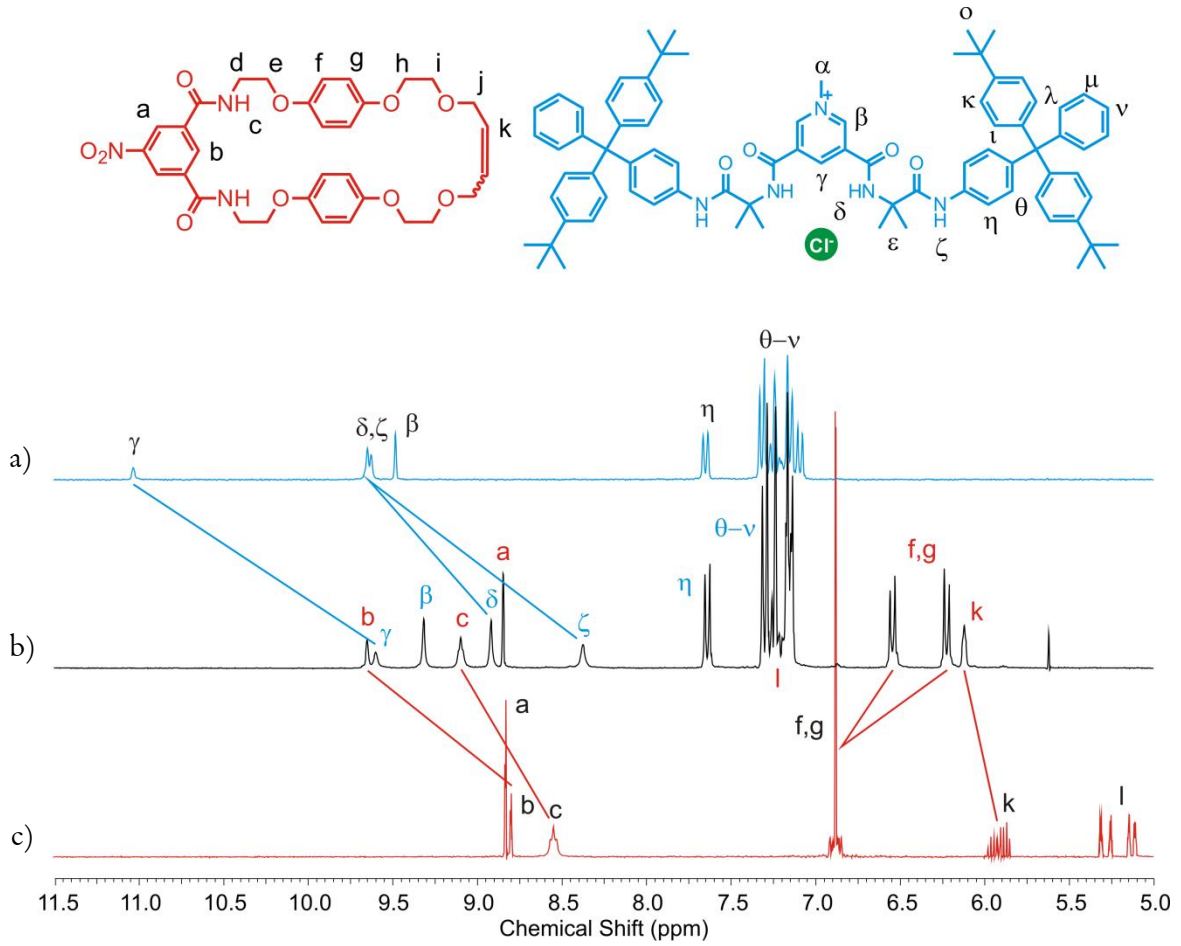


*Figure 5.16. ^{1}H NMR spectra of a) pyridinium chloride axle **150·Cl**, b) [2]rotaxane **155·Cl**, c) macrocycle precursor **99**. (500 MHz, CD_2Cl_2, 293 K).*

A number of typical, diagnostic features are apparent in the rotaxane ^{1}H NMR spectrum. Importantly the disappearance of the multiplet *l*, and the convergence of the vinylic protons multiplet *k* in to a pseudo-singlet demonstrate that the Grubbs'-catalysed RCM clipping reaction of the acyclic precursor was successful. Most notably, the upfield shift and splitting of the signal corresponding to the macrocycle hydroquinone protons *f*,*g* is indicative of aromatic donor–acceptor interactions, consistent with the interpenetration of the axle through the macrocycle. Furthermore, upfield shifts of the pyridinium axle cavity proton *γ* and amide protons *δ* and *ζ* together with concomitant downfield shifts in macrocycle cavity proton *b* and amide protons *c* are all characteristic perturbations arising from the

coordination of the templating chloride anion by the macrocycle isophthalamide group through hydrogen-bonding interactions.

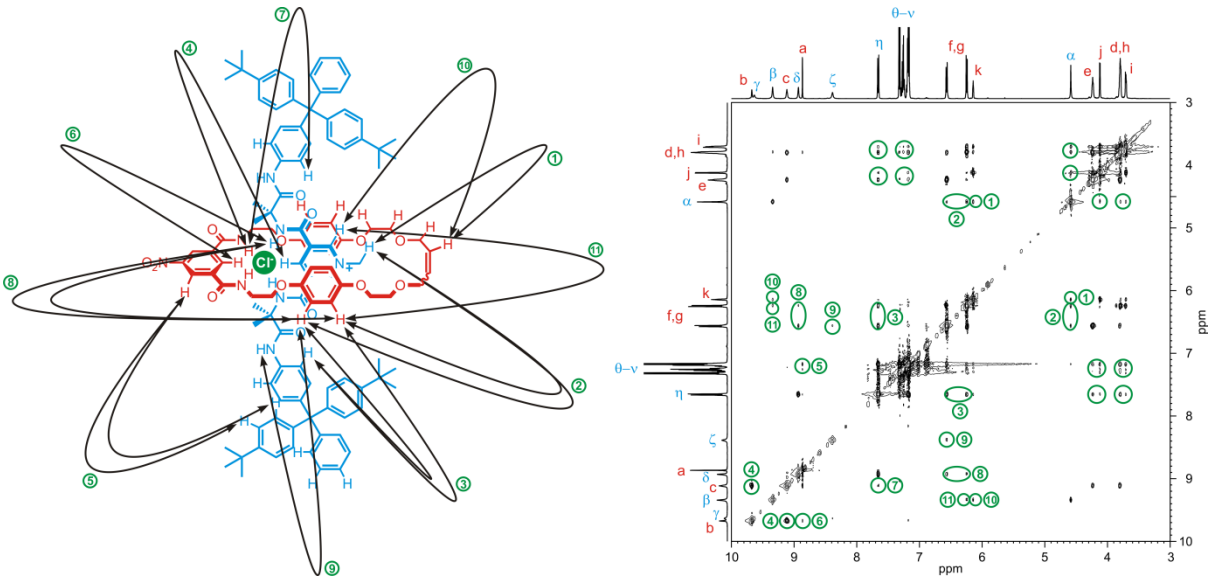


*Figure 5.17. ^{1}H–^{1}H ROESY spectrum of rotaxane **155·Cl**. Assignable inter-component through-space interactions are highlighted (500 MHz, acetone-d_6, 293 K).*

Evidence of the interlocked nature of rotaxane **155·Cl** is compounded by the two-dimensional ^{1}H–^{1}H ROESY NMR spectrum shown in Figure 5.17. Multiple through-space cross-coupling interactions between the two independent, mechanically bonded components confirm the rotaxane is indeed interlocked and in the conformation postulated. In particular, interactions **2** (*f*,*g* → *α*), **8** (*f*,*g* → *δ*), and **11** (*g* → *β*) reveal the macrocycle hydroquinone groups are close to the axle pyridinium unit, whilst interactions **3** (*f*,*g* → *η*) and **9** (*f* → *ζ*) show the hydroquinones are proximal to the stopper groups. The threaded nature of the rotaxane is also highlighted by interactions **5** (*a* → *λ*–*ρ*) and **7** (*c* → *η*). The alkene group, formed in the macrocyclisation reaction, is revealed to be near to the pyridinium methyl and *ortho*-pyridinium protons by interactions **1** (*k* → *α*) and **10** (*k* → *β*). Finally, interactions **4** (*c* → *γ*) and **6** (*b* → *δ*) confirm the protons of both the macrocycle and axle bis-amide anion recognition groups converge into the interlocked binding domain as they hydrogen-bond to the chloride anion guest.

Similar features were observed for rotaxane **156·Cl** in both the one-dimensional two-dimensional ^{1}H NMR spectra (see Experimental and Appendices).

5.3.2.4 Anion recognition properties of novel rotaxanes

The anion recognition properties of both rotaxanes were investigated using ^{1}H NMR spectroscopic titration experiments in 1:1 chloroform-d:methanol-d_4 solvent mixture. Addition of various anions to solutions of the rotaxanes induced downfield shifts in the signals corresponding to the macrocycle cavity proton *b*, and *ortho*- and *para*-pyridinium axle protons *β* and *γ*. Monitoring the chemical shift perturbations of the macrocycle cavity proton *b* (since this is the only proton to give well-fitted data with low errors for all three anions) as a function of anion concentration gave the titration curves shown in Figure 5.18 and winEQNMR analysis of these titration data gave the association constants reported in Table 5.5.

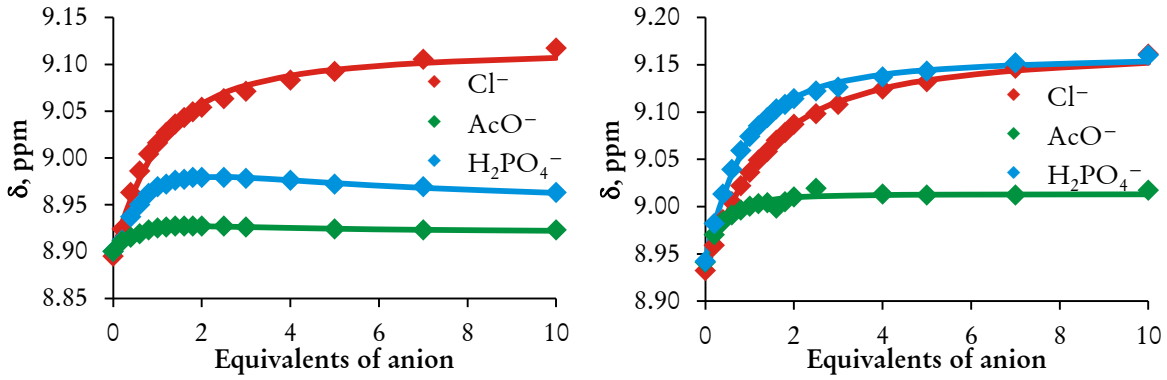


*Figure 5.18. Titration curves for addition of various anions to a) rotaxane **155·PF$_6$** and b) rotaxane **156·PF$_6$** obtained by following the macrocycle cavity proton* b. *1:1 $CDCl_3$:CD_3OD, 293 K. Square data points represent experimental data; continuous lines represent theoretical binding isotherms.*

*Table 5.5. Association constants, K_a (M^{-1}), for addition of various anions to rotaxanes **155·PF$_6$** and **156·PF$_6$**.*

Anion	**155·PF$_6$** K_a (M^{-1})[a]	**156·PF$_6$** K_a (M^{-1})[a]
Cl^-	762(90)	524(9)
AcO^-	K_1 = 579(51) K_2 = 24(3)	K_1 = 1120(10) K_2 = 24(13)
$H_2PO_4^-$	K_1 = 340(67) K_2 = 38(2)	1117(83)

[a]*All anions added as their TBA salt. Association constants were determined by monitoring the downfield shift of the macrocycle cavity proton* b. *Estimated standard errors are given in parentheses. 1:1 $CDCl_3$:CD_3OD, 293 K.*

The methyl-functionalised axle-containing rotaxane **155·PF$_6$** displays a chloride binding affinity which is greater than for acetate or dihydrogen phosphate: K_a = 762 M^{-1} (chloride); 579 M^{-1} (acetate); 340 M^{-1} (dihydrogen phosphate). This implies the shielded binding domain is more suitably sized and shaped for the spherical halide anion than for the more basic oxoanions. In contrast, the control rotaxane, without the integrated axle-methyl groups, **156·PF$_6$** binds both acetate and dihydrogen phosphate oxoanions preferentially over chloride with similar strength of association (K_a = 1120 M^{-1}). Importantly, this observation suggests the axle methyl groups are crucial in achieving chloride anion selectivity. Furthermore, chloride complexation is stronger with rotaxane **155·PF$_6$** than with control rotaxane **156·PF$_6$** (K_a = 762 M^{-1} *versus* K_a = 524 M^{-1}) which indicates the additional methyl functionality is important, not only for achieving preferential halide anion recognition, but also for enhancing chloride guest affinity.

5.4 Conclusions

Following much synthetic effort, four novel [2]rotaxane architectures have been successfully prepared and characterised using one-dimensional and two-dimensional ^{1}H NMR spectroscopy, and electrospray mass spectrometry. The anion binding properties of these systems were probed using ^{1}H NMR spectroscopic titrations.

The rotaxane species incorporating a tetra-methyl-functionalised macrocycle component **130·PF$_6$** displayed a preference for chloride over more basic acetate and dihydrogen phosphate suggesting the interlocked binding cavity is of complementary size for the smaller, spherical halide anion. However, this rotaxane was found to be a weaker anion complexant than the equivalent, unfunctionalised rotaxane reported in the literature **131·PF$_6$**, which may be a result of the additional methyl groups sterically hindering the ability of the anionic guests to penetrate the interlocked binding cavity.

The tetra-methyl-functionalised axle component **136·PF$_6$** showed a promising increase in chloride binding affinity over the non-functionalised analogue. When incorporated into the rotaxane species, however, the anion binding affinities displayed by the interlocked host **137·PF$_6$** were substantially lower than the original rotaxane (**138·PF$_6$**). The small chemical shift perturbations occurring upon addition of chloride were too small to allow accurate determination of an association constant value. This suggests that the additional methyl groups prevent the chloride anionic guest from accessing the binding cavity, whereas oxoanions acetate and dihydrogen phosphate are still able to bind on the periphery of the rotaxane.

Finally, two flexible rotaxane molecules were prepared with a view to enabling anions to access the binding cleft more efficiently. A comparison of their anion binding properties revealed that additional methyl groups served to improve the chloride affinity of this type of rotaxane as well as bestow a degree of halide anion selectivity to the methyl-functionalised structure. Moreover, the unfunctionalised rotaxane **156·PF$_6$** is the first interlocked rotaxane host system to display a preference for oxoanions over chloride guest species.

5.5 References for Chapter Five

[1] M. R. Sambrook, P. D. Beer, J. A. Wisner, R. L. Paul and A. R. Cowley, *J. Am. Chem. Soc.*, 2004, **126**, 15364-15365.
[2] M. R. Sambrook, P. D. Beer, M. D. Lankshear, R. F. Ludlow and J. A. Wisner, *Org. Biomol. Chem.*, 2006, **4**, 1529-1538.
[3] J. A. Wisner, P. D. Beer, M. G. B. Drew and M. R. Sambrook, *J. Am. Chem. Soc.*, 2002, **124**, 12469-12476.

[4] H. W. Gibson, S. H. Lee, P. T. Engen, P. Lecavalier, J. Sze, Y. X. Shen and M. Bheda, *J. Org. Chem.*, 1993, **58**, 3748-3756.
[5] L. M. Hancock, L. C. Gilday, N. L. Kilah, C. J. Serpell and P. D. Beer, *Chem. Commun.*, 2011, **47**, 1725-1727.
[6] A. Charette, A. Gagnon, M. Janes and C. Mellon, *Tetrahedron Lett.*, 1998, **39**, 5147-5150.
[7] L. M. Hancock, L. C. Gilday, S. Carvalho, P. J. Costa, V. Felix, C. J. Serpell, N. L. Kilah and P. D. Beer, *Chem. Eur. J.*, 2010, **16**, 13082-13094.

Chapter Six

Chapter 6 Experimental

6.1 General remarks

6.1.1 Reactants, reagents and solvents

Commercially available reagents and solvents were used without further purification unless otherwise stated. Where anhydrous solvents were used, they were purged with nitrogen, passed through a MBraun MPSP-800 column and then used immediately. Et_3N was distilled from and stored over KOH. H_2O was de-ionised and microfiltered using a Milli-Q® Millipore machine. TBA salts, Grubbs' II catalyst, $[Cu(MeCN)_4]PF_6$, TBTA, $AgPF_6$ were stored in a vacuum dessicator prior to use. $[TBA]_2[SO_4]$ was purchased from Sigma-Aldrich as a 50% aqueous solution, which was concentrated on a rotary evaporator and subsequently dehydrated by azeotroping with toluene and then drying over P_2O_5 in a vacuum desiccator and $TBAF{\cdot}3H_2O$ was used immediately after purchase from Sigma-Aldrich. Column chromatography was performed on silica gel (particle size: 40–63 μm), preparative TLC was performed on 20 × 20 cm plates, with a silica layer of thickness 1 mm. Pyrrole was distilled over CaH_2 under reduced pressure and stored at −25 °C under N_2. Amberlite® was 'loaded' by washing the resin with 10% $NaOH_{(aq)}$, H_2O, either 1 M NH_4Cl or 0.1 M NH_4PF_6, H_2O and finally the solvent to be used in the anion exchange.

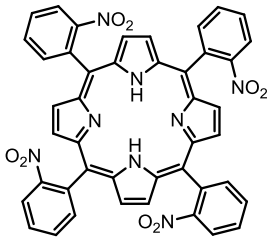
6.1.2 Instrumental methods

Routine NMR spectra were recorded on a Varian Mercury-*vx* 300 spectrometer (with ^1H NMR operating at 300 MHz, ^{13}C at 75.5 MHz, ^{19}F at 282.4 MHz, ^{31}P at 121.6 MHz) or Varian Unity Plus or Bruker Avance III 500 instruments (with ^1H NMR operating at 500 MHz, ^{13}C at 125.8 MHz, ^{19}F at 470.6 MHz, ^{31}P at 202.4 MHz). Mass spectra were obtained using a Micromass LCT Premier XE spectrometer and accurate masses were obtained to four decimal places using a Bruker MicroTOF spectrometer. Reactions carried

out under microwave irradiation used a Biotage Initiator 2.0 Microwave. Where specified, reaction mixtures and samples were sonicated using a bath sonicator.

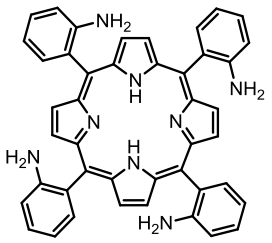
6.2 Experimental procedures for Chapter Two

5,10,15,20-Tetrakis(2-nitrophenyl)porphyrin 1[1]



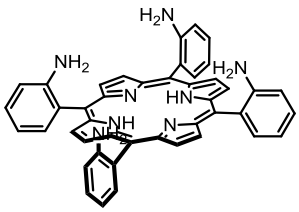
2-Nitrobenzaldehyde (15.0 g, 100 mmol) was dissolved in glacial acetic acid (250 mL) in a 1 L round-bottomed flask. A yellow solution formed which was heated with stirring under N_2 to 115 °C. Freshly distilled pyrrole (8.00 mL, 115 mmol) was added dropwise and the resulting dark mixture was heated at 115 °C for 30 min. The reaction mixture was cooled in an ice bath to 40 °C, during which time $CHCl_3$ (50 mL) was added to prevent coagulation. The mixture was filtered under suction and the precipitate was washed with $CHCl_3$ until the washings were essentially colourless. After drying *in vacuo* for several hours the product was obtained as a purple powder in 12% yield (2.33 g, 2.93 mmol). **^{1}H NMR** (500 MHz, DMSO-d_6) δ (ppm): 8.77 (8H, s, *β*-pyrrole-*H*), 8.16–8.66 (16H, m, *meso*-phenyl-*H*), −2.84 (2H, br s, pyrrole-N*H*); **ESIMS** *m/z*: 817.2 ($[M+Na]^+$, $C_{44}H_{26}N_8NaO_8$ requires 817.2); **UV/Vis** $\lambda_{max}(CHCl_3)$/nm: 421 (ε/M^{-1} cm^{-1} 61 420), 516 (5580), 549 (1900), 592 (1860), 650 (960).

5,10,15,20-Tetrakis(2-aminophenyl)porphyrin 2[2]



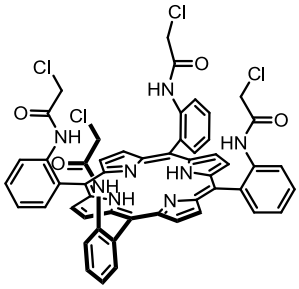
Compound 1 (4.00 g, 5.04 mmol) was dissolved in conc. $HCl_{(aq)}$ (200 mL) in a 1 L round-bottomed flask. A green solution formed, to which a solution of $SnCl_2$ (12.1 g, 64.0 mmol) in conc. $HCl_{(aq)}$ (10 mL) was added. The solution was stirred for 90 min, then heated to 65 °C and stirred under N_2 for a further 25 min. After cooling to rt using an ice bath, the green reaction mixture was cautiously basified using conc. NH_4OH until the solution turned purple (pH > 10). $CHCl_3$ (200 mL) was added and the mixture stirred vigorously for 16 h. The organic layer was separated, H_2O (200 mL) was added to the aqueous layer and this was extracted with $CHCl_3$ (3 × 100 mL). The combined organic layers were washed with H_2O (250 mL containing conc. NH_4OH (10 mL)), dried over anhydrous $MgSO_4$, filtered, and concentrated to ~80 mL *in vacuo*. EtOH (60 mL containing conc. NH_4OH (4 mL)) was added and the volume of the solution reduced to ~70 mL *in vacuo*. EtOH (40 mL) was added and the solution concentrated to ~20 mL *in vacuo*. The mixture was filtered and the purple precipitate washed with EtOH (5 × 10 mL). Compound 2 was isolated in 85% yield as a purple solid (2.90 g, 4.29 mmol). **^{1}H NMR** (300 MHz, $CDCl_3$) δ (ppm): 8.91 (8H, s, *β*-pyrrole-*H*), 7.83–7.90 (4H, m, *meso*-phenyl-*H*), 7.61 (4H, t, ^3J = 7.7 Hz, *meso*-phenyl-*H*), 7.12–7.20 (8H, m, *meso*-phenyl-*H*), 3.55 (8H, d, ^2J = 10.4 Hz, NH_2), −2.68 (2H, br s, pyrrole-N*H*); **ESIMS** *m*/*z*: 675.3 ($[M+H]^+$, $C_{44}H_{35}N_8$ requires 675.3); **UV/Vis** $\lambda_{max}(CHCl_3)$/nm: 420 (ε/M^{-1} cm^{-1} 183 103), 516 (18 140), 549 (5020), 589 (5760), 645 (2080).

α,α,α,α-Tetrakis(2-aminophenyl)porphyrin 2[3]



Silica gel (36.0 g) and toluene (85 mL) were heated in a 250 mL round-bottomed flask to 75 °C and stirred under N_2 for 2 h. Compound 2 (1.00 g, 1.48 mmol) was added and the resulting dark mixture stirred under N_2 at 75 °C for 22 h. The reaction mixture was cooled to rt and the dark slurry poured into a chromatography column. The undesired atropisomers were eluted with 1:1 toluene:Et_2O until the eluent turned a pale red colour and no undesired isomers were observed by TLC. The desired atropisomer was then eluted with 1:1 acetone:Et_2O. The solvents were removed *in vacuo* to give ***α,α,α,α*-2** as a purple powder in 71% yield (712 mg, 1.06 mmol). **^{1}H NMR** (300 MHz, $CDCl_3$) δ (ppm): 8.91 (8H, s, *β*-pyrrole-*H*), 7.87 (4H, d, ^3J = 7.8 Hz, *meso*-phenyl-*H*), 7.62 (4H, t, ^3J = 7.8 Hz, *meso*-phenyl-*H*), 7.18 (4H, t, ^3J = 7.8 Hz, *meso*-phenyl-*H*), 7.13 (4H, d, ^3J = 7.8 Hz, *meso*-phenyl-*H*), 3.54 (8H, s, N*H*$_2$), −2.69 (2H, pyrrole-N*H*); **ESIMS** *m/z*: 675.3 ($[M+H]^+$, $C_{44}H_{35}N_8$ requires 675.3); **UV/Vis** $\lambda_{max}(CHCl_3)$/nm: 419 (ε/M^{-1} cm^{-1} 175 000), 515 (18 980), 549 (5120), 589 (5940), 645 (2240).

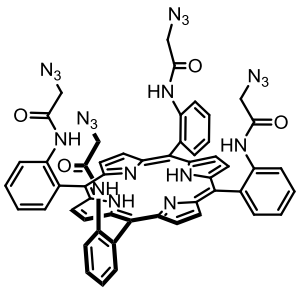
α,α,α,α-Tetrakis(2-chloroacetamidophenyl)porphyrin 3[4]



Compound ***α,α,α,α*-2** (600 mg, 0.9 mmol) and Et_3N (0.75 mL, 5.4 mmol) were dissolved in anhydrous THF and cooled to 0 °C in an ice bath to which a solution of chloroacetyl chloride (0.36 mL, 4.5 mmol) in anhydrous THF was added dropwise. The reaction mixture was

stirred under N_2 for 3 h and the solvent was then removed *in vacuo*. The crude mixture was purified by column chromatography (SiO_2, 95:5 CH_2Cl_2:MeOH) to give compound 3 as purple powder in 72% yield (0.63 g, 0.65 mmol). **^{1}H NMR** (500 MHz, $CDCl_3$) δ (ppm): 8.80 (8H, s, *β*-pyrrole-*H*), 8.73 (4H, d, ^3J = 8.0 Hz, *meso*-phenyl-*H*), 8.08 (4H, d, ^3J = 8.0 Hz, *meso*-phenyl-*H*), 7.99 (4H, s, amide-N*H*), 7.89 (4H, t, ^3J = 8.0 Hz, *meso*-phenyl-*H*), 7.61 (4H, t, ^3J = 8.0 Hz, *meso*-phenyl-*H*), 3.39 (8H, s, CH_2), −2.66 (2H, br s, pyrrole-N*H*); **ESIMS** *m/z*: 1003.2 ([M+Na]$^+$, $C_{52}H_{38}Cl_4N_8NaO_4$ requires 1003.2); **UV/Vis** λ_{max}($CHCl_3$)/nm: 418 (ε/M^{-1} cm^{-1} 491 860), 514 (24 580), 546 (5220), 588 (7664), 643 (1634).

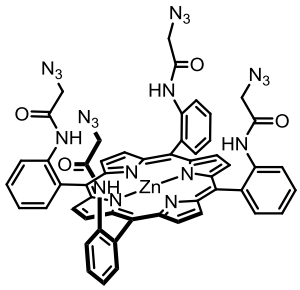
α,α,α,α-Tetrakis(2-azidoacetamidophenyl)porphyrin 4



Compound 3 (500 mg, 0.5 mmol) was dissolved in a 0.5 M solution of NaN_3 in DMSO (10 mL) and the solution was stirred for 16 h. The reaction was cooled in an ice bath to 0 °C and quenched with H_2O (45 mL). The aqueous layer was extracted with $CHCl_3$ (3 × 50 mL). The combined organic extracts were washed with H_2O (2 × 100 mL) and sat. $NaCl_{(aq)}$ (100 mL), dried over anhydrous $MgSO_4$, filtered, and the solvent removed *in vacuo* to give 4 as a purple powder in 61% yield (313 mg, 0.311 mmol). **^{1}H NMR** (300 MHz, $CDCl_3$) δ (ppm): 8.82 (8H, s, *β*-pyrrole-*H*), 8.59 (4H, d, ^3J = 8.0 Hz, *meso*-phenyl-*H*), 7.96 (4H, d, ^3J = 8.0 Hz, *meso*-phenyl-*H*), 7.87 (4H, t, ^3J = 8.0 Hz, *meso*-phenyl-*H*), 7.79 (4H, s, amide-N*H*) 7.56 (4H, t, ^3J = 8.0 Hz, *meso*-phenyl-*H*), 3.31 (8H, s, CH_2), −2.58 (2H, br s, pyrrole-N*H*); **^{13}C NMR** (75.5 MHz, $CDCl_3$) δ (ppm): 164.6, 137.4, 134.9, 131.4, 130.0, 123.8, 121.1, 114.6, 52.5, 40.9; **ESIMS** *m/z*: 1029.3277 ([M+Na]$^+$, $C_{52}H_{38}N_{20}NaO_4$ requires 1029.3301);

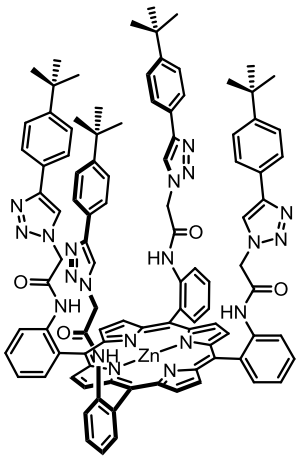
UV/Vis $\lambda_{max}(CHCl_3)$/nm: 420 (ε/M^{-1} cm^{-1} 408 000), 515 (24 240), 547 (6180), 589 (8008), 645 (2500).

α,α,α,α-Tetrakis(2-azidoacetamidophenyl)-zinc(II)-porphyrin 5



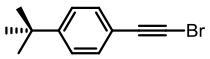
Compound 4 (502 mg, 0.499 mmol) was dissolved in 9:1 CH_2Cl_2:MeOH (100 mL), $Zn(OAc)_2{\cdot}2H_2O$ (1.10 g, 5.50 mmol) was added and the reaction was stirred for 16 h. The solvents were removed *in vacuo* and the resulting dark pink residue redissolved in CH_2Cl_2 (100 mL), washed with H_2O (5 × 100 mL) and sat. $NaCl_{(aq)}$ (100 mL), dried over anhydrous $MgSO_4$, filtered, and the solvent removed *in vacuo* giving compound 5 as a bright purple solid in 74% yield (397 mg, 0.371 mmol). **^{1}H NMR** (300 Hz, $CDCl_3$) δ (ppm): 8.83 (8H, s, *β*-pyrrole-*H*), 8.65 (4H, d, ^3J = 7.7 Hz, *meso*-phenyl-*H*), 7.99 (4H, d, ^3J = 7.7 Hz, *meso*-phenyl-*H*), 7.84 (4H, t, ^3J = 7.7 Hz, *meso*-phenyl-*H*), 7.74 (4H, s, amide-N*H*), 7.55 (4H, t, ^3J = 7.7 Hz, *meso*-phenyl-*H*), 3.16 (8H, s, CH_2); **^{13}C NMR** (75.5 MHz, CDCl3) δ (ppm): 164.1, 150.6, 137.5, 134.5, 132.4, 132.4(*sic*), 132.2, 129.7, 123.6, 120.5, 115.1, 52.6; **ESIMS** *m*/*z*: 1091.2408 ($[M+Na]^+$, $C_{52}H_{36}N_{20}NaO_4Zn$ requires 1091.2412); **UV/Vis** $\lambda_{max}(CHCl_3)$/nm: 425 (ε/M^{-1} cm^{-1} 726 040), 555 (28 440), 592 (3466).

Tetra-triazole-zinc(II)-porphyrin 6



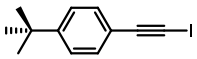
Compound 5 (100 mg, 90 μmol) and 4-*tert*-butylphenylacetylene (76 μL, 66.0 mg, 0.42 mmol) were dissolved in anhydrous CH_2Cl_2. $[Cu(MeCN)_4]PF_6$ (13.4 mg, 36.0 μmol) and TBTA (21.2 mg, 40.0 μmol) were dissolved in anhydrous CH_2Cl_2 and added to the first solution. D*i*PEA (73 μL, 54 mg, 0.42 mmol) was injected dropwise and the reaction stirred for 5 days in the dark under N_2. The solvent was removed *in vacuo* and the crude product purified by column chromatography (SiO_2, 97:3 CH_2Cl_2:MeOH) to give compound 6 as a purple crystalline solid in 80% yield (0.13 g, 72 mmol). **^{1}H NMR** (500 MHz, $CDCl_3$) δ (ppm): 8.70 (8H, s, *β*-pyrrole-*H*), 8.42 (4H, s, amide-N*H*), 8.27 (4H, d, ^3J = 7.8 Hz, *meso*-phenyl-*H*), 8.17 (4H, d, ^3J = 7.8 Hz, *meso*-phenyl-*H*), 7.83 (4H, t, ^3J = 7.8 Hz, *meso*-phenyl-*H*), 7.61 (4H, t, ^3J = 7.8 Hz, *meso*-phenyl-*H*), 7.25 (4H, s, triazole-*H*), 7.17 (8H, d, ^3J = 8.6 Hz, phenyl-*H*), 7.07 (8H, d, ^3J = 8.6 Hz, phenyl-*H*), 3.93 (8H, s, CH_2), 1.21 (36H, s, CH_3); **^{13}C NMR** (125.5 MHz, $CDCl_3$) δ (ppm): 163.1, 151.6, 150.4, 147.4, 137.8, 134.4, 131.7, 128.9, 128.7, 126.3, 125.5, 125.4, 124.3, 121.1, 114.8, 52.7, 34.6, 31.2; **ESIMS** *m/z*: 1725.6824 ($[M+Na]^+$, $C_{100}H_{92}N_{20}NaO_4Zn$ requires 1725.6853); **UV/Vis** $\lambda_{max}(CHCl_3)$/nm: 427 (ε/M^{-1} cm^{-1} 511 000), 557 (22 500) and 597 (4500).

1-(Bromoethynyl)-4-(*tert*-butyl)benzene 7[5]



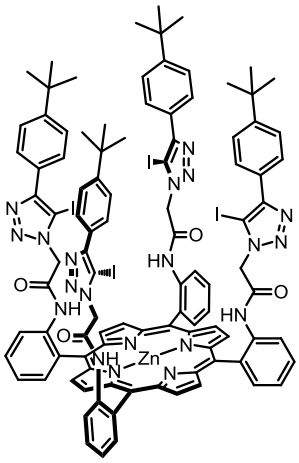
1-*Tert*-butyl-4-ethynyl benzene (0.40 mL, 350 mg, 2.2 mmol) was dissolved in acetone (8 mL). *N*-bromosuccinimide was added (790 mg, 4.4 mmol) followed by $AgNO_3$ (49 mg, cat.) and the reaction mixture was stirred under N_2 at rt in the dark for 4 h. The resulting yellow mixture was filtered through a plug of silica which was subsequently washed with hexanes (5 × 50 mL). The filtrate was collected and the solvent removed *in vacuo* to give compound 7 as an orange solid in 99% yield (520 mg, 2.2 mmol). **^{1}H NMR** (300 MHz, C_6D_6) δ (ppm): 7.33 (2H, d, ^3J = 8.6 Hz, phenyl-*H*), 7.01 (2H, d, ^3J = 8.6 Hz, phenyl-*H*), 1.07 (9H, s CH_3).

1-(Iodoethynyl)-4-(*tert*-butyl)benzene 9[6]



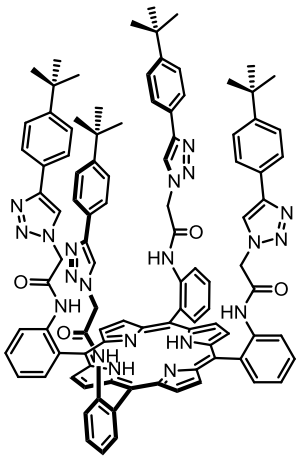
1-*Tert*-butyl-4-ethynyl benzene (1.00 mL, 878 mg 5.55 mmol) was dissolved in acetone (15 mL), *N*-iodosuccinimide (2.50 g, 11.1 mmol) was added followed by $AgNO_3$ (123 mg, cat.) and the reaction mixture stirred under N_2 at rt in the dark for 2 h. The resulting yellow suspension was filtered through a plug of silica which was subsequently washed with hexanes (5 × 50 mL). The pale pink filtrate was collected and the solvent removed *in vacuo* to give compound 9 as a yellow solid in 42% yield (0.67 g, 2.3 mmol). **^{1}H NMR** (300 MHz, C_6D_6) δ (ppm): 7.33 (2H, d, ^3J = 8.6 Hz, phenyl-*H*), 7.00 (2H, d, ^3J = 8.6 Hz, phenyl-*H*), 1.06 (9H, s, CH_3).

Tetra-iodotriazole-zinc(II)-porphyrin 10



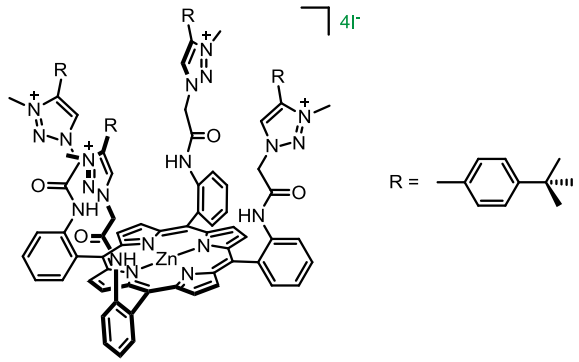
CuI (107 mg, 0.562 mmol) and Et_3N (1.56 mL, 11.2 mmol) were added to anhydrous THF (20 mL) and stirred under N_2 at rt for 20 min. Compound 5 (120 mg, 0.14 mmol) and compound 9 (153 mg, 0.538 mmol) were dissolved in anhydrous THF (20 mL) and added to the first solution. The reaction mixture was stirred under N_2 at rt in the dark for 3 days after which time it was quenched with 10% $NH_4OH_{(aq)}$ solution and the THF was removed *in vacuo*. H_2O (100 mL) was added, the aqueous layer extracted with CH_2Cl_2 (3 × 100 mL) and the combined organics dried over anhydrous $MgSO_4$, filtered, and the solvent removed *in vacuo*. The crude residue was purified by column chromatography (SiO_2, 95:5 CH_2Cl_2:acetone) to give compound **10** as a purple solid in 46% yield (228 mg, 0.103 mmol). **^{1}H NMR** (300 MHz, $CDCl_3$) δ (ppm): 8.75 (8H, s, *β*-pyrrole-*H*), 8.21 (4H, d, ^3J = 8.5 Hz, *meso*-phenyl-*H*), 8.18 (4H, d, ^3J = 8.5 Hz, *meso*-phenyl-*H*), 8.10 (4H, s, amide-N*H*), 7.85 (4H, t, ^3J = 7.5 Hz, *meso*-phenyl-*H*), 7.63 (4H, t, ^3J = 7.5 Hz, *meso*-phenyl-*H*), 7.16 (16H, s, phenyl-*H*), 3.99 (8H, s, CH_2), 1.25 (16H, s, CH_3); **^{13}C NMR** (125.5 MHz, $CDCl_3$) δ (ppm): 162.4, 151.9, 150.4, 149.3, 137.6, 135.6, 134.4, 131.8, 128.9, 126.7, 125.7, 125.3, 124.4, 123.5, 114.9, 78.2, 53.8, 53.1, 34.6, 31.3, 31.2, 29.2, 27.8; **ESIMS** *m/z*: 2227.2660 ($[M+Na]^+$, $C_{100}H_{88}I_4N_{20}NaO_4Zn$ requires 2227.2661); **UV/Vis** $\lambda_{max}(CHCl_3)$/nm: 429 (ε/M^{-1} cm^{-1} 449 000), 559 (13 500), 595 (3530).

Tetra-triazole-porphyrin 11



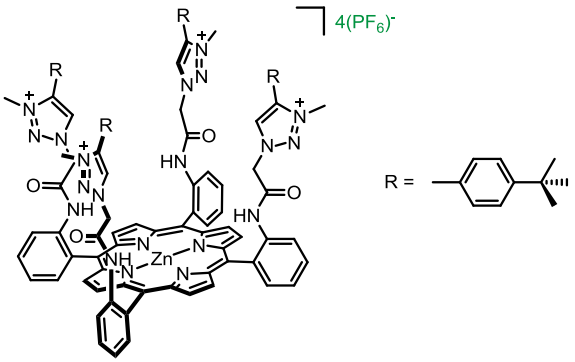
Compound 6 (50 mg, 30 μmol) was dissolved in CH_2Cl_2:TFA (9:1, 10 mL) and the resulting green reaction mixture was stirred at rt for 10 min. Sat. $NaHCO_{3(aq)}$was added until the solution turned purple. The organic phase was separated, washed with sat. $NaHCO_{3(aq)}$ (10 mL), H_2O (10 mL), dried over anhydrous $MgSO_4$, filtered, and the solvent removed *in vacuo*. Following purification using column chromatography (SiO_2, 99:1 CH_2Cl_2:MeOH) compound **11** was isolated as a purple solid in 97% yield (46.8 mg, 28.5 μmol). **^{1}H NMR** (300 MHz, $CDCl_3$) δ (ppm): 8.73 (8H, s, *β*-pyrrole-*H*), 8.35 (4H, d, ^3J = 8.2 Hz, *meso*-phenyl-*H*), 8.13 (4H, d, ^3J = 8.2 Hz *meso*-phenyl-*H*), 7.86 (4H, t, ^3J = 8.2 Hz, *meso*-phenyl-*H*), 7.62 (4H, t, ^3J = 8.2 Hz, *meso*-phenyl-*H*), 7.25 (4H, s, triazole-*H*), 7.15 (8H, d, ^3J = 7.5 Hz, phenyl-*H*), 7.01 (8H, d, ^3J = 7.5 Hz, phenyl-H), 3.83 (8H, s, CH_2), 1.29 (36H, s, CH_3); **^{13}C NMR** (500 MHz, $CDCl_3$) δ (ppm): 163.6, 151.4, 147.2, 137.8, 134.6, 134.2, 129.6, 127.0, 125.5, 124.3, 123.8, 120.9, 115.0, 53.4, 34.6, 31.2; **ESIMS** *m/z*: 1661.7681 ($[M+Na]^+$, $C_{100}H_{94}N_{20}NaO_4$ requires 1661.7659); **UV/vis** λ_{max}(DMSO)/nm: 425 (ε/M^{-1} cm^{-1} 415 120), 519 (15 772), 553 (5122), 593 (5098), 649 (2106).

Tetra-triazolium-zinc(II)-porphyrin iodide ***12·I$_4$***



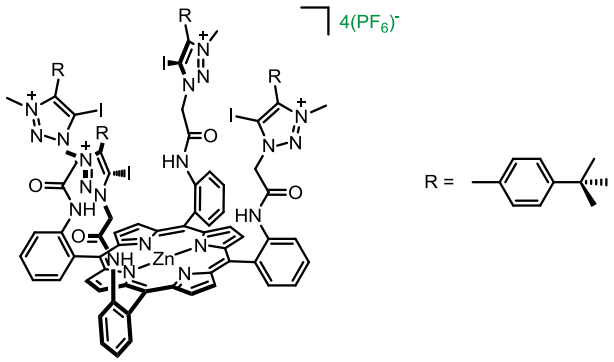
Compound 6 (50 mg, 30 μmol) was suspended in MeI (10 mL) and heated at 40 °C for 7 days. After this time the MeI was removed *in vacuo* and the crude residue purified by preparative thin layer chromatography (SiO_2, 9:1 CH_2Cl_2:MeOH) to give **12·I$_4$** in 82% yield (43.2 mg, 19.0 μmol). **^{1}H NMR** (300 MHz, $CDCl_3$) δ (ppm): 8.92 (4H, s, amide-N*H*), 8.83 (8H, s, *β*-pyrrole-*H*), 8.38 (4H, s, triazole-*H*), 8.28 (4H, d, ^3J = 7.8 Hz, *meso*-phenyl-*H*), 8.24 (4H, d, ^3J = 7.8 Hz, *meso*-phenyl-*H*), 7.77 (4H, t, ^3J = 7.8 Hz, *meso*-phenyl-*H*), 7.60 (4H, t, ^3J = 7.8 Hz, *meso*-phenyl-*H*), 7.48 (8H, d, ^3J = 8.8 Hz, phenyl-*H*), 7.40 (8H, d, ^3J = 8.8 Hz, phenyl-*H*), 4.68 (8H, s, CH_2), 4.07 (12H, s, NCH_3), 1.32 (36H, s, C(CH_3)$_3$); **^{13}C NMR** (75.5 MHz, $CDCl_3$) δ (ppm): 162.8, 155.0, 142.5, 138.3, 135.1, 134.8, 131.7, 129.8, 129.1, 128.6, 126.5, 123.8, 122.9, 119.2, 54.8, 54.0, 38.4, 35.0, 31.0; **ESIMS** *m/z*: Could not characterise by mass spectrometry; **UV/vis** λ_{max}($CHCl_3$)/nm: 429 (ε/M^{-1} cm^{-1} 751 360) (20 116), 596 (3114).

Tetra-triazolium-zinc(II)-porphyrin hexafluorophosphate **12·(PF$_6$)$_4$**



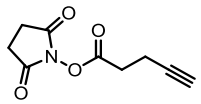
Compound **12·I$_4$** (20 mg, 8.9 μmol) was dissolved in CH_2Cl_2 (20 mL) and stirred vigorously with 0.1 M $NH_4PF_{6(aq)}$ (8 × 10 mL), H_2O, (2 × 10 mL). The solvent was removed and the crude residue dried *in vacuo* to give **12·(PF$_6$)$_4$** as a purple solid in 90% yield (18.5 mg, 7.90 μmol). **^{1}H NMR** (300 MHz, 9:1 $CDCl_3$:pyridine-d_5) δ (ppm): 8.74 (8H, s, *β*-pyrrole-H), 8.30 (4H, d, ^3J = 7.7 Hz, *meso*-phenyl-*H*), 8.10 (4H, d, ^3J = 7.7 Hz, *meso*-phenyl-*H*), 7.94 (8H, br s, triazole-*H* & amide-N*H*), 7.69 (4H, t, ^3J = 7.7 Hz, *meso*-phenyl-*H*), 7.50 (4H, t, ^3J = 7.7 Hz, *meso*-phenyl-*H*), 7.31 (8H, d, ^3J = 8.2 Hz, phenyl-*H*), 7.13 (4H, d, ^3J = 8.2 Hz, phenyl-*H*), 4.26 (8H, s, CH_2), 3.72 (12H, s, NCH_3), 1.16 (36H, s, C(CH_3)$_3$); **^{13}C NMR** (75.5 MHz, 9:1 $CDCl_3$:pyridine-d_5) δ (ppm): 161.4, 155.0, 150.0, 142.4, 137.4, 134.5, 131.7, 128.9, 128.8, 128.5, 126.3, 123.8, 118.4, 114.5, 77.2, 53.9, 37.8, 34.7, 30.7; **^{19}F NMR** (282.5 MHz, 9:1 $CDCl_3$:pyridine-d_5) δ (ppm): −73.3 (d, J = 725 Hz, PF_6); **^{31}P NMR** (121.5 MHz, 9:1 $CDCl_3$:pyridine-d_5) δ (ppm): −145.4 (sept, J = 725 Hz, PF$_6$); **ESIMS** *m/z*: 440.1938 ([M−4PF$_6$]$^{4+}$, $C_{104}H_{104}N_{20}O_4Zn$ requires 440.1955); **UV/vis** λ_{max}(DMSO)/nm: 439 (ε/M^{-1} cm^{-1} 478 950), 565 (17 378), 600 (4144).

Tetra-iodotriazolium-zinc(II)-porphyrin iodide **13·$(PF_6)_4$**



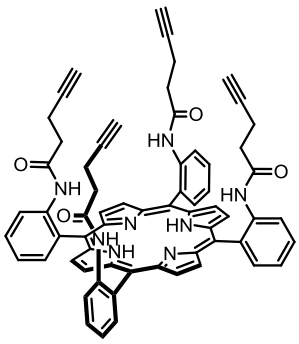
Compound **10** (100 mg, 50 μmol) was dissolved in anhydrous CH_2Cl_2 and $[Me_3O]BF_4$ (30.0 mg, 198 μmol) was added. The reaction mixture was stirred for 16 h after which time it was quenched with 1:1 Et_3N:CH_3OH (5 drops) and the solvents and Et_3N were removed *in vacuo*. The residue was redissolved in CH_2Cl_2 (20 mL) and washed with H_2O (2 × 20 mL), 0.1 M $NH_4PF_{6(aq)}$ (10 × 10 mL), H_2O (2 × 20 mL), dried over anhydrous $MgSO_4$, filtered and the solvent removed *in vacuo*. Following purification using preparative thin layer chromatography (SiO_2, EtOAc) **13·$(PF_6)_4$** was isolated as a purple solid in 15% yield (87.3 mg, 30.7 μmol). **^{1}H NMR** (300 MHz, $CDCl_3$) δ (ppm): 8.87 (8H, s, *β*-pyrrole-*H*), 8.41 (4H, br d, ^3J = 7.9 Hz, *meso*-phenyl-*H*), 8.11 (4H, br s, *meso*-phenyl-*H*), 7.96 (4H, br s, amide-N*H*), 7.82 (4H, t, ^3J = 7.9 Hz, *meso*-phenyl-*H*), 7.61 (4H, t, ^3J = 7.9 Hz, *meso*-phenyl-*H*), 7.42 (8H, br d, ^3J = 7.2 Hz, phenyl-*H*), 7.11 (8H, br s, phenyl-*H*), 4.53 (8H, s, CH_2), 3.91 (12H, s, NCH_3), 1.29 (36H, s, C(CH_3)$_3$); **^{13}C NMR** (125.5 MHz, CD_3OD) δ (ppm) 163.4, 156.9, 151.8, 148.2, 138.7, 137.5, 137.4, 133.1, 130.9, 130.3, 127.7, 125.9, 124.7, 121.0, 117.0, 92.7, 39.6, 36.0, 31.6, 31.5; **^{19}F NMR** (470.4 MHz, $CDCl_3$) δ (ppm): −73.6 (d, J = 720 Hz, PF_6); **^{31}P NMR** (202.4 MHz, $CDCl_3$) δ (ppm): −145.7 (sept, J = 720 Hz, PF_6); **ESIMS** *m/z*: 566.0921 ($[M-4PF_6]^{4+}$, $C_{104}H_{100}I_4N_{20}O_4Zn$ requires 566.0921); **UV/Vis** λ_{max}(DMSO)/nm: 437 (ε/M^{-1} cm^{-1} 543 300), 567 (20 650), 606 (6508).

2,5-Dioxopyrrolidin-1-yl pent-4-ynoate 14[7]



4-pentynoic acid (1.00 g, 10.2 mmol) and *N*-hydroxysuccinimide (1.18 g, 10.2 mmol) were dissolved in 1:1 EtOAc:dioxane (120 mL). After cooling to 0 °C, DCC (2.10 g, 10.2 mmol) was added and the reaction stirred under N_2 at rt for 5 h. The reaction mixture was then filtered and the solvent removed *in vacuo*. The residue was redissolved in EtOAc (200 mL), washed with 5% $NaHCO_{3(aq)}$ (2 × 200 mL), H_2O (200 mL), dried over anhydrous $MgSO_4$, filtered, and the solvent removed *in vacuo*. Recrystallisation from CH_2Cl_2/pentanes afforded compound **14** as a white solid in 42% yield (840 mg, 4.3 mmol). **^{1}H NMR** (300 MHz, $CDCl_3$) δ (ppm): 2.90 (2H, t, ^3J = 6.5 Hz, CH_2), 2.86 (4H, s, succinimide-CH_2), 2.60–2.66 (2H, m, CH_2), 2.06 (1H, t, ^4J = 2.5 Hz, alkyne-*H*).

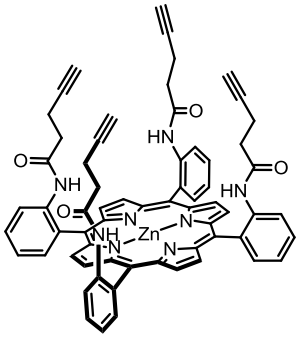
Tetra-alkyne-functionalised porphyrin 15



Compound ***α,α,α,α*-2** (278 mg, 0.412 mmol), 4-pentynoic acid (242 mg, 2.47 mmol), DCC (509 mg, 2.47 mmol) and 4-DMAP (5 mg, cat.) were dissolved in anhydrous CH_2Cl_2 (50 mL) and stirred under N_2 at rt for 16 h. The mixture was filtered and the solvent removed *in vacuo*. The crude residue was purified by column chromatography (SiO_2, 95:5 CH_2Cl_2:acetone) to give **15** as a purple solid in 56% yield (229 mg, 0.230 mmol). **^{1}H NMR** (300 MHz, $CHCl_3$) δ (ppm): 8.84 (8H, s, *β*-pyrrole-*H*), 8.73 (4H, d, ^3J = 8.1 Hz, *meso*-phenyl-*H*), 7.91 (4H, t, ^3J = 8.1 Hz, *meso*-phenyl-*H*), 7.85 (4H, d, ^3J = 8.1 Hz, *meso*-phenyl-*H*), 7.52 (4H, t, ^3J = 8.1 Hz, *meso*-phenyl-*H*), 7.10 (4H, s, amide-N*H*), 1.97 (8H, br t,

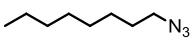
^3J = 6.5 Hz, CH_2), 1.67 (8H, br t, ^3J = 6.5 Hz, CH_2), 0.40 (4H, br s, alkyne-*H*), −2.75 (2H, s, pyrrole-N*H*); **^{13}C NMR** (75.5 MHz, $CDCl_3$) δ (pm): 169.0, 138.1, 135.0, 132.1, 130.8, 130.0, 123.3, 121.6, 115.2, 81.9, 68.8, 35.9, 29.2, 14.1**; ESIMS** *m/z*: 1017.3833 ($[M+Na]^+$, $C_{64}H_{50}N_8NaO_4$ requires 1017.3847); **UV/Vis** $\lambda_{max}(CHCl_3)$/nm: 420 (ε/M^{-1} cm^{-1} 807 480), 514 (21 120), 547 (4900), 587 (6788), 642 (1596).

Tetra-alkyne-functionalised zinc(II)-porphyrin 16



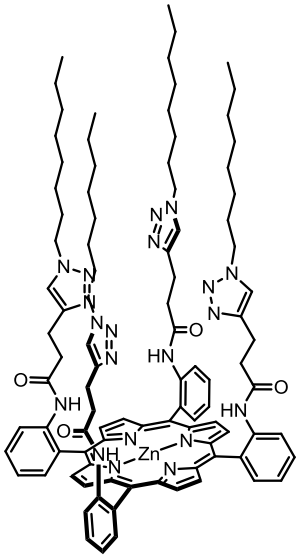
Compound **15** (200 mg, 0.2 mmol) was dissolved in 9:1 CH_2Cl_2:MeOH (10 mL) and $Zn(OAc)_2{\cdot}2H_2O$ (440 mg, 2.0 mmol) was added. The solution was stirred under N_2 at rt for 16 h. The solvent was removed *in vacuo*, the residue redissolved in CH_2Cl_2 and filtered through a plug of silica eluting with CH_2Cl_2. The solvent was removed *in vacuo* and compound **16** was isolated as a bright purple solid in 51% yield (107 mg, 0.101 mmol). **^{1}H NMR** (300 MHz, $CDCl_3$) δ (ppm): 8.84 (8H, s, *β*-pyrrole-*H*), 8.56 (4H, d, ^3J = 8.1 Hz, *meso*-phenyl-*H*), 7.86 (4H, d, ^3J = 8.1 Hz, *meso*-phenyl-*H*), 7.82 (4H, t, ^3J = 8.1 Hz, *meso*-phenyl-*H*), 7.48 (4H, t, ^3J = 8.1 Hz, *meso*-phenyl-*H*), 7.07 (4H, s, amide-N*H*), 1.83 (8H, br s, CH_2), 1.49 (8H, br s, CH_2), 0.50 (4H, s, alkyne-*H*); **^{13}C NMR** (75.5 MHz, $CDCl_3$) δ (ppm): 168.5, 150.2, 137.5, 134.7, 132.2, 129.4, 122.9, 120.8, 115.2, 81.5, 68.6, 35.2, 13.6; **ESIMS** *m/z*: 1079.2993 ($[M+Na]^+$, $C_{64}H_{50}N_8NaO_4Zn$ requires 1079.2982); **UV/Vis** $\lambda_{max}(CHCl_3)$/nm: 421 (ε/M^{-1} cm^{-1} 845 600), 555 (22 936), 592 (3068).

1-*n*-Octylazide 17[8]



1-*n*-Octylbromide (11.2 g, 57.9 mmol) was added to a solution of NaN_3 (4.13 g, 63.5 mmol) in DMSO (130 mL) and the reaction was stirred at rt under N_2 for 16 h. H_2O (250 mL) was added and the aqueous layer was extracted with Et_2O (3 × 150 mL). The combined organic phases were washed with H_2O (100 mL), sat. $NaCl_{(aq)}$ (100 mL), dried over anhydrous $MgSO_4$, filtered, and the solvent removed *in vacuo* to give compound **17** as a colourless oil in 70% yield (7.81 g, 50.3 mmol). **^{1}H NMR** (300 MHz, $CDCl_3$) δ (ppm): 3.26 (2H, t, ^3J = 7.0 Hz, NCH_2), 1.56–1.65 (2H, m, CH_2), 1.29 (10 H, s, CH_2), 0.89 (3H, t, ^3J = 7.0 Hz, CH_3).

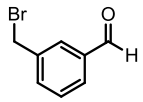
Compound 18



Compound **16** (30 mg, 28 μmol) and compound **17** (19.9 mg, 128 μmol) were dissolved in anhydrous CH_2Cl_2. $[Cu(MeCN)_4]PF_6$ (4.17 mg, 11.1 μmol), TBTA (6.53 mg, 12.3 μmol) and D*i*PEA (2.23 μL, 0.128 mmol) were added and the reaction mixture stirred under N_2 at rt in the dark for 3 days. The solvent was then removed *in vacuo* and the crude residue purified by preparative thin layer chromatography (SiO_2, 93:7 CH_2Cl_2:MeOH) to give compound **18** as a purple solid in 33% yield (15.8 mg, 9.42 μmol). **^{1}H NMR** (300 MHz, $CDCl_3$) δ (ppm):

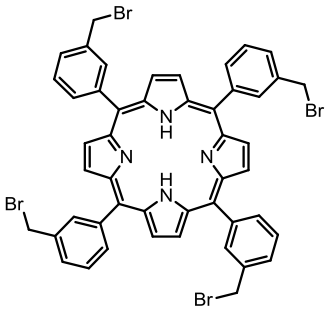
8.52 (8H, s, *β*-pyrrole-*H*), 8.43 (4H, d, ^3J = 8.0 Hz, *meso*-phenyl-*H*), 8.03 (4H, s, amide-N*H*), 7.95 (4H, d, ^3J = 8.0 Hz, *meso*-phenyl-*H*), 7.79 (4H, t, ^3J = 8.0 Hz, *meso*-phenyl-*H*), 7.48 (4H, t, ^3J = 8.0 Hz, *meso*-phenyl-*H*), 7.12 (4H, s, triazole-*H*), 4.04 (8H, t, ^3J = 7.7 Hz, NCH_2), 1.87–1.91 (8H, m, CH_2), 1.67–1.75 (24H, m, CH_2), 1.24 (32H, br s, CH_2), 0.90 (12H, s, CH_3); **^{13}C NMR** (75.5 MHz, $CDCl_3$) δ (ppm): 169.6, 149.7, 144.6, 137.9, 134.2, 134.0, 130.6, 128.4, 122.7, 121.9, 120.6, 114.3, 49.7, 34.8, 31.3, 29.7, 28.7, 28.5, 26.1, 22.2, 20.3, 13.7; **ESIMS** *m/z*: 1699.8659 ($[M+Na]^+$, $C_{96}H_{116}N_{20}NaO_4Zn$ requires 1699.8672); **UV/Vis** $\lambda_{max}(CHCl_3)$/nm: 428 (ε/M^{-1} cm^{-1} 806 600), 558 (28 010), 597 (4878).

3-(Bromomethyl)benzaldehyde 20[9]



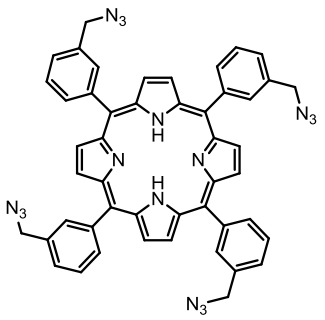
3-(Bromomethyl)benzonitrile (2.50 g, 12.8 mmol) was dissolved in anhydrous toluene (25 mL) and cooled to 0 °C. Dropwise addition of D*i*BAL-H (1 M in toluene, 17.0 mL, 17.0 mmol) was added dropwise to the above solution and the reaction mixture was stirred under N_2 at 0 °C for 2.5 h. $CHCl_3$ (40 mL) and 10% $HCl_{(aq)}$ (100 mL) were added and the reaction was stirred under N_2 at rt for 1 h. The organic layer was then separated and the aqueous layer extracted with $CHCl_3$ (2 × 100 mL). The combined organic layers were washed with H_2O (100 mL), dried over anhydrous $MgSO_4$, filtered, and the solvent removed *in vacuo*. Following recrystallisation from 1:1 toluene:hexane, compound **20** was isolated as colourless crystals in 81% yield (2.23 g, 11.2 mmol). **^{1}H NMR** (300 MHz, $CDCl_3$) δ (ppm): 10.00 (1H, s, C(O)H), 7.92 (1H, s, phenyl-H^2), 7.83 (1H, d, ^3J = 7.6 Hz, phenyl-H^6), 7.68 (1H, d, ^3J = 7.6 Hz, phenyl-H^4), 7.54 (1H, t, ^3J = 7.6 Hz, phenyl-H^5), 4.55 (2H, s, CH_2).

5,10,15,20-Tetrakis(α-bromo-*m*-tolyl)porphyrin 21[10,11]



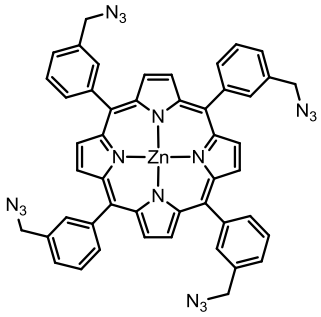
3-(Bromomethyl)benzaldehyde (4.50 g, 22.6 mmol) and pyrrole (1.57 mL, 1.52 g, 22.6 mmol) were dissolved in anhydrous, degassed CH_2Cl_2 (2.5 L) in a three-necked, 3 L round-bottomed flask. EtOH (17.0 mL) was added and the solution was purged with N_2 for 10 min and wrapped in foil. $BF_3{\cdot}OEt_2$ (0.93 mL, 7.5 mmol) was added via syringe and the reaction mixture stirred in the dark at rt for 70 min whilst continuously degassing with N_2. Et_3N (1.26 mL, 915 mg, 9.04 mmol) was added, followed by *p*-chloroanil (4.17 g, 17.0 mmol) and the reaction mixture was refluxed for 1 h. After cooling to rt, all volatiles were removed *in vacuo*. The residue was redissolved in CH_2Cl_2 and passed through a plug of silica, eluting with CH_2Cl_2 to give compound **21** as a purple solid in 30% yield (0.66 g, 0.67 mmol). **^{1}H NMR** (300 MHz, $CDCl_3$) δ (ppm): 8.87 (8H, s, *β*-pyrrole-*H*), 8.27 (4H, s, *meso*-phenyl-*H*), 8.17 (4H, d, ^3J = 7.5 Hz, *meso*-phenyl-*H*), 7.84 (4H, d, ^3J = 7.5 Hz, *meso*-phenyl-*H*), 7.75 (4H, t, ^3J = 7.5 Hz, *meso*-phenyl-*H*), 4.79 (8H, s, CH_2), −2.80 (2H, s, pyrrole-N*H*); **ESIMS** *m*/*z*: 987.0 ($[M+H]^+$, $C_{48}H_{35}Br_4N_4$ requires 987.0); **UV/Vis** λ_{max}(acetone)/nm: 415 (ε/M^{-1} cm^{-1} 631 500) 512 (23920), 546 (11 380), 589 (8360), 644 (6060).

5,10,15,20-Tetrakis(α-azido-m-tolyl)porphyrin 22



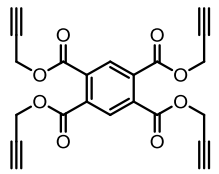
Compound **21** (500 mg, 0.5 mmol) was dissolved in DMSO (100 mL). NaN_3 (329 mg, 5.05 mmol) was added and the reaction stirred at rt under N_2 for 16 h. The reaction mixture was cooled to 0 °C, H_2O (100 mL) was added and the mixture extracted with CH_2Cl_2 (3 × 100 mL). The combined organic phases were washed with H_2O (100 mL), dried over anhydrous $MgSO_4$, filtered, and the solvent removed *in vacuo*. The crude residue was purified by column chromatography (SiO_2, 3:2 CH_2Cl_2:60−80 petroleum ether) to give **22** as a purple solid in 90% yield (382 mg, 0.458 mmol). **Mp**: 192–194 °C; **^{1}H NMR** (300 MHz, $CDCl_3$) δ (ppm): 8.86 (8H, s, *β*-pyrrole-*H*), 8.22 (4H, d, ^3J = 6.5 Hz, *meso*-phenyl-*H*), 8.19 (4H, s, *meso*-phenyl-*H*), 7.76–7.83 (8H, m, *meso*-phenyl-*H*), 4.66 (8H, s, CH_2), −2.79 (2H, s, pyrrole-N*H*); **^{13}C NMR** (75.5 MHz, $CDCl_3$) δ (ppm): 142.6, 134.4, 134.3, 133.8, 131.2, 127.8, 127.3, 119.6, 54.8; **ESIMS** *m/z*: 835.3223 ($[M+H]^+$, $C_{48}H_{35}N_{16}$ requires 835.3225); **UV/Vis** λ_{max}(acetone)/nm: 415 (ε/M^{-1} cm^{-1} 271 000) 512 (19 940), 545 (8280), 589 (5660), 645 (3880).

5,10,15,20-Tetrakis(α-azido-m-tolyl)-zinc(II)-porphyrin 23



Compound **22** (382 mg, 0.458 mmol) was dissolved in 9:1 CH_2Cl_2:MeOH (20 mL) and $Zn(OAc)_2{\cdot}2H_2O$ (502 mg, 2.29 mmol) was added. The reaction was stirred under N_2 at rt for 16 h. The solvent was removed *in vacuo*, the residue redissolved in CH_2Cl_2 (100 mL) and washed with H_2O (5 × 100 mL). The organic layer was dried over anhydrous $MgSO_4$, filtered, and the solvent removed *in vacuo*. The crude residue was purified using column chromatography (SiO_2, CH_2Cl_2) to give **23** as a purple solid in 88% yield (360 mg, 0.40 mmol). **Mp**: decomposed > 200 °C; **^{1}H NMR** (300 MHz, $CDCl_3$) δ (ppm): 8.93 (8H, s, *β*-pyrrole-*H*), 8.21 (4H, d, ^3J = 7.5 Hz, *meso*-phenyl-*H*), 8.14 (4H, s, *meso*-phenyl-*H*), 7.78 (4H, t, ^3J = 7.5 Hz, *meso*-phenyl-*H*), 7.72 (4H, d, ^3J = 7.5 Hz, *meso*-phenyl-*H*), 4.55 (8H, s, C*H*$_2$); **^{13}C NMR** (300 MHz, DMSO-d_6) δ (ppm): 149.3, 143.0, 134.3, 133.9, 131.6, 129.5, 127.8, 127.1, 120.0, 53.6; **ESIMS** *m/z*: 931.1984 ($[M+Cl]^-$, $C_{48}H_{32}ClN_{16}Zn$ requires 931.1981); **UV/Vis** λ_{max}(acetone)/nm: 428 (ε/M^{-1} cm^{-1} 485 000) 560 (20 120), 599 (9120).

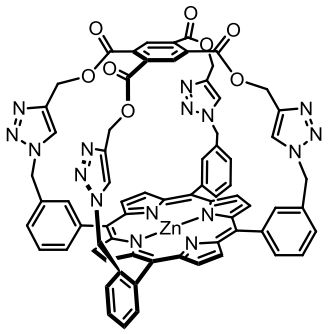
Tetra(prop-2-yn-1-yl)-benzene-1,2,4,5-tetracarboxylate 24[12]



1,2,4,5-Benzenetetracarboxylic acid (1.00 g, 3.93 mmol) was suspended in $SOCl_2$ (20 mL) and DMF (5 drops, cat.) was added. The reaction mixture was heated at reflux under N_2 for 16 h until the solution became homogenous. The $SOCl_2$ was removed by distillation and the residue dissolved in anhydrous CH_2Cl_2 (20 mL). This was added dropwise to a solution of

propargyl alcohol (2.30 mL, 2.20 g, 39.3 mmol) and Et_3N (6.0 mL, 4.4 g, 43 mmol) in anhydrous CH_2Cl_2 (100 mL). The reaction mixture was stirred under N_2 at rt for 16 h after which time it was washed with H_2O (3 × 100 mL), dried over anhydrous $MgSO_4$, filtered, and the solvent removed *in vacuo*. The crude residue was purified by column chromatography (SiO_2, 95:5 CH_2Cl_2:MeOH) to give compound **24** as a white solid in 86% yield (1.37 g, 3.67 mmol). **Mp**: 113–115 °C; **^{1}H NMR** (300 MHz, $CDCl_3$) δ (ppm): 8.17 (2H, s, Ar*H*), 4.96 (8H, d, ^4J = 2.5 Hz, CH_2), 2.58 (4H, t, ^4J = 2.5 Hz, alkyne-*H*); **^{13}C NMR** (75.5 MHz, $CDCl_3$) δ (ppm): 164.7, 133.8, 130.0, 76.6, 76.0, 53.8; **ESIMS** *m/z*: 429.0582 ($[M+Na]^+$, $C_{22}H_{14}NaO_8$ requires 429.0581).

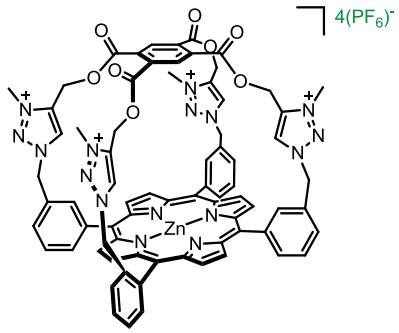
Porphyrin cage 25[adapted from 12]



Porphyrin **23** (90 mg, 0.1 mmol), $[Cu(MeCN)_4]PF_6$ (8.00 mg, 21.5 μmol), and Et_3N (60 μL, 44 mg, 0.43 mmol) were dissolved in anhydrous DMF (200 mL). Capping group **24** (40 mg, 0.10 mmol) was added and the reaction mixture was heated at 75 °C under N_2 for 3 days. The reaction mixture was then cooled and the solvent reduced to ~3 mL *in vacuo*. The residue was redissolved in CH_2Cl_2 (100 mL) and EtOAc (100 mL) and washed with water (2 × 100 mL), filtered, washed with water (2 × 100 mL), dried over anhydrous $MgSO_4$, filtered, and the solvent removed *in vacuo*. The crude residue was purified by preparative thin layer chromatography (SiO_2, 95:5 CH_2Cl_2:MeOH) to give **25** as a purple solid in 17% yield (22.6 mg, 17.3 μmol). **Mp**: decomposed > 245 °C; **^{1}H NMR** (500 MHz, $CDCl_3$) δ (ppm): 8.75 (4H, s, *β*-pyrrole-*H*), 8.71 (4H, s, *β*-pyrrole-*H*), 8.43 (4H, d, ^3J = 7.8 Hz, *meso*-phenyl-*H*), 7.86 (4H, t, ^3J = 7.8 Hz, *meso*-phenyl-*H*), 7.79 (4H, d, ^3J = 7.8 Hz, *meso*-phenyl-*H*),

7.67 (4H, s, triazole-*H*), 7.36 (2H, s, Ar*H*), 7.10 (4H, s, *meso*-phenyl-*H*), 5.95 (4H, d, ^2J = 16.4 Hz, OCH_2), 5.80 (4H, d, ^2J = 16.4 Hz, OCH_2), 5.15 (4H, d, ^2J = 12.8 Hz, NCH_2), 5.06 (4H, d, ^2J = 12.8 Hz, NCH_2); **^{13}C NMR** (125.8 MHz, 9:1 $CDCl_3$:CD_3OD) δ (ppm): 164.9, 149.6, 149.4, 144.1, 141.0, 133.1, 133.0, 132.4, 132.4 (*sic*), 129.0, 126.8, 125.9, 125.5, 119.5, 58.2, 53.4; **ESIMS** *m/z*: 1325.2888 ($[M+Na]^+$, $C_{70}H_{46}NaN_{16}O_8Zn$ requires 1325.2868); **UV/Vis** λ_{max}(acetone)/nm: 422 (ε/M^{-1} cm^{-1} 439 500), 553 (5140), 592 (1600).

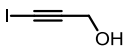
Porphyrin cage 26·(PF$_6$)$_4$



Porphyrin cage **25** (22.0 mg, 16.9 μmol) was dissolved in anhydrous CH_2Cl_2 (10 mL), $[Me_3O]BF_4$ (12.6 mg, 85.2 μmol) was added and the reaction mixture stirred under N_2 at rt for 3 days. MeOH:Et_3N (1:1, 10 drops) was added and the volatiles were removed *in vacuo*. Following purification using preparative thin layer chromatography (SiO_2, 14:2:1 MeCN:H_2O:sat. $KNO_{3(aq)}$) the crude residue was dissolved in acetone:H_2O:sat. $NH_4PF_{6(aq)}$ (100:2:1). The acetone was removed *in vacuo* and the resulting purple precipitate was isolated by filtration as **26·(PF$_6$)$_4$** in 32% yield (10.7 mg, 5.38 μmol). **Mp**: decomposed > 281 °C; **^{1}H NMR** (500 MHz, CD_3CN) δ (ppm): 8.76 (4H, s, *β*-pyrrole-*H*), 8.72 (4H, s, *β*-pyrrole-*H*), 8.55–8.53 (8H, m, triazolium-*H* & *meso*-phenyl-*H*), 7.97 (4H, t, ^3J = 7.7 Hz, *meso*-phenyl-*H*), 7.93 (4H, d, ^3J = 7.7 Hz, *meso*-phenyl-*H*), 7.37 (2H, s, Ar*H*), 7.24 (4H, s, *meso*-phenyl-*H*), 6.15 (8H, s, OCH_2), 5.34 (4H, d, ^2J = 14.4 Hz, NCH_2), 5.14 (4H, d, ^2J = 14.4 Hz, NCH_2), 4.11 (12H, s, NCH_3); **^{13}C NMR** (125.8 MHz, CD_3CN) δ (ppm): 163.6, 149.8, 144.0, 137.4, 133.6, 132.7, 132.3, 132.0, 131.9, 131.9(*sic*), 131.2, 129.6, 127.4, 126.8, 119.6, 56.9, 54.1, 38.61; **^{19}F NMR** (282.4 MHz, CD_3CN) δ (ppm): −72.9 (d, ^1J = 709

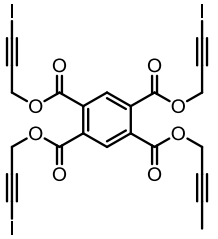
Hz, PF_6); **^{31}P NMR** (121.6 MHz, $CDCl_3$) δ (ppm): −139.3 (sept, J = 709 Hz, PF$_6$); **ESIMS** m/z: 1797.2874 ([M−PF$_6$]$^+$, $C_{74}H_{58}F_{18}N_{16}O_8P_3Zn$ requires 1797.2835); **UV/Vis** λ_{max}(acetone)/nm: 425 (ε/M^{-1} cm^{-1} 409 000), 554 (14 900), 593 (4440).

3-Iodoprop-2-yn-1-ol 27[13]



Propargyl alcohol (0.6 mL, 60 mg, 10 mmol) was dissolved in MeOH (20 mL) and added to a solution of KOH (1.40 g, 25.0 mmol) in H_2O (5 mL) at 0 °C. After stirring for 10 min, I_2 (2.7 g, 10 mmol) was added and the reaction mixture stirred under N_2 at rt for 3 h. After neutralising with 1 M HCl$_{(aq)}$, the mixture was extracted with Et_2O (3 × 20 mL) and the combined organics were washed with sat. $Na_2S_2O_3{\cdot}5H_2O_{(aq)}$ (50 mL) and sat. NaCl$_{(aq)}$ (50 mL), and the solvent removed *in vacuo* to give compound **27** as a pale yellow solid in 81% yield (1.48 g, 8.13 mol). **^{1}H NMR** (300 MHz, DMSO-d$_6$) δ (ppm): 5.29 (1H, t, ^3J = 5.7 Hz, O*H*), 4.16 (2H, d, ^3J = 5.7 Hz, CH_2).

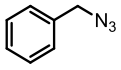
Tetrakis-iodoalkyne-capping group 28



Benzene-1,2,4,5-tetracarboxylic acid (160 mg, 0.63 mmol) and compound **27** (500 mg, 2.75 mmol) were dissolved in anhydrous CH_2Cl_2 (20 mL) and D*i*PEA (0.50 mL, 360 mg, 2.80 mmol) and 4-DMAP (61 mg, 0.50 mmol) were added. The reaction mixture was cooled to 0 °C and EDCI·HCl (530 mg, 2.80 mmol) was added. The reaction was stirred under N_2 at rt for 12 h after which time the solvent was removed *in vacuo*. The crude residue was redissolved in $CHCl_3$ (100 mL), washed with H_2O (100 mL), dried over anhydrous $MgSO_4$, filtered, and the solvent removed *in vacuo*. After purification using column chromatography (SiO_2, CH_2Cl_2), compound **28** was isolated as a white solid in 8% yield (45 mg, 0.056 mmol).

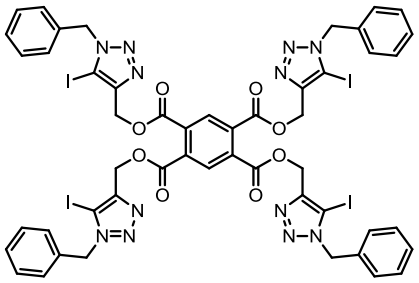
^{1}H NMR (300 MHz, acetone-d_6) δ (ppm): 8.20 (2H, s, Ar*H*), 5.15 (8H, s, CH_2); **^{13}C NMR** (125.8 MHz, acetone-d_6) δ (ppm): 165.4, 135.0, 130.8, 88.0, 55.9, 10.1; **ESIMS** *m/z*: 932.6438 ($[M+Na]^+$, $C_{22}H_{10}I_4NaO_8$ requires 932.6447).

Benzyl azide 29



NaN_3 (5.85 g, 90.0 mmol) was dissolved in DMSO (150 mL) and benzyl bromide (7.14 mL, 10.3 g, 60.0 mmol) was added. The reaction mixture was stirred under N_2 at rt for 16 h after which it was cooled in an ice bath. H_2O (200 mL) was added and stirring continued for a further 20 min. The aqueous phase was then extracted with EtOAc (3 × 150 mL), the combined organic phases were washed with H_2O (4 × 150 mL), sat. $NaCl_{(aq)}$ (200 mL), dried over anhydrous $MgSO_4$, filtered, and the solvent removed *in vacuo* to give compound **29** as a yellow oil in 87% yield (6.97 g, 52.3 mmol). **^{1}H NMR** (300 MHz, $CDCl_3$) δ (ppm): 7.32–7.44 (5H, m, phenyl-*H*), 4.36 (2H, s, CH_2).

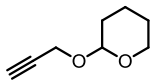
Iodoalkyne-functionalised capping group 30



Iodoalkyne capping group **28** (30 mg, 0.03 mmol) and benzyl azide **29** (22.0 mg, 0.17 mmol) were dissolved in anhydrous THF (10 mL) to which a THF (10 mL) solution of CuI (31 mg, 0.17 mmol) and Et_3N (20 μL, 20 mg, 28 μmol) was added and the reaction stirred under N_2 at rt in the dark for 3 days. After quenching with 10% $NH_4OH_{(aq)}$ solution, the solvent was removed *in vacuo* and the aqueous layer extracted with CH_2Cl_2 (3 × 50 mL). The combined organic layers were washed with H_2O (50 mL), dried over anhydrous $MgSO_4$, filtered, and the solvent removed *in vacuo*. The crude residue was purified by preparative thin layer

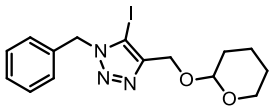
chromatography (9:1 CH_2Cl_2:acetone) to give compound **30** as a white solid in 10% yield (3.0 mg, 3.2 μmol). **^{1}H NMR** (300 MHz, $CDCl_3$) δ (ppm): 8.11 (2H, s, Ar*H*), 7.28–7.37 (20H, m, phenyl-*H*), 5.60 (8H, s, OCH_2), 5.38 (8H, s, NCH_2); **ESIMS** *m*/*z*: 1442.9 ($[M+H]^+$, $C_{50}H_{39}I_4N_{12}O_8$ requires 1442.9).

2-(Prop-2-yn-1-yloxy)tetrahydro-2*H*-pyran 31



Propargyl alcohol (1.00 mL, 0.960 g, 17.2 mmol) and pyridinium *p*-toluene sulfonate (432 mg, 1.72 mmol) were dissolved in degassed acetone (50 mL). Pyran (1.88 mL, 1.74 g, 1.20 mmol) in degassed acetone (10 mL) was added and the reaction mixture stirred under N_2 at rt for 4 days. The solvent was removed *in vacuo* and the crude residue redissolved in CH_2Cl_2 (100 mL) and washed with 1 M $NaOH_{(aq)}$ (100 mL) and H_2O (100 mL). The organic phase was dried over anhydrous $MgSO_4$, filtered, and the solvent removed *in vacuo* to give **31** as a pale yellow oil in 71% yield (1.71 g, 12.1 mmol). **^{1}H NMR** (300 MHz, $CDCl_3$) δ (ppm): 4.83 (1H, t, ^3J = 3.4 Hz, OC*H*O), 4.20–4.34 (2H, m, CH_2), 3.81–3.89 (1H, m, CH_2), 3.51–3.58 (1H, m, CH_2), 2.42 (1H, t, ^4J = 2.3 Hz, alkyne-*H*), 1.53–1.90 (6H, m, CH_2).

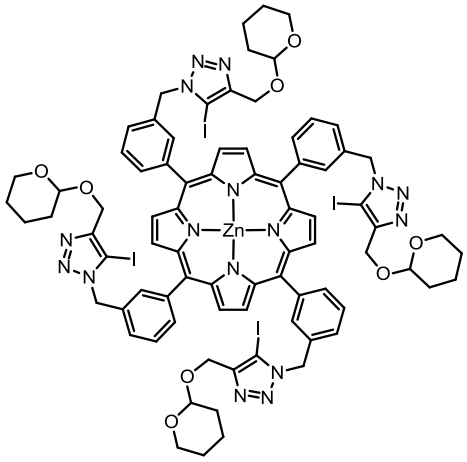
1-Benzyl-5-iodo-4-(((tetrahydro-2*H*-pyran-2-yl)oxy)methyl)-1*H*-1,2,3-triazole 32



Benzyl azide **29** (50 mg, 0.4 mmol) was dissolved in MeCN (5 mL), and NaI (228 mg, 1.52 mmol) and $Cu(ClO_4)_2{\cdot}6H_2O$ (282 mg, 0.761 mmol) were added and the reaction mixture was stirred under N_2 at rt for 5 min. DBU (57 μL, 58 mg, 0.38 mmol) was added followed by **31** (64 mg, 0.46 mmol) and the reaction mixture was stirred under N_2 at rt for 16 h. After diluting with EtOAc (30 mL) the mixture was washed with $NH_4OH_{(aq)}$ (25%, 50 mL), H_2O (50 mL), dried over anhydrous $MgSO_4$, filtered, and the solvent removed *in vacuo* to give **32** as a pale yellow solid in 58% yield (88.3 mg, 0.221 mmol). **^{1}H NMR**

(300 MHz, $CDCl_3$) δ (ppm): 7.23–7.32 (5H, m, phenyl-*H*), 5.55 (2H, s, NCH_2), 4.72–4.77 (2H, m, CH_2O), 4.53 (1H, d, ^3J = 12.3 Hz, OC*H*O), 3.87–3.95 (1H, m, CH_2), 3.49–3.56 (1H, m, CH_2), 1.45–1.83 (6H, m, CH_2); **^{13}C NMR** (75.5 MHz, $CDCl_3$) δ (ppm): 148.9, 134.1, 128.8, 128.5, 127.8, 98.0, 61.8, 60.2, 56.6, 54.2, 30.2, 25.3, 18.9; **ESIMS** *m/z*: 422.0324 ([M+Na]+, $C_{15}H_{18}IN_3NaO_2$ requires 422.0336).

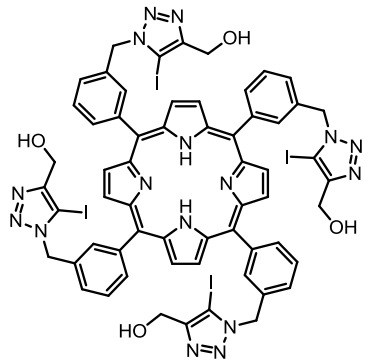
Compound 33



Compound **23** (50 mg, 0.06 mmol) was dissolved in MeCN (10 mL) and THF (1 mL) was added to aid solubility. NaI (134 mg, 0.894 mmol) and $Cu(ClO_4)_2{\cdot}6H_2O$ (165 mg, 0.445 mmol) were added and the reaction mixture stirred under N_2 at rt for 5 min. DBU (33.0 μL, 22.2 μmol) was added followed by compound **31** (63.0 mg, 0.445 mmol) and the reaction mixture was stirred under N_2 at rt for 16 h. After diluting with EtOAc (50 mL) and CH_2Cl_2 (50 mL) the organic phase was washed with $NH_4OH_{(aq)}$ (25%, 100 mL), H_2O (100 mL), dried over anhydrous $MgSO_4$, filtered, and the solvent removed *in vacuo*. The crude residue was purified by column chromatography (SiO_2, 95:5 CH_2Cl_2:MeOH) to give compound **33** as a purple solid in 63% yield (70 mg, 0.04 mmol). **^{1}H NMR** (300 MHz, $CDCl_3$) δ (ppm): 8.83 (8H, s, *β*-pyrrole-*H*), 8.11–8.21 (8H, m, *meso*-phenyl-*H*), 7.63–7.70 (8H, m, *meso*-phenyl-*H*), 5.76 (8H, s, NCH_2), 3.74–4.00 (8H, m, OCH_2), 3.54 (4H, br s, CH_2), 3.23 (4H, br s, CH_2), 2.33 (4H, br s, CH_2), 0.66–1.59 (24H, m, CH_2); **^{13}C NMR** (75.5 MHz, $CDCl_3$) δ (ppm): 149.9, 148.5, 143.6, 134.5, 134.2, 132.4, 132.0, 127.1, 120.0,

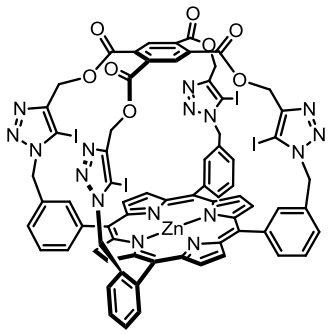
99.9, 96.9, 81.2, 60.5, 59.5, 54.3, 29.2, 24.4, 18.1; **ESIMS** *m/z*: 1983.1421 ($[M+Na]^+$, $C_{80}H_{76}I_4N_{16}NaO_8Zn$ requires 1983.1394; **UV/Vis** λ_{max}(DMSO)/nm: 423 (ε/M^{-1} cm^{-1} 399 440), 552 (20 492), 593 (4754).

Compound 34



Compound **33** (63 mg, 0.032 mmol) was dissolved in CH_2Cl_2:TFA (9:1, 10 mL) and the green solution stirred under N_2 at rt for 20 h. Sat. $NaHCO_{3(aq)}$ was added cautiously until the colour changed from green to purple. The reaction mixture was extracted with CH_2Cl_2 (3 × 50 mL) and the combined organics washed with sat. $NaHCO_{3(aq)}$ (50 mL), H_2O (50 mL), dried over anhydrous $MgSO_4$, filtered, and the solvent removed *in vacuo*. The crude residue was purified by preparative thin layer column chromatography (SiO_2, 95:5 CH_2Cl_2:MeOH) to give compound **34** as a purple solid in 10% yield (4.9 mg, 3.1 μmol). **^{1}H NMR** (300 MHz, 1:1 $CDCl_3$:CD_3OD) δ (ppm): 8.78 (8H, s, *β*-pyrrole-*H*), 8.19 (4H, d, ^3J = 7.6 Hz, *meso*-phenyl-*H*), 8.12 (4H, s, *meso*-phenyl-*H*), 7.78 (4H, t, ^3J = 7.6 Hz, *meso*-phenyl-*H*), 7.72 (4H, br s, *meso*-phenyl-*H*), 5.93 (8H, s, CH_2), 4.63 (8H, s, CH_2); **^{13}C NMR**: not enough sample to acquire a good spectrum; **ESIMS** *m/z*: 782.0 ($[M+2H]^{2+}$, $C_{60}H_{48}I_4N_{16}O_4$ requires 782.0); **UV/Vis** λ_{max}(DMSO)/nm: 420 (ε/M^{-1} cm^{-1} 341 900), 516 (16 072), 551 (7386), 590 (4916), 645 (4062).

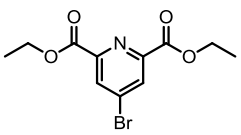
Iodotriazole-porphyrin-cage 35



Compound **23** (50 mg, 0.06 mmol) was dissolved in anhydrous THF (10 mL) and NaI (134 mg, 0.894 mmol) and $Cu(ClO_4)_2 \cdot 6H_2O$ (165 mg, 0.445 mmol) were added. After stirring under N_2 at rt for 5 min, DBU (33 μL, 34 mg, 0.22 mmol) and compound **24** (23 mg, 60 μmol) were added and the reaction mixture left to stir under N_2 at rt for 17 h. After diluting with EtOAc (50 mL) the solution was washed with 25% $NH_4OH_{(aq)}$ (50 mL), H_2O (50 mL), dried over anhydrous $MgSO_4$, filtered, and the solvent removed *in vacuo* to give **35** as a purple solid in 4% yield (4.2 mg, 2.3 μmol). **^{1}H NMR** (500 MHz, $CDCl_3$) δ (ppm): 8.97 (4H, br s, *β*-pyrrole-*H*), 8.78 (4H, br s, *β*-pyrrole-*H*), 8.46 (4H, br s, *meso*-phenyl-*H*), 7.89 (4H, s, *meso*-phenyl-*H*), 7.80 (4H, br s, *meso*-phenyl-*H*), 7.43 (2H, s Ar*H*), 7.09 (4H, br s, *meso*-phenyl-*H*), 6.01 (4H, br s, CH_2), 5.89 (4H, br s, CH_2), 5.30 (4H, br s, CH_2), 5.21 (4H, br s, CH_2); **^{13}C NMR**: not enough sample to acquire a good spectrum; **ESIMS** *m/z*: 1828.8728 ($[M+Na]^+$, $C_{70}H_{42}I_4N_{16}NaO_8Zn$ requires 1828.8734; **UV/Vis** λ_{max}(DMSO)/nm: 428 (ε/M^{-1} cm^{-1} 775 920), 560 (42 028), 599 (19 588).

6.3 Experimental procedures for Chapter Three

Diethyl-4-bromopyridine-2,6-dicarboxylate 36[14]



Chelidamic acid monohydrate (3.00 g, 16.4 mmol) and PBr_5 (25.0 g, 58.1 mmol) were heated to 90 °C and the melt reaction was stirred under N_2 for 3 h. The reaction was cooled to rt,

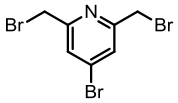
$CHCl_3$ (130 mL) was added followed by dropwise addition of EtOH (60 mL). The reaction was stirred for a further 30 min under N_2 at rt after which the volatiles were removed *in vacuo*. H_2O (100 mL) was added, the mixture filtered and the orange solid washed with water. The solid residue was redissolved in CH_2Cl_2 (100 mL), dried over anhydrous $MgSO_4$, filtered, and the solvent removed *in vacuo* to give **36** as an orange solid in 83% yield (4.10 g, 13.6 mmol). **^{1}H NMR** (300 MHz, $CDCl_3$) δ (ppm): 8.43 (2H, s, pyridine-H^3&H^5), 4.50 (4H, q, ^3J = 7.2 Hz, CH_2), 1.47 (6H, t, ^3J = 7.2 Hz, CH_3); **ESIMS** *m/z*: 324.0 ($[M+Na]^+$, $C_{11}H_{12}BrNNaO_2$ requires 324.0).

(4-Bromopyridine-2,6-diyl)dimethanol 37[14]



Compound **36** (6.04 g, 20.0 mmol) was dissolved in EtOH (250 mL) and $NaBH_4$ (3.40 g, 90.0 mmol) was added in small portions. The reaction mixture was stirred under N_2 at rt for 2 h, after which it was heated at reflux under N_2 for 15 h. The reaction was cooled to rt and the solvent removed *in vacuo*. Saturated $NaHCO_{3(aq)}$ (32 mL) was added, the solution was heated to boiling, and H_2O (45 mL) was added. The mixture was left in the fridge overnight and the resulting crystals were filtered, dried, and purified by Soxhlet extraction with acetone. The acetone was removed *in vacuo* to give **37** as colourless crystals in 76% yield (3.28 g, 15.1 mmol). **^{1}H NMR** (300 MHz, DMSO-d_6) δ (ppm): 7.51 (2H, s, pyridine-H^3&H^5), 5.54 (2H, t, ^3J = 6.0 Hz, OH), 4.52 (4H, d, ^3J = 6.0 Hz, CH_2); **ESIMS** *m/z*: 240.0 ($[M+Na]^+$, $C_7H_8BrNNaO_2$ requires 240.0).

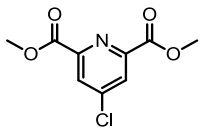
4-Bromo-2,6-bis(bromomethyl)pyridine 38[14]



Compound **37** (2.50 g, 11.5 mmol) was suspended in $CHCl_3$ (70 mL) and a solution of PBr_3 (1.63 mL, 4.68 g, 17.3 mmol) in $CHCl_3$ (40 mL) was added. The reaction mixture was heated

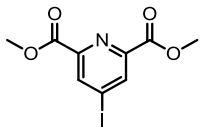
at reflux under N_2 for 16 h. After cooling to rt, the reaction was neutralised with 5% $NaHCO_{3(aq)}$, the organic phase was separated, washed with H_2O (6 × 50 mL), dried over anhydrous $MgSO_4$, filtered, and the solvent removed *in vacuo* to give **38** as a white solid in 70% yield (2.77 g, 8.05 mmol). **^{1}H NMR** (300 MHz, $CDCl_3$) δ (ppm): 7.57 (2H, s, pyridine-H^3&H^5), 4.49 (4H, s, CH_2); **ESIMS** *m/z*: 343.8 ($[M+H]^+$, $C_7H_7Br_3N$ requires 343.8).

Dimethyl-4-chloropyridine-2,6-dicarboxylate 39[adapted from15]



Chelidamic acid monohydrate (250 mg, 1.2 mmol) was suspended in $CHCl_3$ (50 mL). PCl_5 (0.48 mL, 1.0 g, 4.8 mmol) was added and the reaction heated at reflux under N_2 for 72 h. The reaction was cooled to 0 °C, MeOH (50 mL) was added and the reaction mixture stirred at rt under N_2 for 1 h. The reaction mixture was neutralised with sat. $NaHCO_{3(aq)}$ and the volatile solvents removed *in vacuo*. The aqueous layer was extracted with EtOAc (5 × 50 mL) and the combined organic phases were dried over anhydrous $MgSO_4$, filtered, and the solvent removed *in vacuo*. The crude residue was purified by column chromatography (SiO_2, 97:3 CH_2Cl_2:MeOH) to give **39** as a white solid in 42% yield (119 g, 0.518 mmol). **^{1}H NMR** (300 MHz, $CDCl_3$) δ (ppm): 8.31 (2H, s, pyridine-H^3&H^5), 4.05 (6H, s, CH_3); **ESIMS** *m/z*: 230.1 ($[M+H]^+$, $C_9H_9ClNO_4$ requires 230.0).

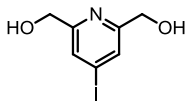
Dimethyl-4-iodopyridine-2,6-dicarboxylate 40[16]



Compound **39** (2.00 g, 8.73 mmol) was dissolved in MeCN (100 mL), NaI (13.1 g, 87.3 mmol) was added and the reaction mixture was sonicated for 30 min. Acetyl chloride (1.86 mL, 26.2 mmol) was added and the reaction mixture sonicated for a further 45 min. CH_2Cl_2 (100 mL) and sat. $Na_2CO_{3(aq)}$ (100 mL) were added, the organic phase was separated

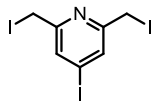
and the aqueous phase extracted with CH_2Cl_2 (3 × 100 mL). The combined organic phases were washed with sat. $Na_2S_2O_3{\cdot}5H_2O_{(aq)}$ (200 mL), H_2O (200 mL), dried over anhydrous $MgSO_4$, filtered, and the solvent removed *in vacuo* to give **40** as a white solid in 74% yield (2.06 g, 6.42 mmol). **^{1}H NMR** (300 MHz, $CDCl_3$) δ (ppm): 8.67 (2H, s, pyridine-*H*^{3}&*H*^{5}), 4.03 (6H, s, C*H*$_3$); **ESIMS** *m/z*: 344.0 ($[M+Na]^+$, $C_9H_8INNaO_4$ requires 343.9).

(4-Iodopyridine-2,6-diyl)dimethanol 41[14]



Compound **40** (750 mg, 2.3 mmol) was dissolved in MeOH (50 mL) and cooled to 0 °C. $NaBH_4$ (266 mg, 7.02 mmol) was added and the reaction mixture heated at reflux for 16 h. After cooling to rt, acetone (20 mL) was added and the solvent removed *in vacuo*. Sat. $NaHCO_{3(aq)}$ (3.5 mL) was added and the suspension heated to boiling forming a yellow solution. H_2O (4.5 mL) was added and the resulting precipitate cooled at 4 °C for 16 h. The mixture was filtered and the solid dried in air to give **41** as a white solid in 68% yield (419 mg, 1.58 mmol). **^{1}H NMR** (300 MHz, acetone-d_6) δ (ppm): 7.78 (2H, s, pyridine-*H*^{3}&*H*^{5}), 4.63 (4H, s, C*H*$_2$), 4.53 (2H, s, O*H*); **ESIMS** *m/z*: 266.0 ($[M+H]^+$, $C_7H_9INO_2$ requires 266.0).

4-Iodo-2,6-bis(iodomethyl)pyridine 42



Compound **41** (300 mg, 1.13 mmol), imidazole (720 mg, 2.74 mmol) and triphenyl phosphine (633 mg, 9.30 mmol) were dissolved in anhydrous CH_2Cl_2 (100 mL). A solution of I_2 (723 mg, 2.85 mmol) in anhydrous CH_2Cl_2 (100 mL) was added in portions and the reaction stirred under N_2 at rt for 16 h. The solvent was removed *in vacuo* and the crude residue purified by column chromatography (SiO_2, CH_2Cl_2) to give **42** as an orange solid in 32% yield (174 mg, 0.359 mmol). **^{1}H NMR** (300 MHz, C_6D_6) δ (ppm): 6.83 (2H, s, pyridine-

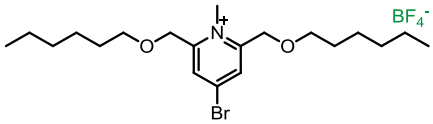
H^3&H^5), 3.72 (4H, s, CH_2); **ESIMS** *m/z*: 485.7710 ([M+H]$^+$, $C_7H_7I_3N$ requires 485.7707). This compound was used without further characterisation.

4-Bromopyridine threading compound 43



NaH (60% dispersion in mineral oil, 960 mg, 24 mmol) was suspended in anhydrous THF (100 mL) under N_2 and cooled to 0 °C. A solution of 1-hexanol (1.48 mL, 1.20 g, 12.0 mmol) in anhydrous THF (50 mL) was added, and the mixture stirred at rt under N_2 for 30 min. Compound **38** (1.00 g, 2.91 mmol) was added and the reaction mixture was stirred at rt for 18 h under N_2. H_2O (100 mL) was added and the THF removed *in vacuo*. The aqueous mixture was extracted with EtOAc (3 × 100 mL), and the combined organic phases dried over anhydrous $MgSO_4$, filtered, and the solvent removed *in vacuo*. The crude residue was purified by column chromatography (SiO_2, 99:1 CH_2Cl_2:MeOH) to give **43** as a yellow oil in 81% yield (906 mg, 2.35 mmol). **^{1}H NMR** (300 MHz, $CDCl_3$) δ (ppm): 7.50 (2H, s, pyridine-H^3&H^5), 4.54 (4H, s, CH_2O), 3.53 (4H, t, ^3J = 6.5 Hz, OCH_2), 1.58–1.68 (4H, m, CH_2), 1.26–1.42 (12H, m, CH_2), 0.88 (6H, t, ^3J = 7.0 Hz, CH_3); **^{13}C NMR** (75.5 MHz, $CDCl_3$) δ (ppm): 159.8, 134.2, 122.8, 72.9, 71.3, 31.6, 29.6, 25.7, 22.5, 14.0; **ESIMS** *m/z*: 386.1674 ([M+H]$^+$, $C_{19}H_{33}BrNO_2$ requires 386.1689).

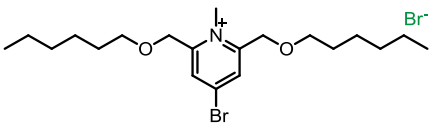
4-Bromopyridinium tetrafluoroborate threading compound 44·BF$_4$



Compound **43** (330 mg, 0.78 mmol) was dissolved in anhydrous CH_2Cl_2 (50 mL). $[Me_3O]BF_4$ (138 mg, 0.933 mmol) was added and the reaction mixture stirred at rt under N_2 for 48 h. MeOH (1 mL) was added and the solvent removed *in vacuo*. The crude residue was purified by column chromatography (SiO_2, 9:1 CH_2Cl_2:MeOH) to give **44·BF$_4$** as a pale orange oil in 75% yield (285 mg, 0.584 mmol). **^{1}H NMR** (300 MHz, $CDCl_3$) δ (ppm): 8.13

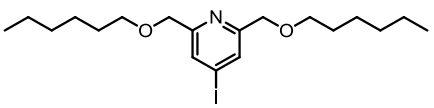
(2H, s, pyridinium-H^3&H^5), 4.84 (4H, s, OCH_2), 4.05 (3H, s, NCH_3), 3.70 (4H, t, ^3J = 6.5 Hz, OCH$_2$CH_2), 1.64–1.73 (4H, m, CH_2), 1.30–1.40 (12H, m, CH_2), 0.91 (6H, t, ^3J = 7.0 Hz, CH_3); **^{13}C NMR** (75.5 MHz, $CDCl_3$) δ (ppm): 156.5, 143.3, 128.7, 72.5, 67.6, 38.9, 31.5, 29.4, 25.7, 22.6, 14.0; **^{19}F NMR** (282.4 MHz, $CDCl_3$) δ (ppm): −152.09–−152.04 (m, BF_4); **ESIMS** *m/z*: 400.1841 ($[M-BF_4]^+$, $C_{20}H_{35}BrNO_2$ requires 400.1846).

4-Bromopyridinium bromide threading compound 44·Br



Compound **44·BF$_4$** (50 mg, 0.1 mmol) was dissolved in $CHCl_3$ (50 mL) and washed with 1 M $NH_4Br_{(aq)}$ (10 × 50 mL), H_2O (2 × 50 mL). The organic phase was dried over anhydrous $MgSO_4$, filtered, and the solvent removed *in vacuo* to give **44·Br** as a pale orange oil in 82% yield (41 mg, 0.084 mmol). **^{1}H NMR** (300 MHz, $CDCl_3$) δ (ppm): 8.16 (2H, s, pyridinium-H^3&H^5), 5.00 (4H, s, OCH_2), 4.28 (3H, s, NCH_3), 3.72 (4H, t, ^3J = 6.5 Hz, CH_2), 1.63–1.70 (4H, m, CH_2), 1.25–1.41 (12H, m, CH_2), 0.90 (6H, t, ^3J = 7.0 Hz, CH_3); **^{13}C NMR** (75.5 MHz, $CDCl_3$) δ (ppm): 156.6, 143.5, 129.1, 72.6, 68.5, 40.8, 31.7, 29.7, 25.8, 22.7, 14.1; **ESIMS** *m/z*: 400.1831 $[M-Br]^+$, $C_{20}H_{35}BrNO_2$ requires 400.1846).

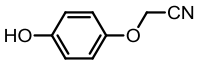
4-Iodopyridine threading compound 45



NaH (60% dispersion in mineral oil, 31 mg, 0.80 mmol) was suspended in anhydrous THF (20 mL) and cooled to 0° C. 1-Hexanol (50 μL, 40 mg, 0.4 mmol) was added and the solution stirred for 30 min. Compound **42** (50 mg, 0.1 mmol) was added and the reaction mixture stirred at rt under N_2 for 4 days. H_2O (50 mL) was added and the THF removed *in vacuo*. The aqueous mixture was extracted with CH_2Cl_2 (3 × 50 mL), and the combined organic phases dried over anhydrous $MgSO_4$, filtered, and the solvent removed *in vacuo*. The crude residue was purified by preparative thin layer chromatography (SiO_2, 95:5 CH_2Cl_2:MeOH) to

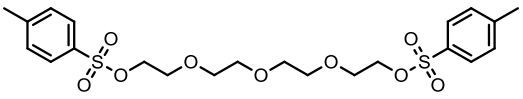
give **45** as a pale yellow solid in 5% yield (2.2 mg, 5.0 μmol). **^{1}H NMR** (500 MHz, 1:1 $CDCl_3$:CD_3OD) δ (ppm): 7.75 (2H, s, pyridine-H^3&H^5), 4.50 (4H, s, CH_2), 3.53 (4H, t, ^3J = 6.5 Hz, CH_2), 1.58–1.65 (4H, m, CH_2), 1.26–1.39 (12H, m, CH_2), 0.87 (6H, t, ^3J = 7.0 Hz, CH_3); **ESIMS** *m/z*: 456.1353 ($[M+Na]^+$, $C_{19}H_{32}INNaO_2$ requires 456.1370).

2-(4-Hydroxyphenoxy)acetonitrile 46[17]



NaOH (8.34 g, 211 mmol) and hydroquinone (11.6 g, 105 mmol) were dissolved in degassed 1:1 dioxane:H_2O (300 mL) which was continuously degassed throughout the reaction. A solution of bromoacetonitrile (7.34 mL, 105 mmol) in degassed dioxane (50 mL) was added and the reaction mixture was stirred at rt under N_2 in the dark for 1 h. The reaction was acidified using 10% $HCl_{(aq)}$ and extracted with CH_2Cl_2 (3 × 150 mL). The combined organic phases were dried over anhydrous $MgSO_4$, filtered, and the solvent removed *in vacuo*. The crude residue was purified by column chromatography (SiO_2, 98:2 CH_2Cl_2:MeOH) to give **46** as a pale yellow oil in 56% yield (9.20 g, 61.7 mmol). **^{1}H NMR** (300 MHz, $CDCl_3$) δ (ppm): 6.91 (2H, d, ^3J = 8.9 Hz, hydroquinone-H), 6.81 (2H, d, ^3J = 8.9 Hz, hydroquinone-H), 5.08 (1H, s, OH), 4.71 (2H, s, CH_2); **ESIMS** *m/z*: 149.0 ($[M-H]^-$, $C_8H_6NO_2$ requires 149.0).

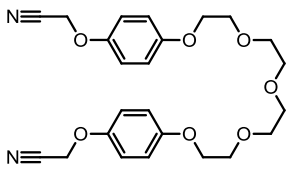
Tetraethylene glycol-bis-*para*-tosylate 47[18,19]



Tetraethylene glycol (5.00 mL, 29.0 mmol) was dissolved in CH_2Cl_2 (50 mL). *p*-Toluenesulfonyl chloride (11.0 g, 58.0 mmol) was added and the reaction mixture was cooled to 0 °C. Powdered KOH (13.0 g, 230 mmol) was added in portions whilst the temperature was maintained at 0 °C. The reaction mixture was stirred at 0 °C under N_2 for 3 h after which CH_2Cl_2 (50 mL) and ice water (100 mL) were added. The phases were separated and the aqueous phase was extracted with CH_2Cl_2 (2 × 50 mL). The combined organic phases were

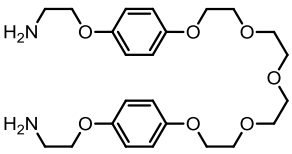
washed with H_2O (50 mL), dried over anhydrous $MgSO_4$, filtered, and the solvent removed *in vacuo* to give **47** as a colourless oil in 93% yield (13.5 g, 26.9 mmol). **^{1}H NMR** (300 MHz, $CDCl_3$) δ (ppm): 7.76 (4H, d, ^3J = 8.1 Hz, SAr*H*), 7.31 (4H, d, ^3J = 8.1 Hz, SAr*H*), 4.12 (4H, t, ^3J = 4.8 Hz, CH_2), 3.64 (4H, t, ^3J = 4.8 Hz, CH_2), 3.58 (8H, s, CH_2), 2.41 (6H, s, CH_3); **ESIMS** *m/z*: 525.1 ($[M+Na]^+$, $C_{22}H_{30}NaO_9S_2$ requires 525.1).

Bis-nitrile macrocycle precursor compound 48[18]



Compound **47** (10.8 g, 21.4 mmol) and compound **46** (6.89 g, 46.2 mmol) were dissolved in anhydrous CH_3CN (300 mL). K_2CO_3 was added (9.50 g, 68.6 mmol) and the mixture heated at reflux under N_2 for 3 days. The reaction was cooled to rt, filtered, and the solvent removed *in vacuo*. The brown residue was redissolved in $CHCl_3$ (200 mL), filtered, and the solvent removed *in vacuo*. The crude pale brown solid was purified by column chromatography (SiO_2, 3:1 EtOAc:hexanes) to give **48** as a white solid in 79% yield (7.69 g, 16.8 mmol). **^{1}H NMR** (300 MHz, $CDCl_3$) δ (ppm): 6.87–6.95 (8H, m, hydroquinone-*H*), 4.71 (4H, s, CH_2CN), 4.09 (4H, t, ^3J = 4.7 Hz, CH_2), 3.85 (4H, t, ^3J = 4.7 Hz, CH_2), 3.68–3.76 (8H, m, CH_2); **ESIMS** *m/z*: 479.2 ($[M+Na]^+$, $C_{24}H_{28}N_2NaO_7$ requires 479.2).

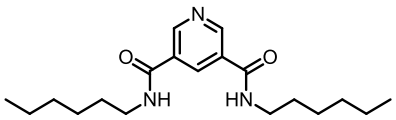
Bis-amine macrocycle precursor compound 49[18]



A 1 M solution of BH_3 in THF (16 mL, 16 mmol) was heated to 70 °C under N_2 and a solution of **48** (0.80 g, 1.94 mmol) in anhydrous THF (40 mL) was added cautiously over 15 min. The reaction stirred at 70 °C under N_2 for 4 h. After cooling to rt, MeOH (50 mL) was added cautiously to quench the reaction followed by conc. $HCl_{(aq)}$ (25 mL) and the

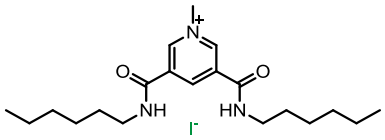
organic solvent removed *in vacuo*. The acidic solution was basified with 10 M $NaOH_{(aq)}$ and the white precipitate filtered, washed with H_2O (50 mL) and dried *in vacuo* over P_2O_5 to give **49** as a white powder in 77% yield (0.68 g, 1.5 mmol). **^{1}H NMR** (300 MHz, $CDCl_3$) δ (ppm): 6.84 (8H, s, hydroquinone-*H*), 4.07 (4H, t, ^3J = 5.3 Hz, CH_2), 3.93 (4H, t, ^3J = 5.3 Hz, CH_2), 3.82 (4H, t, ^3J = 5.0 Hz, CH_2), 3.67–3.75 (8H, m, CH_2), 3.05 (4H, t, ^3J = 5.3 Hz, CH_2NH$_2$), 1.64 (4H, br s, NH_2); **ESIMS** *m/z*: 465.3 ($[M+H]^+$, $C_{24}H_{36}N_2NaO_7$ requires 465.3).

N^3,N^5-Dihexylpyridine-3,5-dicarboxamide 50[20]



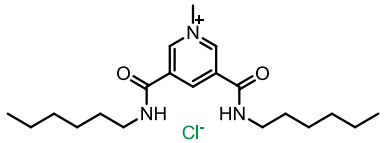
Pyridine-3,5-dicarboxylic acid (3.00 g, 18.0 mmol) was dissolved in $SOCl_2$ (20 mL). DMF (5 drops, cat.) was added and the reaction mixture was heated at reflux under N_2 for 18 h until the solution became homogenous. The $SOCl_2$ was removed by distillation and the residue was immediately redissolved in anhydrous CH_2Cl_2 (50 mL). This solution was added dropwise to a solution of 1-hexylamine (4.73 mL, 3.64 g, 36.0 mmol), and Et_3N (7.50 mL, 5.44 g, 53.8 mmol) in anhydrous CH_2Cl_2 (100 mL). The reaction mixture was stirred at rt under N_2 for 1 h and then washed with 10% citric $acid_{(aq)}$ (3 × 100 mL) and H_2O (2 × 100 mL). The organic phase was dried over anhydrous $MgSO_4$, filtered, and the solvent removed *in vacuo* to give **50** as a white solid in 88% yield (5.30 g, 15.9 mmol). **^{1}H NMR** (300 MHz, $CDCl_3$) δ (ppm): 9.09 (2H, d, ^4J = 2.1 Hz, pyridine-H^2&H^6), 8.45 (1H, t, ^4J = 2.1 Hz, pyridine-H^4), 6.54 (2H, br s, N*H*), 3.45–3.52 (4H, m, NHCH_2), 1.59–1.69 (4H, m, CH_2), 1.30–1.44 (12H, m, CH_2), 0.90 (6H, t, ^3J = 7.1 Hz, CH_3); **ESIMS** *m/z*: 368.2 ($[M+Cl]^-$, $C_{19}H_{31}ClN_3O_2$ requires 368.2).

Compound 51·I[20]



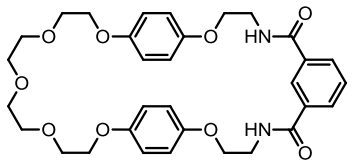
Compound **50** (1.20 g, 3.60 mmol) and MeI (2 mL, excess) were dissolved in $CHCl_3$ (10 mL) and heated at reflux under N_2 for 18 h. After cooling to rt, the solvent and MeI were removed *in vacuo* to give **51·I** as an orange solid in quantitative yield (1.71 g, 3.59 mmol). **^{1}H NMR** (300 MHz, $CDCl_3$) δ (ppm): 9.89 (1H, s, pyridinium-H^4), 9.41 (2H, s, pyridinium-H^2&H^6), 8.69 (2H, t, ^3J = 5.8 Hz, N*H*), 4.56 (3H, s, NCH_3), 3.43–3.50 (4H, m, CH_2), 1.68–1.77 (4H, m, CH_2), 1.29–1.41 (12H, m, CH_2), 0.89 (3H, t, ^3J = 6.8 Hz, CH_3); **ESIMS** *m/z*: 348.3 ($[M-I]^+$, $C_{20}H_{34}N_3O_2$ requires 348.3).

Compound 51·Cl[20]



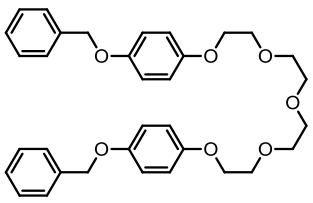
Compound **51·I** (1.85 g, 3.90 mmol) was dissolved in $CHCl_3$ (100 mL) and washed with 1 M $NH_4Cl_{(aq)}$ solution (8 × 100 mL) and H_2O (2 × 100 mL). The organic phase was dried over anhydrous $MgSO_4$, and the solvent removed *in vacuo* to give compound **51·Cl** as a bright orange solid in 75% yield (1.10 g, 2.92 mmol). **^{1}H NMR** (300 MHz, $CDCl_3$) δ (ppm): 10.72 (1H, s, pyridinium-H^4), 9.59 (2H, t, ^3J = 5.2 Hz, N*H*), 9.26 (2H, s, pyridinium-H^2&H^6), 4.54 (3H, s, NCH_3), 3.46–3.52 (4H, m, CH_2), 1.70–1.80 (4H, m, CH_2), 1.26–1.43 (12H, m, CH_2), 0.89 (6H, t, ^3J = 6.8 Hz, CH_3); **ESIMS** *m/z*: 348.3 ($[M-Cl]^+$, $C_{20}H_{34}N_3O_2$ requires 348.3).

Macrocycle 52[17]



Compound **49** (300 mg, 0.7 mmol), **51·Cl** (250 mg 0.65 mmol), Et_3N (0.23 mL, 160 mg, 1.6 mmol) were dissolved in anhydrous CH_2Cl_2 (70 mL) and stirred at rt under N_2 for 30 min. A solution of isophthaloyl dichloride (130 mg, 0.65 mmol) in anhydrous CH_2Cl_2 (10 mL) was added dropwise and the reaction stirred at rt under N_2 for 2 h. The reaction mixture was washed with 10% $HCl_{(aq)}$ (2 × 100 mL), H_2O (2 × 100 mL), dried over anhydrous $MgSO_4$, filtered, and the solvent removed *in vacuo*. Purification using column chromatography (SiO_2, 97:3 CH_2Cl_2:MeOH) gave **52** as a white solid in 25% yield (191 mg, 0.32 mmol). **^{1}H NMR** (300 MHz, $CDCl_3$) δ (ppm): 8.05 (2H, dd, ^3J = 7.6 Hz, ^4J = 1.3 Hz, isophthaloyl-H^4&H^6), 7.96 (1H, t, ^4J = 1.6 Hz, isophthaloyl-H^2), 7.57 (1H, t, ^3J = 7.6 Hz, isophthaloyl-H^5), 6.79 (8H, s, hydroquinone-*H*), 6.71 (2H, br t, ^3J = 6.0 Hz, N*H*), 4.02–4.12 (8H, m, CH_2), 3.83–3.90 (8H, m, CH_2), 3.71 (8H, s, CH_2); **ESIMS** *m/z*: 617.3 ($[M+Na]^+$, $C_{32}H_{38}N_2NaO_9$ requires 617.3).

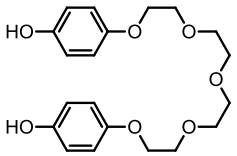
Compound 53



4-Benzyloxyphenol (8.15 g, 40.7 mmol) and compound **47** (8.18 g, 16.3 mmol) were dissolved in anhydrous CH_3CN (100 mL) and K_2CO_3 (6.08 g, 44.0 mmol) was added. The mixture was heated at reflux under N_2 for 72 h after which it was cooled to rt. The reaction mixture was filtered and the solvent removed *in vacuo*. The crude residue was redissolved in $CHCl_3$, filtered, and the solvent removed *in vacuo* to give an orange oil. The residue was dissolved in EtOAc, hexanes added and the resulting precipitate isolated in 80% yield (7.22 g, 12.9 mmol).

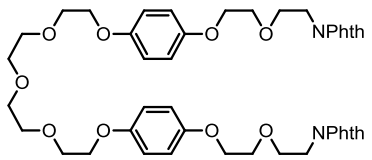
^{1}H NMR (300 MHz, $CDCl_3$) δ (ppm): 7.32–7.45 (10H, m, phenyl-*H*), 6.83–6.92 (8H, m, hydroquinone-*H*), 4.08 (4H, t, ^3J = 4.9 Hz, CH_2), 3.84 (4H, t, ^3J = 4.9 Hz, CH_2), 3.68–3.76 (8H, m, CH_2); **ESIMS** *m/z*: 583.1 ($[M+Na]^+$, $C_{34}H_{38}NaO_7$ requires 581.3).

Compound 54[21]



A solution of compound **53** (2.00 g, 3.58 mmol) in 1:1 $CHCl_3$:MeOH (100 mL) in a 250 mL round-bottomed flask was evacuated and purged with N_2 three times. 10% Pd/C (0.20 g, 10% by wt.) was added and the reaction vessel evacuated and purged three times with N_2 and three times with H_2. The reaction mixture was left to stir at rt under H_2 for 12 h. After evacuating and purging with N_2 three times, the solution was filtered through Celite® and the solvent removed *in vacuo*. The residue was dissolved in $CHCl_3$, filtered, and the solvent removed *in vacuo*. The crude mixture was purified by column chromatography (SiO_2, 95:5 CH_2Cl_2:MeOH) to give **54** as a pale yellow oil in 85% yield (1.16 g, 3.06 mmol). **^{1}H NMR** (300 MHz, $CDCl_3$) δ (ppm): 6.42–6.49 (8H, m, hydroquinone-*H*), 4.35 (2H, br s, O*H*), 3.72 (4H, t, ^3J = 4.6 Hz, CH_2), 3.49 (4H, t, ^3J = 4.6 Hz, CH_2), 3.36–3.41 (8H, m, CH_2); **ESIMS** *m/z*: 401.2 ($[M+Na]^+$, $C_{20}H_{26}NaO_7$ requires 401.2).

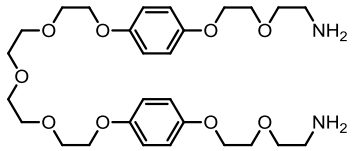
Compound 55



Compound **54** (200 mg, 0.5 mmol) and *N*-phthalimidoethoxy ethanol (453 mg, 1.16 mmol) were dissolved in anhydrous CH_3CN (200 mL). K_2CO_3 (366 mg, 2.65 mmol) was added and the reaction mixture heated to reflux under N_2 for 2 weeks. After cooling to rt, the reaction mixture was filtered and the solvent removed *in vacuo*. The residue was redissolved in $CHCl_3$ (100 mL), filtered, and the solvent removed *in vacuo*. The crude residue was purified by

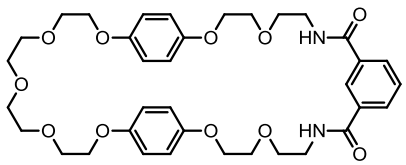
column chromatography (SiO_2, 9:1 CH_2Cl_2:acetone) to give **55** as an oily solid in 77% yield (330 mg, 0.41 mmol). **^{1}H NMR** (300 MHz, $CDCl_3$) δ (ppm): 7.78–7.81 (4H, m, phthalimide-*H*), 7.66–7.68 (4H, m, phthalimide-*H*), 6.71–6.78 (8H, m, hydroquinone-*H*), 4.03 (4H, t, ^3J = 5.0 Hz, CH_2), 3.98 (4H, t, ^3J = 5.0 Hz, CH_2), 3.90 (4H, t, ^3J = 5.5 Hz, CH_2), 3.78–3.81 (12H, m, CH_2), 3.65–3.72 (8H, m, CH_2); **^{13}C NMR** (75.5 MHz, 1:1 $CDCl_3$:CD_3OD) δ (ppm): 168.6, 153.0, 134.1, 132.0, 123.3, 115.5, 70.7, 70.6, 69.8, 69.3, 68.1, 53.5, 37.3, 30.9. **ESIMS** *m/z*: 835.3066 ([M+Na]$^+$, $C_{44}H_{48}NaN_2O_{13}$ requires 835.3049).

Compound 56



Compound **55** (100 mg, 0.1 mmol) was suspended in EtOH (30 mL). $N_2H_4{\cdot}H_2O$ (14 μL, 19 mg, 0.37 mmol) was added and the mixture heated at reflux under N_2 for 3 h. After cooling to rt the reaction mixture was filtered and the solvent removed *in vacuo*. The residue was redissolved in $CHCl_3$, filtered, and the solvent removed *in vacuo* to give **56** as a colourless oil in 97% yield (66 mg, 0.12 mmol). **^{1}H NMR** (300 MHz, $CDCl_3$) δ (ppm): 6.84 (8H, s, hydroquinone-*H*), 4.05–4.09 (8H, m, CH_2), 3.78–3.85 (8H, m, CH_2), 3.67–3.75 (8H, m, CH_2), 3.58 (4H, t, ^3J = 5.5 Hz, CH_2), 2.90 (4H, t, ^3J = 5.5 Hz, CH_2), 2.18 (4H, s, NH_2); **^{13}C NMR** (75.5 MHz, $CDCl_3$) δ (ppm): 153.0, 115.4, 77.2, 73.2, 70.6, 70.5, 69.7, 69.4, 67.9, 41.5; **ESIMS** *m/z*: 553.3120 ([M+Na]$^+$, $C_{28}H_{44}NaN_2O_9$ requires 553.3120).

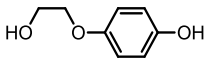
Macrocycle 57



Compound **56** (200 mg, 0.4 mmol), **51·Cl** (140 mg, 0.36 mmol) and Et_3N (0.12 mL, 92.1 mg, 0.91 mmol) were dissolved in anhydrous CH_2Cl_2 (30 mL). A solution of isophthaloyl

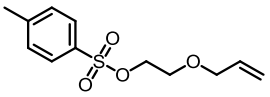
dichloride (74 mg, 0.36 mmol) in anhydrous CH_2Cl_2 (5 mL) was added dropwise and the reaction mixture stirred under N_2 at rt for 16 h. The reaction mixture was washed with 1 M $HCl_{(aq)}$ (2 × 50 mL), H_2O (2 × 50 mL), dried over anhydrous $MgSO_4$, filtered, and the solvent removed *in vacuo*. The crude residue was purified by preparative thin layer chromatography (SiO_2, 95:5 CH_2Cl_2:MeOH) to give **57** as a white solid in 29% yield (71 mg, 0.11 mmol). **^{1}H NMR** (300 MHz, $CDCl_3$) δ (ppm): 8.23 (1H, t, ^4J = 1.7 Hz, isopthaloyl-*H*^{2}), 7.90 (2H, dd, ^3J = 8.0 Hz, ^4J = 1.7 Hz, isophthaloyl-*H*^{4}&*H*^{6}), 7.41 (1H, t, ^3J = 8.0 Hz, isophthaloyl-*H*^{5}), 6.96 (2H, br s, N*H*), 6.79 (8H, s, hydroquinone-*H*), 4.07 (4H, t, ^3J = 4.5 Hz, CH_2), 4.02 (4H, t, ^3J = 4.5 Hz, CH_2), 3.79–3.83 (8H, m, CH_2), 3.65–3.75 (16H, m, CH_2); **^{13}C NMR** (75.5 MHz, $CDCl_3$) δ (ppm): 165.7, 152.3, 151.8, 133.7, 129.1, 127.9, 124.3, 114.7, 76.2, 69.8, 69.8(sic), 68.9, 68.8, 68.5, 67.1, 49.8, 38.8; **ESIMS** *m/z*: 705.2995 ($[M+Na]^+$, $C_{36}H_{46}N_2O_{11}$ requires 705.2994).

4-(2-Hydroxyethoxy)phenol 58[22]



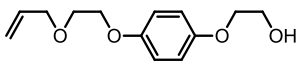
Hydroquinone (10.0 g, 90.8 mmol), 2-chloroethanol (8.33 mL, 9.98 g, 124 mmol) and NaOH (7.10 g, 356 mmol) were dissolved in H_2O (400 mL) heated at reflux under N_2 for 4 h. The mixture was cooled, acidified using 1 M $HCl_{(aq)}$, and extracted with EtOAc (3 × 300 mL). The combined organic phases were dried over anhydrous $MgSO_4$, filtered, and the solvent removed *in vacuo*. The residue was purified using column chromatography (SiO_2, EtOAc) to give compound **58** as an off-white solid in 21% yield (2.96 g, 19.2 mmol). **^{1}H NMR** (300 MHz, $CDCl_3$) δ (ppm): 6.72–6.86 (4H, m, hydroquinone-*H*), 4.62 (1H, s, hydroquinone-O*H*), 4.02–4.05 (2H, m, CH_2OH), 3.93–3.97 (2H, m, OCH_2), 2.06 (1H, s, CH_2O*H*); **ESIMS** *m/z*: 153.1 ($[M-H]^-$, $C_8H_9O_3$ requires 153.1).

2-(4-Allyloxy)ethyl 4-methylbezenesulfonate 59[23]



2-Allyloxyethanol (2.55 g, 25.0 mmol) and *p*-toluenesulfonyl chloride (4.76 g, 25.0 mmol) were dissolved in anhydrous CH_2Cl_2 (100 mL). Anhydrous Et_3N (5.0 mL, 3.8 g, 38 mmol) and 4-DMAP (15 mg, cat.) were added and the mixture stirred at rt under N_2 for 16 h. H_2O (50 mL) was added and the organic phase was separated and washed with H_2O (2 × 50 mL) and sat. $NaCl_{(aq)}$ (50 mL). The combined aqueous phases were re-extracted with CH_2Cl_2 (50 mL). The combined organic phases were dried over anhydrous $MgSO_4$, filtered, and the solvent removed *in vacuo* to give compound **59** as a yellow oil in 94% yield (6.02 g, 23.5 mmol). **^{1}H NMR** (300 MHz, $CDCl_3$) δ (ppm): 7.81 (2H, d, ^3J = 8.0 Hz, Ar*H*), 7.35 (2H, d, ^3J = 8.0 Hz, Ar*H*), 5.76–5.89 (1H, m, C=C*H*), 5.15–5.26 (2H, m, C=CH_2), 4.18 (2H, t, ^3J = 4.5 Hz, SOCH_2), 3.94–3.96 (2H, m, CH_2), 3.62 (2H, t, ^3J = 4.5 Hz, OCH_2CH$_2$S), 2.45 (3H, s, CH_3); **ESIMS** *m/z*: 279.1 ([M+Na]$^+$, $C_{12}H_{16}NaO_4$ requires 279.1).

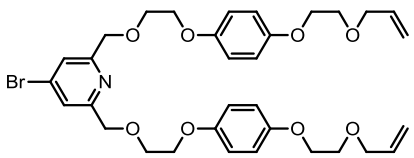
2-(4-(2-(Allyloxy)ethoxy)phenoxy)ethanol 60



Compound **58** (1.80 g, 11.7 mmol), compound **59** (3.00 g, 11.7 mmol) and NaO^{t}Bu (1.27 g, 13.2 mmol) were dissolved in MeCN (150 mL) and heated at reflux under N_2 for 48 h. The mixture was cooled to rt and filtered through Celite®. The solvent was removed *in vacuo* and the resulting residue was purified by column chromatography (SiO_2, EtOAc) to give compound **60** as a cream-coloured solid in 81% yield (2.26 g, 9.48 mmol). **^{1}H NMR** (300 MHz, $CDCl_3$) δ (ppm): 6.83–6.90 (4H, m, hydroquinone-*H*), 5.89–6.02 (1H, m, C=C*H*), 5.19–5.35 (2H, m, C=CH_2), 4.08–4.12 (4H, m, CH_2), 4.03–4.06, (2H, m, CH_2), 3.93–9.97 (2H, m, CH_2), 3.79 (2H, t, ^3J = 5.0 Hz, CH_2), 2.02 (1H, br s, O*H*); **^{13}C NMR**

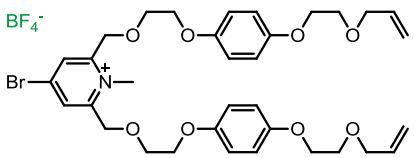
(75.5 MHz, $CDCl_3$) δ (ppm): 153.3, 152.9, 134.5, 117.4, 115.6, 115.4, 72.4, 69.8, 68.6, 68.0, 61.6; **ESIMS** *m/z*: 261.1097 ($[M+Na]^+$, $C_{13}H_{18}NaO_4$ requires 261.1107).

Compound 61



NaH (60% dispersion in mineral oil, 270 mg, 6.8 mmol) was suspended in anhydrous THF (50 mL) and cooled to 0 °C under $N_{2(g)}$. Compound **60** (523 mg, 2.19 mmol) was dissolved in anhydrous THF (20 mL) and added dropwise to the first solution. The mixture was stirred for at rt under N_2 for 30 min. Compound **38** (301 mg, 0.875 mmol) was added and the reaction stirred at rt under N_2 for 6 days. H_2O (50 mL) was added, the volatiles removed *in vacuo* and the aqueous phase was extracted with CH_2Cl_2 (3 × 100 mL). The combined organic phases were dried over anhydrous $MgSO_4$, filtered, and the solvent removed *in vacuo*. The crude residue was purified using column chromatography (SiO_2, 9:1 $CHCl_3$:acetone) to give **61** as a cream-coloured solid in 85% yield (487 mg 0.739 mmol). **^{1}H NMR** (300 MHz, $CDCl_3$) δ (ppm): 7.61 (2H, s, pyridine-H^3&H^5), 6.88 (8H, s, hydroquinone-*H*), 5.89–6.02 (2H, m, C=C*H*), 5.19–5.35 (4H, m, C=CH_2), 4.70 (4H, s, CH_2O), 4.15 (4H, t, ^3J = 4.5 Hz, CH_2), 4.08–4.12 (8H, m, CH_2), 3.91 (4H, t, ^3J = 5.0 Hz, CH_2), 3.79 (4H, t, ^3J = 4.5 Hz, CH_2); **^{13}C NMR** (75.5 MHz, $CDCl_3$): 159.4, 153.2, 153.0, 134.5, 123.2, 117.3, 115.6, 115.5, 73.4, 72.4, 69.7, 68.6, 68.0, 67.9; **ESIMS** *m/z*: 680.1845 ($[M+Na]^+$, $C_{33}H_{40}BrNaNO_8$ requires 680.1830).

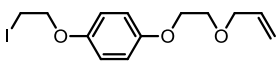
Compound 62·BF$_4$



Compound **61** (50 mg, 0.08 mmol) was dissolved in anhydrous CH_2Cl_2 (30 mL). $[Me_3O]BF_4$ (15 mg, 0.10 mmol) was added and the reaction stirred at rt under N_2 for 4 days. MeOH

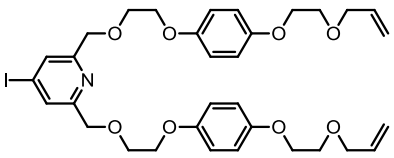
(5 drops) was added and the solvent removed *in vacuo*. The crude residue was purified using preparative thin layer chromatography (SiO_2, 9:1 CH_2Cl_2:MeOH) to give **62·BF$_4$** as a pale orange oil in 38% yield (22 mg, 0.030 mmol). **^{1}H NMR** (300 MHz, $CDCl_3$) δ (ppm): 8.22 (2H, s, pyridinium-*H*^{3}&*H*^{5}), 6.85 (8H, s, hydroquinone-*H*), 5.88–6.01 (2H, m, C=C*H*), 5.19–5.34 (4H, m, C=C*H*$_2$), 4.94 (4H, s, OC*H*$_2$), 4.00–4.14 (16H, m, C*H*$_2$), 3.97 (3H, s, C*H*$_3$), 3.77 (4H, t, ^3J = 5.0 Hz, C*H*$_2$); **^{13}C NMR** (75.5 MHz, $CDCl_3$) δ (ppm): 153.3, 152.6, 143.6, 134.5, 128.7, 117.3, 115.6, 115.4, 72.3, 70.7, 68.6, 68.0, 67.9, 38.8; **^{19}F NMR** (282.4 MHz, $CDCl_3$) δ (ppm): −153.1–−153.2 (m, B*F*$_4$); **ESIMS** *m/z*: 672.2163 ($[M-BF_4]^+$, $C_{34}H_{43}BrNO_8$ requires 672.2167).

Compound 63



Compound **60** (300 mg, 1.26 mmol), imidazole (360 mg, 1.40 mmol) and triphenyl phosphine (408 mg, 1.56 mmol) were dissolved in anhydrous CH_2Cl_2 (100 mL). A solution of I_2 (408 mg, 1.61 mmol) in anhydrous CH_2Cl_2 (100 mL) was added in portions and the reaction stirred under N_2 at rt for 16 h. The solvent was removed *in vacuo* and the crude residue purified by column chromatography (SiO_2, 9:1 CH_3Cl:acetone) to give **63** as a pale yellow solid in 93% yield (407 mg, 1.17 mmol). **^{1}H NMR** (300 MHz, $CDCl_3$) δ (ppm): 6.86 (4H, s, hydroquinone-*H*), 5.88–6.03 (1H, m, C=C*H*), 5.19–5.35 (2H, m, C=C*H*$_2$), 4.20 (2H, t, ^3J = 6.8 Hz, C*H*$_2$), 4.07–4.11 (4H, m, C*H*$_2$), 3.78 (2H, t, ^3J = 5.1 Hz, C*H*$_2$), 3.39 (2H, t, ^3J = 6.8 Hz, C*H*$_2$); **ESIMS** *m/z*: 371.0102 ($[M+Na]^+$, $C_{13}H_{17}INaO_3$ requires 371.0115).

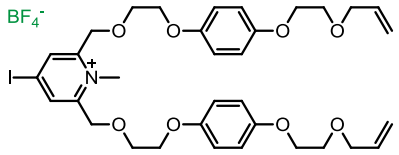
Compound 64



NaH (107 mg, 2.68 mmol) was suspended in anhydrous THF (100 mL) and cooled to 0 °C. Compound **60** (250 mg, 1.05 mmol) was added and the reaction stirred at rt under N_2 for

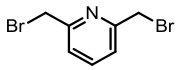
30 min. Compound **42** (174 mg, 0.359 mmol) was added and the reaction stirred at rt under N_2 for 72 h. H_2O (100 mL) was added and the THF removed *in vacuo*. The aqueous mixture was extracted with CH_2Cl_2 (3 × 100 mL) and the combined organic phases dried over anhydrous $MgSO_4$, filtered, and the solvent removed *in vacuo*. The crude residue was purified by column chromatography (SiO_2, 9:1 CH_2Cl_2:acetone) to give **64** as a pale yellow solid in 56% yield (144 mg, 0.20 mmol). **^{1}H NMR** (300 MHz, $CDCl_3$) δ (ppm): 7.82 (2H, s, pyridine-H^3&H^5), 6.88 (8H, s, hydroquinone-*H*), 5.89–6.02 (2H, m, C=C*H*), 5.19–5.35 (4H, m, C=CH_2), 4.68 (4H, s, OCH_2) 4.15 (4H, t, ^3J = 4.7 Hz, CH_2), 4.08–4.11 (8H, m, CH_2), 3.91 (4H, t, ^3J = 4.7 Hz, CH_2), 3.79 (4H, t, ^3J = 5.0 Hz, CH_2); **^{13}C NMR** (75.5 MHz, $CDCl_3$) δ (ppm): 152.7, 152.5, 146.5, 134.1, 128.7, 116.9, 115.2, 115.1, 103.1, 72.8, 71.9, 69.3, 68.2, 67.6, 67.4; **ESIMS** *m/z*: 728.1699 ([M+Na]$^+$, $C_{33}H_{40}INNaO_8$ requires 728.1691).

Compound 65·BF$_4$



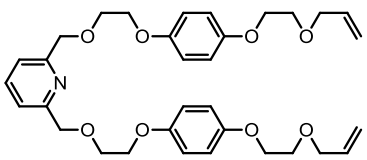
Compound **64** (28 mg, 38 μmol) was dissolved in anhydrous CH_2Cl_2 (10 mL). $[Me_3O]BF_4$ (7.60 mg, 51.4 μmol) was added and the reaction mixture was stirred at rt under N_2 for 48 h. MeOH (5 drops) was added and the solvent removed *in vacuo*. The crude residue was purified by preparative thin layer column chromatography (SiO_2, 95:5 CH_2Cl_2:MeOH) to give **65·BF$_4$** as a pale orange oily solid in 51% yield (15.5 mg, 19.4 μmol). **^{1}H NMR** (300 MHz, $CDCl_3$) δ (ppm): 8.41 (2H, s, pyridinium-H_3&H_5), 6.86 (8H, s, hydroquinone-*H*), 5.88–6.01 (2H, m, C=C*H*), 5.20–5.35 (4H, m, C=CH_2), 4.93 (4H, s, CH_2O), 4.13–4.15 (4H, m, CH_2), 4.07–4.10 (8H, m, CH_2), 4.01–4.04 (4H, m, CH_2), 3.98 (3H, s, CH_3), 3.78 (4H, t, ^3J = 4.9 Hz, CH_2); **^{13}C NMR** (75.5 MHz, $CDCl_3$) δ (ppm): 154.8, 153.3, 152.7, 135.0, 134.5, 117.4, 115.7, 115.5, 72.3, 70.7, 68.6, 68.0, 67.7, 67.5, 38.9; **^{19}F NMR** (282.4 MHz, $CDCl_3$) δ (ppm): −153.1–−153.0 (m, BF_4); **ESIMS** *m/z*: 720.2018 ([M−BF_4]$^+$, $C_{34}H_{43}INO_8$ requires 720.2028).

Compound 66[24]



2,6-Pyridinedimethanol (2.00 g, 14.4 mmol) was suspended in $CHCl_3$ (100 mL) and a solution of PBr_3 (2.02 mL, 5.84 g, 21.6 mmol) in $CHCl_3$ (40 mL) was added. The reaction mixture was heated at reflux under N_2 for 16 h. After cooling to rt, the reaction was neutralised with 5% $NaHCO_{3(aq)}$, the organic phase was separated, washed with H_2O (6 × 50 mL), dried over anhydrous $MgSO_4$, filtered, and the solvent removed *in vacuo* to give **66** as a white solid in 84% yield (3.18 g, 12.1 mmol). **^{1}H NMR** (300 MHz, $CDCl_3$) δ (ppm): 7.12 (1H, t, ^3J = 8.0 Hz, pyridine-H^4), 7.39 (2H, d, ^3J = 8.0 Hz, pyridine-H^3&H^5), 4.55 (4H, s, CH_2); **ESIMS** *m/z*: 265.9 ($[M+H]^+$, $C_7H_8Br_2N$ requires 265.9).

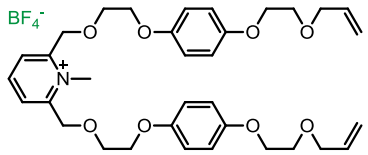
Compound 67



NaH (60% dispersion in mineral oil, 168 mg, 4.20 mmol) was suspended in anhydrous THF (50 mL), cooled to 0 °C and compound **60** (224 mg, 0.940 mmol) in anhydrous THF (10 mL) was added dropwise. After stirring at rt under N_2 for 30 min, compound **66** was added. The reaction mixture was stirred at rt under N_2 for 2 weeks after which H_2O (100 mL) was added and the THF removed *in vacuo*. The aqueous mixture was extracted with CH_2Cl_2 (3 × 100 mL), dried over anhydrous $MgSO_4$, filtered, and the solvent removed *in vacuo*. The crude residue was purified by column chromatography (SiO_2, 9:1 CH_2Cl_2:acetone) to give **67** as a white solid in 82% yield (406 mg, 0.700 mmol). **^{1}H NMR** (300 MHz, $CDCl_3$) δ (ppm): 7.70 (1H, t, ^3J = 8.1 Hz, pyridine-H^4), 7.40 (2H, d, ^3J = 8.1 Hz, pyridine-H^3&H^5), 6.86 (8H, s, hydroquinone-*H*), 5.88–6.01 (2H, m, C=C*H*), 5.18–5.34 (4H, m, C=CH_2), 4.73 (4H, s, CH_2O), 4.06–4.15 (12H, m, CH_2), 3.90 (4H, t, ^3J = 4.8 Hz, CH_2), 3.77 (4H, t, ^3J = 5.0 Hz, CH_2); **^{13}C NMR** (75.5 MHz, $CDCl_3$) δ (ppm): 157.7, 153.0, 137.2, 134.5, 120.0, 117.2, 115.5,

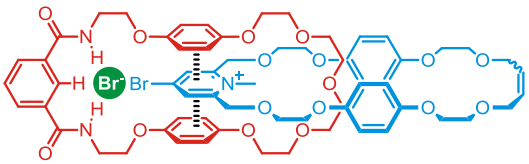
74.0, 72.3, 69.4, 68.5, 67.9, 67.9(*sic*), 30.2, 29.6; **ESIMS** *m/z*: 580.2891 ($[M+H]^+$, $C_{33}H_{42}NO_8$ requires 580.2905).

Compound 68·BF$_4$



Compound **67** (100 mg, 0.2 mmol) was dissolved in anhydrous CH_2Cl_2 (50 mL) and $[Me_3O]BF_4$ (31 mg, 0.21 mmol) was added. The reaction mixture was stirred at rt under N_2 for 72 h after which time MeOH (5 drops) was added and the solvent removed *in vacuo*. The crude residue was purified by column chromatography (SiO_2, 95:5 CH_2Cl_2:MeOH) to give **68·BF$_4$** as a pale yellow oil in 33% yield (33.2 mg, 55.8 μmol). **^{1}H NMR** (300 MHz, $CDCl_3$) δ (ppm): 8.29 (1H, t, ^3J = 8.0 Hz, pyridinium-*H*^{4}), 8.03 (2H, d, ^3J = 8.0 Hz, pyridinium-*H*^{3}&*H*^{5}), 6.80-6.87 (8H, m, hydroquinone-*H*), 5.88–6.01 (2H, m, C=C*H*), 5.19–5.35 (4H, m, C=CH_2), 5.00 (4H, s, CH_2), 4.06–4.14 (15H, m, CH_2 & NCH_3), 4.02–3.99 (4H, m, CH_2), 3.78 (4H, t, ^3J = 4.7 Hz, CH_2); **^{13}C NMR** (75.5 MHz, $CDCl_3$) δ (ppm): 155.5, 153.3, 152.6, 144.7, 134.5, 126.1, 117.3, 115.6, 115.5, 72.3, 70.5, 68.6, 68.0, 67.6, 39.2; **^{19}F NMR** (282.5 MHz, $CDCl_3$) δ (ppm): −153.8–−153.2 (m, B*F*$_4$); **ESIMS** *m/z*: 594.3047 ($[M-BF_4]^+$, $C_{34}H_{44}NO_8$ requires 594.3061).

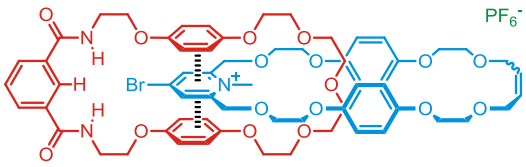
Catenane 69·Br



Compound **52** (50 mg, 80 μmol) and **62·Br** (68.4 mg, 90.8 μmol) were dissolved in anhydrous CH_2Cl_2 (5 mL) and stirred at rt under N_2 for 30 min. Grubbs' II (7 mg, 10% by wt.) was added and the reaction mixture stirred at rt under N_2 for 3 days after which time more Grubbs' II (3.5 mg) was added and the reaction mixture stirred for a further 24 h. The solvent

was removed *in vacuo* and the crude residue purified by preparative thin layer chromatography (95:5 CH_2Cl_2:MeOH and 3:2 MeCN:CH_2Cl_2) to give **69·Br** as a white solid in 8% yield (9.0 mg, 6.8 μmol). **^{1}H NMR** (300 MHz, $CDCl_3$) δ (ppm): 9.30 (1H, s, isophthaloyl-*H*^{2}), 8.84 (2H, br s, amide-N*H*), 8.33 (2H, d, ^3J = 7.6 Hz, isophthaloyl-*H*^{4}&*H*^{6}), 8.03 (2H, s, pyridinium-*H*^{3}&*H*^{5}), 7.59 (1H, t, ^3J = 7.6 Hz, isophthaloyl-*H*^{5}), 6.86 (4H, d, ^3J = 8.9 Hz, hydroquinone-*H*), 6.80 (4H, d, ^3J = 8.9 Hz, hydroquinone-*H*), 6.31 (4H, d, ^3J = 8.8 Hz, hydroquinone-*H*), 6.08 (4H, d, ^3J = 8.8 Hz, hydroquinone-*H*), 5.73 (2H, s, alkene-C*H*), 4.53 (3H, s, NCH_3), 4.26 (4H, br s, CH_2), 4.16 (4H, br s, CH_2), 4.07–4.09 (4H, m, CH_2), 3.97–3.98 (12H, m, CH_2), 3.72–3.74 (4H, m, CH_2), 3.59–3.66 (12H, m, CH_2), 3.46–3.50 (8H, m, CH_2); **^{13}C NMR** (75.5 MHz, $CDCl_3$) δ (ppm): 166.7, 153.6, 153.4, 153.2, 152.2, 151.3, 138.5, 133.8, 131.8, 130.0, 128.9, 128.9, 128.7, 124.6, 115.9, 115.5, 114.9, 114.4, 71.1, 71.1(*sic*), 70.5, 70.0, 69.7, 68.9, 68.3, 67.8, 66.5, 39.8, 29.7; **ESIMS** *m*/*z*: 1238.4457 ([M−Br]$^+$, $C_{64}H_{77}BrN_3O_{17}$ requires 1238.4431).

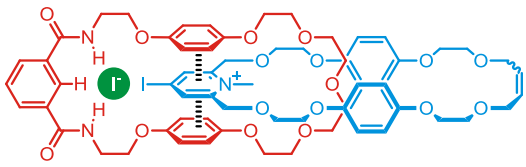
Catenane 69·PF$_6$



Compound **69·Br** (8.50 mg, 6.16 μmol) was dissolved in CH_2Cl_2 (20 mL), washed with 0.1 M $NH_4PF_{6(aq)}$ (10 × 10 mL), H_2O (2 × 10 mL), dried over $MgSO_4$, filtered, and the solvent removed *in vacuo* to give **69·PF$_6$** as an off-white solid in 81% yield (7.66 mg, 5.53 μmol). **^{1}H NMR** (300 MHz, $CDCl_3$) δ (ppm): 8.25 (2H, d, ^3J = 7.8 Hz, isophthaloyl-*H*^{4}&*H*^{6}), 8.12 (1H, s, isophthaloyl-*H*^{2}), 7.61 (1H, t, ^3J = 7.8 Hz, isophthaloyl-*H*^{5}), 7.48 (2H, s, pyridinium-*H*^{3}&*H*^{5}), 7.13 (2H, s, amide-N*H*), 6.79–6.83 (8H, s, hydroquinone-*H*), 6.35 (4H, d, ^3J = 8.8 Hz, hydroquinone-*H*), 6.14 (4H, d, ^3J = 8.8 Hz, hydroquinone-*H*), 5.78 (2H, s, alkene-C*H*), 4.66 (3H, s, NCH_3), 4.22 (4H, s, CH_2), 4.00–4.06 (16H, m, CH_2), 3.90–3.91 (4H, m, CH_2), 3.74–3.75 (4H, m, CH_2), 3.63 (4H, s, CH_2), 3.59 (4H, s, CH_2), 3.50 (8H, s, CH_2), 3.45 (4H, s, CH_2); **^{13}C NMR** (125.8 MHz, $CDCl_3$) δ (ppm): 166.7, 160.6, 153.9, 153.5,

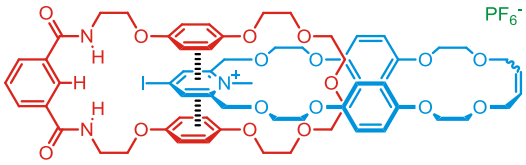
153.2, 152.4, 151.5, 142.7, 140.4, 134.5, 131.7, 129.3, 129.0, 115.7, 115.4, 114.9, 71.1, 70.5, 70.1, 70.1(*sic*), 69.1, 68.2, 68.1, 67.1, 66.7, 66.5, 50.9, 39.6, 29.7; **^{19}F NMR** (282.4 MHz, $CDCl_3$) δ (ppm): −71.1 (d, J = 712 Hz, PF_6); **^{31}P NMR** (202.4 MHz, $CDCl_3$) δ (ppm): −144.0 (sept, J = 712 Hz, PF_6); **ESIMS** *m/z*: 1238.4423 ($[M-PF_6]^+$, $C_{64}H_{77}BrN_3O_{17}$ requires 1238.4431).

Catenane 70·I



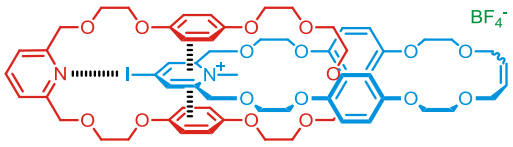
Compound **52** (71 mg, 120 μmol) and compound **65·I** (92.5 mg, 109 μmol) were dissolved in anhydrous CH_2Cl_2 (5 mL) and stirred at rt under N_2 for 30 min. Grubbs' II (9.3 mg, 10% by wt.) was added and the reaction mixture stirred at rt under N_2 for 3 days after which time more Grubbs' II (4.5 mg) was added and the reaction mixture stirred for a further 24 h. The solvent was removed *in vacuo* and the crude residue purified by preparative thin layer chromatography (95:5 CH_2Cl_2:MeOH and 3:2 MeCN:CH_2Cl_2) to give **70·I** as a white solid in 8% yield. (13.5 mg, 9.44 μmol). **^{1}H NMR** (500 MHz, $CDCl_3$) δ (ppm): 9.02 (1H, s, isophthaloyl-H^2), 8.44 (2H, br s, amide-NH), 8.29 (2H, d, ^3J = 7.6 Hz, isophthaloyl-H^4&H^6), 7.95 (2H, s, pyridinium-H^3&H^5), 7.58 (1H ,t, ^3J = 7.6 Hz, isophthaloyl-H^5), 6.83 (8H, s, hydroquinone-H), 6.43 (4H, d, ^3J = 8.8 Hz, hydroquinone-H), 6.12 (4H, d, ^3J = 8.8 Hz, hydroquinone-H), 4.67 (4H, s, CH_2), 4.30–4.32 (4H, m, CH_2), 4.00–4.07 (16H, m, CH_2), 3.79 (3H, s, NCH_3) 3.73–3.75 (4H, m, CH_2), 3.60 (4H, s, CH_2), 3.55 (4H, s, CH_2), 3.46–3.47 (4H, m, CH_2), 3.40 (4H, s, CH_2); **^{13}C NMR** (125.8 MHz, $CDCl_3$) δ (ppm): 166.8, 153.6, 153.3, 152.4, 151.8, 151.4, 135.2, 134.1, 131.9, 128.9, 124.4, 120.3, 115.8, 115.5, 115.0, 114.8, 71.19, 71.12, 70.5, 70.1, 69.8, 69.0, 68.3, 68.0, 67.0, 66.8, 66.7, 39.4, 29.7; **ESIMS** *m/z*: 1286.4300 ($[M-I]^+$, $C_{64}H_{77}IN_3O_{17}$ requires 1286.4292).

Catenane 70·PF$_6$



Compound **70·I** (13.5 mg, 9.44 μmol) was dissolved in CH_2Cl_2 (20 mL), washed with 0.1 M $NH_4PF_{6(aq)}$ (10 × 10 mL), H_2O (2 × 10 mL), dried over $MgSO_4$, filtered, and the solvent removed *in vacuo* to give **70·PF$_6$** as an off-white solid in 67% yield (9.13 mg, 6.37 μmol). **^{1}H NMR** (500 MHz, $CDCl_3$) δ (ppm): 8.23 (2H, d, ^3J = 7.6 Hz, isophthaloyl-*H*^{4}&*H*^{6}), 8.15 (1H, s, isophthaloyl-*H*^{2}), 7.63 (2H, s, pyridinium-*H*^{3}&*H*^{5}), 7.60 (1H, t, ^3J = 7.6 Hz, isophthaloyl-*H*^{5}), 7.13 (2H, br s, amide-N*H*), 6.79–6.88 (8H, m, hydroquinone-*H*), 6.41 (4H, d, ^3J = 8.7 Hz, hydroquinone-*H*), 6.15 (4H, d, ^3J = 8.7 Hz, hydroquinone-*H*), 6.79 (2H, s, alkene-C*H*), 4.68 (4H, s, C*H*$_2$), 4.23 (4H, s, C*H*$_2$), 4.01–4.07 (16H, m, C*H*$_2$), 3.93–3.94 (4H, m, C*H*$_2$), 3.86 (3H, s, NC*H*$_3$), 3.74–3.76 (4H, m, C*H*$_2$), 3.62 (4H, s, C*H*$_2$), 3.57 (4H, s, C*H*$_2$), 3.48 (4H, s, C*H*$_2$), 3.42 (4H, s, C*H*$_2$); **^{13}C NMR** (125.8 MHz, $CDCl_3$) δ (ppm): 166.6, 153.4, 153.2, 152.5, 151.5, 150.6, 134.9, 134.5, 131.7, 129.3, 129.0, 115.6, 115.5, 115.0, 114.9, 71.1, 70.5, 70.0, 69.9, 69.1, 68.2, 68.1, 66.9, 66.7, 66.4, 34.1, 29.0; **^{31}P NMR** (MHz, $CDCl_3$) δ (ppm) −144.0 (sept, *J* = 716 Hz, *P*F$_6$); **ESIMS** m/z: 1286.4287 ([M−PF$_6$]$^+$, $C_{64}H_{77}IN_3O_{17}$ requires 1286.4292).

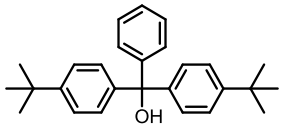
Catenane 74·BF$_4$



Compound **65·BF$_4$** (75.6 mg, 97.0 μmol) and **71** (50.0 mg, 88.0 μmol) were dissolved in anhydrous CH_2Cl_2 (3 mL). Grubbs' II catalyst (7.6 mg, 10% by wt.) was added and the reaction mixture stirred under N_2 at rt for 4 days. A further portion of Grubbs' II catalyst (3.5 mg) was added and the reaction mixture stirred for a further 24 h. The solvent was removed *in vacuo* and the crude residue purified by preparative thin layer column

chromatography (SiO_2, 9:1 CH_2Cl_2:MeOH, 9:1 EtOAc:MeCN and 1:1 CH_2Cl_2:MeCN) to give **74·BF_4** in 6.5% yield (8.56 mg, 6.35 μmol). **^{1}H NMR** (300 MHz, $CDCl_3$) δ (ppm): 7.79 (1H, t, ^3J = 7.6 Hz, pyridine-*H*^{4}), 7.38–7.40 (4H, m, pyridine-*H*^{3}&*H*^{5}, pyridinium-*H*^{3}&*H*^{5}), 6.84–6.87 (4H, m, hydroquinone-*H*), 6.77–6.80 (4H, m, hydroquinone-*H*), 6.43–6.46 (4H, m, hydroquinone-*H*), 6.31–6.34 (4H, m, hydroquinone-*H*), 5.79 (2H, s, alkene-C*H*), 4.89 (4H, s, N(CH_3)CC*H*$_2$), 4.19–4.22 (4H, m, C*H*$_2$), 4.11–4.12 (4H, m, C*H*$_2$), 3.97–4.04 (15H, m, C*H*$_2$, C*H*$_3$), 3.93–3.95 (4H, s, C*H*$_2$), 3.72–3.75 (4H, m, C*H*$_2$), 3.57–3.65 (12H, m, C*H*$_2$), 3.46 (4H, br s, C*H*$_2$); **^{13}C NMR** (125.8 MHz, $CDCl_3$) δ (ppm): 153.1, 152.8, 152.8(*sic*), 152.7, 152.3, 134.4, 128.9, 115.6, 115.4, 115.3, 115.0, 71.1, 70.5, 70.0, 69.9, 69.6, 69.0, 68.2, 68.1, 67.6, 67.1, 66.7, 29.7, 14.1; **^{19}F NMR** (282.4 MHz, acetone-d_6) δ (ppm): −151.83–−151.78 (m, B*F*$_4$); **ESIMS** *m/z*: 1261.4345 ($[M-BF_4]^+$, $C_{63}H_{78}IN_2O_{17}$ requires 1261.4340).

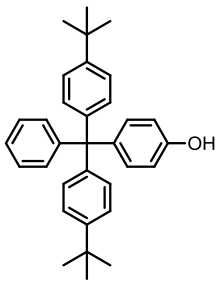
Compound 75[25]



To a flame-dried 250 mL three-necked round-bottomed flask equipped with a condenser, dropping funnel and magnetic stirrer bar were added Mg turnings (6.00 g, 124 mmol) followed by anhydrous THF (enough to cover the turnings) and I_2 (cat.), and the mixture stirred until the iodine colour disappeared. A solution of 1-bromo-4-*tert*-butyl benzene (40.0 mL, 227 mmol) in anhydrous THF (120 mL) was added dropwise and the reaction mixture heated at reflux under N_2 for 2 h. Methyl benzoate (13.6 mL, 108 mmol) in anhydrous THF (15 mL) was added over 30 min and the reaction heated at reflux under N_2 for 18 h. After cooling to rt, the reaction was quenched with 10% $HCl_{(aq)}$, and extracted with hexanes (2 × 20 mL). The combined organic phases were then washed with H_2O (2 × 200 mL), dried over anhydrous $MgSO_4$, filtered, and the solvent removed *in vacuo*. Recrystallisation from MeOH afforded **75** as a white crystalline solid in 80 % yield (32.4 g,

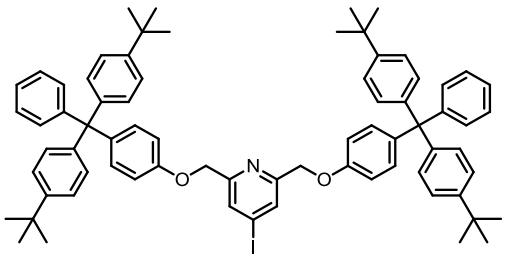
86.9 mmol). **^{1}H NMR** (300 MHz, $CDCl_3$) δ (ppm): 7.23–7.48 (13H, m, Ar*H*), 3.06 (1H, s, O*H*), 1.31 (18H, s, CH_3); **ESIMS** *m/z*: 355.2 ($[M-OH]^+$, $C_{27}H_{31}$ requires 355.2).

Stopper-alcohol compound 76[25]



Compound **75** (6.50 g, 17.4 mmol) was dissolved in molten phenol (25.0 g, 23.3 mL, 266 mmol) and conc. HCl (1 mL, cat.) was added. The reaction mixture was heated at reflux under N_2 for 16 h. The crude mixture was extracted with toluene (3 × 100 mL) and the combined organic phases were washed with H_2O (3 × 250 mL), phases dried over anhydrous $MgSO_4$, filtered, and the solvent removed *in vacuo*. The resulting white solid was washed with hexanes to give pure **76** as an off-white solid in 68% yield (5.32 g, 11.9 mmol). **^{1}H NMR** (300 MHz, $CDCl_3$) δ (ppm): 7.18–7.26 (9H, m, Ar*H*), 7.05–7.11 (6H, m, Ar*H*), 6.71 (2H, d, ^3J = 8.5 Hz, OCC*H*), 4.60 (1H, br s, O*H*), 1.31 (18H, s, C(CH_3)$_3$); **ESIMS** *m/z*: 471.3 ($[M+Na]^+$, $C_{33}H_{36}NaO$ requires 471.3).

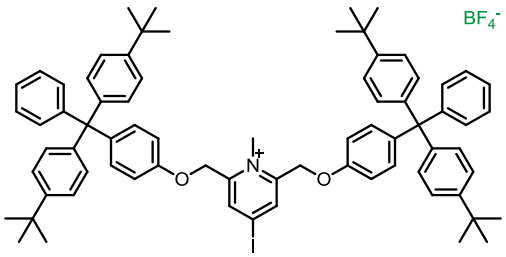
Compound 77



NaH (60% dispersion in mineral oil, 59.6 mg, 1.49 mmol) was suspended in anhydrous THF (20 mL) and cooled to 0° C. Compound **76** (350 mg, 0.77 mmol) was added and the solution stirred at rt under N_2 for 30 min. Compound **42** (94 mg, 0.19 mmol) was added and the reaction mixture stirred at rt under N_2 for 3 weeks. H_2O (50 mL) was added and the THF

removed *in vacuo*. The aqueous mixture was extracted with CH_2Cl_2 (5 × 50 mL), and the combined organic phases dried over anhydrous $MgSO_4$, filtered, and the solvent removed *in vacuo*. The crude residue was purified by preparative thin layer chromatography (SiO_2, 99:1 CH_2Cl_2:acetone) to give **77** as a pale yellow solid in 84% yield (180 mg, 0.16 mmol). **^{1}H NMR** (300 MHz, $CDCl_3$) δ (ppm): 7.91 (2H, s, pyridine-*H*^{3}&*H*^{5}), 7.20–7.28 (16H, m, Ar*H*), 7.10–7.17 (14H, m, Ar*H*), 6.88 (4H, d, ^3J = 8.7 Hz, OCC*H*), 5.14 (4H, s, CH_2O), 1.32 (36H, s, C(CH_3)$_3$); **^{13}C NMR** (75.5 MHz, $CDCl_3$) δ (ppm): 157.6, 155.9, 148.4, 147.2, 143.8, 140.2, 132.3, 131.1, 130.6, 129.3, 127.2, 125.7, 124.1, 113.3, 69.6, 63.4, 34.2, 31.3, 29.7; **ESIMS** *m*/*z*: 1126.4979 ($[M+H]^+$, $C_{73}H_{77}INO_2$ requires 1126.4994).

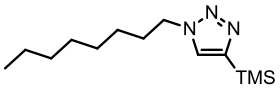
Compound 78·BF$_4$



Compound **77** (110 mg, 0.98 mmol) and $[Me_3O]BF_4$ (22 mg, 0.15 mmol) were dissolved in anhydrous CH_2Cl_2 and stirred for 48 h. MeOH (5 drops) was added and the solvent removed *in vacuo*. The crude residue was purified by preparative thin layer chromatography (95:5 CH_2Cl_2:MeOH) to give **78·BF$_4$** as an off-white solid in 45% yield (54.3 mg, 44.2 mmol). **^{1}H NMR** (300 MHz, $CDCl_3$) δ (ppm): 8.45 (2H, s, pyridinium-*H*^{3}&*H*^{5}), 7.18–7.25 (18H, m, Ar*H*), 7.07–7.11 (12H, m, Ar*H*), 6.90 (4H, d, ^3J = 9.1 Hz, Ar*H*), 5.38 (4H, s, CH_2), 4.19 (3H, s, NCH_3), 1.31 (36H, s, C(CH_3)$_3$); **^{13}C NMR** (300 MHz, $CDCl_3$) δ (ppm): 154.6, 153.3, 148.4, 147.0, 142.0, 136.6, 132.7, 131.0, 130.6, 127.3, 125.8, 124.3, 118.5, 113.7, 65.6, 63.5, 40.2, 34.3, 31.4; **^{19}F NMR** (282.4 MHz, $CDCl_3$) δ (ppm): −153.38–−153.32 (m, B*F*$_4$); **ESIMS** *m*/*z*: 1140.5159 ($[M-BF_4]^+$, $C_{74}H_{79}INO_2$ requires 1140.5150).

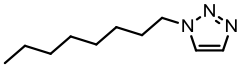
6.4 Experimental procedures for Chapter Four

1-Octyl-4-(trimethylsilyl)-1*H*-1,2,3-triazole 82[26]



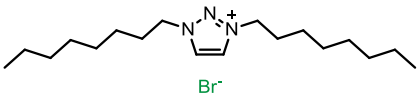
Compound **17** (1.33 g, 8.57 mmol) and trimethlysilylacetylene (1.68 g, 17.1 mmol) were dissolved in anhydrous CH_2Cl_2 (50 mL). $[Cu(MeCN)_4]PF_6$ (0.32 g, 0.86 mmol), TBTA (0.50 g, 0.94 mmol) and D*i*PEA (2.91 mL, 17.1 mmol) were added and the mixture was stirred at rt under N_2 for 48 h. The solvent was removed *in vacuo* and the resulting pale brown oil was purified by column chromatography (SiO_2, 95:5 CH_2Cl_2:acetone) to give compound **82** as a colourless oil in 47% yield (1.03 g, 4.03 mmol). **^{1}H NMR** (300 MHz, $CDCl_3$) δ (ppm): 7.50 (1H, s, triazole-*H*), 4.37 (2H, t, ^3J = 7.5 Hz, NCH_2), 1.86–1.95 (2H, m, CH_2), 1.21–1.38 (10H, m, CH_2), 0.88 (3H, t, ^3J = 7.0 Hz, CH_3), 0.33 (12H, s, CH_3); **ESIMS** *m/z*: 254.2 ($[M+H]^+$, $C_{13}H_{28}N_3Si$ requires 254.2).

1-Octyl-1*H*-1,2,3-triazole 83[26]



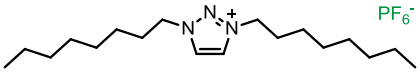
Compound **82** (1.03 g, 4.06 mmol) was dissolved in anhydrous THF (100 mL), TBA·F (1 M solution in THF, 8.13 mL, 8.13 mmol) was added and the reaction was stirred at rt under N_2 for 24 h. The solvent was removed *in vacuo* and the resulting residue was redissolved in 1:1 hexanes:H_2O (400 mL) and stirred vigorously for 15 min. The organic layer was separated, washed with H_2O (2 × 200 mL), and the combined aqueous fractions were extracted with hexanes (100 mL). The combined organic phases were washed with H_2O, dried over anhydrous $MgSO_4$, filtered, and the solvent was removed *in vacuo* to give compound **83** as a colourless oil in 89% yield (0.66 g, 3.6 mmol). **^{1}H NMR** (300 MHz, $CDCl_3$) δ (ppm): 7.70 (1H, s, triazole-*H*), 7.54 (1H, s, triazole-*H*), 4.38 (2H, t, ^3J = 7.5 Hz, NCH_2), 1.86–1.95 (2H, m, CH_2), 1.24–1.31 (10H, m, CH_2), 0.87 (3H, t, ^3J = 7.0 Hz, CH_3).

*1,3-Dioctyl-1*H*-1,2,3-triazol-3-ium bromide 84·Br*



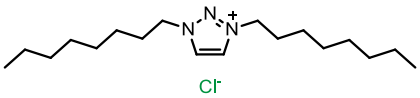
Compound **83** (657 mg, 3.62 mmol) and 1-*n*-octylbromide (10 mL, excess) were heated at 80 °C under N_2 for 5 days. The reaction mixture was cooled to rt and Et_2O (30 mL) was added. The mixture was filtered and the solid was washed with cold Et_2O to give compound **84·Br** as an off-white solid in 83% yield (1.12 g, 2.99 mmol). **^{1}H NMR** (300 MHz, $CDCl_3$) δ (ppm): 9.57 (2H, s, triazolium-*H*), 4.76 (4H, t, ^3J = 7.5 Hz, NCH_2), 2.01–2.11 (4H, m, CH_2), 1.27–1.35 (20H, m, CH_2), 0.88 (3H, t, ^3J = 6.5 Hz, CH_3); **^{13}C NMR** (300 MHz, $CDCl_3$) δ (ppm): 131.6, 54.3, 31.6, 29.6, 28.9, 28.7, 26.1, 22.6, 14.0; **ESIMS** *m/z*: 294.2903 ($[M-Br]^+$, $C_6H_{12}N_3$ requires 294.2904).

*1,3-Dioctyl-1*H*-1,2,3-triazol-3-ium hexafluorophosphate 84·PF$_6$*



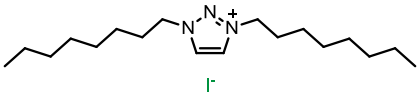
Compound **84·Br** (200 mg, 0.53 mmol) was dissolved in $CHCl_3$ (50 mL) and washed with 0.1 M $NH_4PF_{6(aq)}$ (10 × 10 mL) and H_2O (2 × 10 mL). The organic phase was dried over anhydrous $MgSO_4$, filtered, and the solvent removed *in vacuo* to give compound **84·PF$_6$** as a pale orange oil in 85% yield (198 mg, 0.450 mmol). **^{1}H NMR** (300 MHz, $CDCl_3$) δ (ppm): 8.42 (2H, s, triazolium-*H*), 4.58 (4H, t, ^3J = 7.4 Hz, NCH_2), 1.97–2.06 (4H, m, CH_2), 1.21–1.40 (20H, m, CH_2), 0.88 (6H, t, ^3J = 6.8 Hz, CH_3); **^{13}C NMR** (75.5 MHz, $CDCl_3$) δ (ppm): 130.6, 54.1, 31.6, 29.3, 28.9, 28.7, 26.0, 22.6, 14.0; **^{19}F NMR** (282.4 MHz, $CDCl_3$) δ (ppm): −72.4 (d, J = 712 Hz, PF_6); **^{31}P NMR** (121.5 MHz, $CDCl_3$) δ (ppm): −155.6 (sept, J = 712 Hz, PF_6); **ESIMS** *m/z*: 294.2909 ($[M-PF_6]^+$, $C_{18}H_{26}N_3$ requires 294.2904).

*1,3-Dioctyl-1*H*-1,2,3-triazol-3-ium chloride 84·Cl*



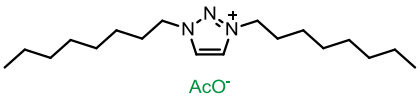
Compound **84·Br** (0.20 g, 0.53 mmol) was dissolved in $CHCl_3$ (50 mL) and washed with sat. $NH_4Cl_{(aq)}$ (10 × 10 mL) and H_2O (2 × 10 mL). The organic phase was dried over anhydrous $MgSO_4$, filtered, and the solvent removed *in vacuo* to give compound **84·Cl** as an off-white solid in 88% yield (0.15 g, 0.47 mmol). **^{1}H NMR** (300 MHz, $CDCl_3$) δ (ppm): 9.41 (2H, s, triazolium-*H*), 4.77 (4H, t, ^3J = 7.4 Hz, NCH_2), 2.04–2.12 (4H, m, CH_2), 1.27–1.36 (20H, m, CH_2), 0.88 (3H, t, ^3J = 6.8 Hz, CH_3); **^{13}C NMR** (300 MHz, $CDCl_3$) δ (ppm): 131.8, 54.1, 31.6, 29.6, 29.0, 28.8, 26.1, 22.6, 14.0; **ESIMS** *m/z*: 294.2907 ($[M-Cl]^+$, $C_{18}H_{26}N_3$ requires 294.2904).

*1,3-Dioctyl-1*H*-1,2,3-triazol-3-ium iodide 84·I*



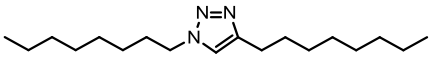
Compound **84·Br** (0.10 g, 0.27 mmol) was dissolved in $CHCl_3$ (30 mL) and washed with sat. $NH_4I_{(aq)}$ (10 × 10 mL) and H_2O (2 × 10 mL). The organic phase was dried over anhydrous $MgSO_4$, filtered, and the solvent removed *in vacuo* to give compound **84·I** as a yellow solid in 79% yield (88.9 mg, 0.211 mmol). **^{1}H NMR** (300 MHz, $CDCl_3$) δ (ppm): 9.77 (2H, s, triazolium-*H*), 4.76 (4H, t, ^3J = 7.4 Hz, NCH_2), 2.01–2.11 (4H, m, CH_2), 1.27–1.35 (20H, m, CH_2), 0.88 (3H, t, ^3J = 6.8 Hz, CH_3); **^{13}C NMR** (300 MHz, $CDCl_3$) δ (ppm): 131.3, 54.3, 31.5, 29.6, 28.9, 28.7, 26.0, 22.5, 13.9; **ESIMS** *m/z*: 294.2909 ($[M-I]^+$, $C_{18}H_{26}N_3$ requires 294.2904).

1,3-Dioctyl-1*H*-1,2,3-triazol-3-ium iodide 84·AcO



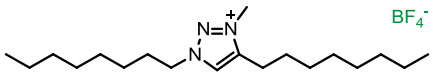
Compound **84·Br** (50 g, 0.13 mmol) was dissolved in $CHCl_3$ (30 mL) and washed with sat. $NH_4AcO_{(aq)}$ (10 × 10 mL) and H_2O (2 × 10 mL). The organic phase was dried over anhydrous $MgSO_4$, filtered, and the solvent removed *in vacuo* to give compound **84·AcO** as a yellow solid in 91% yield (41.6 mg, 0.118 mmol). **^{1}H NMR** (300 MHz, $CDCl_3$) δ (ppm): 9.68 (2H, s, triazolium-*H*), 4.66 (4H, t, ^3J = 7.4 Hz, NCH_2), 1.96–2.02 (7H, m, CH_2 & CH_3), 1.25–1.32 (20H, m, CH_2), 0.86 (3H, t, ^3J = 6.8 Hz, CH_3); **^{13}C NMR** (300 MHz, $CDCl_3$) δ (ppm): 177.4, 132.4, 53.8, 31.6, 29.5, 28.9, 28.7, 26.0, 24.2. 22.5, 14.0; **ESIMS** *m/z*: 294.2902 ($[M-OAc]^+$, $C_6H_{12}N_3$ requires 294.2904).

1,4-Dioctyl-1*H*-1,2,3-triazole 85



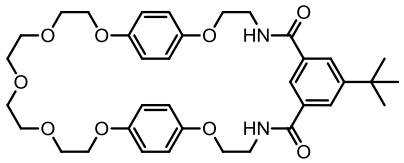
Compound **17** (257 mg, 2.67 mmol) was dissolved in MeOH (15 mL) and sodium L-ascorbate (110 mg, 0.53 mmol), $CuSO_4{\cdot}5H_2O$ (63 mg, 0.40 mmol) and 1-decyne (0.59 mL, 370 mg, 2.70 mmol) were added and the mixture was stirred at rt under N_2 for 3 days. H_2O (70 mL) was added and the aqueous layer extracted with EtOAc (3 × 70 mL). The combined organic phases were washed with sat. $NaCl_{(aq)}$ (70 mL), dried over anhydrous $MgSO_4$, filtered, and the solvent removed *in vacuo*. The resulting residue was purified by column chromatography (SiO_2, 96:4 CH_2Cl_2:MeOH) to give compound **85** as a colourless oil in 27% yield (21 mg, 0.72 mmol). **^{1}H NMR** (300 MHz, $CDCl_3$) δ (ppm): 7.24 (1H, s, triazole-*H*), 4.31 (2H, t, ^3J = 7.5 Hz, NCH_2), 2.71 (2H, t, ^3J = 8.0 Hz, CHCCH_2), 1.84–1.94 (2H, m, NCH_2CH_2), 1.62–1.73 (2H, m, $CHCCH_2CH_2$), 1.24–1.38 (20H, m, CH_2) 0.86–0.90 (6H, m, CH_3); **^{13}C NMR** (75.5 MHz, $CDCl_3$) δ (ppm): 173.3, 119.9, 109.7, 49.7, 31.4, 31.3, 29.9, 29.1, 28.9, 28.9(*sic*), 28.8, 28.6, 28.6(*sic*), 26.1, 25.3, 22.2, 13.7, 13.6; **ESIMS** *m/z*: 294.2900 ($[M+H]^+$, $C_{19}H_{35}N_3$ requires 294.2904).

3-Methyl-1,4-dioctyl-1H-1,2,3-triazol-3-ium tetrafluoroborate 86·BF_4



Compound **85** (210 mg, 0.72 mmol) was dissolved in anhydrous CH_2Cl_2 (40 mL) and $[Me_3O]BF_4$ (212 mg, 1.43 mmol) was added. The mixture was stirred at rt under N_2 for 16 h then MeOH (5 drops) was added. The solvent was removed *in vacuo* and the resulting residue purified by column chromatography (SiO_2, 95:5 CH_2Cl_2:MeOH) to give compound **86·BF_4** in as a pale yellow oil 44% yield (126 mg, 0.319 mmol). **^{1}H NMR** (300 MHz, $CDCl_3$) δ (ppm): 8.33 (1H, s, triazolium-*H*), 4.53 (2H, t, ^3J = 7.6 Hz, NCH_2), 2.82 (2H, t, ^3J = 8.0 Hz, CCH_2), 1.94–2.04 (2H, m, NCH$_2$CH_2), 1.69–1.79 (2H, m, CCH$_2$CH_2), 1.22–1.47 (20H, m, CH_2), 0.86–0.90 (6H, m, CH_3); **^{13}C NMR** (75.5 MHz, $CDCl_3$) δ (ppm): 144.9, 128.2, 54.0, 37.3, 31.7, 31.6, 29.2, 29.1, 29.0, 28.9, 28.8, 26.9, 26.1, 23.3, 22.6, 22.6(*sic*), 14.0; **ESIMS** *m/z*: 308.3060 ($[M-BF_4]^+$, $C_{19}H_{38}N_3$, requires 308.3057).

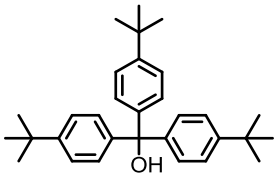
Macrocycle 87[17,27]



5-*tert*-Butylisophthalic acid (240 mg, 1.1 mmol) was suspended in $SOCl_2$ (10 mL) and heated at reflux under N_2 for 18 h until the solution became homogenous. The $SOCl_2$ was removed by distillation and the residue redissolved in anhydrous CH_2Cl_2 (10 mL) and added dropwise to a solution of **49** (500 mg, 1.1 mmol), **51·Cl** (415 mg, 1.08 mmol) and Et_3N (0.38 mL, 270 mg, 2.7 mmol) in anhydrous CH_2Cl_2 (90 mL). The reaction was stirred for 2 h, washed with 10% $HCl_{(aq)}$ (2 × 100 mL), H_2O (2 × 100 mL), dried over anhydrous $MgSO_4$, filtered, and the solvent removed *in vacuo*. The crude residue was purified by column chromatography (SiO_2, 98:2 CH_2Cl_2:MeOH) to give **87** as a white solid in 32% yield (222 mg, 0.341 mmol). **^{1}H NMR** (300 MHz, $CDCl_3$) δ (ppm): 8.08 (2H, s, isophthaloyl-H^4&H^6), 7.77 (1H, s, isophthaloyl-H^2), 6.78–6.86 (2H, m, N*H*), 6.76 (8H, s, hydroquinone-*H*), 4.01–4.09 (8H, br

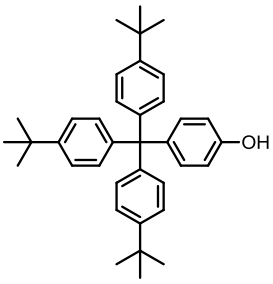
m, CH_2), 3.83–3.86 (8H, m, CH_2), 3.69–3.73 (8H, m, CH_2), 1.35 (9H, s, C(CH_3)$_3$); **ESIMS** *m/z*: 673.3 ([M+Na]$^+$, $C_{36}H_{46}N_2NaO_9$ requires 673.3).

Tris(4-*tert*-butylpheny1)methanol 88[28]



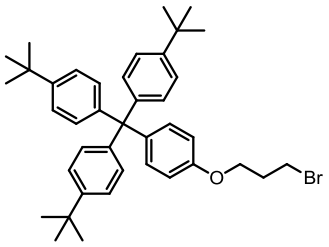
Mg turnings (2.9 g, 0.12 mol) were washed with 60–80 petroleum ether and dried, *in vacuo* with heating, in a three-necked, round-bottomed flask. After cooling to rt anhydrous THF (160 mL) and I_2 (few crystals, cat.) were added. 1-Bromo-4-*tert*-butyl benzene (20 mL, 21.2 g, 0.1 mol) was dissolved in anhydrous THF (60 mL) and 5 mL of this was added to the magnesium suspension under N_2. The remaining 1-bromo-4-*tert*-butyl benzene solution was added continually to maintain a gentle reflux and the mixture was then heated at reflux for 1 h under N_2. Anhydrous diethyl carbonate (4.66 mL, 4.49 g, 38.0 mmol) was dissolved in anhydrous THF and added dropwise to the reaction mixture. The mixture was heated at reflux under N_2 for 1 h and, after cooling to rt, ice (128 g) and conc. H_2SO_4 (11.2 mL) were added. The volume was reduced by half *in vacuo* and the solution extracted with CH_2Cl_2 (3 × 60 mL). The combined organic phases were washed with 5% $Na_2CO_{3(aq)}$ (80 mL) and H_2O (80 mL), dried over anhydrous $MgSO_4$, filtered, and the solvent was removed *in vacuo*. The resulting solid was triturated with hexanes then filtered to give compound **88** as a white powder in 55% yield (8.88 g, 20.7 mmol). **^{1}H NMR** (300 MHz, $CDCl_3$) δ (ppm): 7.32 (6H, d, ^3J = 8.0 Hz, Ar*H*), 7.14–7.25 (6H, m, Ar*H*), 2.73 (1H, s, O*H*), 1.32 (27H, s, CH_3); **ESIMS** *m/z*: 411.3 ([M−OH]$^+$, $C_{31}H_{39}$ requires 411.3).

4-(Tris(4-*tert*-butylpheny1)methyl)phenol 89[29]



Compound **88** (2.00 g, 4.67 mmol) was dissolved in molten phenol (26.0 mL, 27.8 g, excess) by warming in a round-bottomed flask over an oil bath. Conc. $HCl_{(aq)}$ (0.5 mL, cat.) was added and the mixture heated at reflux under N_2 for 24 h. KOH (20 g, 0.36 mol) in H_2O (50 mL) was added and the mixture was extracted with toluene (3 × 55 mL). The combined organic phases were washed with 1 M $NaOH_{(aq)}$ (3 × 200 mL), H_2O (3 × 100 mL), dried over anhydrous $MgSO_4$, filtered, and the solvent removed *in vacuo*. The resulting solid was washed with hexanes and dried *in vacuo* to give compound **89** as an off-white solid in 68% yield (1.60 g, 3.17 mmol). **^{1}H NMR** (300 MHz, $CDCl_3$) δ (ppm): 7.24 (6H, d, ^3J = 8.0 Hz, Ar*H*), 7.04–7.11 (8H, m, Ar*H*), 6.71 (2H, d, ^3J = 9.0 Hz, OCC*H*), 5.31 (1H, s, O*H*), 1.31 (27H, s, $C(CH_3)_3$); **ESIMS** *m/z*: 503.4 ($[M-H]^-$, $C_{37}H_{43}O$ requires 503.3).

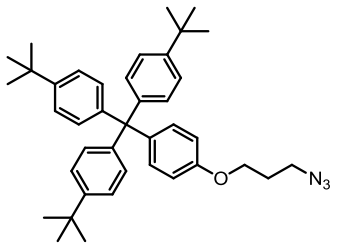
Bromo-functionalised stopper 90[30]



Compound **89** (1.25 g, 2.48 mmol) and 1,3-dibromopropane (3.00 g, 14.9 mmol) were dissolved in anhydrous MeCN (50 mL). K_2CO_3 (0.46 g, 3.3 mmol) was added and the mixture was heated at reflux under N_2 for 16 h. CH_2Cl_2 (50 mL) was added, the mixture was filtered, and the solvent was removed *in vacuo*. The solid was redissolved in CH_2Cl_2 (50 mL), washed with H_2O (3 × 50 mL), dried over anhydrous $MgSO_4$, filtered, and the solvent removed *in vacuo*. The solid was purified by column chromatography (SiO_2, 2:1 40–60

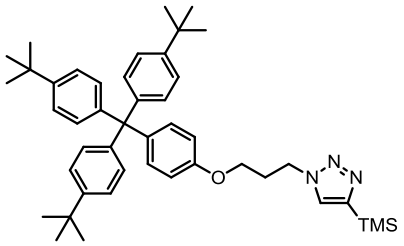
petroleum ether:CH_2Cl_2) to give compound **90** as a white solid in 66% yield (0.96 g, 1.6 mmol). **^{1}H NMR** (300 MHz, $CDCl_3$) δ (ppm): 7.24 (6H, d, ^3J = 8.8 Hz, Ar*H*), 7.07–7.11 (8H, m, Ar*H*), 6.77 (2H, d, ^3J = 8.8 Hz, OCC*H*), 4.09 (2H, t, ^3J = 5.9 Hz, OCH_2), 3.61 (2H, t, ^3J = 6.5 Hz, CH_2Br), 2.24–2.37 (2H, m, CH_2), 1.31 (27H, s, C(CH_3)$_3$); **ESIMS** *m*/*z*: 659.3 ([M+Cl]$^-$, $C_{40}H_{49}ClBrO$ requires 659.3).

Azide-functionalised stopper 91[30]



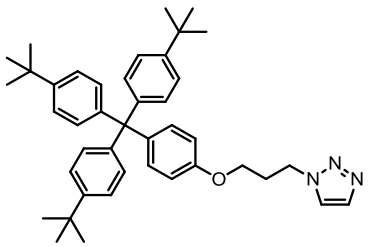
Compound **90** (1.30 g, 2.08 mmol) and NaN_3 (483 mg, 7.44 mmol) were dissolved in DMF (30 mL) and heated at 80 °C under N_2 for 16 h. The mixture was partitioned between EtOAc (125 mL) and H_2O (125 mL), the organic phase was separated and washed with H_2O (2 × 100 mL), dried over anhydrous $MgSO_4$ and filtered. The solvent was removed *in vacuo* and the residue was purified by column chromatography (SiO_2, 2:1 40–60 petroleum ether:CH_2Cl_2) to give compound **91** as a white solid in 68% yield (827 mg, 1.41 mmol). **^{1}H NMR** (300 MHz, $CDCl_3$) δ (ppm): 7.24 (6H, d, ^3J = 9.0 Hz, Ar*H*), 7.05–7.11 (8H, m, Ar*H*), 6.77 (2H, d, ^3J = 9.0 Hz, OCC*H*), 4.03 (2H, t, ^3J = 6.5 Hz, OCH_2), 3.52 (2H, t, ^3J = 7.0 Hz, CH_2N), 2.00–2.09 (2H, m, CH_2), 1.31 (27H, s, C(CH_3)$_3$); **ESIMS** *m*/*z*: 610.4 ([M+Na]$^+$, $C_{40}H_{49}NaN_3O$ requires 610.4).

Trimethylsilyl triazole stopper 92



Compound **91** (0.50 g, 0.86 mmol) and trimethylsilyl acetylene (0.24 mL, 1.7 mmol) were dissolved in anhydrous CH_2Cl_2 (50 mL). $[Cu(MeCN)_4]PF_6$ (32 mg, 85 μmol), TBTA (50.5 mg, 94.0 μmol) and D*i*PEA (0.30 mL, 220 mg, 1.70 mmol) were added and the reaction stirred at rt under N_2 for 48 h. The mixture was washed with 10% $NH_4OH_{(aq)}$ (3 × 50 mL) and the organic phase was dried over anhydrous $MgSO_4$, filtered, and solvent removed *in vacuo*. The resulting solid was purified by column chromatography (SiO_2, 4:1 CH_2Cl_2:acetone) to give compound **92** as a white solid in 80% yield (463 mg, 0.675 mmol). **^{1}H NMR** (300 MHz, $CDCl_3$) δ (ppm): 7.53 (1H, s, triazole-*H*), 7.26 (6H, d, ^3J = 9.0 Hz, Ar*H*), 7.09–7.13 (8H, m, Ar*H*), 6.76 (2H, d, ^3J = 9.0 Hz, OCC*H*), 4.62 (2H, t, ^3J = 6.5 Hz, OCH_2), 3.95 (2H, t, ^3J = 8.0 Hz, CH_2N), 2.36–2.44 (2H, m, CH_2), 1.32 (27H, s, C(CH_3)$_3$), 0.33 (9H, s, Si(CH_3)$_3$); **^{13}C NMR** (75.5 MHz, $CDCl_3$) δ (ppm): 156.2, 148.4, 144.0, 140.1, 133.8, 132.3, 130.7, 124.0, 123.9, 112.9, 110.0, 63.8, 63.0, 46.9, 34.3, 31.4, 30.0; **ESIMS** *m*/*z*: 686.4499 ($[M+H]^+$, $C_{45}H_{60}N_3OSi$ requires 686.4500).

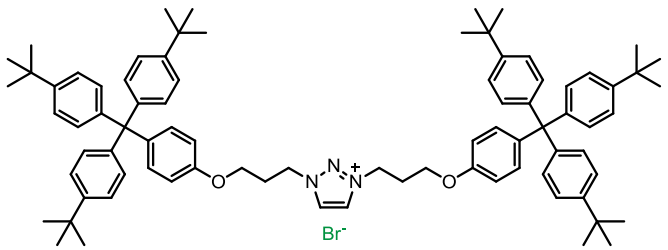
Triazole stopper 93



TBA·F (1 M in THF, 0.15 mL, 0.15 mmol) was added to a solution of compound **92** (50 mg, 73 μmol) in anhydrous THF (25 mL). The mixture was stirred at rt under N_2 for 48 h and the reaction followed by TLC. The solvent was removed *in vacuo* and the residue was purified

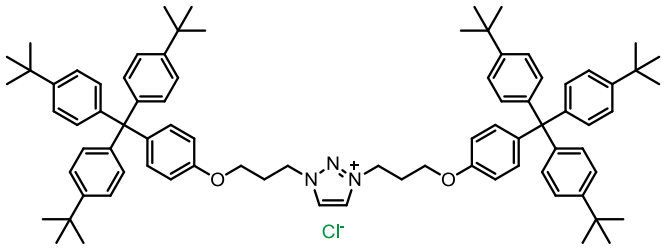
using column chromatography (SiO_2, 1:1 EtOAc:hexanes) to give compound **93** as a white solid in 93% yield (41.7 mg, 68.0 μmol). **^{1}H NMR** (300 MHz, $CDCl_3$) δ (ppm): 7.71 (1H, s, triazole-*H*), 7.57 (1H, s, triazole-*H*) 7.25 (6H, d, ^3J = 9.0 Hz, Ar*H*), 7.06–7.12 (8H, m, Ar*H*), 6.76 (2H, d, ^3J = 9.0 Hz, Ar*H*), 4.63 (2H, t, ^3J = 6.6 Hz, OCH_2), 3.94 (2H, t, ^3J = 5.7 Hz, CH_2N), 2.36–2.45 (2H, m, CH_2), 1.31 (27H, s, CH_3); **^{13}C NMR** (75.5 MHz, $CDCl_3$) δ (ppm): 163.6 158.7, 148.4, 144.0, 140.1, 135.1, 132.4, 130.7, 124.1, 112.9, 110.0, 63.7, 46.6, 34.3, 31.4, 30.0; **ESIMS** *m/z*: 636.3932 ([M+Na]$^+$, $C_{42}H_{51}NaN_3O$ requires 636.3924).

Bromide triazolium axle 94·Br



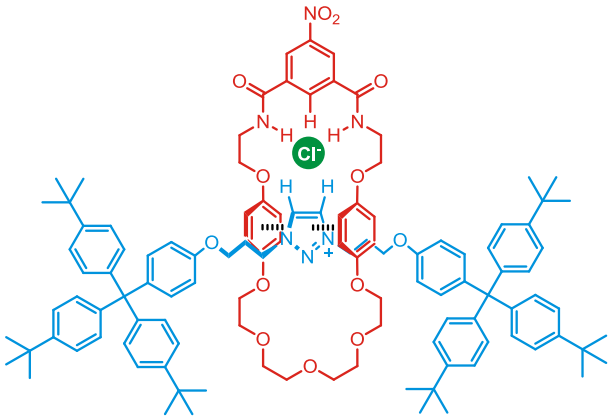
Compound **93** (200 mg, 0.3 mmol) and compound **91** (410 mg, 0.65 mmol) and NaI (10 mg, cat.) were heated at 150 °C in acetone (4 mL) in a sealed vial under microwave radiation for 3 h. The solvent was removed *in vacuo* and the resulting solid was purified using column chromatography (SiO_2, 95:5 CH_2Cl_2:MeOH), after removal of the starting materials the eluent polarity was gradually increased (9:1 CH_2Cl_2:MeOH) to elute compound **94·Br** as an off-white solid in 61% yield (246 mg, 0.198 mmol). **^{1}H NMR** (300 MHz, $CDCl_3$) δ (ppm): 9.21 (2H, s, triazolium-*H*), 7.22 (12H, d, ^3J = 8.6 Hz, Ar*H*), 7.03–7.09 (16H, m, Ar*H*), 6.62 (4H, d, ^3J = 9.0 Hz, OCC*H*), 4.96 (4H, t, ^3J = 6.6 Hz, OCH_2), 3.99 (4H, t, ^3J = 5.7 Hz, CH_2), 2.44–2.53 (4H, m,CH_2), 1.29 (54H, s, CH_3); **^{13}C NMR** (75.5 MHz, $CDCl_3$) δ (ppm): 155.7, 148.4, 143.9, 140.5, 132.4, 131.5, 130.6, 124.1, 112.8, 63.7, 63.0, 53.4, 52.0, 34.3, 31.4; **ESIMS** *m/z*: 1158.7798 ([M−Br]$^+$, $C_{82}H_{100}N_3O$ requires 1158.7810).

Chloride triazolium axle 94·Cl



Compound **94·Br** (77.0 mg, 62.1 μmol) was dissolved in $CHCl_3$ (50 mL) and washed with sat. $NH_4Cl_{(aq)}$ (10 × 25 mL) and H_2O (2 × 25 mL). The organic phase was dried over anhydrous $MgSO_4$, filtered, and the solvent removed *in vacuo* to give compound **94·Cl** as a yellow solid in 73% yield (52.0 mg, 45.0 μmol). **^{1}H NMR** (300 MHz, $CDCl_3$) δ (ppm): 9.81 (2H, s, triazolium-*H*), 7.21 (12H, d, ^3J = 8.6 Hz, Ar*H*), 7.04–7.08 (16H, m, Ar*H*), 6.60 (4H, d, ^3J = 9.1 Hz, OCC*H*), 4.96 (4H, t, ^3J = 6.6 Hz, OCH_2), 3.96 (4H, t, ^3J = 5.7 Hz, CH_2), 2.45–2.53 (4H, m, CH_2), 1.29 (54H, s, CH_3); **^{13}C NMR** (75.5 MHz, $CDCl_3$) δ (ppm): 155.8, 148.3, 143.9, 140.3, 132.3, 131.9, 130.6, 124.1, 112.8, 63.8, 63.0, 51.6, 34.3, 31.4, 29.3; **ESIMS** *m/z*: 1158.7795 ($[M-Cl]^+$, $C_{82}H_{100}N_3O$ requires 1158.7810).

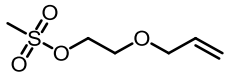
Rotaxane 95·Cl



5-Nitroisophthalic acid (100 mg, 0.48 mmol) was suspended in $SOCl_2$ (10 mL) and heated at reflux under N_2 for 16 h until the solution became homogenous. The $SOCl_2$ was removed by distillation and the residue immediately redissolved in anhydrous CH_2Cl_2 (10 mL). This was added dropwise to a solution of compound **49** (223 mg, 0.480 mmol), compound **94·Cl**

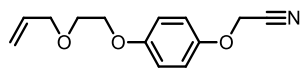
(200 mg, 0.2 mmol) and Et_3N (0.17 mL, 1.2 mmol) in anhydrous CH_2Cl_2 (20 mL) that had been stirred vigorously for 30 min at rt under N_2. The mixture was stirred at rt under N_2 for 2 h then washed with 10% citric $acid_{(aq)}$ (2 × 50 mL) and H_2O (50 mL), dried over $MgSO_4$, filtered, and the solvent was removed *in vacuo*. The crude mixture was purified by column chromatography (SiO_2, 9:1 CH_2Cl_2:MeOH) and preparative thin layer chromatography (SiO_2, 1:1 CH_2Cl_2:MeCN) to give **95·Cl** as a white solid in 0.5% yield (1.4 mg, 0.76 μmol). **^{1}H NMR** (500 MHz, $CHCl_3$) δ (ppm): 9.85 (1H, br s, isophthaloyl-*H*^{2}), 9.31 (2H, br s, amide-N*H*), 9.05 (2H, s, isophthaloyl-*H*^{4}&*H*^{6}), 8.33 (2H, br s, triazolium-*H*), 7.24 (6H, d, ^3J = 8.6 Hz, axle-Ar*H*), 7.17 (4H, d, ^3J = 9.1 Hz, axle-Ar*H*). 7.10 (6H, d, ^3J = 8.6 Hz, axle-Ar*H*), 6.75 (4H, d, ^3J = 9.1, axle-Ar*H*), 6.57 (4H, d, ^3J = 8.8 Hz, hydroquinone-*H*), 6.32 (4H, d, ^3J = 8.8 Hz, hydroquinone-*H*), 4.45 (4H, t, ^3J = 6.6 Hz, CH_2), 4.23 (4H, br s, CH_2), 3.94 (8H, t, ^3J = 4.9 Hz, CH_2), 3.68–3.69 (4H, m, CH_2), 3.56–3.62 (8H, m, CH_2), 2.22 (4H, br quin, ^3J = 5.7 Hz, CH_2), 1.30 (54H, s, CH_3); **ESIMS** *m/z*: 1798.0256 ($[M-Cl]^+$, $C_{114}H_{137}N_6O_{13}$ requires 1798.0238).

2-(Allyloxy)ethyl methyl sulfonate 96[31]



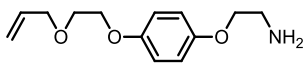
2-Allyloxyethanol (7.50 mL, 7.16 g, 70.1 mmol) and Et_3N (20.2 mL, 14.8 g, 145 mmol) were dissolved in anhydrous CH_2Cl_2 (100 mL) and stirred at 0 °C under N_2. Methanesulfonyl chloride (6.40 mL, 9.47 g, 82.7 mmol) dissolved in anhydrous CH_2Cl_2 (100 mL) was added dropwise. The mixture was stirred at rt under N_2 for 1 h then washed with H_2O (2 × 75 mL), 1 M $HCl_{(aq)}$ (3 × 50 mL) and sat. $NaCl_{(aq)}$ (3 × 75 mL). The organic phase was dried over anhydrous $MgSO_4$, filtered, and the solvent removed *in vacuo* to give compound **96** as an orange oil in 89% yield (12.1 g, 66.9 mmol). **^{1}H NMR** (300 MHz, $CDCl_3$) δ (ppm): 5.84–5.98 (1H, m, C=C*H*), 5.27–5.34 (1H, m, C=CH_2), 5.20–5.25 (1H, m, C=CH_2), 4.38–4.41 (2H, m, CH_2CH_2OS), 3.71–3.74 (2H, m, OCH_2CH_2OS), 3.07 (3H, s, SCH_3); **ESIMS** *m/z*: 203.0 ($[M+Na]^+$, $C_6H_{12}NaO_4S$ requires 203.0).

2-(4-(2-(Allyloxy)ethoxy)phenoxy)acetonitrile 97[32]



Compound **46** (3.30 g, 22.0 mmol), compound **96** (3.98 g, 22.0 mmol) and K_2CO_3 (7.70 g, 48.0 mmol) were suspended in anhydrous CH_3CN (250 mL) and heated at reflux under N_2 for 16 h. The mixture was cooled to rt, filtered, and the solvent removed *in vacuo*. The residue was dissolved in CH_2Cl_2 (50 mL) and washed with 1 M $HCl_{(aq)}$ (2 × 50 mL), H_2O (2 × 50 mL), 10% $NaOH_{(aq)}$ (2 × 50 mL), H_2O (2 × 50 mL) and sat. $NaCl_{(aq)}$ (2 × 50 mL). The organic phase was dried over anhydrous $MgSO_4$, filtered, and the solvent removed *in vacuo*. The residue was purified by column chromatography (SiO_2, 7:3 hexanes:EtOAc) to give compound **97** as a clear yellow oil in 44% yield (2.28 g, 9.80 mmol). **^{1}H NMR** (300 MHz, $CDCl_3$) δ (ppm): 6.89–6.96 (4H, m, hydroquinone-*H*), 5.89–6.02 (1H, m, C=C*H*), 5.29–5.36 (1H, m, C=CH_2), 5.20–5.24 (1H, m, C=CH_2), 4.72 (2H, s, CH_2CN), 4.09–4.16 (4H, m, CH_2), 3.78–3.81 (2H, m, CH_2); **ESIMS** *m/z*: 256.1 ($[M+Na]^+$, $C_{13}H_{15}NaNO_3$ requires 256.1).

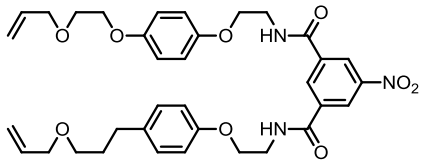
2-(4-(2-(Allyloxy)ethoxy)phenoxy)ethanamine 98[32]



Compound **97** (2.28 g, 9.77 mmol) was dissolved in anhydrous Et_2O (100 mL) and added dropwise to a suspension of $LiAlH_4$ (0.64 g, 17 mmol) in anhydrous Et_2O (100 mL). The mixture was heated at reflux under N_2 for 3 h then cooled to rt. $Na_2SO_4{\cdot}10H_2O$ (3.00 g, 9.32 mmol) was added and the mixture stirred at rt under N_2 for 2 h then filtered. The filtrate was dried with anhydrous $MgSO_4$, filtered, and the solvent removed *in vacuo* to give compound **98** as an orange oil in 85% yield (1.97 g, 8.30 mmol). **^{1}H NMR** (300 MHz, $CDCl_3$) δ (ppm): 6.72–6.97 (4H, m, hydroquinone-*H*), 5.88–6.01 (1H, m, C=C*H*), 5.29–5.35 (1H, m, C=CH_2), 5.17–5.23 (1H, m, C=CH_2), 4.01–4.14 (4H, m, CH_2), 3.94 (2H, t,

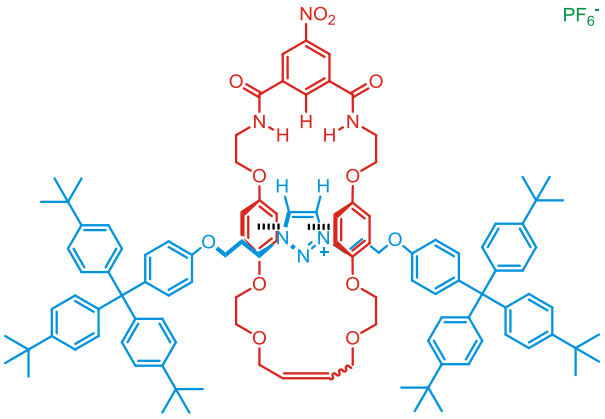
^3J = 5.0 Hz, CH_2), 3.78 (2H, t, ^3J = 4.5 Hz, CH_2), 3.06 (2H, t, ^3J = 5.0 Hz, NCH_2), 1.65 (2H, br s, NH_2); **ESIMS** *m/z*: 238.2 ($[M+H]^+$, $C_{13}H_{20}NO_3$ requires 238.1).

Bis-vinyl-appended macrocycle precursor 99[33]



5-Nitroisophthalic acid (675 mg, 3.20 mmol) was suspended in $SOCl_2$ (10 mL), DMF (5 drops, cat.) was added and the mixture was heated at reflux under N_2 for 16 h until the solution became homogenous. The $SOCl_2$ was removed by distillation and the resulting solid was redissolved in anhydrous CH_2Cl_2 and added dropwise to a solution of compound **98** (1.50 g, 6.34 mmol) and Et_3N (13.5 mL, 9.81 g, 96.9 mmol) in anhydrous CH_2Cl_2 (100 mL) that had been stirred for 10 min. The mixture was stirred at rt under N_2 for 1 h then washed with 10% $HCl_{(aq)}$ (3 × 100 mL) and H_2O (3 × 100 mL). The organic phase was dried over anhydrous $MgSO_4$, filtered, and the solvent removed *in vacuo*. The resulting residue was purified by column chromatography (SiO_2, 7:3 EtOAc:CH_2Cl_2) to give compound **99** as a yellow solid in 23% yield (0.52 g, 0.80 mmol). **^{1}H NMR** (300 MHz, $CDCl_3$) δ (ppm): 8.75 (2H, s, isophthaloyl-H^4&H^6), 8.54 (1H, s, isophthaloyl-H^2), 6.82–6.89 (10H, m, amide-N*H* & hydroquinone-*H*), 5.88–6.02 (2H, m, C=C*H*), 5.19–5.35 (4H, m, C=CH_2), 4.04–4.17 (12H, m, CH_2), 3.87–3.92 (4H, m, CH_2), 3.77–3.80 (4H, m, CH_2); **ESIMS** *m/z*: 672.3 ($[M+Na]^+$, $C_{34}H_{39}NaN_3O_{10}$ requires 672.3).

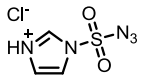
Rotaxane 100·PF$_6$



Compound **94·Cl** (0.20 g, 170 μmol) and compound **99** (217 mg, 335 μmol) were dissolved in anhydrous CH_2Cl_2 (5 mL) and stirred at rt under N_2 for 30 min. Grubbs' II catalyst (21.7 mg, 10% by wt.) was added and the reaction mixture stirred at rt under N_2 for 3 days. Di(ethylene glycol) vinyl ether (14.0 μL, 102 μmol) was added to quench the Grubbs' II catalyst and the solvent was removed *in vacuo* without heating. Following purification using column chromatography (SiO_2, 9:1 CH_2Cl_2:MeOH) and preparative thin layer chromatography (SiO_2, 1:1 CH_2Cl_2:MeCN) **100·Cl** was isolated as an off-white solid (1.3% yield, 4.2 mg, 2.2 μmol). This was dissolved in $CHCl_3$ (10 mL) and washed with 0.1 M $NH_4PF_{6(aq)}$ (10 × 10 mL), H_2O (2 × 10 mL), dried over anhydrous $MgSO_4$, filtered, and the solvent removed *in vacuo* to give **100·PF$_6$** as a pale yellow oily solid in 1.2% over two steps (3.97 mg, 2.00 μmol). **^{1}H NMR** (500 MHz, 1:1 $CDCl_3$:CD_3OD) δ (ppm): 8.81 (2H, d, ^4J = 1.4 Hz, isophthaloyl-H^4&H^6), 8.74 (2H, t, ^3J = 5.4 Hz, amide-N*H*), 8.57 (1H, br t, ^4J = 1.4 Hz, isophthaloyl-H^2), 8.17 (2H, s, triazolium-*H*), 7.21 (12H, d, ^3J = 8.6 Hz, axle-Ar*H*), 7.11 (4H, d, ^3J = 9.0 Hz, axle-Ar*H*), 7.07 (12H, d, ^3J = 8.6 Hz, axle-Ar*H*), 6.62 (4H, d, ^3J = 9.0 Hz, axle-Ar*H*), 6.59 (4H, d, ^3J = 9.2 Hz, hydroquinone-*H*), 6.44 (4H, d, ^3J = 9.2 Hz, hydroquinone-*H*), 5.70 (2H, br s, alkene-*H*), 4.38 (4H, t, ^3J = 7.4 Hz, NCH_2), 4.00 (4H, t, ^3J = 4.7 Hz, CH_2), 3.84 (4H, br s, CH_2), 3.72–3.74 (12H, m, CH_2), 3.58–3.59 (4H, m, CH_2), 2.06 (4H, quin, ^3J = 6.7 Hz, CH_2); **^{13}C NMR** (125.8 MHz, 4:1 MeCN:$CHCl_3$) δ (ppm): 156.9, 153.6, 149.5, 149.1, 145.3, 140.8, 136.8, 132.5, 131.8, 131.1,

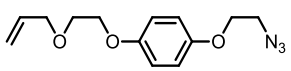
129.7, 126.1, 125.2, 116.1, 115.4, 114.2, 71.4, 69.9, 68.6, 67.5, 64.9, 63.8, 55.0, 51.7, 40.6, 34.9, 31.6, 30.2, 29.1; **^{19}F NMR** (470.6 MHz, 1:1 $CDCl_3$:CD_3OD) δ (ppm): −74.4 (d, J = 729 Hz, PF_6); **ESIMS** *m*/*z*: 1780.0153 ($[M-PF_6]^+$, $C_{114}H_{135}N_6O_{12}$ requires 1780.0133).

1-(Azidosulfonyl)-1*H*-imidazol-3-ium chloride 101·HCl[34]



NaN_3 (6.50 g, 0.100 mol) was dissolved in anhydrous MeCN (100 mL) and sulfuryl chloride (8.11 mL, 1.35 g, 0.100 mol) was added dropwise at 0 °C. The mixture was stirred at rt under N_2 for 16 h, imidazole (13.0 g, 190 mmol) was added portionwise at 0 °C and the mixture was stirred at rt for a further 3 h. EtOAc (200 mL) was added and the reaction mixture was washed with H_2O (2 × 200 mL) and sat. $NaHCO_{3(aq)}$ (2 × 200 mL), and dried over anhydrous $MgSO_4$ and filtered. A solution of HCl in EtOH was prepared by adding acetyl chloride (10.7 mL) to EtOH (40 mL) in an ice bath and this was added to the dried organic phase at 0 °C. The mixture was chilled in the ice bath, filtered, and the solid was washed with cold EtOAc (3 × 50 mL) to give compound **101·HCl** as colourless needles in 69% yield (12.0 g, 69.5 mmol). **^{1}H NMR** (300 MHz, D_2O) δ (ppm): 8.70–8.72 (1H, m, NC*H*N), 7.77–7.78 (1H, m, SNC*H*CHN), 7.33–7.34 (1H, m, SNCHC*H*N); **ESIMS** *m*/*z*: 174.0 ($[M-Cl]^+$, $C_3H_4N_5O_2S$ requires 174.0).

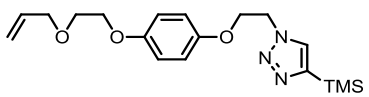
Vinyl-appended azide 102



Compound **98** (3.00 g, 12.6 mmol) was dissolved in MeOH (150 mL) and K_2CO_3 (4.20 g, 30.3 mmol), compound **101·HCl** (3.17 g, 15.2 mmol) and $CuSO_4·5H_2O$ (31.0 mg, 1.26 mmol) were added. The suspension was stirred at rt under N_2 for 72 h. The mixture was concentrated to ~5 mL *in vacuo*, diluted with H_2O (50 mL), acidified with conc. $HCl_{(aq)}$ and then extracted with EtOAc (3 × 50 mL). The combined organic phases were washed with sat. $NaCl_{(aq)}$ (50 mL) and anhydrous $MgSO_4$, filtered, and the solvent removed *in vacuo*. The

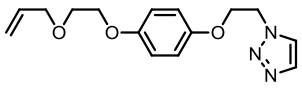
resulting residue was purified by column chromatography (SiO_2, 2:1 40–60 petroleum ether:EtOAc) to give compound **102** as a colourless oil in 48% yield (1.61 g, 6.11 mmol). **^{1}H NMR** (300 MHz, $CDCl_3$) δ (ppm): 6.83–6.92 (4H, m, hydroquinone-*H*), 5.89–6.02 (1H, m, C=C*H*), 5.20–5.36 (2H, m, C=CH_2), 4.09–4.13 (6H, m, CH_2), 3.79 (2H, t, ^3J = 5.0 Hz, CH_2), 3.58 (2H, t, ^3J = 5.0 Hz, CH_2); **^{13}C NMR** (75.5 MHz, $CDCl_3$) δ (ppm): 153.4, 152.5, 134.5, 117.3, 115.6, 115.6(*sic*), 72.4, 68.6, 68.0, 67.6, 50.2; **ESIMS** *m/z*: 286.1166 ($[M+Na]^+$, $C_{13}H_{17}NaN_3O_3$ requires 286.1162).

Vinyl-appended trimethylsilyl triazole 103



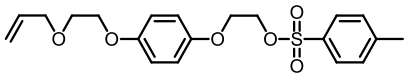
Compound **102** (1.00 g, 3.80 mmol) and trimethylsilyl acetylene (1.08 mL, 7.60 mmol) were dissolved in anhydrous CH_2Cl_2 (100 mL). $[Cu(MeCN)_4]PF_6$ (142 mg, 0.380 mmol), D*i*PEA (1.32 mL, 982 mg, 7.60 mmol) and TBTA (222 mg, 0.380 mmol) were added and the mixture was stirred at rt under $N_2$for 48 h. The mixture was washed with 10% $NH_4OH_{(aq)}$ (3 × 50 mL) and H_2O (50 mL) then dried over anhydrous $MgSO_4$, filtered, and the solvent was removed *in vacuo*. The resulting residue was purified by column chromatography (SiO_2, 95:5 CH_2Cl_2:MeOH) to give compound **103** as a cream-coloured solid in 88% yield (1.20 g, 3.32 mmol). **^{1}H NMR** (300 MHz, $CDCl_3$) δ (ppm): 7.70 (1H, s, triazole-*H*), 6.77–6.88 (4H, m, hydroquinone-*H*), 5.88–6.01 (1H, m, C=C*H*), 5.19–5.35 (2H, m, C=CH_2), 4.77 (2H, t, ^3J = 5.0 Hz, CH_2), 4.31 (2H, t, ^3J = 5.0 Hz, CH_2), 4.07–4.11 (4H, m, CH_2), 3.77–3.80 (2H, m, CH_2), 0.33 (9H, s, Si(CH_3)$_3$); **^{13}C NMR** (75.5 MHz, $CDCl_3$) δ (ppm): 134.5, 130.0, 117.4, 115.7, 115.6, 72.3, 68.5, 68.0, 68.0(*sic*), 67.3, 49.2, −1.1; **ESIMS** *m/z*: 384.1708 ($[M+Na]^+$, $C_{18}H_{27}NaN_3O_3Si$ requires 384.1714).

Vinyl-appended triazole 104



Compound **103** (1.00 g, 2.77 mmol) was dissolved in anhydrous THF (50 mL), TBA·F (1 M solution in THF, 5.53 mL, 5.53 mmol) was added and the reaction was stirred at rt under N_2 for 24 h. The solvent was removed *in vacuo* and the resulting residue was purified by column chromatography (SiO_2, 95:5 CH_2Cl_2:MeOH) to give compound **104** in 89% yield (0.71 g, 2.5 mmol). **^{1}H NMR** (300 MHz, $CDCl_3$) δ (ppm): 7.77 (1H, s, triazole-*H*), 7.72 (1H, s, triazole-*H*), 6.77–6.88 (4H, m, hydroquinone-*H*), 5.88–6.02 (1H, m, C=C*H*), 5.19–5.35 (2H, m, C=CH_2), 4.78 (2H, t, ^3J = 5.0 Hz, CH_2), 4.32 (2H, t, ^3J = 5.0 Hz, CH_2), 4.07–4.11 (4H, m, CH_2), 3.78 (2H, t, ^3J = 5.0 Hz); **^{13}C NMR** (75.5 MHz, $CDCl_3$) δ (ppm): 115.0, 113.4, 95.8, 95.2, 85.9, 78.7, 38.8, 38.3, 37.9, 33.6, 29.8, 29.3, 28.4; **ESIMS** *m/z*: 312.1324 ($[M+Na]^+$, $C_{15}H_{19}NaN_3O_3$ requires 312.1319).

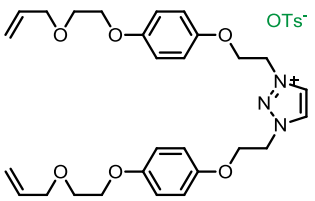
2-(4-(2-(Allyloxy)ethoxy)phenoxy)ethyl-4-methylbezenesulfonate 105



Compound **60** (0.84 g, 2.5 mmol), *p*-toluenesulfonyl chloride (0.52 g, 2.7 mmol), Et_3N (0.53 mL, 0.38 g, 3.8 mmol) and 4-DMAP (5 mg, cat.) were dissolved in anhydrous CH_2Cl_2 (150 mL) and stirred at rt under N_2 for 72 h. The mixture was washed with 1 M $HCl_{(aq)}$ (100 mL), H_2O (100 mL) and sat. $NaCl_{(aq)}$ (100 mL), dried over anhydrous $MgSO_4$, filtered, and the solvent removed *in vacuo*. The residue was purified by column chromatography (SiO_2, 98:2 CH_2Cl_2:MeOH) to give compound **105** as a white solid in 77% yield (0.65 g, 1.7 mmol). **^{1}H NMR** (300 MHz, $CDCl_3$) δ (ppm): 7.82 (2H, d, ^3J = 8.0 Hz, Ar*H*), 7.35 (2H, d, ^3J = 8.0 Hz, Ar*H*), 6.83 (2H, d, ^3J = 9.0 Hz, hydroquinone-*H*), 6.72 (2H, d, ^3J = 9.0 Hz, hydroquinone-*H*), 5.88–6.02 (1H, m, C=C*H*), 5.19–5.35 (2H, m, C=CH_2), 4.35 (2H, t, ^3J = 5.0 Hz, CH_2), 4.07–4.12 (6H, m, CH_2), 3.78 (2H, t, ^3J = 5.0 Hz, CH_2), 2.46 (3H, s, CH_3); **^{13}C NMR** (75.5 MHz, $CDCl_3$) δ (ppm): 152.2, 144.9, 134.5, 132.9, 129.8, 128.0, 117.3,

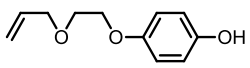
115.6, 115.5, 72.3, 68.5, 68.2, 68.0, 66.1, 53.4, 21.6; **ESIMS** *m/z*: 415.1173 ($[M+Na]^+$, $C_{20}H_{24}NaO_6S$ requires 415.1186).

Macrocycle precursor 106·OTs



Compound **104** (0.15 g, 0.52 mmol) and compound **105** (0.24 g, 0.62 mmol) were dissolved in acetone (10 mL), NaI (5 mg, cat.) was added and the mixture was heated at 150 °C in a sealed vial under microwave radiation for 2 h. The solvent was removed *in vacuo* and the resulting residue was purified by column chromatography (SiO_2, 95:5 CH_2Cl_2:MeOH then 9:1 CH_2Cl_2:CH_3OH) to give compound **106·OTs** as a white solid in 14% yield (50 mg, 0.07 mmol). **^{1}H NMR** (300 MHz, CD_3OD) δ (ppm): 8.85 (2H, s, triazolium-*H*), 7.72 (2H, d, ^3J = 8.0 Hz, SAr*H*), 7.22 (2H, d, ^3J = 8.0 Hz, SAr*H*), 6.75–6.82 (4H, m, hydroquinone-*H*), 5.86–5.99 (2H, m, C=C*H*), 5.15–5.42 (4H, m, C=CH_2), 5.05 (4H, t, ^3J = 5.0 Hz, NCH_2), 4.42 (4H, t, ^3J = 5.0 Hz, NCH$_2$CH_2), 4.01–4.07 (8H, m, CH_2), 3.73–3.76 (4H, m, CH_2), 2.35 (3H, s, CH_3); **^{13}C NMR** (75.5 MHz, CD_3OD) δ (ppm): 155.0, 153.2, 143.2, 141.7, 135.8, 132.5, 129.7, 126.8, 117.3, 116.7, 116.5 73.0, 69.7, 69.0, 66.9, 54.7, 21.2; **ESIMS** *m/z*: 510.2595 ($[M-OTs]^+$, $C_{28}H_{36}N_3O_6$ requires 510.2599).

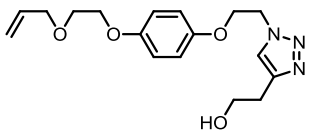
4-(2-(Allyloxy)ethoxy)phenol 107[32]



Compound **59** (2.00 g, 7.80 mmol), hydroquinone (3.44 g, 31.2 mmol) and K_2CO_3 (1.19 g, 8.58 mmol) were suspended in EtOH (50 mL) and heated at reflux under N_2 for 18 h. The suspension was cooled to rt, filtered, and the solvent removed *in vacuo*. The residue was dissolved in H_2O (40 mL) and acidified to pH 3 using 1 M $HCl_{(aq)}$, then extracted with $CHCl_3$ (3 × 40 mL). The combined organic phases were dried over anhydrous $MgSO_4$,

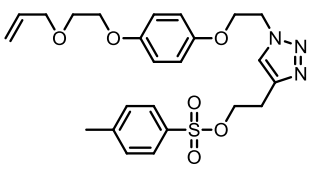
filtered, and the solvent was removed *in vacuo*. The resulting residue was purified using column chromatography (SiO_2, 3:2 hexane:EtOAc) to give compound **107** as a brown oil in 67% yield (1.02 g, 5.23 mmol). **^{1}H NMR** (300 MHz, $CDCl_3$) δ (ppm): 6.73–6.86 (4H, m, hydroquinone-*H*), 5.89–6.02 (1H, m, C=C*H*), 5.19–5.35 (2H, m, C=CH_2), 4.57 (1H, s, O*H*), 4.07–4.12 (4H, m, CH_2), 3.77–3.80 (2H, m, CH_2); **ESIMS** *m/z*: 217.1 ($[M+Na]^+$, $C_{11}H_{14}NaO_3$ requires 217.1).

Vinyl-appended alcohol 108



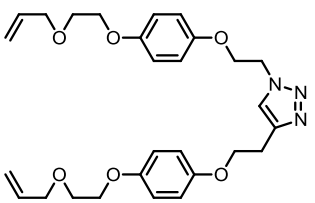
Compound **102** (1.00 g, 3.80 mmol) was dissolved in MeOH (30 mL) and sodium L-ascorbate (0.15 g, 0.75 mmol), $CuSO_4{\cdot}5H_2O$ (0.14 g, 0.56 mmol) and 3-butyn-1-ol (0.29 mL, 210 mg, 3.80 mmol) were added. The mixture was stirred at rt under N_2 for 72 h then diluted with H_2O (100 mL) and extracted with EtOAc (3 × 150 mL). The combined organic phases were washed with 10% $NH_4OH_{(aq)}$ (3 × 50 mL) and sat. $NaCl_{(aq)}$ (50 mL), dried over anhydrous $MgSO_4$, filtered, and the solvent removed *in vacuo* to give compound **108** as a cream-coloured solid in 80% yield (1.01 g, 3.04 mmol). **^{1}H NMR** (300 MHz, $CDCl_3$) δ (ppm): 7.60 (1H, s, triazole-*H*), 6.78–6.88 (4H, m, hydroquinone-*H*), 5.88–6.01 (1H, m, C=C*H*), 5.19–5.35 (2H, m, C=CH_2), 4.73 (2H, t, ^3J = 5.0 Hz, CH_2), 4.31 (2H, t, ^3J = 5.0 Hz, CH_2), 4.05–4.13 (4H, m, CH_2), 3.92–4.00 (2H, m, CH_2), 3.87 (2H, t, ^3J = 4.5 Hz, CH_2), 2.96 (2H, t, ^3J = 6.0 Hz, CH_2); **^{13}C NMR** (75.5 MHz, $CDCl_3$) δ (ppm): 153.7, 152.1, 145.6, 134.5, 122.7, 117.4, 115.6, 72.4, 68.5, 68.0, 67.1, 61.7, 53.4, 49.8, 28.6; **ESIMS** *m/z*: 334.1767 ($[M+H]^+$, $C_{17}H_{24}N_3O_4$ requires 334.1761).

Vinyl-appended tosylate 109



Compound **108** (652 mg, 1.96 mmol), *p*-toluenesulfonyl chloride (4.03 g, 2.11 mmol), Et_3N (0.41 mL, 3.0 mg, 2.9 mmol) and 4-DMAP (5 mg, cat.) were dissolved in anhydrous CH_2Cl_2 (50 mL) and the mixture was stirred at rt under N_2 for 18 h. H_2O was added to quench the reaction and the organic phase was washed with H_2O (2 × 50 mL) and sat. $NaCl_{(aq)}$ (50 mL). The combined aqueous phases were re-extracted with CH_2Cl_2 (50 mL) and then the combined organic phases were dried over anhydrous $MgSO_4$, filtered, and the solvent removed *in vacuo*. The resulting residue was purified by column chromatography (SiO_2, 95:5 CH_2Cl_2:MeOH) to give compound **109** as an off-white solid in 79% yield (749 mg, 1.54 mmol). **^{1}H NMR** (300 MHz, $CDCl_3$) δ (ppm): 7.74 (2H, d, ^3J = 8.0 Hz, SAr*H*), 7.62 (1H, s, triazole-*H*), 7.30 (2H, d, ^3J = 8.0 Hz, SAr*H*), 6.79–6.89 (4H, m, hydroquinone-*H*), 5.88–6.03 (1H, m, C=C*H*), 5.20–5.35 (2H, m, C=CH_2), 4.69 (2H, t, ^3J = 5.0 Hz, CH_2), 4.27–4.31 (4H, m, CH_2), 4.07–4.11 (4H, m, CH_2), 3.78 (2H, t, ^3J = 5.0 Hz, CH_2), 3.11 (2H, t, ^3J = 6.5 Hz, CH_2), 2.44 (3H, s, CH_3); **^{13}C NMR** (75.5 MHz, $CDCl_3$) δ (ppm): 152.0, 142.8, 134.5, 132.7, 129.9, 127.9, 123.2, 117.4, 115.7, 115.6, 77.2, 72.4, 69.0, 68.5, 68.1, 67.1, 49.8, 25.9, 21.6; **ESIMS** *m/z*: 510.1669 ($[M+Na]^+$, $C_{24}H_{29}NaN_3O_6S$ requires 510.1663).

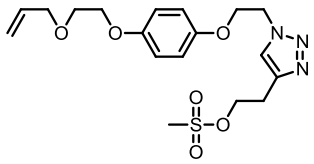
Bis-vinyl-appended triazole 110



Compound **107** (305 mg, 1.57 mmol) and compound **111** (538 mg, 1.31 mmol) were dissolved in anhydrous DMF (50 mL). K_2CO_3 (1.81 g, 13.1 mmol) was added and the mixture heated at 85 °C under N_2 for 72 h. The solvent was removed *in vacuo* and the residue was dissolved in

CH_2Cl_2 (100 mL) and washed with H_2O (3 × 100 mL). The organic phase was dried over anhydrous $MgSO_4$, filtered, and the solvent removed *in vacuo*. The residue was purified by column chromatography (SiO_2 2:1 EtOAc:hexanes then EtOAc) to give compound **110** as an off-white solid in 44% yield (294 mg, 0.58 mmol). **^{1}H NMR** (300 MHz, $CDCl_3$) δ (ppm): 7.65 (1H, s, triazole-*H*), 6.74–6.87 (8H, m, hydroquinone-*H*), 5.89–6.04 (2H, m, C=C*H*), 5.20–5.35 (4H, m, C=CH_2), 4.71 (2H, t, ^3J = 5.0 Hz, CH_2), 4.29 (2H, t, ^3J = 5.0 Hz, CH_2), 4.19 (2H, t, ^3J = 6.5 Hz, CH_2), 4.06–4.11 (8H, m, CH_2), 3.77–3.80 (4H, m, CH_2), 3.20 (2H, t, ^3J = 6.0 Hz, CH_2); **^{13}C NMR** (75.5 MHz, $CDCl_3$) δ (ppm): 153.7, 152.9, 152.1, 134.6, 134.5, 123.1, 117.4, 117.3, 115.7, 115.7(*sic*), 115.6, 115.6(*sic*), 115.5, 72.4, 68.6, 68.6(*sic*), 68.1, 68.0, 67.4, 67.2, 49.8, 30.9, 26.2; **ESIMS** *m/z*: 510.2590 ($[M+H]^+$, $C_{28}H_{36}N_3O_6$ requires 510.2599).

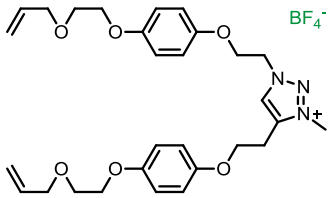
Vinyl-appended mesylate 111



Compound **108** (0.50 g, 1.5 mmol) and Et_3N (0.42 mL, 300 mg, 3.00 mmol) were dissolved in anhydrous CH_2Cl_2 (20 mL) and stirred in an ice bath under N_2 for 10 min. Methanesulfonyl chloride (0.13 mL, 1.6 mmol) in anhydrous CH_2Cl_2 (20 mL) was added dropwise. The mixture was allowed to warm to rt and stirred under N_2 for 1 h then washed with H_2O (2 × 75 mL), 1 M $HCl_{(aq)}$ (3 × 50 mL) and sat. $NaCl_{(aq)}$ (3 × 75 mL). The organic phase was dried over anhydrous $MgSO_4$, filtered, and the solvent removed *in vacuo* to give compound **111** as a pale yellow solid in 88% yield (0.55 g, 1.3 mmol). **^{1}H NMR** (300 MHz, $CDCl_3$) δ (ppm): 7.66 (1H, s, triazole-*H*), 6.78–6.88 (4H, m, hydroquinone-*H*), 5.88–6.01 (1H, m, C=C*H*), 5.19–5.35 (2H, m, C=CH_2), 4.72 (2H, t, ^3J = 5.0 Hz, CH_2), 4.53 (2H, t, ^3J = 6.5 Hz, CH_2), 4.30 (2H, t, ^3J = 5.0 Hz, NCH_2), 4.06–4.10 (4H, m, CH_2), 3.78 (2H, t, ^3J = 5.0 Hz, CH_2), 3.20 (2H, t, ^3J = 6.5 Hz, CH_2), 2.92 (3H, s, SCH_3); **^{13}C NMR** (75.5 MHz, $CDCl_3$) δ (ppm): 153.6, 151.9, 142.7, 134.4, 132.3, 117.3, 115.6, 115.5, 72.2, 68.4,

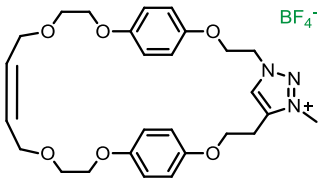
68. (*sic*), 68.0, 67.0, 50.0, 37.2, 25.9; **ESIMS** *m/z*: 421.1535 ($[M+H]^+$, $C_{18}H_{26}N_3O_6S$ requires 421.1537).

Macrocycle precursor 112·BF$_4$



Compound **111** (200 mg, 0.4 mmol) was dissolved in anhydrous CH_2Cl_2 (25 mL), $[Me_3O]BF_4$ (116 mg, 0.790 mmol) was added and the mixture was stirred at rt under N_2 for 18 h. The reaction was quenched with MeOH (5 drops) and the solvent removed *in vacuo*. Purification by column chromatography (SiO_2, 95:5 CH_2Cl_2:MeOH) gave compound **112·BF$_4$** as an orange oil in 54% yield (111 mg, 0.210 mmol). **^{1}H NMR** (300 MHz, $CDCl_3$) δ (ppm): 8.51 (1H, s, triazolium-*H*), 6.75–6.83 (8H, m, hydroquinone-*H*), 5.87–6.01 (2H, m, C=C*H*), 5.19–5.34 (4H, m, C=CH_2), 4.87 (2H, t, ^3J = 4.5 Hz, CH_2), 4.39 (2H, t, ^3J = 4.5 Hz, CH_2), 4.27 (3H, s, NCH_3), 4.22–4.26 (2H, m, CH_2), 4.03–4.10 (8H, m, CH_2), 3.75–3.78 (4H, m, CH_2), 3.31 (2H, t, ^3J = 5.5 Hz, CH_2); **^{13}C NMR** (75.5 MHz, $CDCl_3$) δ (ppm): 153.9, 153.7, 151.8, 151.7, 142.7, 136.9, 134.5, 129.7, 117.4, 115.8, 115.7, 115.7, 115.7, 115.4, 77.2, 72.4, 68.5, 68.0, 65.6, 65.5, 53.5, 24.0; **ESIMS** *m/z*: 524.2754 ($[M-BF_4]^+$, $C_{29}H_{38}N_3O_6$ requires 524.2755).

Macrocycle 113·BF$_4$

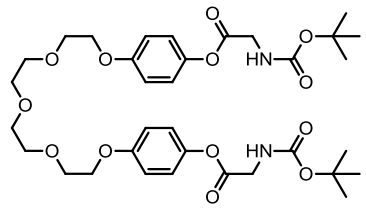


Compound **112·BF$_4$** (30 mg, 0.05 mmol) and Grubbs' II catalyst (3.0 mg, 10% by wt.) were dissolved in anhydrous CH_2Cl_2 (100 mL) and the mixture was stirred at rt under N_2 for 72 h. The solvent was removed *in vacuo* and the resulting residue was purified by preparative thin

layer chromatography (SiO_2, 9:1 CH_2Cl_2:MeOH) to give compound **113·BF_4** as a white solid in 31% yield (9 mg, 0.02 mmol). **^{1}H NMR** (300 MHz, 1:1 **114·BF_4**:TBA·Cl, $CDCl_3$) δ (ppm): 9.19 (1H, s, triazolium-*H*), 6.75 (2H, d, ^3J = 9.2 Hz, hydroquinone-*H*), 6.68 (2H, d, ^3J = 8.8 Hz, hydroquinone-*H*), 6.61 (2H, d, ^3J = 8.8 Hz, hydroquinone-*H*), 6.54 (2H, d, ^3J = 9.2 Hz, hydroquinone-*H*), 5.88–5.90 (2H, m, alkene-*H*), 5.07 (2H, t, ^3J = 4.5 Hz, CH_2), 4.42 (2H, t, ^3J = 4.5 Hz, CH_2), 4.37 (3H, s, CH_3), 4.26 (2H, t, ^3J = 5.5 Hz, CH_2), 4.10 (4H, t, ^3J = 4.0 Hz, CH_2), 4.03 (2H, t, ^3J = 4.5 Hz, CH_2), 3.98 (2H, t, ^3J = 4.5 Hz, CH_2), 3.75-3.79 (4H, m, CH_2), 3.47 (2H, t, ^3J = 5.5 Hz, CH_2), 3.27–3.31 (8H, m, TBA·Cl), 1.60–1.66 (8H, m, TBA·Cl), 1.39–1.46 (8H, m, TBA·Cl), 0.98 (8H, t, ^3J = 7.5 Hz, TBA·Cl); **ESIMS** *m/z*: 496.2419 ($[M-BF_4]^+$, $C_{27}H_{34}N_3O_6$ requires 496.2442).

6.5 Experimental procedures for Chapter Five

Compound 114



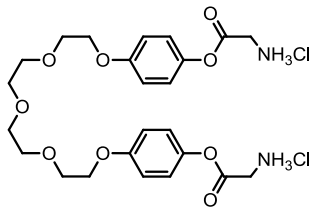
Method A: *N*-Boc-glycine (93 mg, 0.53 mmol) was dissolved in EtOAc (20 mL) and **54** (100 mg, 0.3 mmol) and DCC (123 mg, 0.596 mmol) were added. The reaction mixture was stirred at rt under N_2 for 16 h after which time the mixture was filtered, and the solvent removed *in vacuo*. The crude residue was redissolved in $CHCl_3$ (50 mL) and washed with sat. $NaHCO_{3(aq)}$ (50 mL), H_2O (50 mL), dried over anhydrous $MgSO_4$, filtered, and the solvent removed *in vacuo*. Recrystallisation from EtOAc:hexanes gave **114** as a pale yellow solid in 22% yield (38.8 mg, 56.0 μmol).

Method B: *N*-Boc-glycine (222 mg, 1.26 mmol), and EDCI·HCl (242 mg, 1.26 mmol) were dissolved in 1:1 DMF:EtOAc (50 mL) at 0 °C. Compound **54** (165 mg, 0.436 mmol) and 4-

DMAP (14.1 mg, cat.) in 1:1 DMF:EtOAc (10 mL) were added and the reaction mixture stirred at rt under N_2 for 3 days. The solvent was removed *in vacuo* and the crude residue purified by column chromatography (SiO_2, 9:1 CH_2Cl_2:MeOH) to give **114** as a pale yellow oil in 12% yield (35.1 mg, 50.7 μmol).

Method D: *N*-Boc-glycine (92.8 mg, 0.530 mmol) was dissolved in anhydrous CH_2Cl_2 (20 mL). DCC (120 mg, 0.58 mmol) and *N*-hydroxysuccinimide (71.8 mg, 0.624 mmol) were added and the reaction mixture was stirred at rt under N_2 for 18 h. The reaction mixture was filtered and the filtrate added dropwise to a solution of **54** (0.10 g, 0.26 mmol) and Et_3N (0.10 mL, 66 mg, 0.65 mmol) in anhydrous CH_2Cl_2 (20 mL). This solution was stirred at rt under N_2 for 72 h. The solvent was removed *in vacuo* and the crude residue purified by column chromatography (SiO_2, 75:23:2 CH_2Cl_2:acetone:MeOH) to give **114** as a pale yellow oil in 42% yield (76.3 mg, 0.110 mmol). **^{1}H NMR** (300 MHz, $CDCl_3$) δ (ppm): 6.99 (4H, d, ^3J = 8.9 Hz, hydroquinone-*H*), 6.89 (4H, d, ^3J = 8.9 Hz, hydroquinone-*H*), 5.14 (2H, br s, N*H*), 4.14 (4H, d, ^3J = 5.8 Hz, CH_2NH), 4.09 (4H, t, ^3J = 4.9 Hz, CH_2), 3.84 (4H, t, ^3J = 4.9 Hz, CH_2), 3.66–3.74 (8H, m, CH_2), 1.47 (18H, s, CH_3); **^{13}C NMR** (75.5 MHz, $CDCl_3$) δ (ppm): 169.3, 156.6, 155.7, 143.8, 122.0, 115.2, 80.1, 70.8, 70.6, 69.6, 67.8, 42.5, 28.3; **ESIMS** *m/z*: 715.3054 ($[M+Na]^+$, $C_{34}H_{48}N_2NaO_{13}$ requires 715.3049).

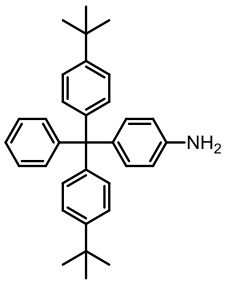
Compound 115



Acetyl chloride (2.8 mL) was added dropwise to MeOH (5 mL) at 0 °C, to form anhydrous HCl *in situ*, and the solution was stirred at rt under N_2 for 20 min. Compound **114** (0.10 g, 0.14 mmol) was dissolved in anhydrous CH_2Cl_2 (20 mL) and added to the acidic solution. The reaction mixture was stirred at rt under N_2 for 1.5 h during which time the product precipitated as a white power and was collected by filtration to give **115** in 46% yield

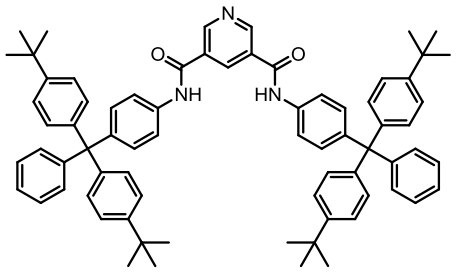
(45.6 mg, 80.6 μmol). **^{1}H NMR** (300 MHz, $CDCl_3$) δ (ppm): 8.40 (6H, br s, N*H*$_3$Cl), 7.01 (4H, d, ^3J = 8.7 Hz, hydroquinone-*H*), 7.00 (4H, d, ^3J = 8.7 Hz, hydroquinone-*H*), 4.07–4.10 (8H, m, C*H*$_2$), 3.74 (4H, br s, C*H*$_2$), 3.56–3.57 (8H, m, C*H*$_2$); **^{13}C NMR** (75.5 MHz, DMSO-d_6) δ (ppm): 169.0, 166.9, 156.5, 151.3, 143.2, 122.4, 115.8, 115.3, 70.0, 68.9, 67.6; **ESIMS** *m/z*: 493.2175 ($[M-2Cl-H]^+$, $C_{24}H_{33}N_2O_9$ requires 493.2181).

Stopper-amine compound 116[25]



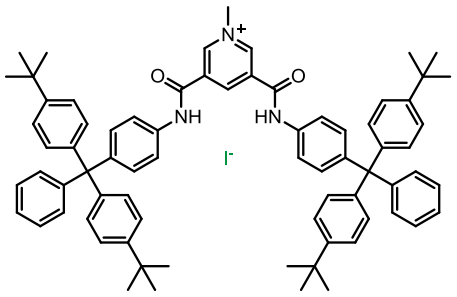
Compound **75** (6.00 g, 16.1 mmol) was dissolved in acetyl chloride (30 mL) and heated at reflux under N_2 for 18 h. After cooling to rt, the acetyl chloride was removed by distillation and the residue redissolved immediately in aniline (30 mL). The reaction mixture was heated to 105 °C under N_2 for 48 h during which time the colour changed from orange to purple. The reaction mixture was cooled to rt, poured onto 10% $HCl_{(aq)}$ (300 mL) and stirred vigorously for 20 min forming a purple precipitate. The solid was collected by filtration, washed with sat. $K_2CO_{3(aq)}$ (50 mL) and H_2O (50 mL), and then redissolved in CH_2Cl_2 (150 mL), dried over anhydrous $MgSO_4$ and filtered. The solvent volume was reduced by ¾, the solution filtered through a plug of silica, and the solvent removed *in vacuo* to give a pale brown solid. Recrystallisation from toluene/hexanes gave **116** as a white solid in 68% yield (4.91 g, 20.0 mmol). **^{1}H NMR** (300 MHz, $CDCl_3$) δ (ppm): 7.17–7.26 (9H, m, Ar*H*), 7.08 (4H, d, ^3J = 8.8 Hz, Ar*H*), 7.03 (2H, d, ^3J = 8.8 Hz, Ar*H*), 6.73 (2H, d, ^3J = 8.8 Hz, Ar*H*), 1.04 (18H, s, C*H*$_3$); **ESIMS** *m/z*: 470.3 ($[M+Na]^+$, $C_{33}H_{37}NNa$ requires 470.3).

Pyridine-3,5-bis-amide axle compound 117[35]



Pyridine-3,5-dicarboxylic acid (0.37 g, 2.2 mmol) was suspended in $SOCl_2$ (10 mL) and the mixture was heated at reflux under N_2 for 16 h until the solution became homogenous. The $SOCl_2$ was removed by distillation and the resulting solid redissolved in anhydrous CH_2Cl_2 (10 mL). This was added dropwise to a solution of compound **116** (2.00 g, 4.46 mmol) and Et_3N (2 mL, excess) in CH_2Cl_2 and stirred at rt under N_2 for 2 h. The solvent was removed *in vacuo* and EtOH (40 mL) added to the residue. The mixture was heated at reflux under N_2 for 1 h and then filtered to give compound **117** as a pale yellow solid in 83% yield (1.91 g, 1.86 mmol). **^{1}H NMR** (300 MHz, $CDCl_3$) δ (ppm): 9.25 (2H, s, pyridine-H^2&H^6), 8.69 (1H, s, pyridine-H^4), 8.18 (2H, s, N*H*), 7.57 (4H, d, ^3J = 8.9 Hz, NCC*H*) 7.11–7.24 (30H, m, Ar*H*), 1.31 (36H, s, C(CH_3)$_3$); **ESIMS** *m/z*: 1060.6 ($[M+Cl]^-$, $C_{73}H_{75}ClN_3O_2$ requires 1060.6).

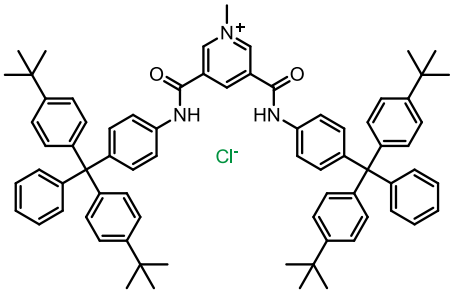
Pyridinium-3,5-bis-amide iodide axle compound 118·I[35]



Compound **117** (1.00 g, 0.974 mmol) and MeI (10.0 mL, 0.161 mol) were heated at reflux under N_2 for 48 h. After cooling to rt, the MeI was removed *in vacuo* to give **118·I** as a yellow solid in quantitative yield (1.13 g, 0.967 mmol). **^{1}H NMR** (300 MHz, DMSO-d_6) δ (ppm): 10.94 (2H, br s, N*H*), 9.64 (2H, s, pyridinium-H^2&H^6), 9.49 (1H, s, pyridinium-H^4), 7.68

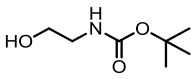
(4H, d, ^3J = 8.7 Hz, NCC*H*), 7.09–7.35 (30H, m, ArH), 4.49 (3H, s, NCH_3), 1.27 (36H, s, C(CH_3)$_3$); **ESIMS** *m/z*: 1040.6 $[M-I]^+$, $C_{74}H_{78}N_3O_2$ requires 1040.6).

Pyridinium-3,5-bis-amide chloride axle compound 118·Cl[35]



Compound **118·I** (200 mg, 0.2 mmol) was dissolved in $CHCl_3$ (200 mL) and washed with 1 M $NH_4Cl_{(aq)}$ (10 × 200 mL) and H_2O (2 × 100 mL). The organic phase was dried over anhydrous $MgSO_4$, filtered, and the solvent removed *in vacuo* to give **118·Cl** as a bright yellow solid in 95% yield (175 mg, 0.163 mmol). **^{1}H NMR** (300 MHz, $CDCl_3$) δ (ppm): 11.01 (2H, s, N*H*), 10.65 (1H, s, pyridinium-H^4), 8.82 (2H, s, pyridinium-H^2&H^6), 7.82 (4H, d, ^3J = 8.8 Hz, NCC*H*), 7.15–7.30 (30H, m, Ar*H*), 3.91 (3H, s, NCH_3), 1.30 (36H, s, C(CH_3)$_3$); **ESIMS** *m/z*: 1040.7 ($[M-Cl]^+$, $C_{74}H_{78}N_3O_2$ requires 1040.6).

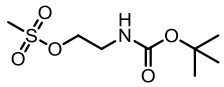
***Tert*-butyl-(2-hydroxyethyl)carbamate 120**



Ethanolamine (8.5 mL, 8.6 g, 140 mol) was dissolved in anhydrous CH_2Cl_2 (200 mL), Et_3N (20.3 mL, 15.6 g, 154 mol) was added and the reaction mixture stirred for 30 min. After dropwise addition of a solution of $(Boc)_2O$ (35.4 mL, 33.6 g, 154 mol) in CH_2Cl_2 (50 mL), the reaction mixture was stirred at rt under N_2 for 16 h. The reaction was quenched with sat. $NH_4Cl_{(aq)}$, and the aqueous phase separated and extracted with CH_2Cl_2 (2 × 100 mL). The combined organic phases were washed with sat. $NaCl_{(aq)}$, dried over anhydrous $MgSO_4$, filtered, and the solvent removed *in vacuo* to give **120** as a pale yellow oil in 57% yield (12.9 g, 80.0 mol). **^{1}H NMR** (300 MHz, CD_3OD) δ (ppm): 6.55 (2H, t, ^3J = 5.9 Hz, CH_2), 3.15 (2H,

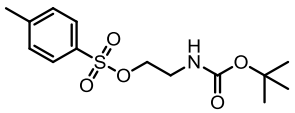
t, ^3J = 5.9 Hz, CH_2), 1.44 (9H, s, C(CH_3)$_3$); **ESIMS** *m/z*: 184.1 ([M+Na]$^+$, $C_7H_{15}NNaO_3$ requires 184.1).

2-((*Tert*-butoxycarbonyl)amino)ethyl methanesulfonate 121



Compound **120** (1.00 g, 6.20 mmol) was dissolved in anhydrous CH_2Cl_2 (50 mL), Et_3N (1.3 mL, 0.94 g, 9.3 mmol) and 4-DMAP (0.19 g, cat.) were added and the solution cooled to 0 °C. After dropwise addition of a solution of methanesulfonyl chloride (0.58 mL, 0.85 g, 7.4 mmol) in CH_2Cl_2 (10 mL), the solution was left to stir at rt under N_2 for 3 h. After this time the reaction mixture was washed with 10% citric acid$_{(aq)}$ (2 × 15 mL), sat. NaCl$_{(aq)}$ (3 × 15 mL), dried over anhydrous $MgSO_4$, filtered, and the solvent removed *in vacuo* to give **121** as an orange oil in 64% yield (0.96 g, 4.0 mmol). **^{1}H NMR** (300 MHz, $CDCl_3$) δ (ppm): 4.92 (1H, s, N*H*), 4.29 (2H, t, ^3J = 5.0 Hz, CH_2), 3.47 (2H, q, ^3J = 5.0 Hz, CH_2), 3.04 (3H, s, SCH_3), 1.45 (9H, s, C(CH_3)$_3$); **ESIMS** *m/z*: 262.1 ([M+Na]$^+$, $C_8H_{17}NNaO_5S$ requires 262.1).

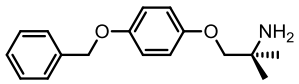
2-((*Tert*-butoxycarbonyl)amino)ethyl-4-methylbenzenesulfonate 122



Compound **120** (1.00 g, 6.20 mmol) was dissolved in CH_2Cl_2 (30 mL), *p*-toluenesulfonyl chloride (1.18 mg, 6.20 mmol) was added and the solution was cooled to 0 °C. Powdered KOH (3.48 mg, 62.0 mmol) was added whilst the temperature was maintained below 0 °C. The reaction mixture was stirred at rt for 3 h, after which time CH_2Cl_2 (50 mL) and H_2O (50 mL) were added. The aqueous layer was separated and extracted with CH_2Cl_2 (3 × 50 mL). The combined organic phases were combined, washed with H_2O (50 mL), dried over anhydrous $MgSO_4$, filtered, and the solvent removed *in vacuo* to give **122** as an off-white solid in 48% yield (0.94 g, 3.0 mmol). **^{1}H NMR** (300 MHz, $CDCl_3$) δ (ppm): 7.79 (2H, d,

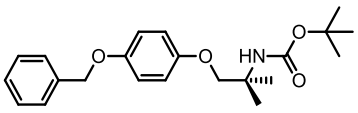
^3J = 8.3 Hz, Ar*H*), 7.35 (2H, d, ^3J = 8.3 Hz, Ar*H*), 4.88 (1H, br s, N*H*), 4.06 (2H, t, ^3J = 4.8 Hz, CH_2), 3.37 (2H, q, ^3J = 4.8 Hz, CH_2), 2.45 (3H, s, SCH_3), 1.40 (9H, s, C(CH_3)$_3$); **ESIMS** *m/z*: 338.2 ([M+Na]$^+$, $C_{14}H_{21}NNaO_5S$ requires 338.1).

Compound 124[36]



Compound **123** (5.00 g, 20.9 mmol) was dissolved in anhydrous toluene (150 mL) and cooled in a $CO_{2(s)}$/MeCN slush bath to −40 °C. Ti(O^{i}Pr)$_4$ (6.50 mL, 6.25 g, 22.0 mmol) and the resulting yellow solution was stirred for 15 min. Following dropwise addition of MeMgBr (21.5 mL, 187 mmol), the solution was stirred at rt under N_2 for 18 h. Dilute $NH_4OH_{(aq)}$ (100 mL) and Et_2O (100 mL) were added and the mixture stirred for a further 18 h. The layers were separated and the aqueous layer extracted with Et_2O (3 × 100 mL). The combined organic layers were washed with H_2O (300 mL), dried over anhydrous $MgSO_4$, filtered, and the solvent removed *in vacuo*. The crude residue was purified by column chromatography (SiO_2, 95:5 CH_2Cl_2:MeOH) to give **124** as a pale orange solid in 92% yield (5.21 g, 19.2 mmol). **^{1}H NMR** (300 MHz, $CDCl_3$) δ (ppm): 7.32–7.46 (5H, m, phenyl-*H*), 6.92 (2H, d, ^3J = 9.5 Hz, hydroquinone-*H*), 6.85 (2H, d, ^3J = 9.5 Hz, hydroquinone-*H*), 5.03 (2H, s, CH_2Ph), 3.65 (2H, s, CH_2), 1.23 (6H, s, C(CH_3)$_2$); **^{13}C NMR** (75.5 MHz, $CDCl_3$) δ (ppm): 153.5, 153.0, 137.2, 128.5, 127.8, 127.4, 115.8, 115.4, 78.3, 70.7, 50.0, 27.2; **ESIMS** *m/z*: 272.1643 ([M+H]$^+$ $C_{17}H_{22}NO_2$ requires 272.1645).

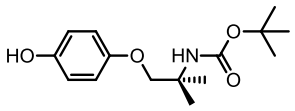
Compound 125



Compound **124** (1.00 g, 3.68 mmol) and di-*tert*-butyl dicarbonate (1.20 g, 5.52 mmol) were dissolved in anhydrous CH_2Cl_2 and stirred at rt under N_2 for 18 h. All volatiles were removed *in vacuo* to give a yellow oil which was purified by column chromatography (SiO_2, CH_2Cl_2)

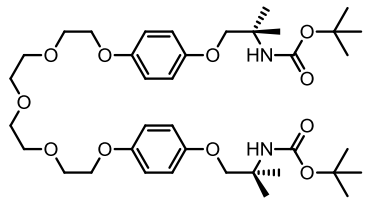
to give **125** as a pale yellow oil which solidified on standing in quantitative yield (1.36 g, 3.68 mmol). **^{1}H NMR** (300 MHz, $CDCl_3$) δ (ppm): 7.32–7.45 (5H, m, phenyl-*H*), 6.91 (2H, d, ^3J = 9.5 Hz, hydroquinone-*H*), 6.86 (2H, d, ^3J = 9.5 Hz, hydroquinone-*H*), 5.02 (2H, s, CH_2Ph), 4.79 (1H, br s, N*H*), 3.89 (2H, s, CH_2) 1.43 (9H, s, C(CH_3)$_3$), 1.41 (6H, s, C(CH_3)$_2$); **^{13}C NMR** (75.5 MHz, $CDCl_3$) δ (ppm): 153.3, 153.1, 146.7, 137.2, 128.5, 127.8, 127.4, 115.8, 85.2, 74.3, 70.6, 52.5, 28.4, 27.4, 24.3; **ESIMS** *m/z*: 394.1977 ([M+Na]$^+$, $C_{22}H_{29}NNaO_4$ requires 394.1989).

Compound 126



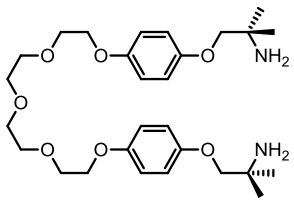
A solution of **125** (2.00 g, 5.38 mmol) in 1:1 $CHCl_3$:MeOH (100 mL) in a 250 mL round-bottomed flask was evacuated and purged with N_2 three times. 10% Pd/C (20 mg, 10% by wt.) was added and the reaction vessel evacuated and purged three times with N_2 and then three times with H_2. The reaction mixture was left to stir under H_2 for 12 h. After evacuating and purging with N_2 three times, the solution was filtered through Celite® and the solvent removed *in vacuo*. The residue was dissolved in $CHCl_3$ the precipitate filtered off and the solvent removed *in vacuo*. Trituration of the crude residue with hexanes gave **126** as a white solid in 92% yield (1.40 g, 4.97 mmol). **^{1}H NMR** (300 MHz, $CDCl_3$) δ (ppm): 6.81 (2H, d, ^3J = 9.5 Hz, hydroquinone-*H*), 6.75 (2H, d, ^3J = 9.5 Hz, hydroquinone-*H*), 4.77 (1H, br s, N*H*), 4.61 (1H, br s, O*H*), 3.88 (2H, s, CH_2), 1.43 (9H, s, C(CH_3)$_3$), 1.40 (6H, s, C(CH_3)$_2$); **^{13}C NMR** (75.5 MHz, $CDCl_3$) δ (ppm): 152.9, 149.9, 116.0, 115.9, 79.2, 74.3, 52.6, 28.4, 24.4; **ESIMS** *m/z*: 282.1694 ([M+H]$^+$, $C_{15}H_{24}NO_4$ requires 282.1700).

Compound 127



Compound **126** (500 mg, 1.78 mmol), compound **47** (426 mg, 0.848 mmol) were dissolved in anhydrous MeCN (100 mL). K_2CO_3 (2.50 g, 17.8 mmol) was added and the reaction was heated at reflux under N_2 for 48 h. After cooling to rt, the reaction mixture was filtered and the solvent removed *in vacuo*. The residue was dissolved in $CHCl_3$ (100 mL), filtered, and the solvent removed *in vacuo*. The crude mixture was purified by column chromatography (SiO_2, EtOAc:hexanes 1:3 to 1:1) to give compound **127** as a viscous yellow oil in 35% yield (449 mg, 0.623 mol). **^{1}H NMR** (300 MHz, $CDCl_3$) δ (ppm): 6.80 (8H, s, hydroquinone-*H*), 4.79 (2H, br s, N*H*), 4.04 (4H, m, CH_2), 3.84 (4H, s, CH_2), 3.79 (4H, s, CH_2), 3.64–3.70 (8H, m, CH_2), 1.39 (18H, s, C(CH_3)$_3$), 1.36 (12H, s, C(CH_3)$_2$); **^{13}C NMR** (75.5 MHz, $CDCl_3$) δ (ppm): 171.1, 153.1, 115.5, 74.3, 70.6, 69.8, 68.0, 60.3, 53.4, 52.5, 28.4, 24.3, 21.0, 14.2; **ESIMS** *m/z*: 743.4090 ($[M+Na]^+$, $C_{38}H_{60}N_2NaO_{11}$ requires 743.4089).

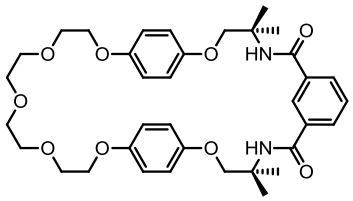
Compound 128



Compound **127** (450 mg, 0.63 mmol) was dissolved in $CHCl_3$ (50 mL). TFA (5 mL, excess) was added and the reaction was stirred at rt, under N_2 for 18 h. The reaction mixture was basified with 10% $NaOH_{(aq)}$ and then extracted with $CHCl_3$ (3 × 100 mL). The combined organic extracts were washed with H_2O (3 × 75 mL), and the combined aqueous layer were re-extracted with $CHCl_3$ (100 mL). The combined organic phases were dried over anhydrous $MgSO_4$, filtered, and the solvent removed *in vacuo* giving **128** as a white oily solid in 88%

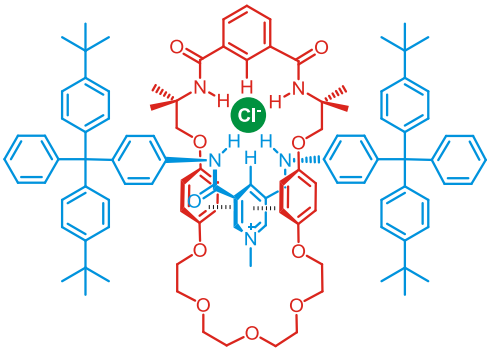
yield (286 mg, 0.549 mmol). **^{1}H NMR** (300 MHz, $CDCl_3$) δ (ppm): 6.82 (8H, s, hydroquinone-*H*), 4.06 (4H, t, ^3J = 5.0 Hz, CH_2), 3.82 (4H, t, ^3J = 5.0 Hz, CH_2), 3.66–3.73 (8H, m, CH_2), 3.61 (4H, s, CH_2), 1.50 (4H, br s, NH_2), 1.19 (12H, s, CH_3); **^{13}C NMR** (75.5 MHz, $CDCl_3$) δ (ppm): 153.4, 152.8, 115.4, 115.2, 78.3, 70.6, 70.5, 69.7, 67.9, 49.8, 27.2; **ESIMS** *m/z*: 521.3208 ($[M+H]^+$, $C_{28}H_{45}N_2O_7$ requires 521.3221).

Macrocycle 129



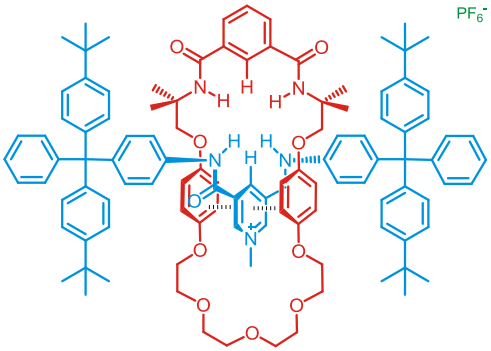
Compound **128** (150 mg, 0.29 mmol) and **51·Cl** (111 mg, 0.289 mmol) were dissolved in anhydrous CH_2Cl_2 (100 mL). The solution was stirred at rt under N_2 for 20 min and Et_3N (0.10 mL, 73 mg, 0.72 mmol) was added, followed by a solution of isophthaloyl dichloride (59 mg, 0.29 mmol) in anhydrous CH_2Cl_2 (10 mL). The reaction mixture was stirred at rt under N_2 for 16 h and then washed with 10% $HCl_{(aq)}$ (2 × 100 mL), H_2O (2 × 100 mL), dried over anhydrous $MgSO_4$, filtered, and the solvent removed *in vacuo*. The crude residue was purified by column chromatography (SiO2, 9:1 CH_2Cl_2:MeOH and 1:1 CH_2Cl_2:EtOAc) to give **129** as a white powder in 65% yield (124 mg, 0.191 mmol). **^{1}H NMR** (300 MHz, CD_2Cl_2) δ (ppm): 7.96 (1H, t, ^4J = 1.9 Hz, isophthaloyl-H^2), 7.84 (dd, ^3J = 7.6 Hz, ^4J = 1.9 Hz, isophthaloyl-H^4&H^6), 7.48 (1H, t, ^3J = 7.6 Hz, isophthaloyl-H^5), 6.79 (8H, s, hydroquinone-*H*), 6.30 (2H, s, N*H*), 4.03 (4H, s, CH_2), 4.00 (4H, t, ^3J = 4.7 Hz, CH_2), 3.77 (4H, t, ^3J = 4.7 Hz, CH_2), 3.60–3.66 (8H, m, CH_2) 1.55 (12H, s, C(CH_3)$_2$); **^{13}C NMR** (75.5 MHz, CD_2Cl_2) δ (ppm): 166.6, 153.3, 153.0, 136.0, 129.8, 128.9, 124.4, 115.7, 73.9, 70.8, 70.7, 69.7, 68.2, 54.3, 24.2; **ESIMS** *m/z*: 673.3076 ($[M+Na]^+$, $C_{36}H_{46}N_2NaO_9$ requires 673.3096).

Rotaxane 130·Cl



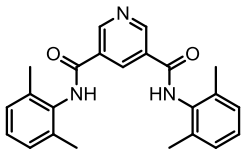
Compound **129** (24.0 mg, 46.0 μmol) and compound **118·Cl** (50.0 mg, 46.0 μmol) were dissolved in anhydrous CH_2Cl_2 (10 mL) and stirred vigorously for 30 min. Et_3N (16.0 μL, 11.7 mg, 116 μmol) was added, followed immediately by isophthaloyl dichloride (9.34 mg, 46.0 μmol). The reaction mixture was stirred at rt under N_2 for 2 h and then washed with 10% $HCl_{(aq)}$ (2 × 25 mL) and H_2O (2 × 25 mL), dried over anhydrous $MgSO_4$, filtered, and the solvent removed *in vacuo*. The crude mixture was purified by preparative thin layer chromatography (SiO_2, 95:5 $CHCl_3$:MeOH and 1:1 acetone:60−80 petroleum ether) to give the pure [2]rotaxane **130·Cl** in 58% yield (45.7 mg, 26.0 μmol). **^{1}H NMR** (300 MHz, CD_2Cl_2) δ (ppm): 10.45 (2H, br s, axle-N*H*), 10.10 (1H, s, pyridinium-H^4), 8.98 (2H, s, pyridinium-H^2&H^6), 8.72 (1H, s, isophthaloyl-H^2), 8.29 (2H, br s, macrocycle-N*H*), 7.93 (4H, d, ^3J = 9.5 Hz, axle-Ar*H*), 7.69 (2H, dd, ^3J = 7.9 Hz, ^4J = 1.5 Hz, isophthaloyl-H^4&H^6), 7.11–7.33 (30H, m, axle-Ar*H*), 7.00 (1H, t, ^3J = 7.9 Hz, isophthaloyl-H^5), 6.38 (4H, d, ^3J = 8.9 Hz, hydroquinone-*H*), 6.14 (4H, d, ^3J = 8.9 Hz, hydroquinone-*H*), 4.68 (3H, s, NCH_3), 3.81 (4H, s, CH_2), 3.71–3.76 (16H, m, CH_2), 1.47 (12H, s, macrocycle-C(CH_3)$_2$), 1.33 (36H, s, axle-C(CH_3)$_3$); **^{13}C NMR** (75 MHz, $CDCl_3$) δ (ppm): 167.7, 158.2, 153.9, 151.7, 148.4, 147.0, 145.0, 144.2, 143.6, 135.4, 135.2, 133.7, 131.6, 131.1, 130.9, 130.6, 128.4, 127.3, 125.8, 125.1, 124.3, 119.8, 119.8(*sic*), 114.7, 114.5, 75.5, 70.7, 70.5, 70.0, 68.3, 63.8, 54.3, 49.7, 34.3, 31.4, 23.1; **ESIMS** *m/z*: 1690.9314 ([M−Cl]$^+$, $C_{110}H_{124}N_5O_{11}$ requires 1690.9292).

Rotaxane 130·PF$_6$



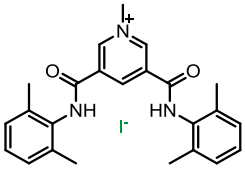
Compound **130·Cl** (42.6 mg, 24.7 μmol) was dissolved in $CHCl_3$ (15 mL) and washed with 0.1 M $NH_4PF_{6(aq)}$ (10 × 10 mL) and H_2O (2 × 10 mL). The organic phase was dried over anhydrous $MgSO_4$, filtered, and the solvent removed *in vacuo* to give **130·PF$_6$** as a yellow solid in 96% yield (43.4 mg, 23.6 μmol). **^{1}H NMR** (300 MHz, CD_2Cl_2) δ (ppm): 9.37 (2H, s, axle-N*H*), 9.15 (1H, s, pyridinium-*H*^{4}), 8.53 (2H, s, pyridinium-*H*^{2}&*H*^{6}), 8.30 (1H, s, isophthaloyl-*H*^{2}), 7.86 (2H, d, ^3J = 7.7 Hz, isophthaloyl-*H*^{4}&*H*^{6}), 7.66 (4H, d, ^3J = 8.2 Hz, axle-Ar*H*), 7.48 (1H, t, ^3J = 7.7 Hz, isophthaloyl-*H*^{5}), 7.18–7.33 (30H, m, axle-Ar*H*), 6.57 (4H, d, ^3J = 8.9 Hz, hydroquinone-*H*), 6.50 (2H, s, macrocycle-N*H*), 6.34–6.37 (4H, d, ^3J = 8.9 Hz, hydroquinone-*H*), 4.03 (3H, s, NC*H*$_3$), 3.88 (4H, s, C*H*$_2$), 3.63–3.72 (16H, m, C*H*$_2$), 1.43 (12H, s, macrocycle-C(C*H*$_3$)$_2$), 1.32 (36H, s, axle-C(C*H*$_3$)$_3$); **^{13}C NMR** (75.5 MHz, CD_2Cl_2) δ (ppm): 167.0, 158.8, 153.9, 152.5, 149.3, 147.7, 145.4, 144.3, 141.6, 136.4, 135.4, 134.8, 132.2, 131.4, 131.0, 130.2, 129.2, 128.1, 126.4, 126.2, 125.0, 120.4, 115.8, 115.6, 110.6, 78.1, 73.9, 71.2, 71.1, 70.6, 68.4, 64.4, 50.0, 34.8, 31.6, 24.5; **^{19}F NMR** (282.4 MHz, CD_2Cl_2) δ (ppm): −71.4 (d, *J* = 715 Hz, P*F*$_6$); **^{31}P NMR** (202.4 MHz, $CDCl_3$) δ (ppm): −143.9 (sept, *J* = 715 Hz, *P*F$_6$); **ESIMS** *m*/*z*: 1690.9249 ([M−PF$_6$]$^+$, $C_{110}H_{124}N_5O_{11}$ requires 1690.9292).

Pyridine-3,5-bis-amide thread compound 132



Pyridine-3,5-dicarboxylic acid (1.31 g, 7.84 mmol) was suspended in $SOCl_2$ (20 mL), DMF (5 drops, cat.) was added and the mixture heated at reflux under N_2 for 18 h until the solution became homogenous. The $SOCl_2$ was removed by distillation, the residue was redissolved in anhydrous CH_2Cl_2 (20 mL) and added dropwise to a solution of 2,6-dimethylaniline (2.40 mL, 2.38 g, 19.6 mmol) and Et_3N (3.30 mL, 2.37 g, 23.5 mmol) in anhydrous CH_2Cl_2 (30 mL). The reaction was stirred at rt under N_2 for 18 h, washed with 10% citric $acid_{(aq)}$ (2 × 50 mL), H_2O (2 × 50 mL), dried over anhydrous $MgSO_4$, filtered, and the solvent removed *in vacuo*. The crude residue was purified by column chromatography (SiO_2, 97:3 CH_2Cl_2:MeOH) to give **132** as a white solid in 33% yield (968 mg, 2.59 mmol). **^{1}H NMR** (300 MHz, DMSO-d_6) δ (ppm): 10.17 (2H, s, N*H*), 9.34 (2H, s, pyridine-H^2&H^6), 8.84 (1H, s, pyridine-H^4), 7.15 (6H, s, aniline-*H*), 2.22 (12H, s, CH_3); **^{13}C NMR** (75.5 MHz, 1:1 $CDCl_3$:CD_3OD) δ (ppm): 165.1, 151.5, 136.4, 136.0, 134.4, 131.1, 128.9, 128.4, 58.1; **ESIMS** *m/z*: 396.1672 ($[M+Na]^+$, $C_{23}H_{23}N_3NaO_2$ requires 396.1682).

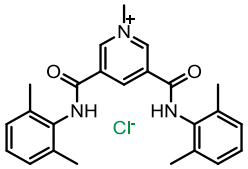
Pyridinium-3,5-bis-amide iodide axle compound 133·I



Compound **132** (500 mg, 1.34 mmol) was dissolved in 1:1 $CHCl_3$:acetone (5 mL). MeI (5 mL) was added and the suspension heated at 40 °C under N_2 for 3 days. The yellow solution was cooled to rt and the solvent removed *in vacuo* to give **133·I** as a bright yellow solid in 85% yield (587 mg, 1.14 mmol). **^{1}H NMR** (300 MHz, DMSO-d_6) δ (ppm): 10.55 (2H, s, N*H*), 9.68 (2H, s, pyridinium-H^2&H^6), 9.53 (1H, s, pyridinium-H^4), 7.19 (6H, s, aniline-*H*), 4.53 (3H, s, NCH_3), 2.25 (12H, s, CH_3); **^{13}C NMR** (75.5 MHz, DMSO-d_6) δ

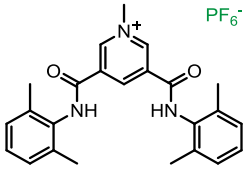
(ppm): 159.6, 147.4, 140.9, 135.1, 133.6, 132.8, 127.8, 127.1, 48.4, 17.8; **ESIMS** *m/z*: 388.2018 ($[M-I]^+$, $C_{24}H_{26}N_3O_2$ requires 388.2020).

Pyridinium-3,5-bis-amide chloride axle compound 133·Cl



Compound **133·I** was converted to **139·Cl** using filtration through Amberlite® IRA-402 Cl (approx. 5 mL) in a 10 mL disposable syringe. Compound **133·I** (50 mg, 100 μmol) was dissolved in acetone:water (7:3, 100 mL) and passed through the Amberlite® column. The column was washed further with acetone:water (7:3, 100 mL) and the washings combined with the other product-containing fractions. The solvents were removed *in vacuo* and the solid dried under vacuum to give **133·Cl** as a pale orange solid in 63% yield (25.8 mg, 60.8 μmol). **^{1}H NMR** (300 MHz, DMSO-d_6) δ (ppm): 10.71 (2H, s, N*H*), 9.72 (3H, s, pyridinium-H^2,H^4&H^6), 7.10 (6H, aniline-*H*), 4.52 (3H, NCH_3), 2.25 (12H, s, CH_3); **^{13}C NMR** (75.5 MHz, 1:1 $CDCl_3$:CD_3OD) δ (ppm): 160.9, 148.0, 143.2, 136.2, 135.0, 133.7, 128.9, 128.7, 24.2, 18.6; **ESIMS** *m/z*: 388.2017 ($[M-Cl]^+$, $C_{24}H_{26}N_3O_2$ requires 388.2020).

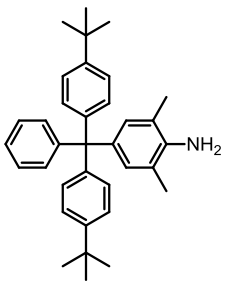
Pyridinium-3,5-bis-amide hexafluorophospate axle compound 133·PF$_6$



Compound **139·I** was converted to **133·PF$_6$** using filtration through an Amberlite® column. IPA-402 Cl (approx. 5 mL) was loaded into a 10 mL disposable syringe and washed with H_2O (100 mL), 1 M NaOH (100 mL), H_2O (100 mL), 0.1 M $NH_4PF_{6(aq)}$ (100 mL), H_2O (100 mL) and acetone:water (7:3, 100 mL). Compound **133·I** (100 mg, 20 mmol) was dissolved in acetone:water (7:3, 100 mL) and passed through the Amberlite® column. The column was washed with further acetone:water (7:3, 100 mL) and the washings combined with the other

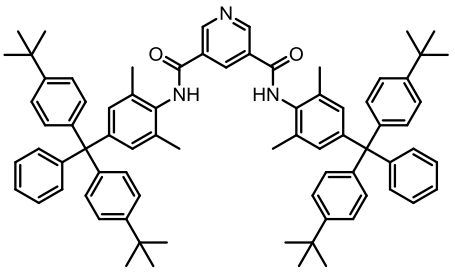
product-containing fractions. The solvent was removed *in vacuo* and the resulting off-white solid dried under vacuum to give **133·PF$_6$** in 39% yield (40 mg, 0.07 mmol). **^{1}H NMR** (300 MHz, CD_2Cl_2) δ (ppm): 9.43 (1H, s, pyridinium-*H*^{4}), 9.31 (2H, s, pyridinium-*H*^{2}&*H*^{6}), 8.55 (2H, s, N*H*), 7.13–7.24 (6H, m, aniline-*H*), 4.49 (3H, s, NC*H*$_3$), 2.24 (12H, s, C*H*$_3$); **^{13}C NMR** (75.5 MHz, acetone-d_6) δ (ppm): 161.8, 148.6, 142.6, 136.7, 135.6, 134.7, 129.1, 128.7, 18.5; **^{19}F NMR** (282.4 MHz, CD_2Cl_2) δ (ppm): −71.5 (d, *J* = 712 Hz, P*F*$_6$); **^{31}P NMR** (121.6 MHz, CD_2Cl_2) δ (ppm): −144.3 (sept, d, *J* = 712 Hz, *P*F$_6$); **ESIMS** *m/z*: 388.2008 ([M−PF$_6$]$^+$ $C_{24}H_{26}N_3O_2$ requires 388.2020).

Stoppered-amine compound 134



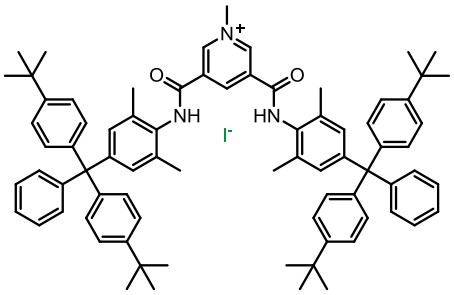
Compound **75** (1.50 g, 4.00 mmol) was dissolved in anhydrous benzene, acetyl chloride (0.70 mL) was added and the solution was heated at reflux for 30 min. After cooling to rt, hexanes (12 mL) were added and the solution cooled at 4 °C for 18 h. The resulting white crystals were filtered, redissolved in 2,6-dimethylaniline (10 mL) and heated to 125 °C under N_2 for 3 days. The reaction mixture was cooled to rt, poured onto 10% $HCl_{(aq)}$ and stirred for 20 min. The pale purple mixture was filtered and the residue washed with sat. $K_2CO_{3(aq)}$ (50 mL) and H_2O (50 mL), and purified by column chromatography (SiO_2, CH_2Cl_2) to give **134** as a white solid in 65% yield (1.23 g, 2.59 mmol). **^{1}H NMR** (300 MHz, $CDCl_3$) δ (ppm): 7.21–7.24 (9H, m, Ar*H*), 7.09–7.12 (4H, m, Ar*H*), 6.76 (2H, s, Ar*H*), 2.11 (6H, s, C*H*$_3$), 1.31 (18H, s, C(C*H*$_3$)$_3$); **^{13}C NMR** (75.5 MHz, $CDCl_3$) δ (ppm): 147.6, 147.4, 143.9, 139.8, 138.0, 136.1, 130.8, 130.7, 130.3, 127.1, 126.6, 125.0, 123.6, 33.8, 31.0, 17.5; **ESIMS** *m/z*: 498.3114 ([M+Na]$^+$, $C_{35}H_{41}NNa$ requires 498.3131).

Pyridine-3,5-bis-amide axle compound 135



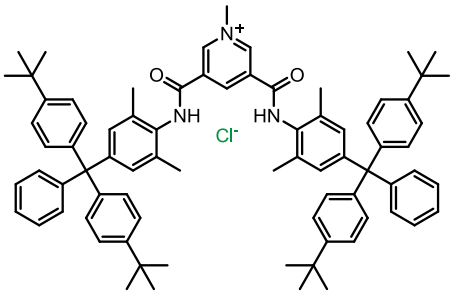
Pyridine-3,5-dicarboxylic acid (175 mg, 1.05 mmol) was suspended in $SOCl_2$ (10 mL), DMF (5 drops, cat.) was added and the mixture heated at reflux under N_2 for 18 h until the solution became homogenous. The $SOCl_2$ was removed by distillation and the yellow residue redissolved in anhydrous CH_2Cl_2. This was added dropwise to a solution of **134** (1.00 g, 2.01 mmol) and Et_3N (1.00 mL, excess) in anhydrous CH_2Cl_2 that had been stirred vigorously under N_2 for 30 min. The reaction mixture was stirred at rt under N_2 for 2 h. The solvent was removed *in vacuo*, EtOH was added and the mixture heated at reflux for 1 h, cooled to rt, and filtered to give **135** as an off-white solid in 38% yield (428 mg, 0.395 mmol). **^{1}H NMR** (300 MHz, $CDCl_3$) δ (ppm): 9.31 (2H, d, ^4J = 2.1 Hz, pyridine-H^2&H^6), 8.76 (1H, t, ^4J = 2.1 Hz, pyridine-H^4), 7.59 (2H, s, N*H*), 7.24–7.26 (18H, m, Ar*H*), 7.12–7.15 (8H, m, Ar*H*), 7.00 (4H, s, Ar*H*), 2.18 (12H, s, CH_3), 1.31 (36H, s, C(CH_3)$_3$); **^{13}C NMR** (75.5 Hz, $CDCl_3$) δ (ppm): 163.1, 152.7, 150.8, 148.8, 148.4, 146.7, 143.5, 137.0, 133.9, 131.2, 131.1, 130.7, 130.2, 127.3, 125.7, 124.2, 120.8, 34.3, 31.4, 18.8; **ESIMS** *m/z*: 1104.6380 ($[M+Na]^+$, $C_{73}H_{75}N_3NaO_2$ 1104.6378).

Pyridinium-3,5-bis-amide iodide axle compound 136·I



Compound **135** (350 mg, 0.32 mmol) was dissolved in MeI and heated at reflux under N_2 for 5 days. The reaction mixture was cooled to rt, poured into Et_2O and filtered to give **136·I** as a bright yellow solid in 77% yield (301 mg, 0.246 mmol). **^{1}H NMR** (300 MHz, $CDCl_3$) δ (ppm): 10.19 (1H, s, pyridinium-*H*^{4}), 10.09 (2H, s, N*H*), 9.18 (2H, s, pyridinium-*H*^{2}&*H*^{6}), 7.16–7.32 (30H, m, Ar*H*), 7.04 (4H, s, Ar*H*), 3.77 (3H, s, NC*H*$_3$), 2.22 (12H, s, C*H*$_3$), 1.31 (36H, s, C(C*H*$_3$)$_3$); **^{13}C NMR** (75.5 MHz, $CDCl_3$) δ (ppm): 160.1, 148.4, 147.3, 147.1, 147.0, 143.7, 141.9, 134.4, 134.1, 131.1, 131.0, 130.5, 127.5, 125.7, 124.4, 64.0, 48.4, 34.3, 31.4, 29.3, 19.4; **ESIMS** *m/z*: 1096.6714 ([M−I]$^-$, $C_{78}H_{86}N_3O_2$ requires 1096.6751).

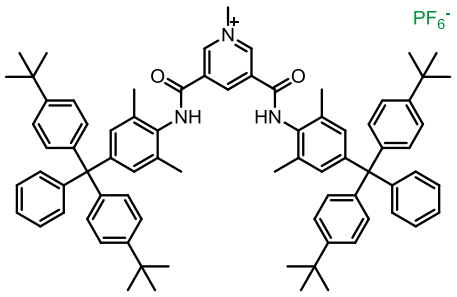
Pyridinium-3,5-bis-amide chloride axle compound 136·Cl



Compound **136·I** (400 mg, 0.3 mmol) was dissolved in $CHCl_3$ (200 mL) and washed with 1 M $NH_4Cl_{(aq)}$ (10 × 200 mL) and H_2O (2 × 100 mL). The organic phase was dried over anhydrous $MgSO_4$, filtered, and the solvent removed *in vacuo* to give **136·Cl** as a bright yellow solid in 92% yield (340 mg, 0.30 mmol).**^{1}H NMR** (300 MHz, $CDCl_3$) δ (ppm): 11.01 (2H, br s, N*H*), 10.08 (1H, s, pyridinium-*H*^{4}), 9.12 (2H, s, pyridinium-*H*^{2}&*H*^{6}), 7.16–7.34 (30H, m, Ar*H*), 7.05 (4H, s, Ar*H*), 3.42 (3H, s, NC*H*$_3$), 2.19 (12H, s, C*H*$_3$), 1.30 (36H, s, C(C*H*$_3$)$_3$); **^{13}C NMR** (75.5 MHz, $CDCl_3$) δ (ppm): 159.9, 148.3, 147.4, 146.9, 146.7, 143.8,

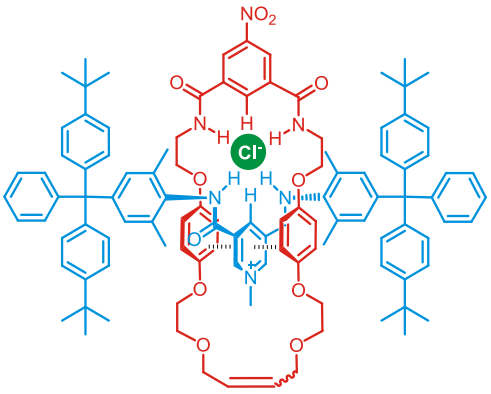
142.4, 134.7, 134.1, 131.1, 131.0, 130.9, 130.5, 127.5, 125.6, 124.4, 64.0, 47.8, 34.3, 31.4, 19.1; **ESIMS** *m/z*: 1096.6707 ($[M-Cl]^+$, $C_{78}H_{86}N_3O_2$ requires 1096.6751).

Pyridinium-3,5-bis-amide hexafluorophosphate axle compound 136·PF$_6$



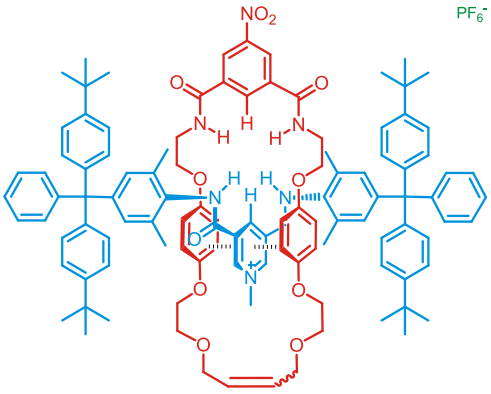
A solution of **136·I** (100 mg, 82 μmol) in $CHCl_3$ (30 mL) was washed with 0.1 M $NH_4PF_{6(aq)}$ (10 × 20 mL), H_2O (2 × 20 mL), dried over anhydrous $MgSO_4$ and filtered. The solvent was removed *in vacuo* to give **136·PF$_6$** as a bright yellow solid in 93% yield (94.8 mg, 76.4 μmol). **^{1}H NMR** (300 MHz, $CDCl_3$) δ (ppm): 9.28 (1H, s, pyridinium-*H*^{4}), 8.95 (2H, s, pyridinium-*H*^{2}&*H*^{6}), 8.67 (2H, br s, N*H*), 7.15–7.33 (30H, m, Ar*H*), 7.06 (4H, s, Ar*H*), 3.87 (3H, s, NC*H*$_3$), 2.08 (12H, s, C*H*$_3$), 1.34 (36H, s, C(C*H*$_3$)$_3$); **^{13}C NMR** (300 MHz, $CDCl_3$) δ (ppm): 159.8, 148.4, 147.2, 147.1, 143.6, 135.2, 134.1, 131.1, 131.0, 130.6, 130.5, 130.2, 127.4, 125.7, 124.4, 48.2, 34.3, 31.5, 31.3, 18.4; **^{19}F NMR** (282.4 MHz, $CDCl_3$) δ (ppm): −70.9 (d, *J* = 715 Hz, P*F*$_6$); **^{31}P NMR** (121.6 MHz, $CDCl_3$) δ (ppm): −144.7 (sept, *J* = 715 Hz, *P*F$_6$); **ESIMS** *m/z*: 1096.6703 ($[M-PF_6]^+$ $C_{78}H_{86}N_3O_2$ requires 1096.6715).

Rotaxane 137·Cl



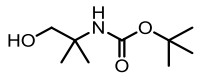
Compound **136·Cl** (100 mg, 0.09 mmol) and compound **99** (115 mg, 0.178 mmol) were dissolved in anhydrous CH_2Cl_2 (30 mL). Grubbs' II catalyst (11 mg, 10% by wt.) was added and the reaction mixture stirred at rt under N_2 for 4 days. After this time more Grubbs' II catalyst was added (6 mg) and the reaction left to stir for a further 3 days. The solvent was removed *in vacuo* and the crude residue purified by preparative thin layer chromatography (8:2 CH_2Cl_2:acetone, 2:1 60–80 petroluem ether:acetone and 1:1 CH_2Cl_2:MeCN) to give **137·Cl** as a yellow solid in 10% yield (14.7 mg, 8.38 μmol). **^{1}H NMR** (500 MHz, 1:1 $CDCl_3$:CD_3OD) δ (ppm): 9.49 (1H, s, pyridinium-*H*^{4}), 9.27 (2H, s, pyridinium-*H*^{2}&*H*^{6}), 9.13 (1H, s, isophthaloyl-*H*^{2}), 8.86 (2H, s, isophthaloyl-*H*^{4}&*H*^{6}), 7.22–7.27 (12H, m, axle-Ar*H*), 7.16–7.18 (6H, m, axle-Ar*H*), 7.08 (8H, d, ^3J = 8.8 Hz, axle-Ar*H*), 6.94 (4H, s, axle-Ar*H*), 6.50 (4H, d, ^3J = 8.9 Hz, hydroquinone-*H*), 6.37 (4H, d, ^3J = 8.9 Hz, hydroquinone-*H*), 6.01 (2H, alkene-C*H*), 4.45 (3H, s, NCH_3), 4.04 (4H, s, CH_2), 3.96 (4H, br t, ^3J = 5.0 Hz, CH_2), 3.88–3.89 (4H, m, CH_2), 3.75–3.77 (4H, m, CH_2), 3.62 (4H, br t, ^3J = 5.0 Hz, CH_2), 2.17 (12H, s, macrocycle-C(CH_3)$_2$), 1.27 (36H, s, axle-C(CH_3)$_3$); **^{13}C NMR** (125.8 MHz, 1:1 $CDCl_3$:CD_3OD) δ (ppm): 167.0, 160.8, 154.1, 153.7, 150.0, 148.5, 148.3, 144.9, 137.4, 135.5, 135.4, 135.0, 133.2, 132.5, 132.3, 132.0, 131.8, 131.3, 128.7, 127.2, 126.6, 125.6, 116.4, 116.1, 72.2, 70.6, 69.4, 67.5, 65.2, 41.3, 35.5, 33.2, 30.9, 23.9, 20.0; **ESIMS** *m*/*z*: 1717.9039 ([M−Cl]$^+$, $C_{110}H_{121}N_6O_{12}$ requires 1717.9037).

Rotaxane 137·PF$_6$



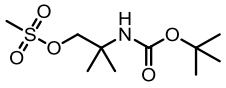
Compound **137·Cl** (16.7 mg, 9.52 μmol) was dissolved in $CHCl_3$ (50 mL) and washed with 0.1 M $NH_4PF_{6(aq)}$ (10 × 50 mL) and H_2O (2 × 50 mL). The organic phase was dried over anhydrous $MgSO_4$, filtered, and the solvent removed *in vacuo* to give **137·PF$_6$** as a pale yellow solid in 85% yield (15.4 mg, 8.05 μmol). **^{1}H NMR** (300 MHz, 1:1 $CDCl_3$:CD_3OD) δ (ppm): 9.45 (1H, s, pyridinium-*H*^{4}), 9.08 (2H, d, ^4J = 1.0 Hz, pyridinium-*H*^{2}&*H*^{6}), 9.03 (1H, t, ^4J = 1.7 Hz, isophthaloyl-*H*^{2}), 8.86 (2H, d, ^4J = 1.7 Hz, isophthaloyl-*H*^{4}&*H*^{6}), 7.24–7.28 (12H, m, axle-Ar*H*), 7.17–7.20 (6H, m, axle-Ar*H*), 7.08 (8H, d, ^3J = 8.5 Hz, axle-Ar*H*), 6.95 (4H, s, axle-Ar*H*), 6.50 (4H, d, ^3J = 9.0 Hz, hydroquinone-*H*), 6.37 (4H, d, ^3J = 9.0 Hz, hydroquinone-*H*), 6.03 (2H, s, alkene-C*H*), 4.44 (3H, s, NCH_3), 4.05–4.06 (4H, m, CH_2), 3.93 (4H, t, ^3J = 4.8 Hz, CH_2), 3.88–3.89 (4H, m, CH_2), 3.76–3.78 (4H, m, CH_2), 3.61 (4H, t, ^3J = 4.8 Hz, CH_2), 2.16 (12H, s, macrocycle-C(CH_3)$_2$), 1.28 (36H, s, axle-C(CH_3)$_3$); **^{13}C NMR** (125.8 MHz, 1:1 $CDCl_3$:CD_3OD) δ (ppm): 167.0, 160.8, 154.1, 153.7, 150.0, 149.9, 148.5, 148.3, 144.9, 137.4, 135.5, 135.4, 132.3, 131.9, 131.8, 131.3, 128.7, 127.2, 126.6, 125.6, 116.4, 116.1, 72.2, 70.6, 69.4, 67.5, 41.3, 35.5, 33.2, 30.9, 23.9, 20.0; **^{19}F NMR** (470.6 MHz, $CDCl_3$) δ (ppm): −73.7 (d, *J* = 712 Hz, P*F*$_6$); **ESIMS** *m/z*: 1717.9052 ([M−PF$_6$]$^+$, $C_{110}H_{121}N_6O_{12}$ requires 1717.9037).

Tert-butyl-(1-hydroxy-2-methylpropan-2-yl)carbamate 139[37]



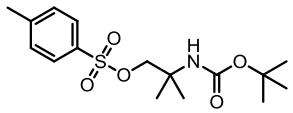
2-Amino-2-methyl propanol (5.00 mL, 4.67 g, 52.4 mmol) and di-*tert*-butyl dicarbonate (17.2 g, 78.6 mmol) were dissolved in anhydrous CH_2Cl_2 (150 mL). The reaction mixture was stirred at rt under N_2 for 16 h after which the solvent was removed *in vacuo*. The crude residue was dissolved in a minimum amount of hot pentane and the solution was cooled to −20 °C for 72 h. Compound **139** was isolated by filtration as a white solid in 66% yield (6.55 g, 34.6 mmol). **^{1}H NMR** (300 MHz, $CDCl_3$) δ (ppm): 4.73 (1H, br s, N*H*), 4.17 (1H, br s, O*H*), 3.56 (2H, d, ^3J = 5.9 Hz, CH_2), 1.42 (9H, s, C(CH_3)$_3$), 1.24 (6H, s, C(CH_3)$_2$); **ESIMS** *m*/*z*: 188.1 ([M−H]$^-$, $C_9H_{18}NO_3$ requires 188.1).

2-((_Tert_-butoxycarbonyl)amino)-2-methylpropyl methanesulfonate 140[37]



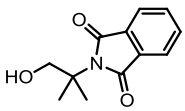
Compound **139** (1.00 g, 5.28 mmol) and Et_3N (1.50 mL, 1.07 g, 10.6 mmol) were dissolved in anhydrous CH_2Cl_2 (50 mL) and cooled to 0 °C. Methanesulfonyl chloride (0.810 mL, 1.21 g, 10.6 mmol) was added dropwise and the solution stirred at rt under N_2 for 1 h. The reaction mixture was washed with H_2O (2 × 50 mL), dried over anhydrous $MgSO_4$, filtered, and the solvent removed *in vacuo* to give compound **140** as a pale yellow liquid in 99% yield (1.40 g, 5.25 mmol). **^{1}H NMR** (300 MHz, $CDCl_3$) δ (ppm): 4.53 (1H, br s, N*H*), 4.32 (2H, s, CH_2), 3.01 (3H, s, SCH_3), 1.43 (9H, s, C(CH_3)$_3$), 1.33 (6H, s, C(CH_3)$_2$); **ESIMS** *m*/*z*: 290.1 ([M+Na]$^+$, $C_{10}H_{21}NaO_5S$ requires 290.1).

Compound 141



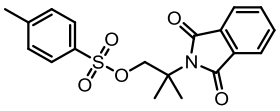
Compound **139** (1.00 g, 5.29 mmol) was dissolved in anhydrous CH_2Cl_2 (100 mL) and Et_3N (1.5 mL, 1.1 g, 11 mmol), *p*-toluenesulfonyl chloride (1.01 g, 5.29 mmol) and 4-DMAP (10 mg, cat.) were added. The reaction mixture was stirred at rt under N_2 for 16 h and H_2O (50 mL) was added. The reaction mixture was stirred vigorously and neutralised with 10% citric $acid_{(aq)}$. The organic phase was separated, washed with H_2O (2 × 50 mL), dried over anhydrous $MgSO_4$, filtered, and the solvent removed *in vacuo* to give **141** as a yellow oil that solidified on standing in 65% yield (1.17 g, 3.42 mmol). **^{1}H NMR** (300 MHz, $CDCl_3$) δ (ppm): 7.78 (2H, d, ^3J = 8.2 Hz, Ar*H*), 7.33 (2H, d, ^3J = 8.2 Hz, Ar*H*), 4.52 (1H, br s, N*H*), 4.05 (2H, s, CH_2), 2.44 (3H, s, CH_3), 1.43 (6H, s, C(CH_3)$_2$), 1.37 (9H, s, C(CH_3)$_3$); **^{13}C NMR** (75.5 MHz, $CDCl_3$) δ (ppm): 141.0, 130.6, 129.3, 128.4, 126.1, 77.5, 73.6, 73.6(*sic*), 31.0, 27.6, 22.5, 21.5; **ESIMS** *m/z*: 366.1335 ($[M+Na]^+$, $C_{16}H_{25}NNaO_5S$ requires 366.1346).

Compound 142[38]



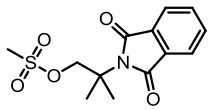
Phthalic anhydride (14.8 g, 0.10 mol) and 2-amino-2-methyl propanol (9.2 g, 0.10 mol) were heated at 160−180 °C under N_2 for 30 min. The reaction mixture was poured on ice water, the aqueous phase extracted with $CHCl_3$ (3 × 200 mL), and the combined organic phases dried over anhydrous $MgSO_4$, filtered, and the solvent removed *in vacuo*. The crude residue was purified by column chromatography (SiO_2, 7:3 hexanes:EtOAc) to give **142** as a white solid in 54% yield (11.9 g, 54.3 mmol). **^{1}H NMR** (300 MHz, $CDCl_3$) δ (ppm): 7.73–7.77 (2H, m, phthalimide-*H*), 7.66–7.70 (2H, m, phthalimide-*H*), 3.90 (2H, d, ^3J = 7.6 Hz, CH_2), 3.56 (1H, t, ^3J = 7.6 Hz, O*H*), 1.56 (6H, s, C(CH_3)$_2$); **ESIMS** *m/z*: 274.1 ($[M+Na+CH_3OH]^+$, $C_{13}H_{17}NNaO_4$ requires 274.1).

Compound 143



Compound **142** (1.00 g, 4.57 mmol) was dissolved in anhydrous CH_2Cl_2 (50 mL) and Et_3N (1.27 mL, 0.920 g, 9.11 mmol), *p*-toluenesulfonyl chloride (0.87 g, 4.6 mmol) and 4-DMAP (10 mg, cat.) were added. The reaction mixture was stirred at rt under N_2 for 16 h giving a dark orange solution. H_2O (30 mL) was added, the solution was stirred vigorously and neutralised with 10% citric $acid_{(aq)}$. The organic phase was separated, washed with H_2O (2 × 50 mL), dried over anhydrous $MgSO_4$, filtered, and the solvent removed *in vacuo*. The crude residue was purified by column chromatography (SiO_2, 9:1 CH_2Cl_2:acetone) to give **143** as a pale yellow solid in 20% yield (333 mg, 0.892 mmol). **^{1}H NMR** (300 MHz, $CDCl_3$) δ (ppm): 7.68–7.73 (6H, s, phthalimide-*H*), 7.20 (2H, d, ^3J = 7.7 Hz, phthalimide-*H*), 4.44 (2H, s, CH_2), 2.38 (3H, s, CH_3), 1.68 (6H, s, C(CH_3)$_2$); **^{13}C NMR** (75.5 MHz, $CDCl_3$) δ (ppm): 169.0, 144.7, 133.9, 132.6, 131.6, 129.7, 127.8, 127.0, 122.7, 58.8, 42.0, 24.2, 21.6; **ESIMS** *m/z*: 396.0870 ($[M+Na]^+$, $C_{19}H_{19}NNaO_5S$ requires 396.0876).

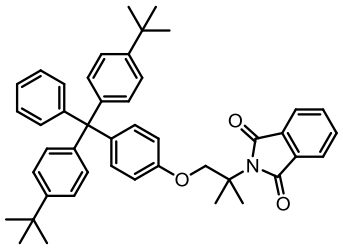
Compound 144



Compound **143** (1.00 g, 4.57 mmol) and Et_3N (1.28 mL, 0.930 g, 9.18 mmol) were dissolved in anhydrous CH_2Cl_2 (100 mL) and cooled to 0 °C. A solution of methanesulfonyl chloride (0.71 mL, 1.1 g, 9.2 mmol) in anhydrous CH_2Cl_2 (10 mL) was added dropwise, the reaction mixture warmed to rt and stirred under N_2 for 1 h. The solution was washed with H_2O (2 × 100 mL), 1 M $HCl_{(aq)}$ (3 × 100 mL), sat. $NaCl_{(aq)}$ (1 × 100 mL), dried over anhydrous $MgSO_4$, filtered, and the solvent removed *in vacuo*. The crude residue was purified by column chromatography (SiO_2, 9:1 CH_2Cl_2:acetone) to give **144** as a pale orange solid in quantitative yield (1.35 g, 4.54 mmol). **^{1}H NMR** (300 MHz, $CDCl_3$) δ (ppm): 7.79–7.82 (2H, m,

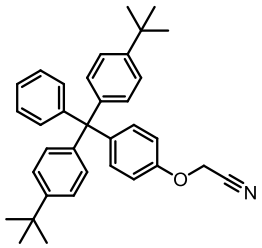
phthalimide-*H*), 7.71–7.73 (2H, m, phthalimide-*H*), 4.68 (2H, s, CH_2), 3.02 (3H, s, CH_3), 1.76 (6H, s, C(CH_3)$_2$); **^{13}C NMR** (75.5 MHz, $CDCl_3$) δ (ppm): 168.2, 134.1, 131.7, 122.9, 73.4, 58.8, 37.2, 24.2; **ESIMS** *m/z*: 320.0566 ([M+Na]$^+$, $C_{13}H_{15}NNaO_5S$ requires 320.0563).

Compound 145



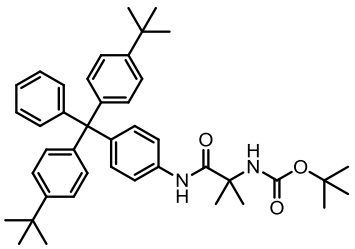
Compound **144** (264 mg, 0.888 mmol), compound **76** (200 mg, 0.5 mmol) and K_2CO_3 (608 mg, 4.40 mmol) were dissolved in anhydrous DMF (30 mL). The reaction mixture was heated to 80 °C for 72 h and the solvent removed *in vacuo*. H_2O (100 mL) was added and the aqueous phase extracted with CH_2Cl_2 (3 × 100 mL). The combined organic phases was dried over anhydrous $MgSO_4$, filtered, and the solvent removed *in vacuo*. The crude residue was purified by column chromatography (SiO_2, 2:1 hexanes:EtOAc) and preparative thin layer chromatography (4:1 60–80 petroleum ether:acetone) to give **145** as a white solid in 17% yield (50.0 mg, 77.0 µmol). **^{1}H NMR** (300 MHz, $CDCl_3$) δ (ppm): 7.87–7.90 (1H, m, phthalimide-*H*), 7.59–7.81 (1H, m, phthalimide-*H*), 7.56–7.59 (2H, m, phthalimide-*H*), 7.23–7.29 (11H, m, Ar*H*), 7.10–7.15 (6H, m, OCC*H*), 4.08 (2H, s, CH_2), 1.34 (6H, s, C(CH_3)$_2$), 1.32 (18, s, C(CH_3)$_3$); **^{13}C NMR** (75.5 MHz, $CDCl_3$) δ (ppm): 165.9, 148.8, 148.6, 147.0, 144.7, 143.5, 132.2, 131.5, 131.1, 130.7, 130.5, 130.0, 129.5, 128.8, 127.3, 124.3, 119.9, 79.8, 68.1, 63.8, 28.2; **ESIMS** *m/z*: 672.3448 ([M+Na]$^+$, $C_{45}H_{47}NNaO_3$ requires 672.3448).

Stopper-nitrile 146



Compound **76** (0.500 g, 1.11 mmol) and bromoacetonitrile (0.12 mL, 0.20 g, 1.7 mmol) was dissolved in anhydrous DMF (50 mL). K_2CO_3 (0.800 g, 5.79 mmol) was added and the reaction mixture heated at 80 °C under N_2 for 16 h. The solvent was removed *in vacuo*, H_2O (100 mL) was added and the aqueous layer extracted with EtOAc (3 × 100 mL). The organic phases were combined, dried over anhydrous $MgSO_4$, filtered, and the solvent removed *in vacuo*. The crude residue was purified by column chromatography (SiO_2, CH_2Cl_2) to give **146** as a white crystalline solid in 54% yield (291 mg, 0.597 mmol). **^{1}H NMR** (300 MHz, $CDCl_3$) δ (ppm): 7.16–7.26 (11H, m, Ar*H*), 7.08 (4H, d, ^3J = 9.1 Hz, Ar*H*), 6.85 (2H, d, ^3J = 9.1 Hz, OCC*H*), 4.75 (2H, s, CH_2), 1.30 (18H, s, C(CH_3)$_3$); **^{13}C NMR** (75.5 MHz, $CDCl_3$) δ (ppm): 154.4, 148.5, 147.0, 143.6, 142.0, 132.6, 131.1, 130.6, 127.3, 125.8, 124.2, 115.2, 113.5, 63.5, 53.4, 34.3, 31.3; **ESIMS** *m/z*: 510.2749 ([M+Na]$^+$, $C_{35}H_{37}NNaO$ requires 510.2767).

Compound 147

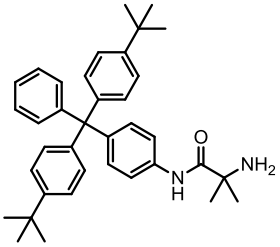


Method A: Boc-Aib-OH (51 mg, 0.25 mmol) was dissolved in anhydrous CH_2Cl_2 (10 mL) and D*i*PEA (87.1 µL, 64.4 mg, 0.50 mmol) and pyBOP (128 mg, 0.25 mmol) were added. The reaction mixture was stirred at rt under N_2 for 15 min and added dropwise to a solution of **116** (100 mg, 0.2 mmol) in anhydrous CH_2Cl_2 (10 mL). After stirring the solution at rt under

N_2 for 16 h, the solvent was removed *in vacuo*. The crude residue was purified by column chromatography (SiO_2, CH_2Cl_2) to give **147** in 25% yield (35 mg, 55 μmol).

Method B: Boc-Aib-OH (45 mg, 0.22 mmol) was dissolved in anhydrous CH_2Cl_2 (25 mL). EDCI (50 mg, 0.3 mmol) was added, followed by HOBt (35.1 mg, 0.260 mmol). This was added dropwise to a solution of **116** (100 mg, 0.2 mmol) in anhydrous CH_2Cl_2 (25 mL) at 0 °C. The reaction mixture was stirred at rt under N_2 for 16 h and quenched with 1 M $HCl_{(aq)}$. The organic phase was separated and the aqueous layer extracted with CH_2Cl_2 (3 × 50 mL). The combined organic phases were washed with sat. $NaHCO_{3(aq)}$ (100 mL) and sat. $NaCl_{(aq)}$ (100 mL), dried over anhydrous $MgSO_4$, filtered, and the solvent removed *in vacuo*. The crude residue was purified by column chromatography (SiO_2, CH_2Cl_2) to give **147** as a white solid in 62% yield (86.6 mg, 0.137 mmol). **^{1}H NMR** (300 MHz, $CDCl_3$) δ (ppm): 7.40 (2H, d, ^3J = 8.8 Hz, Ar*H*), 7.09–7.25 (15H, m, Ar*H*), 4.86 (1H, br s, amide-N*H*), 1.57 (6H, s, C(CH_3)$_2$), 1.45 (9H, s, OC(CH_3)$_3$), 1.31 (18H, s, C(CH_3)$_3$); **^{13}C NMR** (75.5 MHz, $CDCl_3$) δ (ppm): 172.6, 155.3, 148.4, 147.1, 143.7, 142.9, 135.8, 131.7, 131.1, 130.6, 127.3, 125.7, 124.1, 118.6, 63.7, 57.7, 53.4, 34.3, 31.4, 28.3, 25.7; **ESIMS** *m/z*: 655.3876 ($[M+Na]^+$, $C_{42}H_{52}N_2NaO_3$ requires 655.3870).

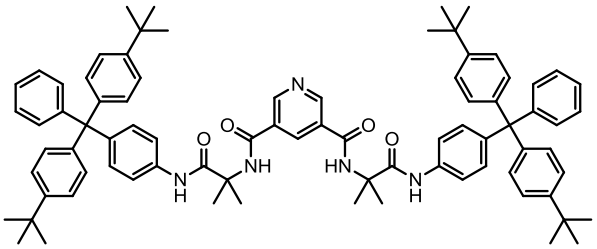
Compound 148



Compound **147** (796 mg, 1.26 mmol) was dissolved in $CHCl_3$ (20 mL). TFA (2 mL) was added and the resulting yellow solution stirred at rt under N_2 for 16 h. After basifying with 10% $NaOH_{(aq)}$ the aqueous layer was extracted with $CHCl_3$ (3 × 50 mL). The combined organic phases were washed with H_2O (100 mL), dried over anhydrous $MgSO_4$, filtered, and the solvent removed *in vacuo*. The crude residue was purified by column chromatography (SiO_2, 95:5 CH_2Cl_2:MeOH) to give **148** as a white crystalline solid in 73% yield (487 mg,

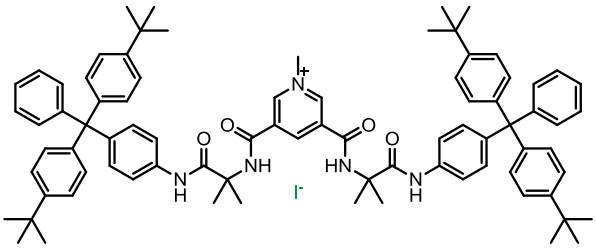
0.91 mmol). **^{1}H NMR** (300 MHz, $CDCl_3$) δ (ppm): 9.88 (1H, br s, amide-N*H*), 7.53 (2H, d, ^3J = 8.8 Hz, NCC*H*), 7.15–7.32 (15H, m, Ar*H*), 1.76 (2H, br s, NH_2), 1.49 (6H, s, $C(CH_3)_2$), 1.35 (18H, s, $C(CH_3)_3$); **^{13}C NMR** (75.5 MHz, $CDCl_3$) δ (ppm): 175.6, 148.4, 147.2, 143.7, 142.7, 135.6, 131.7, 131.1, 130.6, 127.3, 125.7, 124.2, 118.0, 63.7, 55.3, 34.3, 31.4, 29.2; **ESIMS** *m/z*: 533.3534 ($[M+H]^+$, $C_{37}H_{45}N_2O$ requires 533.3526).

Pyridine-3,5-bis-amide axle compound 149



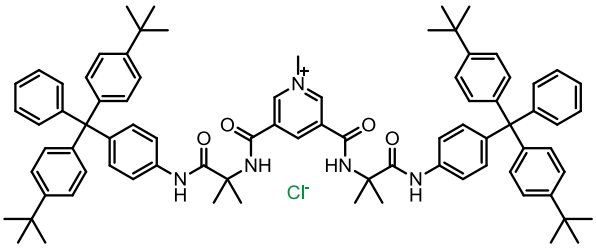
Pyridine-3,5-dicarboxylic acid (44 mg, 0.26 mmol) was suspended in $SOCl_2$ (5 mL). DMF (5 drops, cat.) was added and the reaction mixture was heated at reflux under N_2 for 16 h until the solution became homogenous. The $SOCl_2$ was removed by distillation, the residue redissolved in anhydrous CH_2Cl_2 (10 mL) and added dropwise to a solution of **148** (303 mg, 0.569 mmol), and Et_3N (0.10 mL, 73 mg, 0.72 mmol) in anhydrous CH_2Cl_2 (50 mL). The reaction mixture was stirred at rt under N_2 for 16 h during which time a white precipitate formed. The mixture was filtered to give **149** as a white solid and the filtrate was washed with 10% citric $acid_{(aq)}$ (50 mL), H_2O (50 mL), dried over anhydrous $MgSO_4$, filtered and concentrated to 10 mL. The resulting with precipitate was isolated by filtration and combined with the initial precipitate to give **149** in 66% yield (204 mg, 0.170 mmol). **^{1}H NMR** (300 MHz, 1:1 $CDCl_3$:CD_3OD) δ (ppm): 9.07 (2H, d, ^4J = 1.75 Hz, pyridine-H^2&H^6), 8.98 (2H, br s, amide-N*H*), 8.55 (1H, s, pyridine-H^4), 8.24 (2H, br s, amide-N*H*), 7.37 (4H, d, ^3J = 8.8 Hz, NCC*H*), 7.03–7.19 (30H, m, Ar*H*), 1.67 (12H, s, $(CH_3)_2$), 1.24 (36H, s, $(CH_3)_3$); **^{13}C NMR** (75.5 MHz, DMSO-d_6) δ (ppm): 172.8, 164.1, 147.9, 147.1, 143.8, 137.1, 130.4, 130.1, 129.3, 127.7, 124.5, 119.2, 63.3, 57.2, 42.2, 40.4, 34.1, 31.2, 25.0; **ESIMS** *m/z*: 1230.6602 ($[M+Cl]^-$, $C_{81}H_{89}ClN_5O_4$ requires 1230.6609).

Pyridinium-3,5-bis-amide iodide axle compound 150·I



Compound **149** (50 mg, 40 μmol) and MeI (5 mL) were heated at 40 °C for 72 h. MeI was removed *in vacuo* and the crude residue purified by column chromatography (95:5 CH_2Cl_2:MeOH) to give **150·I** as a yellow solid in 86% yield (48.2 mg, 36.0 μmol). **^{1}H NMR** (300 MHz, $CDCl_3$) δ (ppm): 10.21 (1H, br s, pyridinium-H^4), 9.04 (2H, br s, amide-N*H*), 8.79 (4H, br s, pyridinium-H^2&H^6, amide-N*H*), 7.41 (4H, d, ^3J = 8.8 Hz, NCC*H*), 7.16–7.23 (18H, m, Ar*H*), 7.05–7.11 (12H, m, Ar*H*), 3.37 (3H, s, NCH_3), 1.66 (12H, s, $C(CH_3)_2$), 1.27 (36H, s, $C(CH_3)_3$); **^{13}C NMR** (75.5 MHz, $CDCl_3$) δ (ppm): 172.3, 160.7, 149.0, 147.5, 147.0, 144.0, 143.5, 136.4, 131.8, 131.3, 130.9, 127.9, 126.3, 124.8, 91.1, 64.1, 59.8, 49.0, 34.7, 31.8, 25.8; **ESIMS** *m/z*: 1210.7179 ($[M-I]^+$, $C_{82}H_{92}N_5O_4$ requires 1210.7144).

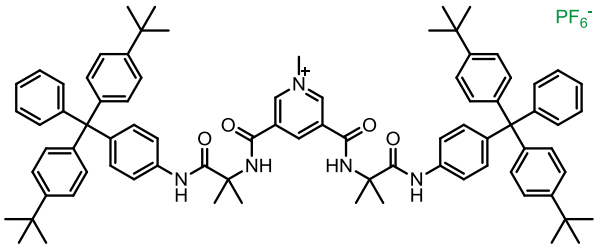
Pyridinium-3,5-bis-amide chloride axle compound 150·Cl



Compound **150·I** (48.2 mg, 36.0 μmol) was dissolved in $CHCl_3$ (50 mL) and washed with 1 M $NH_4Cl_{(aq)}$ (10 × 50 mL), H_2O (2 × 50 mL), dried over anhydrous $MgSO_4$, filtered, and the solvent removed *in vacuo* to give **150·Cl** as a yellow solid in 88% yield (39.4 mg, 31.6 μmol). **^{1}H NMR** (300 MHz, $CDCl_3$) δ (ppm): 10.57 (1H, br s, pyridinium-H^4), 9.26 (2H, br s, amide-N*H*), 9.07 (2H, br s, amide-N*H*), 8.87 (2H, s, pyridinium-H^2&H^6), 7.33 (4H, d, ^3J = 8.8 Hz, NCC*H*), 7.13–7.22 (18H, m, Ar*H*), 7.05–7.09 (12H, m, Ar*H*), 3.88 (3H, s, NCH_3), 1.66 (12H, s, $C(CH_3)_2$), 1.27 (36H, s, $C(CH_3)_3$); **^{13}C NMR** (75.5 MHz, $CDCl_3$)

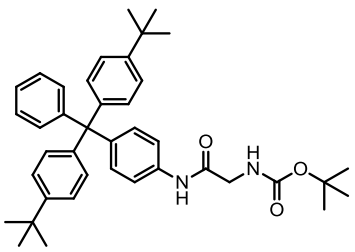
δ (ppm): 172.0, 160.5, 148.4, 147.1, 146.4, 143.7, 143.1, 135.9, 133.8, 131.4, 130.9, 130.5, 127.4, 125.7, 124.3, 118.8, 63.7, 59.1, 34.3, 31.3, 25.1; **ESIMS** *m/z*: 1210.7111 ($[M-Cl]^+$, $C_{82}H_{92}N_5O_4$ requires 1210.7144).

Pyridinium-3,5-bis-amide hexafluorophosphate axle compound 150·PF$_6$



Compound **150·I** (50.0 mg, 37.4 μmol) was dissolved in $CHCl_3$ (30 mL) and washed with 0.1 M $NH_4PF_{6(aq)}$ (8 × 10 mL), H_2O (2 × 20 mL), dried over anhydrous $MgSO_4$, filtered, and the solvent removed *in vacuo* to give **150·PF$_6$** as a pale yellow solid in 84% yield (39.4 mg, 31.6 μmol). **^{1}H NMR** (300 MHz, acetone-d_6) δ (ppm): 9.70 (1H, s, pyridinium-*H*^{4}), 9.60 (2H, s, pyridinium-*H*^{2}&*H*^{6}), 9.25 (2H, br s, amide-N*H*), 8.86 (2H, br s, amide-N*H*), 7.55 (4H, d, ^3J = 8.8 Hz, Ar*H*), 7.21–7.33 (18H, m, Ar*H*), 7.11–7.18 (12H, m, Ar*H*), 4.75 (3H, s, NCH_3), 1.69 (12H, s, C(CH_3)$_2$), 1.28 (36H, s, C(CH_3)$_3$); **^{13}C NMR** (75.5 MHz, acetone-d_6) δ (ppm): 161.3, 149.3, 148.3, 145.0, 143.2, 142.7, 138.1, 134.9, 131.9, 131.7, 131.5, 128.4, 126.8, 125.3, 19.8, 119.7, 59.5, 34.9, 31.7, 25.3; **^{19}F NMR** (282.4 MHz, acetone-d_6) δ (ppm): −72.3 (d, J = 724 Hz, PF_6); **ESMS** *m/z*: 1210.7098 ($[M-PF_6]^+$, $C_{82}H_{92}N_5O_4$ requires 1210.7144.

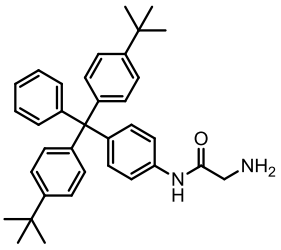
Compound 151



Boc-Gly-OH (196 mg, 1.12 mmol) was dissolved in anhydrous CH_2Cl_2 (25 mL), ECDI·HCl (257 mg, 1.34 mmol) and HOBt (181 mg, 1.34 mmol) were added and the solution added

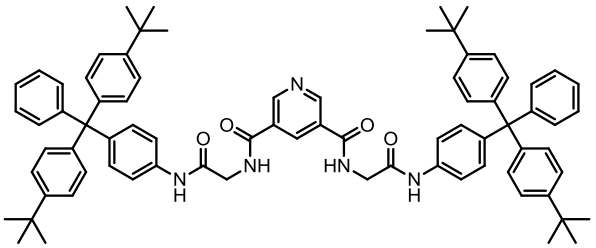
dropwise to a solution of compound **116** (500 mg, 1.12 mmol) in anhydrous CH_2Cl_2 (25 mL) at 0 °C. The reaction mixture was stirred at rt under N_2 for 16 h after which is was quenched with 1 M $HCl_{(aq)}$. The organic layer was separated and washed with sat. $NaHCO_{3(aq)}$ (50 mL), H_2O (50 mL), dried over anhydrous $MgSO_4$, filtered, and the solvent removed *in vacuo*. The crude residue was purified by column chromatography (SiO_2, CH_2Cl_2) to give **151** as a white solid in 94% yield (638 mg, 1.05 mmol). **^{1}H NMR** (300 MHz, $CDCl_3$) δ (ppm): 8.13 (1H, s, ArN*H*), 7.43 (2H, d, ^3J = 8.1 Hz, NCC*H*), 7.21–7.31 (11H, m, Ar*H*), 7.15 (4H, d, ^3J = 8.4 Hz, Ar*H*), 5.27 (1H, s, amide-N*H*), 3.95 (2H, s, CH_2), 1.52 (9H, s, OC(CH_3)$_3$), 1.35 (18H, s, C(CH_3)$_3$); **^{13}C NMR** (75.5 MHz, $CDCl_3$) δ (ppm): 167.8, 156.4, 148.4, 147.0, 143.6, 143.5, 135.0, 131.7, 131.1, 130.6, 127.3, 125.7, 124.2, 118.8, 63.7, 53.4, 45.5, 34.3, 31.3, 28.3; **ESIMS** *m/z*: 603.3618 ([M+H]$^+$, $C_{40}H_{47}N_2O_3$ requires 603.3592).

Compound 152



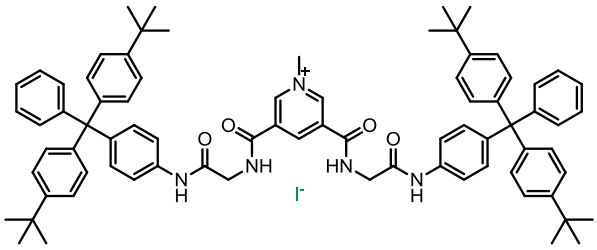
Compound **151** (500 mg, 0.8 mmol) was dissolved in CH_2Cl_2 (20 mL) and TFA (2 mL) was added. The reaction mixture was stirred at rt under N_2 for 16 h and then basified with 10% $NaOH_{(aq)}$. The organic phase was separated and the aqueous phase extracted with $CHCl_3$ (3 × 50 mL). The combined organic phases were dried over anhydrous $MgSO_4$, filtered, and the solvent removed *in vacuo*. The crude residue was purified by column chromatography (SiO_2, 95:5 CH_2Cl_2:MeOH) to give **152** as a colourless solid in quantitative yield (418 mg, 0.828 mmol). **^{1}H NMR** (300 MHz, $CDCl_3$) δ (ppm): 9.40 (1H, s, amide-N*H*), 7.51 (2H, d, ^3J = 8.6 Hz, NCC*H*), 7.22–7.31 (11H, m, Ar*H*), 7.17 (4H, d, Ar*H*), 3.47 (2H, s, CH_2), 1.74 (2H, s, NH_2), 1.36 (18H, s, C(CH_3)$_3$); **^{13}C NMR** (75.5 MHz, $CDCl_3$) δ (ppm): 170.6, 148.4, 147.1, 143.7, 143.0, 135.1, 131.7, 131.0, 130.6, 127.2, 125.7, 124.2, 118.3, 63.7, 45.0, 34.2, 31.3; **ESIMS** *m/z*: 505.3213 ([M+H]$^+$, $C_{35}H_{41}N_2O$ requires 505.3211).

Pyridine-3,5-bis-amide axle compound 153



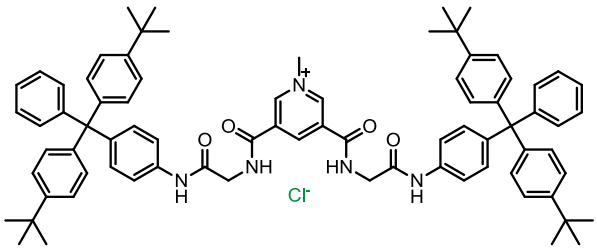
Pyridine-3,5-dicarboxylic acid (26.4 mg, 158 μmol) was suspended in $SOCl_2$ (5 mL), DMF (5 drops, cat.) was added and the mixture heated to 85 °C under N_2 for 16 h until the solution became homogenous. The $SOCl_2$ was removed by distillation and the residue redissolved in anhydrous CH_2Cl_2 (10 mL). This was added dropwise to a solution of **152** (200 mg, 40 μmol) and Et_3N (0.70 mL, 510 mg, 0.48 mmol) in anhydrous CH_2Cl_2 (50 mL) and the reaction mixture was stirred at rt under N_2 for 16 h. The mixture was washed with 10% citric $acid_{(aq)}$ (100 mL), H_2O (100 mL), dried over anhydrous $MgSO_4$, filtered, and the solvent removed *in vacuo*. After purifying by column chromatography (SiO_2, 97:3 CH_2Cl_2:MeOH), the product-containing fractions were combined and the solvent removed *in vacuo*. The residue was redissolved in CH_2Cl_2 and addition of 60–80 petroleum ether gave **153** as a white precipitate which was isolated by filtration in 67% yield (121 mg, 10.6 μmol). **^{1}H NMR** (300 MHz, 1:1 $CDCl_3$:CD_3OD) δ (ppm): 9.20 (2H, br s, pyridine-H^2&H^6), 8.88 (1H, s, pyridine-H^4), 7.43 (4H, d, ^3J = 9.0 Hz, NCCH), 7.12–7.22 (22H, m, ArH), 7.07 (8H, d, ^3J = 8.3 Hz, ArH), 4.20 (4H, s, CH_2), 1.26 (36H, s, C(CH_3)$_3$); **^{13}C NMR** (75.5 MHz, DMSO-d_6) δ (ppm): 171.5, 167.8, 165.3, 148.3, 147.3, 144.0, 142.1, 135.6, 131.1, 130.7, 130.4, 128.1, 126.2, 126.1, 124.9, 118.8, 63.7, 55.3, 34.5, 31.5; **ESIMS** *m/z*: 1162.6123 ($[M+Na]^+$, $C_{77}H_{81}N_5NaO_4$ requires 1162.6181).

Pyridinium-3,5-bis-amide iodide axle compound 154·I



Compound **153** (110 mg, 96 μmol) and MeI (10 mL) were heated at 40 °C under N_2 for 3 days. The MeI was removed *in vacuo* at the crude residue purified by column chromatography (SiO_2, 95:5 CH_2Cl_2:MeOH) to give **154·I** as a yellow solid in 54% yield (66.8 mg, 52.1 μmol). **^{1}H NMR** (300 MHz, 1:1 $CDCl_3$:CD_3OD) δ (ppm): 9.48 (2H, s, pyridinium-H^2&H^6), 9.43 (1H, br s, pyridinium-H^4), 7.43 (4H, d, ^3J = 9.1 Hz, NCCH), 7.12–7.22 (22H, m, ArH), 7.06 (8H, d, ^3J = 8.4 Hz, ArH), 4.45 (3H, s, NCH_3), 4.25 (4H, s, CH_2), 1.26 (36H, s, C(CH_3)$_3$); **^{13}C NMR** (75.5 MHz, 1:1 $CDCl_3$:CD_3OD) δ (ppm): 168.0, 162.6, 149.1, 147.8, 144.4, 144.2, 136.1, 134.4, 132.2, 131.7, 131.3, 128.0, 126.4, 124.9, 119.7, 64.4, 44.3, 39.7, 34.8, 31.8; **ESIMS** *m/z*: 1154.6497 ($[M-I]^+$, $C_{78}H_{84}N_5O_4$ requires 1154.6518).

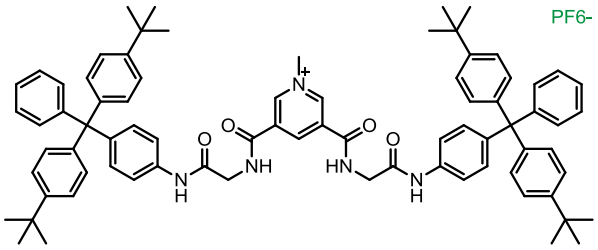
Pyridinium-3,5-bis-amide chloride axle compound 154·Cl



Compound **154·I** (66.8 mg, 52.1 μmol) was dissolved in $CHCl_3$ (50 mL) and washed with 1 M $NH_4Cl_{(aq)}$ (10 × 50 mL), H_2O (2 × 50 mL), dried over anhydrous $MgSO_4$, filtered, and the solvent removed *in vacuo* to give **154·Cl** as a yellow solid in 79% yield (48.6 mg, 40.8 μmol). **^{1}H NMR** (300 MHz, 1:1 $CDCl_3$:CD_3CN) δ (ppm): 10.27 (1H, s, pyridinium-H^4), 9.70 (2H, br t, ^3J = 5.2 Hz, amide-NHCH$_2$), 9.42 (2H, s, pyridinium-H^2&H^6), 9.33 (2H, s, ArNH), 7.44 (4H, d, ^3J = 8.7 Hz, NCCH), 7.16–7.22 (15H, m, ArH), 7.07–7.10 (15H, m, ArH), 4.29

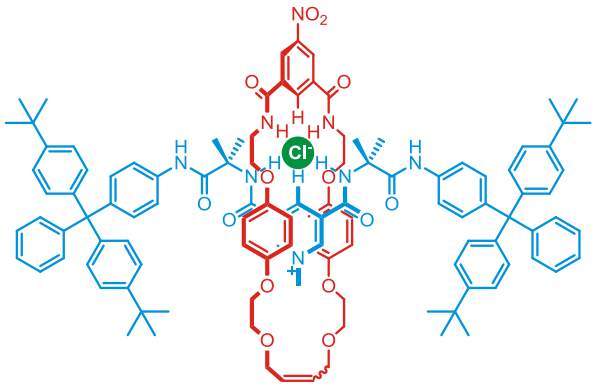
(3H, s, NCH_3), 4.16 (4H, d, ^3J = 5.2 Hz, CH_2), 1.23 (36H, s, C(CH_3)$_3$); **^{13}C NMR** (75.5 MHz, 1:1 $CDCl_3$:CD_3CN) δ (ppm): 167.3, 161.6, 148.8, 147.7, 144.4, 143.3, 136.3, 136.2, 133.6, 131.5, 131.2, 130.8, 128.0, 126.2, 124.9, 119.3, 64.1, 49.4, 44.5, 34.6, 31.5; **ESIMS** *m/z*: 1154.6520 ([M−Cl]$^+$, $C_{78}H_{84}N_5O_4$ requires 1154.6518).

Pyridinium-3,5-bis-amide hexafluorophosphate axle compound 154·PF$_6$



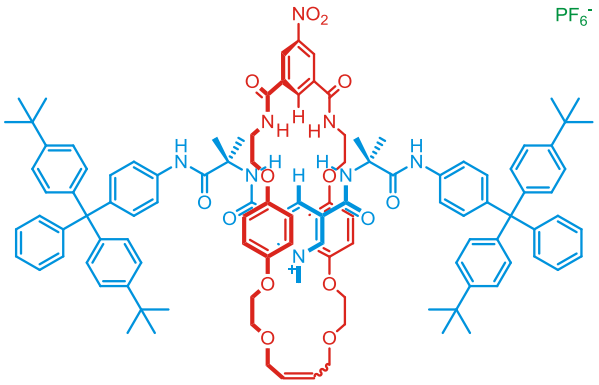
Compound **154·I** (16.7 mg, 14.0 μmol) was dissolved in $CHCl_3$ (50 mL) and washed with 0.1 M $NH_4PF_{6(aq)}$ (10 × 20 mL), H_2O (2 × 20 mL), dried over anhydrous $MgSO_4$, filtered, and the solvent removed *in vacuo* to give **154·PF$_6$** as an off-white solid in 89% yield (15.0 mg, 11.5 μmol). **^{1}H NMR** (500 MHz, DMSO-d_6) δ (ppm): 10.31 (2H, s, pyridinium-H^2&H^6), 10.10 (2H, s, ArNH), 9.59 (1H, s, pyridinium-H^4), 9.53 (2H, s, amide-NHCH_2), 7.52 (4H, d, ^3J = 8.4 Hz, NCCH), 7.26–7.30 (12H, m, ArH), 7.13–7.18 (6H, m, ArH), 7.04–7.08 (12H, m, ArH), 4.44 (3H, s, NCH_3), 4.12 (4H, s, CH_2), 1.25 (36H, s, C(CH_3)$_3$); **^{13}C NMR** (125.8 MHz, DMSO-d_6) δ (ppm): 161.5, 147.9, 147.3, 146.8, 141.6, 136.5, 132.7, 130.6, 130.0, 127.6, 124.4, 118.6, 63.2, 34.0, 31.1; **^{19}F NMR** (470.6 MHz, DMSO-d_6) δ (ppm): −70.2 (d, J = 712 Hz, PF_6); **^{31}P** NMR (202.4 MHz, DMSO-d_6) δ (ppm): −144.2 (sept, J = 712 Hz, PF$_6$); **ESIMS** *m/z*: 1154.6474 ([M−PF$_6$]$^+$, $C_{78}H_{84}N_5O_4$ requires 1154.6518).

Rotaxane 155·Cl



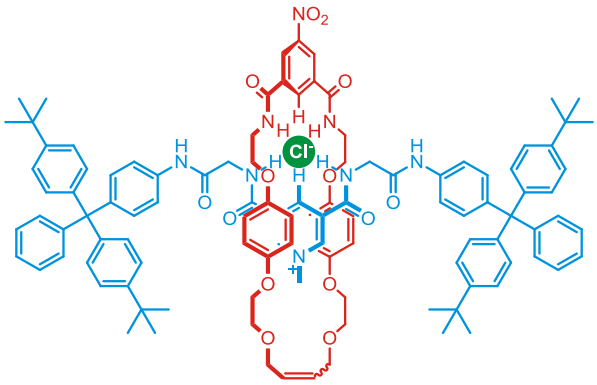
Compound **150·Cl** (100 mg, 0.08 mmol) and compound **99** (62.5 mg, 0.100 mmol) were dissolved in anhydrous CH_2Cl_2 (5 mL). Grubbs' II catalyst (6.3 mg, 10% by wt.) was added and the reaction mixture stirred at rt under N_2 for 3 days. The solvent was removed *in vacuo* and the crude residue purified by preparative thin layer column chromatography (9:1 CH_2Cl_2:MeOH, 1:1 CH_2Cl_2:MeCN and 9:1 EtOAc:MeOH) to give **155·Cl** as a yellow solid in 26% yield (38.8 mg, 20.5 μmol). **^{1}H NMR** (300 MHz, acetone-d_6) δ (ppm): 9.65 (1H, s, isophthaloyl-*H*^{2}), 9.60 (1H, s, pyridinium-*H*^{4}), 9.31 (2H, s, pyridinium-*H*^{2}&*H*^{6}), 9.10 (2H, br s, amide-N*H*), 8.92 (2H, s, amide-N*H*), 8.85 (2H, s, isophthaloyl-*H*^{4}&*H*^{6}), 8.37 (2H, s, amide-N*H*), 7.64 (4H, d, ^3J = 8.8 Hz, NCC*H*), 7.22–7.31 (16H, m, Ar*H*), 7.13–7.17 (14H, m, Ar*H*), 6.55 (4H, d, ^3J = 8.4 Hz, hydroquinone-*H*), 6.23 (4H, d, ^3J = 8.4 Hz, hydroquinone-*H*), 6.12 (2H, s, alkene-*H*), 4.56 (3H, s, NCH_3), 4.20–4.23 (4H, m, CH_2), 4.09–4.10 (4H, m, CH_2), 3.76–3.78 (8H, m, CH_2), 3.68–3.69 (4H, m, CH_2), 1.72 (12H, s, C(CH_3)$_2$), 1.28 (36H, s, C(CH_3)$_3$); **^{13}C NMR** (75.5 MHz, acetone-d_6) δ (ppm): 172.3, 171.0, 164.9, 160.9, 153.9, 153.2, 149.7, 149.3, 148.2, 147.4, 145.0, 143.5, 137.8, 137.0, 133.9, 132.0, 131.7, 131.4, 131.2, 128.4, 126.7, 126.3, 125.3, 120.2, 116.0, 115.5, 71.5, 69.9, 68.8, 67.2, 64.7, 60.6, 59.8, 49.6, 41.8, 34.9, 31.7, 25.7; **ESIMS** *m/z*: 1831.9467 ($[M-Cl]^+$, $C_{114}H_{127}N_8O_{14}$ requires 1831.9466).

Rotaxane 155·PF$_6$



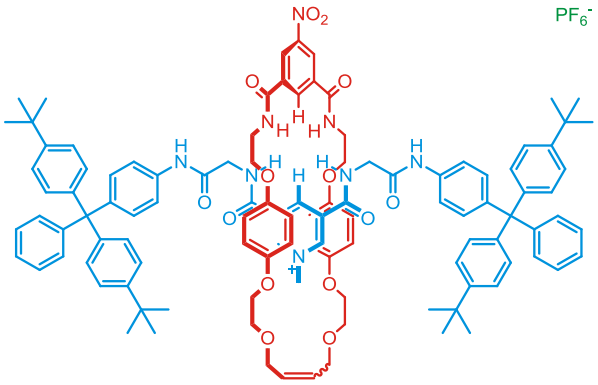
Compound **155·Cl** (38.8 mg, 20.5 μmol) was dissolved in $CHCl_3$ (20 mL) and washed with 0.1 M $NH_4PF_{6(aq)}$ (10 × 10 mL), H_2O (2 × 10 mL), dried over anhydrous $MgSO_4$, filtered, and the solvent removed *in vacuo* to give **155·PF$_6$** as a yellow solid in quantitative yield (44.5 mg, 20.5 μmol). **^{1}H NMR** (300 MHz, acetone-d_6) δ (ppm): 9.17 (1H, br s, pyridinium-*H*^{4}), 9.16 (2H, s, pyridinium-*H*^{2}&*H*^{6}), 9.03 (1H, br s, isophthaloyl-*H*^{2}), 8.92 (2H, s, axle-N*H*), 8.81 (2H, d, ^4J = 1.6 Hz, isophthaloyl-*H*^{4}&*H*^{6}), 8.46 (2H, br s, macrocycle-N*H*), 8.43 (2H, s, axle-N*H*), 7.57 (4H, d, ^3J = 8.5 Hz, NCC*H*), 7.14–7.31 (30H, m, Ar*H*), 6.47 (4H, d, ^3J = 9.4 Hz, hydroquinone-*H*), 6.37 (4H, d, ^3J = 9.4 Hz, hydroquinone-*H*), 6.01 (2H, br t, ^3J = 2.6 Hz, alkene-*H*), 4.54 (3H, m, NCH_3), 4.06–4.07 (4H, m, CH_2), 3.84–3.89 (8H, m, CH_2), 3.71–3.74 (4H, m, CH_2), 3.62–3.64 (4H, m, CH_2), 1.63 (12H, s, C(CH_3)$_2$), 1.27 (36H, s, C(CH_3)$_3$); **^{13}C NMR** (75.5 MHz, acetone-d_6) δ (ppm): 172.6, 165.8, 161.3, 153.8, 153.6, 151.5, 149.5, 145.2, 143.9, 137.8, 137.5, 135.0, 133.4, 132.2, 131.9, 131.6, 130.8, 128.7, 127.0, 125.8, 125.6, 120.1, 116.2, 115.9, 71.7, 70.1, 69.2, 67.3, 64.9, 59.9, 50.5, 40.9, 35.2, 32.0, 25.3; **^{19}F NMR** (282.4 MHz, acetone-d_6) δ (ppm): –71.6 (d, *J* = 724.2 Hz, PF_6); **ESIMS** *m*/*z*: 1831.9476 ($[M-PF_6]^+$, $C_{114}H_{127}N_8O_{14}$ requires 1831.9466).

Rotaxane 156·Cl



Compound **154·Cl** (56.3 mg, 47.3 μmol), compound **99** (36.8 mg, 56.6 μmol) and Grubbs' II catalyst (3.7 mg, 10% by wt.) were dissolved in anhydrous CH_2Cl_2 (5 mL) and stirred at rt under N_2 for 2 days. The solvent was removed *in vacuo* and the residue purified by preparative thin layer chromatography (SiO_2, 9:1 CH_2Cl_2:MeOH and 3:2 CH_2Cl_2:MeCN) to give **156·Cl** as a bright yellow solid in 25% yield (21.8 mg, 11.6 μmol). **^{1}H NMR** (300 MHz, acetone-d_6) δ (ppm): 9.54 (1H, s, isophthaloyl-*H*^{2}), 6.52 (1H, s, pyridinium-*H*^{4}), 9.21 (2H, s, axle-N*H*), 9.19 (2H, s, pyridinium-*H*^{2}&*H*^{6}), 8.85–8.91 (4H, m, axle-N*H* & macrocycle-N*H*), 8.73 (2H, s, isophaloyl-*H*^{4}&*H*^{6}), 7.53 (4H, d, ^3J = 9.4 Hz NCC*H*), 7.10–7.34 (30H, m, Ar*H*), 6.58 (4H, d, ^3J = 9.4 Hz, hydroquinone-*H*), 6.25 (4H, d, ^3J = 9.4 Hz, hydroquinone-*H*), 6.16 (2H, s, alkene-*H*), 4.62 (3H, s, NCH_3), 4.24 (4H, t, ^3J = 4.6 Hz, CH_2), 4.14–4.18 (8H, m, CH_2), 3.80–3.81 (4H, m, CH_2), 3.72 (8H, m, CH_2), 1.29 (36H, s, C(CH_3)$_3$); **^{13}C NMR** (75.5 MHz, acetone-d_6) δ (ppm): 167.4, 165.0, 161.6, 154.3, 153.4, 149.8, 149.5, 148.5, 147.5, 145.2, 143.7, 139.3, 137.7, 137.2, 133.6, 132.6, 132.1, 131.7, 131.3, 131.0, 128.6, 127.0, 126.7, 125.5, 119.4, 116.0, 115.6, 71.7, 70.3, 68.9, 66.6, 64.9, 50.1, 44.8, 35.2, 32.0; **ESIMS** *m/z*: 1775.8778 ($[M-Cl]^+$, $C_{110}H_{119}N_8O_{14}$ requires 1775.8840).

Rotaxane 156·PF$_6$



Compound **156·Cl** (21.8 mg, 11.6 μmol) was dissolved in $CHCl_3$ (20 mL) and washed with 0.1 M $NH_4PF_{6(aq)}$ (10 × 10 mL), H_2O (2 × 10 mL), dried over anhydrous $MgSO_4$, filtered, and the solvent removed *in vacuo* to give **156·PF$_6$** as a yellow solid in 99% yield (22.8 mg, 11.5 mmol). **^{1}H NMR** (300 MHz, 1:1 $CDCl_3$:acetone-d_6) δ (ppm): 9.17 (4H, s, pyridinium-*H*^{2},*H*^{4}&*H*^{6}, isophthaloyl-*H*^{2}), 9.06 (2H, s, ArN*H*), 8.74 (2H, s, isophthaloyl-*H*^{4}&*H*^{6}), 8.66 (2H, br s, amide-N*H*), 8.51 (2H, br s, amide-N*H*), 7.44 (4H, d, ^3J = 8.8 Hz, Ar*H*), 7.17–7.25 (16H, m, Ar*H*), 7.08–7.15 (14H, s, Ar*H*), 6.51 (4H, d, ^3J = 9.4 Hz, hydroquinone-*H*) 6.28 (4H, d, ^3J = 9.4 Hz, hydroquinone-*H*), 6.07 (2H, br s, alkene-*H*), 4.52 (3H, s, NC*H*$_3$), 4.17–4.19 (4H, m, C*H*$_2$), 4.05–4.09 (8H, m, C*H*$_2$), 3.82–3.83 (4H, m, C*H*$_2$), 3.69–3.75 (8H, m, C*H*$_2$), 1.25 (36H, s, C(C*H*$_3$)$_3$); **^{13}C NMR** (75.5 MHz, 1:1 $CDCl_3$:acetone-d_6) δ (ppm): 166.6, 165.13, 161.0, 153.3, 152.8, 148.7, 144.3, 136.5, 133.3, 131.8, 131.3, 131.0, 130.5, 127.8, 126.1, 124.7, 118.7, 115.5, 115.0, 78.6, 71.1, 69.5, 68.3, 64.1, 34.5, 31.5, 36.1; **^{19}F NMR** (470.6 MHz, 1:1 $CDCl_3$:acetone-d_6) δ (ppm): −67.4 (d, J = 711, P*F*$_6$); **^{31}P NMR** (202.4 MHz, 1:1 $CDCl_3$:acetone-d_6) δ (ppm): −144.6 (sept, J = 711 Hz, *P*F$_6$); **ESIMS** *m*/*z*: 1775.8778 ([M–PF$_6$]$^+$, $C_{110}H_{119}N_8O_{14}$ requires 1775.8840).

6.6 ^{1}H NMR titration protocols

^{1}H NMR titration spectra were recorded on a Varian Unity Plus or Bruker Avance III 500 spectrometer. A solution of guest was added to a solution of host (0.5 ml) at 298 K. The chemical shift(s) of specific host proton(s) were monitored for seventeen titration points (for

0.0, 0.2, 0.4, 0.6, 0.8, 1.0, 1.2, 1.4, 1.6, 1.8, 2.0, 2.5, 3.0, 4.0, 5.0, 7.0, and 10.0 equivalents of added guest). The resulting data were analysed using the WinEQNMR2 computer program[39] in experiments where association of guest and host was fast on the NMR timescale.

A summary of the concentration of host and guest species, along with solvent for every ^{1}H NMR titration is given in Table A.1. The volumes of the salt solution added were 10 × 2 μL, 2 × 5 μL, 2 × 10 μL, 1 × 20 μL and 1 × 30 μL.

Binding stoichiometries were investigated by visual analysis of the titration data, and using approximations of Job plots. A graph of $\Delta\delta \cdot \chi_H$ against χ_H was plotted, with a 1:1 binding stoichiometry corresponding to a maximum $\delta.\chi_H \sim 0.5$ (χ_H = mole fraction of host, $\Delta\delta$ = change in chemical shift relative to free host).

When using the WinEQNMR2 computer program, estimates for the association constant and the limiting chemical shifts were added to the program's input file. The parameters were refined by non-linear least-squares analysis using WinEQNMR2 to achieve the best fit between observed and calculated chemical shifts. The input parameters for the final chemical shift and association constant were adjusted based on the program output until convergence was reached. Comparison of the calculated and experimental binding isotherms demonstrated that an appropriate model with an appropriate stoichiometry was being used.

WinEQNMR2 also provides an estimate of the error of the measurement, which is included with all data. This error is a measure of the standard deviation of the association constant value reported. To avoid introduction of inaccuracies by rounding, the absolute values of an association constant and its error are given in the text. This has the disadvantage that values are often given to more significant figures than is statistically valid, but this is taken into account when discussing the similarities and differences between association constants. It should also be noted that these estimated standard errors only account for the fitting of a

binding isotherm to the titration data, they do not consider systematic error behind such data, for example an incorrect concentration of the titrant solution.

Table A.1. Host and guest concentrations, and solvent, of ^{1}H NMR titrations

[Host]	[Guest]	Solvent
Porphyrin 6, **10**	Cl^-, Br^-, I^-, OAc^-, $H_2PO_4^-$, PF_6^-	$CDCl_3$
Porphyrin **11**	Cl^-, Br^-, I^-	$CDCl_3$
Porphyrin **25**	Cl^-	acetone-d_6
Axles **137·PF$_6$**, **152·PF$_6$**	Cl^-, AcO^-, $H_2PO_4^-$	1:1$CDCl_3$:CD_3OD
Catenanes **69·PF$_6$**, **70·PF$_6$**	Cl^-, Br^-, I^-	1:1 $CDCl_3$:CD_3OD
Threads **84·PF$_6$**, **86·BF$_4$**	Cl^-, Br^-, I^-, AcO^-	$CDCl_3$
Macrocycle **87**	Threads **84·Cl, 84·Br, 84·I, 84·AcO, 86·Cl**	$CDCl_3$
Rotaxane **134·PF$_6$**	Cl^-, AcO^-, $H_2PO_4^-$	45:45:10 $CDCl_3$:CD_3OD:D_2O
Rotaxanes **134·PF$_6$**, **157·PF$_6$**, **158·PF$_6$** (1.91×10^{-3} M)	Cl^-, AcO^-, $H_2PO_4^-$ (0.094 M)	1:1 $CDCl_3$:CD_3OD
Macrocycles **52**, **57**	Thread **44·Br**, **44·BF$_4$**, Cl^-	$CDCl_3$
Macrocycle **52**, **57** + Cl^-	Thread **44·BF$_4$**	$CDCl_3$
Macrocycle **52** + Br^-	Thread **62·BF$_4$**, **65·BF$_4$**	$CDCl_3$
Macrocycle **52** + I^-	Thread **62·BF$_4$**, **65·BF$_4$**	$CDCl_3$
Macrocycle **133** (3.94×10^{-3} M)	Thread **51·Cl** (0.182 M)	$CDCl_3$
Macrocycle **71** (5.54×10^{-3} M)	Threads **62·BF$_4$**, **65·BF$_4$**, **68·BF$_4$** (0.139 M)	CD_2Cl_2
Rotaxane **101·PF$_6$** (2×10^{-3} M)	Cl^- (0.1 M)	1:1 $CDCl_3$:CD_3OD
Rotaxane**140·PF$_6$** (1.52×10^{-3} M)	Cl^-, AcO^-, $H_2PO_4^-$ (0.076 M)	1:1$CDCl_3$:CD_3OD
Porphyrin 6 (4.77×10^{-4} M)	Ag^+, Cu^+ (0.024 M)	acetone-d_6

6.7 UV/visible titration protocols

UV/visible experiments were carried out on a PG instruments T60U spectrometer at 293 K. Aliquots of guest were added to a 2.5 mL solution of host in a 1 cm cuvette. Spectra were recorded after each addition and the sample was mixed thoroughly before each measurement. The concentration of host species was chosen to give an absorbance between 0.5 and 1.0. The concentration of the guest species was varied according to the strength of binding in order to obtain suitable experimental data for association constant determination.

Stability constants were obtained by analysis of the resulting titration data using the Specfit® computer program. The parameters were refined by global analysis using singular value decomposition and non-linear modeling by the Levenberg-Marquardt method. The parameters were varied until the values for the stability constants converged. Comparison of the theoretical binding isotherms, calculated concentration profiles and calculated spectra of the complexes with the experimental data confirmed that the models used were correct. Estimated standard errors are also reported.

6.8 References and notes for Chapter Six

[1] T. N. Sorrell, *Inorg. Synth.*, 1980, **20**, 161.
[2] J. P. Collman, R. R. Gagne, C. Reed, T. R. Halbert, G. Lang and W. T. Robinson, *J. Am. Chem. Soc.*, 1975, **97**, 1427-1439.
[3] J. Lindsey, *J. Org. Chem.*, 1980, **45**, 5215-5215.
[4] J. P. Collman, B. Boitrel, L. Fu, J. Galanter, A. Straumanis and M. Rapta, *J. Org. Chem.*, 1997, **62**, 2308-2309.
[5] J. Leroy, *Synth. Commun.*, 1992, **22**, 567-572.
[6] J. E. Hein, J. C. Tripp, L. B. Krasnova, K. B. Sharpless and V. V. Fokin, *Angew. Chem. Int. Ed.*, 2009, **48**, 8018-8021.
[7] D. C. Kennedy, C. S. McKay, M. C. B. Legault, D. C. Danielson, J. A. Blake, A. F. Pegoraro, A. Stolow, Z. Mester and J. P. Pezacki, *J. Am. Chem. Soc.*, 2011, **133**, 17993-18001.
[8] S. G. Alvarez and M. T. Alvarez, *Synthesis-Stuttgart*, 1997, 413-414.
[9] L. Q. Wen, M. Li and J. B. Schlenoff, *J. Am. Chem. Soc.*, 1997, **119**, 7726-7733.
[10] J. S. Lindsey and R. W. Wagner, *J. Org. Chem.*, 1989, **54**, 828-836.
[11] B. C. Bookser and T. C. Bruice, *J. Am. Chem. Soc.*, 1991, **113**, 4208-4218.
[12] J. E. A. Webb, F. Maharaj, I. M. Blake and M. J. Crossley, *Synlett*, 2008, 2147-2149.
[13] R. Xu, W. B. Schweizer and H. Frauenrath, *Chem. Eur. J.*, 2009, **15**, 9105-9116.
[14] H. Takalo, P. Pasanen and J. Kankare, *Acta Chem. Scand. Ser. B.*, 1988, **42**, 373-377.
[15] S. Bhattacharya, K. Snehalatha and V. P. Kumar, *J. Org. Chem.*, 2003, **68**, 2741-2747.
[16] A. Picot, C. Feuvrie, C. Barsu, F. Malvolti, B. Le Guennic, H. Le Bozec, C. Andraud, L. Toupet and O. Maury, *Tetrahedron*, 2008, **64**, 399-411.

[17] L. M. Hancock and P. D. Beer, *Chem. Eur. J.*, 2009, **15**, 42-44.
[18] K.-Y. Ng, V. Felix, S. M. Santos, N. H. Rees and P. D. Beer, *Chem. Commun.*, 2008, 1281-1283.
[19] K. M. Bonger, R. J. B. H. N. van den Berg, L. H. Heitman, A. P. Ijzerman, J. Oosterom, C. M. Timmers, H. S. Overkleeft and G. A. van der Marel, *Biorg. Med. Chem.*, 2007, **15**, 4841-4856.
[20] J. A. Wisner, P. D. Beer and M. G. B. Drew, *Angew. Chem. Int. Ed.*, 2001, **40**, 3606-3609.
[21] B. L. Allwood, N. Spencer, H. Shahriari-Zavareh, J. F. Stoddart and D. J. Williams, *J. Chem. Soc., Chem. Commun.*, 1987, 1061-1064.
[22] L. Crombie, A. P. Ryan, D. A. Whiting and S. O. Yeboah, *J. Chem. Soc., Perkin Trans. 1*, 1987, 2783-2786.
[23] P. Nilsson, M. Larhed and A. Hallberg, *J. Am. Chem. Soc.*, 2001, **123**, 8217-8225.
[24] P. Roquette, C. König, O. Hübner, A. Wagner, E. Kaifer, M. Enders and H.-J. Himmel, *Eur. J. Inorg. Chem.*, 2010, **2010**, 4770-4782.
[25] H. W. Gibson, S. H. Lee, P. T. Engen, P. Lecavalier, J. Sze, Y. X. Shen and M. Bheda, *J. Org. Chem.*, 1993, **58**, 3748-3756.
[26] S. I. Fukuzawa, E. Shimizu and K. Ogata, *Heterocycles*, 2009, **78**, 645-655.
[27] M. R. Sambrook, P. D. Beer, J. A. Wisner, R. L. Paul, A. R. Cowley, F. Szemes and M. G. B. Drew, *J. Am. Chem. Soc.*, 2005, **127**, 2292-2302.
[28] W. Zhang and H. Yamamoto, *J. Am. Chem. Soc.*, 2006, **129**, 286-287.
[29] P. R. Ashton, D. Philp, N. Spencer and J. F. Stoddart, *J. Chem. Soc., Chem. Commun.*, 1992, 1124-1128.
[30] H. Zheng, W. Zhou, J. Lv, X. Yin, Y. Li, H. Liu and Y. Li, *Chem. Eur. J.*, 2009, **15**, 13253-13262.
[31] T. M. Weathers, Y. Wang and M. P. Doyle, *J. Org. Chem.*, 2006, **71**, 8183-8189.
[32] M. D. Lankshear, N. H. Evans, S. R. Bayly and P. D. Beer, *Chem. Eur. J.*, 2007, **13**, 3861-3870.
[33] M. R. Sambrook, P. D. Beer, M. D. Lankshear, R. F. Ludlow and J. A. Wisner, *Org. Biomol. Chem.*, 2006, **4**, 1529-1538.
[34] E. D. Goddard-Borger and R. V. Stick, *Org. Lett.*, 2007, **9**, 3797-3800.
[35] J. A. Wisner, P. D. Beer, M. G. B. Drew and M. R. Sambrook, *J. Am. Chem. Soc.*, 2002, **124**, 12469-12476.
[36] A. Charette, A. Gagnon, M. Janes and C. Mellon, *Tetrahedron Lett.*, 1998, **39**, 5147-5150.
[37] T. P. Shiau, A. Houchin, S. Nair, P. Xu, E. Low, R. Najafi and R. Jain, *Bioorg. Med. Chem. Lett.*, 2009, **19**, 1110-1114.
[38] J. W. Lown and R. R. Koganty, *J. Am. Chem. Soc.*, 1986, **108**, 3811-3818.
[39] M. J. Hynes, *J. Chem. Soc., Dalton Trans.*, 1993, 311-312.

Chapter Seven

Chapter 7 Conclusion

The work described in this thesis has underscored the importance of halogen and hydrogen bonding in achieving strong, and selective, recognition and sensing of negatively charged species. The superiority of halogen bonding over complementary hydrogen bonding for the binding of anions has been demonstrated, providing further evidence to support the integration of halogen-bond-donor groups into both cyclic anion hosts and anion-templated interlocked molecular frameworks.

The preparation of four novel triazole- and triazolium-containing zinc(II)-metalloporphyrin-based anion receptors which operate through halogen- and hydrogen-bonding interactions was described in Chapter Two. The anion binding properties of the two neutral triazole- and iodotriazole-containing porphyrin receptors were investigated in chloroform, acetone and acetonitrile and the strength of anion recognition correlated with the hydrogen-bond-donor ability of the solvent as measured using the Gutmann acceptor number. Importantly, the halogen-bonding iodotriazole-porphyrin-based anion host displayed halide anion binding affinities which were substantially larger than the protic-functionalised hydrogen-bonding analogue and a reduced strength of acetate oxoanion complexation. The related positively charged triazolium porphyrin-based receptors were able to sense anions strongly in competitive DMSO solvent, and similar selectivity trends in halogen *versus* hydrogen bonding were observed. The role of anion ligation to the zinc(II) metal centre of the porphyrin receptor was also found to be significant. In addition, two cyclic triazole- and triazolium-containing porphyrin-cage anion receptors were prepared and the neutral host demonstrated to be a potent colorimetric anion sensor. The positively charged porphyrin cage was able to sense anions in competitive aqueous solvent media and displayed an impressive selectivity for sulfate in a 15% water:acetone solvent mixture.

The strategic exploitation of halogen-bonding in the solution-phase construction of anion-templated interlocked structures is in its infancy. In Chapter Three a series of new bromo- and iodopyridinium species were prepared, and their ability to form anion-templated halogen-

bonding pseudorotaxanes with an isophthalamide-containing macrocycle investigated. Such interpenetrated assemblies were determined to be more stable when halogen bonding was employed. Specifically, bromide- and iodide-templated pseudorotaxane assemblies containing the iodopyridinium threading component were more stable compared with analogous bromo- or protic-pyridinium threaded components, which reflects the greater halogen-bond-donor ability of the more polarisable iodine atom. The stability of the anion-templated halogen-bonded pseudorotaxane architectures, formed between an isophthalamide macrocycle and bis-vinyl-appended halopyridinium threading derivatives, was exploited in the preparation of novel interlocked catenane species via a Grubbs' RCM clipping methodology. Both bromo- and iodopyridinium-containing catenanes were found to bind halides with similar magnitude in the order iodide > bromide > chloride. Through the design and synthesis of a suitable halogen-bond-acceptor pyridine-containing macrocycle, interpenetrative assembly and interlocked catenane construction with a complementary iodo-functionalised pyridinium halogen-bond-donating threading component, driven by a single charge-assisted halogen-bond was also highlighted.

Chapter Four described the preparation of a novel 1,3-disubtituted-triazolium anion recognition motif whose halide and acetate anion binding affinities were found to be greater than 1,4-disubstituted-triazolium or 2-methylimidazolium motifs. Chloride-anion-templation was used to prepared a rotaxane host system containing a 1,3-disubstituted-triazolium axle which displayed a moderate chloride binding affinity in the competitive 1:1 chloroform:methanol solvent mixture.

With a view to enhancing the anion recognition properties of rotaxane host systems by shielding their interlocked binding domains from competing solvent molecules, Chapter Five discussed attempts to prepare alkyl-functionalised rotaxanes. The rotaxanes incorporating either tetra-methyl-functionalised macrocycle or axle components were found to be weaker anion complexants than their unfunctionalised analogues, which may be a result of the additional methyl groups sterically hindering the ability of chloride to penetrate the

interlocked binding cavity or acetate and dihydrogen phosphate to associate on the periphery. The anion binding properties of more flexible rotaxane molecules revealed that additional methyl groups served to improve the chloride binding affinity of these systems, as well as bestow a degree of halide selectivity to the methyl-functionalised structure.

Overall, the results described in this thesis demonstrate that both halogen- and hydrogen-bonding interactions can effect strong anion binding with a high degree of recognition in both cyclic and interlocked host systems. In particular, halogen-bonding has been shown to dramatically improve halide anion binding affinities as well as to reduce the strength of oxoanion complexation. Also, importantly, the real potential of solution phase halogen-bonding interactions to template the formation of interlocked structures and for anion recognition applications has been highlighted.

Appendices

Appendices

A.1 Additional titration curves for titration experiments

A.1.1 Titration curves for Chapter Two

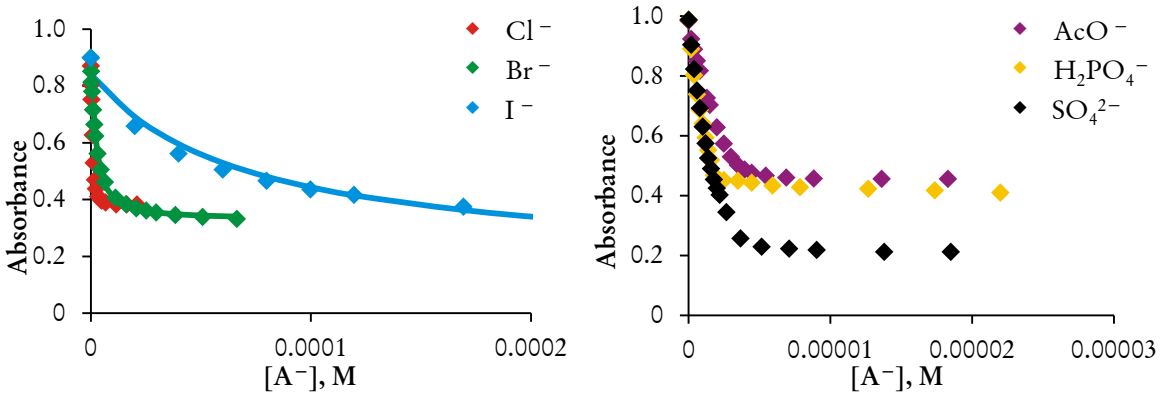


Figure A.1. Titration curves for complex formation between porphyrin 6 and various anions obtained by monitoring perturbations of the Soret band at 425 nm. Acetone, 293 K. Square data points represent experimental data; continuous lines represent theoretical binding isotherms.

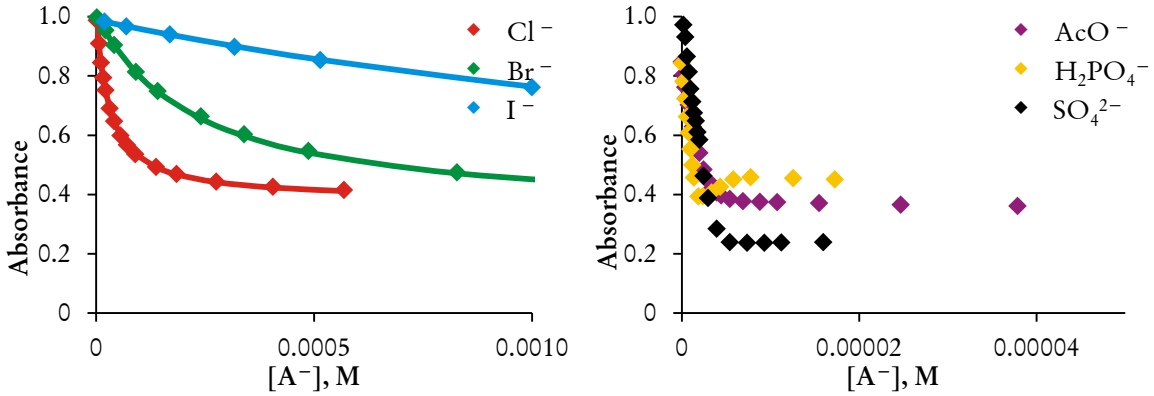


Figure A.2.Titration curves for complex formation between porphyrin 6 and various anions obtained by monitoring perturbations of the Soret band at 425 nm. Acetonitrile, 293 K. Square data points represent experimental data; continuous lines represent theoretical binding isotherms.

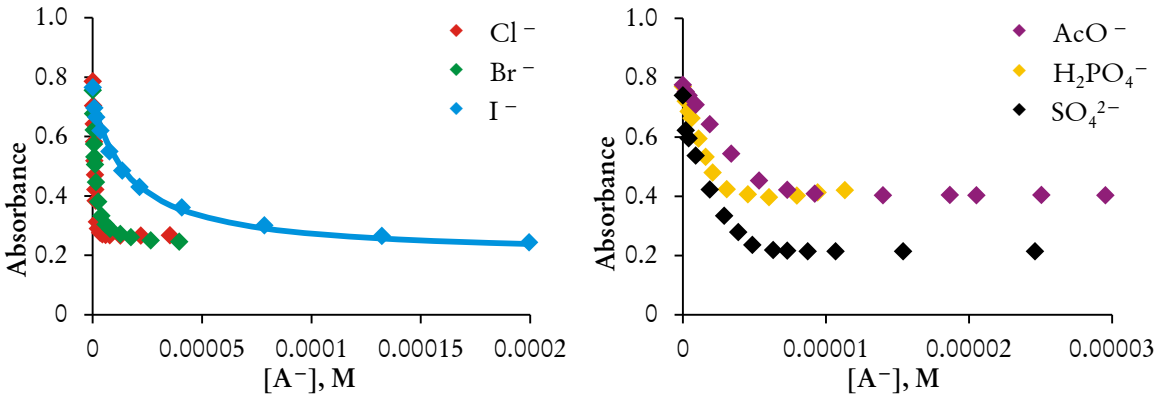


*Figure A.3. Titration curves for complex formation between porphyrin **10** and various anions obtained by monitoring perturbations of the Soret band at 425 nm. Acetone, 293 K. Square data points represent experimental data; continuous lines represent theoretical binding isotherms.*

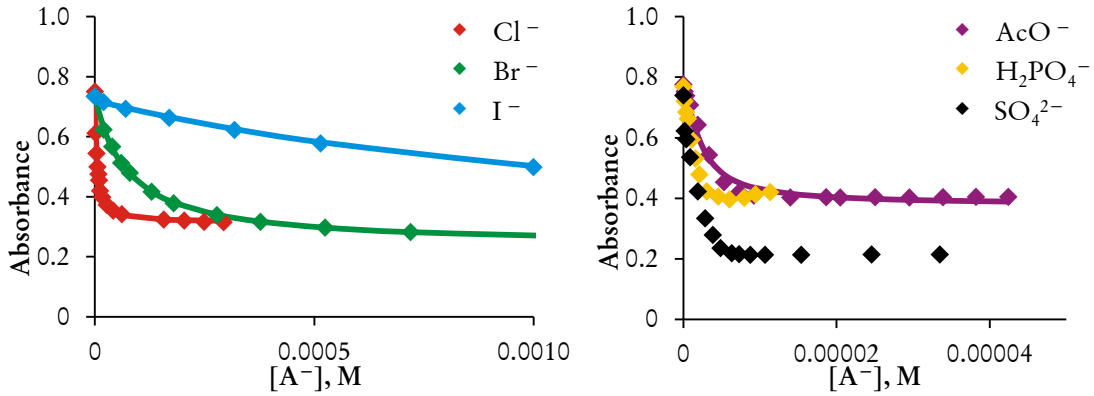


*Figure A.4. Titration curves for complex formation between porphyrin **10** and various anions obtained by monitoring perturbations of the Soret band at 425 nm. Acetonitrile, 293 K. Square data points represent experimental data; continuous lines represent theoretical binding isotherms.*

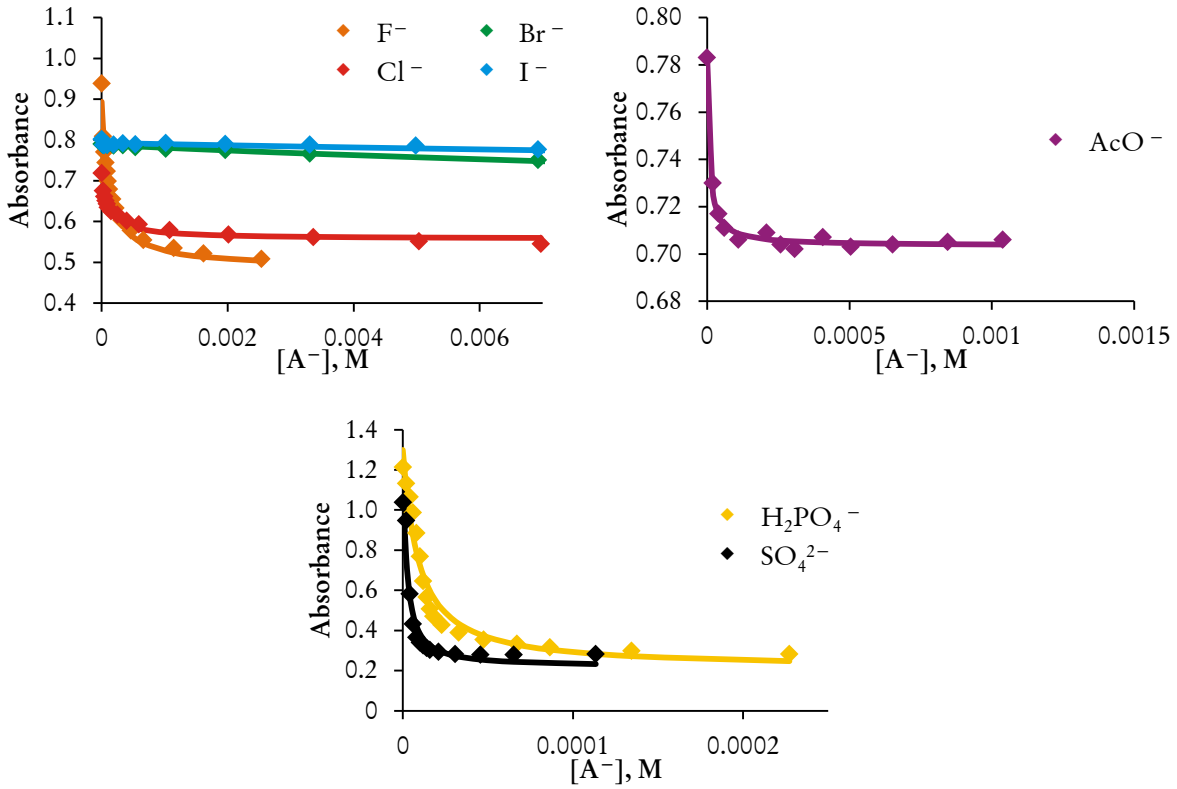


Figure A.5. Titration curves for complex formation between porphyrin ***26*****·(PF$_6$)$_4$** *and various anions obtained by monitoring perturbations of the Soret band at 425 nm. 5% H_2O/acetone, 293 K. Square data points represent experimental data; continuous lines represent theoretical binding isotherms.*

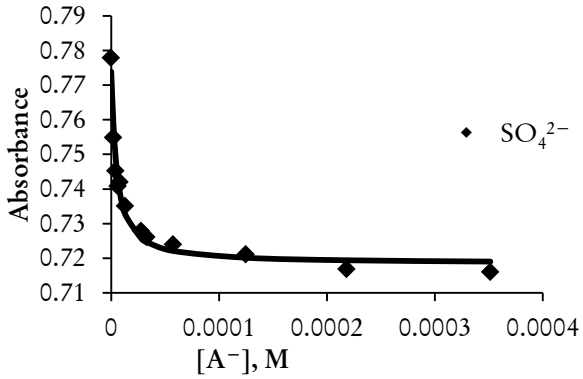


Figure A.6. Titration curves for complex formation between porphyrin ***26*****·(PF$_6$)$_4$** *and sulfate obtained by monitoring perturbations of the Soret band at 423 nm. 15% H_2O/acetone, 293 K. Square data points represent experimental data; continuous lines represent theoretical binding isotherms.*

A.1.2 Titration curves for Chapter Three

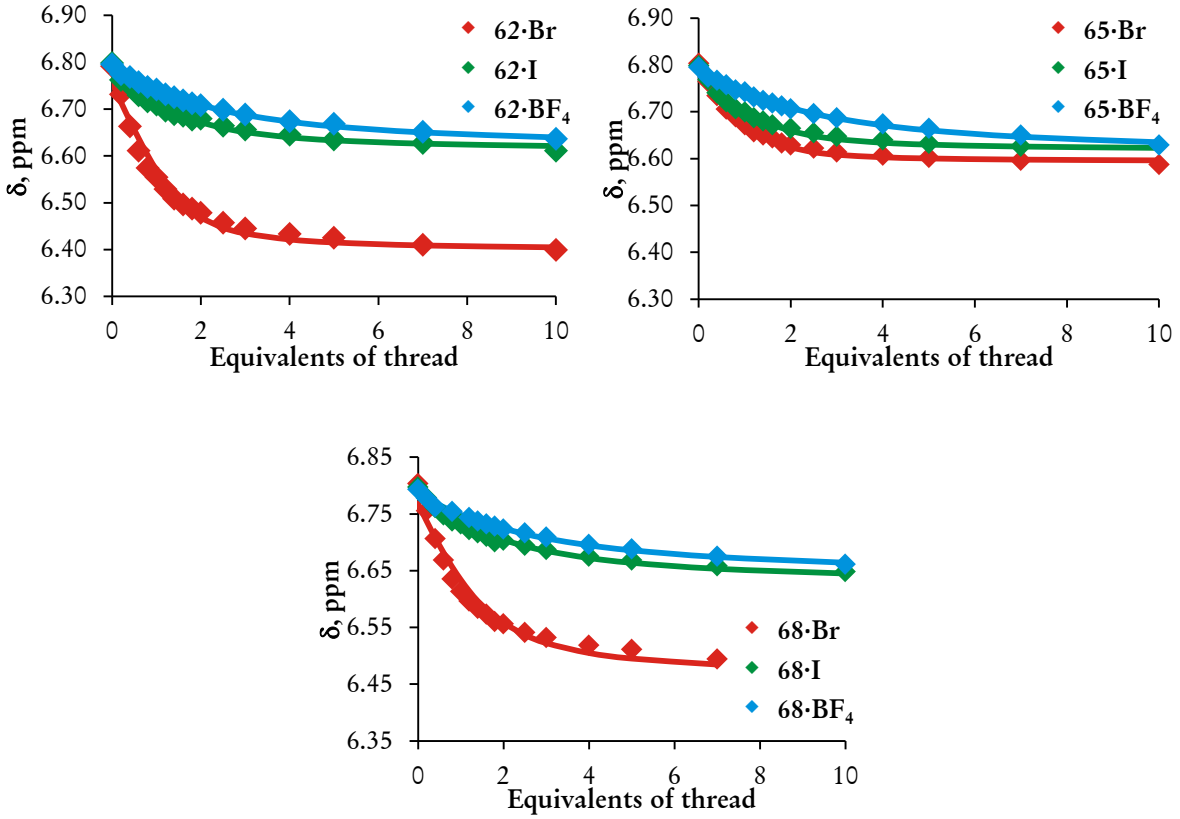


Figure A.7. Titration curves for pseudorotaxane formation between macrocycle ***52*** *and threading compounds a)* ***62·A****, b)* ***65·A*** *and c)* ***68·A*** *obtained by monitoring perturbations of the hydroquinone protons. 500 MHz, $CHCl_3$, 293 K. Square data points represent experimental data; continuous lines represent theoretical binding isotherms.*

A.2 Additional information for Chapter Five

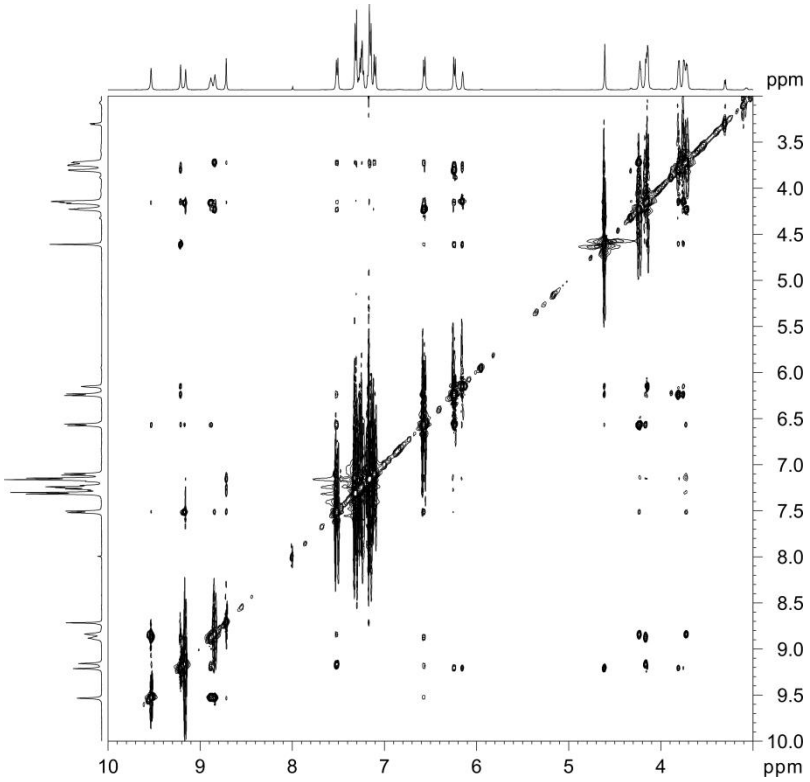


Figure A.8. Partial ^1H–^1H ROESY NMR of rotaxane ***157·PF$_6$*** *(500 MHz, acetone-d_6, 293 K).*

A.3 Crystal structure data

A.3.1 General notes

Unless otherwise stated, crystals suitable for single crystal structure determination were grown by the author, while data acquisition and structure determination were carried out by N. G. White stated with each structure.

Data was collected using one of the following:

(a) graphite monochromated Mo Kα radiation (λ = 0.71073 Å) on a Nonius KappaCCD diffractometer;

(b) mirror monochromated Cu Kα radiation (λ = 1.54180 Å) on an Oxford Diffraction Dual Source SuperNova diffractometer;

(c) silicon double crystal monochromated synchtrotron radiation (λ = 0.66890 Å) at Diamond Light Source beamline I19 on a custom built Rigaku diffractometer (when crystals were too small or weakly diffracting).

All diffractometers were equipped with a Cryostream N_2 open-flow cooling device,[1] and data were collected at 150(2) or 100(2) K.

When using the Nonius machine series of ω-scans were typically performed in such a way as to collect every independent reflection to a maximum resolution of 0.77 Å. Cell parameters and intensity data (including inter-frame scaling) were processed using the DENZO-SMN package.[2]

When using the Oxford machine series of ω-scans were performed in such a way as to collect every independent reflection to a maximum resolution of 0.80 Å. Cell parameters and intensity data (including inter-frame scaling) were processed using the CrysAlisPro package.[3]

When using synchrotron radiation, ω-scans were performed such that a half-sphere of data was collected to a maximum resolution of 0.77 Å. Cell refinement, data reduction, and scaling were performed using the CrystalClear package.[4]

The structures were solved by direct methods using the SIR92 software[5] or by charge flipping using Superflip.[6] Structures were refined using full-matrix least-squares on F^2 or F within the CRYSTALS suite.[7] Non-hydrogen atoms were refined with anisotropic displacement parameters, unless specified otherwise. Disordered portions were modelled using refined partial occupancies. Geometric and vibrational restraints were applied where appropriate to ensure physically reasonable models. Hydrogen atoms were usually located in the difference map, but those attached to carbon atoms were repositioned geometrically. Protic hydrogen atoms which could not be located in the difference map were positioned to satisfy hydrogen bonding requirements. Hydrogen atoms were initially refined with soft restraints on the bond lengths and angles to regularise their geometry, after which the positions were refined with riding constraints.

In some cases the molecular structure within solvent voids could not be resolved in the difference map, and PLATON SQUEEZE[8, 9] was used in these cases to account for the residual electron density in the refinement.

After the construction of a stable, physically reasonable, and complete model, the weights were optimised,[10, 11] anomalous reflections were omitted, and absent high-angle data (in the case of poorly diffracting samples) were pruned using the Wilson plot. This generally led to convergence of the refinement, giving the final structure.

For the more challenging structures in which the refinement did not converge immediately, initially half-shifts, then restraints, and finally rigid body refinement were used to overcome this problem.

IUCr CheckCIF/PLATON[12] was used to validate the structures, and warnings were dealt with as appropriate or justified using validation reply forms.

Additional notes and parameters for each structure are given below. Where crystallographic data have been deposited with the Cambridge Crystallographic Data Centre, the CCDC number is given in the summary table.

A.3.2 Crystal structure of tetra-azide-functionalised zinc(II)-metalloporphyrin 5

Structure determined by N. G. White

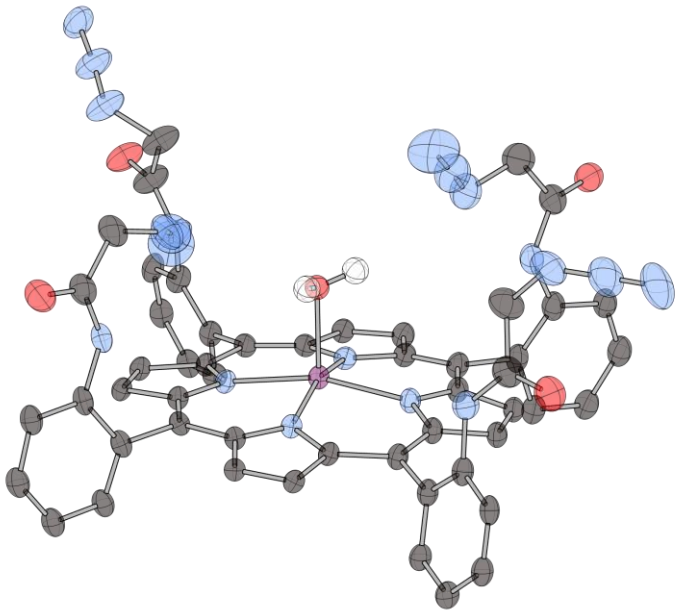


Figure A.9. X-ray structure of porphyrin ***5****. Thermal ellipsoids displayed at 30% probability.*

Table A.2. Crystal structure data for tetra-azide-functionalised zinc(II)-metalloporphyrin 5.

Compound reference	5
Chemical formula	$C_{52}H_{36}N_{20}O_4Zn{\cdot}CHCl_3$
Formula Mass	1208.77
Crystal system	Triclinic
a/Å	13.1226 (16)
b/Å	14.3173 (19)
c/Å	15.820 (3)
α/°	74.846 (10)
β/°	74.743 (7)
γ/°	71.641 (7)
Unit cell volume/Å^3	2669.3 (7)
Temperature/K	150 K
Space group	*P*1̄
No. of formula units per unit cell, *Z*	2
No. of reflections measured	5827
No. of independent reflections	3426
R_{int}	0.177
Final R_1 values ($I > 2\sigma(I)$)	0.1592
Final $wR(F^2)$ values ($I > 2\sigma(I)$)	0.3251
Final R_1 values (all data)	0.2495
Final $wR(F^2)$ values (all data)	0.4147

A.3.3 Crystal structure of tetrakis-iodotriazole-functionalised zinc(II)-metalloporphyrin 10

Structure determined by N. G. White

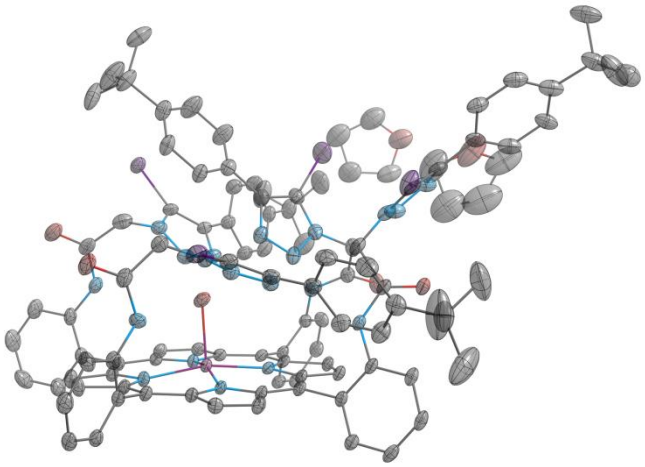


*Figure A.10. X-ray crystal structure of porphyrin **10**. Thermal ellipsoids are shown at 30% probability. Hydrogen atoms are omitted for clarity.*

*Table A.3. Crystal structure data for tetrakis-iodotriazole-functionalised zinc(II)-metalloporphyrin **10**.*

Compound reference	**10**
Chemical formula	$C_{100}H_{90}I_4N_{20}O_4Zn{\cdot}2C_4H_8O$
Formula Mass	2369.12
Crystal system	Triclinic
a/Å	11.1168 (5)
b/Å	15.8537 (7)
c/Å	31.3514 (14)
α/°	84.171 (4)
β/°	83.870 (4)
γ/°	81.378 (4)
Unit cell volume/Å^3	5411.12 (4)
Temperature/K	150 K
Space group	$P\bar{1}$
No. of formula units per unit cell, Z	2
No. of reflections measured	22322
No. of independent reflections	45284
R_{int}	0.064
Final R_1 values ($I > 2\sigma(I)$)	0.0635
Final $wR(F^2)$ values ($I > 2\sigma(I)$)	0.1471
Final R_1 values (all data)	0.0834
Final $wR(F^2)$ values (all data)	0.1773
CCDC number	953393

A.3.4 Crystal structure of triazole-functionalised zinc(II)-metalloporphyrin cage anion receptor 25

Structure determined by N. G. White

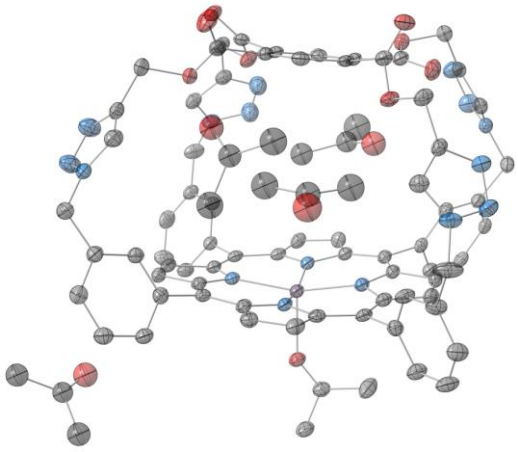


Figure A.11. X-ray crystal structure of asymmetric unit of porphyrin cage compound ***25*****·5(**C_3H_6O**).** *Thermal ellipsoids are shown at 50% probability. Hydrogen atoms are omitted for clarity.*

Table A 4. Crystal structure data for porphyrin cage compound ***25****.*

Compound reference	**25**
Chemical formula	$C_{73}H_{52}N_{16}O_9Zn{\cdot}4(C_3H_6O)$
Formula Mass	1595.02
Crystal system	Monoclinic
a/Å	14.7594(2)
b/Å	19.6725(2)
c/Å	26.8029(3)
α/°	90
β/°	99.6681(11)
γ/°	90
Unit cell volume/Å^3	7671.81(16)
Temperature/K	150
Space group	$P2_1/c$
No. of formula units per unit cell, Z	4
Absorption coefficient, λ/mm^{-1}	1.079
No. of reflections measured	56994
No. of independent reflections	16008
R_{int}	0.0427
Final R_1 values ($I > 2\sigma(I)$)	0.0560
Final $wR(F^2)$ values ($I > 2\sigma(I)$)	0.1563
Final R_1 values (all data)	0.0639
Final $wR(F^2)$ values (all data)	0.1612
Goodness of fit on F^2	1.0464
CCDC number	863074

A.3.5 Crystal structure of 1,3-dialkyltriazolium threading species 84·Br

Structure determined by N. G. White

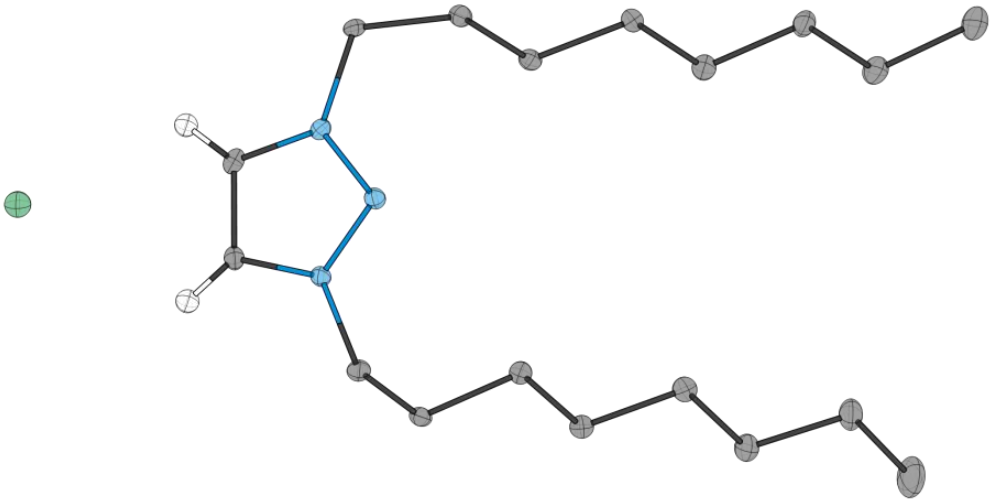


*Figure A.12. X-ray crystal structure of 1,3-dialkyltriazolium threading compound **84·Br**. Thermal ellipsoids are shown at 30% probability. Hydrogen atoms not involved in anion binding are omitted for clarity.*

*Table A.5. Crystal structure data for 1,3-dialkyltriazolium threading compound **84·Br**.*

Compound reference	**84·Br**
Chemical formula	$C_{18}H_{36}N_3$·Br
Formula Mass	374.41
Crystal system	Triclinic
a/Å	4.9534 (5)
b/Å	8.31112 (9)
c/Å	25.3767 (19)
α/°	92.999 (7)
β/°	92.685 (7)
γ/°	105.284 (9)
Unit cell volume/Å^3	1004.39 (17)
Temperature/K	150 K
Space group	$P\bar{1}$
No. of formula units per unit cell, *Z*	2
No. of reflections measured	8881
No. of independent reflections	4137
R_{int}	0.043
Final R_1 values ($I > 2\sigma(I)$)	0.048
Final $wR(F^2)$ values ($I > 2\sigma(I)$)	0.138
Final R_1 values (all data)	0.0525
Final $wR(F^2)$ values (all data)	0.1382

A.3.6 Crystal structure of 1,4-disubstituted triazolium-based macrocycle 113·BF_4

Structure determined by N. G. White

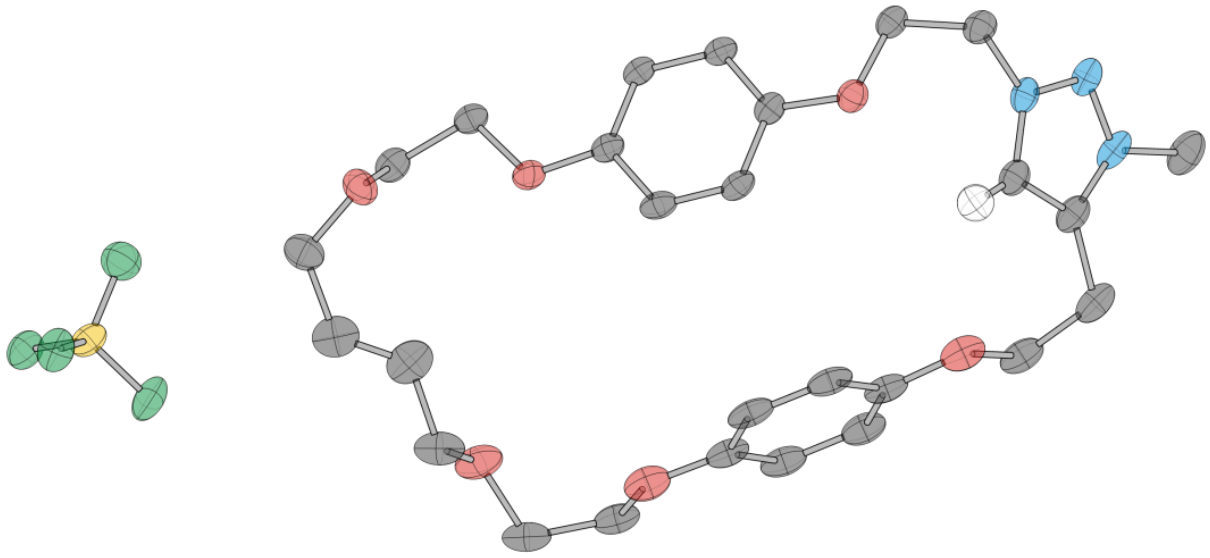


Figure A.13. X-ray crystal structure of macrocycle ***113·BF$_4$****. Thermal ellipsoids are shown at 30% probability. Hydrogen atoms are omitted for clarity.*

Table A.6. Crystal structure data for macrocycle ***113·BF$_4$****.*

Compound reference	**113·BF_4**
Chemical formula	$C_{27}H_{34}N_3O_6 \cdot BF_4$
Formula Mass	583.38
Crystal system	Monoclinic
a/Å	16.0495 (6)
b/Å	8.2498 (3)
c/Å	21.6094 (7)
α/°	90
β/°	98.384 (3)
γ/°	90
Unit cell volume/Å^3	2830.61 (18)
Temperature/K	150 K
Space group	*P*21/C
No. of formula units per unit cell, *Z*	4
No. of reflections measured	9612
No. of independent reflections	36864
R_{int}	0.0495
Final R_1 values ($I > 2\sigma(I)$)	0.0950
Final $wR(F^2)$ values ($I > 2\sigma(I)$)	0.1744
Final R_1 values (all data)	0.1022
Final $wR(F^2)$ values (all data)	0.1753

A.3.7 Crystal structure of macrocycle 129

Structure determined by N. G. White

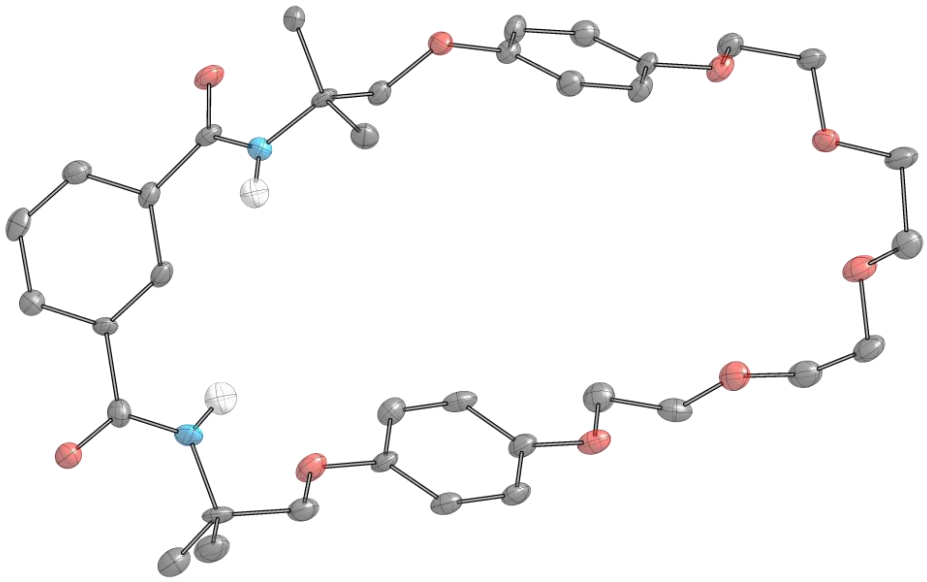


*Figure A.14. X-ray crystal structure of macrocycle **129**. Thermal ellipsoids are shown at 30% probability. Hydrogen atoms are omitted for clarity.*

*Table A.7. Crystal structure data for macrocycle **129**.*

Compound reference	**129**
Chemical formula	$C_{36}H_{47}N_2O_9 \cdot Cl_{1.5}$
Formula Mass	710.46
Crystal system	Triclinic
a/Å	9.9710 (6)
b/Å	18.8322 (12)
c/Å	20.1910 (11)
α/°	89.081 (5)
β/°	79.619 (5)
γ/°	76.018 (5)
Unit cell volume/Å^3	3617.3 (4)
Temperature/K	150 K
Space group	*P*1̄
No. of formula units per unit cell, *Z*	4
No. of reflections measured	7812
No. of independent reflections	15730
R_{int}	0.0782
Final R_1 values ($I > 2\sigma(I)$)	0.0943
Final $wR(F^2)$ values ($I > 2\sigma(I)$)	0.2514
Final R_1 values (all data)	0.1371
Final $wR(F^2)$ values (all data)	0.2980

A.3.8 Crystal structure of 133·Cl

Structure determined by N. G. White

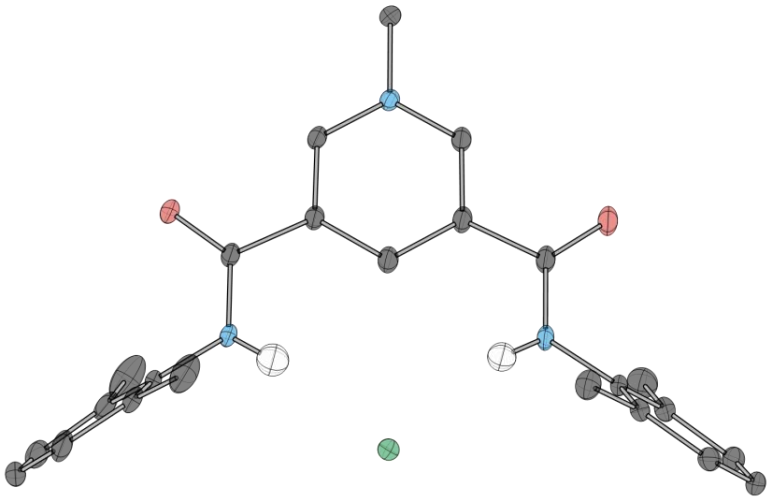


Figure A.15. X-ray crystal structure of compound ***133·Cl****. Thermal ellipsoids are shown at 30% probability. Hydrogen atoms are omitted for clarity.*

Table A 8. Crystal structure data for compound ***133·Cl****.*

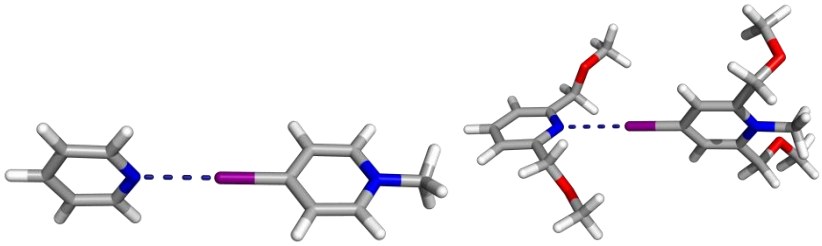
Compound reference	**133·Cl**
Chemical formula	$C_{24}H_{26.3}N_3O_{2.15}\cdot Cl$
Formula Mass	426.64
Crystal system	Monoclinic
a/Å	14.7582 (2)
b/Å	11.0760 (2)
c/Å	14.5795 (2)
α/°	90
β/°	112.840 (2)
γ/°	90
Unit cell volume/Å^3	2196.33 (7)
Temperature/K	150 K
Space group	*P*121/C1
No. of formula units per unit cell, *Z*	4
No. of reflections measured	4559
No. of independent reflections	11553
R_{int}	0.0191
Final R_1 values ($I > 2\sigma(I)$)	0.0416
Final $wR(F^2)$ values ($I > 2\sigma(I)$)	0.1036
Final R_1 values (all data)	0.0432
Final $wR(F^2)$ values (all data)	0.1047

A.4 Molecular modelling carried out by Prof. Vitor Félix

A.4.1 Computational Details.

A.4.1.1 DFT calculations and halogen bond parameterization for Molecular Dynamics simulations

The ability of [2]catenane **74·BF$_4$** to form C–I···N halogen-bonding interactions, was investigated by classical Molecular Dynamics (MD) simulations, using a similar procedure reported by Félix and co-workers in references [1] and [2]. The specific force field parameters used to describe these interactions were developed as follows. DFT calculations were performed with Gaussian 09[3] using the hybrid functional B3LYP[4,5] on systems **A1**, and **B1** (see Figure A.16), models for the I···N interaction in **74·BF$_4$**. System **B1** contains two *meta*-methoxy substituents as mimetic groups of the ether linkages of the two interlocked macrocycles on the [2]catenane assembly.



A1 **B1**

*Figure A.16. Optimised B3LYP gas phase structures of **A1** and **B1** models used in the parameterisation of C–I···N charged assisted interactions.*

For C, O, H, and N the standard 6-311+G** basis set was used while I was described by the aug-cc-pVDZ-PP basis set and pseudo potential taken from the EMSL Basis Set Exchange website.[6] The geometries were optimized in the gas phase and, for the larger model **B1**, solvent effects ($CHCl_3$) were also considered by means of IEFPCM calculation with radii and non-electrostatic terms for Truhlar and co-workers' SMD solvation model.[7] The relevant structural parameters are collect in Table A.9.

*Table A.9. Optimised B3LYP gas phase relevant distances (Å) for models **A1**, and **B1**. In parenthesis are shown the optimised distances in $CHCl_3$ using a Polarizable Continuum Model.*

	A1	B1	
C–I	2.138	2.122	(2.121)
I···N	2.720	2.896	(3.061)

It is evident that the halogen bond distance increases slightly with the presence of larger substituents whereas the use of an implicit solvent model indicates that the C–I···N halogen bonds are ~ 3.0 Å long.

Taking this in consideration, Félix and Costa proceeded with the parameterization of the possible C–I···N halogen bond interactions present in **74·BF_4**. Parameterisations were performed with the addition of a specific term to the General Amber Force Field (GAFF)[8] parameters used to describe the macrocycle components of the [2]catenane interlocked assembly as suggested in references [9] and [10]. The positive region on the electrostatic potential of the iodopyridinium moiety centred on the iodine atom is represented by a pseudo-atom (DU) with a van de Waals parameter set to zero, a C–I–DU bond angle set to 180°, and a bending force constant of 150 kcal mol^{-1} $Å^{-2}$. The optimal I–DU equilibrium distance was evaluated using several I–DU distances and computing the electrostatic potential and the Restricted Electrostatic Potential (RESP) charges for each new DU position. This was followed by a Molecular Mechanics (MM) minimisation of the corresponding assembled catenane structures in Amber 12[11]. Subsequently, the MM optimised distances (I···N) were compared with the DFT data (Table A.10). The electrostatic potential for the two individual macrocycles was calculated at the HF/6-31G* level, with the aug-cc-pVDZ-PP basis set for iodine using previously optimised B3LYP geometries at the theory level reported above for the model systems, and the atomic point charges for the individual macrocycles were determined according to the RESP methodology[12] using a single conformation and Gaussian

IOp (6/42=6) in agreement with the original GAFF reference.[8] The MM optimised I···N and C–I distances are reported in Table A.10 along with the relevant RESP charges.

Table A.10. Gas phase MM optimised distances (Å) as a function of the I–DU distance together with the DU and iodine RESP charges.

I-DU distance	C–I	I···N	DU charge	I charge
2.00	2.091	3.118	0.108788	-0.111542
2.10	2.092	3.062	0.097845	-0.090483
2.20	2.093	2.963	0.088007	-0.070660
2.35	2.164	2.600	0.074972	-0.042888
without DU	2.092	---	---	0.186479

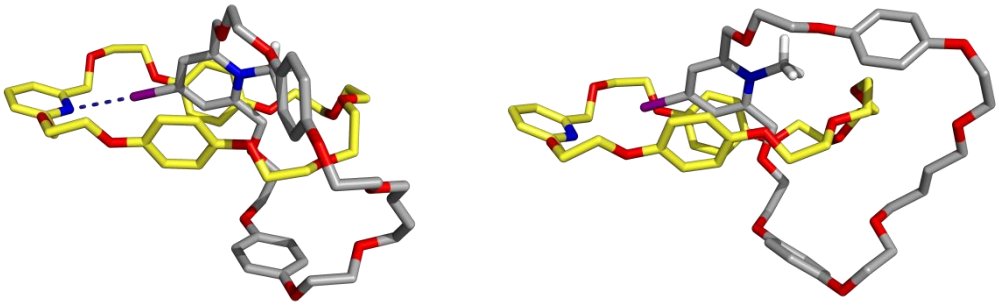


*Figure A.17. MM minimized interlocked structures of **74·BF$_4$** (top) with DU (I–DU distance 2.10 Å, left) and without DU (right) for the C–I···N halogen bond.*

If a DU atom is not used, the halogen-bond interactions are lost whereas the addition of the DU atom, independently of the distance, enables the description of the halogen bonds (see Figure A.17). However, values of I–DU larger than 2.10 Å are not suitable since atom clashes occur during the subsequent MD simulations performed either in gas phase or in explicit CH_3Cl solution. The I–DU = 2.10 Å leading to an I···N distance of 3.062 Å, which compares well with the 3.061 Å value obtained for the DFT model **B1** in $CHCl_3$ continuum solvent model, is the optimum value to describe I···N interactions and was selected for the further MD simulations reported in this work.

Moreover, preliminary gas phase MM calculations on the iodopyridinium macrocycle showed that default potential energy barrier (V_n) of 0.3 kcal for the X-*ca*-*na*-X torsion angle (where *ca* and *na* are the atom types assigned to the pyridinium ring carbon atoms and nitrogen atom, respectively, and X means any other atom type) led to a slight bending of the *N*-methyl group relatively to pyridinium ring plane. This structural imprecision was corrected using the torsion force field parameters available in the GAFF for the related X-*cd*-*na*-X torsion angle (4 / 6.8 / 180.0 / 2), where *cd* is a sp^2 carbon in non-pure aromatic systems.

A.4.1.2 Generation of starting structures for the MD simulations

Since there is no X-ray structure for catenane **74·BF$_4$** and given its conformational freedom, the starting structures for the MD simulations were generated by a protocol based on a gas-phase quenched dynamics simulation.[13] The previous MM optimised structure with I–DU = 2.10 Å was subjected to a 5 ns MD run at 500 K saving a trajectory with 10000 structures that should sample most of the conformational space. All these structures were minimised by MM and clustered by RMSD similarity. Two structures corresponding to representative conformations of the most populated clusters were selected. These structures shown in Figure A.18 as **S1A** and **S1B** present an C–I···N halogen bond and π–π donor-acceptor interactions between the iodopyridinium and the hydroquinone rings of the macrocycle **71**. These two co-conformations basically differ in the conformation adopted by the iodopyridinium macrocycle leading to slightly different binding scenarios.

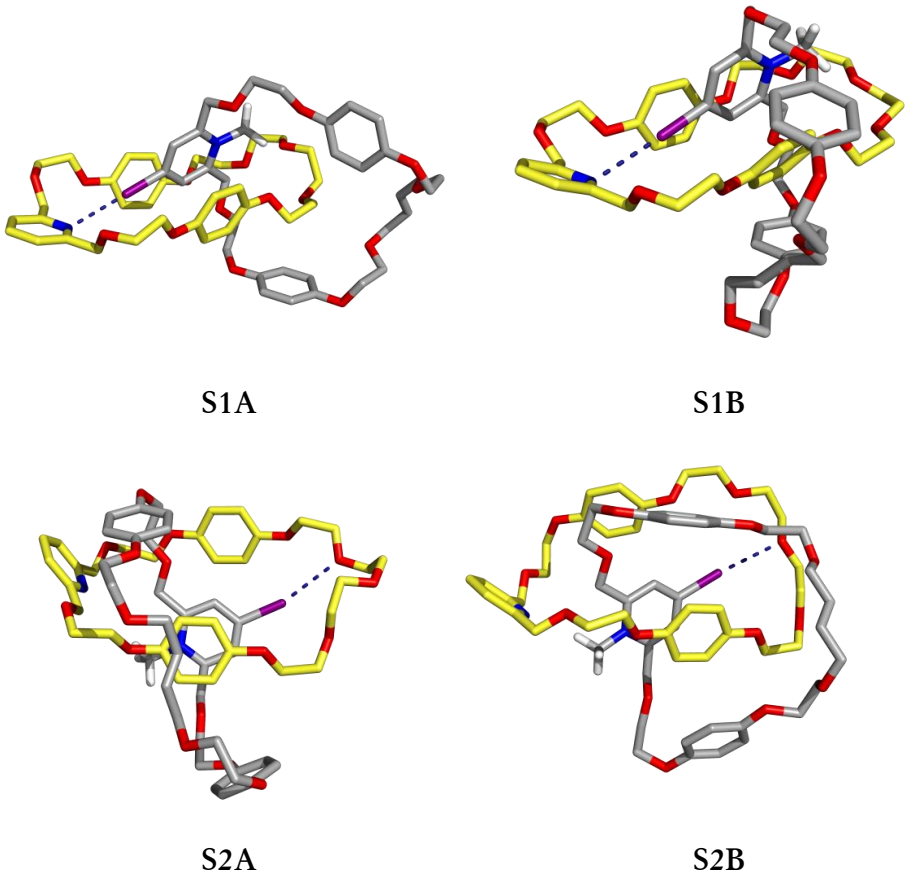


*Figure A.18. Starting co-conformations used in the MD simulations, **S1A** and **S1B** exhibit a C–I···N halogen bond and **S2A** and **S2B** present an C–I···O halogen bond.*

In order to increase the sampling, the iodopyridinium macrocycle in a structure similar to **S1A** was rotated affording an interlocked assembly with the C–I bond pointing away from the N of the pyridine ring. This struture was subjected to the same protocol mentioned earlier yielding two starting co-conformations **S2A** and **S2B** presented in Figure A.18, where the C–I bond is pointing towards an oxygen atom from the polyether loop of the macrocycle **71**.

A.4.1.3 Molecular Dynamics simulations

The MM minimised conformations shown in Figure A.18 were immersed in cubic box of $CHCl_3$ molecules[14] (~43 Å side, after equilibration). One BF_4^- anion, with charges and parameters from reference[15], was used as counter-ion. All systems were simulated using the following multi-stage protocol. The solvent was initially relaxed keeping the solute fixed with

a strong positional restraint (500 kcal mol^{-1} $Å^{-2}$). Then, the restraint was removed and a MM energy minimisation of entire system was performed followed by a heating stage (0 to 300 K) during 50 ps using the Langevin thermostat with a collision frequency of 1 ps^{-1} in an NVT ensemble and a weak positional restraint on the solute (10 kcal mol^{-1} $Å^{-2}$). The system was then equilibrated for 5 ns in a NPT ensemble at 1 atm with isotropic pressure scaling using relaxation time of 2 ps and data collection was performed for 50 ns. All simulations were carried out with the pmemd.cuda AMBER executable, able to accelerate explicit solvent Particle Mesh Ewald (PME) calculations[16,17] trough the use of GPUs.[18,19] All bonds involving hydrogen atoms were constrained using SHAKE[20] allowing the usage of 2 fs time step. A 10 Å cut-off was used for the non-bonded van der Waals interactions. Trajectory analysis was performed with the cpptraj utility of AmberTools12 while the molecular representations were drawn with PyMOL.[21] Plots were performed with Gnuplot.[22] Representative co-conformations from the MD trajectories in solution were obtained by clustering the structures by RMSD similarity, using the average-linkage clustering algorithm.[23] A frame from the most populated cluster was chosen as representative of the simulation.

A.4.2 MD simulations extended analysis.

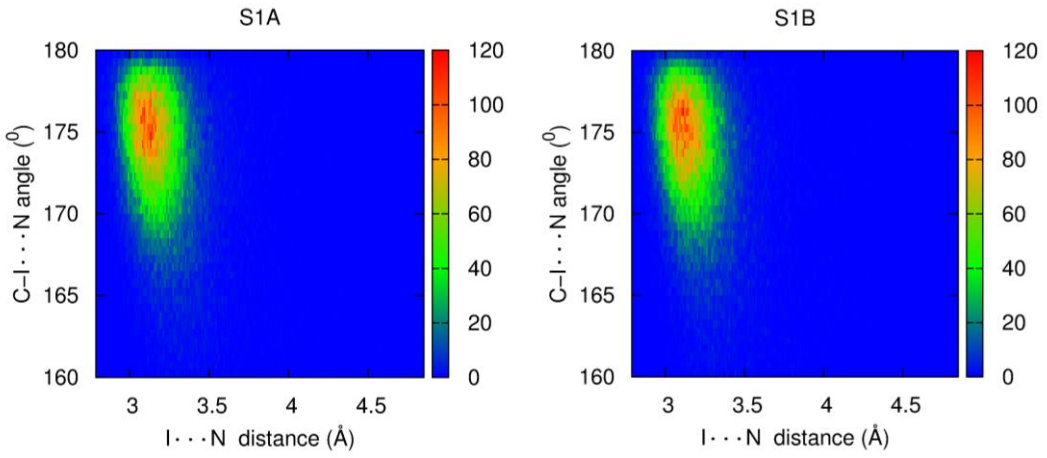


*Figure A.19. Histograms for the distribution of the I···N distances (Å) and the C–I···N angles (°) for simulations with **S1A** and **S1B**. Data were collected for 50 ns.*

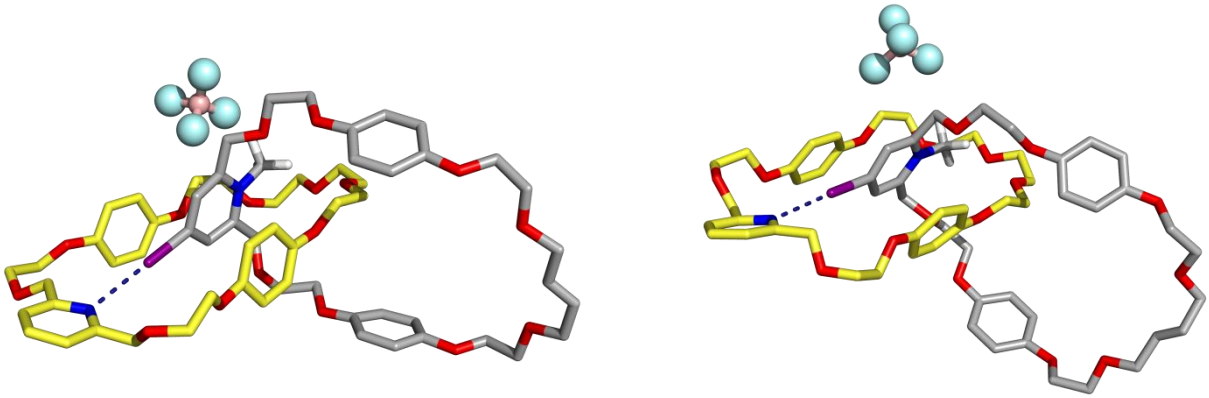


Figure A.20. Representative co-conformations of ***74·BF$_4$*** *for simulations with* ***S1A*** *(left) and* ***S1B*** *(right).*

A.4.2.1 Extended discussion on simulations with S2A and S2B

In the **S2** scenarios (**A** and **B**), a C–I···O halogen bond is possible between the iodopyridinium and the three available oxygen atoms of the polyether loop numbered O1, O2, and O3 (see Figure A.21). In these simulations the distribution of the I···O distances and C–I···O angles was also monitored, and the results are plotted in Figure A.21. It is clear that the results are very similar and independent of the starting co-conformation (**A** or **B**). Concerning the interaction with O1 or O3, the distances are too long and the angles are too low to be considered halogen bonds. For the C-I interaction with O2, the values are distributed around values more compatible with the presence of an halogen bond with average I···O distances and C–I···O angles of 3.60 Å and 164° for **A** and 3.51 Å and 164° for **B** co-conformations. However, contrary to what was found for simulations of C–I···N halogen bonds in **S1A** and **S1B**, the distributions of I···O distances for the simulations with **S2A** and **S2B** structures are very diffuse with respect to the C–I···O angle as evident when the corresponding histograms for these two types of halogen bonds are compared (Figure A.19 *versus* Figure A.21 middle). This is an indication that the possible C–I···O halogen bond is not sufficiently stable for halogen-bond templation as it is the charged assisted I···N halogen bond.

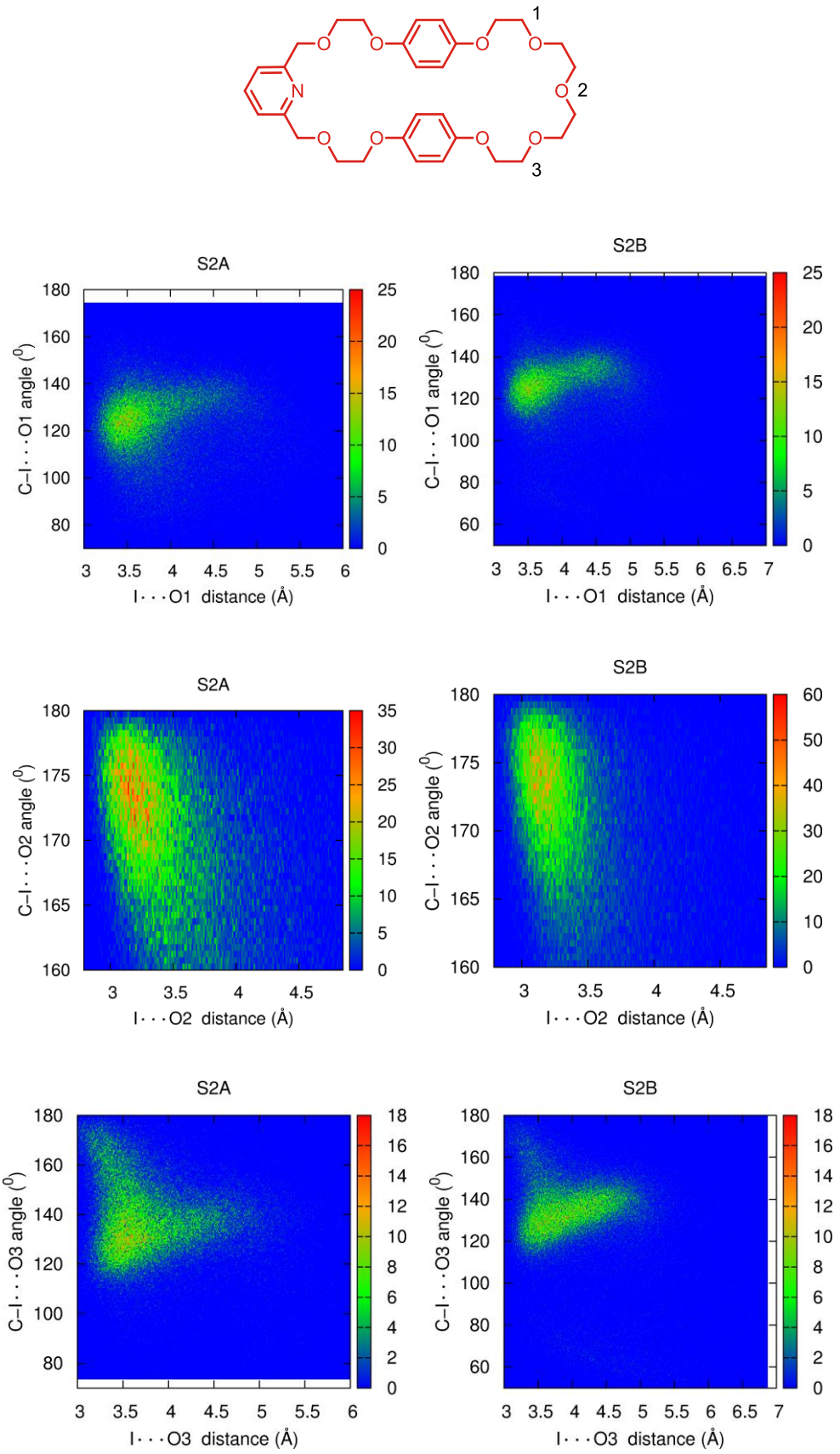


Figure A.21. Histograms for the distribution of the I···O distances (Å) and the C–I···O angles (°) for simulations with ***S2A*** *and* ***S2B****. Data were collected for 50 ns. The numbering scheme used for oxygen atoms is shown at the top.*

A.5 References and notes for Appendices

[1] A. Caballero, F. Zapata, N. G. White, P. J. Costa, V. Felix and P. D. Beer, *Angew. Chem. Int. Ed.*, 2012, **51**, 1876-1880.
[2] F. Zapata, A. Caballero, N. G. White, T. D. W. Claridge, P. J. Costa, V. Felix and P. D. Beer, *J. Am. Chem. Soc.*, 2012, **134**, 11533-11541.
[3] M. J. Frisch, G. W. Trucks, H. B. Schlege, G. E. Scuseria, M. A. Robb, J. R. Cheeseman, J. J. A. Montgomery, T. Vreven, K. N. Kudin, J. C. Burant, J. M. Millam, S. S. Iyengar, J. Tomasi, V. Barone, B. Mennucci, M. Cossi, G. Scalmani, N. Rega, G. A. Petersson, H. Nakatsuji, M. Hada, M. Ehara, K. Toyota, R. Fukuda, J. Hasegawa, M. Ishida, T. Nakajima, Y. Honda, O. Kitao, H. Nakai, M. Klene, X. Li, J. E. Knox, H. P. Hratchian, J. B. Cross, V. Bakken, C. Adamo, J. Jaramillo, R. Gomperts, R. E. Stratmann, O. Yazyev, A. J. Austin, R. Cammi, C. Pomelli, J. W. Ochterski, P. Y. Ayala, K. Morokuma, G. A. Voth, P. Salvador, J. J. Dannenberg, V. G. Zakrzewski, S. Dapprich, A. D. Daniels, M. C. Strain, O. Farkas, D. K. Malick, A. D. Rabuck, K. Raghavachari, J. B. Foresman, J. V. Ortiz, Q. Cui, A. G. Baboul, S. Clifford, J. Cioslowski, B. B. Stefanov, G. Liu, A. Liashenko, P. Piskorz, I. Komaromi, R. L. Martin, D. J. Fox, T. Keith, M. A. Al-Laham, C. Y. Peng, A. Nanayakkara, M. Challacombe, P. M. W. Gill, B. Johnson, W. Chen, M. W. Wong, C. Gonzalez and J. A. Pople, *Gaussian 09*, Gaussian Inc., Wallingford CT, 2009.
[4] A. D. Becke, *J. Chem. Phys.*, 1993, **98**, 5648-5652.
[5] C. Lee, W. Yang and R. G. Parr, *Physical Review B*, 1988, **37**, 785-789.
[6] K. L. Schuchardt, B. T. Didier, T. Elsethagen, L. Sun, V. Gurumoorthi, J. Chase, J. Li and T. L. Windus, *J. Chem. Inf. Model.*, 2007, **47**, 1045-1052.
[7] A. V. Marenich, C. J. Cramer and D. G. Truhlar, *J. Phys. Chem. B*, 2009, **113**, 6378-6396.
[8] J. Wang, R. M. Wolf, J. W. Caldwell, P. A. Kollman and D. A. Case, *J. Comput. Chem.*, 2004, **25**, 1157-1174.
[9] M. A. A. Ibrahim, *J. Comput. Chem.*, 2011, **32**, 2564-2574.
[10] S. Rendine, S. Pieraccini, A. Forni and M. Sironi, *PCCP*, 2011, **13**, 19508-19516.
[11] D. A. Case, T. A. Darden, I. T. E. Cheatham, C. L. Simmerling, J. Wang, R. E. Duke, R. Luo, R. C. Walker, W. Zhang, K. M. Merz, B. Roberts, S. Hayik, A. Roitberg, G. Seabra, J. Swails, A. W. Götz, I. Kolossváry, K. F. Wong, F. Paesani, J. Vanicek, R. M. Wolf, J. Liu, X. Wu, S. R. Brozell, T. Steinbrecher, H. Gohlke, Q. Cai, X. Ye, J. Wang, M.-J. Hsieh, G. Cui, D. R. Roe, D. H. Mathews, M. G. Seetin, R. Salomon-Ferrer, C. Sagui, V. Babin, T. Luchko, S. Gusarov, A. Kovalenko and P. A. Kollman, *AMBER12*, University of California, San Francisco, 2012.
[12] C. I. Bayly, P. Cieplak, W. Cornell and P. A. Kollman, *J. Phys. Chem.*, 1993, **97**, 10269-10280.
[13] A. Rappe and C. Casewit, *Molecular Mechanics Across Chemistry*, University Science Books, Sausalito, CA, 1997.
[14] P. Cieplak, J. Caldwell and P. Kollman, *J. Comput. Chem.*, 2001, **22**, 1048-1057.
[15] X. Wu, Z. Liu, S. Huang and W. Wang, *PCCP*, 2005, **7**, 2771-2779.
[16] T. Darden, D. York and L. Pedersen, *J. Chem. Phys.*, 1993, **98**, 10089-10092.
[17] U. Essmann, L. Perera, M. L. Berkowitz, T. Darden, H. Lee and L. G. Pedersen, *J. Chem. Phys.*, 1995, **103**, 8577-8593.
[18] *see* http://ambermd.org/gpus/ Accessed 2012/10/10.
[19] A. W. Goetz, R. Salomon-Ferrer, D. Poole, S. L. Grand and R. C. Walker, *Routine microsecond molecular dynamics simulations with AMBER - Part II: Particle Mesh Ewald (in preparation)*, 2011.
[20] J. P. Ryckaert, G. Ciccotti and H. J. C. Berendsen, *Journal of Computational Physics*, 1977, **23**, 327-341.
[21] *PyMOL Molecular Graphics System*, DeLano Scientific LLC, 2009.
[22] T. Williams and C. Kelley, *Gnuplot 4.4: An Interactive Plotting Program*, 2009, http://www.gnuplot.info.
[23] J. Shao, S. W. Tanner, N. Thompson and T. E. Cheatham, *J. Chem. Theory Comput.*, 2007, **3**, 2312-2334.